NUREG/CP-0166
Vol. 3

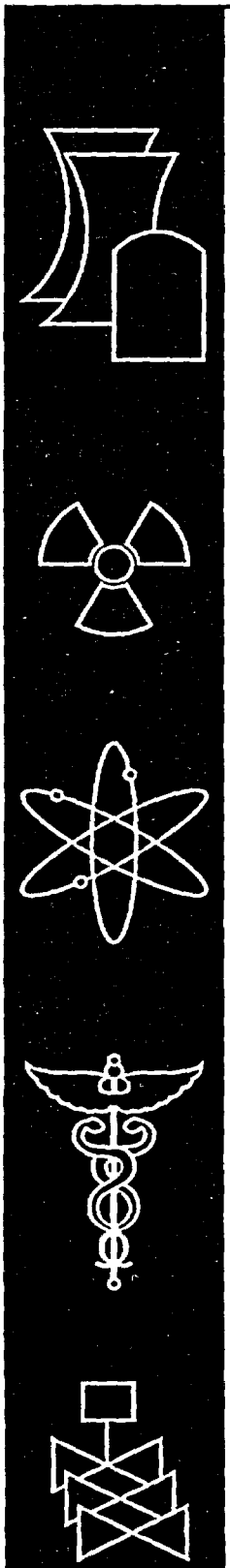

Proceedings of the Twenty-Sixth Water Reactor Safety Information Meeting

Volume 3
– Thermal Hydraulic Research
– Plant Aging I — Plant Life Management
– High Burn-up Fuel
– Plant Aging II — Cable Aging

Held at
Bethesda Marriott Hotel
Bethesda, Maryland
October 26–28, 1998

U.S. Nuclear Regulatory Commission
Office of Nuclear Regulatory Research

Proceedings prepared by
Brookhaven National Laboratory

AVAILABILITY NOTICE

Availability of Reference Materials Cited in NRC Publications

NRC publications in the NUREG series, NRC regulations, and *Title 10, Energy,* of the *Code of Federal Regulations,* may be purchased from one of the following sources:

1. The Superintendent of Documents
   U.S. Government Printing Office
   P.O. Box 37082
   Washington, DC 20402–9328
   <http://www.access.gpo.gov/su_docs>
   202–512–1800

2. The National Technical Information Service
   Springfield, VA 22161–0002
   <http://www.ntis.gov/ordernow>
   703–487–4650

The NUREG series comprises (1) brochures (NUREG/BR-XXXX), (2) proceedings of conferences (NUREG/CP-XXXX), (3) reports resulting from international agreements (NUREG/IA-XXXX), (4) technical and administrative reports and books [(NUREG-XXXX) or (NUREG/CR-XXXX)], and (5) compilations of legal decisions and orders of the Commission and Atomic and Safety Licensing Boards and of Office Directors' decisions under Section 2.206 of NRC's regulations (NUREG-XXXX).

A single copy of each NRC draft report is available free, to the extent of supply, upon written request as follows:

Address: Office of the Chief Information Officer
Reproduction and Distribution
Services Section
U.S. Nuclear Regulatory Commission
Washington, DC 20555–0001
E-mail: <DISTRIBUTION@nrc.gov>
Facsimile: 301–415–2289

A portion of NRC regulatory and technical information is available at NRC's World Wide Web site:

<http://www.nrc.gov>

All NRC documents released to the public are available for inspection or copying for a fee, in paper, microfiche, or, in some cases, diskette, from the Public Document Room (PDR):

NRC Public Document Room
2120 L Street, N.W., Lower Level
Washington, DC 20555–0001
<http://www.nrc.gov/NRC/PDR/pdr1.htm>
1–800–397–4209 or locally 202–634–3273

Microfiche of most NRC documents made publicly available since January 1981 may be found in the Local Public Document Rooms (LPDRs) located in the vicinity of nuclear power plants. The locations of the LPDRs may be obtained from the PDR (see previous paragraph) or through:

<http://www.nrc.gov/NRC/NUREGS/SR1350/V9/lpdr/html>

Publicly released documents include, to name a few, NUREG-series reports; *Federal Register* notices; applicant, licensee, and vendor documents and correspondence; NRC correspondence and internal memoranda; bulletins and information notices; inspection and investigation reports; licensee event reports; and Commission papers and their attachments.

Documents available from public and special technical libraries include all open literature items, such as books, journal articles, and transactions, *Federal Register* notices, Federal and State legislation, and congressional reports. Such documents as theses, dissertations, foreign reports and translations, and non-NRC conference proceedings may be purchased from their sponsoring organization.

Copies of industry codes and standards used in a substantive manner in the NRC regulatory process are maintained at the NRC Library, Two White Flint North, 11545 Rockville Pike, Rockville, MD 20852–2738. These standards are available in the library for reference use by the public. Codes and standards are usually copyrighted and may be purchased from the originating organization or, if they are American National Standards, from—

American National Standards Institute
11 West 42nd Street
New York, NY 10036–8002
<http://www.ansi.org>
212–642–4900

NUREG/CP-0166
Vol. 3

Proceedings of the Twenty-Sixth Water Reactor Safety Information Meeting

Volume 3
– Thermal Hydraulic Research
– Plant Aging I — Plant Life Management
– High Burn-up Fuel
– Plant Aging II — Cable Aging

Held at
Bethesda Marriott Hotel
Bethesda, Maryland
October 26–28, 1998

Manuscript Completed: May 1999
Date Published: June 1999

Compiled by: Susan Monteleone

S. Nesmith, NRC Project Manager

Office of Nuclear Regulatory Research
U.S. Nuclear Regulatory Commission
Washington, DC 20555-0001

Proceedings prepared by
Brookhaven National Laboratory

ABSTRACT

This three-volume report contains papers presented at the Twenty-Sixth Water Reactor Safety Information Meeting held at the Bethesda Marriott Hotel, Bethesda, Maryland, October 26-28, 1998. The papers are printed in the order of their presentation in each session and describe progress and results of programs in nuclear safety research conducted in this country and abroad. Foreign participation in the meeting included papers presented by researchers from France, Germany, Italy, Japan, Norway, Russia, Sweden and Switzerland. The titles of the papers and the names of the authors have been updated and may differ from those that appeared in the final program of the meeting.

PROCEEDINGS OF THE
26TH WATER REACTOR SAFETY INFORMATION MEETING

OCTOBER 26-28, 1998

Published in Three Volumes

GENERAL INDEX

Volume 1

Volume 2

Volume 3

REGISTERED ATTENDEES
26TH WATER REACTOR SAFETY MEETING

D. C. AGARWAL
U.S. DEPT. OF ENERGY
19901 GERMANTOWN RD. GERMANTOWN
MD 20585 USA
Phone: 301 903 3919
Fax: 301 903 5057
E-Mail: duli.agarwal@hq.doe.gov

R. AMADOR-GARCIA
COMISION NACIONAL DE SEGURIDAD
NUCLEAR
BARRAGAN DR. #779 MEXICO, D.F. 03020
MEXICO
Phone: 525-590-8113
Fax: 525-590-6103
E-Mail:

F. AMMIRATO
EPRI NDE CENTER
1300 HARRIS BLVD. CHARLOTTE NC 28262
USA
Phone: 704 547 6129
Fax: 704 547 6168
E-Mail: fammirat@epri.com

S. ANGHAIE
U. FLORIDA, DEPT. NUCLEAR &
RADIOLOGICAL ENG.
ROOM 202, NUCLEAR SCIENCES CENTER
GAINESVILLE FL 32611 USA
Phone: 352 392 1421
Fax: 352 392 8656
E-Mail: anghaie@ufl.edu

A. R. ANKRUM
BATTELLE PNNL
PO BOX 999, K8-28 RICHLAND WA 99352
USA
Phone: 509 372 4095
Fax: 509 372 6242
E-Mail: ar_ankrum@pnl.gov

W. H. BAMFORD
WESTINGHOUSE
PO BOX 355 PITTSBURGH PA 15238 USA
Phone: 412 374 6515
Fax: 412 374 6277
E-Mail: bamfordwh@westinghouse.com

S. BANERJEE
UNIVERSITY OF CALIFORNIA
DEPT. OF CHEMICAL ENGINEERING
SANTA BARBARA CA 93106 USA
Phone: 805 893 3456
Fax: 805 893 4731
E-Mail: banerjee@anemone.ucsb.edu

R. E. BEEDLE
NUCLEAR ENERGY INSTITUTE
1776 EYE ST., NW, SUITE 400
WASHINGTON DC 20006 USA
Phone: 202 739 8101
Fax: 202 785 1898
E-Mail: rb@nei.org

E. BEK
PJSC MASHINOSTROITELNY ZAVOD
ELECTROSTAL MOSCOW REGION 144001
RUSSIA
Phone: 7 95 7029731
Fax: 7 96 5750947
E-Mail:

K. D. BERGERON
SANDIA NATIONAL LABORATORIES
PO BOX 5800, DEPT. 6421/MS0739
ALBUQUERQUE NM 87185-0739 USA
Phone: 505 844 2507
Fax: 505 844 8719
E-Mail: kdberge@sandia.gov

C. E. BEYER
BATTELLE/PNNL
BATTELLE BLVD. RICHLAND WA 99352
USA
Phone: 509-372-4605
Fax: 509-372-4439
E-Mail: carl.beyer@pnl.gov

D. BHARGAVA
VIRGINIA POWER
5000 DOMINION BLVD. GLEN ALLEN VA
23060 USA
Phone: 804 273 3638
Fax: 804 293 3448
E-Mail: divakar_bhargava@vapower.com

M. BILLONE
ARGONNE NATIONAL LAB
9700 S. CASS AVE ARGONNE IL
60439-4838 USA
Phone: 630 252 7146
Fax: 630 252 9232
E-Mail: billone@anl.gov

N. E. BIXLER
SANDIA NATIONAL LABORATORIES
P.O. BOX 5800, DEPT. 6421/MS0739
ALBUQUERQUE NM 87185-0739 USA
Phone: 505 845 3144
Fax: 505 844 8719
E-Mail: nbixler@sandia.gov

J. E. BONDARYK
ENGINEERING TECHNOLOGY CENTER
84 SHERMAN ST. CAMBRIDGE MA 02148
USA
Phone: 617 864 1944
Fax: 617 864 1953
E-Mail: jbondaryk@etc.atinc.com

G. A. BROWN
AEA TECHNOLOGY
THOMSON HOUSE, RISLEY WARRINGTON
CHESHIRE WA3 6AT ENGLAND
Phone: 44 19 25 254473
Fax: 44 19 25 254473
E-Mail: geoff.brown@aeat.co.uk

T. J. BROWN
SANDIA NATIONAL LABORATORIES
P.O. BOX 5800 ALBUQUERQUE NM
87185-0736 USA
Phone: 505 844 5247
Fax:
E-Mail: tjbrown@sandia.gov

D. A. BROWNSON
IDAHO NATIONAL ENGINEERING &
ENVIRONMENTAL LAB
PO BOX 1625 IDAHO FALLS ID 83415-3850
USA
Phone: 208 526 9460
Fax: 208 526 2930
E-Mail: dov@inel.gov

W. T. BRUNSON
FRAMATOME COGEMA FUELS
3315 OLD FOREST RD. LYNCHBURG VA
24503 USA
Phone: 804 832 2687
Fax: 804 832 3663
E-Mail: wbrunson@framatech.com

J. W. BRYANT
LOCKHEED MARTIN IDAHO
TECHNOLOGIES CO.
PO BOX 1625 IDAHO FALLS ID 83415-3114
USA
Phone: 208 526 3981
Fax: 208 526 4902
E-Mail: bryajw@inel.gov

J. C. BUTLER
NUCLEAR ENERGY INSTITUTE
1776 EYE ST., NW, SUITE 400
WASHINGTON DC 20006 USA
Phone: 202 739 8000
Fax: 202 785 1898
E-Mail: jcb@nei.org

S. T. BYRNE
ABB
2000 DAY HILL RD., MC 9483-1903
WINDSOR CT 06095 USA
Phone: 860 285 3469
Fax: 860 285 4232
E-Mail: stephen.t.byrne@ussev.mail.abb.com

A. L. CAMP
SANDIA NATIONAL LABORATORIES
PO BOX 5800, MS 0747 ALBUQUERQUE NM
87185-0747 USA
Phone: 505 844 5960
Fax: 505 844 3321
E-Mail: alcamp@sandia.gov

J. J. CAREY
EPRI
3412 HILLVIEW AVE PALO ALTO CA 94304
USA
Phone: 650 855 2105
Fax: 650 855 7945
E-Mail: jcarey@epri.com

Y.C. CHI
DEPT. OF NUCLEAR REG., ATOMIC ENERGY COMM.
67 LANE 144, KEELUNG RD, SEC. 4 TAIPEI TAIWAN 10660 REP. CHINA
Phone: 886 2 23634180
Fax: 886 2 23635377
E-Mail: chiyc@cc22.aec.gov.tw

W. G. CHOE
TU ELECTRIC
1601 N. BRYAN ST. DALLAS TX 75201-3411 USA
Phone: 214 812 4371
Fax: 214 812 8687
E-Mail: whee.choe@tuelectric.com

H. M. CHUNG
ARGONNE NATIONAL LAB
9700 S. CASS AVE ARGONNE IL 60439-4838 USA
Phone: 630 252 5111
Fax: 630 252 3604
E-Mail: hee_chung@qmgate.anl.gov

A. B. COHEN
ARGONNE NATIONAL LAB
9700 S. CASS AVE ARGONNE IL 60439-4838 USA
Phone: 630 252 5179
Fax: 630 252 9232
E-Mail: adam.cohen@anl.gov

A. S. COHLMEYER
VPA CORPORATION
1768 BUSINESS CENTER DRIVE RESTON VA 20190 USA
Phone: 703 438 3911
Fax: 703 438 3911
E-Mail:

L. CONNOR
DOC-SEARCH ASSOCIATES
PO BOX 34 CABIN JOHN MD 20818 USA
Phone: 301 346 0119
Fax: 503 973 5037
E-Mail: lynnbc@compuserve.com

K. O. COZENS
NUCLEAR ENERGY INSTITUTE
1776 EYE ST., NW, SUITE 400
WASHINGTON DC 20006 USA
Phone: 202 739 8000
Fax: 202 785 1898
E-Mail: koc@nei.org

D. CRAWFORD
ARGONNE NATIONAL LABORATORY
P.O. BOX 2528 IDAHO FALLS ID 83403 USA
Phone: 208 533 7456
Fax: 208 533 7863
E-Mail: doug.crawford@anlw.anl.gov

M. E. CUNNINGHAM
PACIFIC NORTHWEST NATIONAL LAB
P.O. BOX 999 RICHLAND WA 99337 USA
Phone: 509 372 4987
Fax: 509 372 4989
E-Mail: mitch.cunningham@pnl.gov

G. L. DARDEN
VIRGINIA POWER
5000 DOMINION BLVD, IN3S GLEN ALLEN VA 23060 USA
Phone: 804 273 3497
Fax: 804 273 3543
E-Mail: gary_darden@vapower.com

R. S. DAUM
PENNSYLVANIA STATE UNIVERSITY
231 SACKETT BLDG., DEPT OF NUC ENG
STATE COLLEGE PA 16802 USA
Phone: 814 863 3512
Fax: 814 865 8499
E-Mail: rsd12r@psu.edu

J. S. DE BOR
DE BOR AND ASSOCIATES, INC.
3630 NO. 21 AVE. ARLINGTON VA 22207 USA
Phone: 703 524 3222
Fax: 703 524 2427
E-Mail: cc001331@mindspring.com

M. S. DESAI
UNDERWRITERS LAB
12 LABORATORY DRIVE, P.O. BOX 13995
RESEARCH TRIANGLE PARK NC 27709 USA
Phone: 919 549 1610
Fax: 919 547 6110
E-Mail: desaim@ul.com

T. L. DICKSON
LOCKHEED MARTIN ENERGY RESEARCH
PO BOX 2008 OAK RIDGE TN 37831 USA
Phone: 423 574 0650
Fax: 423 576 0651
E-Mail: tyd@oml.gov

I. DOR
CEA GRENOBLE/DRN/DTP/SMTH
17 RUE DES MARTYRS GRENOBLE CEDEX 9 38054 FRANCE
Phone: 33 4 76885970
Fax: 33 47 6889453
E-Mail: isabelle.dor@cea.fr

S. DOROFEEV
RUSSIAN RESEARCH CENTER, KURCHATOV INSTITUTE
KIRCHATOV SQ. 1 MOSCOW 123182 RUSSIA
Phone:
Fax:
E-Mail:

R. L. DOTY
PP&L, INC.
2 N. NINTH ST. (GENA93) ALLENTOWN PA 18101 USA
Phone: 610 774 7932
Fax: 610 774 7205
E-Mail: rldoty@papl.com

J. D. DUNKLEBERGER
NEW YORK STATE HEALTH DEPT.
II UNIVERSITY PLACE ALBANY NY 12203 USA
Phone: 518 458 6458
Fax: 518 458 6434
E-Mail: jdd08@health.state.ny.us

B. M. DUNN
FRAMATOME TECHNOLOGIES, INC.
OLD FOREST RD. LYNCHBURV VA 24501 USA
Phone: 804 832 2427
Fax:
E-Mail: bdunn@framatech.com

F. A. DURAN
SANDIA NATIONAL LABORATORIES
PO BOX 5800, MS0747, DEPT 6412
ALBUQUERQUE NM 87185-0747 USA
Phone: 505 844 4495
Fax: 505 844 3321
E-Mail: faduran@sandia.gov

F. A. EMERSON
NUCLEAR ENERGY INSTITUTE
1776 EYE ST., NW, SUITE 400
WASHINGTON DC 20006 USA
Phone: 202 739 8000
Fax: 202 785 1898
E-Mail: fae@nei.org

R. C. EVANS
NUCLEAR ENERGY INSTITUTE
1776 EYE ST., NW, SUITE 400
WASHINGTON DC 20006 USA
Phone: 202 739 8000
Fax: 202 785 1898
E-Mail: rce@nei.org

M. L. EYRE
PECO NUCLEAR
965 CHESTERBROOK BLVD., 62A-5 WAYNE PA 19087-5691 USA
Phone: 610 640 6829
Fax: 610 640 6797
E-Mail: meyre@peco-energy.com

J. A. FORESTER
SANDIA NATIONAL LABORATORIES
PO BOX 5800, MS 0747 ALBUQUERQUE NM 87185-0747 USA
Phone: 505 844 0578
Fax: 505 844 3321
E-Mail: jafores@sandia.gov

L FRANKL
STOLLER NUCLEAR FUEL/NAC INTERNATIONAL
485 WASHINGTON AVENUE
PLEASANTVILLE NY 10570 USA
Phone: 914-741-1200
Fax: 914-741-2093
E-Mail: lfrankl@nacintl.com

Y. FUJIKI
TOSHIBA INTERNATIONAL CORP.
175 CURTNER AVENUE SAN JOSE CA USA
Phone: 408-925-6592
Fax: 408-925-4945
E-Mail: yasunobu.fujiki@toshiba.co.jp

M. FUJITA
KANSAI ELECTRIC POWER CO., INC.
2001 L ST., NW, SUITE 801 WASHINGTON DC 20036 USA
Phone: 202 659 1138
Fax: 202 457 0272
E-Mail: mfujita@kansai.com

T. FUKETA
JAPAN ATOMIC ENERGY RESEARCH INSTITUTE
TOKAI IBARAKI 319-1195 JAPAN
Phone: 81 29 282 6386
Fax: 81 29 282 6160
E-Mail: toyo@nsrr.tokai.jaeri.go.jp

F. GANTENBEIN
INSTITUT DE PROTECTION ET DE SURETE NUCLEAIRE
BP 6 FONTENAY-AUX-ROSES CEDEX
92265 FRANCE
Phone:
Fax
E-Mail: francase.gantenbein@ipsn.fr

G. GAUTHIER
CEA/IPSN/DES/SAMS/BASME
BP 6 FONTENAY-AUX-ROSES 92265
FRANCE
Phone: 01 46 54 90 16
Fax: 01 47 46 10 14
E-Mail:

P. H. GENOA
NUCLEAR ENERGY INSTITUTE
1776 EYE ST., NW, SUITE 400
WASHINGTON DC 20006 USA
Phone: 202 739 8000
Fax: 202 785 1898
E-Mail: phg@nei.org

G. GIGGER
WESTINGHOUSE
P.O. BOX 79 WEST MIFFLIN PA 15122 USA
Phone: 412 476 7365
Fax
E-Mail:

K. T. GILLEN
SANDIA NATIONAL LABORATORY
ORG. 1811 - M/S 1407, P.O. BOX 5800
ALBUQUERQUE NM 87185-1407 USA
Phone: 505 844 7494
Fax: 505 844 9624
E-Mail: ktgille@sandia.gov

R. M. GODFREY
AUSTRALIAN NUCLEAR SCIENCE & TECH. ORG.
EMBASSY OF AUSTRALIA, 1601 MASS. AVE., NW WASHINGTON DC 20036 USA
Phone: 202 797 3042
Fax: 202 483 5156
E-Mail:

M. GOMOLINSKI
INSTITUT DE PROTECTION ET DE SURETE NUCLEAIRE
BP 6 FONTENAY-AUX-ROSES 92265
FRANCE
Phone: 146548177
Fax: 146548925
E-Mail: maurice.gomolinski@ipsn.fr

A. L. GRAHAM
COUNCIL FOR NUCLEAR SAFETY
PO BOX 7106 CENTURION GAUTENG
00046 SOUTH AFRICA
Phone: 27 12 6635500
Fax: 27 12 6635513
E-Mail: agraham@cns.co.za

D. F. GRAND
CEA - NUCLEAR REACTORS DIRECTORATE
17 RUE DES MARTYRS GRENOBLE CEDEX 9 38054 FRANCE
Phone: 33 4 7688 3933
Fax: 33 4 7688 5179
E-Mail: grand@dtp.cea.fr

C. GRANDJEAN
INSTITUT DE PROTECTION ET DE SURETE NUCLEAIRE
CEA CADARACHE ST PAUL LEZ DURANCE
13108 FRANCE
Phone: 33 4 4225 4480
Fax: 33 4 4225 6142
E-Mail: claude.grandjean@ipsn.fr

M. GREEN
OECD HALDEN REACTOR PROJECT
P.O. BOX 173, N-1751 HALDEN NORWAY
Phone: 47 69212200
Fax: 47 69212201
E-Mail:

M. GREGORIC
SLOVENIAN NUCLEAR SAFETY ADMINISTRATION
VOJKOVA 59 LJUBLJANA SI 01113
SLOVENIA
Phone: 386 61 172 11 00
Fax: 386 61 172 11 99
E-Mail: miroslav.gregoric@rujv.sigov.mail.si

J. HA
KOREA ATOMIC ENERGY RESEARCH INSTITUTE
150 DUKJINDONG, YUSUNG-KU TAEJON
305-353 KOREA
Phone: 82 42 8682755
Fax: 82 42 8688374
E-Mail: jjha@nanum.kaeri.re.kr

B. P. HALLBERT
LOCKHEED-MARTIN
P.O. BOX 1625 IDAHO FALLS ID 83415 USA
Phone: 208 526 9867
Fax:
E-Mail: hallbp@inel.gov

R. O. HARDIES
BGE
1650 CALVERT CLIFFS PKWY LUSBY MD 20732 USA
Phone: 410-495-6577
Fax: 410-492-6577
E-Mail: robert.o.hardies@bge.com

J. J. HARTZ
WESTINGHOUSE ELECTRIC
P.O. BOX 355 PITTSBURGH PA 15230 USA
Phone: 412 374 5185
Fax:
E-Mail: hartzjj@westinghouse.com

R. C. HARVIL
CONSUMERS ENERGY, PALISADES NUCLEAR PLANT
27780 BLUE STAR MEMORIAL HWY
COVERT MI 49043 USA
Phone: 616 764 2954
Fax: 616 764 2060
E-Mail:

L. HENDRICKS
NUCLEAR ENERGY INSTITUTE
1776 EYE ST., NW, SUITE 400
WASHINGTON DC 20006 USA
Phone: 202 739 8000
Fax: 202 785 1898
E-Mail: bxh@nei.org

J.Y. HENRY
CEA/IPSN/DES/SAMS/BASP
BP 6 FONTENAY-AUX-ROSES 92265
FRANCE
Phone: 01 46 54 90 16
Fax: 01 47 46 10 14
E-Mail: jean.yves-henry@ipsn.fr

D. C. HERRELL
MPR ASSOCIATES, INC.
320 KING ST. ALEXANDRIA VA 22314 USA
Phone: 703 519 0200
Fax: 703 519 0220
E-Mail: dherrell@mpra.com

C. HERRERA
CHUBU ELECTRIC POWER CO.
900 17TH ST, NW, STE 1220 WASHINGTON DC 20006 USA
Phone: 202 775 1960
Fax: 202 331 9256
E-Mail: carolina@chubudc.com

J. C. HIGGINS
BROOKHAVEN NATIONAL LABORATORY
PO BOX 5000, BLDG. 130 UPTON NY 11973-5000 USA
Phone: 516 344 2432
Fax: 516 344 3957
E-Mail: higgins@bnl.gov

J. S. HOLM
SIEMENS POWER CORP.
2101 HORN RAPIDS RD. RICHLAND WA 99352 USA
Phone: 509 375 8142
Fax: 509 375 8775
E-Mail: jerrys_holm@nfuel.com

T. HSU
VIRGINIA POWER
5000 DOMINION BLVD. GLEN ALLEN VA 23060 USA
Phone:
Fax:
E-Mail:

H. T. HUNTER
LOCKHEED MARTIN ENERGY RESEARCH
PO BOX 2008 OAK RIDGE TN 37831-6362 USA
Phone: 423 576-6297
Fax: 423 574 6182
E-Mail: h30@ornl.gov

J. E. HUTCHINSON
EPRI
1300 HARRIS BLVD. CHARLOTTE NC 28262 USA
Phone: 704 547 6086
Fax: 704 547 6035
E-Mail: jhutchin@epri.com

J.P. C. HUTIN
ELECTRICITE DE FRANCE
DEPT. 1, PLACE PLEYEL ST DENIS CEDEX 93282 FRANCE
Phone: 33 1 43693051
Fax: 33 1 43693495
E-Mail: jean-pierre.hutin@edfgdf.fr

J. R. IRELAND
LOS ALAMOS NATIONAL LABORATORY
PO BOX 1663, MS F606 LOS ALAMOS NM 87545 USA
Phone: 505 667 4567
Fax: 505 665 5204
E-Mail: john.ireland@lanl.gov

S. K. ISKANDER
OAK RIDGE NATIONAL LABORATORY
MS 6151, BLDG. 45005, P.O. BOX 2008 OAK RIDGE TN 37831-6151 USA
Phone: 423-574-4468
Fax: 423-574-5118
E-Mail: ski@ornl.gov

R. IWASAKI
NUCLEAR POWER ENGINEERING CORP.
FUJITA KANKO TORANOMON BLDG, 6F
MINATO-KU TOKYO 105-0001 JAPAN
Phone: 81 3 3438 3068
Fax: 81 3 5470 5544
E-Mail:

R. JANATI
DEPT. OF ENVIR. PROT., DIV. OF NUCLEAR SAFETY
PO BOX 8469, 400 MARKET ST.
HARRISBURG PA 17105 USA
Phone: 717 787 2163
Fax: 717 783 8965
E-Mail: janati.rich@91.dep.state.pa.us

J. V. JANERI
UNDERWRITERS LABORATORIES, INC.
12 LABORATORY DR. RESEARCH TRIANGLE PARK NC 27709 USA
Phone: 919 549 1902
Fax: 919 547 6113
E-Mail: janerij@ul.com

J. JANSKY
BTB-JANSKY GmbH
GERLINGERSTR. 151 LEONBERG 71229 GERMANY
Phone: 07152 41058
Fax: 07152 73868
E-Mail: btbjansky1@aol.com

T-E. JIN
KOREA POWER ENGINEERING CO.
360-9 MABUK-RI, KUSONG-MYON
YONGIN-CITY KYUNG GI-DD 449713 KOREA
Phone: 0331 289 7579
Fax: 0331 289 4517
E-Mail: jinte@ns.kopec.co.kr

B. W. JOHNSON
UNIVERSITY OF VIRGINIA
THORNTON HALL CHARLOTTESVILLE VA 22903-2442 USA
Phone: 804 924 7623
Fax: 804 924 8818
E-Mail: bwj@virginia.edu

W. V. JOHNSTON
RETIRED
2 RUTH LAND DOWNINGTOWN PA 19335 USA
Phone: 610 873 7182
Fax: 610 873 7182
E-Mail: wjohn@nni.com

C. R. JONES
TECHNIDIGM ORG.
13624 HARTSBOURNE DR. GERMANTOWN MD 20874 USA
Phone: 301-972-2017
Fax: 301-428-9341
E-Mail: tech2000@ix.netcom.com

E. KAPLAR
RUSSIAN RESEARCH CENTER, KURCHATOV INSTITUTE
KIRCHATOV SQ. 1 MOSCOW 123182 RUSSIA
Phone: 7 095 196 9725
Fax: 7 095 196 1702
E-Mail: asmolov@nsi.kiae.ru

T. M. KARLSEN
OECD HALDEN REACTOR PROJECT
P.O. BOX 173, N-1751 HALDEN NORWAY
Phone: 47 69212200
Fax: 47 69212201
E-Mail:

L. M. KAUFMAN
UNIVERSITY OF VIRGINIA
THORNTON HALL CHARLOTTESVILLE VA 22901 USA
Phone: 804 924 6083
Fax: 804 924 8818
E-Mail: lori@virginia.edu

P. J. KERSTING
KW CONSULTING, INC.
PO BOX 101567 PITTSBURGH PA 15237 USA
Phone: 412 635 7333
Fax: 412 367 2195
E-Mail: paul@kwconsulting.com

H. KIM
COMMONWEALTH EDISON
1400 OPUS DR., STE. 400 DOWNERS GROVE IL 60515 USA
Phone: 630 663 3072
Fax: 630 663 7181
E-Mail: hak-soo.kim@ucm.com

B. L. KIRK
OAK RIDGE NATIONAL LABORATORY
BLDG. 6025, PO BOX 2008 OAK RIDGE TN 37831-6362 USA
Phone: 423 574 6176
Fax: 423 574 6182
E-Mail: blk@ornl.gov

R. W. KNOLL
FLORIDA POWER CORP.
1022 POWERLINE ROAD CRYSTAL RIVER FL
Phone:
Fax:
E-Mail:

T. S. KRESS
U.S. NRC/ACRS
102-B NEWRIDGE RD. OAK RIDGE TN
37830 USA
Phone: 423 483 7548
Fax: 423 462 7548
E-Mail: tskress@aol.com

K. KUGIMIYA
MITSUBISHI HEAVY INDUSTRIES
AMERICA, INC.
105 MALL BLVD, EXPO MART 339E
MONROEVILLE PA 15146 USA
Phone: 412 374 7395
Fax: 412 374 7377
E-Mail: keiichi_kugimiya@mhiahq.com

S. KURATA
CHUBU ELECTRIC POWER CO.
900 17TH ST, NW, STE 1220 WASHINGTON
DC 20006 USA
Phone: 202 775 1960
Fax: 202 331 9256
E-Mail: kurata@chubudc.com

K. F. KUSSMAUL
UNIVERSITY OF STUTTGART
PFAFFENWALDRING 32 STUTTGART
D70569 GERMANY
Phone: 49 711 685 3582
Fax: 49 711 685 2635
E-Mail: kussmaul@mpa.uni-stuttgart.de

J. A. LAKE
LOCKHEED MARTIN IDAHO
TECHNOLOGIES CO.
P.O. BOX 1625 IDAHO FALLS ID 83415-3860
USA
Phone: 208 526 7670
Fax: 208 526 2930
E-Mail: lakeja@inel.gov

C. LECOMTE
INSTITUT DE PROTECTION ET DE SURETE
NUCLEAIRE
BP 6 FONTENAY-AUX-ROSES 92265
FRANCE
Phone: 01 46 54 77 36
Fax: 01 46 54 79 71
E-Mail: catherine.lecomte@ipsn.fr

C.M. LEE
KOREA POWER ENGINEERING CO.
360-9 MABUK-RI, KUSONG-MYON
YONGIN-CITY KYUNG GI-DO 449713
KOREA
Phone: 0331 289 3579
Fax: 0331 289 4517
E-Mail: cmlee@ns.kopec.co.kr

Y. LIU
ARGONNE NATIONAL LABORATORY
9700 S. CASS AVENUE ARGONNE IL 60439
USA
Phone: 630-252-5127
Fax: 630-252-3250
E-Mail: yylin@anl.gov

M. LIVOLANT
INSTITUT DE PROTECTION ET DE SURETE
NUCLEAIRE
BP 6 FONTENAY-AUX-ROSES CEDEX
92265 FRANCE
Phone:
Fax
E-Mail:

R. LOFARO
BROOKHAVEN NATIONAL LABORATORY
PO BOX 5000, BLDG. 130 UPTON NY
11973-5000 USA
Phone: 516 344 7191
Fax: 516 344 5569
E-Mail: lofaro@bnl.gov

V. K. LUK
SANDIA NATIONAL LABORATORIES
PO BOX 5800, INS DEPT. 6403
ALBUQUERQUE NM 87185-0744 USA
Phone: 505 844 5498
Fax: 505 844 1648
E-Mail: vkluk@sandia.gov

E. S. LYMAN
NUCLEAR CONTROL INSTITUTE
1000 CONNECTICUT AVE., NW, STE 804
WASHINGTON DC 20036 USA
Phone: 202 822 8444
Fax: 202 452 0892
E-Mail: lyman@nci.org

S. MAJUMDAR
ARGONNE NATIONAL LAB
9700 S. CASS AVE ARGONNE IL
60439-4838 USA
Phone: 630 252 5136
Fax: 630 252 9232
E-Mail: saurin_majumdar@qmgate.anl.gov

V. MALOFEEV
RUSSIAN RESEARCH CENTER,
KURCHATOV INSTITUTE
KIRCHATOV SQ. 1 MOSCOW 123182
RUSSIA
Phone: 7 095 196 7466
Fax: 7 095 196 1702
E-Mail: malofeev@nsi.kiae.ru

A. MARION
NUCLEAR ENERGY INSTITUTE
1776 EYE ST., NW, SUITE 400
WASHINGTON DC 20006 USA
Phone: 202 739 8000
Fax: 202 785 1898
E-Mail: am@nei.org

P. MARSILI
AGENZIA NAZIONALE PROTEZIONE
AMBIENTS
VIA VITALIANO BRANCANTI 48 ROME
00144 ITALY
Phone:
Fax
E-Mail:

M. MASSOUD
BGE NUCLEAR ENGINEERING UNIT
1650 CALVERT CLIFFS PARKWAY, NEF-1
LUSBY MD 20657 USA
Phone: 410 495 6522
Fax: 410 495 4498
E-Mail: mahmoud.massoud@bge.com

B. MAVKO
JOSEF STEFAN INSTITUTE
JAMOVA LJUBLJANA 01000 SLOVENIA
Phone: 386 61 1885330
Fax: 386 61 1612258
E-Mail: borut.mavko@ijs.si

R. K. McGUIRE
RISK ENGINEERING, INC.
4155 DARLEY AVE, SUITE A BOULDER CO
80303 USA
Phone: 303 499 3000
Fax: 303 499 4850
E-Mail: info@riskeng.com

J.C. MELIS
INSTITUT DE PROTCTION ET DE SURETE
NUCLEAIRE
BLDG. 250 CE CADARACHE ST PAUL LEZ
DURANCE 01368 FRANCE
Phone: 33 4 4225 8722
Fax: 33 4 4225 2971
E-Mail: jean-claude.melis@ipsn.fr

D. W. MILLER
ILLINOIS POWER CO.
P.O. BOX 678 CLINTON IL 61727 USA
Phone: 217-935-8881
Fax: 217-935-4632
E-Mail:

D. B. MITCHELL
FRAMATOME COGEMA FUELS
3315 OLD FOREST ROAD LYNCHBURG VA
24506-0935 USA
Phone: 804 832 3438
Fax: 804 832 3200
E-Mail: dmitchell@framatech.com

D. J. MODEEN
NUCLEAR ENERGY INSTITUTE
1776 EYE ST., NW, SUITE 400
WASHINGTON DC 20006 USA
Phone: 202 739 8000
Fax: 202 785 1898
E-Mail: djm@nei.org

S. MONTELEONE
BROOKHAVEN NATIONAL LABORATORY
BLDG. 130, 32 LEWIS ROAD UPON NY
11973-5000 USA
Phone: 516 344 7235
Fax: 516 344 3957
E-Mail: monteleo@bnl.gov

R. J. MORANTE
BROOKHAVEN NATIONAL LABORATORY
BLDG. 475C UPTON NY 11973-5000 USA
Phone: 516 344 5860
Fax: 516 344 4255
E-Mail: morante@bnl.gov

J. E. MORONEY
MPR ASSOCIATES, INC.
320 KING ST. ALEXANDRIA VA 22314 USA
Phone: 703 519 0200
Fax: 703 519 0224
E-Mail: jmoroney@mpra.com

M. MURATA
NUCLEAR POWER ENGINEERING CORP.
FUJITA KANKO TORANOMON BLDG. 6F
17-1 MINATO-KU TOKYO 105 0001 JAPAN
Phone:
Fax
E-Mail:

D. P. MURTLAND
SCIENCE & ENGINEERING ASSOCIATES, INC.
7918 JONES BRANCH DR, SUITE 500
MCLEAN VA 22102 USA
Phone: 703 761 4100
Fax: 703 761 4105
E-Mail:

R. K. NADER
DUKE ENERGY CORP.
7812 ROCHESTER HWY. SENECA SC 29679 USA
Phone: 864 885 4166
Fax: 864 885 3401
E-Mail: rknader@duke-energy.com

R. K. NANSTAD
OAK RIDGE NATIONAL LABORATORY
PO BOX 2008, MS6151 OAK RIDGE TN 37831-6151 USA
Phone: 423 574 4471
Fax: 423 574 5118
E-Mail: nanstadrk@ornl.gov

L. A. NEIMARK
ARGONNE NATIONAL LABORATORY
9700 S. CASS AVE. ARGONNE IL 60439-4838 USA
Phone: 630 252 5177
Fax: 630 252 9232
E-Mail: laneimark@anl.gov

J. NESTELL
MPR ASSOCIATES, INC.
320 KING STREET ALEXANDRIA VA 22314 USA
Phone: 703 519 0200
Fax: 703 519 0224
E-Mail: jnestell@mpra.com

H. P. NOURBAKHSH
BROOKHAVEN NATIONAL LABORATORY
PO BOX 5000, BLDG. 130 UPTON NY 11973-5000 USA
Phone: 516-344-5405
Fax: 516 344 3957
E-Mail: nour@bnl.gov

A. NUNEZ-CARRERA
COMISION NACIONAL DE SEGURIDAD NUCLEAR
BARRAGAN DR. #779 MEXICO, D.F. 03020 MEXICO
Phone: 525-590-5113
Fax: 525-590-6103
E-Mail:

J. M. O'HARA
BROOKHAVEN NATIONAL LABORATORY
PO BOX 5000, BLDG. 130 UPTON NY 11973-5000 USA
Phone: 516 344 3638
Fax: 516 344 4900
E-Mail: ohara@bnl.gov

N. ORTIZ
SANDIA NATIONAL LABORATORIES
PO BOX 5800, DEPT. 6400/MS0736
ALBUQUERQUE NM 87185-0736 USA
Phone: 505 844 0577
Fax: 505 844 0955
E-Mail: nrortiz@sandia.gov

D. J. OSETEK
LOS ALAMOS TECHNICAL ASSOCIATES
BLDG. 1, SUITE 400, 2400 LOUISIANA BLVD. NE ALBUQUERQUE NM 87110 USA
Phone: 505 880 3407
Fax: 505 880 3560
E-Mail: djosetek@lata.com

F. OWRE
OECD HALDEN REACTOR PROJECT
P.O. BOX 173, N-1751 HALDEN NORWAY
Phone: 47 69212200
Fax: 47 69212201
E-Mail:

J. PAPIN
INSTITUT DE PROTECTION ET DE SURETE NUCLEAIRE
CEA CADARACHE ST PAUL LEZ DURANCE 13108 FRANCE
Phone: 33 4 4225 3463
Fax: 33 4 4225 6143
E-Mail: joelle.papin@ipsn.fr

K.B. PARK
KOREA ATOMIC ENERGY RESEARCH INSTITUTW
PO BOX 105, YUSONG DAEJON 305-600 KOREA
Phone: 82 42 8682239
Fax: 82 42 8688990
E-Mail: kbpark2@nanum.kaeri.re.kr

W. E. PENNELL
LOCKHEED MARTIN ENERGY RESEARCH
PO BOX 2008 OAK RIDGE TN 37831 USA
Phone: 423 576 8571
Fax: 423 576 0651
E-Mail: pq5@ornl.gov

H. PETTERSSON
VATTENFALL FUEL
FAOK STOCKHOLM S16287 SWEDEN
Phone: 46 87395328
Fax: 46 8128640
E-Mail: hakan@fuel.vattenfall.se

M. PEZZILLI
ENEA
C.R. CASACCIA VIA ANGUILLA RESE.301
ROME 00060 ITALY
Phone: 39 06 30484197
Fax: 39 06 30486308
E-Mail: pezzilli@casaccia.enea.it

L. PHILLIPS
UTILITY RESOURCE ASSOCIATES CORP.
1901 RESEARCH BOULEVARD, SUITE 405
ROCKVILLE MD 20850-3164 USA
Phone: 301 294 3069
Fax: 301 294 7879
E-Mail: lepi@urac.com

R. POST
NUCLEAR ENERGY INSTITUTE
1776 EYE ST., NW, SUITE 400
WASHINGTON DC 20006 USA
Phone: 202 739 8000
Fax: 202 785 1898
E-Mail: rep@nei.org

G. A. POTTS
GENERAL ELECTRIC NUCLEAR ENERGY
CASTLE HAYNE RD., MIC K12, PO BOX 780
WILMINGTON NC 28402-0780 USA
Phone: 910 675 5708
Fax: 910 675 6966
E-Mail: gerald.potts@gene.ge.com

D. POWERS
NRC/ACRS
7964 SARTAN WAY, NEW ALBUQUERQUE NM 08709 USA
Phone: 505-821-2735
Fax: 505-821-0245
E-Mail: dapowers.sandia.gov

J. PUGA
UNESA
FRANCISCO GERYAS 3 MADRID SPAIN
Phone: 34 915674800
Fax: 34 915674988
E-Mail: nuclear@unesa.es

C. PUGH
OAK RIDGE NATIONAL LABORATORY
P.O. BOX 2009, M/S 8063 OAK RIDGE TN 37831 USA
Phone: 423-574-0422
Fax: 423-241-5005
E-Mail: pug@ornl.gov

J. R. RASHID
ANATECH
5435 OBERLIN DRIVE SAN DIEGO CA 92121 USA
Phone: 619-455-6350
Fax: 619-455-1094
E-Mail: joe@anatech.com

N. K. RAY
IDAHO NATIONAL ENG. & ENV. LAB
19901 GERMANTOWN ROAD
GERMANTOWN MD 20874 USA
Phone: 301-903-4126
Fax: 301-903-9902
E-Mail: knr@inel.gov

S. RAY
WESTINGHOUSE ENERGY CENTER
NORTHERN PIKE MONROEVILLE PA 15146 USA
Phone: 412 374 2101
Fax: 412 374 2045
E-Mail: rays@westinghouse.com

P. REGNIER
CEA/IPSN/DES/SAMS/BASP
BP 6 FONTENAY-AUX-ROSES 92265 FRANCE
Phone: 01 46 54 90 16
Fax: 01 47 46 10 14
E-Mail:

I. C. RICKARD
ASEA BROWN BOVERI ENGINEERING SVCS.
200 DAY HILL RD. WINDSOR CT 06095 USA
Phone: 860 285 9678
Fax: 860 285 3253
E-Mail:

J. W. RIVERS
JASON ASSOCIATES CORP.
262 EASTGATE DR., SUITE 335 AIKEN SC 29803 USA
Phone: 803-648-6989
Fax: 803-648-0499
E-Mail: jrivers@scescape.net

G. D. ROBISON
DUKE ENERGY CORP.
526 S. CHURCH ST. CHARLOTTE NC 28202 USA
Phone: 704 382 8685
Fax: 704 382 0368
E-Mail: gdrobiso@duke-energy.com

H. S. ROSENBAUM
EPRI CONSULTANT
917 KENSINGTON DRIVE FREMONT CA 94539 USA
Phone: 510 657 2740
Fax:
E-Mail: hermrosenb@aol.com

T. M. ROSSEEL
OAK RIDGE NATIONAL LABORATORY
PO BOX 2008 OAK RIDGE TN 37631-6158 USA
Phone: 423 574 3380
Fax: 423 574 5118
E-Mail: rosseeltm@ornl.gov

J. G. ROYEN
OECD NUCLEAR ENERGY AGENCY
LE SEINE-ST. GERMAIN-12 BLVD. DES ILES
ISSY-LES-MOULINEAUX F92130 FRANCE
Phone: 33 1 4524 1052
Fax: 33 1 4524 1129
E-Mail: jackques.royen@oecd.org

L. P. RUIZ
COMISION NACIONAL DE SEGURIDAD NUCLEAR
DR. BARRAGAN 779 COL. NARVARTE
MEXICO, D.F. 03020 MEXICO
Phone: 525 590 5054
Fax: 525 590 7508
E-Mail: gsn1@servidor.uncm.mx

A. RYDL
NUCLEAR RESEARCH INSTITUTE REZ
25068 REZ NEAR PRAGUE REZ 25068
CZECH REPUBLIC
Phone: 420 266172471
Fax: 420 220941029
E-Mail: ryd@nri.cz

O. SANDERVAG
SWEDISH NUCLEAR POWER INSPECTORATE
STOCKHOLM 10658 SWEDEN
Phone: 46 8 6988463
Fax: 46 8 6619086
E-Mail: oddbjorn@ski.se

P. A. SCHEINERT
BETTIS ATOMIC POWER LABORATORY
PO BOX 79 WEST MIFFLIN PA 15521-0079 USA
Phone: 412 476 5974
Fax: 412 476 6937
E-Mail:

C. S. SCHLASEMAN
MPR ASSOCIATES, INC.
320 KING STREET ALEXANDRIA VA 22314 USA
Phone: 703 519 0200
Fax: 703 519 0224
E-Mail: cschlaseman@mpra.com

F. K. SCHMITZ
INSTITUT DE PROTECTION ET DE SURETE NUCLEAIRE
CEA CADARACHE ST PAUL LEZ DURANCE 13108 FRANCE
Phone: 33 4 4225 7035
Fax: 33 4 4225 2971
E-Mail: franz.schmitz@ipsn.fr

M. SCHWARZ
INSTITUT DE PROTECTION ET DE SURETE NUCLEAIRE
CENTRE D'ETUDES DE CADARACHE, BAT. 250 ST PAUL LEZ DURANCE 13108 FRANCE
Phone: 33 4 4225 7748
Fax: 33 4 4225 2971

E. SCOTT DE MARTINVILLE
C E A
60, GAL LECLERC FONTENAY AUX ROSES 92265 FRANCE
Phone: 33 1 46548202
Fax: 33 1 46543264
E-Mail:

S. Y. SHIM
ATOMIC ENERGY CONTROL BOARD
280 SLATER ST. OTTAWA ONTARIO K1P5S9 CANADA
Phone: 613 947 1443
Fax: 613 995 2125
E-Mail: shim.s@atomcon.gc.ca

F. A. SIMONEN
PACIFIC NORTHWEST NATIONAL LABORATORY
P.O. BOX 999 RICHLAND WA 99352 USA
Phone: 509-375-2067
Fax: 509-375-3614
E-Mail: fa_simonen@pnl.gov

B.P. SINGH
JUPITOR CORPORATION
2730 UNIVERSITY BLVD. W, STE 900
WHEATON MD 20902 USA
Phone: 301 946 8088
Fax: 301 946 6539
E-Mail: bhupinder.singh@hq.doe.gov

T. SIVERTSEN
OECD HALDEN REACTOR PROJECT
P.O. BOX 173, N-1751 HALDEN NORWAY
Phone: 47 69212200
Fax: 47 69212201
E-Mail:

W. H. SLAGLE
WESTINGHOUSE ELECTRIC
P.O. BOX 355 PITTSBURGH PA 15230 USA
Phone: 412 374 2088
Fax: 412 374 2045
E-Mail: slaglewh@westinghouse.com

L. SLEGERS
SIEMENS
POSTFACH 101063 OFFENBACH D63010
GERMANY
Phone:
Fax:
E-Mail:

A. SMIRNOV
RIAR
ULJANOVSK, DIMITROVGRAD RUSSIA
Phone: 7 84235 32350
Fax: 7 84235 64163
E-Mail:

V. SMIRNOV
RIAR
ULJANOVSK, DIMITROVGRAD RUSSIA
Phone: 7 84235 32350
Fax: 7 84235 64163
E-Mail:

C. L. SMITH
INEEL
2525 FREEMONT IDAHO FALLS ID 83415
USA
Phone: 208 526 9804
Fax:
E-Mail: cls2@inel.gov

G. P. SMITH
ABB COMBUSTION ENGINEERING
NUCLEAR POWER
2000 DAY HILL ROAD WINDSOR CT
06095-0500 USA
Phone: 860-687-8070
Fax: 860-687-8051
E-Mail:

P. SOO
BROOKHAVEN NATIONAL LABORATORY
PO BOX 5000, BLDG. 130 UPTON NY
11973-5000 USA
Phone: 516 344 4094
Fax: 516 344 5569
E-Mail: soo@bnl.gov

S. SPALJ
FER-ZAGREB
PRISAVLJE 8 ZAGREB CROATIA
Phone: 385-16129994
Fax: 385-16129890
E-Mail: srdjan.spalj@fer.hr

K. SPANG
INGEMANSSON TECHNOLOGY AB
SWEDEN
Phone: 46 31 774 7401
Fax: 46 31 774 7474
E-Mail: kjell.spang@ingemanssen.se

N. N. SRINIVAS
DETROIT EDISON
2000 SECOND AVE, WSC H-60 DETROIT MI
48226 USA
Phone: 313 897 1198
Fax: 313 897 1440
E-Mail: srinivasn@dte.com

R. G. STARCK
MPR ASSOCIATES, INC.
320 KING ST. ALEXANDRIA VA 22314 USA
Phone: 703 519 0200
Fax: 703 519 0224
E-Mail:

J. STONE
MPR ASSOCIATES, INC.
320 KING ST. ALEXANDRIA VA 22314 USA
Phone:
Fax:
E-Mail:

P. STOREY
HSE
ST. PETERS HOUSE BOOTLE LIVERPOOL
L203PT UK
Phone: 44 1519514172
Fax: 44 1519513942
E-Mail: peter.storey@HSE.gov.uk

Y. TAKAHASHI
TOKYO ELECTRIC POWER CO.
1-3-1 UCHISAIWAI CHO CHIYODAKU
TOKYO 100-0011 JAPAN
Phone: 81 34216 4951
Fax: 81 33596 8571
E-Mail: to560565@pmail.tepco.co.jp

T. TAMINAMI
TOKYO ELECTRIC POWER CO.
1901 L ST, NW, STE 720 WASHINGTON DC
20036 USA
Phone: 202 457 0790
Fax: 202 457 0810
E-Mail: taminami@tepco.com

J. H. TAYLOR
BROOKHAVEN NATIONAL LABORATORY
PO BOX 5000, BLDG. 130 UPTON NY
11973-5000 USA
Phone: 516 344 7005
Fax: 516 344 3957
E-Mail: jtaylor@bnl.gov

V. H. TESCHENDORFF
GESELLSCHAFT FUR ANLAGEN UND
REAKTORSICHERHEIT
FORSCHUNGSGELANDA GARCHING
D85748 GERMANY
Phone: 49 89 32004423
Fax: 49 89 32004599
E-Mail: tes@grs.de

H. O. TEZEL
ATOMIC ENERGY CONTROL BOARD
280 SLATER STREET ONTARIO K1P559
CANADA
Phone: 613 995 3896
Fax:
E-Mail: tezel.h@atomcon.gc.ca

H. D. THORNBURG
CONSULTANT
901 S. WARFIELD DR. MT. AIRY MD 21771
USA
Phone: 301 831 7328
Fax: 301 829 0874
E-Mail: matt@erols.com

G. J. TOMAN
NUTHERM INTERNATIONAL, INC.
501 SO. 11 ST MT VERNON IL 62864 USA
Phone: 618 244 6000
Fax: 618 244 6641
E-Mail: nutherm@midwest.net

R. L. TREGONING
NAVAL SURACE WARFARE CENTER
9500 MACARTHUR BLVD. WEST
BETHESDA MD 20817 USA
Phone: 301-227-5145
Fax: 301-227-5548
E-Mail: tregonin@metels.dt.navy.mil

S. TSURUMAKI
NUCLEAR POWER ENGINEERING CORP.
SHUWA-KAMIYACHO BLDG., 2F 3-13, 4
CHOME MINATO-KU TOKYO JAPAN
Phone: 81 3 3434 4551
Fax: 81 3 3434 9487
E-Mail:

A. C. UPTON
UMDNJ-RWJ MEDICAL SCHOOL
170 FRELINGHUYSEN RD. PISCATAWAY
NJ 08854 USA
Phone: 732 445 0795
Fax: 732 445 0959
E-Mail: acupton@eohsi.rutgers.edu

R. A. VALENTIN
ARGONNE NATIONAL LABORATORY
9700 S. CASS AVE., BLDG. 308 ARGONNE
IL 60439 USA
Phone: 630 252 4483
Fax: 630 252 3250
E-Mail: richv@anl.gov

K. K. VALTONEN
RADIATION & NUCLEAR SAFETY
AUTHORITY
PO BOX 14 HELSINKI 00881 FINLAND
Phone: 358 9 759 88 331
Fax: 358 9 759 88 382
E-Mail: keijo.valtonen@stuk.fi

J. L. VILLADONIGA
CONSEJO DE SEGURIDAD NUCLEAR
JUSTO DORADO, 11 MADRID 28040 SPAIN
Phone: 34 91 3460240
Fax: 34 91 3460588
E-Mail: jivt@csn.es

M. VILLARAN
BROOKHAVEN NATIONAL LABORATORY
PO BOX 5000, BLDG. 130 UPTON NY
11973-5000 USA
Phone: 516 344 3833
Fax: 516 344 5569
E-Mail: villaran@bnl.gov

G. L. VINE
EPRI
2000 L. ST. NW, SUITE 805 WASHINGTON
DC 20036 USA
Phone: 202-293-6347
Fax: 202-293-2697
E-Mail: gvine@epri.com

C. VITANZA
OECD HALDEN REACTOR PROJECT
OS ALLE 13, PO BOX 173 HALDEN 01751
NORWAY
Phone: 47 69212200
Fax: 47 69212201
E-Mail: carlo.vitanza@hrp.no

R. VON ROHR
INST. OF PROCESS ENGINEERING, ETH
ZURICH
SONNEGGSTRASSE 3, PO BOX ZURICH
CH 8092 SWITZERLAND
Phone: 4116322488
Fax: 4116321141
E-Mail: vonrohr@ivuk.mavt.ethz.ch

N. WAECKEL
ELECTRICITE DE FRANCE SEPTEN
12-14 AV DUTRIEVOS VILLEURBANNE
69628 FRANCE
Phone: 33 4 7282 7571
Fax: 33 4 7282 7713
E-Mail: nicolas.waeckel@edfgdf.fr

L. WARNKEN
SIEMENS KWU NLE
PO BOX 2032 ERLANGEN BAYERN 91050
GERMANY
Phone: 49 91 3118 3336
Fax: 49 91 3118 6362
E-Mail: lueder.warnken@erl11.siemens.de

R. A. WEINER
KW CONSULTING, INC.
PO BOX 101567 PITTSBURGH PA 15237
USA
Phone: 412 635 7732
Fax: 412 687 3965
E-Mail: bob@kwconsulting.com

W. WIESENACK
OECD HALDEN REACTOR PROJECT
P.O. BOX 173, N-1751 HALDEN NORWAY
Phone: 47 69212200
Fax: 47 69212201
E-Mail:

L. E. WILLERTZ
PP&L, INC.
2 NO. NINTH ST., GENA62 ALLENTOWN PA
18101 USA
Phone: 610 774 7646
Fax: 610 774 7830
E-Mail: lewillertz@papa.com

D. H. WILLIAMSON
SAIC
Phone: 703-827-4896
Fax:
E-Mail:

R. T. WOOD
OAK RIDGE NATIONAL LABORATORY
PO BOX 2008, BLDG. 3500, MS6010 OAK
RIDGE TN 37831-6010 USA
Phone: 423 574 5578
Fax: 423 576 8380
E-Mail: woodrt@ornl.gov

R. YANG
EPRI
3412 HILLVIEW AVE. PALO ALTO CA 94024
USA
Phone: 650 855 2481
Fax: 650 855 1026
E-Mail: ryang@epri.com

P.C. YEH
DEPT. OF NUCLEAR REG., ATOMIC
ENERGY COMM.
67 LANE 144, KEELUNG RD, SEC. 4 TAIPEI
TAIWAN 10660 REP. CHINA
Phone: 886 2 23634180
Fax: 886 2 23635377
E-Mail: pcyeh@aec.gov.tw

T. YONOMOTO
JAERI, DEPT. OF REACTOR SAFETY
ENGR.
SHIRAKATA TOKAI IBARAKI 319-11 JAPAN
Phone: 81 29 2825262
Fax: 81 29 2826728
E-Mail: yonomoto@lstf3.tokai.jaeri.go.jp

K. K. YOON
FRAMATOME TECHNOLOGIES
3315 OLD FOREST RD. LYNCHBURG VA
24506-0935 USA
Phone: 804 832 3280
Fax:
E-Mail:

D. ZANOBETTI
UNIV. OF BOLOGNA
VIALE RISORGIMENTO 2 BOLOGNA I40136
ITALY
Phone: 39 051 6443471
Fax: 39 051 6443470
E-Mail: dino.zanobetti@mail.ing.unibo.it

G. L. ZIGLER
ITS CORPORATION
6000 UPTOWN BLVD., NE, STE 300
ALBUQUERQUE NM 87123 USA
Phone: 505 872 1064
Fax: 505 872 0233
E-Mail: gzigler@itsc.com

Proceedings of the
26th Water Reactor Safety Information Meeting
October 26-28, 1998

Contents - Volume 3

High Burn-up Fuel
Chair: R. Meyer

Page

Plant Aging II - Cable Aging
Chair: J. Vora

Scaling in the safety of next generation reactors

S. Banerjee[a], M. G. Ortiz[b], T. K. Larson[b], and D. L. Reeder[c]

[a] *Department of Chemical Engineering, University of California, Santa Barbara, CA 93106 USA*
[b] *Idaho National Engineering and Environmental Laboratory, PO Box 1625, Idaho Falls, ID 83415 USA*
[c] *Consultant, Santa Barbara, CA 93110 USA*

Abstract

A technique was developed to evaluate the applicability of data from small scale facilities for validation of codes for analysis of nuclear safety with emphasis on the next generation of reactors. The technique first divides an accident into phases based on the components that come into play as the accident evolves. Conservation equations, resolved to the component level and their interconnections, are derived for the active components in each phase. The equations are then nondimensionalized and reference parameters are selected such that the dependent variables, other than the system response of interest, are of order 1. Order of magnitude analysis is then performed for each equation and then between equations, based on the numerical values of the nondimensional coefficients for each term, with only the large order terms being retained. The resulting equations then contain terms whose impact on key system responses (e.g., reactor vessel level) are ordered in terms of the magnitude of the nondimensional groups multiplying the O[1] dependent variables. The reduced set of equations and nondimensional groups are validated with experimental data where possible. The validation process is meant to demonstrate that the important terms have been retained and enhance confidence in the system of equations used to capture the main processes occurring in each phase.

The methodology was demonstrated by evaluating the applicability of small-scale facility data for next generation reactor SBLOCA. Based on the nondimensional equations, the dominant nondimensional groups, and hence the dominant physical mechanisms and their dependence on geometric and operational parameters, were identified for a particular scenario, an AP600 cold leg break, starting from the initiating event through long term cooling. The important parameters entering the groups included elevation differences between the reactor vessel and other components, PRHR heat transfer rates, fluid thermophysical properties, liquid levels in tanks, flow resistances in the CMT lines and IRWST lines, flow resistance in the pressurizer surge line, and pressurizer drain rate. It was also shown that, after the beginning of CMT draining and accumulator injection, the dominant processes do not depend on break size provided they are small. The dominant processes were dependent on plant geometry and the operation of engineered safety features, such as the automatic depressurization system. The same transient events were evaluated for three experimental facilities and the same nondimensional groups, and hence mechanisms, were shown to be important. It was found that these nondimensional groups covered the range expected in the AP600, indicating that while there may be some distortions in scaling for a particular facility, between them, the important phenomena were captured and the small-scale facility data appear applicable for SBLOCA in the AP600 system.

In more general terms, the methodology appears suitable for assessing scaling of various facilities for other postulated accidents and for other reactor concepts.

1. Introduction

In this study a method was developed for assessing the applicability of data, obtained in reduced-scale experimental facilities, to the validation of computer codes used in reactor safety analysis. The method was demonstrated by application to a small break loss of coolant accident (SBLOCA) for the advanced pressurized water reactor concept - the AP600.

In this procedure, the SBLOCA transient was divided into several phases based on the process identification and ranking table (PIRT), in each of which different phenomena or components come in to play. Each phase was

described in terms of a set of conservation equations resolved down to the relevant component and component interaction levels. These conservation equations were then nondimensionalized such that all dependent variables other than the key system response that was to be determined, were of O[1]. The magnitude of the nondimensional groups multiplying each term involving dependent variables (of O[1]), then gave a measure of the impact of each term on the system response of interest. To ascertain whether the hierarchy of nondimensionalized equations captured the dominant phenomena in each phase, each equation was checked against experimental data to the extent feasible.

The result of this process was a set of nondimensional groups for each phase whose magnitudes were a measure of their effect on a key system response such as reactor vessel mass inventory. These groups involved quantities like elevation differences, flow resistances of lines, component volumes, and thermophysical properties - all of which could be obtained from design information for each facility and the AP600. By comparing the dominant groups between facilities and with the AP600, conclusions were drawn as to whether the AP600 and the various facilities were in the same region of nondimensional parameter space from the viewpoint of their response in a SBLOCA. Variations in the ordering of the magnitudes of these groups and their relative magnitudes were noted. The effects of these differences in magnitude on key system responses were assessed to determine if distortions in response would be expected in any of the experimental facilities. Thus the method resulted in an assessment of how well a facility was scaled vis-à-vis the AP600 for each phase of a SBLOCA, and hence, how applicable the data from a given facility in a specific phase were to code validation.

The method was demonstrated primarily by assessment of data for one-inch (equivalent) cold leg breaks, though for some phases, scaling with regard to other break sizes and locations, was also touched on.

Applicability of data from several test facilities has been assessed in the scaling methodology demonstration. For the AP600, these include the SPES facility (Rigamonti, 1994) in Italy, the Advanced Plant Experiment (APEX) facility (Westinghouse Electric Company, 1994) at Oregon State University, and the Rig of Safety Assessment (ROSA) facility (Japan Atomic Energy Research Institute, 1996) at the Japanese Atomic Energy Research Institute (JAERI). Relative to the AP600, SPES and ROSA are full-height, full-pressure, volume and power scaled facilities. Scale factors for SPES and ROSA are 1/395 and 1/30.5, respectively, meaning that system fluid volumes, flow areas, and mass flow rates should be approximately in these ratios relative to AP600. As SPES and ROSA are full-height and full-pressure facilities, fluid velocities and transit times should be approximately the same as the AP600. The APEX facility is a reduced pressure, 1/4 height system relative to the AP600. APEX scale factors are as follows: fluid velocity and transit times scale at 1/2, relative elevation and lengths are scaled at 1/4, flow areas are scaled at 1/48, core power and mass flows are scaled at 1/96, and fluid volumes are scaled at 1/192.

While the main intent of this paper is to show that the methodology developed captures the effect of various scales on the system responses of interest, e.g. vessel inventory, an aspect which is also important - a sort of by product so far as this paper is concerned - is that the facilities assessed are shown to produce data applicable to assessment of AP600 SBLOCA analysis codes.

2. Outline of system design features

Before outlining the scaling approach and demonstrating its application, it is necessary to outline the features of the advanced reactor design so the discussion is understandable. The AP600 reactor design is an advanced PWR concept that relies on a number of passive safety features. The design includes low core volumetric heat generation rates, low peak-to-average fuel heat flux ratio, reliance on gas pressurization and gravity heads for safety system operation, and dependence on natural circulation and condensation for safety system performance. All passive safety systems are an integral part of the reactor containment which incorporates heat exchange facilities for removing core decay heat from the reactor system and eventually from the containment to the environment.

A brief overview of the plant will be given here. Figure 1 shows a sketch of the containment and reactor system. The AP600 design is a two-loop system consisting of two hot legs and four cold legs. The AP600 contains many components found in current generation pressurized water reactor designs (e.g., steam generators, pressurizer). A significant difference relative to current commercial systems is that passive emergency core cooling systems are included in the design. These systems are automatically activated in the event of loss of coolant from the primary

system to replenish and maintain the reactor system inventory. An "S signal", which can be generated by off-normal plant operating conditions such as low pressurizer pressure, low cold leg temperature, low steam line pressure, or high containment pressure, generates a core scram signal, reactor coolant pump trip signal, main feedwater pump and turbine trip, and also activates many of the passive safety systems.

The passive systems consist of accumulators pressurized with nitrogen gas, core makeup tanks (CMTs) which contain cold water and are pressure balanced with the primary reactor system, and a large in-containment refueling water storage tank (IRWST) that is pressure balanced with the containment. The CMTs are activated (and thus can start recirculating by natural circulation) by pressurizer or steam generator low level setpoints or by receipt of the S signal which also activates the IRWST system valves. The bottoms of the CMTs and the IRWST are located at elevations above the reactor cold legs to provide the head necessary for coolant injection. Although the S signal activates the IRWST system, flow from the IRWST into the primary can not commence until the primary pressure decreases below the IRWST hydrostatic head. Once the IRWST tank inventory has been discharged, the containment liquid level will exceed the elevation of the coolant loops allowing liquid to be injected back into the primary system via sump valves. Steam in the containment (generated by flashing of primary coolant) is condensed on the interior walls of the containment, collected, and then returned to the IRWST. Gravity-driven evaporative cooling external to the containment provides passive containment cooling.

To help ensure the proper functioning of the gravity driven passive safety systems, an automatic depressurization system (ADS) is incorporated into the AP600 design to limit the primary system-to-containment differential pressure (i.e., depressurize the primary system). The ADS consists of four different stages of valves (ADS-1, ADS-2, ADS-3, and ADS-4) to provide primary system pressure relief. ADS-1, ADS-2, and ADS-3 are connected to the top of the pressurizer and discharge through a sparger into the IRWST. The CMT actuation signal activates the ADS-1,-2,-3 valves. ADS-1 fires when the CMT level reaches specified level and the second and third ADS stages open based on elapsed time from the previous stage opening. ADS-4 valves are connected to the reactor hot legs and discharge directly to containment. ADS-4 valves are triggered by a low CMT level setpoint in conjunction with an elapsed time from ADS-3 actuation. Core decay heat is rejected to the IRWST via a passive decay heat removal system (PRHR) which is capable of removing full decay heat and can operate at full system pressure.

Unlike existing operating reactors whose safety systems rely primarily on pump heads for operation, the AP600 design relies on gravity dominated forces for safety system operation. The current research program is focused on the evaluation of these systems and the processes that influence their operation.

3. The scaling approach

The approach developed involves a multi-step process that builds on the Phenomena Identification and Ranking Table (PIRT) (Fletcher, 1995; Burtt, 1997) description of the accident scenario. The steps include:

1. Define the phenomenologically distinct phases of the transient identifying initiating and ending events, for example, when the CMT level drops to a specified value (the specified setpoint), ADS-4 is activated and the "ADS-4 Phase" is initiated. Figure 2 illustrates the phases considered in this study for a SBLOCA. It is important that the start and ending of each phase be defined in a clear and logical way.
2. Identify subsystems, components, and interactions of importance in each phase.
3. Develop a diagram of the system indicating subsystems, components, and interconnections identified in Step 2.
4. Define the governing equations for each component, in each phase and their interconnections as identified in Step 3 using a lumped parameter approach to develop integral forms of the conservation of mass, energy, and momentum equations.
5. Nondimensionalize the equations developed in Step 4.
6. Select reference scales such that the nondimensionalization process leads to the dependent variables, except those characterizing the key system response in each equation, being ~O(1).
7. Order the terms in the nondimensional equations in terms of the magnitude of the nondimensional coefficients and retain only the dominant terms in each equation clarifying the impact of each remaining term on the system response of interest.

8. Evaluate the reduced nondimensional equations using data from experimental facilities to determine their validity in predicting the system responses of interest.
9. Compare the nondimensional groups that dominate the system response of interest, for the AP600 and experimental facilities, and thereby evaluate the applicability of the experimental data to assessments of AP600 analysis methods.

The results of Steps 4-6 in the methodology provide a set of nondimensionalized equations that are used to predict a key system response such as vessel mass inventory. This closed set may contain certain requirements for closure relationships that eventually may be supplied by more detailed analysis since resolution is limited to the component and interconnection levels. For example, nondimensionalized equations for the IRWST refill phase contain a nondimensional group involving the pressurizer surge line density. This may not be specified in detail at this stage, but may be refined if necessary. Characteristics of this top-down equation set which allows the calculation of a key system response, such as the reactor vessel mass inventory, are:

- All nondimensional variables except the key system response, are approximately O[1], with nondimensional coefficient groups which then determine the magnitude of each term
- Then groups can be evaluated so that their magnitudes can be compared to identify the dominant terms in each equation and their impact on the key system response. Based on this comparison, only the dominant groups in each equation are retained
- The dominant groups for each transient phase for each facility and the reference plant are then compared to help clarify distortions

Validation increases confidence that the dominant nondimensional groups, and correct reference scales, for each phase have been identified, that important phenomena have not been excluded, and helps identify the important closure relationships. After going through this process, if for a given facility, one or more of the dominant groups for a particular phase are significantly different from the reference plant, then the data for that phase must be carefully examined for applicability.

The sketch in Figure 3 illustrates the process of validation for each hierarchical level in the system of nondimensionalized equations resulting from the order of magnitude analysis. In essence for each equation, the integral of the left hand side of the equation can be plotted against the integral of the right hand side of the equation. If the result is near the $y = x$ line as indicated on the sketch, then there is reasonable assurance that the necessary terms have been accounted for in the equation and the retained nondimensional groups capture the main phenomena. This type of check ultimately should be done for each phase and for each equation in the hierarchy for that phase. For example, the equations starting with the vessel mass balance, then for the mass in flows and out flows, then for the head terms governing the flows, and so forth. This process also allows determination of the order of magnitude of the nondimensionalized dependent variable in each equation and ensures that the reference scales are selected such that they are ~O[1].

4. Scaling methodology demonstration

The methodology was applied to all phases of the transient shown in Figure 2. The ADS-4 blowdown phase and the IRWST injection phase, are expected to be more complex and a significant test of the methodology as well as being the phases with the highest priorities from the viewpoint of the system response. To keep this paper to reasonable length, only the ADS-4 phase is discussed in detail in order to demonstrate the methodology. The same level of detail was necessary for the IRWST injection phase, and somewhat less for the other phases. In all cases the process was validated by comparisons with experimental data. It is worth noting at the onset that the key to successful application of the methodology lies in carefully selecting the reference parameters to scale the dependent variables O[1] within a phase.

4.1. ADS-4 blowdown phase

This phase corresponds to the ADS-4 Blowdown Phase described in the shown in Figure 2. It is initiated when the level drops to a specified (low-level) setpoint in the CMTs and ends when IRWST injection commences.

4.1.1. *Step 1: ADS-4, Phase description*

The CMTs are the active source of coolant for the core and, at the ADS-4 actuation signal, the CMTs will contain some fraction of their initial inventory.

The pressurizer has a significant liquid inventory due to accumulation of water entrained into it by the blowdown through ADS-1-3 valves in the previous phase. When the ADS-4 valves open the system depressurization rate increases, and flow through ADS-1,-2,-3 transitions from choked to friction dominated. Flow through the pressurizer and ADS-1-3 decreases to a negligible quantity when compared to the ADS-4 flows. The system is mostly saturated, except perhaps for the liquid in the CMTs. The CMTs deliver this liquid to the vessel downcomer through the CMT/DVI lines.

4.1.2. *Step 2: ADS-4, Identification of key components or subsystems*

As depicted in Figure 4, the participating components are the CMTs, the vessel, the pressurizer, the ADS-4 Valves, the CMT injection line, the pressurizer surge line, and the hot legs. There are two steam bubbles in the system: one in the vessel upper head and one in the steam space of the pressurizer. The upper head bubble is part of a larger steam space that includes the steam generators, hot legs, etc. but is assumed not to participate in this subphase of the transient. After the ADS-1,-2,-3 flow transitions from choked to friction dominated flow the steam space above the pressurizer liquid is affected by the level of immersion of the sparger in the IRWST. It is assumed that the steam space in the pressurizer is at constant pressure related to the head of water above the sparger in the IRWST. Furthermore, the CMTs and the upper head are at the same pressure as they communicate via the downcomer bypass, the loops, and PBLs. Other assumptions made include; the accumulators are empty; break flow can be ignored as the beak area is much less than the ADS-4 area; there is no significant pressurizer draining; there is no flow between the hot legs and steam generators; and injected CMT fluid does not get to the cold legs since the downcomer level is beneath the cold leg nozzle elevation.

4.1.3. *Step 4: ADS-4, Governing equations*

The system of equations for the configuration shown in Figure 4 were derived from basic conservation laws of mass, energy, and momentum. The resulting nondimensionalized equations are presented below. Quantities with an asterisk in these equations denote division by a reference value.

The vessel mass balance is

$$\frac{dV_l^*}{dt^*} = \frac{dL_V^*}{dt^*} = \Pi_{7-V}(\Pi_{16}Q_{CMT}^* - \dot{m}_{ADS-4}^*) \tag{1}$$

where the CMT mass flow rate is defined as

$$\dot{m}_{CMT}^* = \Pi_{16}Q_{CMT}^* \tag{2}$$

and it is assumed that the pressurizer flow is negligible and that there is no flow from the hot legs into the steam generators (or vice versa) so that the hot leg flow is equal to the ADS-4 flow.

The CMT mass balance in terms of the nondimensionalized CMT level and volumetric flow rate is given by

$$\frac{dL_{CMT}^*}{dt^*} = -\Pi_{15-CMT}Q_{CMT}^* \tag{3}$$

The CMT discharge line flow is given by

$$\frac{dQ_{CMT}^*}{dt^*} = -\Pi_{2-CMT}\left[\Pi_{17}L^* - \Pi_{18}L_{CMT}^* - \Delta Y^*\right] - \Pi_{3-CMT}Q_{CMT}^2 \tag{4}$$

where L^* is the vessel level and is constrained by the DVI nozzle elevation (L_{DVI}^*) as follows

$$L^* = L_V^* \text{ for } L_V^* \geq L_{DVI}^*$$
$$= L_{DVI}^* \text{ for } L_V^* < L_{DVI}^* \tag{5}$$

An energy balance on the lower plenum fluid assuming that the CMT temperature is approximately constant yields the following expression for the mixing

$$\frac{d(T_{CMT} - T_{lp})^*}{dt^*} = -\Pi_{9-lp} Q_{CMT}^* (T_{CMT} - T_{lp})^* \tag{6}$$

The variables with asterisks in the above equations are specified as

$$V_l^* = \frac{V_l}{V_0}; t^* = \frac{t}{t_0}; L_V^* = \frac{L_V}{V_0/A_0}; \dot{m}_{ADS-4}^* = \frac{\dot{m}_{ADS-4}}{\dot{m}_0};$$
$$Q_{CMT}^* = \frac{Q_{CMT}}{Q_{CMT,0}}; L_{CMT}^* = \frac{L_{CMT}}{L_{CMT,0}}; \Delta Y^* = \frac{\Delta Y}{\Delta Y_{CMT,0}} \tag{7}$$
$$(T_{CMT} - T_{lp})^* = \frac{(T_{CMT} - T_{lp})}{\Delta T_0}$$

where the terms with subscript "0" denote reference values.

These equations require additional relationships in order to constitute a closed system. To complete the analysis from a top-down perspective, the following assumptions were made about the form of these relationships.

As stated above, the ADS-4 flowrate is assumed to be equal to the hot leg flow rate and the ADS-4 discharge is given by the homogeneous equilibrium model (HEM) (Hall and Czapary, 1980) evaluated at the ADS-4 quality or

$$\dot{m}_{hl}^* = \dot{m}_{ADS-4}^* = G_{HEM}(x_{ADS-4}) A_{ADS-4} / \dot{m}_0 \tag{8}$$

where the ADS-4 quality is specified by an energy balance across the core

$$x_{ADS-4} = \frac{\dot{q}_f - Q_{CMT}\rho_l C_p (T_{sat} - T_{lp})}{\rho_l Q_{CMT} h_{fg}} \tag{9}$$

The nondimensional groups in the above equations are summarized in Table 1.

4.1.4. Step 6: ADS-4, Selection of reference parameters

The reference values, subscripted by "0," were chosen to obtain numerical values of the Π s that can be used to compare the facilities and their behavior with that of the plant and with each other. Reference parameters are selected such that the normalized variables in each equation are of O[1] and the time scale of the system is selected as the residence time of the mass inventory in the vessel above the bottom of the heated length (e.g. $\Pi_{7\text{-}V}$ is taken as unity). Choosing the coefficient of the vessel mass inventory equation, Π_7, to define the reference time focuses the analysis on the dynamic processes that participate in the emptying and filling of the vessel.

Reference parameters were selected for the AP600 and for the experimental facilities. The reference pressure was taken to be the pressurizer pressure plus the hydrostatic head due to the pressurizer level (assumed to be half full). The pressurizer pressure is assumed to be atmospheric pressure plus the hydrostatic head due to the sparger submergence in the IRWST. Also note that the reference CMT flow is defined as

$$Q_{cmt,0} = \sqrt{\frac{g\Delta Y_{cmt,0}}{\left.\frac{K}{2A^2}\right|_{cmt,0}}} \tag{10}$$

and the reference mass flow rate ($\dot{m}_0$) is based on the HEM model evaluated using the quality from Equation (8) and the ADS-4 area (SPES is an exception as discussed below). As mentioned above, setting $\prod_{7\text{-}v}$ to unity and solving for t_0 using reference parameter values produces a time scale. Table 2 shows the resulting values for t_0. Also shown in this table are the time scales that result from using reference mass flow rates obtained from experimental data to compute t_0.

Note that for ROSA and OSU, there is quite good agreement between the external (based on experiment) and internal (HEM model) values.

In Table 2 multiple values are listed for the SPES experiment. This stems from the manner in which the experiment was conducted. The ADS-4 valves opened approximately 300 s after the specified CMT level set point for ADS-4 activation was reached. Due to the fact that the ADS-1-3 train in the SPES facility discharges to atmosphere (rather than to the IRWST sparger as in the other experimental facilities), the ADS1-3 train is assumed to be a part of ADS-4 blowdown for the purpose of this analysis. Thus it was assumed that the when specified CMT level was reached, flow out the ADS1-3 train is included as part of ADS-4 flow. The experimental data value for SPES is an average of both flows over the time frame between specified CMT level for ADS-4 opening and the end of ADS-4 blowdown. The time scales shown in Table 2 appear reasonable in that ROSA is reasonably close to the plant value and OSU is on the order of half the plant value as expected based on the reduced height scaling for the APEX facility. The SPES time scales are as expected in light of the fact that the ADS-4 train is oversized by a factor of approximately 2.5 and the ADS1-3 train discharges to atmosphere rather than to the IRWST.

4.1.5. Step 7: ADS-4, Order of magnitude analysis

Table 3 lists numerical values for the groups listed in Table 1 using values from Table 2 and reference parameter values. In this table two values are listed for the SPES facility as appropriate for the different time scales noted above.

Note from Table 3 that the values of the $\Pi_{2\text{-cmt}}$ and $\Pi_{3\text{-cmt}}$ groups are large and with the definition used in Equation (10), they are numerically equal. Because the values are much larger than the other groups, Equation (4) can be divided through by $\Pi_{2\text{-cmt}}$ making the LHS of the equation much smaller than the RHS. The equation describing the CMT flow then becomes

$$Q^*_{cmt} = \left[\Pi_{18}L^*_{CMT} - \Pi_{17}L^* + \Delta Y^*\right]^{1/2} \tag{11}$$

This result indicates that the line inertias are not a dominant factor in the CMT flow determination. Observation of the remaining Π values in Table 3 indicates that the experimental facility values tend to bound the values calculated for the plant and, for the large part, are reasonably close to the plant value. To further illustrate this, Table 4 gives the ratios of the Π groups for the facilities to that of the plant. With the exception of the $\Pi_{2\text{-cmt}}$ and $\Pi_{3\text{-cmt}}$ groups which are of little consequence on the CMT flow rate as noted above, the ratios are reasonably close to unity.

Based on Table 4, the three facilities should do a reasonable job at either individually representing or, as a group, enveloping AP600 behavior for the ADS 4 phase. The biggest consideration is the time scale for the SPES facility due to the oversized nature of the ADS-4 valves and the manner in which this particular experiment was conducted. It is clear from this analysis that the line resistance of the CMT line is an important parameter, for it defines the rate and duration of water delivery to the vessel. In general, the groups that influence the vessel mass directly (Π_{16} Π_{17}, and Π_{18} from Equations (1) and (11)) are fairly well preserved in the facilities.

The equations for the CMT and ADS-4 flows can be substituted into the vessel mass balance to provide the following expression

$$\frac{dV^*}{dt^*} = \frac{t_0}{V_0}\left(\frac{g_0L_0}{R'_0}\right)^{1/2}\left[\frac{g^*}{R'^*}\left(L^*_{CMT} - L^*_{DC} + \Delta Y^*\right)\right]^{1/2} - \frac{G_0A_0t_0}{V_0\rho_0}\frac{G^*A^*}{\rho^*} \tag{12}$$

These dimensionless groups were evaluated using reference parameters and the time scales in Table 2. For the experimental facilities the data values of the time were used. The numerical values of the dimensionless groups are

summarized in Table 5 with the ratio of ADS-4 flow to CMT flow. The ratio of ADS flow to CMT flow is greater than 1 in the full pressure facilities and less than 1 in OSU. The ratio in ROSA is ~30 % large relative to AP600 while in SPES the value is ~ 220 % larger than in AP600. These differences are consistent with the differences in the ratios of ADS-4 flow area to vessel volume in the full pressure facilities. The reason for the ratio of ADS-4 flow to CMT flow being less than 1 in OSU is less clear. It may be due to the flow in APEX not being choked. The effect of the differences in the ratios of ADS-4 flow to CMT flow can be expected to affect the amount of vessel mass loss occurring during ADS-4 blowdown. Based on these values the full pressure experimental facilities would be expected to lose a larger fraction of vessel inventory than the AP600 while OSU would be expected to lose less. Note that the last row in Table 5 is a ratio of values from the second and first rows.

4.1.6. Step 8: ADS-4, Verification with data

Using the methodology previously described, each of the important equations is verified with data to show that the equations and nondimensional groups are correct. We now proceed to demonstrate this process starting with the vessel mass inventory balance and then work outward to the flows that influence the vessel inventory. Liquid inventory in the vessel is the primary consideration as this inventory is the controlling factor for core cooling.

Vessel mass balance

With respect to the vessel (see schematic in Figure 5), Equations (1) and (2) can be combined to get the following nondimensional mass balance

$$\Pi_7^{-1}\frac{dV_l^*}{dt^*} = \dot{m}_{cmt}^* - \dot{m}_{ads4}^* \tag{13}$$

where

$$\Pi_7 = \frac{t_0\dot{m}_0}{\rho_0 V_0} \tag{14}$$

and is unity for the time scale used and variables with an asterisk are defined in Equation (7).

Equation (13) can be integrated with respect to the dimensionless time variable to provide an expression for the vessel dimensionless liquid volume.

$$\int_{t_0^*}^{t^*}\frac{dV_l^*}{dt^*}dt^* = \int_{t_0^*}^{t^*}\dot{m}_{cmt}^* dt^* - \int_{t_0^*}^{t^*}\dot{m}_{ads4}^* dt^*. \tag{15}$$

or

$$V_l^*(t^*) - V_l^*(t_0^*) - \int_{t_0^*}^{t^*}\dot{m}_{CMT}^* dt^* = -\int_{t_0^*}^{t^*}\dot{m}_{ads4}^* dt^* \tag{16}$$

where $V_l^*(t_0^*)$ is a constant of integration. Equation (16) can be applied to the experimental data from each facility to calculate the nondimensional vessel liquid volume change with dimensionless time for the ADS-4 phase. This equation will balance if the mass inflows and outflows have been correctly accounted for. Furthermore, if reasonable reference scales have been chosen, the variables will be O[1] and plotting the LHS of the equation against the RHS should produce a slope near unity.

Figure 6 shows the result of evaluating Equation (16) with the ROSA, SPES, and OSU experimental data. In this figure, the ordinate corresponds to the LHS of Equation (16) and the abscissa corresponds to the RHS of the equation. The integrals were computed over the range $-0.8 \le t^* \le 0$ where the lower limit corresponds to the start of ADS-4 blowdown and the upper limit to the start of IRWST injection. The reference line labeled y = x is included on the figure.

The results in Figure 6 indicate that a relatively good mass balance on the vessel has been achieved as the data are near the y = x line as expected. The figure shows remarkably good agreement given the experimental uncertainty associated with mass flow measurements. It was expected that the mass balance would likely be within about 10 - 20% at best. This result suggests that the major sinks and sources of mass have been properly accounted for. Note that in Figure 6 the two different time scales have been represented for the SPES result.

Figure 7 shows the integrals of the nondimensional mass flows used in Figure 6. In this figure, the integral of the CMT flow has been plotted against the integral of the ADS-4 flow. The deviation in the data from the y = x line is, of course, the inventory change in the vessel. This figure illustrates the significance of the CMT inventory in the overall mass balance on the vessel. Furthermore, the relationship among the facilities is similar in terms of magnitude and in that the CMT inventory supplies a fairly large fraction of the flow that is exiting the system through the ADS-4. Note that the significant slope change in the SPES curve is related to the actual opening of the ADS-4 valves.

This illustrates how the methodology can also lead to insight as to what the important processes impacting key system response are. The results presented in Figures 6 and 7 show that the process of scaling the experimental data with the nondimensional residence time of the vessel (Π_7) was successful and that the behavior of the nondimensional flows in the facilities is reasonably similar. The results shown indicate that a reasonable mass balance can be effected for each of the facilities using the equations developed. Furthermore, it appears that reasonable reference scales have been determined since, for all the facility data sets, the range of the left hand side of Equation (16) is between similar limits as is the range of the right hand side of the equation. This result suggests that a common basis has been developed so that in nondimensional coordinate space, the data collapse.

The reference scales developed in this analysis appear to be reasonable in light of the design of the individual facilities. For example, the reference time scales for the AP600 plant and for the ROSA facility are approximately equal as expected. Also, the OSU facility reference time scale is on the order of half the reference time scale for the AP600 and the ROSA facility. This is reasonable since the design philosophy of the OSU system was to approximate one-half time scale for the all of important transport processes. The SPES time scale results because the SPES ADS-4 valve area is oversized by a factor of approximately 2.5. This fact helps to explain the noticeable effect of the ADS-4 valve opening.

Vessel outflow

We now proceed to examine the flows that influence the vessel mass balance, i.e., the terms appearing on the RHS of Equation (15). First, we examine the facility measured ADS-4 flow rates in light of the reference scales selected to show that the scale choices were reasonable and adequate.

A frozen flow assumption can be used to estimate a reference ADS-4 mass flow rate assuming no knowledge of the ADS-4 discharge quality. This assumption involves computing a critical mass flux by multiplying the vapor sound speed (Karplus, 1961) and vapor density at the reference pressure conditions. Figure 8 shows a comparison of the measured integrated ADS-4 mass flux and the integrated mass flux computed with the HEM model for various qualities using the measured upper head pressure as input for the ROSA experiment. Both the HEM result and the measured result were divided by the frozen value for normalization.

The results shown in Figure 8 indicate that the integrated normalized ADS-4 mass flux for ROSA AP-CL-03 is approximately bounded on the high side by the HEM result for quality of 0.3 for a fair portion of the ADS-4 blowdown. By inspection, it is seen that the mass flux based on the frozen flow model approximates the average of the measured mass flux. For the ROSA experiment, the average measured mass flow was about 1.7 kg/s whereas the frozen model mass flux of 778 kg/m^2-s gives a reference flow of 1.86 kg/s. The information in Figure 8 shows that the reference flow scale picked using HEM (without knowledge of the data) for the ROSA ADS-4 flow is reasonable as both the time and reference flow scales are of order unity as desired.

Figure 9 shows the SPES experiment data displayed on the same integrated ratio basis as the ROSA data on Figure 8. As shown, the frozen assumption is a reasonable representation of the upper bound of the measured integrated flow rate until t* ~0.2 when the data become larger. For reference, the average measured total ADS flow rate (including the ADS1-3 train and the ADS-4 train) was 0.27 kg/s for the SPES experiment. Using this average

value with the combined ADS1-3 and ADS-4 flow area produces an average mass flux of 837 kg/m^2-s which is only about 7% higher than the reference mass flux value used. The measured integrated data in Figure 9 are reasonably bounded by the HEM 30% quality line indicating that the reference flow scale selected without knowledge of the data is reasonable.

Figure 10 indicates that the measured ADS-4 mass flux in OSU is considerably higher than predicted using the frozen flow assumption. This result is the reason that the measured average ADS-4 flow rate was used to establish the reference flow rate. The results in Figure 10 indicate that the HEM model evaluated at low quality ($\lesssim$-0.05) bounds the measured OSU data and that the friction dominated discharge flow rate can be approximated by HEM evaluated at low quality as was done above to establish a reference flowrate value.

The data shown in the previous figures indicate that reasonable flow scales have been determined for the ROSA and SPES facilities since the integrated outflow from the system is in reasonable agreement with the integrated reference mass flux. As indicated, the HEM model for a quality of 20-30% produces reasonable reference flow values for the ROSA and SPES experiments. The frozen flow assumption did not work for the OSU experiment as the data suggest that the ADS-4 flow was not choked. The data indicate the flow contains significant liquid and in this case, the ADS-4 flowrate is bounded by the HEM model at low (~1- 5%) quality.

Vessel inflow

As shown in Equation (15), the CMT flows along with the hot leg flows influence the vessel mass balance. We now examine the CMT flows in light of the CMT tank and line equations with the goal of showing that the equations collapse the experimental data and hence the equations and the Π groups in them are correct. We note from the previous sections that the CMT equations contain Π groups that contain line resistance and line inertia parameters and the reference flow for the CMT along with the system time scale. Based on the order of magnitude analysis shown previously, the $\Pi_{2\text{-cmt}}$ and $\Pi_{3\text{-cmt}}$ groups are quite large indicating that the transient term on the left hand side of the CMT line equation can be neglected so that Equation (11) applies.

Using Equations (2) and (11) gives the following

$$\begin{aligned} \dot{m}^*_{cmt} &= \Pi_{16} Q^*_{cmt} \\ &= \Pi_{16}\left[\Pi_{18} L^*_{CMT} - \Pi_{17} L^* + \Delta Y^*\right]^{1/2} \end{aligned} \tag{17}$$

Both sides of Equation (17) can be integrated and the resulting equation

$$\begin{aligned} \int \dot{m}^*_{cmt} dt^* &= \int \Pi_{16} Q^*_{cmt} \\ &= \int \Pi_{16}\left[\Pi_{18} L^*_{CMT} - \Pi_{17} L^* + \Delta Y^*\right]^{1/2} dt^* \end{aligned} \tag{18}$$

was used to examine the experimental data. Figures 11 - 13 show the results for the facility data where the integral of the nondimensional CMT flow rates are plotted versus the RHS of Equation (18). As is shown in these figures, all of the data are near the y = x line as expected.

Analytic solution for vessel level

An analytic solution for the vessel level equation was developed for the ADS-4 blowdown. Solutions for the vessel level greater than or equal to the DVI nozzle elevation and the vessel level less than the DVI nozzle are developed. For the vessel level greater than or equal to the DVI nozzle, the solution is

$$V_i^*(t^*) - V_i^*(0) = \left[\Pi_{16} Q^*_{CMT}(0) - 1\right] t^* + \frac{\Pi_{16}\hat{\Pi}_{19}}{2Q^*_{CMT}(0)}\left[Q^*_{CMT}(0) + \frac{\Pi_{17}}{\hat{\Pi}_{19}}\right]\frac{t^{*2}}{2} + \ldots \tag{19}$$

where

$\hat{\Pi}_{19} = (\Pi_{18}\Pi_{15} - \Pi_{17}\Pi_{16})$ for $L_v^* \geq L_{DVI}^*$ and it is assumed that the nondimensionalized ADS-4 flowrate is 1. Note that Equation (19) applies mainly to the ROSA experiment because of the relationship between the vessel level and the DVI elevation.

For the case of the vessel level less than the DVI nozzle, the solution is

$$V_l^* - V_l^*(0) = \left[\Pi_{16} Q_{CMT}^*(0) - \dot{m}_{ADS4}^*\right] t^* + \frac{\Pi_{16}\Pi_{18}\Pi_{15}}{4} t^{*2} \quad \text{for} \quad L_v^* < L_{DVI}^* \tag{20}$$

Figure 14 shows a comparison of the experimental data for the one inch cold leg break experiments with Equations (19) and (20). The nature of the agreement provides additional evidence for the validity of the equations and scale assumptions.

Analytic solution for vessel level during IRWST refill

Following an approach similar to that outlined above for the ADS-4 blowdown phase, an analytic solution for the vessel level equation during the IRWST refill phase was developed. For brevity, details of the development are omitted here. The vessel level equation can be simplified and solved analytically with asymptotic solutions for the cases of nondimensional time being large and small. The short time solution is

$$V_l^*(t^*) = \frac{2}{3}\Pi_{20}\left[\left(\Pi_{22}\Pi_{15}\dot{m}_{prz}^* - \Pi_{20}\frac{dP_{prz}^*}{dt^*}\right)^{1/3}\right] t^{*3/2} - \left(\dot{m}_{ADS4}^* - \dot{m}_{prz}^*\right) t^* + V_l^*(0) \tag{21}$$

which takes on the following coefficients for the experimental facilities.

ROSA: $V_l^*(t^*) - V_l^*(0) = 1.4t^{*3/2} - 0.74t^*$

SPES: $V_l^*(t^*) - V_l^*(0) = 3.9t^{*3/2} - 1.32t^*$

OSU: $V_l^*(t^*) - V_l^*(0) = 1.13t^{*3/2} - 0.82t^*$.

The solution for large values of t^* is

$$V_l^*(\infty) - V_l^*(t^*) = \left[V_l^*(\infty) - V_l^*(0)\right] \exp\left[-\Pi_{22}\Pi_{19} t^* / (2Q_{DVI}^*(\infty))\right] \tag{22}$$

which takes on the following coefficients for the experimental facilities.

ROSA: $V_l^*(t^*) = 0.72 - 0.26e^{-1.16t^*}$

SPES: $V_l^*(t^*) = 0.70 - 0.43e^{-1.17t^*}$

OSU: $V_l^*(t^*) = 0.72 - 0.20e^{-1.16t^*}$

These solutions are plotted with data from 1" CLB experiments in Figures 15, 16, and 17 for the experimental facilities. The agreement with data is generally good at early and late times. This quality of agreement provides additional credence for the scaling estimates of the dominant processes for the IRWST refill phase.

A word of caution is in order regarding Equations (21) and (22) and their solutions. A very simple closure model was used to estimate pressurizer draining rate (flow rate was specified as $C(g\, D_{prz\text{-}sl})^{1/2}$ where C is a constant). This simple model does not account for flooding effects, bend effects, etc. in the surge line. While this simple model produced reasonable results, modeling of the pressurizer drain rate is a topic that should be more thoroughly investigated using the bottom-up approach since the drain rate has a significant influence on the solutions.

Discussion of reference parameters - selection with and without data knowledge

If no experimental information is available, reference parameters must be selected in a blind fashion, that is without benefit of the data. However, if experimental information is available, it can support or confirm reference parameter selection. In the present case, there is no plant data so reference parameters must be selected without data knowledge. Since experimental facility data is available, reference parameters can be first selected assuming no data knowledge for the facilities and then these selections can be examined/confirmed using the data. Such a process helps to verify that reasonable reference values for the plant have been chosen. Here we summarize observations

regarding selection of reference parameters both with and without data knowledge referred to hereafter as "with-data" and "without-data."

For both situations (without-data and with-data), the vessel time scale was determined in the same fashion via the Π_7 group and the same reference vessel volume was chosen by design. For the with-data view, the reference pressures were chosen based on the measured data. For the without-data view, the reference pressure was chosen to be the pressurizer steam dome pressure (as determined by the IRWST head and ADS lines connecting the sparger to the top of the pressurizer) plus the head of liquid in the pressurizer and surge line. The liquid level in the pressurizer was assumed to be at a position approximately midway between the top of the pressurizer and an elevation corresponding to the IRWST level. For the ROSA and SPES experiments, the view without-data resulted in reference pressures that were somewhat lower (20 - 40 kPa) than those based on the data. For the OSU experiment, the two views yielded basically the same reference pressure. Part of the minor difference in reference pressure for the SPES experiment is due to the fact that part of the ADS 1-3 blowdown was considered as ADS-4 blowdown as discussed above. The reference pressure differences had little effect on the resulting selection of reference saturated liquid densities and temperatures for the facilities.

Reference ADS-4 outflow scales for the experimental facilities (and plant) without-data view were based on the HEM model as discussed above. The ADS-4 discharge quality was estimated from the core vapor generation rate and a reference CMT flow rate. This quality estimate was then used with the HEM model to compute a reference discharge rate. The quality so estimated was of the order of 20-30% for the plant and the ROSA experiment, approximately 14% for the SPES experiment, and about 7% for the OSU experiment. These reference flow rate scales, in conjunction with the reference volume and density, produced vessel time scales for ADS-4 blowdown consistent with the duration of the ADS-4 blowdown which was the desired result.

Reference ADS-4 outflow for the with-data view was evaluated with application of a simple frozen flow model for the ROSA and SPES facilities (and the plant) since the actual ADS-4 discharge quality is not known. The ADS-4 discharge was assumed to be saturated steam leaving the system at the vapor sound speed for a quality of unity. For the OSU experiment the measured average flow was used as the reference ADS-4 flow since the ADS-4 flow does not appear to be choked and the frozen assumption did not apply. Review of these results and the data indicated that the reference flow scales selected are reasonably consistent with the HEM model results discussed above for the without-data view although for the OSU experiment, the without-data procedure results in a reference flow rate that is slightly low relative to the data (most likely due to a quality estimate that is slightly large). The resulting effect is a vessel time scale slightly larger than the duration of ADS-4 blowdown in the OSU experiment. A better estimate would be made using a lower quality with the HEM model to estimate a reference ADS-4 scale for the OSU experiment.

From the without-data viewpoint, reference flow values selected using the approach described above produced vessel time scale estimates that were close to those estimated from the with-data view as might be expected based on the discussion of the data above. Based on evaluation of the data, both selections were shown to provide reasonable reference flow scales for the facilities.

Nominal geometric parameters for the plant and facilities such as hardware elevation changes, initial levels, etc. are used in the without-data approach. It is recognized that situations arise wherein the value of an experiment parameter may be different than the expected nominal value based on evaluation of experiment results data. Tank levels are an example in that levels may deviate from an expected value for a variety of reasons. Such differences could impact the results obtained from the with-data approach relative to the without-data approach if this initial level factors into the computation of a reference flow or a reference length in a dimensionless group. An example is the SPES experiment delayed ADS-4 activation as discussed above. In general, deviation from nominal values has not been a significant issue to date.

4.1.7. Conclusions for the demonstration

Values of the dimensionless groups resulting from the ADS-4 phase indicate that the facility values bound the plant values. This result suggests that the plant performance is bounded by the experimental data and that the data are applicable for code adequacy evaluations.

5. Summary of methodology demonstration

This section collects together the main results and conclusions for the demonstration, including a brief recapitulation of the ADS-4 discharge phase for completeness.

Subcooled depressurization

For the 1 inch cold leg break, the system mass response during the initial portion of the subcooled blowdown phase were found to be dominated by the break flow rate. The break volumetric flow is the controlling term for the depressurization response as the net heat flows in and out of the system were nearly balanced. Order of magnitude analysis showed that effects due to convecting energy out the break and pressurizer heating were each an order of magnitude smaller than the break volumetric flow. Data from various facilities scaled with a time nondimensionalized by the break discharge rate and the initial coolant mass in the pressurizer.

Intermediate phase

Following pressurizer draining and reactor scram, the balance of core, steam generator, and PRHR heat flows and break flow play an important role in the pressure response. The mass loss continues to depend on the break flow. Based on the values of the nondimensional groups, the same processes control the mass balance in the AP600 and the experimental facilities for all three subphases of the Intermediate Phase.

During the initial passive cooling phase, mass inventory changes depend on the break flow until the accumulator draining and CMT draining begin. In this interval the depressurization rate is related to the balance of core and PRHR heat flows and break volumetric flow. Following the initiation of accumulator injection and CMT draining, these flows govern the mass balance until ADS flow begins. The low temperatures of these flows determine the depressurization process primarily by decreasing the average specific volume of the system. From this point on, the depressurization transient is controlled by the actions of the engineered safety systems. All this can be phrased in terms of nondimensionalized equations, with nondimensional coefficients for the O[1] nondimensional variables that for the experimental facilities, lie in the same range as in the AP600 with some differences. For example, during this phase the heat in and out flows are distorted in SPES, though the overall effect on the subphase response does not appear to be significant as far as the ultimate outcome, coolant inventory before ADS-4 opens, is concerned. Also, the PRHR heat transfer appears to be oversized in the ROSA facility relative to the AP600 whereas it is somewhat undersized in the SPES and OSU facilities. These distortions appeared to have little effect on the overall transient response, however.

After the ADS-1,-2,-3 flows begin they, in addition to the accumulator and CMT flows, influence the system coolant inventory and depressurization rate. The ADS influence on the depressurization rate is accentuated by the discharge being of high quality. In the experimental facilities, essentially these same processes are dominant. In the full pressure facilities, the effect of the cooler accumulator and CMT fluid on depressurization occurred primarily by mixing with subcooled liquid. In the OSU APEX facility, the effect occurred more by mixing with saturated fluid. This difference does not appear to have a significant effect on the overall phase outcome.

A preliminary assessment of the presence of accumulator nitrogen in the primary system on the processes occurring during the intermediate phase was made. The two situations evaluated to provide a comparison included assuming the primary system vapor volume contained only steam and assuming the vapor space contained nitrogen. Results of this much simplified estimate indicate that the numeric values of the nondimensional groups for the two cases are different but the relative rankings for the groups for a given facility are the same. In both cases for all the facilities, the ADS-1,-2,-3 volumetric flow was the major factor affecting depressurization.

From the analysis of the Intermediate Phase, the conclusion is drawn that the nondimensional pressure and inventory are relatively independent of break size provided the break is small (<< ADS-1,-2,-3 area). These nondimensional parameters do depend on accumulator and CMT mass and to a lesser extent on the details of the net heating from core decay heat and steam generator and PRHR heat transfer. The experimental data tend to support this conclusion.

ADS-4 blowdown

During the ADS-4 blowdown the vessel mass inventory is determined by the balance between CMT and ADS-4 flow rates. The CMT head relative to the vessel liquid level, CMT line resistance, and ADS-4 quality are important parameters during this phase. Temperature of the CMT liquid and mixing in the lower plenum affect the ADS-4 quality. In the full pressure facilities, the ratio of ADS-4 flow to CMT flow was greater than in AP600. This difference would cause these facilities to lose more mass during ADS-4 blowdown than the AP600. In OSU, the ratio of ADS-4 flow to CMT flow was less than in the AP600 which would cause OSU to lose less vessel inventory during ADS-4 blowdown than in the AP600.

IRWST injection

During the initial vessel refill the vessel mass inventory is determined by the balance between IRWST, pressurizer surge line, and ADS-4 flow rates. The IRWST and pressurizer heads relative to the vessel level, IRWST line resistance, resistance to draining through the pressurizer surge line, and ADS-4 quality are important parameters during this phase. Temperature of the IRWST liquid and mixing in the lower plenum affect the ADS-4 quality. The effects of oscillatory pressurizer draining were observed but did not significantly affect the vessel refill process. In the experimental facilities the same processes were dominant and the relative ordering of the flow magnitudes was the same. In OSU the ADS-4 flow appeared to be somewhat low relative to the other facilities. Conditions in the experimental facilities cover the range, in nondimensional parameter space, expected in the AP600.

IRWST drain(long term cooling)

The OSU facility is the only experimental facility equipped to run transients through the IRWST draining phase. For this phase, the drain time for the IRWST is the relevant time scale and is much larger than the vessel residence time scale. The drain is essentially a series of steady-state points in which the flow rate through the DVI, core, and out the ADS-4 valves depends primarily on the IRWST water level and, to a lesser extent, the ratio of the hydraulic resistances in the DVI and ADS-4 trains. These ratios are well preserved in the OSU facility suggesting that similar performance should be observed in the plant.

IRWST/Sump injection (long term cooling)

Sump injection commences after the Sump level has increased to a point that causes check valves and eventually motor operated valves to open and allow communication between the IRWST and Sump. The head imposed on the primary system by the Sump level remains constant at that point and the system operation is basically steady-state wherein coolant from the IRWST/Sump enters the system via the DVI lines, flows through the vessel, and out the ADS-4 valves. The vessel collapsed level settles at an elevation near the DVI nozzle during this phase implying a relatively constant vessel mass since other experiment parameters are not changing. Based on test data, the vessel nondimensional mass (in OSU) is approximately 0.85. Experimental data suggests that significant phase separation occurs in the upper core region and upper plenum. In effect, a significant fraction of the liquid in the mixture flowing out the top of the heated region separates and/or de-entrains in the upper plenum. Scaling analysis results predicted a nondimensional vessel mass lower than the experiment value. This result is a consequence of simplifying assumptions that were made in the analysis since the void profile above the core is not known The essence of the problem is that a more detailed, local effects description of the phase distribution is needed for the particular geometry in the upper plenum and various tee connections leading to the ADS-4 valves.

6. Main conclusions

The overall conclusion of the study was that the methodology outlined was useful and gave quantitative results that were validated by the experimental data, i.e. the nondimensional groups identified captured the data in all the facilities. As such, the methodology would be useful for other accidents and other systems. With regard to the detailed objectives, the magnitudes of the nondimensional coefficients in the reduced conservation equations were similar for the experimental facilities and the AP600 system. From this, the same important processes occurred in the experimental facilities as might be expected in the AP600. This similarity indicates that the experimental results are useful for understanding the response of the AP600 system. It further indicates that the data from the experimental facilities are in the same parameter range as the AP600, and hence are applicable to assessment of computer codes.

The important phenomena identified from the scaling analysis for the one inch cold leg break were in general agreement with those identified in the PIRT. Several phenomena were determined to play a primary role in the accident sequence that were not listed as high priority in the original PIRT (the rankings of these phenomena have been elevated in the current PIRT). These phenomena included:

- The CMT level and line resistance during the ADS-4 Blowdown and IRWST Phases
- The IRWST/DVI flow resistance during the IRWST Phase
- The initial pressurizer inventory at the start of the IRWST Phase
- Pressurizer drain rate during the IRWST phase.

However the scaling of these in terms of the important nondimensional groups was such that significant distortions were not identified. Table 6 below summarizes the important nondimensional groups for the transient phases.

7. Nomenclature

c_p	specific heat
d	diameter
e	energy per unit mass
f	friction factor
g	gravitational acceleration
h	specific enthalpy
l	length or characteristic dimension
$\dot{m}$	mass flow
p	pressure
q	decay heat
r	radius
t	time
u or v	velocity
x	quality
A	area
C	coefficient for Intermediate Phase
C_P	specific heat
D	diameter or characteristic dimension
G	mass flux
H	height or elevation
K	loss coefficient
L	pipe length or level (tanks)
LHS	left hand side
M or m	mass
P	pressure
Q	volumetric flow
R	ideal gas constant or radius
R'	line resistance parameter
RHS	right hand side
T	temperature
V	volume
Y	elevation or elevation difference
Z	elevation difference

Greek symbols

α	void fraction

β	thermal expansion coefficient
γ	specific heat ratio
φ	nondimensional coefficient
Δ	difference (as in ΔT)
ρ	density
ν	specific volume
μ	viscosity or specific internal energy
π	ratio of reference values
Φ	nondimensional coefficient[1]
Π	nondimensional coefficient
Ψ	nondimensional coefficient
Subscripts	
0	reference or initial value
acc	accumulator
ads	ADS system
ads123	stages 1, 2, and 3 automatic depressurization system
ads4	stage 4 automatic depressurization system
b	vessel upper head bubble
break	break value
cc	concrete
cmt	core makeup tank
cont	containment value
core	core value
crit	choked flow value
dc	downcomer
dvi	direct vessel injection
f	saturated liquid value
fg	saturated vapor - saturated liquid
g	gas or vapor value
head	manometric parameter
hl	hot leg parameter
i	ith component
in	control volume inlet
it	IRWST value
j	jth component
l	liquid parameter
lp	lower plenum
m	mixture
net	net value
out	control volume outlet
p	constant pressure
pzr	pressurizer
sat	saturation value
sl	surge line
tank	value for tank
uh	upper head
up	upper plenum
v	vessel or constant volume
w	wall
ACC	accumulator
ADS-1,2,3	stages 1, 2, and 3 automatic depressurization system
ADS-4	stage 4 automatic depressurization system

[1] For clarity, different Greek symbols are used to denote nondimensional coefficients for the different transient phases. For example, Φ is used for the Early Depressurization Phase, Ψ is used for the Intermediate Phase, and Π is used for other phases.

C	cold
CMT	core makeup tank
DC	downcomer
DVI	direct vessel injection
H	hot
HEM	homogeneous equilibrium
IRWST	in reactor refueling water storage tank
N	nitrogen/steam
PRHR	passive residual heat removal system
PZR	pressurizer
S	Sump
SG	steam generator
SL	pressurizer surge line
V	vessel

Superscripts

*	normalized value

8. References

Burtt, J.D., et al., 1997. Interim Phenomena Identification and Ranking Tables for Westinghouse AP600 Small Break Loss-of-Coolant Accident, Main Steam Line Break, and Steam Generator Tube Rupture Scenarios. Idaho National Engineering and Environmental Laboratory, INEL-94/0061, Revision 2, March 1997.

Fletcher, C.D., et al., 1995. Interim Phenomena Identification and Ranking Tables for Westinghouse AP600 Small Break Loss-of-Coolant Accident, Main Steam Line Break, and Steam Generator Tube Rupture Scenarios, Appendix H - Summary of Plant Systems and Automatic Actions (Proprietary). Idaho National Engineering Laboratory, INEL-94/0061, Revision 1, July 1995.

Hall, D.G. and Czapary, L.S., 1980. Tables of Homogeneous Equilibrium Critical Flow Parameters for Water in SI Units. Idaho National Engineering Laboratory, EGG-2056, September 1980.

Japan Atomic Energy Research Institute, 1996. Large Scale Test Facility; System Description for the ROSA/AP600 and ROSA-V Configurations (for the Third Installed Core), Revision A, Draft, March 1996.

Karplus, H.B., 1961. Propagation of Pressure Waves in a Mixture of Steam and Water. ARF, 4132 12, pp. 39, January 1961.

Rigamonti, M., 1994. SPES-2 Facility Description. Sezione Reattori Innovativi (SIET), 00183RI92, Revision 0 (Proprietary), April 1994.

Westinghouse Electric Company, 1994. Westinghouse AP600 Long Term Cooling Test at Oregon State University, Facility Drawings, Piping and Instrumentation Diagrams. Westinghouse Electric Company Report LTCT-T3-300 (Proprietary), December 1994.

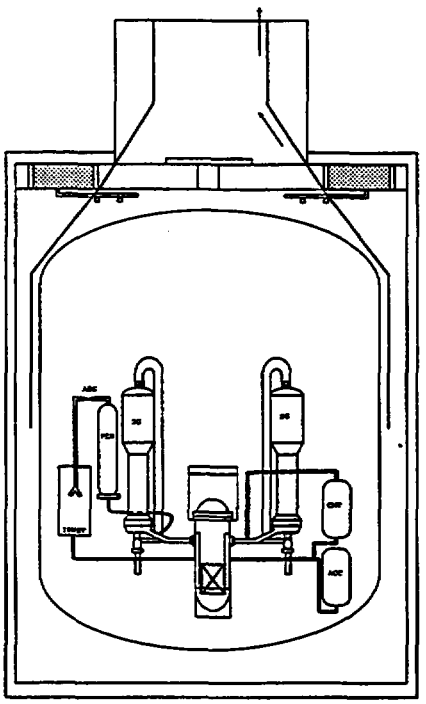

Figure 1. Sketch showing main AP600 components; SG - steam generator, PZR - pressurizer, RV - reactor vessel, ACC - accumulator, CMT - core makeup tank, IRWST - in-containment refueling water storage tank, ADS - automatic depressurization system.

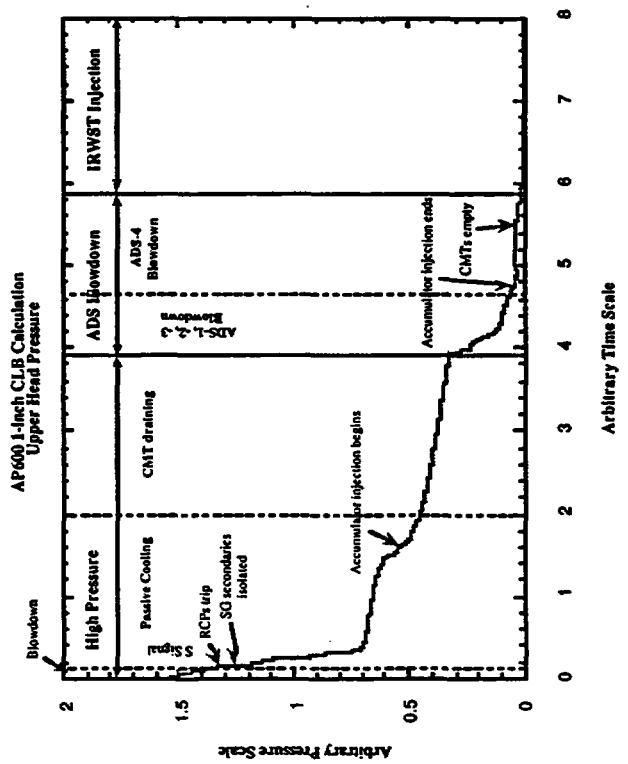

Figure 2. A typical SBLOCA transient showing the various phases for an AP600 cold leg.

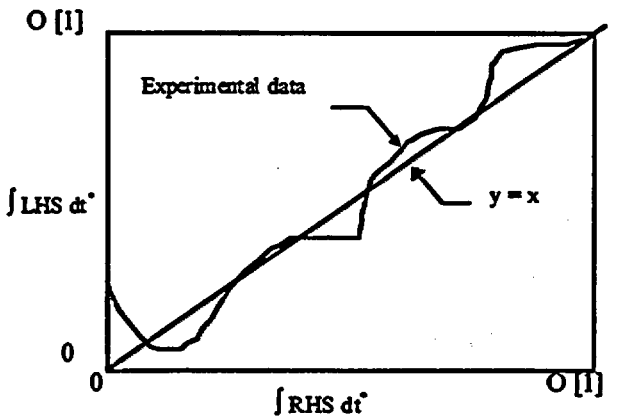

Figure 3. Sketch illustrating verification process to evaluate whether the dominant terms retained in each equation are sufficient to capture the experimental data.

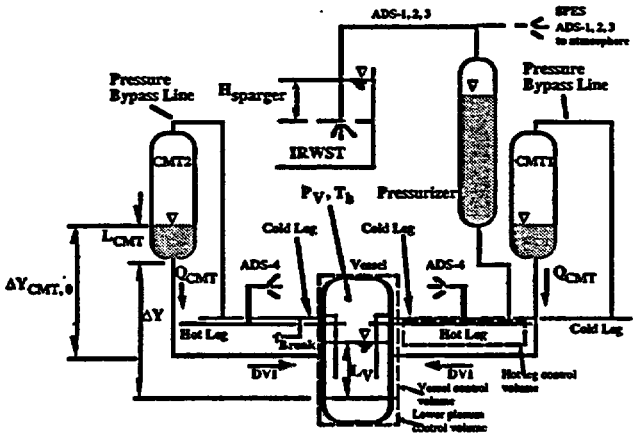

Figure 4. ADS-4 Blowdown Phase: schematic and important components.

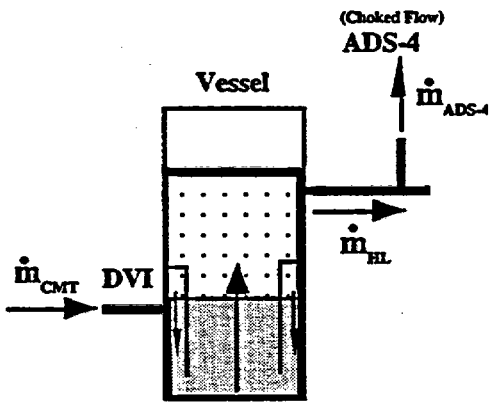

Figure 5. Vessel control volume for ADS-4 blowdown.

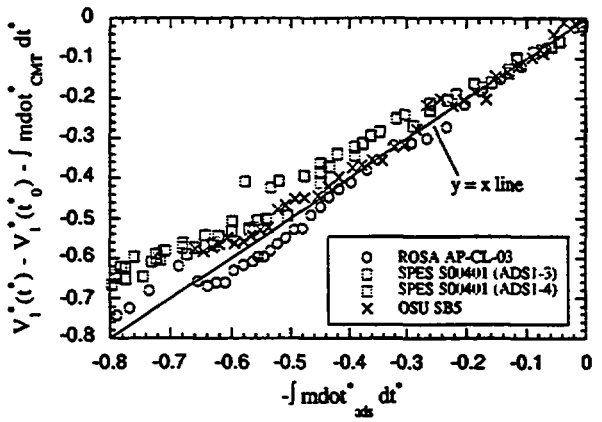

Figure 6. ROSA, SPES, and OSU mass balances in nondimensional coordinates for the ADS-4 phase.

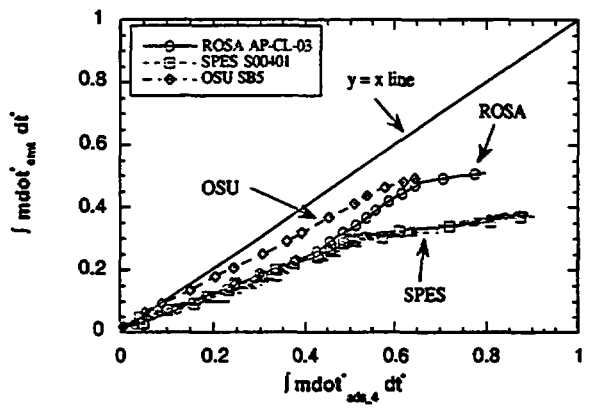

Figure 7. ROSA, SPES, and OSU nondimensional flow integrals for ADS-4 phase.

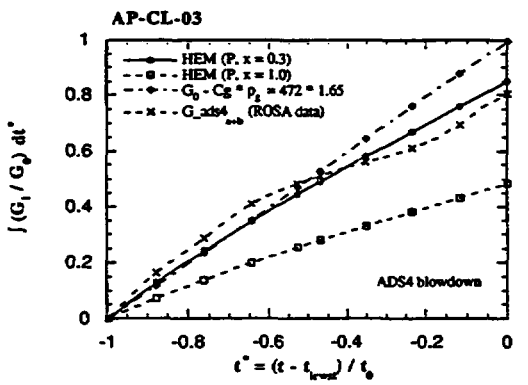

Figure 8. ROSA experiment AP-CL-03 ADS-4 mass flux.

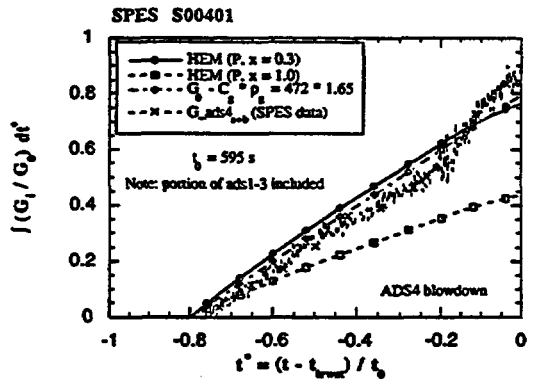

Figure 9. SPES experiment S00401 ADS-4 mass flux for ADS-4 blowdown.

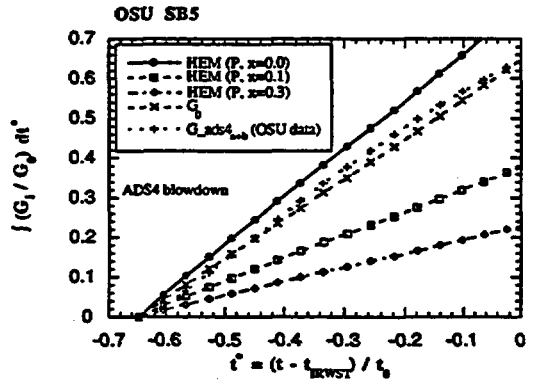

Figure 10. OSU experiment SB5 ADS-4 mass flux for ADS-4 blowdown.

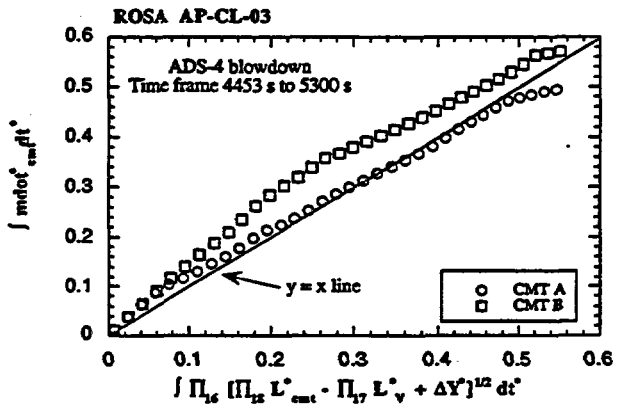

Figure 11. ROSA AP-CL-03 CMT line equation.

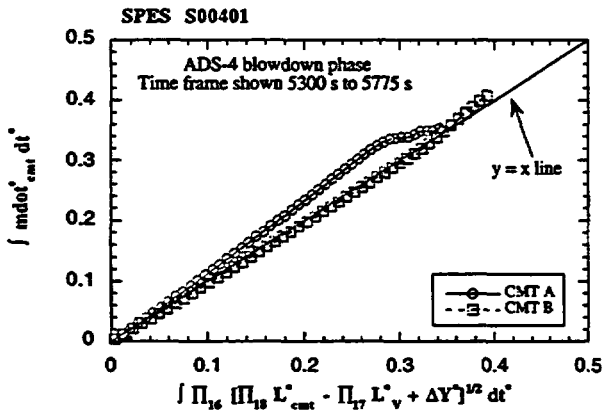

Figure 12. SPES S00401 CMT line equation.

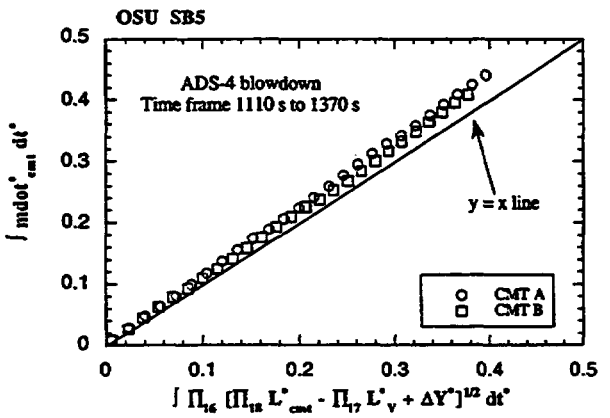

Figure 13. OSU SB5 CMT line equation.

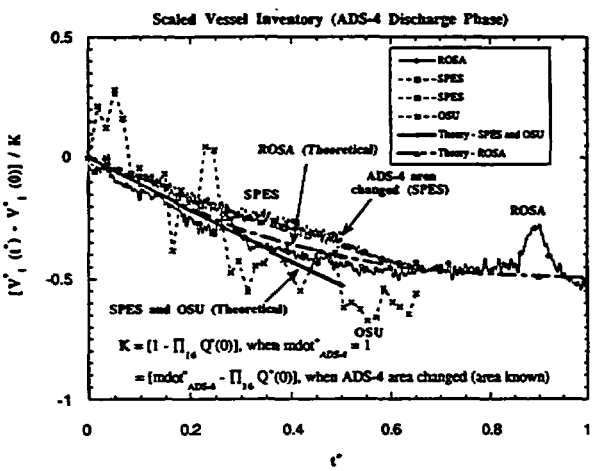

Figure 14. Analytic solution for vessel level during ADS-4 blowdown.

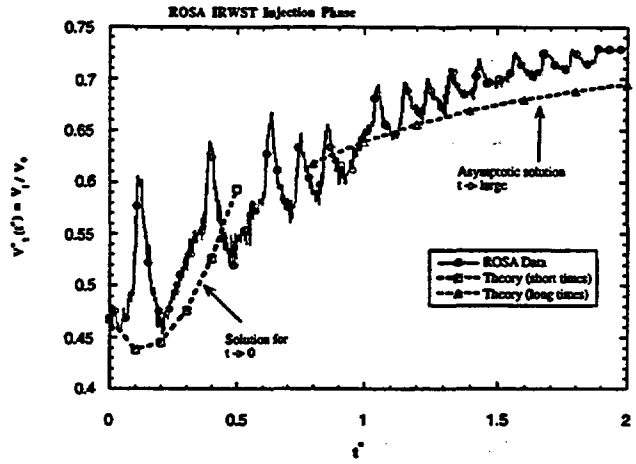

Figure 15. Analytic solution for vessel level with data from ROSA experiment AP-CL-03.

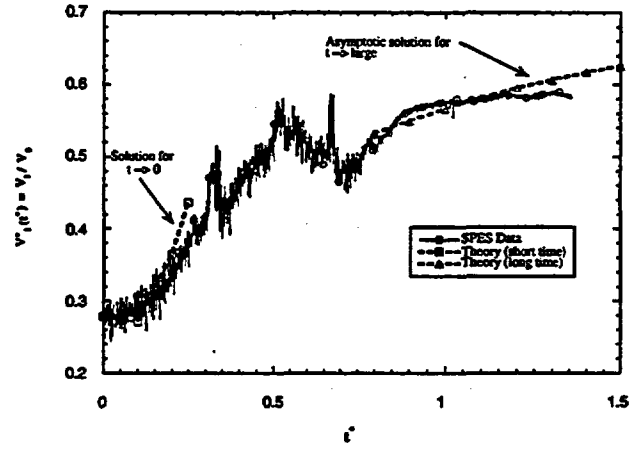

Figure 16. Analytic solution for vessel level with data from SPES experiment S00401.

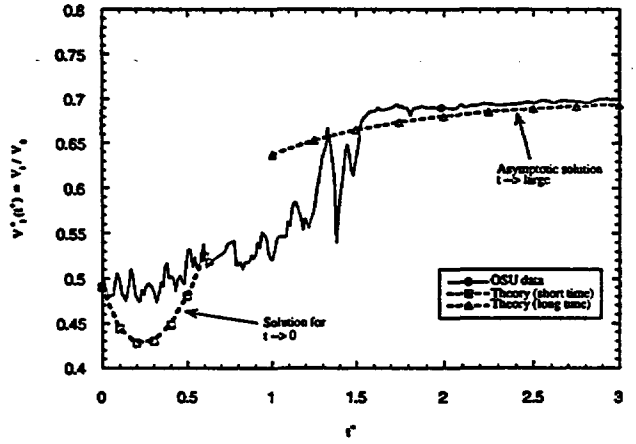

Figure 17. Analytic solution for vessel level with data from OSU experiment SB5.

Table 1. Dimensionless coefficients for ADS-4 phase.

Dimensionless Coefficient	Algebraic Description	Physical interpretation
$\Pi_{2\text{-CMT}}$	$\frac{g\Delta Y_{CMT,0}t_0}{Q_{CMT,0}L/A)_{CMT,0}}$	Ratio of hydrostatic and acceleration forces
$\Pi_{3\text{-CMT}}$	$\frac{Q_{CMT,0}t_0\dot{R}_{CMT,0}}{L/A)_{CMT,0}}$	Ratio of friction and acceleration forces
$\Pi_{7\text{-V}}$	$\frac{\dot{m}_0 t_0}{\rho_l V_0}$	Vessel nondimensional residence time
$\Pi_{9\text{-lp}}$	$\frac{Q_{CMT,0}t_0}{V_{lp+dc,0}}$	Lower plenum mixing time
$\Pi_{15\text{-CMT}}$	$\frac{Q_{CMT,0}t_0}{A_{CMT,0}L_{CMT,0}}$	Ratio of vessel and CMT emptying times
Cross groups		
Π_{16}	$\frac{\rho_l}{\dot{m}_0}\left(\frac{g\Delta Y_{CMT,0}}{\dot{R}_{CMT,0}}\right)^{1/2}$	Ratio of CMT flow to reference flow
Π_{17}	$\frac{V_0}{A_0\Delta Y_{CMT,0}}$	Ratio of head in vessel to CMT line head
Π_{18}	$\frac{L_{CMT,0}}{\Delta Y_{CMT,0}}$	Ratio of CMT level to CMT line head

Table 2. Time scales for ADS-4 blowdown.

Parameter	AP600	ROSA	SPES	OSU
t_0 (s)	1157	880	714 (ADS-1-3) 300 (ADS-1-4)	537
		892 (data)	599 (data)	524 (data)

Table 3. Π values for the ADS-4 Blowdown Phase.

Π	AP600	ROSA	SPES	OSU
$\Pi_{2\text{-}cmt}$	2393	6797	2907	7586
$\Pi_{3\text{-}cmt}$	2393	6797	2907	7586
$\Pi_{7\text{-}v}$	1	1	1	1
$\Pi_{9\text{-}lp\text{-}dc}$	3.5	2.93	3.0[a] 1.26[b]	5.71
$\Pi_{15\text{-}cmt}$	1.62	1.38	1.74[a] 0.73[b]	2.11
Π_{16}	0.53	0.58	0.63[a] 0.26[b]	0.89
Π_{17}	1.86	2.07	2.87	2.17
Π_{18}	0.36	0.29	0.35	0.33

a. SPES based on time scale of 714 s.
b. SPES based on time scale of 300 s.

Table 4. Π ratios between facilities and AP600 for the ADS-4 Blowdown Phase.

Ratio	ROSA/AP600	SPES/AP600	OSU/AP600
$\Pi_{7\text{-}v}$	1	1	1
$\Pi_{2\text{-}cmt}$	2.84	1.21	0.46
$\Pi_{3\text{-}cmt}$	2.84	1.21	0.46
$\Pi_{9\text{-}lp}$	0.85	0.87[a] 0.37[b]	1.7
$\Pi_{15\text{-}cmt}$	0.85	1.08[a] 0.45[b]	1.35
Π_{16}	1.10	1.18[a] 0.5[b]	1.73
Π_{17}	1.11	1.54	1.17
Π_{18}	0.81	0.97	0.92

a. SPES based on time scale of 714 s.
b. SPES based on time scale of 300 s.

Table 5. Dimensionless groups for ADS-4 vessel mass balance.

Dimensionless Group	Physical Meaning	AP600	ROSA	SPES	OSU
$\frac{t_0}{V_0}\left(\frac{g_0 L_0}{R_0'}\right)^{1/2}$	Ratio of CMT flow to vessel volume	0.82	0.82	0.77	1.21
$\frac{G_0 A_0 t_0}{V_0 \rho_0}$	Ratio of ADS flow to vessel volume	0.96	1.26	2.00	0.98
$\frac{G_0 A_0}{\rho_0}\left(\frac{R_0'}{g_0 L_0}\right)^{1/2}$	Ratio of ADS flow to CMT flow	1.18	1.54	2.58	0.81

Table 6. Summary of Important Nondimensional Groups by Transient Phase.

Dimensionless group	Algebraic form	Physical meaning	AP600	ROSA	SPES	OSU
High Pressure Subcooled depressurization Phase						
Φ_4	$\frac{\dot{m}_0 t_0 v_0}{p_0 M_0}\frac{\mu_{fg0}}{v_{fg0}}\frac{\partial p}{\partial \mu}\Big\|_{v_0}$	Ratio of pressure change, due to volumetric outflow, to the reference pressure	0.41	0.41	0.41	NA
Φ_6	$\frac{\dot{m}_0 t_0}{M_0}$	Ratio of mass loss to total mass in volume	1.0	1.0	1.0	NA
Intermediate Phase Subphase I						
Ψ_3	$\frac{C_{1,1,0}\dot{q}_{SG,0} t_0}{P_0}$	Ratio of pressure change, due to change in specific energy of the subcooled field from heat transfer, to the reference pressure	1.33	0.63	2.03	NA
Ψ_{10}	$\frac{C_{2,0} v_{1,0} \dot{m}_0 t_0}{P_0}$	Ratio of pressure change, due to change in specific volume of the subcooled field, to the reference pressure	-0.031	-0.017	-0.099	NA
π_{core}	$q_{core,0}/q_{SG,0}$	Ratio of heat addition by core to heat removal by steam generator	0.03	0.032	0.069	NA
Ψ_{13}	$\frac{\dot{m}_0 t_0}{M_0}$	Ratio of integrated mass flow to reference mass	1.0	1.0	1.0	NA

Table 6. Summary of Important Nondimensional Groups by Transient Phase (continued).

Dimensionless group	Algebraic form	Physical meaning	AP600	ROSA	SPES	OSU
Intermediate Phase Subphase II						
Ψ_3	$\frac{C_{l,l,0}\dot{q}_{core,0}t_0}{P_0}$	Ratio of pressure change, due to change in specific energy of the subcooled field from heat transfer, to the reference pressure	0.11	0.12	0.53	0.06
Ψ_4	$(C_{l,l}(h_f-u_l)-C_{l,m}(h_m-u_m))_0\dot{m}_{0,ss}t_0/P_0$	Ratio of pressure change, due to change in specific energy of the saturated field from mass inflows, to the reference pressure	-0.023	-0.025	-0.024	-0.01
Ψ_{10}	$\frac{C_{2,0}v_{l,0}\dot{m}_0t_0}{P_0}$	Ratio of pressure change, due to change in specific volume of the subcooled field, to the reference pressure	-0.20	-0.20	-0.20	-0.09
π_{PRHR}	$q_{PRHR,0}/q_{Core,0}$	Ratio of reference heat removal rate from PRHR and heat addition rate by core	2.03	2.59	0.52	1.0
Ψ_{13}	$\frac{\dot{m}_0t_0}{M_0}$	Ratio of integrated mass flow to reference mass	1.0	1.0	1.0	1.0
Intermediate Phase Subphase III						
Ψ_1	$\frac{C_{l,l,0}\dot{m}_{0,ADS}(h_{in}-u_l)_0t_0}{P_0}$	Ratio of pressure change, due to change in specific energy of the subcooled field from mass inflows, to the reference pressure	13.12	19.84	14.57	1.27
Ψ_3	$\frac{C_{l,l,0}\dot{q}_0t_0}{P_0}$	Ratio of pressure change, due to change in specific energy of the subcooled field from heat transfer, to the reference pressure	0.46	0.74	2.99	0.28
Ψ_6	$\frac{C_{l,m,0}\dot{q}_0t_0}{P_0}$	Ratio of pressure change, due to change in specific energy of the saturated field from heat transfer, to the reference pressure	2.74	2.97	15.57	10.55
Ψ_{10}	$\frac{C_{2,l,0}v_0\dot{m}_{0,ADS}t_0}{P_0}$	Ratio of pressure change, due to change in specific volume of the subcooled field, to reference pressure	-23.16	-33.34	-25.75	-4.92
Ψ_{11}	$\frac{C_{2,m,0}v_0\dot{m}_{0,ADS}t_0}{P_0}$	Ratio of pressure change, due to change in specific volume of the saturated field, to reference pressure	-125.5	-216.9	-146.7	-33.9
Ψ_{13}	$\frac{\dot{m}_{0,ADS}t_0}{M_0}$	Ratio of integrated mass flow to reference mass	11.4	12.4	10.0	5.5
M^*_{ACC}	M_{ACC}/M_0	Ratio of accumulator mass to reference mass	0.51	0.50	0.51	0.51
M^*_{CMT}	M_{CMT}/M_0	Ratio of CMT mass to reference mass	0.61	0.62	0.61	0.61
M^*_{PCS}	$M_{PCS,0}/M_0$	Ratio of PCS mass to reference mass	1.16	1.2	1.13	1.3

Table 6. Summary of Important Nondimensional Groups by Transient Phase (continued).

Dimensionless group	Algebraic form	Physical meaning	AP600	ROSA	SPES	OSU
Intermediate Phase Subphase III (cont'd)						
Time ratio	$(t_0-\hat{t}_0)/t_0$	Time ratio	0.053	0.048	0.061	0.11
π_{break}	$\dot{m}_{0,break}/\dot{m}_{0,ADS}$	Ratio of break and ADS-1,-2,-3 reference flows	0.038	0.035	0.044	0.083
π_{ACC}	$\dot{m}_{0,ACC}/\dot{m}_{0,ADS}$	Ratio of accumulator and ADS-1,-2,-3 reference flows	0.34	0.28	0.38	1.19
π_{CMT}	$\dot{m}_{0,CMT}/\dot{m}_{0,ADS}$	Ratio of CMT and ADS-1,-2,-3 reference flows	0.12	0.10	0.15	0.35
ADS-4 Blowdown Phase						
Term in Eq. (12)	$\frac{t_0}{V_0}\left(\frac{g_0L_0}{\dot{R}_0}\right)^{1/2}$	Ratio of CMT flow to vessel volume	0.82	0.82	0.77	1.21
Term in Eq. (12)	$\frac{G_0A_0t_0}{V_0\rho_0}$	Ratio of ADS flow to vessel volume	0.96	1.26	2.00	0.98
Term in Eq. (12)	$\frac{G_0A_0}{\rho_0}\left(\frac{\dot{R}_0}{g_0L_0}\right)^{1/2}$	Ratio of ADS flow to CMT flow	1.18	1.54	2.58	0.81
IRWST Refill Phase						
	$\sqrt{\frac{g_0L_0t_0^2}{V_0^2\dot{R}'_0}}$	Ratio of IRWST flow to vessel volume	1.48	1.44	1.44	0.99
	$\frac{G_{crit_0}A_0t_0}{\rho_0V_0}$	Ratio of ADS-4 flow to vessel volume	0.59	0.59	0.50	0.22
	$\frac{0.1t_0A_0\sqrt{g_0D_0}}{V_0}$	Ratio of pressurizer surge line flow to vessel volume	0.19	0.06	0.04	0.04
IRWST Drain Phase						
$Z^*_{dvi}+Z^*_{dc\text{-}dvi}$	$(Z_{dvi}+Z_{dc\text{-}dvi})/(Z_{dvi}+Z_{dc\text{-}dvi}+L_{IRWST,0})$	Nondimensional distance from bottom of IRWST to bottom of core	0.43	NA	NA	0.40
$\Pi_{2\text{-}ads4}/\Pi_{2\text{-}dvi}$	$\Delta Z_4/Y_0$	Ratio between ADS-4 height and IRWST initial level	0.63	NA	NA	0.58
$\Pi_{3\text{-}dvi}/\Pi_{2\text{-}dvi}$ $+\Pi_{3\text{-}ads}/\Pi_{2\text{-}dvi}$		Ratio between the sum of ADS-4 and IRWST injection line frictional losses and reference head	0.37	NA	NA	0.42

Table 6. Summary of Important Nondimensional Groups by Transient Phase (continued).

IRWST/Sump Injection Phase						
Dimensionless group	Algebraic form	Physical meaning	AP600	ROSA	SPES	OSU
$\Pi_{\rho_{dvi}}$	$\frac{v_{g_0}}{v_{f_0}}$	Vapor to liquid specific volume ratio	981.9	NA	NA	1373.
$\Pi_{Z_{dvi}}$	$\frac{\rho_{H0}}{\rho_0}\frac{\Delta Z_{4_0}}{L_0}$	Ratio of head on the ADS side to the head on the IRWST side	0.944	NA	NA	0.81
$\Pi_{\dot{R}_{dvi}}$	$\frac{\rho_0}{\rho_{H0}}\left(\frac{\dot{R}_{ads_0}}{\dot{R}_{dvi_0}}\right)$	Density weighted ratio of ADS-4 and DVI line resistances	0.054	NA	NA	0.19
Π_{SUB}	$\frac{C_{p_0}\Delta T_0}{h_{fg_0}}$	Subcooling number	0.029	NA	NA	0.009
$\Pi_{\dot{q}}$	$\frac{\dot{q}_0}{\dot{m}_{S_0} h_{fg_0}}$	Phase change number	0.046	NA	NA	0.053

THERMAL-HYDRAULIC RESEARCH ON PASSIVE SAFETY SYSTEMS FOR NEXT-GENERATION PWRS USING ROSA/LSTF

Taisuke YONOMOTO
Department of Reactor Safety Research
Japan Atomic Energy Research Institute
Tokai, Ibaraki, Japan, 319-11

Abstract

A thermal-hydraulic research on next generation passive PWRs has been conducted at JAERI using the ROSA-V/Large Scale Test Facility (LSTF), focusing on phenomena related to passive safety systems. This paper summarizes test results conducted for this research, including small break loss-of-coolant accident (SBLOCA) tests, and separate effect tests for a low pressure steady-state natural circulation (NC) and a flashing-driven safety injection system (FDIS). The SBLOCA tests investigated a combined use of a SG secondary-side automatic depressurization system (SADS) and a gravity-driven injection system (GDIS) to mitigate SBLOCAs. The results have shown that the primary loop can be depressurized to the GDIS actuation pressure of 0.2 MPa by the SADS alone, the core decay heat can be removed to the SG secondary side by the stable NC flow at low pressure, and the FDIS is a promising injection system which can be designed to have the safety functions similar to those for the nitrogen-gas driven accumulator injection system. The assessment using the test data revealed several problems of the RELAP5/MOD3 code to predict the primary depressurization due to the SADS and low pressure NC behavior.

1.INTRODUCTION

Passive safety systems are considered to have significant potential to simplify a reactor safety system, and thus, enhance its reliability, safety and economy. Several designs of next-generation pressurized-water-reactors (PWRs), therefore, utilizes passive systems for mitigation of consequences of accidents. Such reactor designs include the Westinghouse AP600[1], Mitsubishi New PWR-21 (NP-21)[2], the Japan Atomic Energy Research Institute's JPSR[3], and the Russian V-407 (or VVER 640)[4].

One of main safety characteristics of these designs is that the stable long-term core cooling is achieved automatically by the use of passive safety systems. That is, an automatic depressurization system (ADS) is used to depressurize the primary loop to the actuation pressure of a gravity-driven safety injection system (GDIS), and the GDIS is used to maintain the coolant inventory during the long-term cooling phase. The depressurization of the primary loop is achieved generally by relieving steam directly from the primary loop and/or cooling the primary coolant using a dedicated heat exchanger or steam generators (SGs). In order to maintain the core coolant inventory during the depressurization phase, these reactor designs have a medium-pressure range safety injection system similar to or the same as the existing accumulator injection system (AIS).

To assess and optimize such passive safety system designs, their performance should be evaluated against various accident scenarios. The current computer codes for doing this job, however, may have large uncertainties in predicting phenomena occurring in new components which the current-generation PWRs do not have, and those occurring under the thermal-hydraulic conditions which are not expected to occur in the current PWRs. For example, the long-term core cooling relies on pump-driven cooling systems for the current PWRs, which are operable when the pressure is lower than ~1 MPa. Therefore, the low pressure natural circulation (NC) behavior in the primary loop has not been investigated in detail.

Furthermore, because passive safety systems generally have a very small driving force for the injection and circulation, its behavior tends to be affected very easily by phenomena occurring in different locations and/or components. Such thermal-hydraulic interaction, called system effects, should be carefully investigated to assess the performance of passive safety systems. An experimental study using an integral facility is considered to be one of the best tools for the investigation of the system effects. Indeed, the ROSA/AP600 test program was conducted not only to provide the experimental data for the assessment of the analysis code but also to investigate the system effects[5].

Motivated by this background, a thermal-hydraulic research program was initiated on next-generation PWR designs using the ROSA-V/Large Scale Test Facility (LSTF)[6]. This research aims to improve the understanding on thermal hydraulic phenomena related to passive-safety systems and contribute the advancement of a safety assessment technique, the development of a reactor design, and the decision making for the selection of a next-generation reactor.

So far, four small break LOCA (SBLOCA) tests, and two separate effect tests for low pressure NC and a flashing-driven safety injection system (FDIS) have been conducted for this test program[7,8,9,10]. The FDIS is a new safety injection system proposed by JAERI as will be described later[7]. These tests focused mainly on a safety system based on the combined use of a SG secondary-side automatic depressurization system (SADS) and a GDIS for the long-term core cooling. The primary loop is depressurized to the GDIS actuation pressure mainly by the SADS in this safety system. Because of several advantages of this depressurization system, the SADS is adopted in the design of NP-21[2].

In this paper, the results of these tests will be summarized after a short description of the test facility and test methodology. The results discussed in this paper include the effectiveness of the SADS on the primary depressurization, thermal-hydraulic behaviors related to the low pressure NC and the FDIS, and other identified important phenomena. The analysis results by the RELAP5/MOD3 code are also discussed.

2.TEST FACILITY

The LSTF was originally built as a 1/48 volumetrically-scaled, full-height, full-pressure simulator of the current-generation Westinghouse-type four-loop (3423 MW thermal power) PWR[6]. The core is simulated by a 10 MW electric heater rod assembly which consists of ~1000 heater rods. The four loops of the reference PWR are lumped into two model loops (see Fig. 1). Each loop has a SG consisting of 141 full-size (19.6 mm id.) inverted-U-tubes, a reactor coolant pump, a hot leg and a cold leg.

The passive safety injection systems, currently available in the LSTF, include the GDIS, the conventional nitrogen gas-driven AIS, and the FDIS[7].

The GDIS consists of a tank holding water of ambient temperature and pressure. An injection line connects the bottom of the tank to the cold leg, or to the vessel downcomer. The line includes a check valve so that the liquid injection automatically initiates when the system pressure decreases sufficiently.

The LSTF has two tanks designed to simulate the AIS in the current-generation PWR. One of the two tanks has the design pressure of 11.7 MPa. This high-pressure AIS tank can be used for the FDIS. It utilizes steam, generated by flashing, to pressurize the coolant for injection. An apparent advantage of the FDIS over the current nitrogen-driven AIS design is that it would not bring any noncondensable gases into the primary system. Such gases would deteriorate the heat transfer performance of heat exchangers or SGs. Thus, this advantage would be significant for reactor designs which rely on heat exchangers or SGs for the system depressurization and core decay heat removal.

An ADS for the primary system can be simulated by up to three sets of a remote-control valve and a flow restriction orifice in the lines connected to the pressurizer top. Each valve can be controlled independently. The SADS can be simulated by up to two sets of a remote-control valve and a flow restriction orifice in the lines connected to each SG steam dome.

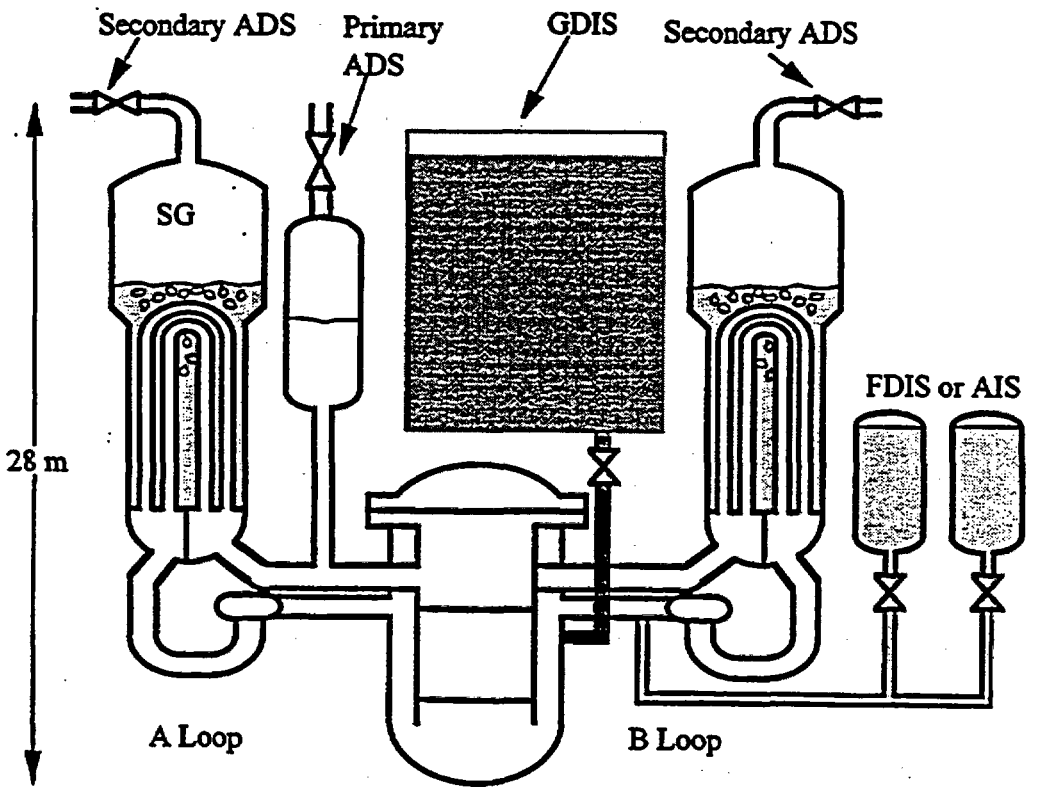

Fig.1 Geometry of LSTF

3.TEST CONDITIONS

As mentioned in the previous section, it is of significant importance to understand and predict the system effects for the safety assessment of a passive safety system. Since the system effects are generally dependent on a reactor design, the consideration of a total safety system design is necessary for a test to investigate the system effects in this research program. In this section, it is discussed how to specify test conditions to give realistically meaningful boundary conditions for each passive system.

3.1.How to specify test conditions

The safety functions of passive safety systems to mitigate effects of a SBLOCA may be classified into four functions for the proposed passive PWR designs, that is, 1) the maintenance of the core liquid inventory during the long-term cooling phase, 2) the decay heat removal during the long-term cooling phase, 3) the primary depressurization, and 4) the maintenance of the core liquid inventory during the depressurization phase.

Several passive safety systems are proposed to realize the above-mentioned safety functions. For the maintenance of the core liquid inventory during the long-term cooling phase, the GDIS is used for almost all the proposed passive reactors. For the decay heat removal during the long-term cooling phase, two-types of passive safety systems are proposed, that is, those relying on the containment cooling (passive containment cooling system; PCCS) or the SG secondary side cooling. For the purpose of the primary depressurization, two types of the depressurization system are proposed, i.e., the steam-relief type ADS and the cooling-induced type ADS using SGs or a dedicated heat exchanger. For the maintenance of the core cooling during the depressurization, the AIS is mainly used.

If the proposed safety systems for each required function are tested changing its specification, such as water inventory for the injection system, as a parameter, the total number of the tests may become unrealistically large, and an unrealistic combination of the safety systems may be included. Such concern may be avoided considering the following points. The first point is that the proposed next-generation passive PWRs are more or less similar to the current-generation PWRs. For example, the geometry of the pressure vessel and the nominal thermal-hydraulic condition are not so different. The second point is that the thermal-hydraulic behavior during the refill and reflood phase of a large break LOCA are designed to be almost the same between the current PWRs and next-generation passive PWRs. The third point is that the selection of the depressurization system is closely connected to the selection of the decay heat removal system during the long-term cooling phase, that is, if the SG secondary side depressurization is used for the primary depressurization, then the decay heat is removed by the system used for the primary depressurization, i.e., the SG secondary side cooling system for this case. If steam is relieved to the containment for the primary depressurization, it is quite natural that the PCCS is used to condense steam and remove the core decay heat.

Considering these three points, the most important parameter which characterizes the system response during a test is the selection of the primary depressurization system. The actuation logic and the depressurization rate are parameters to be investigated. Because the AIS condition has significant influences on thermal-hydraulic behavior during a large break LOCA, the AIS condition

may not be changed although the enhancement of its performance is likely as in the case for the NP-21 design. For the high-pressure range safety injection system, whether it is necessary or not in a total safety system may be an important test parameter to be investigated, in addition to the actuation logic and the water inventory. For the GDIS condition, the test parameter may be the relative elevation of the GDIS tank to the core, although the range is limited because of the size of the containment. Other test conditions such as logic of the core scram, pump coastdown, etc. may be based on those for the current-generation PWR.

3.2.Test Conditions Conducted So Far

The safety concept based on the combined use of the SADS and GDIS has been mainly investigated for this research program so far. The reasons for this are 1) the SADS is beneficial in avoiding the additional primary coolant loss required for the steam relief type ADS, 2) the thermal-hydraulic behavior caused by the steam-relief type ADS was studied in the ROSA/AP600 program tests in detail, and 3) the experimental data are non-existent for the primary depressurization to almost the atmospheric pressure by the SG secondary side depressurization, and for the low pressure NC in the primary loop. Four small break LOCA tests were conducted to investigate this safety system. In addition to the integral tests, two separate effects tests were conducted, i.e., one for the low pressureNC cooling in the primary loop and one for the FDIS. The test conditions are summarized in Table 1.

For SBLOCA tests, a system break was assumed to be at the cold leg of the loop without the pressurizer (loop B). The break diameter ranged form 6.8 to 31.9 mm. These corresponded, for an area scaling factor of 1/48, to 1.9-8.7 in.-diameter break in the reactor. The SG secondary sides were depressurized, by relieving steam, at different rates for the four tests. For Test SB1, the

TABLE 1 TEST CONDITIONS

(a) Small Break LOCA Tests

Test I.D.	Break Size[1]	Secondary ADS	Safety Injection	Steam-relief type ADS
SB1	2 inch	-100 K/h	FDIS	No
SB2	1.9 inch	2 Stage	AIS[2]	Yes
SB3	8.7 inch	2 Stage	AIS	Yes
SB4	4.4 inch	2 Stage	FDIS	No

1 : Based on scaling factor of 1/48
2 : Nitrogen-driven AIS and Pump-driven Injection

(b) Steady-state Natural Circulation Test

Test I.D.	SG Pressure	Core Power
NC1	0.14 MPa	0.94 MW(1.3% of the nominal power)

(c) Flashing-Driven Safety Injection System (FDIS) Test

Test I.D.	Initial Pressure	Initial Temperature Distribution
FDIS1	4.5 MPa	see Fig. 11

depressurization rate was -100K/h in saturation temperature. The used flow restriction orifices for the SADS were the same as those used for the current generation PWR simulation. The other three tests simulated the two-step depressurization. Tests SB2 and SB3 used the tentative setpoints for the Mitsubishi NP-21. Makeup water was injected into the SG secondary sides during depressurization. For Tests SB1, 2 and 4, a pump-driven auxiliary feedwater system was used, with a flow rate based on that for the current-generation 4-loop reactor. For Test SB3, the GDIS was used to feed the coolant to the SG secondary sides.

For the safety injection to the primary loop, the FDIS with the initial pressure of 4.6 and 5.5 MPa were used for Tests SB1 and SB4, respectively, and the AIS was used for the Tests SB2 and SB3. The fluid temperature in the FDIS was uniform and saturated. The GDIS with the constant liquid level of 12.5 m above the cold leg elevation was used for all the four tests.

A steady-state NC test NC1 was conducted by decreasing a primary mass inventory step-wisely as a test parameter, and controlling the core power at 0.94 MW (1.3% of the nominal core power) and the SG secondary pressure at 0.14 MPa.

For the separate effect test of the FDIS, the FDIS tank was directly connected to the break flow catch tank to simulate a rapid liquid injection required during a large break LOCA.

4.RELAP5 ANALYSIS

The SBLOCA and NC tests were analyzed using the RELAP5/MOD3[11]. The primary and secondary loops were modeled using 235 volumes and 204 heat structures. The measured data were used for the temperature and flowrate of the feedwater. For the analysis of the NC test, the SG secondary pressure was controlled at the measured pressure of 0.14 MPa by adjusting the vapor discharge flow from the main steam line.

For the analysis of the FDIS test, the number of calculation cells used are 30 both for the FDIS tank and the injection line. The break storage tank was model with a time-dependent volume. Measured values were given for the initial values of the tank pressure, fluid temperature distribution, and liquid level.

5.SUMMARY OF TEST RESULTS

5.1.Primary pressure

The pressure responses measured in the tests SB1 and SB4 are shown in Figs.2 and 3, where the primary pressure is represented by that measured in the upper plenum. Both axes of these figures are scaled logarithmically to clearly show the pressure difference between the primary and secondary sides over the whole range of pressure during the tests. The pressure difference is more important than for existing PWRs since it directly reflects the effectiveness of the SADS on the primary depressurization. Even minor pressure difference can affect significantly the timing of the GDIS injection.

Major events observed in Test SB4 can be summarized as follows. The test was initiated by opening a break simulation valve. The primary side was depressurized quickly toward the SG

secondary-side pressure. During this initial depressurization, several trip-initiated events occurred. The scram signal was generated at 19 s after break, at a primary-side pressure of 12.97 MPa, and the safety system actuation (S) signal at 24 s, at 12.25 MPa. The scram signal initiated the simulated core power decay, pump coastdown and isolation of the SG secondary sides from the feedwater and steam lines. The S signal actuated the first stage of SADS (SADS-1).

Liquid injection from the FDIS occurred between 331 and 387 s, as the primary-side pressure decreased below the FDIS initial pressure of 5.5 MPa. The primary depressurization was accelerated immediately after the second stage of SADS (SADS-2) was actuated at 407 s. When the primary pressure decreased to ~0.2 MPa, the GDIS injection initiated at 3435 s. After the GDIS actuation, a stable long-term cooling condition was established; the primary pressure at the upper plenum was almost constant at ~0.2 MPa, the decay heat was transferred to SGs by NC, and the break flowrate was balanced with the GDIS injection flowrate. This constant pressure is almost equal to atmospheric pressure plus the water head corresponding to the elevation difference between the upper plenum and the GDIS tank water level. The core was always covered with liquid water or two-phase mixture through the experiment. The experiment was terminated at 14000 s, approximately three hours after the GDIS initiation, by closing the break valve.

The pressure difference between the primary and secondary sides was affected by the flow condition inside the SG U-tubes. As indicated in Fig. 3 for Test SB4, the pressure difference was markedly smaller when the U-tube primary side was steam-filled (i.e., when the primary-side heat

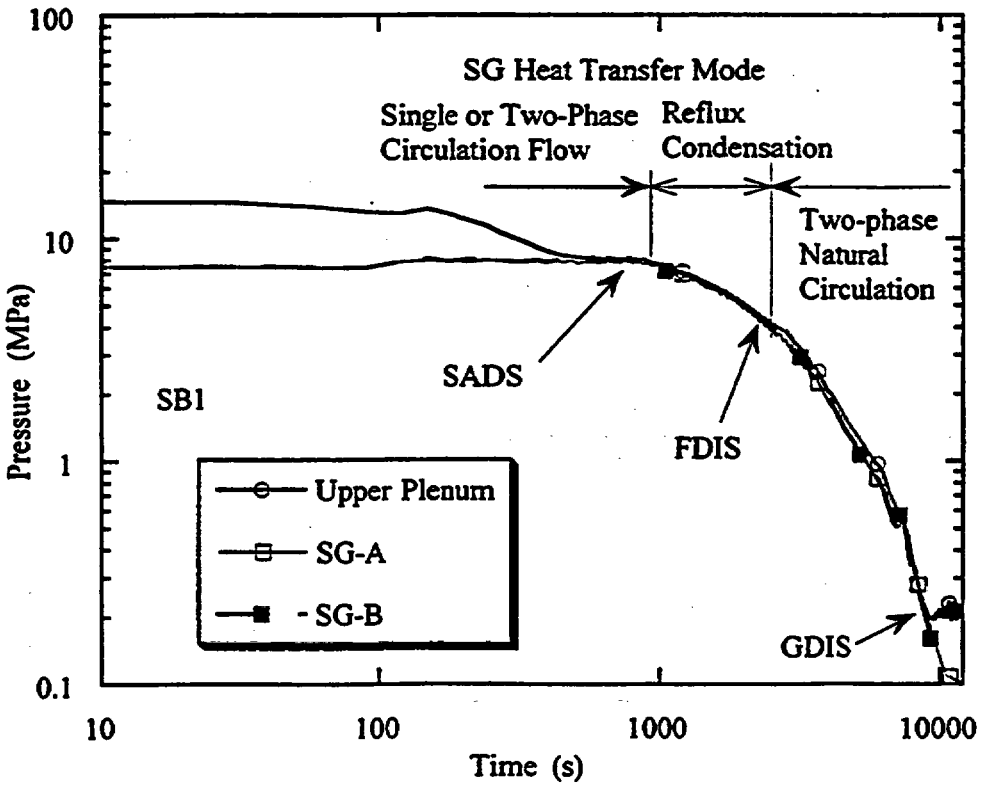

Fig.2 Pressure responses during Test SB1

transfer was in the reflux condensation mode) than when there was liquid circulation. For Test SB1, on the other hand, the pressure difference was always small after the SADS actuated, irrespective of the U-tube flow mode as shown in Fig. 2. This is because the SG heat transfer rate was too small to create the measurable temperature difference between the primary and secondary of the SG due to the slow secondary-side depressurization for this test. Note that the size of the flow restriction orifice for the simulation of the SADS for the test SB1 was the same as that for the LSTF reference reactor, i.e., the current-generation PWR. These results indicate that the analysis of the pressure difference, i.e., the NC heat transfer at the SG becomes important for next-generation PWRs if the depressurization rate is much faster than for the current generation PWR. The depressurization rate is likely to be faster for the next-generation passive PWRs when the maintenance of the core coolant inventory during the depressurization phase relies on the safety injection from tanks such as the AIS.

The primary depressurization caused by the SADS actuation was relatively well predicted by the RELAP5 code before the actuation of the second stage of the SADS (SADS-2), as shown in Fig.4. The depressurization rate was, however, overpredicted at lower pressure. Because of the overpredicted depressurization, the GDIS actuation was predicted to occur about 1500 s earlier than the experiment as shown in Fig.4. The cause of this will be discussed in the later section.

5.2.Natural circulation and SG U-tube flow behavior during SBLOCA tests

The NC through U-tubes affected the SG heat transfer performance, and thus the primary-side

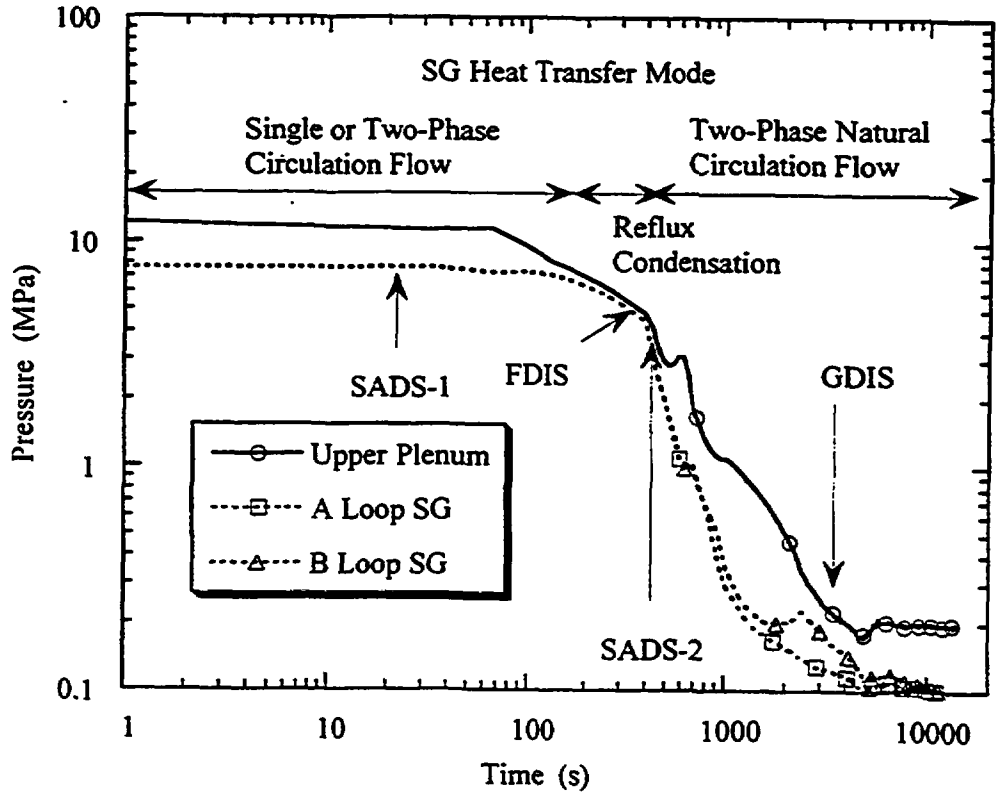

Fig.3 Pressure responses during Test SB4

depressurization especially when the depressurization rate was relatively fast as observed for Test SB4. The figure 5 shows the loop flowrate measured at the pump suction for Test SB4. The loop flowrate decreased rapidly due to the pump coastdown immediately after the break, took the minimum due to the flow mode transition from the NC to the reflux condensation, and increased rapidly after the FDIS actuation due to the resumption of two-phase NC. After that, the stable NC continued. Because of this stable NC, the core cooling mode was changed from the two-phase cooling to almost single-phase cooling at ~4500 s.

Nonuniform flow behavior among U-tubes was observed both during the blowdown phase and low pressure long-term core cooling phase[8,9,10]. The behavior was characterized by the coexistence of concurrent condensing flow in some tubes and stagnant two-phase stratification in the other tubes as shown in Fig.6. For U-tubes with the stagnant two-phase stratification, liquid levels in the tubes changed very slowly with time, and the fluid temperatures inside and outside of the tube were the same except for some tubes showing fluid saturation in the bottom region of the inlet side. This means the heat transfer occurs primarily through U-tubes with the concurrent condensing flow.

The stable two-phase stratification in U-tubes during the blowdown phase was caused mainly by the temporal liquid level drop in the secondary side. The secondary side liquid level temporarily decreased down to 40% of the U-tube height due to the coolant loss from the SADS valves[8,9]. This decreased the condensation in the U-tube top region and resulted in the stable existence of vapor

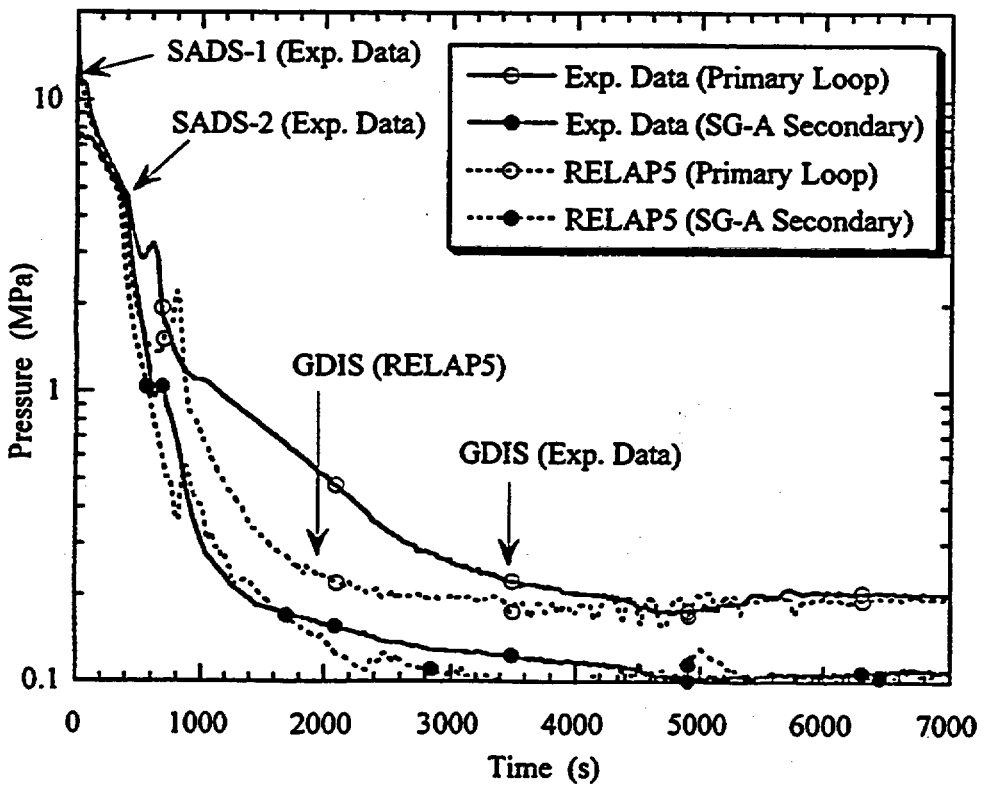

Fig.4 Comparison of primary and secondary pressures between Test SB4 and RELAP5

space above liquid columns in there.

On the other hand, the two-phase stratification during the long-term core cooling phase occurred when entire U-tubes were covered with the two-phase mixture in the secondary side. This stratification was caused by the secondary side temperature distribution as will be discussed in the next section describing the NC test.

Since the heat transfer occurs primarily in the U-tubes with the concurrent condensing flow, the nonuniform behavior effectively reduces the heat transfer area at SG. This characteristic is very important when the test result is compared with the RELAP5 code which does not have an appropriate physical model to take into account this effect.

The NC flowrate calculated by the RELAP5 code was very oscillatory when compared with the experimental data as shown in Fig.5. This was caused by the above-mentioned inability of the code to deal with the nonuniform U-tube flow. The overestimated heat transfer area caused excess condensation in the U-tube, which resulted in the flow oscillation including the flow reversal. The exaggerated oscillation of the NC flow affected the prediction of the core cooling. Although the core fluid changed to single-phase liquid from two-phase mixture after ~4500 s in the test, such transition was not predicted at all.

The inability of the code to predict the NC behavior is noteworthy when compared with the

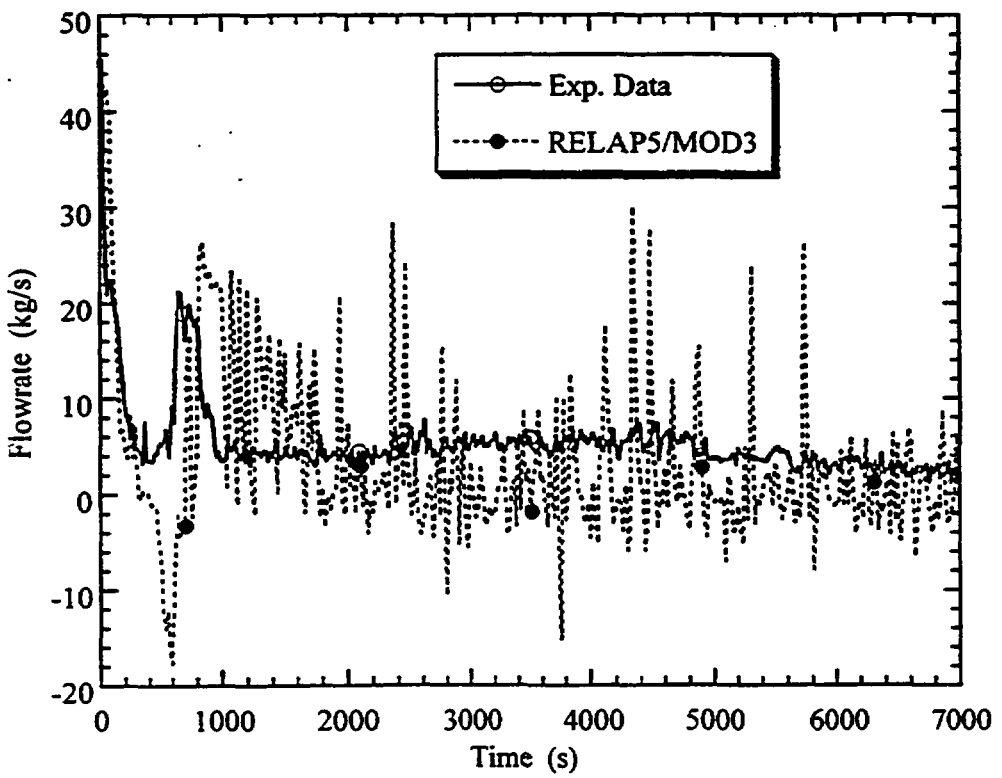

Fig.5 Comparison of loop flowrates between Test SB4 and RELAP5/MOD3

code assessment results using the high pressure NC data. Even using a lumped flow channel for U-tubes, the loop flow rate under various two-phase flow modes, including a fill and dump mode, was somehow calculated[12,13]. These results stress the importance of a calculation model for the nonuniform behavior in order for the prediction of the low pressure NC.

The overprediction of the depressurization rate shown in Fig.4 can be also explained by the inability of the code to deal with the nonuniform behavior. Since the pressure and mixture level responses in the SG secondary side were predicted well, the overprediction of the primary depressurization was caused by the overprediction of the effective heat transfer area at SG. When the effective reduction of the heat transfer area at SG is not taken into account, the overprediction of the heat transfer is inevitable.

5.3.Natural circulation and SG U-tube flow behavior during Test NC1

Figure 7 shows the loop flowrate vs. the primary mass inventory observed in the test NC1. With decreasing the mass inventory, the loop flowrate increased due to the transition from the single-phase NC to the two-phase NC, peaked at ~90%, and then decreased. The reflux condensation was observed for the mass inventory below ~40%.

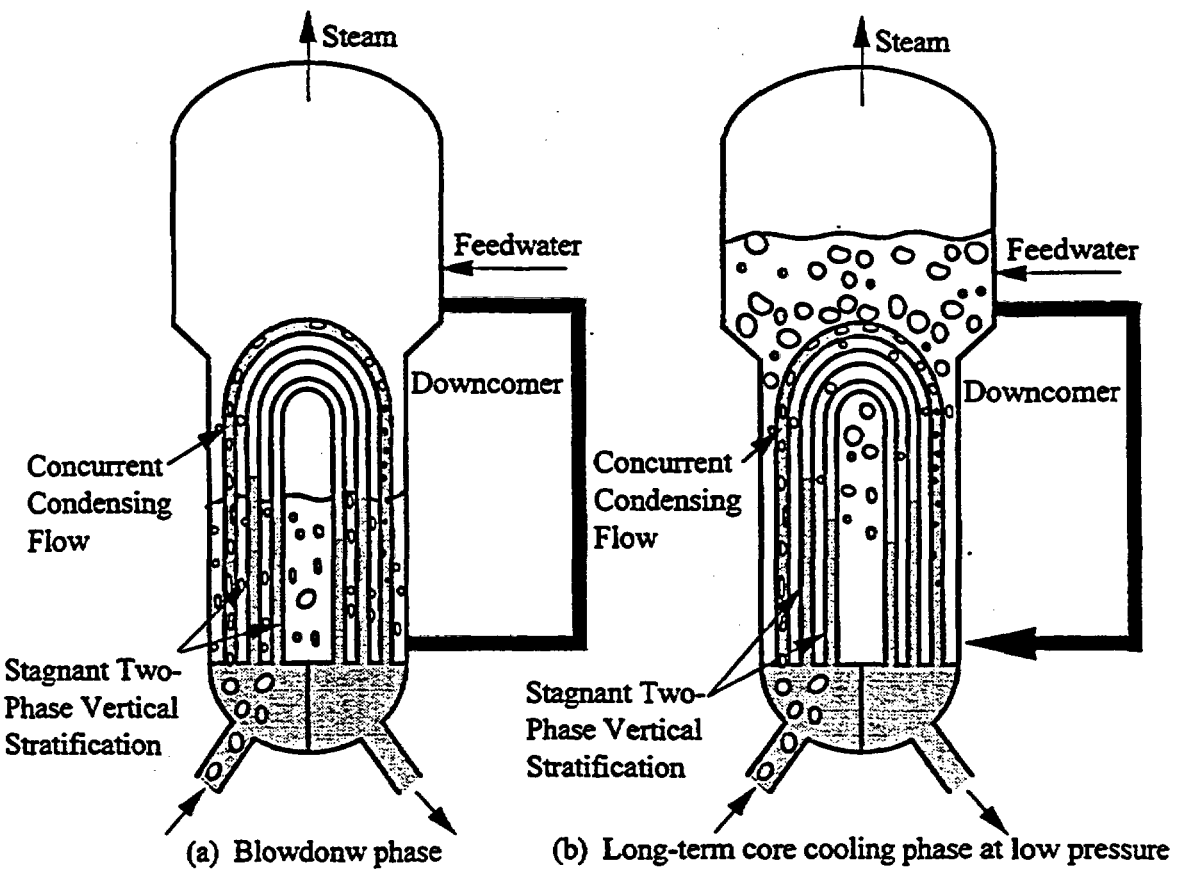

Fig.6 Nonuniform flow behaivor observed among U-tubes

The nonuniform two-phase flow behavior similar to that observed in the SBLOCA tests was observed when the primary mass inventory was between 70 and 91%. Among six instrumented SG U-tubes in the loop-A, the stagnant two-phase stratification was observed in five U-tubes, while the concurrent condensing flow was observed only in one U-tube.

The existence of the stable two-phase stratification suggests that the vapor mass does not change with time in the vapor continuous regions above the liquid levels in such U-tubes. Note that all the core power was transferred to the SG secondary sides during the test, that is, the average primary temperature was higher than that in the secondary side. Only condensation was seemingly possible in U-tubes under this condition.

The mechanism for the stagnant stratification can be understood from the measured secondary side temperature distribution showing the lowest temperature at the top and bottom regions and the highest around the midplane as shown in Fig.8. This was caused by the saturation temperature difference corresponding to the static pressure difference, and the recirculation in the SG secondary side. The condensation occurring around the tube top was balanced with the evaporation occurring around the midplane in the U-tube with the stratification. This enabled the stable existence of vapor space above the liquid levels in the U-tube. This behavior is one of characteristic behaviors at low pressure where the pressure is comparable to the water head. On the other hand, such coexistence of evaporation and condensation in a tube is impossible to occur at high pressure where the secondary side temperature is generally uniform[13]. The above-mentioned mechanism for the stagnant two-

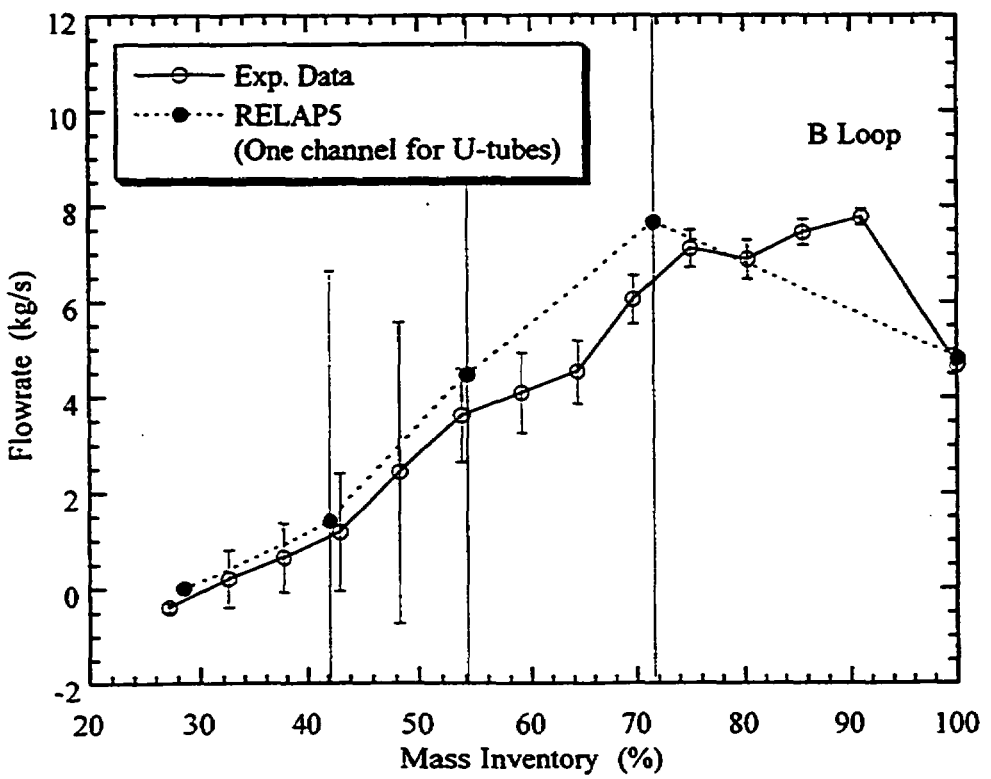

Fig.7 Comparison of loop flowrates at cold leg vs. primary mass inventory for Test NC1 and RELAP5 analysis

phase vertical stratification was confirmed by the RELAP5 analysis using a partial SG model[10]. In this analysis, only the SG primary side was modeled with a pipe component. The measured data were used for the inlet and outlet pressure and qualities, and the secondary side fluid temperatures. The result has indicated that such balance of condensation and evaporation rates are possible in the U-tube.

The concurrent condensing flow behavior was also analyzed using the SG partial model to investigate the mechanism of the nonuniform behavior[10]. It is concluded that the fraction of the tubes with the concurrent condensing flow is determined so that the complete condensation and stable flow behavior are possible in the tube. The flow behavior in the other tubes can be stable with the two-phase stratification.

Based on the mechanism of the nonuniform flow behavior at low pressure, the simple tentative RELAP5 analysis procedure was proposed[10]. In this tentative approach, the SG primary side was modeled with two parallel flow passes representing the tubes with the condensing flow and the two-phase stratification. A very high flow resistance (of the order of 10^5) was imposed for the flow channel representing the two-phase stratification. Such an artificial adjustment may be justified because it does not affect the calculation results if the flow velocity is small enough, that is, the resistance coefficient has an influence on the result only when the flow exists. The fraction of U-tubes with the condensing flow was changed as a calculation parameter. When the fraction was 25%, the calculated behavior was similar to the measured NC flow rate at 70% mass inventory. The

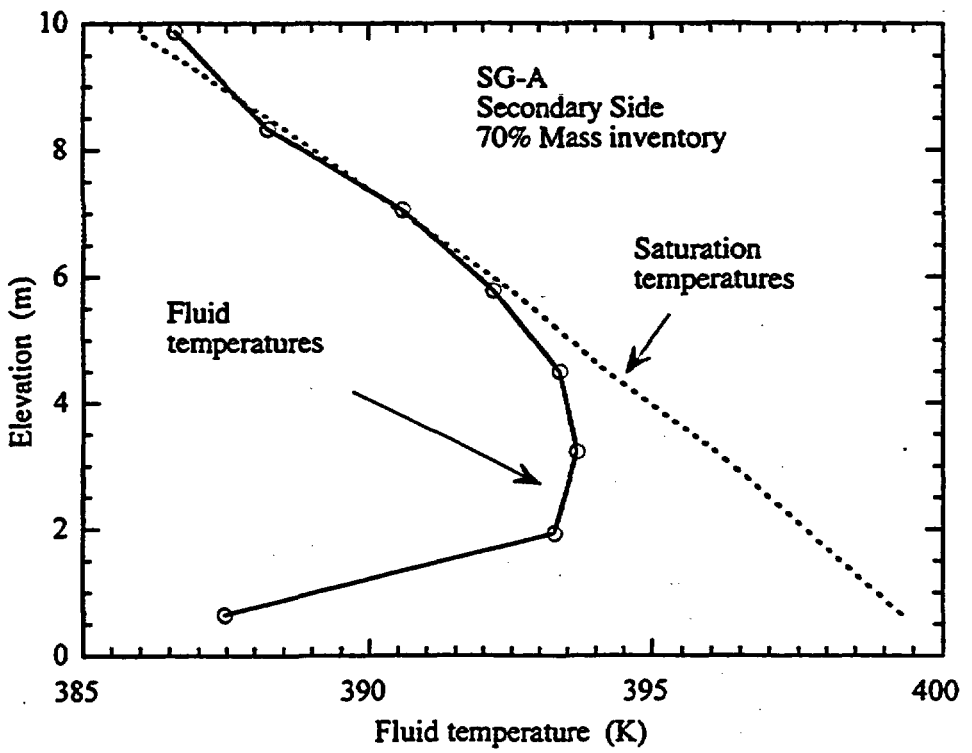

Fig.8 Comparison of SG-A Secondary side fluid and saturation temperatures at 70% mass inventory for Test NC1

oscillation was suppressed significantly by using this procedure, although there still exists disagreements between the data and calculation. For more accurate prediction of the low pressure NC behavior, the heat transfer correlations for the condensing flow should be investigated in addition to the physical model development to determine the fraction of the U-tubes with the concurrent flow. At the present time, the low pressure NC behavior may be investigated, at least qualitatively, by using this procedure and changing the fraction as a calculation parameter.

5.4.Flashing-Driven Safety Injection System (FDIS)

As mentioned in the previous sections, the FDIS has a significant advantage when it is used with the cooling-induced ADS such as the SADS. Considering this, we have proposed to use the FDIS as an alternative system of the current-generation AIS. The AIS has two safety functions; the maintenance of the core coolant inventory during the depressurization phase for a SBLOCA and a rapid coolant injection for a large break LOCA (LBLOCA). The FDIS has to satisfy these two safety functions in order to be used as an alternative safety system.

The proposed FDIS is shown in Fig.9, which consists of a water tank, a pressure balance line, and an injection line. Thermally stratified borated water is stored in the tank, that is, hot and room temperature water is stored in the upper and lower part of the tank, respectively. Flashing occurs in the hot liquid region when the system is depressurized, and the resultant volume expansion pushes the cold water into the primary loop. The use of the stratified water is beneficial in avoiding the choking of the hot fluid flow in the injection line. To establish such a thermal stratified layer in the tank during the normal operation condition, a heater is installed in the upper part of the tank. The

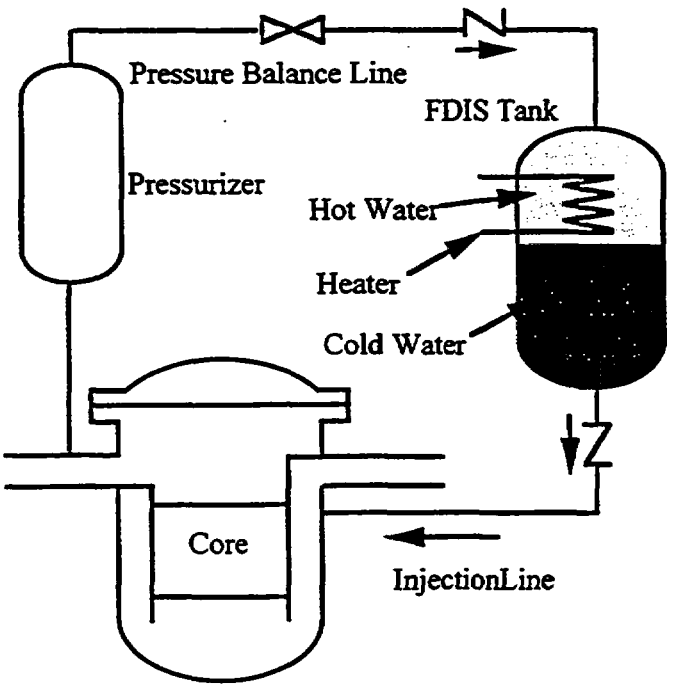

Fig.9 Flashing-Driven Safety Injection System

pressure balance line between the FDIS tank top and the pressurizer is to take into account an accident with the loss of electric power for the heater. By opening the valve in the pressure balance line, the liquid level in the FDIS tank is expected to change according to that in the pressurizer for a slow transient such as a SBLOCA, because of the manometric balance between the FDIS and pressurizer.

One of main concerns of the combined use of the FDIS and SADS during a SBLOCA is whether the injection of the hot liquid and steam by the FDIS may have an undesirable effect to slow the depressurization. The FDIS was used for Tests SB1 and SB4 as shown in Figs.2 and 3. For both tests, the fluid temperature in the tank was uniform and saturated to give adverse effects on the primary depressurization. The pressure difference between the primary and secondary sides indeed increased after the FDIS actuation during the tests. This occurred because the mass addition by the FDIS changed the U-tube flow mode from the reflux condensation to two-phase NC, and thereby increased the thermal resistance on the U-tube primary side. Since this increase of the thermal resistance is caused by the increase of the primary inventory, this may not create safety problems related to the core cooling.

Thermal-hydraulic behavior occurring in the FDIS tank with the thermally stratified layer is similar to that in the CMT or the boron injection tank proposed by Mitsubishi[14]. The CMT behavior was investigated in detail in the ROSA/AP600 tests. The test results have shown that the thermal stratified layer is created due to the ingress of the hot water from the cold leg through the

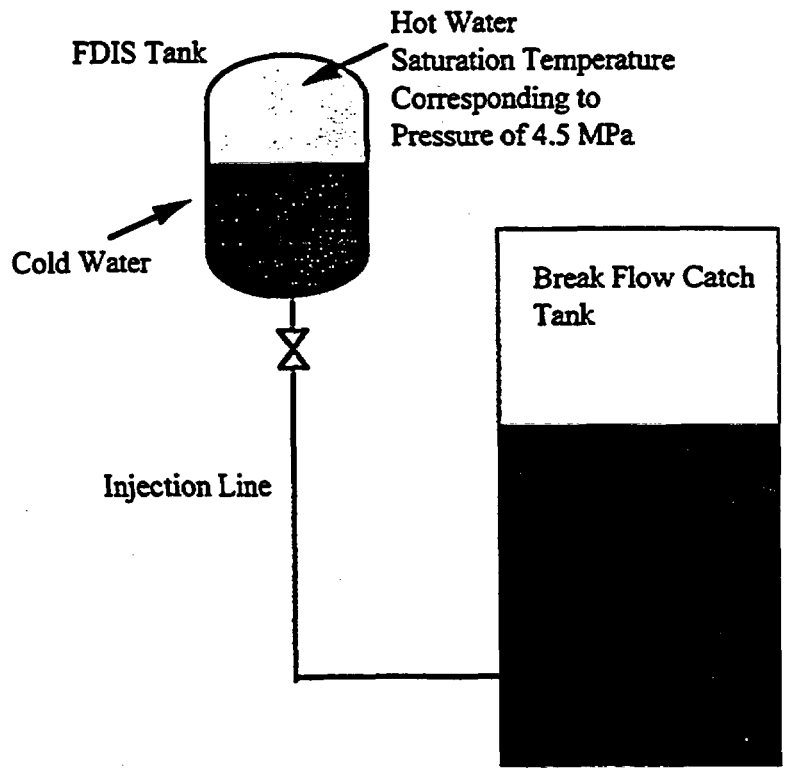

Fig.10 Separate Effects Tests for FDIS

tank top nozzle before the liquid level is formed in the tank, and the flow behavior in the tank is very stable and one-dimensional when the layer moves downward due to the flashing of the hot water[15]. Because the liquid velocity in the tank is expected to be much faster for a LBLOCA condition than that observed in the CMT during SBLOCA tests for the ROSA/AP600 program, the stability of the thermally stratified layer was investigated in the FDIS separate effect test. For this test, the simulated FDIS tank was connected directlyto the break flow catch tank as shown in Fig.10. The initial temperature distribution in the tank is shown in Fig.11, which has the saturated fluid layer of ~2 m and the cold liquid layer of ~3 m. Here the cold layer is defined as that having liquid temperature of lower than 373 K. Because the heater was located in the bottom part of the tank used for this test, the thermally stratified layer was created first by heating water of ~2m height in the bottom part of the tank up to the specified temperature, and then by injecting cold water from the bottom. The slope of the temperature distribution can be, therefore, much steeper in the proposed system having the heater in the upper part of the tank. The initial tank pressure was 4.5 MPa. The test was initiated by opening a valve in the injection line.

The test results showed that thermal-stratified layer was stable, and the shape of the vertical temperature distribution as a function of the distance relative to the liquid level did not change significantly with time, except for the saturation temperature, as shown in Fig.11. This indicates the

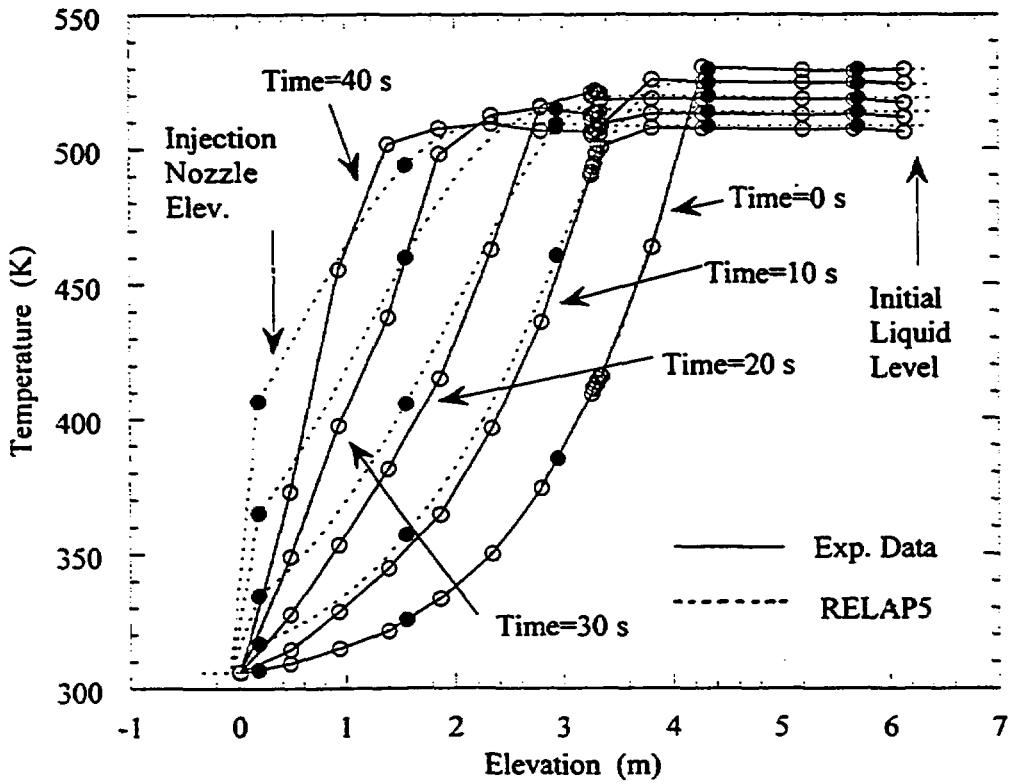

Fig.11 Comparison of temperature distributions in FDIS tank between Test FDIS1 and RELAP5

fluid mixing was not significant in the tank. The measured maximum flowrate of 53 kg/s corresponds to the fluid velocity in the tank of ~7 cm/s, which is the same order of the maximum liquid velocity in the AIS tank for the LSTF reference reactor during a LBLOCA. As expected from the simple behavior in the tank, the measured flowrate was predicted very well by the RELAP5 code as shown in Fig.12. The fluid temperatures are also well predicted as shown in Fig.11, although they are slightly overpredicted in the lower part of the tank probably due to a numerical diffusion as observed in the analysis of the CMT behavior[16].

The above-mentioned results indicate that it may be possible to design the FDIS by using the RELAP5 code. The required flowrate for the AIS during a LBLOCA is available in literature. For example, the high flow rate of an advanced accumulator, proposed by Mitsubishi, is based on the required flowrate[17]. The advanced AIS is characterized by an automatic, passive decrease in the injection flowrate from the high to low flow mode, which occurs when the tank water level drops to a certain predetermined level. This automatic flow reduction is intended to avoid the coolant spillover from the break.

The FDIS injection flowrate was calculated by the RELAP5 so that the injection rate becomes similar to that required for the LBLOCA by changing the initial thickness of the hot water region and the injection line flow resistance, while the initial tank pressure was set to be 4.5 MPa. The comparison in Fig.13 shows that the FDIS injection rate can be at least similar to that for the high flowrate mode, i.e., the flow rate required for the conventional PWR during the LBLOCA. These

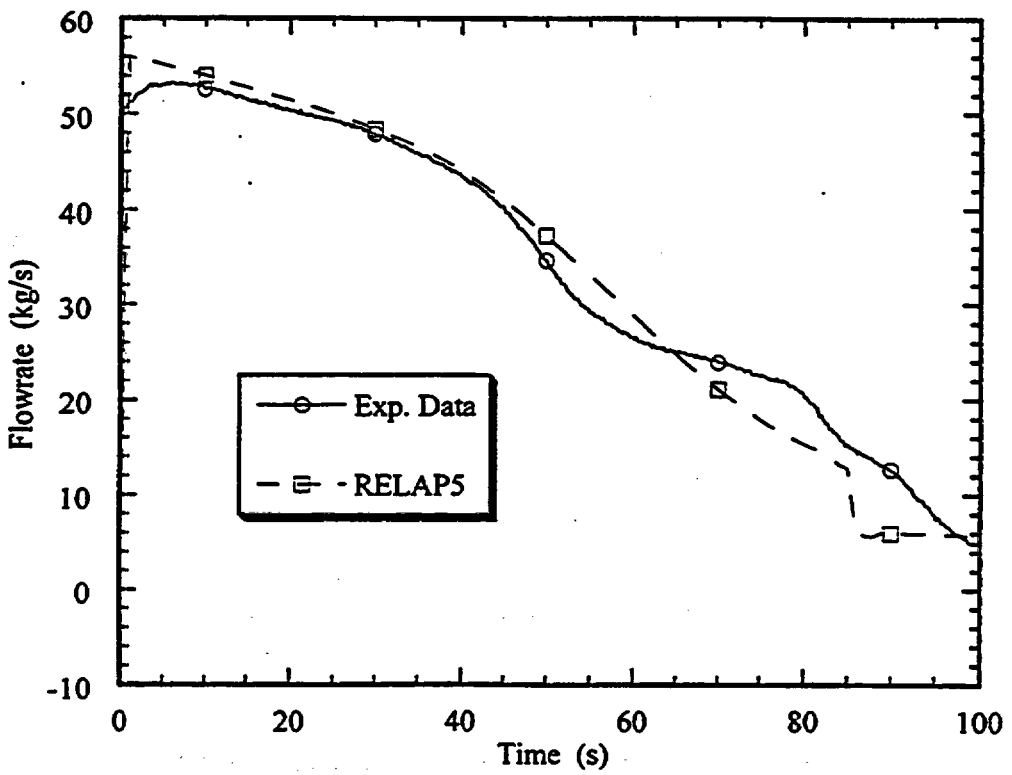

Fig.12 Comparison of FDIS Injection Flowrates between Test FDIS1 and RELAP5

results indicate the promising nature of the FDIS as an alternative safety component for the next-generation PWR.

5.5.Other important thermal-hydraulic behaviors

5.5.1.Accumulation of Non-Condensable Gas

Accumulation of noncondensable gases in the SG U-tubes was observed in the SBLOCA tests The gases were found to have originated mainly from the dissolved gas in the coolant injected by the safety systems[8,9]. The total gas volume at the end of experiment was 0.080 m^3 for Test SB1, 0.072 m^3 for Test SB2, and 0.258 m^3 for Test SB4, where the gas volumes correspond to those at a temperature of 273.15 K and a pressure of 0.1013 MPa. The differences in the gas volumes among the tests were caused by the differences in the injected mass from the GDIS, which was 2180 kg for Test SB1, 2750 kg for Test SB2 and 14000 kg for Test SB4.

The effect of the accumulation would become more significant for longer transients and for low pressures. The accumulation will deteriorate the SG heat transfer and adversely affect the GDIS performance. The prediction of the gas accumulation behavior will be therefore important for plant designs which rely heavily on SGs or heat exchangers for the primary system depressurization and cooling. Note that most of existing LOCA analysis codes do not take into account the dissolved gas behavior. Also, devices and procedures should be developed for effective gas venting from the

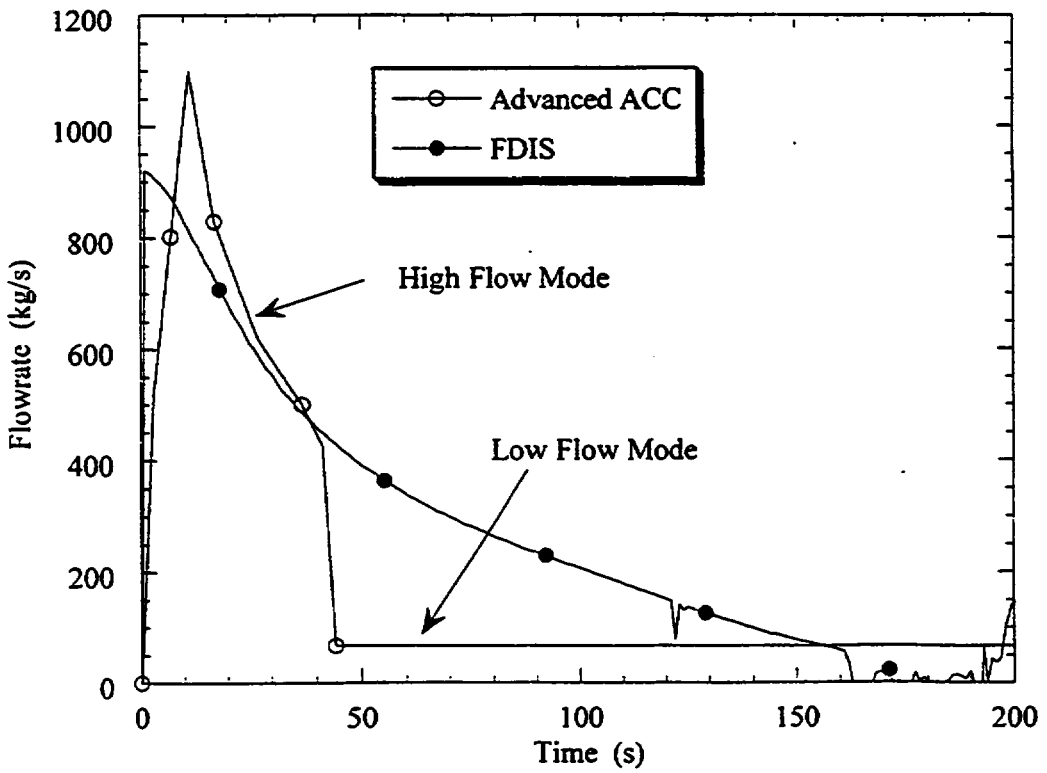

Fig.13 Comparison of flowrates from FDIS and Mitsubishi advanced accumulator for a large break LOCA condition

primary system.

5.5.2. Liquid holdup in U-tubes due to CCFL

The liquid holdup in U-tubes was observed during Test SB3 due to the counter-current flow limitation (CCFL). The liquid holdup corresponded to the maximum collapsed liquid level of ~2 m. This was observed only in Test SB3 with the largest break area among the tests which caused the fastest primary depressurization rate. Note that such liquid holdup is believed to be unlikely for the conventional PWRs when the SG secondary side is depressurized as an accident management measure because the depressurization rate is not large enough. It is known that the RELAP5 code has a difficulty in predicting the amount of the liquid which is held in the U-tubes due to CCFL[18]. Thus, there may be need for the prediction of CCFL-induced liquid holdup for the optimization of the SADS design.

5.5.3. System-Wide Long-Term Oscillation

The system-wide long-term oscillations occurred during Tests SB1 and SB2 as a result of interactions among several phenomena. The oscillated parameter includes the pressurizer liquid level, NC flow rate, the primary pressure, the GDIS flowrate, and so on. Although the core was kept cooled adequately during the oscillations, the core subcooling margin and the GDIS flowrate fluctuated. It is thus would be desirable not only to predict the phenomena but also to find a way to suppress the oscillations to achieve stable plant cooldown. Similar behavior was observed during the ROSA/AP600 tests, after the forth stage ADS was actuated[19]. Periodic refill and drain-down of the pressurizer affected the hot leg level and thus the steam venting rate from the ADS. There was no NC flow through the U-tubes during the long-term core cooling phase in the ROSA/AP600 tests. In the present tests, however, oscillations occurred even when the pressurizer was empty (Test SB1), the fluctuation in the NC flow rate played an important role. On the other hand, such oscillation was not observed in the Test SB4 in which the steam-relief type ADS was not used. Further study is necessary to identify the conditions for the oscillations to occur.

6. CONCLUSIONS

Thermal-hydraulic safety research program is currently being conducted by using the ROSA-V/LSTF, to better understand the phenomena related to passive safety systems for the next generation PWRs. The test data also are useful for assessment and improvement of computer codes. This paper describes a summary of the small break loss-of-coolant accident (SBLOCA) tests for the investigation of the combined use of a gravity-driven injection system (GDIS) and a SG secondary-side automatic depressurization system (SADS), and two separate effects tests for low-pressure steady-state natural circulation (NC) and a flashing-driven safety injection system (FDIS). The results of the tests and RELAP5/MOD3 analysis can be summarized as follows.

1. The primary system was depressurized, by means of the SADS, successfully to the GDIS injection pressure of 0.2 MPa, even when the steam was not relieved directly from the primary loop. Stable long-term passive core cooling by the NC flow, with the GDIS injection flow balanced with the break flow, was established at low pressure. These results confirm the effectiveness of the combined use of the SADS and GDIS.

2. Nonuniform flow behavior was observed among SG U-tubes during the low-pressure NC core cooling phase both in the SBLOCA and NC tests. The behavior was characterized by the

coexistence of U-tubes with condensing concurrent flow and those with stagnant vertical two-phase stratification. The heat transfer occurred primarily through U-tubes with the two-phase concurrent condensing flow. This causes the reduction of the effective heat transfer area in the SG.

3. The primary depressurization rate was overpredicted by the RELAP5/MOD3 code using one lumped U-tube model when the depressurization rate was large enough as observed in Test SB4. The calculated low-pressure NC flow was excessively oscillatory, and the observed stable core cooling by a single-phase liquid flow was not predicted. These are caused mainly by the inability of the code to take into account the above-mentioned effective reduction of the heat transfer area.

4. The FDIS is proposed as an alternative system to replace the nitrogen gas-driven accumulator injection system (AIS). The proposed system consists of a tank storing thermally stratified water: hot water in the upper part and cold water in the lower part, an injection line with a check valve connected the tank bottom to the primary loop, and a pressure balance line to the pressurizer. The apparent advantage of the FDIS over the current-generation AIS is that there is no possibility of unintentional noncondensable gas ingress into the primary loop. The FDIS, therefore, has an advantage to be used with a cooling-induced type ADS such as the SADS.

5. The actuation of FDIS did not give significant adverse effects on the primary depressurization during the two SBLOCA tests SB1 and SB4, for which the tank initial temperature was uniform and saturated to give adverse effects on the depressurization.

6. The thermally stratified layer in the FDIS tank was very stable and one-dimensional under the condition simulating the rapid liquid injection during a large break LOCA (LBLOCA). Because of this observed simple behavior, the behavior was well predicted by the RELAP5/MOD3 code, indicating that the code can be an appropriate tool for the design of the FDIS. The RELAP5 calculation has shown that the FDIS injection flowrate can be similar to that required for a LBLOCA condition for the current generation PWR by adjusting the thickness of the hot water layer, the tank pressure, and the flow resistance in the injection line. These results indicate a promising nature of the FDIS as an alternative safety injection system to replace the current-generation AIS.

ACKNOWLEDGMENTS

The authors express their thanks to Mr. Etsuo Ohtani of Nihon Computer Bureau and Ms. Kazue Toyoda of Information Technologies Japan Inc. for their contribution to the RELAP5 analysis.

NOMENCLATURE

ADS : Automatic Depressurization System
AIS : Accumulator Injection System
FDIS : Flashing-Driven Safety Injection System

GDIS : Gravity-Driven Safety Injection System
LOCA : Loss-Of-Coolant Accident
LBLOCA : Large Break Loss-Of-Coolant Accident
NC : Natural Circulation
SADS : Steam Generator Secondary Side Automatic Depressurization System
SADS-1 : First Stage of SADS
SADS-2 : Second Stage of SADS
SBLOCA : Small Break Loss-Of-Coolant Accident
SG : Steam Generatour

REFERENCES

[1] TOWER, S.N., SCHULZ, T. L. AND VIJUK, R. P., "Passive and simplified system features for the advanced Westinghouse 600 MWe PWR", Nucl. Eng. Des. **109** (1988) 147-154.

[2] MATSUOKA, T. et al., "Safety features of the simplified Mitsubishi pressurized reactor", Nuclear Safety, **33** (1992) 196-208.

[3] MURAO, Y., ARAYA, F. AND IWAMURA, T., "A concept of JAERI passive safety light water reactor system (JPSR)", Proc. of the 7th Int. Mtg. on Nucl. Reac. Thermal-Hydraulics NURETH-7, NUREG/CP--0142-Vol.2 (1995) 1169-1195.

[4] INTERNATIONAL ATOMIC ENERGY AGENCY, Review of design approaches of advanced pressurized LWRs, IAEA-TECDOC-861, Vienna (1996).

[5] Kukita, Y., Yonomoto, T., Nakamura, H., "Major outcomes from the ROSA/AP600 testing program," Proc. of 10th Pacific basin nuclear conference, 1, Kobe, Japan, (1996) 317-324.

[6] ROSA-IV GROUP, "ROSA-IV Large Scale Test Facility (LSTF) System Description for Second simulated fuel assembly", JAERI-M90-176 (1990).

[7] YONOMOTO, T., KONDO, M. AND KUKITA, Y., "PWR small break loss-of-coolant-accident experiment at ROSA-V/LSTF with a combination of secondary-side depressurization and gravity-driven safety injection", Nucl. Sci. Tech., **34** (1997) 571-581.

[8] YONOMOTO, T. et al., "Small break LOCA tests at ROSA-IV/LSTF on next generation PWR designs", Proc. of Eighth International Topical Meeting on Nuclear Reactor Thermal-Hydraulics (NURETH-8), 1, Kyoto, Japan (1997) 535-542.

[9] YONOMOTO, T., OHTSU I., AND ANODA, Y., "Thermal-hydraulic characteristics of a next-generation reactor relying on steam generator secondary side cooling for primary depressurization and long-term passive core cooling", To be published in Nuclear Engineering and Design (1998).

[10] YONOMOTO, T., ANODA, Y., "Thermal-hydraulic research on next generation PWRs using ROSA/LSTF," To be published in Proc. of 1998 IAEA tech. mtg. on experimental tests and qualification of analytical methods to address thermohydraulic phenomena in advanced water cooled reactor, Paul Scherrer Institute, Villigen, Switzerland, Sep. 14-17, 1998.

[11] RELAP5 DEVELOPMENT TEAM, "RELAP5/MOD3 code manual", NUREG/CR-5535, INEL-95/0174, 1~4 (1995).

[12] SCHULTZ, R. R., CHAPMAN, J.C., KUKITA, Y., et al., "Single and two-phase natural circulation in Westinghouse pressurized water reactor simulators: phenomena, analysis and scaling", Proc. of the Winter Annual Meeting of ASME, Boston, MA, FED-Vol. 61, HTD-Vol. 92 (1987) 59-70.

[13] KUKITA, Y., NAKAMURA, H. AND TASAKA, K., "Nonuniform steam generator U-tube flow distribution during natural circulation tests in ROSA-IV Large scale test facility", Nucl. Sci. Eng., 99 (1988) 289-298.
[14] OKABE, K., NAITO, T., UENO, T., "Thermal hydraulic experiments and analysis for new passive heat removal concept utilizing steam generator (hybrid safety system for new PWR-21)," Proc. of NUTHOS-5, Beijing, (1997).
[15] YONOMOTO, T. et al., "Core makeup tank behavior observed during the ROSA-AP600 experiments," Nuclear Technology, 119 (1997) 112-122.
[16] YONOMOTO, T., KUKITA, Y., "RELAP5 analysis of a gravity-driven injection experiments at ROSA-V/Large Scale Test Facility," 93-WA/HT-74, Proc. Winter Annual Mtg., New Orleans, Louisiana, 1993, ASME (1993).
[17] SHIRAISHI, T., et al., "Development of the flow controlled accumulator," Proc. of ANP92 (1992) 36.4-1~6.
[18] YONOMOTO, T.; ANODA, Y.; KUKITA, Y. ; PENG, Y., "CCFL characteristics of PWR steam generator U-tubes," Proc. of ANS Int. Topical Mtg. Safety of Thermal Reactors, Portland, (1991)
[19] YONOMOTO, T., KUKITA, "Long-term oscillations of pressurizer liquid level observed during ROSA/AP600 experiments," Proc. of the 1995 international joint power generation conference - v.2: Minneapolis, MN, United States (1995) 25-31.

Computational Two-Phase Flow Dynamics and Heat Transfer for Analysis of LWR Transients

Samim Anghaie and Gary Chen

Department of Nuclear & Radiological Engineering
University of Florida
Gainesville, FL 32611
Tel: (352) 392-1427
Fax: (352) 392-8656
anghaie@ufl.edu, gary@inspi.ufl.edu

ABSTRACT

A Computational Fluid Dynamic (CFD) model is developed to simulate the fluid flow and heat transfer with phase change. The CFD model is based on the Navier-Stokes formulation in conjunction with a k-ε turbulence model and a set of constitutive relationships for water-steam system. The model combines the high-resolution capability of the state-of-the-art CFD methods with a novel approach that allow for the tracking and delineation of the dynamic interfacial water-steam boundary. Reynolds number and Raleigh number are included in the parabolic-type governing equations to identify the flow and heat transfer regimes in water, vapor and two-phase regions. In this method the need for temporal and spatial averaging is completely eliminated. The geometrical void fraction in this formulation is replaced by a dynamic vapor-phase fraction, which plays a pivotal role in tracking the liquid-vapor interfacial boundary. Preliminary results have demonstrated the computational efficiency and the applicability of the powerful CFD methodology to a variety of two-phase flow and heat transfer problems of interest to light water reactor (LWR) safety.

I. INTRODUCTION

Computational analysis of two-phase flow dynamics and boiling heat transfer is a complicated task due to the order of magnitude type change in some flow properties across the liquid-vapor interface boundary [1]. In particular, the large step change in the density results in a singular-like behavior in Navier-Stokes equations. Equally important, is the quantum jump in the magnitude of the thermal conductivity, which controls the rate of heat transfer in the thermal boundary sub-layer. Surface tension is also a key term, which plays a pivotal role in the boiling nucleation and bubble dynamics. Calculation of the surface tension tem, which requires the determination of the interfacial boundary curvature, needs special treatment. Conventional approaches in computational thermal hydraulic modeling have been largely based on using macroscopic cells with ensemble averaging in both time and space. This modeling approach has necessitated the introduction of the void fraction as a pseudo-dependent parameter in two-phase governing equations. The use of ensemble averaged parameters such as void fraction, which has no local or instantaneous value, limits the application of these models to cases where high-resolution calculation is needed. Furthermore, the lack of microscopic details in the physical model has brought a

high level of dependency on using empirical data and closure relationships to describe mass, momentum and energy transport at the wall and through the interfacial boundary.

Over the past decade, numerical modeling and simulation of the phase change processes have been the focus of many investigations. A variety of approaches to numerical modeling of phase change problems could be found in the published works of Huang [2], Jang[3], Poirier[4], Samarskii[5], Shyy[6,7] and Voller[8]. Their numerical modeling has focused on parabolic flow condensation problems where the forced convection plays a dominant role. In this type of condensation problem, the vapor pressure, saturation temperature and latent heat have been treated as constant properties. Empirical relationships are also used to approximate the transport processes through the liquid-vapor interface. This paper presents a new approach for simultaneous calculation and tracking of the water-steam interfacial boundary as well as for the calculation of temperature, pressure, and flow fields. In this approach the pressure is treated as a dependent variable and using an internal energy based iterative scheme, the interfacial boundary is delineated and tracked throughout the system. The interfacial transport terms are directly calculated by solving Navier-Stokes equations for the thermal and flow fields in computational cells on and in the vicinity of the interfacial boundary.

II. Mathematical Models

The three-dimensional Navier-Stokes equations for two-phase single-component flow in Cartesian coordinate system could be written as[9]:

$$\frac{\partial \rho}{\partial t} + \nabla \cdot (\rho \vec{V}) = 0 \tag{1}$$

$$\frac{D\vec{V}}{Dt} = -\nabla P + \nabla \cdot \vec{\tau} + \rho \vec{g} \tag{2}$$

$$\rho C_p \frac{DT}{Dt} = -\frac{DP}{Dt} + \nabla \cdot (\kappa \nabla T) + Q \tag{3}$$

where $\frac{D}{Dt} = \frac{\partial}{\partial t} + \vec{V}.\nabla$ is substantial derivative, $\vec{V} = V(u, v, w)$ is velocity vector, $\vec{\tau}$ is the stress tensor, $\vec{g}$ is the gravitational acceleration vector, and Q is heat source. For two-dimensional flow in a cylindrical tube, the conservation equations for transient, compressible flow in the liquid and vapor phases are reduced to the following form:

$$\frac{\partial \rho_i}{\partial t} + \nabla \cdot (\rho_i \vec{V}) = 0 \tag{4}$$

$$\frac{\partial \rho_i u}{\partial t} + \nabla \cdot (\rho_i \vec{V} u) = -\frac{\partial p}{\partial x} + \nabla \cdot (\mu_i \nabla u) - \rho_i g \tag{5}$$

$$\frac{\partial \rho_i v}{\partial t} + \nabla \cdot (\rho_i \vec{V} v) = -\frac{\partial p}{\partial r} + \nabla \cdot (\mu_i \nabla v) \tag{6}$$

$$\frac{\partial \rho_i c_v T}{\partial t} + \nabla \cdot (\rho_i \vec{V} c_v T) = \kappa_i \nabla^2 T - \Delta e \frac{\partial (\rho_i f)}{\partial t} \tag{7}$$

where the subscript i=l *or* v denotes the liquid and vapor phases, respectively, and $\rho_{v,0}$ is the reference vapor density. The thermal expansion coefficient, β, is introduced into the u-momentum equation to include the buoyancy force term, according to the Boussinesq approximation:

$$\rho_i = \rho_{i,0}[1-\beta_i(T-T_0)] \tag{8}$$

Substituting Equation (8) into the last term in Equation (5) yields

$$-\rho_i g = g\rho_{i,0}[\beta_i(T-T_0)-1] \tag{9}$$

The first term in Equation (9) represents the thermal expansion induced buoyancy effect and the second term is the phase change induced buoyancy force. In liquid-vapor two-phase systems the second term in Equation (9) is much greater than the first term.

Using scaling laws, Equations (4) - (7) can be reduced to dimensionless forms:

Continuity:

$$\frac{\partial \overline{\rho}_i}{\partial \tau}+\frac{\partial \overline{\rho}_i U}{\partial X}+\frac{\partial \overline{\rho}_i V}{\partial R}=0 \tag{10}$$

Axial Momentum:

$$\frac{\partial \overline{\rho}_i U}{\partial \tau}+\frac{\partial(\overline{\rho}_i UU)}{\partial X}+\frac{\partial(\overline{\rho}_i UV)}{\partial R}=-\frac{\partial \overline{p}}{\partial X}+\frac{1}{\mathrm{Re}_v}\nabla\cdot(\overline{\mu}_i\nabla U)+\frac{\overline{g}Ra_{E,v}}{\mathrm{Re}_v^{\,2}\,\mathrm{Pr}_v}\cdot[\overline{\beta}_i\overline{\rho}_{i,0}\theta+\frac{(1-\overline{\rho}_{i,0})}{\beta_v\Delta T}] \tag{11}$$

Radial Momentum:

$$\frac{\partial \overline{\rho}_i V}{\partial \tau}+\frac{\partial(\overline{\rho}_i VU)}{\partial X}+\frac{\partial(\overline{\rho}_i VV)}{\partial R}=-\frac{\partial \overline{p}}{\partial R}+\frac{1}{\mathrm{Re}_v}\nabla\cdot(\overline{\mu}_i\nabla V) \tag{12}$$

Energy:

$$\frac{\partial \overline{\rho}_i\theta}{\partial \tau}+\frac{\partial(\overline{\rho}_i U\theta)}{\partial X}+\frac{\partial(\overline{\rho}_i V\theta)}{\partial R}=\frac{\overline{\kappa}_i}{\mathrm{Re}_v\,\mathrm{Pr}_v}\nabla^2\theta-\frac{1}{\mathrm{Re}_v\,\mathrm{Pr}_v\,St}\frac{\partial(\overline{\rho}_i f)}{\partial \tau}-\frac{1}{\mathrm{Re}_v\,\mathrm{Pr}_v\,St}\nabla\cdot(\overline{\rho}_i f\overline{V}) \tag{13}$$

The external Rayleigh number representing the buoyancy effect in the vapor phase is defined

$$Ra_{E,v}=\frac{g\beta_v\Delta TL^3}{\alpha_{v,0}\nu_{v,0}} \tag{14}$$

The Stefan number representing the latent heat is defined

$$St=\frac{C_p\Delta T}{\Delta e} \tag{15}$$

The Prandtl number for vapor phase is

$$\mathrm{Pr}_v = \frac{\nu_{v,0}}{\alpha_{v,0}} \tag{16}$$

and the Reynolds number is

$$\mathrm{Re}_v = \frac{u_0 D}{\nu_{v,0}} \tag{17}$$

In obtaining the Equations (7)-(10), the following dimensionless variables are used

$$\begin{aligned}
\tau &= \frac{t u_0}{R} \\
X &= \frac{x}{R} \\
Y &= \frac{y}{R} \\
U &= \frac{u}{u_0} \\
V &= \frac{v}{u_0} \\
\theta &= \frac{(T - T_0)}{(T_1 - T_0)} \\
\overline{\rho}_i &= \frac{\rho_i}{\rho_{v,0}} \\
\overline{p} &= \frac{p}{\rho_{v,0} u_0^{\,2}} \\
\overline{k}_i &= \frac{k_i}{k_v} \\
\overline{\mu}_i &= \frac{\mu_i}{\mu_v} \\
\overline{V} &= U e_x + V e_r
\end{aligned} \tag{18}$$

Additional constitutive relationships are included to complete the governing equations. Based on the Clausius-Clapeyron equation, the relationship between the saturation temperature T_{sat} and saturation pressure p_{sat} is defined as:

$$T_{sat} = \frac{C}{D - \ln(p_{sat})} \tag{19}$$

Equation (19) can be reduced to non-dimensional form by using a set of reference temperature and pressure,

$$\theta_{sat} = \frac{T_{sat} - T_0}{\Delta T} = \frac{1}{\Delta T}\left[\frac{C}{D - \ln(\bar{p}_v \cdot p_0)} - T_0\right] = \frac{C'}{D' - \ln(\bar{p}_v \cdot p_0)} - A' \tag{20}$$

where $C'=C/\Delta T$, $D'=D+ln(p_0)$, $A'=T_0/\Delta T$.

The saturation pressure, or the vapor pressure, can be obtained from the equation of state and the mass conservation in which the bulk vapor density and temperature are used:

$$\begin{aligned} p_{sat} &= p_{vap} = \frac{m_v}{V_{vap}} R T_{b,vap} \\ m_{total} &= m_v + m_l = Constant \end{aligned} \tag{21}$$

where R is the gas constant for the vapor phase.

To solve the governing equations for three different regions, i.e. liquid, vapor and two-phase, a relationship between the vapor phase fraction f and the temperature θ or the internal energy e should be formulated. For a pure substance undergoing evaporation or condensation, the total internal energy is a discontinuous function of the temperature. However, from a computational viewpoint, discontinuities are difficult to track and it is often necessary to smear the phase change over a small temperature range to attain numerical stability. Thus the following relationships are used:

$$\begin{aligned} \bar{e} &= S_l \cdot \theta && \theta < \theta_l \\ \bar{e} &= S_l \cdot \theta_l + (\theta - \theta_l)/(\theta_v - \theta_l) && \theta_l < \theta < \theta_v \\ \bar{e} &= S_l \cdot \theta + 1 && \theta_v < \theta \end{aligned} \tag{22}$$

A formulation expressing the vapor phase fraction as a function of the total internal energy, rather than the temperature or enthalpy, is developed in this work. According to the classical thermodynamic definition, the relationship between the vapor phase fraction and the internal energy is

$$f = \frac{e - e_l}{e_v - e_l} \tag{23}$$

This is used for the iterative update of the vapor phase fraction. This update procedure is referred to as the E-based update method, which is analogous to the isothermal case discussed by Swaminathan[10]. In particular, The E-based method does not need to use a phase change window and can be conveniently used for all kinds of phase change problems. Furthermore, it has also the advantage for cases where the value of latent heat is relatively larger than the sensible internal energy. In such cases, the vapor phase fraction varies slowly with respect to the total internal energy. This enhances the stability of the update procedure. The implementation of the E-based method is relatively straightforward and does not need any pre-conditioning. The internal energy is updated first, with the current values of saturation temperature and latent heat,

$$\bar{e}_p^{\,k} = S_l \theta_p^{\,k} + f^{k-1} \qquad 0 < f^{k-1} < 1 \tag{24}$$

Then the vapor phase fraction is updated with the current internal energy,

$$f^k = \bar{e}_P^{\,k} - \bar{e}_l^{\,k} \qquad \bar{e}_l^{\,k} < \bar{e}_P^{\,k} < \bar{e}_v^{\,k} \tag{25}$$

The density for two-phase region is defined as a function of f according to the following relationship:

$$\rho(f) = \frac{\rho_L \rho_V}{\rho_L f + \rho_V (1-f)} \tag{26}$$

The viscosity and conductivity for two-phase region is the average of what is defined by McAdams's and Cichetti's formula [11]:

$$\mu(f) = \frac{1}{2}\left(\frac{\mu_L \mu_V}{\mu_L f + \mu_V (1-f)} + f\mu_V + (1-f)\mu_L \right) \tag{27}$$

$$k(f) = \frac{1}{2}\left(\frac{k_L k_V}{k_L f + k_V (1-f)} + f k_V + (1-f) k_L \right) \tag{28}$$

III. NUMERICAL METHODS

The numerical procedure for predicting the transient behavior of the flow and tracking of the two-phase flow interface is based on Patankar's SIMPLE scheme (Semi-Implicit Method for Pressure-Linked Equations)[12]. In this method a cyclic series of guess-and-correct operations are used to solve the governing equations. An iterative solution scheme is developed in which three different regions are determined using the current field values of the internal energy. Then the velocity, pressure and temperature are updated, accordingly. This procedure is continued until a steady-state condition is reached. The numerical procedure is as follows:

1. Initialize the pressure, temperature, density and velocity fields.
2. Assume the pressure drop is equal to zero.
3. Solve the momentum equation to obtain intermediate velocity fields.
4. Solve new pressure field.
5. Calculate real velocity fields.
6. Solve the energy equation to obtain the temperature field.
7. Determine density and interface from the equation of state.
8. Repeat steps 3-7 for each time step until the velocity and temperature residuals are smaller than pre-assigned values.

To solve the discretized equations, the TDMA (Tri-diagonal Matrix Algorithm) and Gauss-Seidel Line-by-line iterative method are used to obtain the velocity and temperature fields. A general relationship for the thermal conductivity is developed based on the analysis of the heat flux in a computational cell. In the thermal conductivity formulation, *P* is the nodal point of the computational cell; *E, W, N* and *S* are nodal points for eastern, western, northern, and southern surrounding computational cell, respectively. The eastern, western, northern, and southern computational cell boundaries are

represented by *e*, *w*, *n*, and *s*, respectively. In 2-D, axisymmetric coordinates, the linear heat flux is expressed as:

$$q_r = -2\pi r\kappa\frac{\partial T}{\partial r} = 2\pi\kappa_n\frac{(T_P - T_N)}{\ln(r_N / r_P)} = 2\pi\kappa_N\frac{(T_n - T_N)}{\ln(r_N / r_n)} = 2\pi\kappa_P\frac{(T_P - T_n)}{\ln(r_n / r_P)} \tag{29}$$

Using the relation

$$T_P - T_N = T_P - T_n + T_n - T_N \tag{30}$$

The thermal conductivity at the north surface boundary, K_n, is obtained as following:

$$\kappa_n = \frac{\kappa_N\kappa_P\ln(r_N / r_P)}{\kappa_P\ln(r_N / r_n) + \kappa_N\ln(r_n / r_P)} \tag{31}$$

The thermal conductivity at the east surface boundary takes a more simple form,

$$\kappa_e = \left(\frac{1 - f_e}{\kappa_P} + \frac{f_e}{\kappa_E}\right)^{-1} \tag{32}$$

where f_e is a ratio defined

$$f_e \equiv \frac{(\delta x)_{e+}}{(\delta x)_{e+} + (\delta x)_{e-}} \tag{33}$$

The thermal conductivity at the south and west surface boundaries could be obtained in a similar fashion. To achieve stability and convergence, a multi-scheme procedure is used for the calculation. The first-order upwind scheme is utilized for solving the convection terms. Before the steady-state condition is reached, the numerical scheme is switched to second-order central difference scheme to improve the accuracy of the steady-state results. This procedure guarantees the high accuracy with stability and convergence during unsteady phase of the phase-change process. For typical cases presented in this paper, a 101 x 51 uniform grid are used. About 2000 iterations are needed achieve convergence. The CPU time on a Pentium workstation is about 16 hours.

IV. k-ε TERBULENCE MODELING

The turbulence model used in this analysis is Kolmogorov-Prandtl Model [13,14]. The effects of the turbulence are simulated in terms of the eddy viscosity coefficient, μ_t, which is determined according to the following formula:

$$\mu_t = \frac{C_\mu\rho k^2}{\varepsilon} \tag{34}$$

In order to obtain eddy viscosity coefficient, μ_t, two additional transport equations, the kinetic energy of turbulence k and its dissipation rate ε have to be solved:

Turbulence kinetic energy equation

$$\frac{\partial \bar{\rho}_i k}{\partial \tau}+\frac{\partial(\bar{\rho}_i kU)}{\partial X}+\frac{\partial(\bar{\rho}_i kV)}{\partial R}=\frac{1}{\mathrm{Re}_r}\nabla\cdot(\Gamma_k\nabla k)+G-\rho\varepsilon \tag{35}$$

Turbulence dissipation rate

$$\frac{\partial \bar{\rho}_i \varepsilon}{\partial \tau}+\frac{\partial(\bar{\rho}_i \varepsilon U)}{\partial X}+\frac{\partial(\bar{\rho}_i \varepsilon V)}{\partial R}=\frac{1}{\mathrm{Re}_r}\nabla\cdot(\Gamma_\varepsilon\nabla \varepsilon)+C_1 G\frac{\varepsilon}{k}-C_2\rho\frac{\varepsilon^2}{k} \tag{36}$$

where

$$\Gamma_k=\mu_l+\frac{\mu_t}{\sigma_k} \tag{37}$$

$$\Gamma_\varepsilon=\mu_l+\frac{\mu_t}{\sigma_\varepsilon} \tag{38}$$

$$G=\mu_t\left\{2\left[\left(\frac{\partial U}{\partial X}\right)^2+\left(\frac{\partial V}{\partial R}\right)^2\right]+\left(\frac{\partial V}{\partial X}+\frac{\partial U}{\partial R}\right)^2-\frac{2}{3}\left(\frac{\partial U}{\partial X}+\frac{\partial V}{\partial R}\right)^2\right\} \tag{39}$$

The constants used for this model are listed below:

$C_\mu=0.09$

$C_1=1.44$

$C_2=1.92$

Equations (35), (36) are subjected to the following boundary conditions:

$$Y=\delta_l, k=\varepsilon=0$$

$$Y=Y_G, u_G\frac{dk_G}{dX}=-\varepsilon_G, u_G\frac{d\varepsilon_G}{dX}=-C_{\varepsilon 2}\frac{{\varepsilon_G}^2}{k_G}$$

The above set of equations is solved using a pressure-correction type of semi-implicit finite volume formulation. Because of the stiff nonlinear terms in the ε equation, the two-equation turbulence model often causes instability. A decoupled line-by-line TDMA (Tri-diagonal Matrix Algorithm) is used to solve the equations sequentially over the entire computational domain. Using the velocity scale obtained from solving the governing equation for k and a time scale obtained from a combination of k and ε, an expression for the turbulent viscosity is obtained.

V. RESULTS AND DISCUSSION

To demonstrate the capabilities of the two-phase computational fluid dynamics and heat transfer model, a few cases involving bulk evaporation, condensation and flow boiling are simulated. Due to the generalized nature of the developed method, the simulation of all these cases requires the use of the same model. To match the physical conditions of the simulated cases, only the boundary conditions are needed to be changed A mesh of 101x51 uniform and fixed grids is adopted for the liquid and vapor in the channels. The time step size of 10^{-3} is chosen for the computation of the transient behavior of the phase change process. A second order central difference is used to calculate all spatial derivative terms and a fully implicit difference is employed for the time marching.

V.a. Bulk Evaporation and Condensation in a Constant Volume Container

The first simulated case is involved a cylindrical container, which is filled with multi-phase nuclear fuel. The fuel undergoes liquid-vapor phase change (evaporation and condensation), due to a variable neutron flux. The internal heat generation due to the nuclear fission reaction evaporates the liquid, while the sidewall cooling tends to condense the vapor. Globally, the evaporation of liquid and condensation of vapor take place simultaneously. The evaporation and condensation processes could be driven by either pure heat conduction or by both heat conduction and convection, depending mainly on the gravity field [15,16]. Under zero gravity condition, the buoyancy driven convection is nonexistent. However, under nonzero gravity conditions, buoyancy induced convection is present. The location of the liquid-vapor interface may vary depending on the internal heat generation intensity and its spatial distribution, as well as the gravity field. To solve the phase change problem numerically, the free and moving interface is not known in advance, so the solution to this heat transfer problem is quite complex [17]. Assumptions made for solving this problem are included: (1) the liquid-vapor interface is kept at saturation temperature, (2) proper boundary conditions on the walls are imposed to activate the bulk evaporation or condensation, and also to avoid the buoyancy effect and bubble growth, (3) while keeping the side wall insulated, only heating the top wall or cooling the bottom wall induce evaporation or condensation, respectively, and (4) the scaling analysis indicates that this convection effect is quite weak and negligible. It can be reasonably assumed that the phase change processes are driven entirely by the conduction and the release or absorption of latent heat at the phase change interface.

All the boundary and initial conditions are maintained the same for nonzero cases of 10^{-3} –g and 1-g. Figure 1 shows the schematics of the constant volume bulk vaporization-condensation problem. The topology of the liquid-vapor interface and the temperature distribution at various time instants are displayed in Figures 2, 3, 4, and 5, respectively.

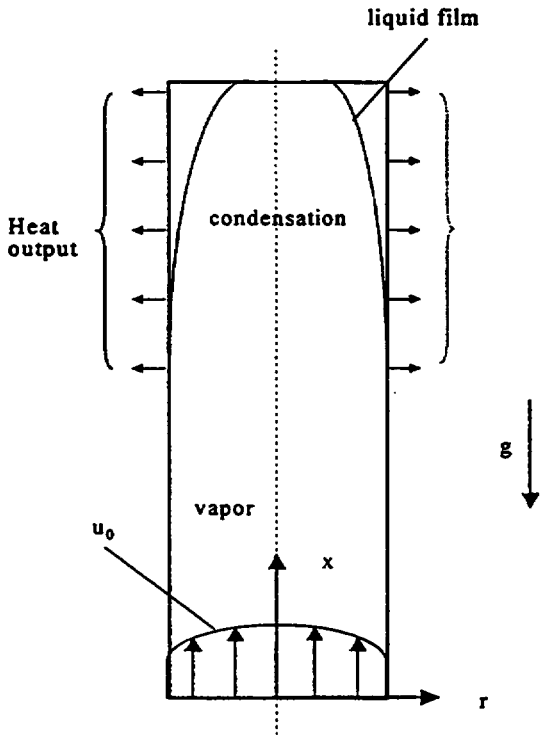

Figure 1. Coordinate system (not to scale).

Significant differences appear for cases involving 1-g and 10^{-3}-g. First, under the normal gravity condition, the liquid film grows more slowly and thinner, compare with the 10^{-3}-g case. Under 1-g condition, the liquid film under the influence of a much larger gravitational force is drawn faster to the liquid pool. As a result, the position of the horizontal surface of the liquid pool is higher than that of 10^{-3}-g case. Second, the horizontal surface of the liquid pool becomes wavy, particularly in the position near the end of the liquid film. Such phenomenon does not appear under the reduced gravity condition of 10^{-3}-g. The liquid film, though thinner, carries more momentum owing to the greater gravity effect. It impacts the liquid pool and distorts the pool surface. Third, the temperature distribution and its gradient are quite different at different levels of gravity. In particular, the temperature gradient across the liquid film under normal gravity condition is significantly smaller than that of the vapor phase. This is mainly due to the higher conductivity and very small thickness of the liquid film.

Figure 6 shows the flow fields in the vapor and liquid phases under 10^{-3}-g and 1-g conditions. The rate of forced convection under 1-g condition is much smaller than that of 10^{-3}-g case. Due to the higher level of gravity, the rate of natural convection is much higher under 1-g condition. Condensation of the vapor phase in the upper part of the container forms the liquid film on the wall. The thinner liquid film under 1-g condition is due to the higher rate of liquid fall back. This countercurrent flow condition results in net zero flow condition in parts of the container and is commonly known as "reflux." The differences and the dependence of the phase change performance on gravity can be observed more clearly in Figure 7, in which, the temperature distribution under the steady state condition are plotted and compared. Under low gravity conditions, conductive heat transfer controls the thermal hydraulic process. Under normal gravity condition, both conductive heat transfer and natural convection control the process. As higher levels of

gravity the thickness of the liquid decreases. The temperature gradient inversely varies with the thickness of the liquid film [18].

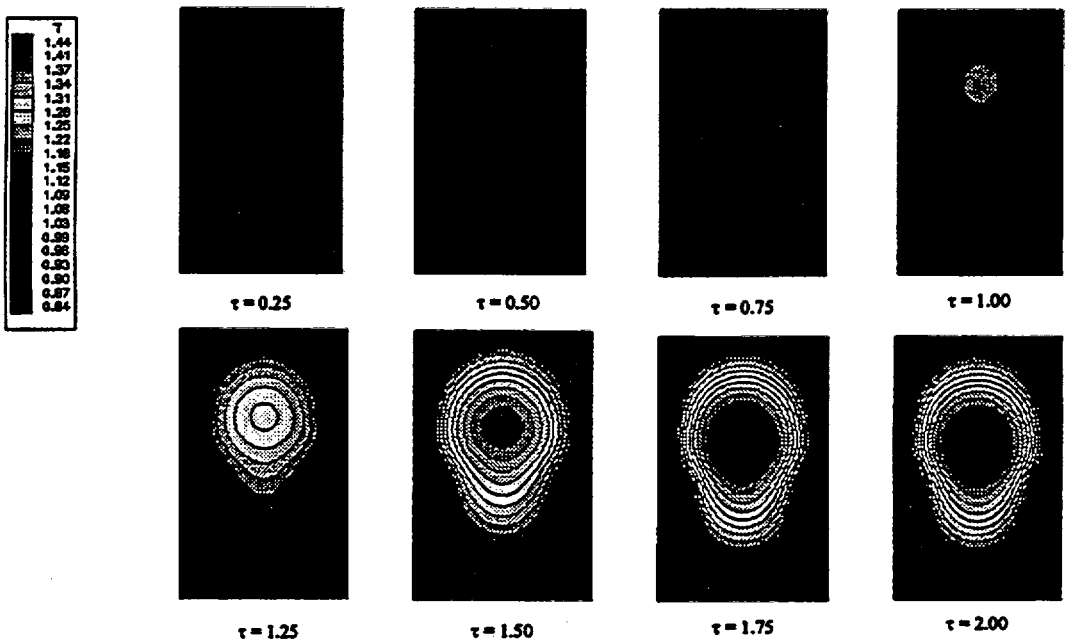

Figure 2. Evolution of temperature contour at g = 0.001.

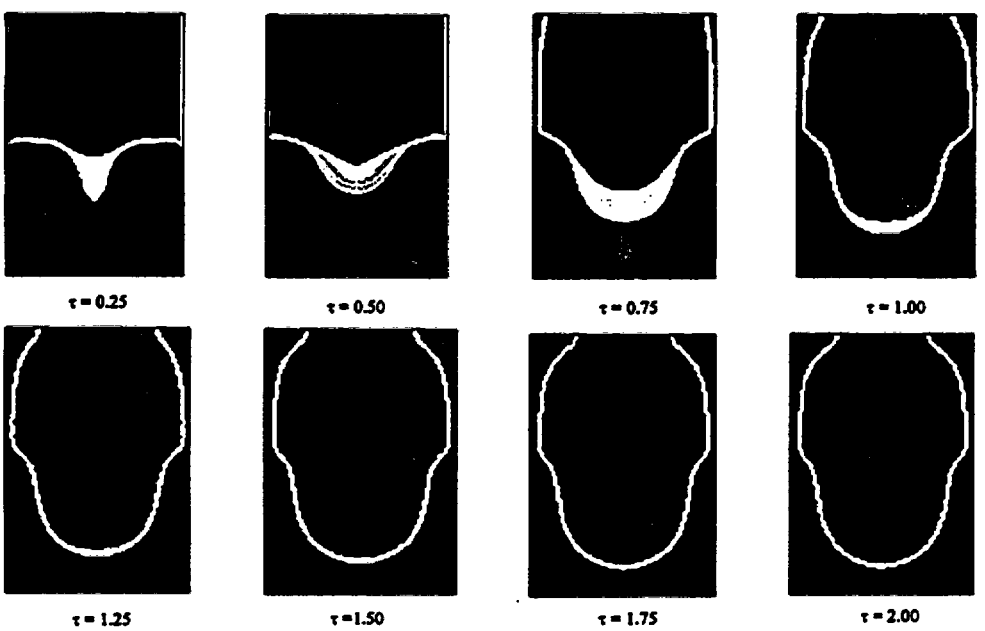

Figure 3. Evolution of water-vapor interface at g = 0.001.

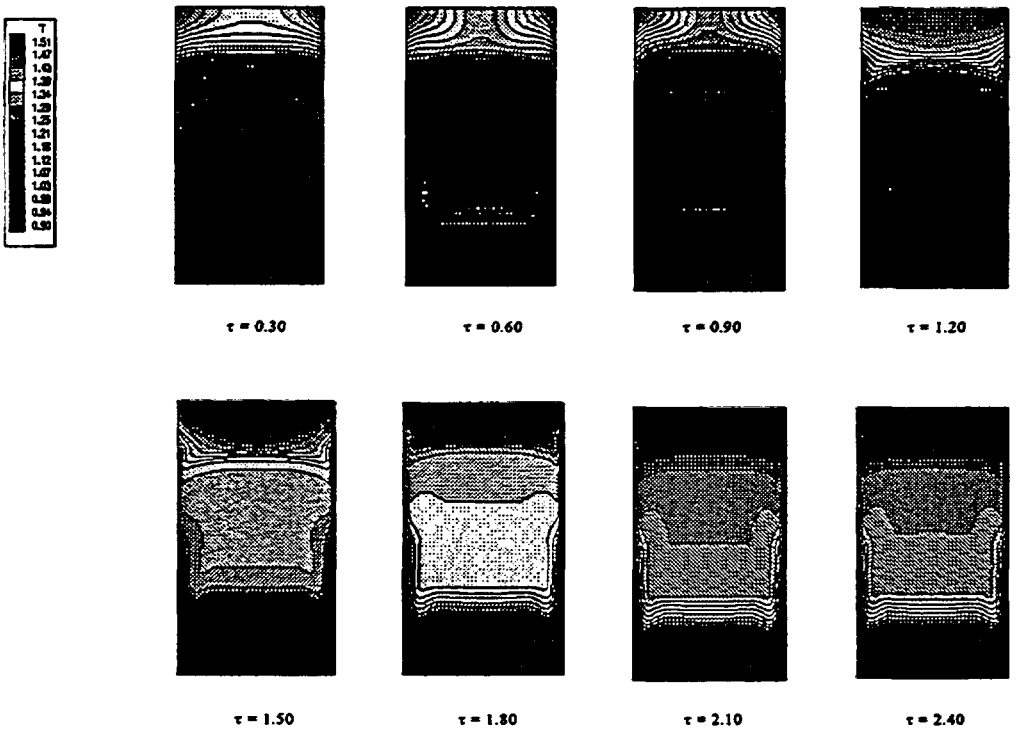

Figure 4. Evolution of temperature contour at g = 1.

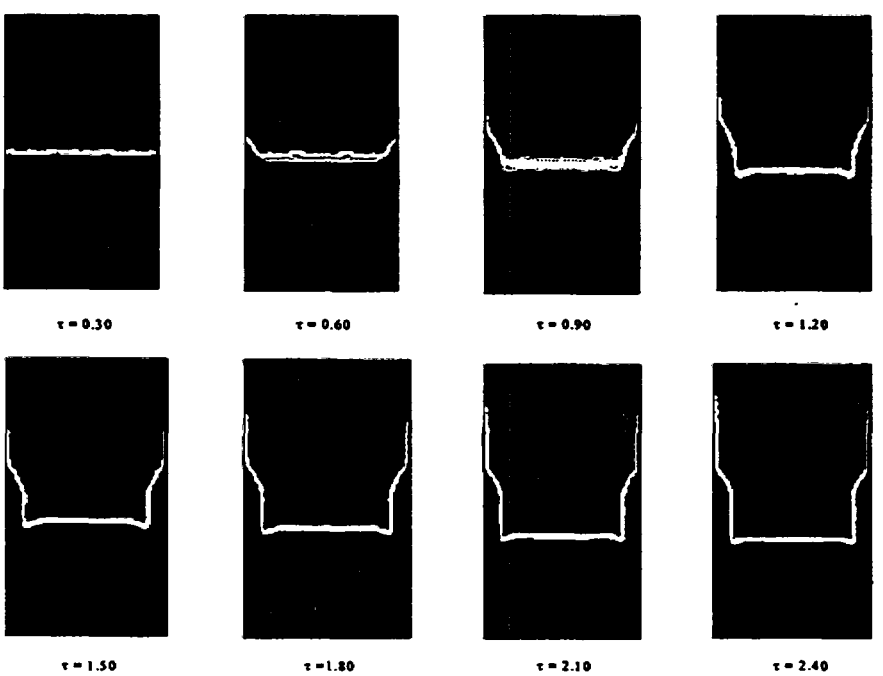

Figure 5. Evolution of water-steam interface at g = 1.

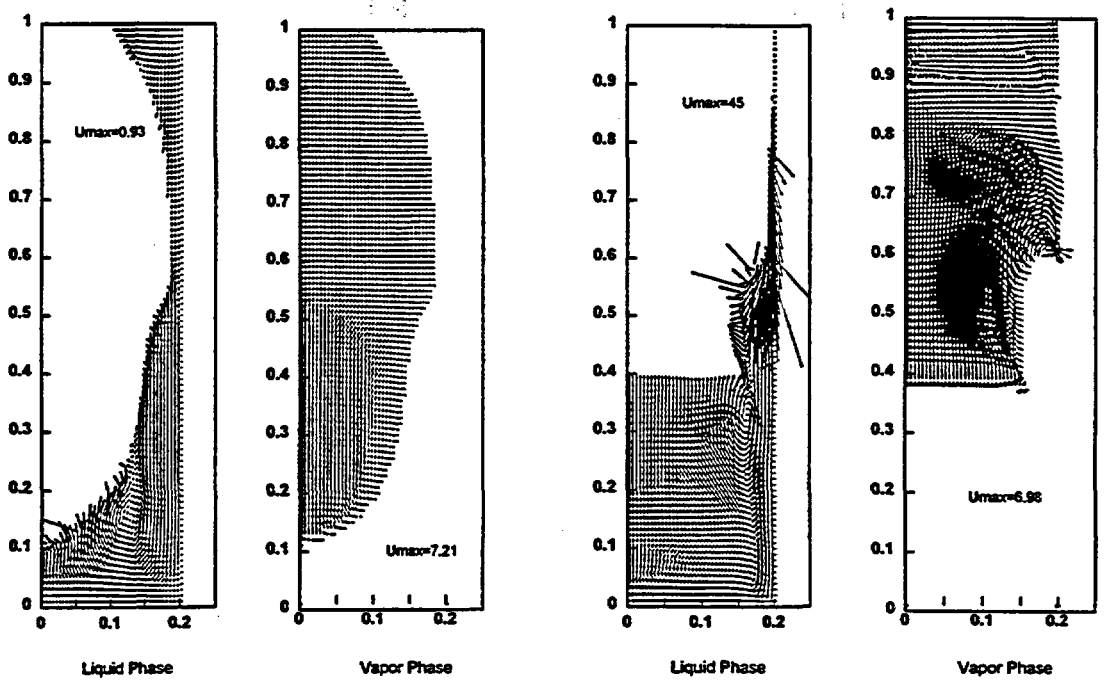

Figure 6. Comparison of flow pattern at g = 0.001 and g = 1.

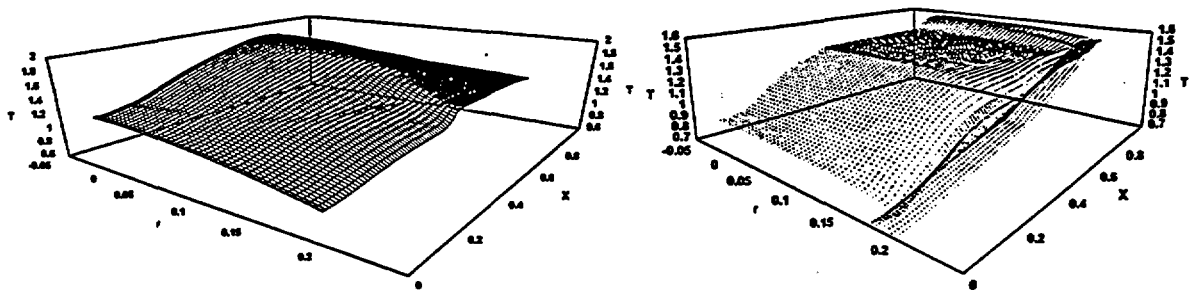

Figure 7. Comparison of temperature distribution at g = 0.001 and g = 1.

V.b Bulk Condensation in a Steam Generator Tube

Modeling of the transient condensation process inside steam generator tubes is a challenging issue due to the effects of lateral heat transfer and the gravitational force. In recent years many investigators [19-21] have treated the problem as a parabolic flow condensation problem, where the forced convection plays a dominant role. In this type of condensation modeling, the vapor pressure, saturation temperature, and latent heat are treated as constant parameters. This type of treatment is not applicable to transient cases, where the flow parameters could rapidly change [22]. The use of the two-phase Navier-Stokes equations

solver does not require the use of oversimplifying assumptions such as constant flow parameters, and it is directly applicable to all types of transient condensation problems

Solving the governing equations requires simultaneous calculation of the water-steam interfacial boundary as well as the temperature and flow fields. In this method the film thickness is calculated as a function of stream-wise location and the transient time. The calculation of the liquid film thickness allows for the determination of heat transfer coefficients and temperature gradients in steam generator tubes. Accurate prediction of the temperature gradients is of critical importance to the calculation of thermal stresses in steam generator tubes. Similar to the previous case, the value of the gravitational force is used as a variable to achieve convergence. Under low gravity conditions, the convergence is achieved without the use of optimum relaxation factor. To find the optimum value of the relaxation factor, the value of the gravity is gradually changed. Figure 8 shows the forced flow condensation of saturated and superheated steam under low gravity conditions. The flow reversal and the reflux condition are present along the two-phase region of the tube. Due to the low gravity level (~0.01-g), the liquid film is rather thick and the fall back process is not very pronounced. The evolution of temperature contour and evolution of the interfacial boundary are shown in Figures 9 and 10, respectively.

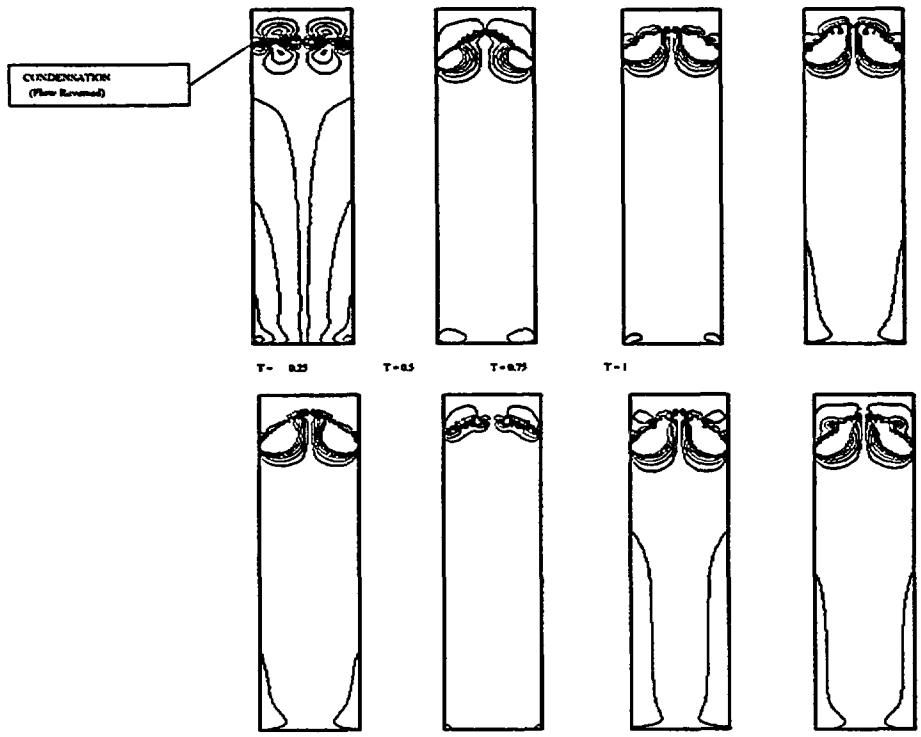

Figure 8. Evolution of velocity contour in a vertical tube.

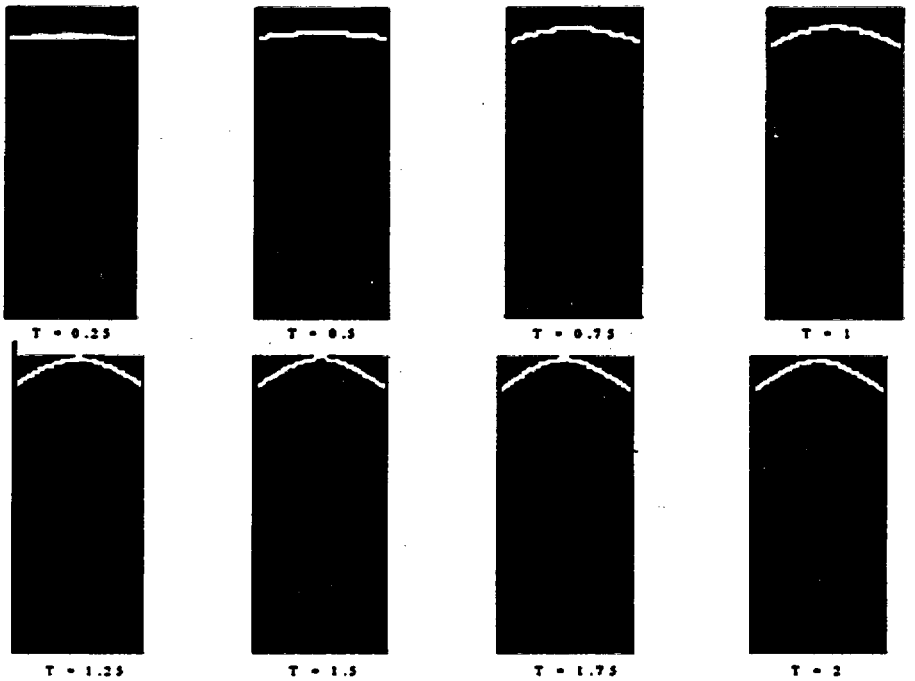

Figure 9. Evolution of water-steam interface in a vertical tube.

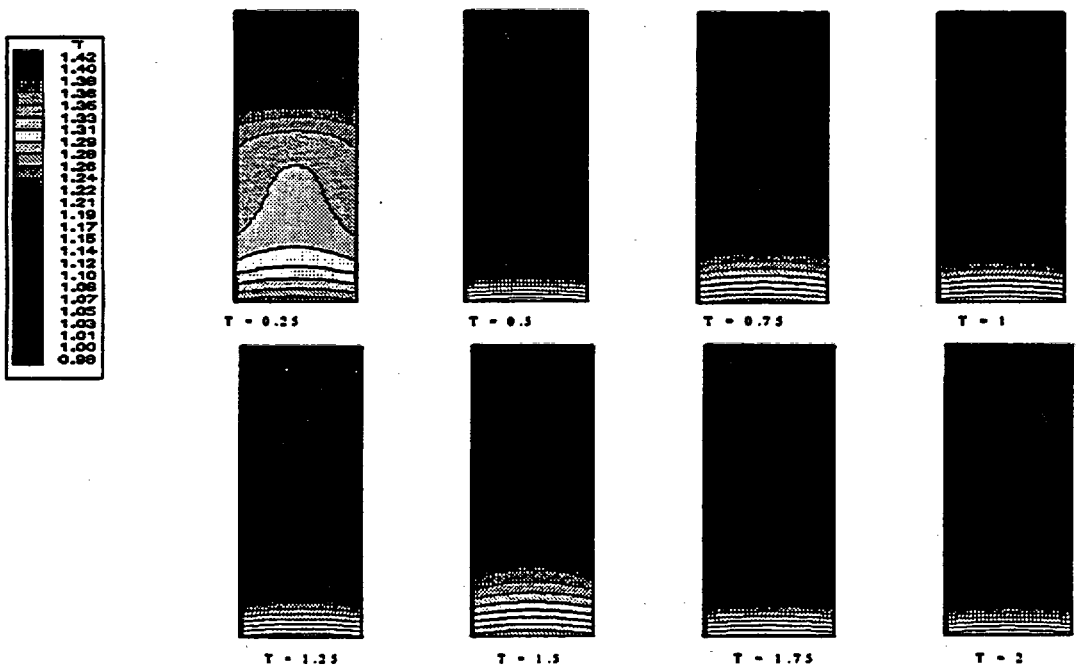

Figure 10. Evolution of temperature contour for a vertical tube.

V.c Bubble Nucleation and Growth

Bubble nucleation, growth, and transport play a major role in two-phase boiling heat transfer processes. Since the flow velocity and other system parameters influence the bubble dynamics, the process is highly non-linear and complex. To date, most heat-transfer correlations for flow boiling heat transfer are based on using empirical data. Due to complication of bubble dynamics and transport, a complete theoretical model for the process is not yet available. Although there are a few numerical investigations for bubble formation and growth, it is often assumed that the bubble is in a complete hemispherical shape. This assumption is not valid for relatively high flow velocities, where the bubble deformation is caused as a result of the flow shear force. Moreover, there is a significant change in the bubble shape during the growth and departure stages. In the model presented in this work, the bubble deformation is an integral part of the bubble dynamic modeling.

The buoyancy force, surface tension, shear stress, hydraulic pressure gradient and the latent heat for phase change govern the bubble formation and growth processes. In this boiling heat transfer model, all the parameters influencing the bubble nucleation are included in the Navier-Stokes equations:

$$\frac{\partial \bar{\rho}_i U}{\partial \tau}+\frac{\partial(\bar{\rho}_i UU)}{\partial X}+\frac{\partial(\bar{\rho}_i UV)}{\partial R}=-\frac{\partial \bar{p}}{\partial X}+\frac{1}{\mathrm{Re}_v}\nabla\cdot(\bar{\mu}_i\nabla U)++\frac{\sigma k n_X}{\mathrm{Re}_v}\delta(X-X^B)\frac{Ra_{E,v}}{\mathrm{Re}_v^{\,2}\,\mathrm{Pr}_v}\left[\bar{\beta}_i\bar{\rho}_{i,0}\theta+\frac{(1-\bar{\rho}_{i,0})}{\beta_v\Delta T}\right] \quad (40)$$

$$\frac{\partial \bar{\rho}_i V}{\partial \tau}+\frac{\partial(\bar{\rho}_i VU)}{\partial X}+\frac{\partial(\bar{\rho}_i VV)}{\partial R}=-\frac{\partial \bar{p}}{\partial R}+\frac{1}{\mathrm{Re}_v}\nabla\cdot(\bar{\mu}_i\nabla V)+\frac{\sigma k n_R}{\mathrm{Re}_v}\delta(R-R^B) \quad (41)$$

In these equations, σ is the surface tension coefficient, k is the curvature with respect to the arc length of bubble surface, n_X and n_R are x and R components of the unit normal vector representing the bubble surface, and $\delta(X-X^B)$ and $\delta(R-R^B)$ are delta function, which are non-zero only on the bubble surface where $X=X^B$ or $R=R^B$. The inclusion of surface tension force gives a body-force-like term in the momentum equations. The inclusion of the surface tension allows for the timely detachment of the bubble as a result of buoyancy and shear force.

The growth of a bubble or the formation of a vapor patch on the wall must be treated as a three dimensional problem. Preliminary results are obtained in a two-dimensional channel for a "two-dimensional bubble", which is generated on the wall as a result of a high local heat flux in a computational cell with a nucleation site The purpose of the 2-D modeling in this work is the assessment of the feasibility of the CFD model for solving problems involving bubble nucleation and growth.

Figure 11 shows the growth of a large bubble on a pre-defined nucleation site. The bubble shape at t=12ms is very similar to experimentally observed results [23]. In the early stages of bubble growth, the surface tension force is dominant and the growth rate in the radical direction is faster than in the axial direction [24]. As the bubble size increases with time, the buoyancy and shear forces become dominant. These forces are the main cause of bubble deformation and tilt in upward direction. Figure 12 shows the temperature distribution inside the bubble. Due to lower conductivity, the temperature gradient inside the bubble is much larger than the temperature gradient in the water. The temperature distribution in and around the bubble is shown in Figure 13.

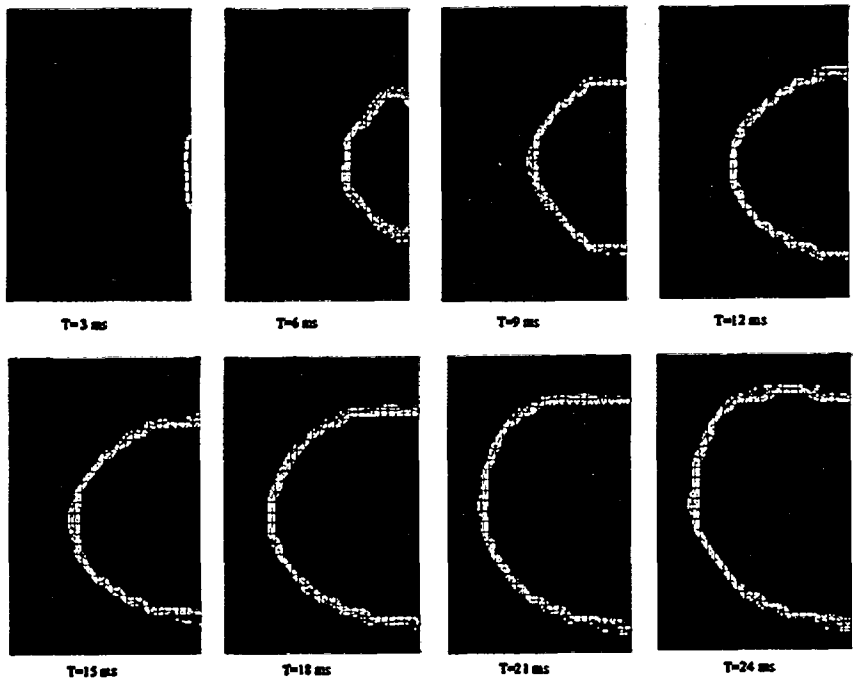

Figure 11. Sub-cooled bubble growth under vertical upward flow condition..

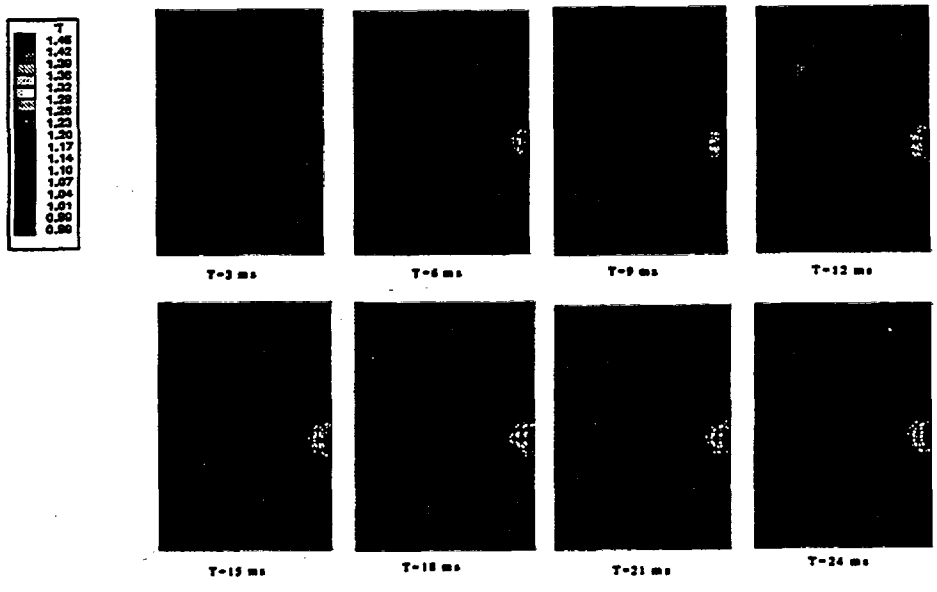

Figure 12. Evolution of temperature contour during bubble growth

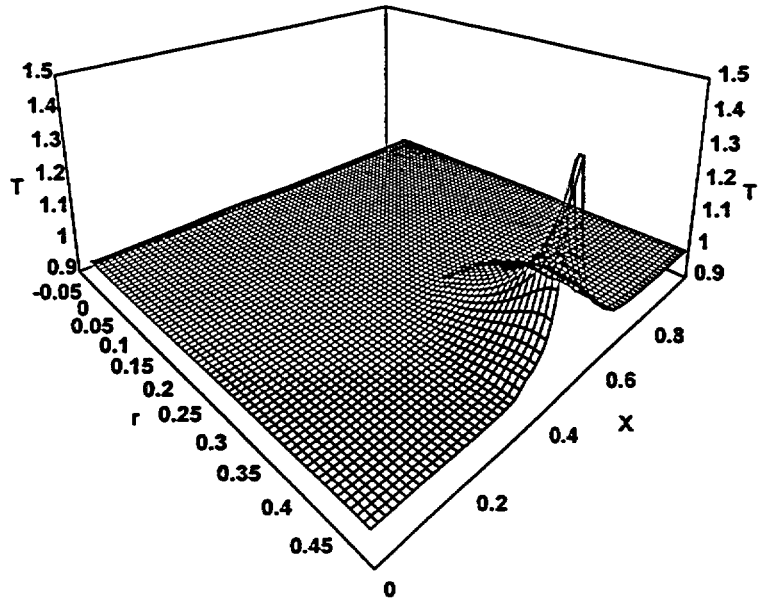

Figure 13. Temperature distribution in and around a single bubble.

VI. CONCLUSIONS

A two-phase computational fluid dynamics and heat transfer model is developed and implemented. The fluid dynamic model is complemented with an energy-based iterative scheme that is used to detect and track the vapor-liquid interfacial boundary. The governing equations are based on fully compressible Navier-Stokes equations. The turbulent viscosity is determined by solving the two-equation k-ε turbulence model. To assess the performance of the model, three cases involving bulk condensation and evaporation in a cylindrical container, bulk condensation in a vertical flowing channel, and vapor bubble formation and growth, are simulated and analyzed. Results have demonstrated the developed model's capabilities for prediction of density, velocity, pressure and temperature fields in 2-D two-phase systems. The detection and tracking of the vapor-liquid interfacial boundary allows for accurate prediction of momentum and energy transport across the phase change boundary.

ACNOWLEDGMENTS

The work presented in this paper is supported by the US Nuclear Regulatory Commission (NRC), Office of Nuclear Regulatory Research under contract number NRC-04-98-053, with Mr. Christopher Boyd as the technical manager.

NOMENCLATURE

A, C, D	constants
E	internal energy [J]
H	enthalpy [J]

T	temperature [K]
V	volume [m^3]
U	velocity [m/s]
X, R	dimensionless coordinates
c_v, c_p	specific heat at constant volume and constant pressure [J/kg/K]
e	specific internal energy [J/kg]
h	specific enthalpy [J/kg]
f	vapor phase fraction
l	length scale [m]
p	pressure [bar]
t	time [s]
x, r	cylindrical coordinates [m]

Non-dimensional Characteristic Numbers

Pr	Prandtl number $\mathrm{Pr}_v = \frac{\nu_{v,0}}{\alpha_{v,0}}$
Re	Reynolds number $\mathrm{Re}_v = \frac{v_0 L}{\upsilon_{v,0}}$
Ra	Raleigh number $Ra_{E,v} = \frac{g\beta_v \Delta T L^3}{\alpha_{v,0}\nu_{v,0}}$
St	Stefan number $St = \frac{Cp\Delta T}{\Delta e}$

Greek symbols

α	thermal diffusivity [m^2/s], or thermal diffusivity ratio
β	thermal expansion coefficient
κ	thermal conductivity [W/K/m], or its ratio
θ	dimensionless temperature
ρ	density [kg/m^3]
τ	dimensionless time

Subscripts

f	interface position, mixed phase
i	interface
l	liquid phase
r	characteristic scale
s, sat	saturation point
v, vap	vapor phase

REFERENCES

1. Anghaie, S. and Ding, Z., "Thermal-Hydraulic Analysis of Bulk Evaporation and Condensation in A Multiphase Nuclear Fuel Cell", *Nuclear Technology*, vol. 120, pp. 57-70, 1997.

2. Hung, C. I., Shyy, W. and Ouyang, H., "Transient Natural Convection and Conjugate Heat Transfer in a Crystal Growth Device", *Inernational ournal of. Heat Mass Transfer*, Vol.38, pp.701-712, 1995.
3. Jang, J. H., Faghri, A., Chang, W. S. and Mahefkey, E. T., "Mathematical Modeling and Analysis of Heat Pipe Start-up from the Frozen State", *Journal of Heat Transfer*, Vol. 112, pp. 586-594, 1990.
4. Poirier, O. and Salcudean, M., "On Numerical Methods Used in Mathematical Modeling of Phase Change in liquid Metals", *Journal of. Heat Transfer*, Vol. 110, pp.562-570, 1988.
5. Samarskii, A. A., Vabishchevich, P. N., Iliev, O. P. and Churbanov, A. G., "Numerical Simulation of Convection/Diffusion Phase Change Problems-A Review", *International Journal of Heat and Mass Transfer*, Vol. 36, pp. 4095-4106, 1993.
6. Shyy, W., *Computational Modeling for Fluid Flow and Interfacial Transport*, Elsevier, Amsterdam, The Netherlands, 1994.
7. Shyy, W. and Rao, M. M., "Enthalpy Based Formulations for Phase-Change Problems with Application to g-jitters", *Microgravity Science and Technology*, Vol. 7, pp. 41-49, 1994.
8. Voller, V. R. and Swaminathan, C. R., "General Source-Based Method for Solidification Phase Change", *Numerical Heat Transfer*, Part B, VOL. 19, pp. 175-189, 1991.
9. Warren M. Rohsenow, James P. Hartnett, Ejup N. Ganic, *Handbook of Heat Transfer Fundamentals*, McGraw-Hill, New York, Vol. 2, p. 5-70, 1985.
10. Shamsundar, N. and Sparrow, E. M., "Analysis of Multidimensional Conduction Phase Change via the Enthalpy model", *Journal of Heat Transfer*, Vol. 97, pp. 333-340, 1975.
11. Todreas, N. E. and Kazimi, M. S., *Nuclear System I Thermal Hydraulic Fundamentals*, Hemisphere Publishing Corporation, New York, 1990.
12. Patankar, S. V., *Numerical Heat Transfer and Fluid Flow*, Hemisphere Publication Corporation., New York, 1980.
13. B.E. Launder and D. B. Spalding, "The Numerical Computation of Turbulent Flows", *Computer Methods and Applications in Mechanical Engineering*, Vol. 3, pp.269-283, 1974.
14. Jones, W. P. and Renz, U., "Condensation from a Turbulent Stream onto a Vertical Surface", *International. Journal of. Heat and Mass Transfer*, Vol. 17, pp. 1019-1028, 1974.
15. Buckle, V. and Peric, M., "Numerical Simulation of Buoyant and Thermocapillary Convection in a Square Cavity", *Numerical Heat Transfer*, Part A, Vol. 21, pp. 121-141, 1992.
16. Carpenter, B. M. and Homsy, G. M., "Combined Buoyant-Thermocapillary Flow in a Cavity", *Journal of Fluid Mechanics*, Vol. 207, pp. 121-132, 1989.
17. Ostrach, S., "Low-Gravity Fluid Flows", *Journal of Fluid Mechanics*, Vol. 14, pp. 313-345, 1982.
18. Crank, J., *Free and Moving Boundary Problems*, Clarendon Press, Oxford, 1984.
19. Filk, M. I. and Tien, C. L., "An Approximate Analysis for General Film Condensation Transients", *Journal of Heat Transfer*, Vol. 111, pp. 511-517, 1989.
20. Sparrow, E. M. and Lin, S. H., "Condensation Heat Transfer in the Presence Noncondensable Gas", *Journal of Heat Transfer*, Vol. 86, pp. 430-436, 1964.
21. Sparrow, E. M., Minkowycz, W. J. and Saddy, M., "Forced Convection Condensation in the Presence of Noncondensables and Interfacial Resistance", *International Journal of Heat and Mass Transfer*, Vol. 10, pp. 1829-1845, 1967.
22. Tournier, J. M. and El-Genk, M. S., ""HPTAM" Heat-Pipe Transient Analysis Model: An Analysis of Water Heat Pipes", *Proceedings of 9th Symposium for Space Nuclear Power Systems*, 1992.
23. Sjoerd van Stralen and Robert Cole, *Boiling Phenomena: Physicochemical and Engineering Fundamentals and Applications*, Hemisphere Publishing Corporation, New York, Vol. 2, 1979.
24. Chen C. L. and Dhir V. K., "Hydrodynamics of a Bubble Formed at Vent Pipe Exit", *International Journal of Multiphase Flow*, Vol. 8, pp. 147-163, 1982.

FASTNET: proposal for a ten-year effort in thermal-hydraulic research

Dominique F. GRAND
CEA/ DRN
Department of Thermal-Hydraulics and Physics
17, rue des Martyrs 38054 Grenoble Cedex 9 France

Abstract

This paper deals with proposals for thermal-hydraulic research applied to nuclear reactors. After an evaluation of the challenges in terms of the competitiveness and safety of nuclear energy, areas are identified where increased knowledge and advances in thermal-hydraulics are expected. They are in two complementary directions: the improvement of the two-fluid model by inclusion of additional transport equations and the development of the simulation of the fine scales of the flow. The greater computing efficiency can be fully used if the modeling is enhanced, i.e. it becomes more generic end flexible. Recommendations are made for the development of instrumentation and definition of new experiments able to provide the needed information. An outline is given for the progression of the program from present day tools to future tools based on advanced two-fluid model and modeling of local phenomena.

1. Introduction

In 1996, CEA/DRN launched a project to define new avenues of research in thermal-hydraulics and establish guidelines for the next ten years. A group of experts in thermal-hydraulics worked under the acronym FASTNET, for Future Advances in Sciences and Technology for Nuclear Engineering Thermal-Hydraulics, and issued a number of scientific proposals. The project was later extended to CEA's French partners, IPSN, EDF and FRAMATOME.

This presentation is the result of the collective effort. As the name indicates, these proposals are put into the perspective of the main challenges in the area of nuclear engineering. The identification of the challenges and the motivation for improved methods and tools were the primary concerns of the representatives from EDF, FRAMATOME, IPSN and CEA/DRN. The group established guidelines for a research and development program for the next decade.

Hereafter, the paper will try to summarize the results of this work. First, it briefly presents the industrial challenges foreseen for the next decade and the resulting needs in thermal-hydraulics. Then it presents the general development of the R and D program and the expected milestones concerning the development of software which will be the end result of this program. One important aspect is the transition between the present generation and the next generation of software. However, thermal-hydraulics cannot progress without a parallel

improvement in modeling and experimental investigations. Thus, we need an evaluation of the state of the art and of new trends in thermal-hydraulic research in its four major activities: experimental techniques and instrumentation, physical modeling, numerical techniques and software. This is the subject of section 4, which gives the main recommendations, and section 5, which deals with the state of the art and the proposals in these activities.

Developments are to be shared with the international community of thermal-hydraulics, as exchanges in the past, such as the meetings organized in 1996 and 1997 by ODCE on Transient thermal-hydraulics and Neutronic code requirements or on Advanced Instrumentation, have been very fruitful.

2. R&D is needed to meet industrial challenges

2.1. Industrial challenges

With 57 reactors in operation providing more than 75% of the production of electricity, France will need no new plants before the older ones begin to retire. The extension of the life span of this generation and the preparation of the next generation are the main elements of context for R and D in thermal-hydraulics.

The primary objective is to sustain the economic competitiveness of energy production by nuclear reactors while continuing to ensure safe operations. This can be achieved by:

- a better evaluation of margins of operation and safety
- a reduction of the duration and cost of design and development

The main industrial challenges are:

- Better design
- Optimization of experimental qualification before start up
- Improvement of the performance and availability of existing and future reactors
- Extension of the lifetime of reactors
- Safety: greater knowledge of operating events and accidents
- Design innovations

Under each of these challenges, nearly 35 specific requests were listed.
Two generic challenges come into play in the above topics:

- 'Best estimate' calculations to reduce bounds that are too conservative: quantification of uncertainty on results of thermal-hydraulic codes.
- Reduction of investment cost by optimization of the experimental programs and by limiting the need for integral test facilities.

2.2. Related R and D problems

Methods are already well-established and efficient. Thus a qualitative jump in the description of the physics is required for a significant improvement of an already good situation.

A detailed analysis was carried out in order to associate the physical phenomena related to the industrial problems identified in section 2. This analysis was summarized in a table relating industrial problems and categories of flow situations encountered or categories of physical models involved. Figure 1 gives a global result of this analysis. It plots in abscissa the number of industrial problems which fall into the different categories of physical problems: flow regimes, heat transfer mode and geometry.

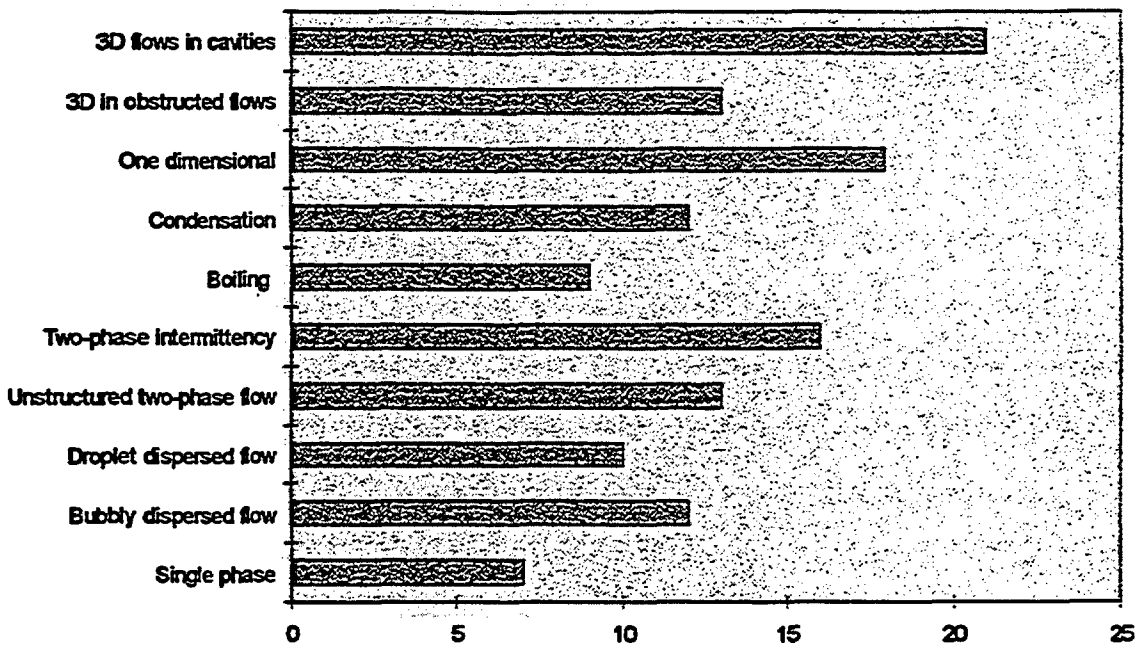

Fig 1 Number of industrial problems relevant to different types of physical phenomena

Some examples of the physical problems identified are:

- Boiling crisis and CHF limitation quantified by costly experimental qualification
- Direct contact condensation under unstable flow conditions: e.g. safety injection and water hammer induced by condensation
- Distribution of two-phase flows in manifolds, application to heat exchangers
- Countercurrent flows in complex geometry
- Thermal stripping: interaction of temperature fluctuations with the thermal-mechanical evolution of structures
- Interference of subcooled boiling and heat transfer on corrosion of the clad

These physical problems require improvements in modeling. Figure 2 gives a summary of the impact of such improvements on the practical problems by counting the number of industrial challenges which could benefit from these improvements.

Below are more detailed examples of critical issues in physical modeling.

- Closure relationships for 3D models are extrapolated from 1D models: lack of turbulence modeling, idealized friction tensors in rod bundles (diagonal tensors)
- Closure relationships for 1D flows do not take into account the spatial distribution of variables which are generally 3D

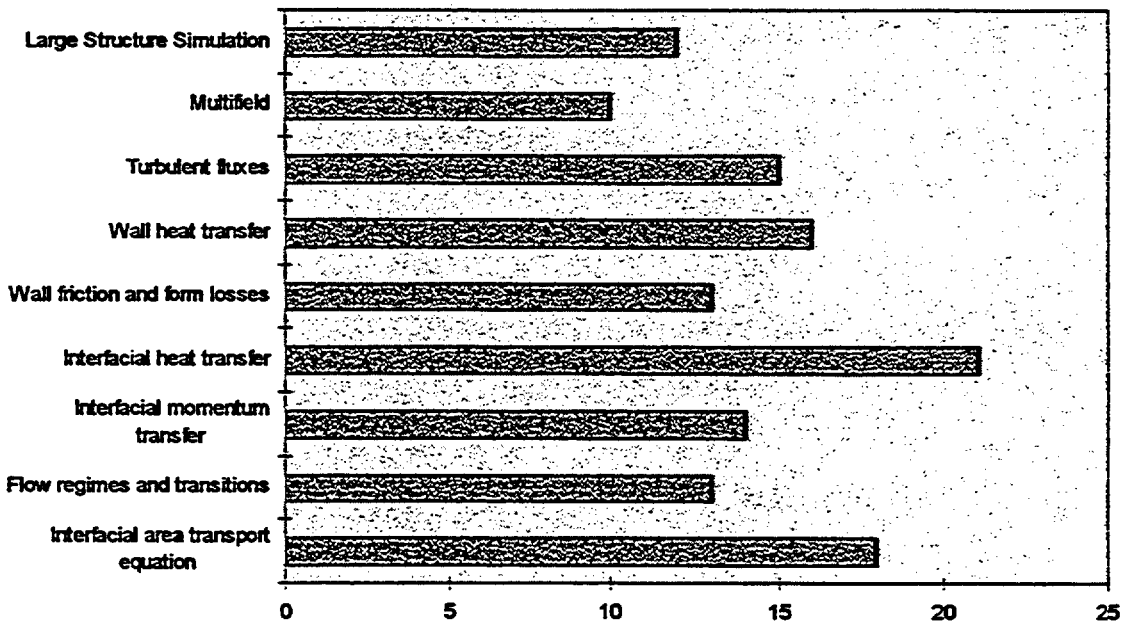

Fig 2 Number of industrial challenges impacted by improvement of modeling issues

- Algebraic expressions used for closure relationships are derived from steady and spatially established flows. They implicitly assume that all physical phenomena adjust instantaneously to the local conditions. They are no longer valid when relaxation times are of the order of magnitude of the travel time in a regular portion of the duct.
- Flow pattern maps and transitions: based on an algebraic criterion, they do not represent the phenomena governing the transition e.g. transition from bubbly to stratified flow where the separation of phase is induced by buoyancy and is limited by turbulence. Flow pattern maps give the result: they are geometry dependent, and the data base is missing for high pressure steam-water flows in large pipes.

3. General development of the R&D program

3.1. The different levels of development

R and D must be carried out in the context of existing and proven tools like CATHARE and SCAR for which industrial versions are programmed for the near future. In this context, three levels are identified:

- existing tools: new versions have been planned and will not be greatly impacted by the developments mentioned above.
- next generation tools with improved multifluid models: an evolution of the two-fluid model with extension to other fields and the incorporation of transport equations for the interfacial area will mostly benefit from the developments in the middle range time frame
- advanced developments: local modeling of two-phase flow with phase change in a new frame different from the averaged two-fluid models can be initiated today, e.g. Direct Numerical Simulation (DNS) with interface tracking. Today these models can only be used on very fundamental issues, although they may be the initial bricks of long-term development of industrial tools.

3.2. *Connections between these levels*

The development of computers makes it possible to increase considerably the volume of the discretization mesh and to refine the physical description to smaller length and time scales.

It can be assumed that when the modeling of physical phenomena is devoted to the small scales it will be simpler and more universal than when it has to deal with all flow scales. The large scales are strongly dependent on the geometry of the flow domain. Thus they are very specific to a given configuration and cannot be extrapolated without additional validation and development from one configuration to the other. On the contrary, small scales are more related to the local and instantaneous conditions of the flow. Solving numerically the large scale and limiting the modeling to small scales may lead to more universal computational models.

This idea is still a conjecture and not a rigorous result. However, this trend is shown in the simulation of turbulent single phase flows or dispersed two-phase flows by the success encountered by Large Eddy Simulation (LES) and its growing share in the simulation of industrial flows over the averaged models. In two-phase flows the knowledge of the links between small scales and large scales is not as advanced as in turbulent single phase flows (there is no equivalent to the Kolmogorov law), and further work is needed to confirm this trend.

At this stage, the prospect of very detailed simulation applied to industrial situations and the development of industrial tools on this basis is a reasonable assumption for the long term (more than 10 years).

In the meantime, this type of simulation should be developed for academic and basic flow situations (e.g. local study of boiling in the thermal boundary layer along a heated wall.) This can give feedback on the industrial tools developed in a shorter time frame: it may provide information to complement experimental results useful for the elaboration of models implemented in these tools.

4. Main recommendations

4.1. *Single phase flows*

In the area of single phase turbulent flows, the direct simulation of the large scales of the flow is making rapid progress thanks to computing capacities and progress in the modeling of small scales. The first applications to industrial flows are underway. Together with the Reynolds Averaged Navier-Stokes modeling, this will provide powerful solution methods for turbulent flows in industrial contexts. One recommendation is to pursue the development of CFD in this area and to advance in the modeling of small scales of the flow particularly in the vicinity of solid walls.

CEA and EDF are working on a joint project in association with French universities. It consists in the development of software for Large Eddy Simulation: PRICELES. This new software is developed in a Object Oriented Method, written in C++ and designed to run on parallel computers. The objective is to run computations of industrial flows on meshes of more than 10 million cells.

4.2. *Averaged two-fluid model*

The extension and development of an advanced generation of the two-fluid model is the second recommendation. The idea is to remove current limitations of the two-fluid model and to continue in this frame which still has good potential for improvement. The physical extensions identified are:

- addition of a transport equation for the interfacial area in order to provide more physical transition between flow regimes.
- addition of averaged equations for the turbulent characteristics of the flow, addition of other fields (e.g. in the case of dispersed annular flow, separation of the liquid phase into two fields - droplets and film - which may have different dynamic behavior),
- improvement of heat transfer models.

These developments can first be carried out on 1D models where some of the difficulties of physical modeling are more tractable and whose results can be very useful for the system codes. Thus it may consist in a well-identified project which results in a pilot code for the next generation of system codes for reactor safety.

The transposition and extension of this model to the 3D geometry can be carried out in close connection and result in the development of multiD models for components like the core or steam generator or other industrial components as well as a 3D module for system codes.

4.3. Microscopic simulation of two-phase flow

This covers the challenge of the development of an approach that is more closely related to simulation in two-phase flows. This is an open field where various attempts are underway, but no unanimous viewpoint exists within the scientific community as to the modeling approaches or experimental efforts to be promoted. The subject must be initiated now in a way that leaves the options relatively open. We recommend the implementation of platforms for numerical and modeling developments on the one hand and instrumentation development on the other hand. In particular, it is recommended to explore the possible extension to two-phase flows of methods available for single phase flows such as Large Eddy Simulation (LES) or Direct Numerical Simulation (DNS).

4.4. Development in time

Figure 3 summarizes the preceding discussion and provides a map for the development of codes for the next 10 years, with the three categories identified: existing tools, next generation with improved multifluid models and advanced local modeling. It illustrates the evolution of these categories in time and their connections:

- today's generation of industrial codes which will enter a maintenance phase with reduced effort after the development phase: T/H system code or component codes for two-phase flows, CFD codes mostly devoted to single phase flows but with increased capacities in two-phase flows.
- the next generation of industrial tools should be based on improved modeling, the advanced two-fluid model in particular which will first be developed at a pilot stage in the laboratory.
- the development of microscopic simulation (the bottom or more fundamental layer) provides inputs to the elaboration of the improved fluid modeling thus complementing experimental developments which will be the main source for elaboration of the models.

The development of this new generation of products is an opportunity for greater convergence or at least the coupling of tools that are separated today.

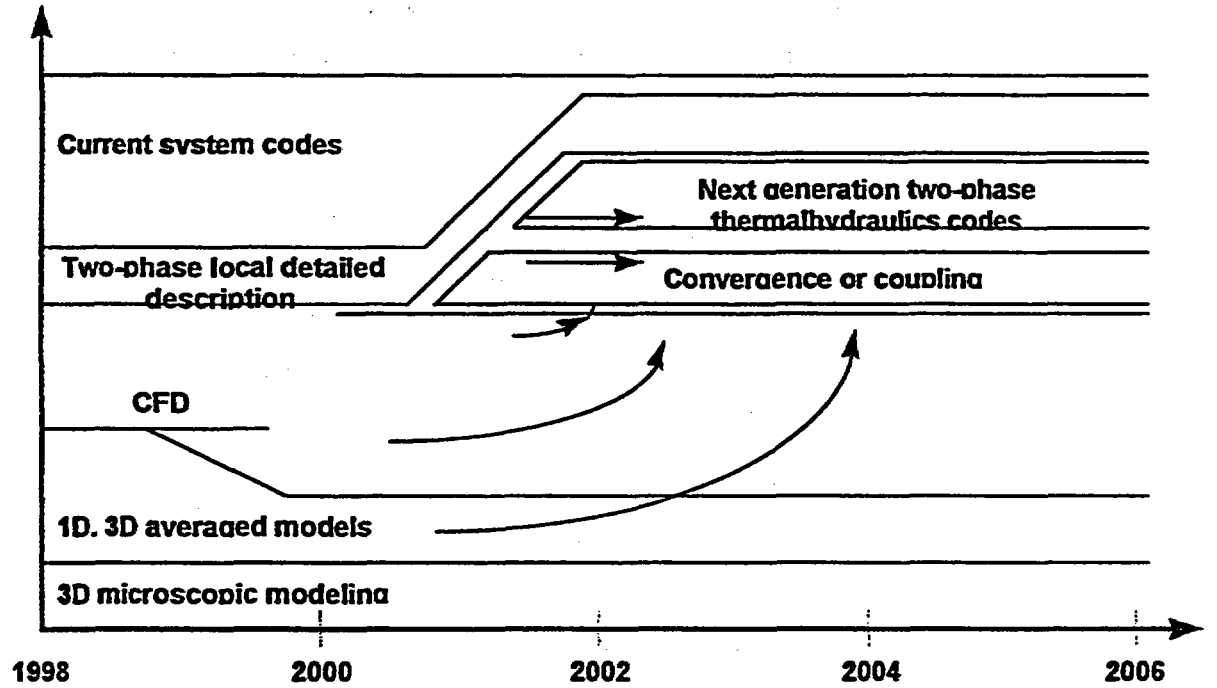

Fig 3 Map for code development and R and D program

4.5. A general recommendation

The discussion in the preceding sections focused on software because software is one end product of research that can be transmitted to industry or safety authorities. We must now acknowledge the real effort devoted to the acquisition of this knowledge.

The planned software will simulate the physical reality at unmatched levels of accuracy. The quality of the information produced by this software can be guaranteed for a long period only through comparisons with physical reality. Thus basic data must be drawn from reality by conducting physically relevant experiments with fine and accurate instrumentation. Thus the real effort of development results from different specialties working in synergy for the elaboration of scientific strategy:

- instrumentation
- experimental methods
- physical modeling
- numerical methods and software development

5. Research axes

5.1. Physical modeling

Table 1 summarizes the recommendations for physical modeling. For each area listed in the first column, (single phase flows, two-fluid model 1D and 3D), the second column presents the current limitations, and the third column the proposals made to remove these limitations. For example, the development of a transport equation for the interfacial area found in the third cell of the last column should remove the limitations on closure relationships due to the absence of relaxation time in the current modeling frame and the brutal transition between flow regimes.

The last proposal for multi-D two-phase flow is relevant to the advanced local modeling, while the other proposals can progress in the frame of the advanced two-fluid model using averaged equations.

Table 1 Proposals in physical modeling

Area	Current limitations	Proposals
Single phase turbulent flows	Coefficients of closure relationships	Develop the application of LES to complex flow configurations characteristic of industrial applications
	Homogenization in rod bundles	
	Wall functions in separated flows and for heat transfer	Improve wall functions with strong heat transfer.
Two-fluid model 1D	Closure relationships	Interfacial area transport equation with modeling of bubble breakup, coalescence
	Transitions between flow regimes	
	No relaxation time and assumption of instantaneous adjustment to local conditions	
	Flow regimes where two fields of the same phase are weakly coupled (e.g. liquid film and droplets)	Multifield models e.g.: dispersed annular flow, bubbly stratified flow
Two-fluid multi D	Closure relationships	Development of models for interfacial transfer and fluid-to-wall transfer
	Filtering turbulent and two-phase intermittence	Transport equation for k,e to obtain characteristic scales for turbulence and two-phase intermittence
	Turbulence description limited to dispersed and diluted two-phase flows (averaged models or SGE)	Extension from dispersed flow to all flow regimes requires combined efforts on Averaged two-fluid model and DNS
	Direct Numerical simulation for the description of elementary two-phase flows with few « particles »	DNS with simulation of interfaces and account of phase changes

5.2. Numerical simulation and software development

We will now consider the current limitations of numerical simulation including numerical schemes, software architecture and development and user interfaces (preparation of simulation and post-processing of results).

Table 2: Proposals in numerical simulation and software development.

Area	Current limitations	Proposals
Time discretization	Different time scales (e.g.: phase change, acoustic waves, convection) result in stiffness	Develop implicit schemes even for transient simulations
	Nonlinear stiff source terms	Solution methods
Spatial discretization	Impossibility to refine locally with structured meshes	Finite Volume or Finite Element Methods on unstructured meshes
		Adaptive methods to track small structures associated with error indicator
		Domain coupling
	Precision vs robustness	Develop schemes characterized by 'soberness' (optimum balance of order, precision, robustness and flexibility)
Solution algorithm	Efficiency of matrix inversion techniques (large contribution to computing time)	Improve preconditioning methods for nonsymmetric matrices
		Multigrid methods with increased robustness for anisotropic meshes
		Develop parallelism, preferably in new code design combined with domain decomposition
Code design		Object Oriented Method
Preparation of simulations		Coupling with CAD and mesh generation software
Interpretation of results	Evaluation of uncertainty of the results limited to 1D and small variations	Extend to 3D and large variations of physical parameters
		Use of automatic differentiation software
	Synthesis of the result	4D visualization software with extraction of quantitative results
	Conservation of results	Improve specialized data base with results from experiment and simulation.

5.3. Instrumentation

A necessary condition for the development of advanced simulation is the availability of instrumentation providing the data needed for the elaboration of the models or their verification. Ideally the instrumentation should fulfill the following conditions:

- Give information with a spatial and temporal resolution compatible with the numerical model
- Have a negligible influence on the flow
- Work in a wide range of two-phase flow regimes
- Work for adiabatic flows and flows with heat transfer and phase change

Table 3 gives a rough summary of the techniques available for measuring different physical quantities characteristic of the flow (void fraction, interfacial area, velocity, temperature), their limitations, and the proposed developments to remove some of these limitations.

Table 3 Proposals in instrumentation

Area	Current limitations	Type	Proposals
One dimensional models	Cost of X ray densitometry	Impedance densitometry	Extend impedance densitometry to nonisothermal flows
	Adiabatic flows		Explore electromagnetic inductance
		Flow metering or anemometry	Extend use of electromagnetic flowmeters
			Nuclear Magnetic Resonance for densitometry and flow metering
		Wall transfers	MEMS fluxmeters and shear gauges
			Electrochemical techniques for wall shear stress measurements.
	Detection of transition between flow regimes		Time-frequency analysis and neural networks
Three-dimensional dispersed flow	Perturbation by intrusive probes	Void fraction and interfacial area	Optical or electrical multiple probes: miniaturization
			Ultrasonic tomography
		Liquid velocity	Extend Particle Image Velocimetry with stereoscopic imaging.
			Miniaturization of electomagnetic velocimetry probes.
		Temperature and velocity	Extension of hot film probes to nonisothermal flows and measurement of turbulent shear stress and heat flux.
			Temperature of superheated vapor
Three-dimensional unstructured flows		Void fraction and interfacial area	Optical or electrical multiple probes: signal processing for interfacial area (density, orientation of normal vector).
			Adaptation of X Ray tomography to fast transients
		Local void fraction and velocities	Adaptation of Nuclear Magnetic Resonance

5.4. Experimentation

The next generation of computer codes should increase the genericness of the physical phenomena described and the universality of their application. The experiments designed for their validation should move along two lines:

- analytical experiments devoted to the quantification of a local isolated phenomenon

- validation experiment assessing the ability of a model to represent more complex situations coupling different phenomena.

The following list gives suggestions in the methodology, the design and the realization of experiments along these lines:

- Simulant fluids : use of fluid different from the prototypic one is often a good compromise between difficulty and cost of the experiment, availability of the instrumentation and quality of the results.Look for new fluids to replace Freons for the simulation of high pressure boiling water. Associated scaling procedures should be developed.
- Close interaction between modeling and experimental experts
- Experiments on :
    - two-phase flow turbulence, e.g. mixing layer
    - flow regimes and interfacial area topology
- Development of technology in areas like :
    - flow visualization : windows, endoscopes, infrared visualization. Application to nucleate boiling
    - heating elements
- Development of experimental procedures
    - control of the loop parameters in steady state or for slowly varying transients
    - real time pre-analysis of the results (quality control)

5.5. Coupling of thermal-hydraulics with other disciplines

The last item is at the boundary of the disciplines but must be considered in the definition of the strategy. It concerns the links between thermal-hydraulics and other scientific disciplines which are also involved in the resolution of practical problems.

Table 4 Proposals in coupling thermal-hydraulics with other disciplines

Area	Current limitations	Proposals
T/H Physical chemistry	Simplified physical properties	Coupling with software providing the properties by minimization of free energy of the mixture (severe accidents, waste storage)
T/H Aerosols	One-way coupling	Retroaction of vapor condensation on aerosols
T/H corrosion or		Mechanistic approach to clad corrosion by local description of boundary layer
T/H Mechanics		Fluid elastic coupling LES & Thermomechanical for thermal stripping Large amplitude vibrations modifying boundaries of flow domain.
T/H Neutronic		Coupling with 3D Neutronic codes
T/H Electromagnetism		

6. Conclusion:

The preparation of the new generation of thermal-hydraulic methods and tools for the next decade should be launched without delay. The end tools of R and D are software gathering the knowledge under a transmissible form. To produce the software, the R and D program must include a good balance of modeling, instrumentation improvements, experimental programs related to the modeling issues and numerical developments.

The reflection initiated two years ago on both industrial challenges and scientific breakthroughs has led to the results presented here.

International cooperation is of utmost importance. Reflection nourished by international workshops like OECD meetings feeds the discussion at later meetings and initiates further exchanges in these highly challenging issues.

Acknowledgments : The author wishes to associate his co-workers: D. Bestion, P. Clement, JP Caminade, JM Delhaye, P. Dumaz, J. Garnier, E. Hervieu, O. Lebaigue, H. Lemonnier, C. Lhuillier, P. Mercier, JR Pages, I. Toumi, M . Villand, D. Besnard from CEA , G. Le Coq, C. Simeon and G. Houdayer from EDF, L. Catalani from FRAMATOME and M. Durin from IPSN.

References:

Proceedings of the OECD/CSNI Workshop on Transient Thermal-Hydraulic and Neutronic Codes Requirements, Annapolis, MA, Nov. 5-8, 1996 NUREG/CP-0159 NEA/CSNI/R(97)4

Proceedings of the OECD/CSNI Specialist Meeting on Advanced Instrumentation and Measurement Techniques, Santa Barbara, CA, March 17-20, 1997.

Containment/RCS Analysis of a Large Break Loss-of-Coolant Accident in the AP600 Using RELAP5/MOD3

Abstract

Several large break loss-of-coolant accident (LBLOCA) calculations were performed for the Westinghouse AP600 using RELAP5/MOD3 with a containment module developed to assess containment effects on AP600 reactor coolant system (RCS) behavior. The first calculation used AP600 FSAR mass and energy flows from the RCS as boundary conditions for the containment and was used as a benchmark to compare basic containment models against similar calculations using CONTAIN and WGOTHIC. The calculated containment pressure was comparable to the CONTAIN and WGOTHIC results. For the second calculation, the containment module was linked to the RELAP5 AP600 RCS Long Term Cooling Model, and an integrated RCS/containment LBLOCA was performed. In this case the second and highest pressure peak disappears, because: 1) the FSAR mass and energy release is significantly higher than the release calculated by RELAP5, and 2) the excess energy in the FSAR release goes upward as steam to the upper containment, because of the conservative energy partition assumed by Westinghouse.

A sensitivity study to internal containment shell heat transfer showed that a factor of three reduction still does not result in a high second pressure peak for the integrated model with. A second sensitivity study was done by varying the outside containment heat transfer . This indicated that a substantial margin exists in the time required to initiate PCCS cooling compared to what would be required using the conservative FSAR energy release.

Integrated containment/RCS analyses proved to be very helpful in assessing the conservatism of certain design basis FSAR assumptions used for containment analysis.

Abbreviations

ADS	Automatic Depressurization System
ADS123	ADS combined first three stages
ADS4	ADS fourth stage
AP600	Advanced Passive 600 MWe Reactor
CMT	Core Makeup Tank
CONTAIN	General Purpose Containment Analysis Program
CONTEMPT	Simplified Containment Analysis Program
CVCS	Chemical Volume and Control System
ECCS	Emergency Core Cooling System
FSAR	Final Safety Analysis Report
IRWST	In-containment Refueling Water Storage Tank
LBLOCA	Large Break Loss-of-Coolant Accident
LOCA	Loss-of-Coolant Accident

LTCM	Long Term Cooling Model
PCCS	Passive Containment Cooling System
PRHR	Passive Residual Heat Removal System
RCDT	Reactor Coolant Drain Tank
RCS	Reactor Coolant System
RELAP5	General Purpose Reactor Analysis Program
SBLOCA	Small Break LOCA
SG	Steam Generator
WGOTHIC	Westinghouse containment analysis program

1. INTRODUCTION

The Westinghouse AP600 design integrates the containment and RCS performance to a much greater degree than is the case for current generation operating pressurized water reactors (PWRs).

In Reference 1 the effects of containment modeling on RCS/ECCS behavior were explored for a one-inch cold leg break. Reference 1 describes a RELAP5 containment module developed for the one-inch break study. The purpose of the containment portion of the RELAP5 small break LOCA calculations was not containment design audit, but determination of coolant mass and energy disposition in the lower containment, since that is the coolant source for the RCS in the long term.

The physical computer models contained within RELAP5 and used for the containment module were not specifically developed for containment design analysis. They were also not assessed against experiments associated with containment design. In order to obtain an idea of the viability of the RELAP5 containment features, the module was benchmarked against WGOTHIC, CONTAIN, and CONTEMPT calculations for a large break LOCA in AP600. This benchmark calculation is described in Appendix A of Reference 1 and shows a reasonable comparison against calculations which were done several years earlier.

After review of more recent WGOTHIC and CONTAIN analyses (References 2 and 3), it became clear that the RELAP5 containment module was out of date and could not be successfully benchmarked against the calculations in References 2 and 3. Therefore, the RELAP5 containment module was substantially modified to improve the heat structures, volumes, elevations, flow paths, and containment shell heat transfer using the more recent AP600 design information. The new module with new mass and energy boundary conditions was then benchmarked against the recent WGOTHIC and CONTAIN calculations for a large break LOCA.

Since an integrated RCS/containment calculation was performed for a one-inch cold leg break in Reference 1, it was relatively easy to perform a similar integrated calculation for a large break LOCA.

In this report, the new RELAP5 Long Term Cooling Model (LTCM) with emphasis on the containment module is briefly contrasted to the model described in Reference 1; the new benchmark and integrated calculations are described; and relevant sensitivity studies are performed and described.

2. MODIFIED RELAP5 LONG TERM COOLING MODEL

Figure 1 is a schematic diagram of the linkage between the principal components used for the two basic models used in this study. Both models use the same input for the containment and the IRWST. The benchmark model, however, does not use a PRHR heat exchanger in the IRWST. In a later section, this will be shown to be insignificant for containment analysis. The RCS model used for the integrated

Figure 1. RELAP5 AP600 Large Break LOCA
Containment/RCS Modeling

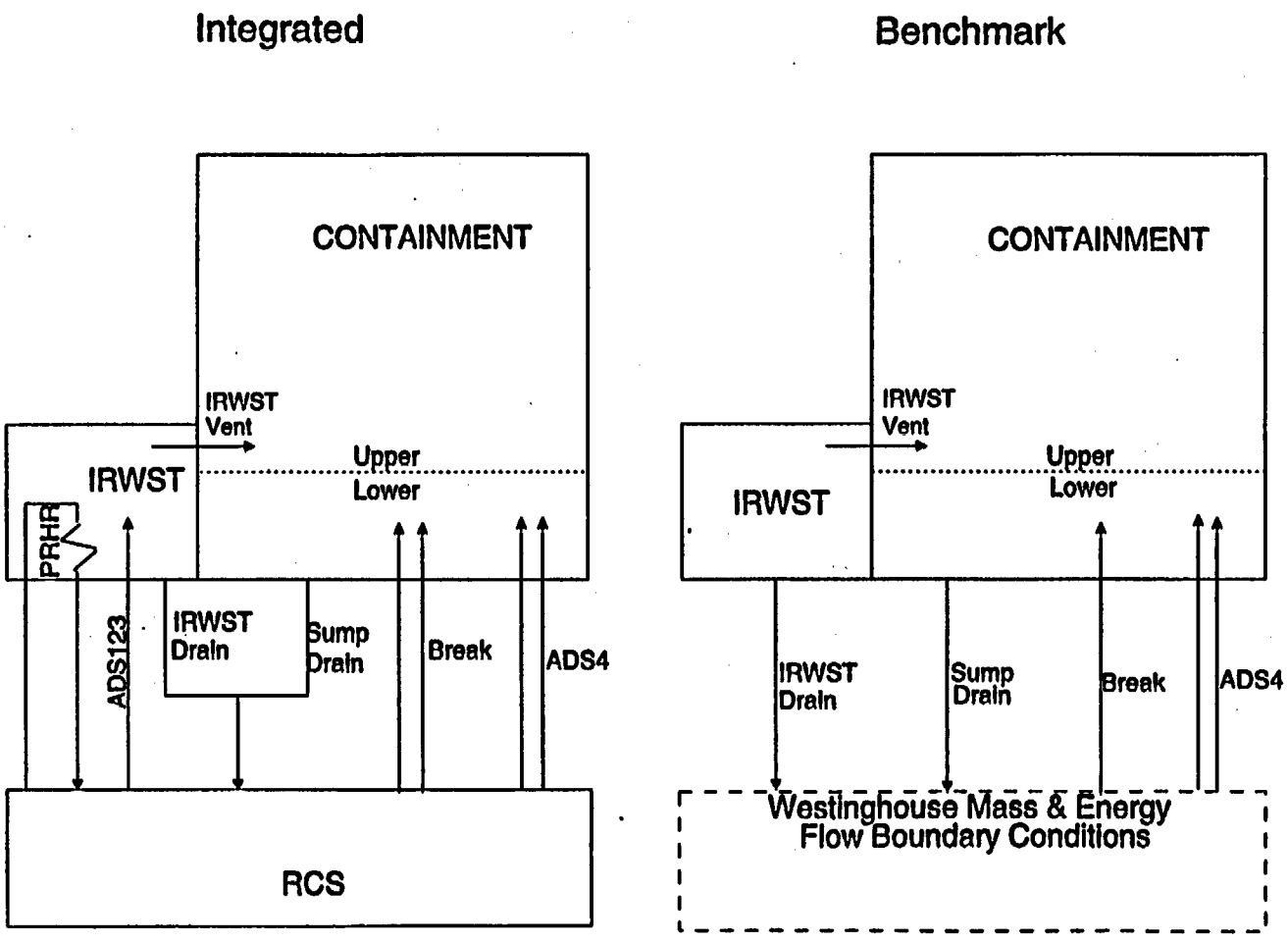

analysis includes accumulators, CMTs, and a simplified secondary system. In Reference 4, the basic 100 node RELAP5 RCS model is described and assessed against OSU small break experiments. In the benchmark model, the RCS is replaced by mass and energy flow boundary conditions obtained from the revised AP600 FSAR.

Experience with the RCS model connected to various containment models has indicated the need to make some changes to the 100 node RCS model. In order to avoid substantive reverse flow through accumulator and CMT check valves, the surge lines upstream of these valves is now modeled with the homogeneous flow option. This does not have a large effect on the results, but essentially avoids this anomaly. The ADS123 outlet line to the sparger has been re-nodalized and re-initialized to avoid unrealistic oscillations encountered at the beginning of the problem. The 100 node RCS model is used for all of the integrated RCS/containment calculations.

In Reference 1, the LTCM analysis concentrates on the IRWST and sump injection phases of an SBLOCA in AP600. This focus requires more detail in the containment compartments below the operating deck than is usual for containment design analysis. Figure 2 shows the 32 nodes of the active primary sump below the containment operating deck. After reviewing Reference 2, several modifications were made to the primary sump, compared to Reference 1. First, a separate access tunnel component was created with connections only to the lower sump, CMT room, and sump recirculation lines. The sump recirculation lines are unchanged from Reference 1. A separate refueling canal component was added with an always active drain line to the lower sump and a small flow path to the vessel cavity. Upper containment components were separated from sump components. Junctions to the RCS are those used in the integrated calculation.

Figure 3 is nearly identical to Figure 2. The only difference is the time dependent volumes and junctions used to simulate mass and energy flow to and from the RCS for the benchmark model. Thermodynamic conditions for the time dependent volumes and phasic flows for the junctions are derived from Chapter 6 of the Westinghouse FSAR (Reference 5). The time dependent volumes are shaded in gray.

Figure 4 shows the three rooms that comprise the "normally non-flooded" rooms or secondary sump. These are the two accumulator rooms and the CVCS room. In order to show the relationship to the CMT room, that component is included in the figure , even though it appears in Figures 2 and 3. There are no changes from Reference 1 except the junction designation from the CMT room to the upper containment.

Figure 5 shows the 8 volumes and associated junctions that comprise the upper containment. Compared to Reference 1, the cylindrical portion of the containment is a separate component and volume and junction designations are changed accordingly.

The large break study in Appendix A of Reference 1 used average external containment shell PCCS heat transfer coefficients from an old CONTAIN large break calculation (Reference 6). The integrated small break analysis in Reference 1 used a four region external shell heat transfer model with coefficients obtained from a CONTAIN small break analysis (Reference 7) done as part of the small break assessment. The PCCS external heat transfer coefficients used for this study were obtained from Reference 3 and are shown in Figure 6. Since RELAP5 does not have heat transfer models designed to simulate the curved upper surface of the containment shell, the vertically oriented containment annulus shown in Figure 5 translates to vertical containment walls. As shown in Figure 5, that portion of the containment shell adjacent to the three lower volumes is assumed to be 90% "wet". That is the heat transfer coefficients used are from the curve labeled "wet" in Figure 6. The remaining 10% of the shell surface adjacent to the lower three volumes uses the coefficients from the curve labeled "dry" in Figure 6. The upper annulus and cylindrical nodes in Figure 5 represent the dome region of the AP600 containment. The water

Figure 2. RELAP5 AP600 "Primary Sump" Model
for Integrated RCS/Containment Analysis

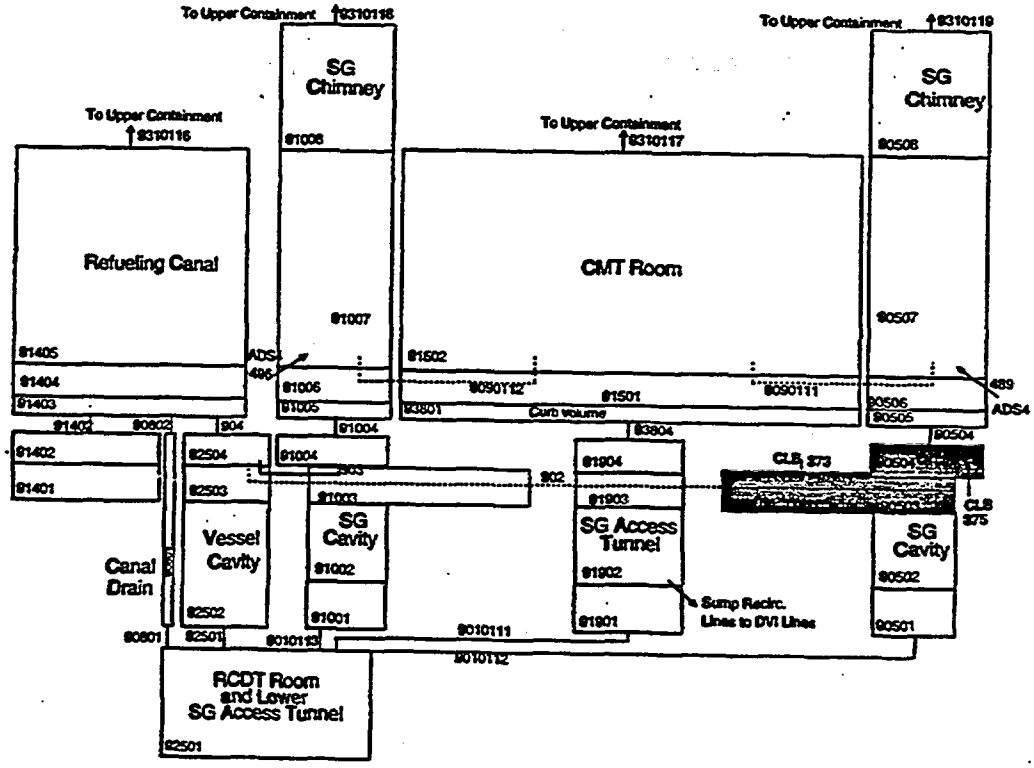

Figure 3. RELAP5 AP600 "Primary Sump" Model
for Benchmark Containment Analysis

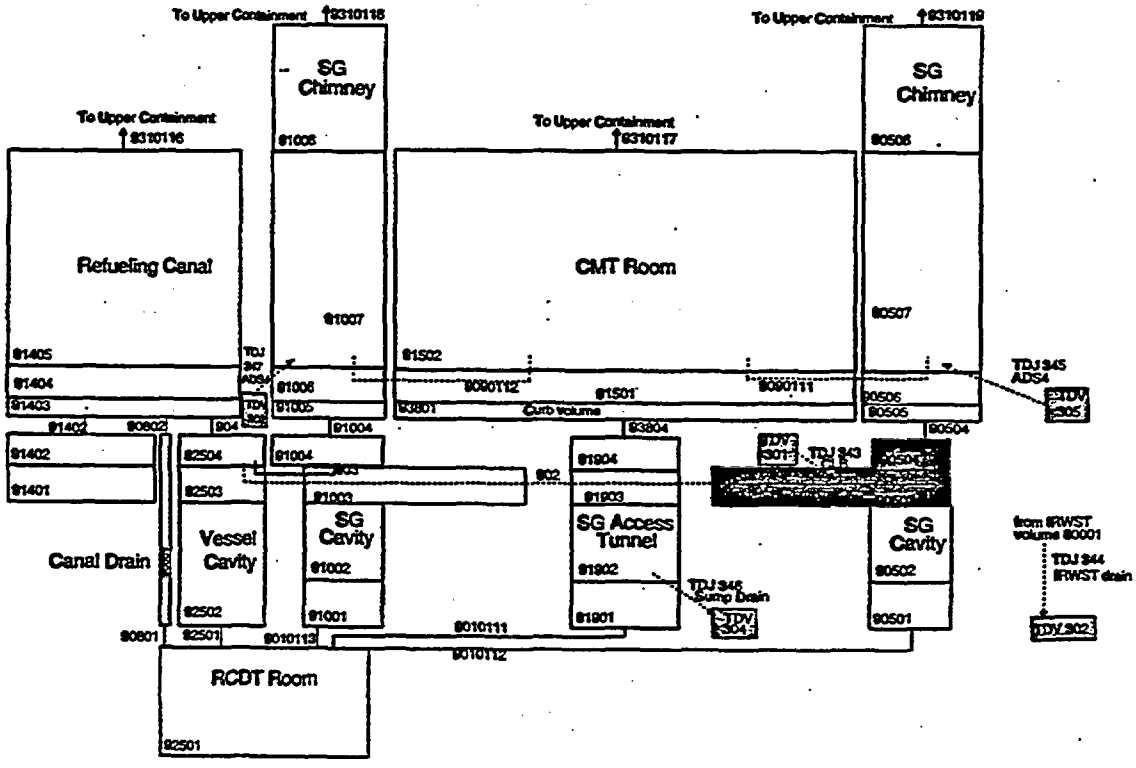

Figure 4. RELAP5 AP600 Model
"Secondary Sump" Rooms and CMT Room

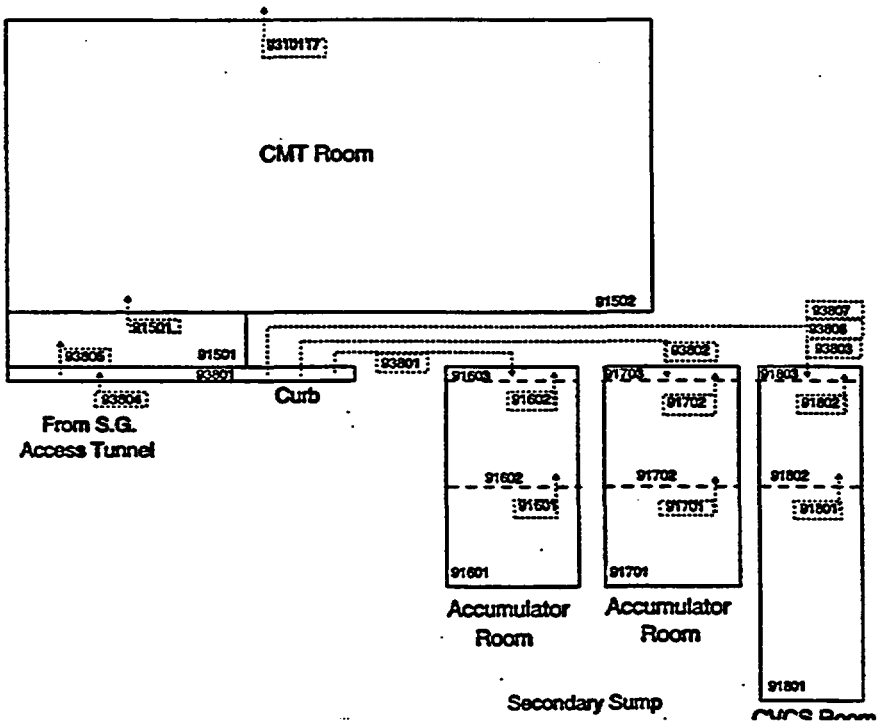

Figure 5. RELAP5 AP600 Model
Upper Containment Model

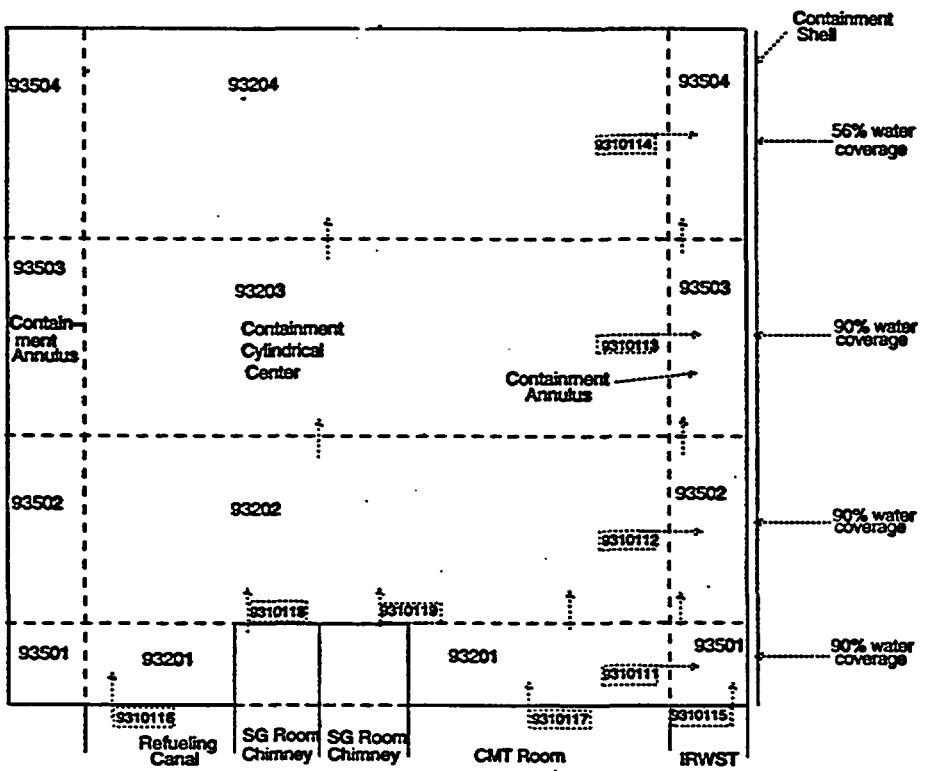

Figure 6. CONTAIN Calculated Large Break LOCA
Average PCCS Film Coefficients

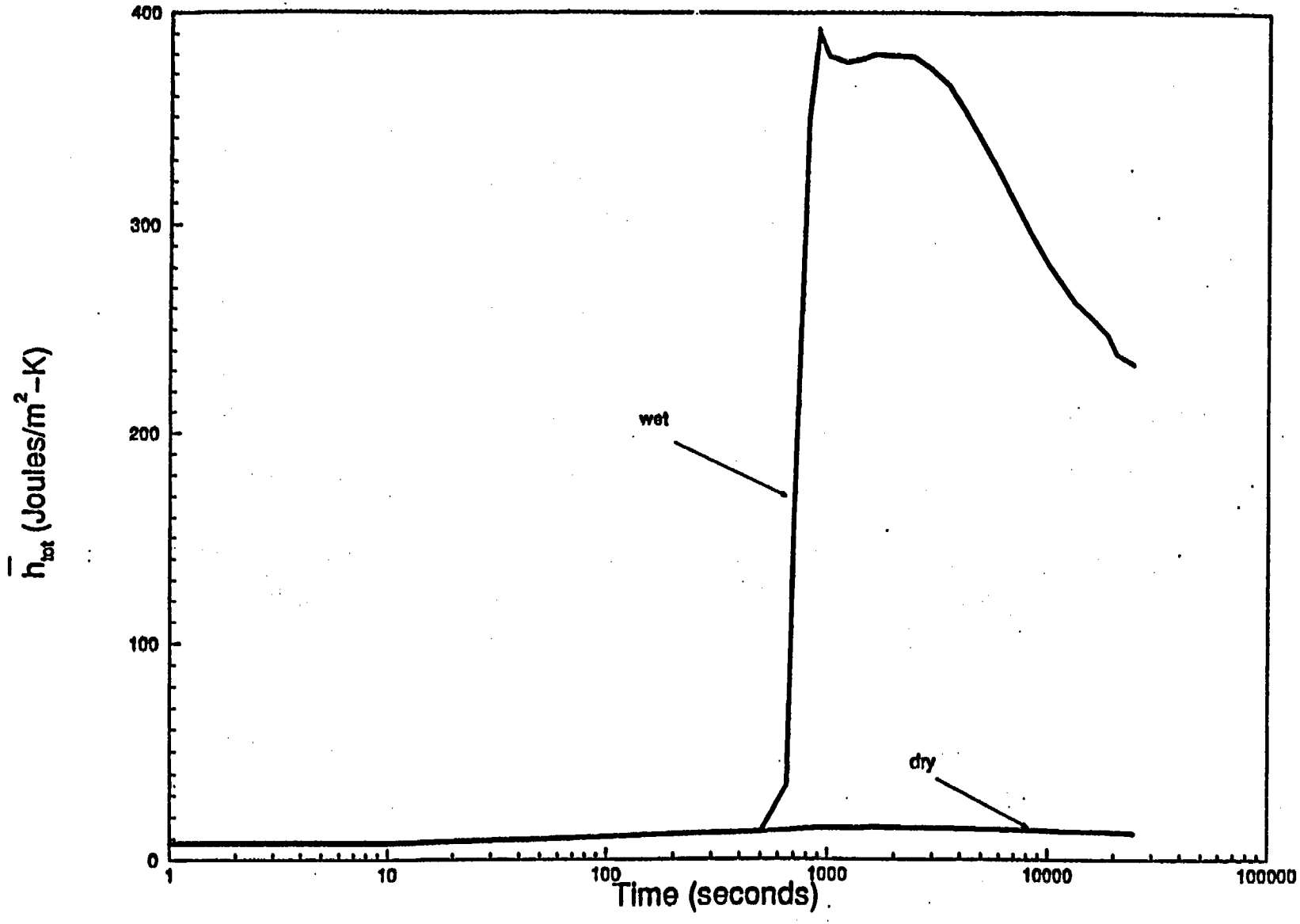

[data7/ap600/library/LT_D_B.HCOEF.REV3]

coverage for vertical shell adjacent to this region is assumed to be 56% with the same "wet" and "dry" coefficients being applied. Coverage values and heat transfer areas are from Reference 2.

The inner containment shell heat transfer model used in Reference 1 included an interim condensation heat transfer option which is no longer recommended. This study uses the improved standard RELAP5 default model contained in version IG (Reference 8). After sufficient warm water vapor has accumulated in the upper containment (<10 seconds), the heat transfer mode is condensation in the presence of non-condensables. If the outer surface is dry, the inside heat transfer mode reverts to a convection mode after that portion of the wall heats up. For those portions of the wall that are wetted on the outside, the heat transfer remains in the condensation mode on the inside.

The current condensation model for this geometry (Reference 8) uses a combination of the Nusselt and Shah correlations for convection through the liquid film. The Colburn-Hougen method is then used to balance the heat transferred by condensing steam with the heat transferred through the condensate film. This is done by iterating for the interface temperature (steam partial pressure). The diffusion of steam through the non-condensables to the interface is according to the heat/mass transfer analogy, using the Churchill-Chou correlation for natural convection to a vertical surface.

All of the old internal containment heat structures were removed and replaced with heat structures that are geometrically similar to those described in Reference 2. Carbo-zinc paint and air gap thermal properties were added to simulate these heat structure materials. For these calculations, heat structures were not turned on and off as Westinghouse did in their analyses in Reference 2.

3. ANALYSES PERFORMED

The first set of analyses compare the RELAP5 benchmark and integrated analyses with comparable CONTAIN and WGOTHIC analyses. The second set is a sensitivity to variation in the internal containment shell heat transfer. The third set is a sensitivity to external containment shell heat transfer. RELAP5/MOD3 Version IG was chosen for these analyses. This version is a predecessor to the forthcoming generally released Version 3.3. For these analyses it appears to be more stable and slightly faster than Version 3.2.1.2. The mass error also seems to be generally improved.

3.1 COMPARISON OF RELAP5 ANALYSES WITH WGOTHIC AND CONTAIN

In Reference 2, Westinghouse presents the results of their design basis containment analysis using WGOTHIC. The methodology used for providing RCS mass and energy release boundary conditions for the containment analysis is described briefly in the AP600 FSAR (Reference 5). Reference 3 presents an NRC audit analysis using the CONTAIN code and the same mass and energy boundary conditions used by Westinghouse. For this study, an analysis was performed using the RELAP5 benchmark model described in Section 2. The same mass and energy release was used as was used for the WGOTHIC and CONTAIN analyses. A second RELAP5 calculation was performed using the integrated model described in Section 2. A summary of nodalization and boundary conditions for the four calculations is given in Table 1.

Table 1. Input Summary for Base Case LBLOCA Analyses

Code/ Reference	RCS Nodes	Lower Containment Nodes	Upper Containment Nodes (Inside/Outside)	Containment Boundary Conditions	RCS Boundary Conditions
WGOTHIC/ Reference 2	0	15	74/16	N/A	Reference 5 Mass & Energy Flow Rates
CONTAIN/ Reference 3	0	8	7/10	N/A	Reference 5 Mass & Energy Flow Rates
RELAP5 Benchmark/ This report	0	41	8/0	Reference 3 heat transfer coefficients	Reference 5 Mass & Energy Flow Rates
RELAP5 Integrated/ This report	100	41	8/0	Reference 3 heat transfer coefficients	N/A

Whenever a code input model does not contain the capability to analyze a particular aspect of the transient, a zero appears in the applicable noding column of Table 1. Thus the containment codes have no RCS capability and no RCS noding. Under such circumstances, boundary conditions are required and are given in the last column of the table. In the case of RELAP5, there is no outer shell PCCS heat transfer model. Therefore, heat transfer coefficients are used from Reference 3.

Figure 7 is a containment pressure comparison of the four calculations described in Table 1. The WGOTHIC and CONTAIN results are reproduced directly from Reference 3. The RELAP5 benchmark, which uses the same mass and energy release as the WGOTHIC and CONTAIN analyses, shows a result very similar to the other two codes. This is characterized by an initial peak pressure at the end of blowdown (30-40 seconds) of about 3.4 bar, and a higher peak of about 4 bar between 1000 and 1200 seconds. The RELAP5 integrated calculation shows no second pressure peak at all. The only difference between the two RELAP5 calculations is the mass and energy release boundary conditions. In the benchmark case, the flow conditions are provided by Reference 5 tables. In the integrated case, the 100 node RCS model generates its own conditions at the interfacing junctions between the containment and the RCS. .

3.2 COMPARISON OF MASS AND ENERGY RELEASE FOR THE TWO RELAP5 CALCULATIONS

Because the only difference between the two RELAP5 calculations is mass and energy release, it was decided to explore the quantitative difference between those two cases for those parameters. This also provides a measure of understanding of the difference between the "best estimate" RELAP5 mass and energy release and the AP600 FSAR release which in part follows the Standard Review Plan containment release methodology.

3.2.1 SMALL EFFECT OF ADS4 RELEASE AND IRWST VENT FLOW

As shown in Figures 2 and 3, the mass and energy sources to the containment are the break flow, ADS4 flow, and IRWST vent flow in the RELAP5 model. In the cases using the FSAR boundary condition prescription (CONTAIN, WGOTHIC, and RELAP5 benchmark), the ADS4 does not discharge to the

Figure 7. AP600 Large Break LOCA
Containment Pressure Comparison

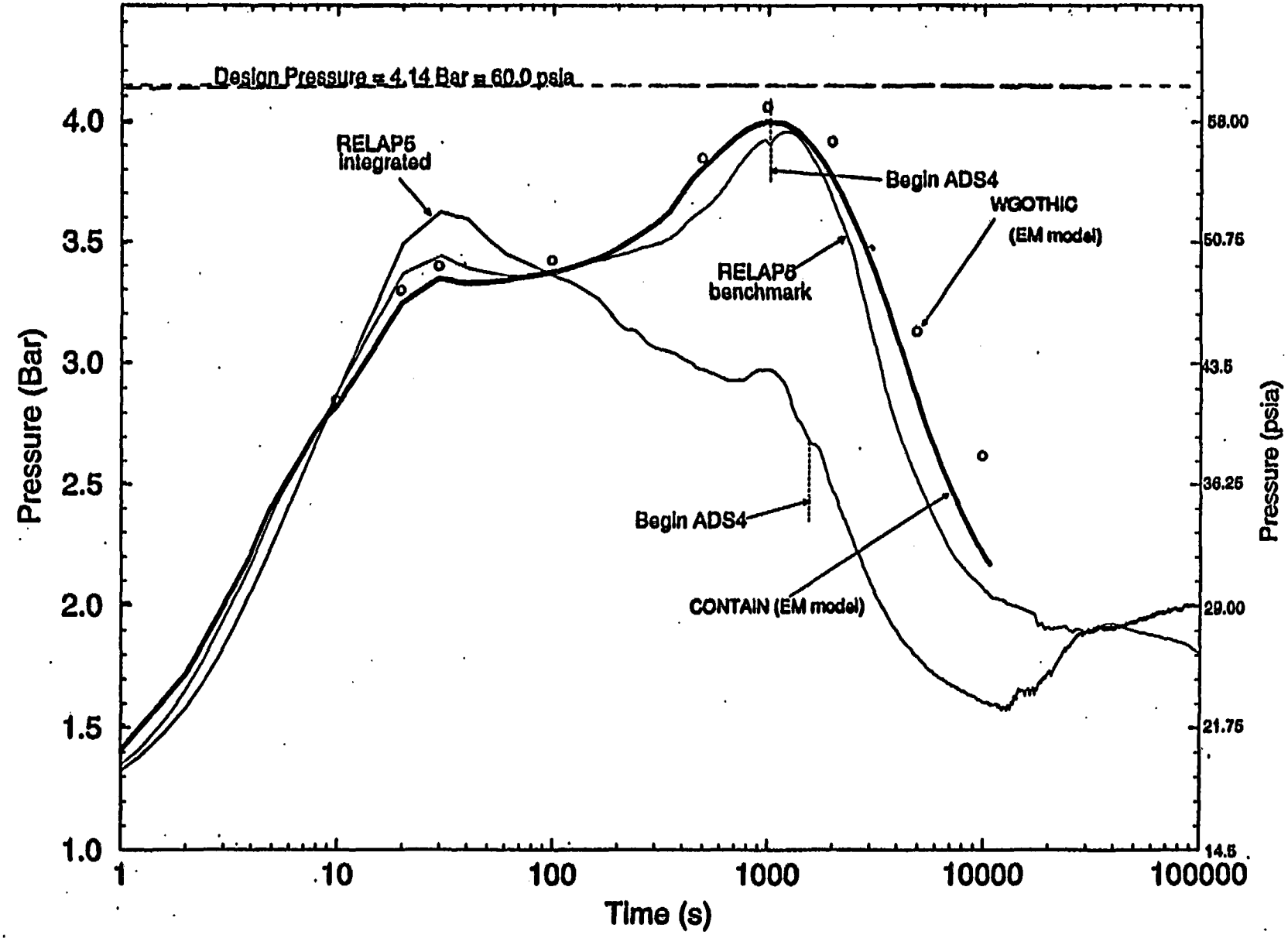

containment until 1000 seconds. In the RELAP5 integrated case, ADS4 does not discharge until about 1560 seconds. In the RELAP5 benchmark the small effect of ADS4 can be seen at 1000 seconds in Figure 7. At this time, the pressure has just turned over when the energy release from ADS4 causes a very small rise of about .05 bar (0.7 psi) over the next 200 seconds. From 900 seconds onward, the PCCS external shell heat transfer coefficients have reached such high values (see Figure 6), that additional energy release from ADS4 does not have a significant effect on containment pressure.

Figure 8 shows the integrated IRWST vent energy release for the two RELAP5 cases. As the figure shows, the slope is negative, indicating that mass and energy are actually flowing into the IRWST from the upper containment. Thus for this break, energy from ADS123 and the PRHR is not enough to warm the large volume of IRWST water to cause steam venting to the containment. Rather the calculations indicate that a small amount of warm steam from the upper containment flows down into the IRWST and is condensed. For the approximate time of interest (40 to 1040 seconds), there is less than 1000 MJ difference in integrated energy flow between the IRWST and upper containment for the two cases.

3.2.2 LARGE EFFECT OF BREAK ENERGY RELEASE

Figure 9 shows an integrated break energy release comparison for the two RELAP5 cases for the first 2000 seconds. It is the energy release during the first 40 seconds that determines the first pressure peak. During this initial period, the energy release is similar for the benchmark model using the Westinghouse AP600 FSAR release and the integrated model using the RELAP5 "best estimate" RCS release. The benchmark model is based on a Westinghouse SATAN-VI RCS analysis described in Reference 2. Therefore, conservative assumptions, necessary after 40 seconds when Westinghouse did not use an RCS analysis for mass and energy release, are not required during this initial period. Also RELAP5 and SATAN-VI both use the Henry-Fauske break flow model with a break coefficient of 1.0. Thus, it is not surprising that the mass and energy release based on SATAN-VI is similar to that based on RELAP5.

For the 40 to 1040 second time interval, 100,000 MJ more energy is released for the benchmark case (See Figure 9). This difference is the main reason why there is a second pressure peak in the RELAP5 benchmark, WGOTHIC, and CONTAIN calculations and not in the RELAP5 integrated calculation. Figure 10 shows that for the same time interval, the break mass release is similar for the two RELAP5 cases. Thus with the higher energy release and similar mass release for the benchmark case, the specific energy of the break effluent is higher.

Without the benefit of an RCS analysis after 40 seconds, Westinghouse made conservative assumptions regarding the energy state of the RCS and the speed at which stored metal and secondary fluid energy are released to the primary system and then to the containment. It was not possible to separate and quantify the various components of the Westinghouse release model to compare it to the more phenomenological RELAP5 RCS model. However two of the effects were estimated based on the two RELAP5 calculations.

The effect of different decay heat models appears to be very small. Westinghouse uses the 1979 ANS decay heat standard with a 2σ uncertainty added. The RELAP5 analysis used the same standard without the uncertainty. The effect of the uncertainty is about 3.6% and amounts to only about 1,600 MJ over the 1000 second time interval.

The effect of rapidly releasing secondary energy could be very significant. Figure 11 shows the total integrated energy gain of the fluid flowing through the steam generator tubes after 30 seconds for the RELAP5 integrated model case. This start time is the beginning time for the Westinghouse rapid exponential secondary energy release used in the benchmark case. As shown in the figure, the primary system energy gain through steam generator heat transfer during the 30 to 1030 second time interval is

Figure 8. RELAP5 AP600 Large Break LOCA
IRWST Vent Energy Flow Comparison

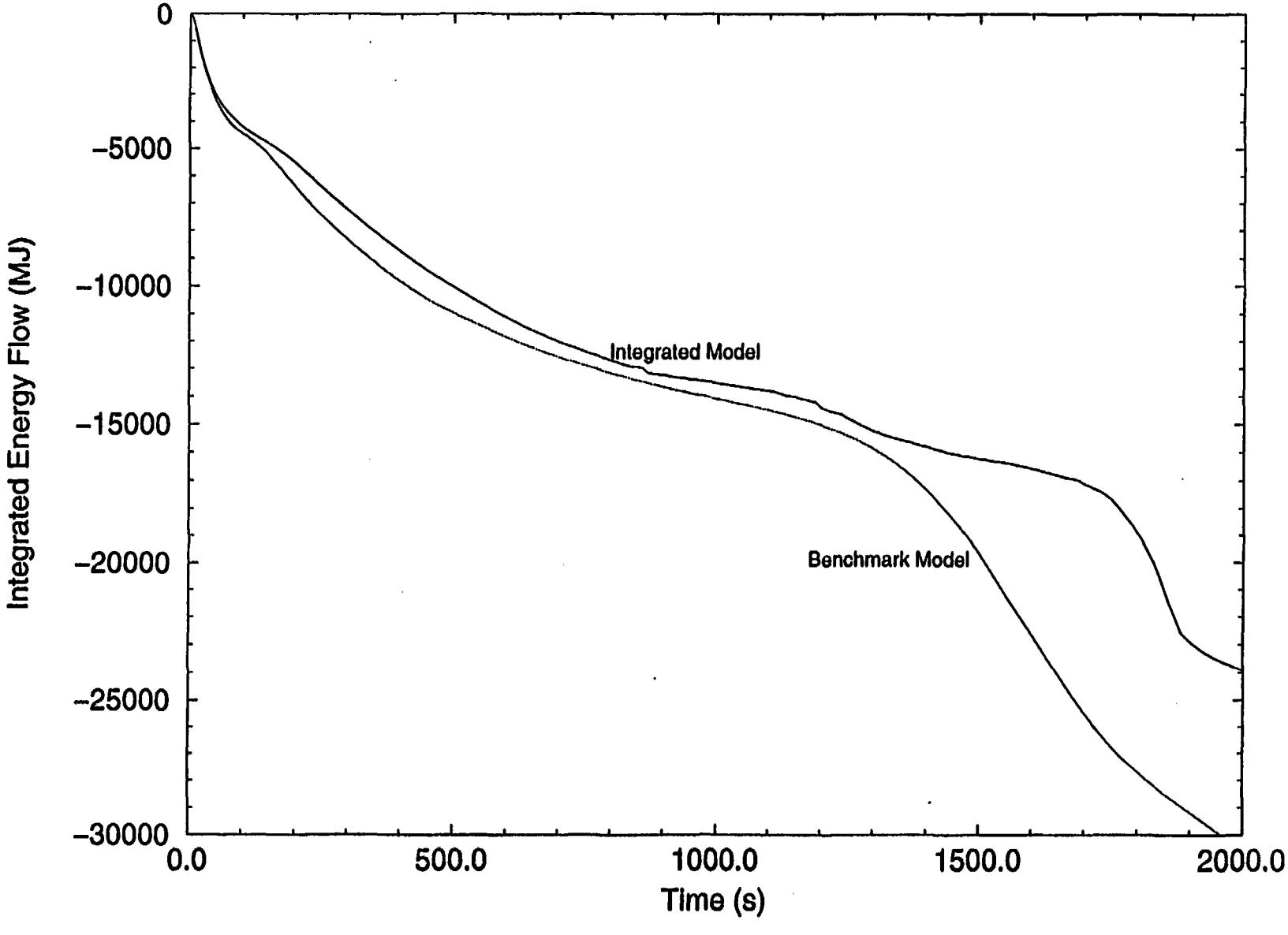

Figure 9. RELAP5 AP600 Large Break LOCA
Break Energy Release Comparison

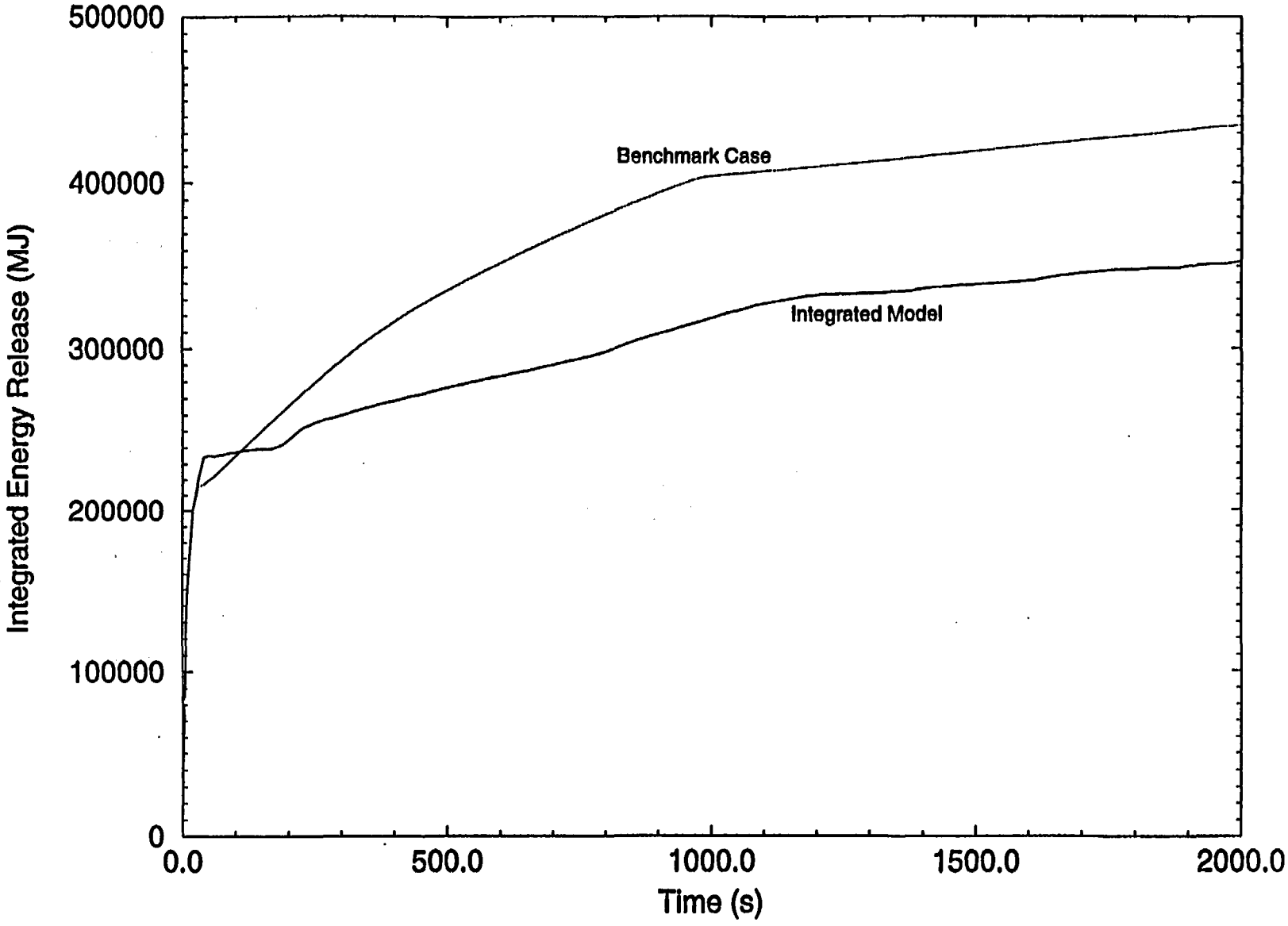

Figure 10. RELAP5 AP600 Large Break LOCA
Break Mass Release Comparison

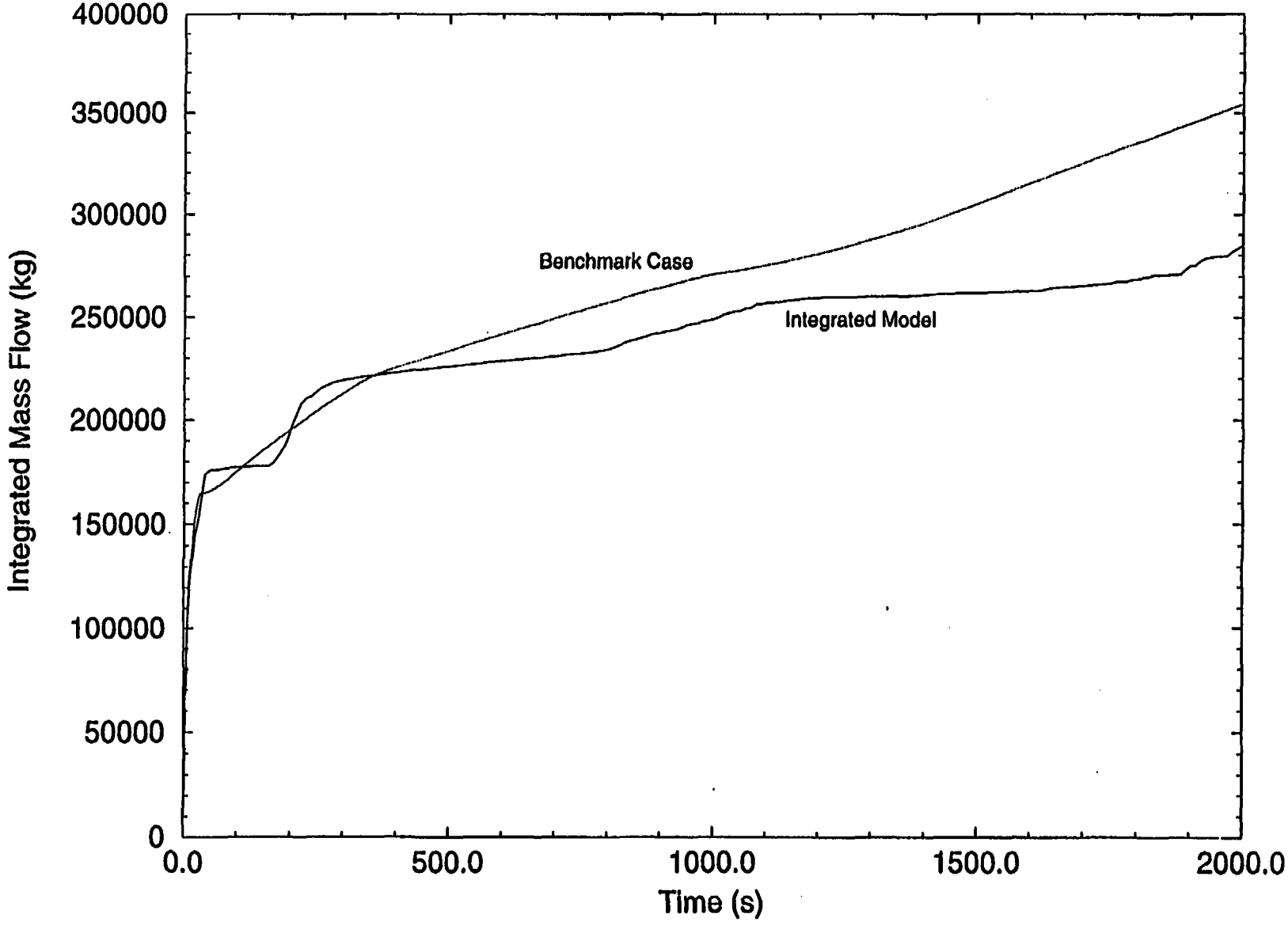

Figure 11. RELAP5 AP600 LBLOCA Integrated Model
Integrated Primary Steam Generator Energy Pickup

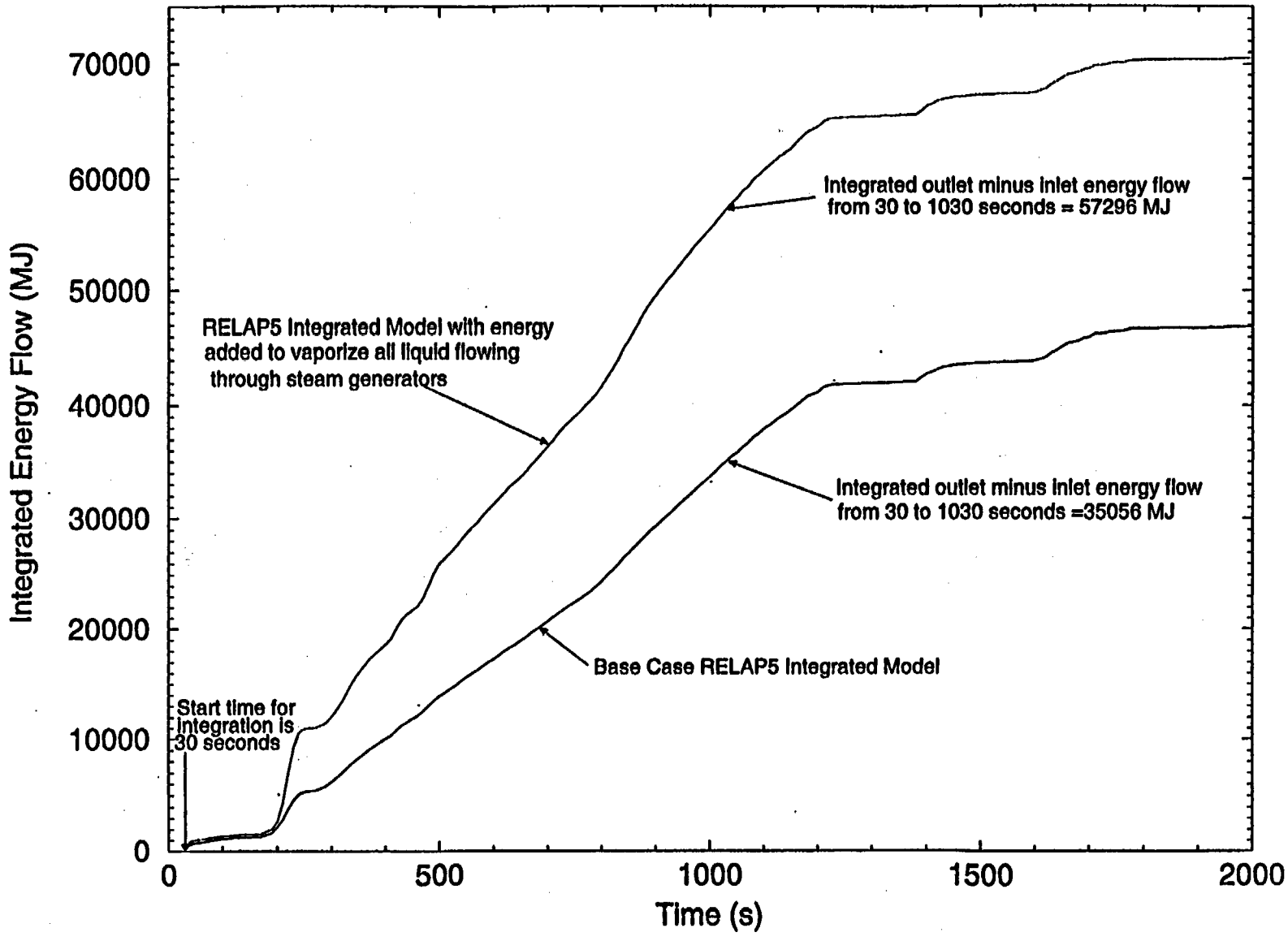

35,056 MJ for the integrated case. Also shown on the figure is the energy gain for the same time period if all of the vapor flowing through the steam generators, that was not vaporized, is now vaporized regardless of the heat transfer. The value for this energy gain is 57,296 MJ. This is a measure of the maximum possible secondary to primary heat transfer, since the outlet enthalpy is assumed to be all vapor and the secondary side temperature has not dropped accordingly to produce the extra primary energy gain. Also the steam generator primary side exit temperatures are nearly equilibrated to the secondary side temperature. The difference between these two cases is about 22,000 MJ or only about 22% of the energy release difference between the integrated and benchmark cases.

In their post-blowdown energy release model Westinghouse uses a value of 260F (400K) for the final equilibrium temperature. For the exponential, they assume that the secondary temperature of the broken loop steam generator has decayed to 99% of that value in 1830 seconds (one-half hour after end of blowdown). For the intact loop generator, the time is one hour after end of blowdown. In the RELAP5 integrated analysis, the steam generators are isolated within 15 seconds. That is, the feedwater flow is isolated and the main steam isolation valves are closed. Thus, the principal change in secondary energy content is via heat transfer through the SG tubes. Thus, a measure of the heat loss to the primary system is to track the water temperature in the SG secondary. Figure 12 shows the secondary side liquid temperature of each generator. Figure 12 also shows the secondary side temperatures assuming the temperature decay model used in Westinghouse energy release model and using the temperatures calculated by RELAP5 at 30 seconds as the starting temperatures for the exponential temperature decay. The temperature drop is about 2.8 times greater for each generator during the 1000 second time interval. If that factor is applied to the best estimate energy release shown in Figure 11, the energy gain by the primary due to heat transfer from the secondary assuming the Westinghouse exponential release model would be about 98,000 MJ. Nearly all of this energy would then be released through the break during this time period. Thus, the rapid secondary to primary heat release assumed by Westinghouse could account for most of the "excess" energy release to the containment during the time preceding the second containment pressure peak.

3.2.3 EFFECT OF BREAK FLOW PHASIC ENERGY SPLIT

Reference 1 showed that the phasic energy split of the break effluent can have a substantial effect on containment pressure for a small break. That is, if more energy is discharged as steam, it will rise in the gas phase to the upper containment and contribute to a higher containment pressure. However, if more energy is associated with warmer effluent water, this will contribute more to warmer sump water and less to a higher containment pressure.

For this study a break repository was defined in order to evaluate mass and energy disposition in the containment nearest the break junctions. The repository was taken as volumes 90503 and 90504 (See Figure 2). In the integrated case these are the containment volumes that receive break effluent from the RCS. In the benchmark case break effluent is deposited only in volume 90503 (See Figure 3). However, to make a consistent comparison, the repository is still taken as both volumes 90503 and 90504. In addition to the break, there are three junctions connecting the repository to the rest of the containment. One junction goes upward from the repository to the steam generator chimney from whence it goes to the upper containment. The second junction goes downward to the sump. The third junction connects the vessel cavity to the repository via the hot and cold leg pipeways.

To explore the energy and mass disposition in the repository, the average values of mass and energy flows were derived from integrated flows during the 40 to 1040 second interval. Figure 13 shows the average energy flow through the four repository junctions over the time interval for the two cases. In addition, the average energy flow to the heat structures is shown. Figure 13 shows that the larger break energy flow in

Figure 12. RELAP5 AP600 LBLOCA Integrated Model
Steam Generator Secondary Temperatures

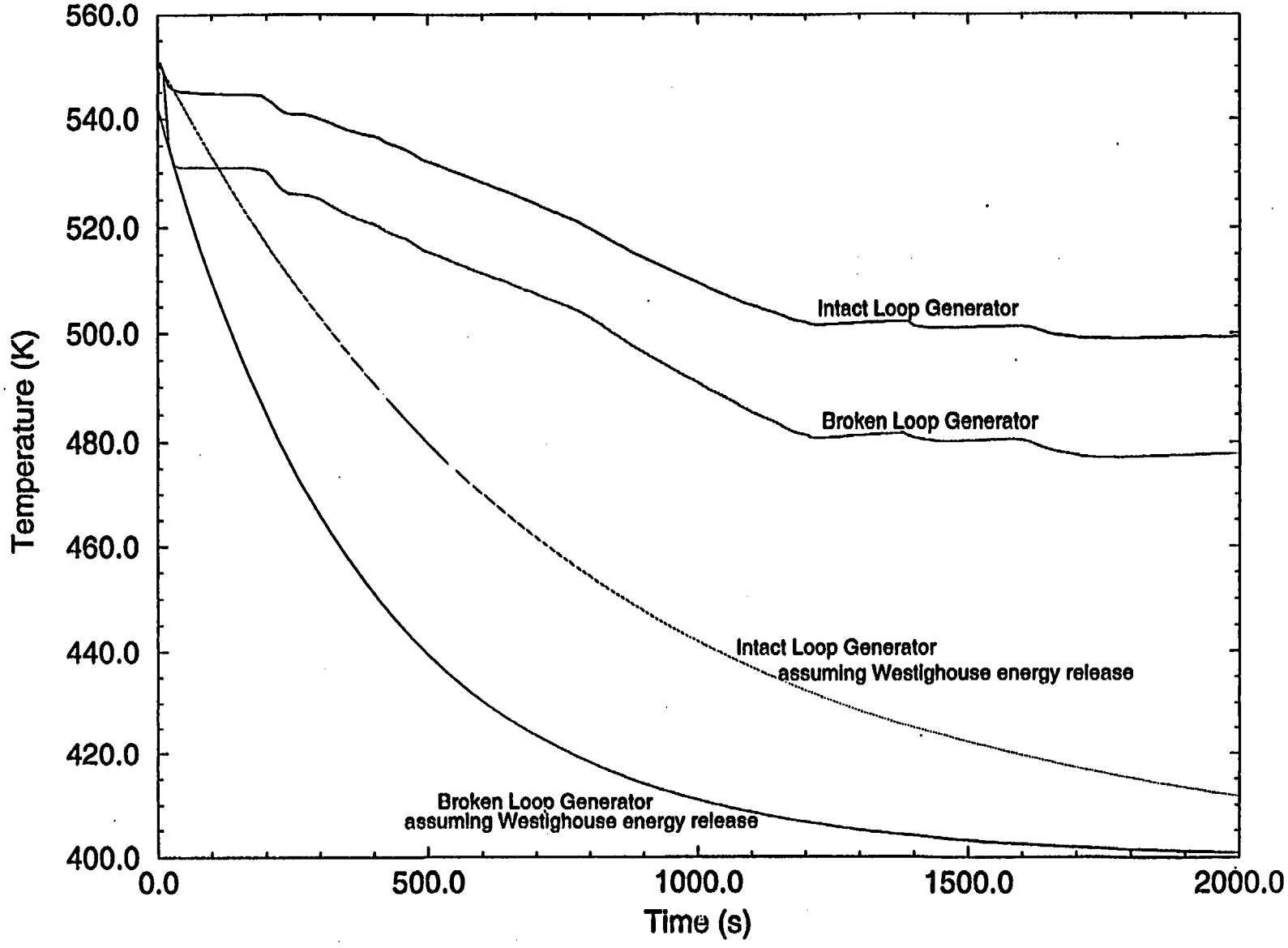

Figure 13. RELAP5 AP600 Large Break LOCA
Break Repository Average Energy Flow from 40 to 1040 Seconds

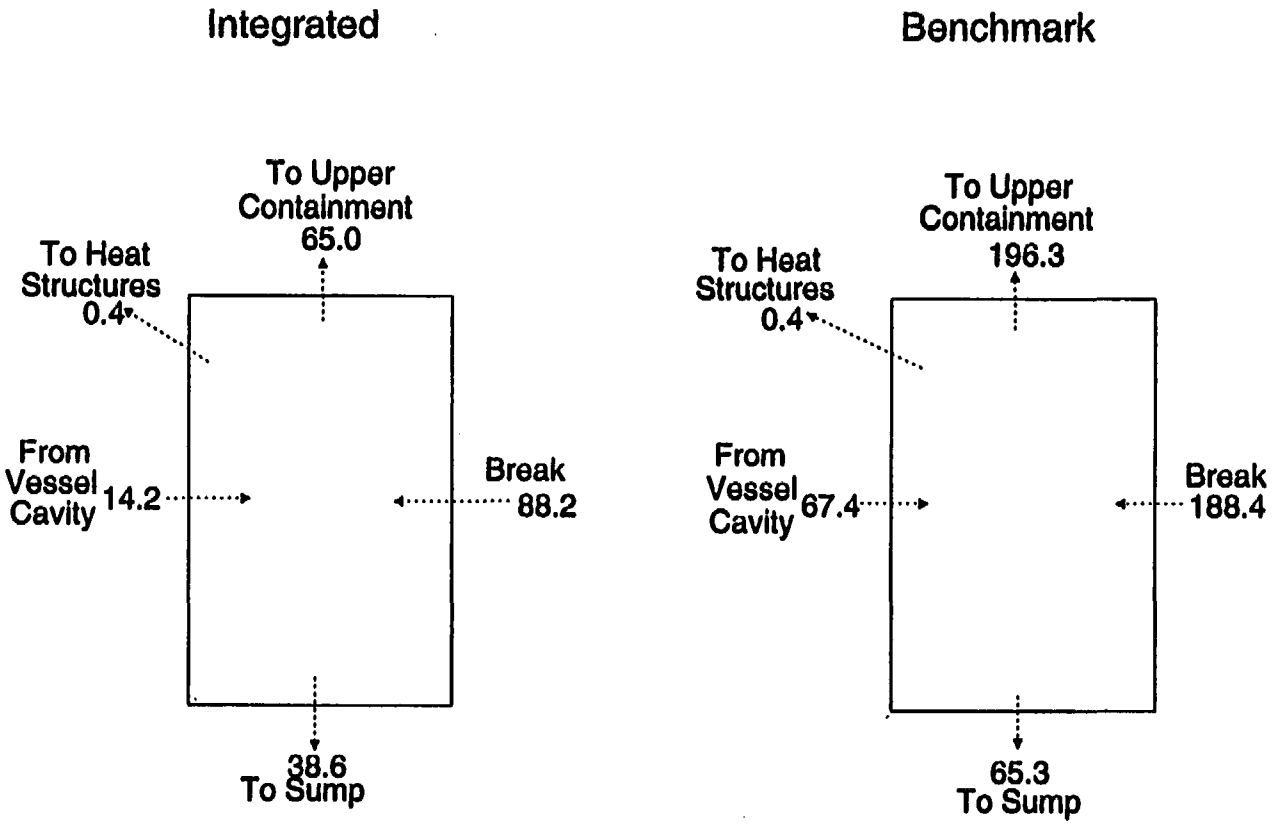

Average Energy Flows in MW

the benchmark case results in a much larger energy flow to the upper containment. Also the buoyant effect of the additional heat causes more gas to be convected across from the vessel cavity.

The average mass flows for the repository junctions are shown in Figure 14. The figure shows that relatively little phase change occurs in the repository in either case The water that comes in from the break goes down toward the sump. Steam that comes in from the break goes up to the upper containment. Since most of the excess break energy is associated with the steam in the benchmark case, it is not at all surprising that most of that energy goes to the upper containment and contributes to the higher second pressure peak.

3.3 SENSITIVITY TO INTERNAL CONTAINMENT SHELL HEAT TRANSFER

References 2 and 3 provide a number of sensitivity studies using CONTAIN and WGOTHIC and the FSAR mass and energy release. Since energy release played such a dominant role in the results of the two RELAP5 calculations, it was decided to explore the effect of a key parameter (internal containment shell heat transfer) when the "best estimate" RELAP5 release model is used in the integrated calculation. Although the RELAP5 natural convection condensation heat transfer model should be reasonably applicable to inside vertical containment walls, it may not be applicable to the inner containment dome and has not been specifically assessed against AP600 or other containment data. If the internal shell heat transfer is thought to be too "optimistic," the importance of the effect of energy release on containment pressure could be questioned.

Figure 15 illustrates the effect of multiplying the internal shell heat transfer coefficient by factors of 1/3 and 3 on the containment pressure for the integrated case. As can be seen, even a reduction by a factor of three in the heat transfer coefficient does not result in a second pressure peak. Increasing the heat transfer by a factor of three has relatively little effect, because the limiting resistance is the external shell PCCS heat transfer.

3.4 SENSITIVITY TO EXTERNAL CONTAINMENT SHELL HEAT TRANSFER

Analysis of the OSU experimental data demonstrated the substantial heat removal capability of the core makeup tanks (CMTs) and the IRWST for the long term (Reference 9). These two heat sinks provide the required RCS cooling until sump injection begins sometime after about 20,000 seconds. For this reason it was postulated that with a "best estimate" RCS energy release to the containment, significant external containment heat removal may not be required until much later than the 300 to 1000 seconds assumed in the Westinghouse design basis analysis. Therefore, two sensitivity studies were performed using the integrated model and varying the external shell heat transfer coefficients.

In the first study, the "dry" heat transfer coefficients shown in Figure 6 were applied to all external shell surfaces, to simulate no PCCS cooling. In the second study, "wet" coefficients were applied only to 56% of the dome and not at all to the cylindrical shell. That is, PCCS water coverage was only applied to 20% of the total available containment surface. Figure 16 shows the results of the two sensitivity studies compared to the base case integrated RELAP5 calculation. As postulated, the heat sink capability of the CMTs and IRWST is sufficient to prevent a significant containment pressure increase for all cases including the "dry" wall case until about 20,000 seconds. For that case, the design pressure is not reached until nearly 100,000 seconds. The case with the "dry" cylindrical shell (20% total coverage) is well below the design pressure at 100,000 seconds and does not appear to be heading for a significant second pressure peak. Calculations using a "best estimate" energy release from an integrated RCS/containment model show significant margin for the time required to cool the containment shell , even for severely degraded PCCS cooling.

Figure 14. RELAP5 AP600 Large Break LOCA
Break Repository Average Mass Flow from 40 to 1040 Seconds

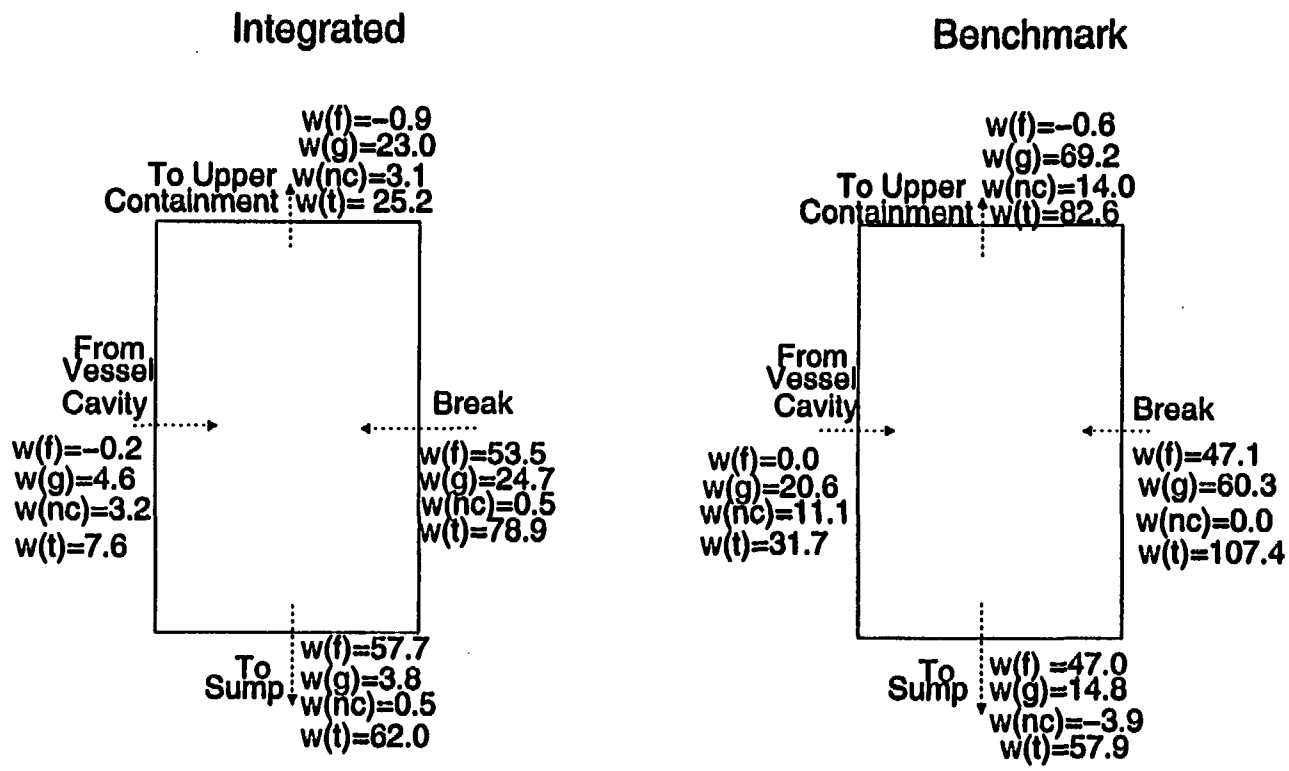

w(f) – liquid flow
w(g) – steam flow
w(nc) – non-condensable flow
w(t) – total junction flow

Average Mass Flows in kg/sec

Figure 15. AP600 LBLOCA Integrated RELAP5 Model
Containment Pressure Sensitvity to Inside Wall Heat Transfer

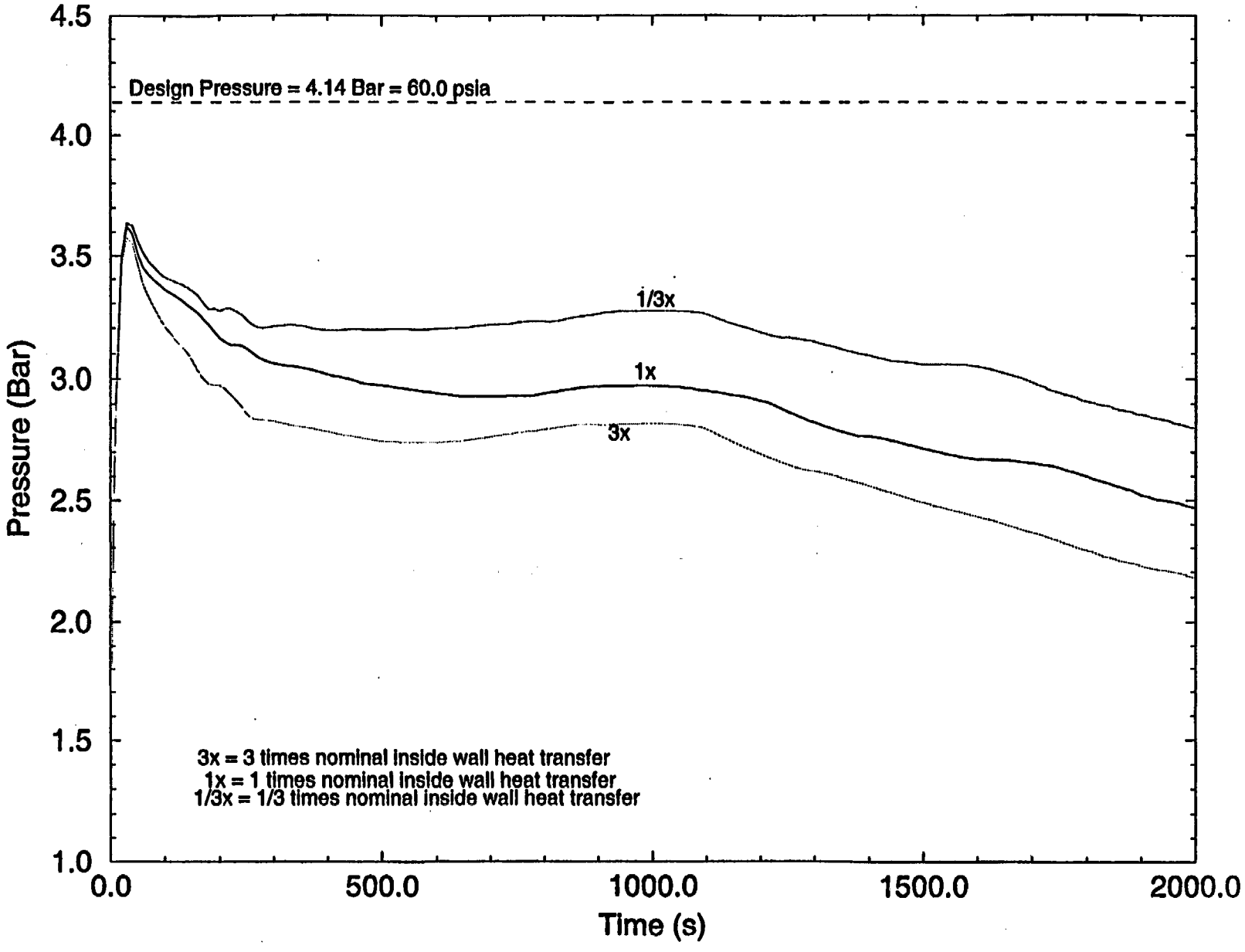

Figure 16. AP600 LBLOCA Integrated RELAP5 Model
Containment Pressure Sensitivity to PCCS External Heat Transfer

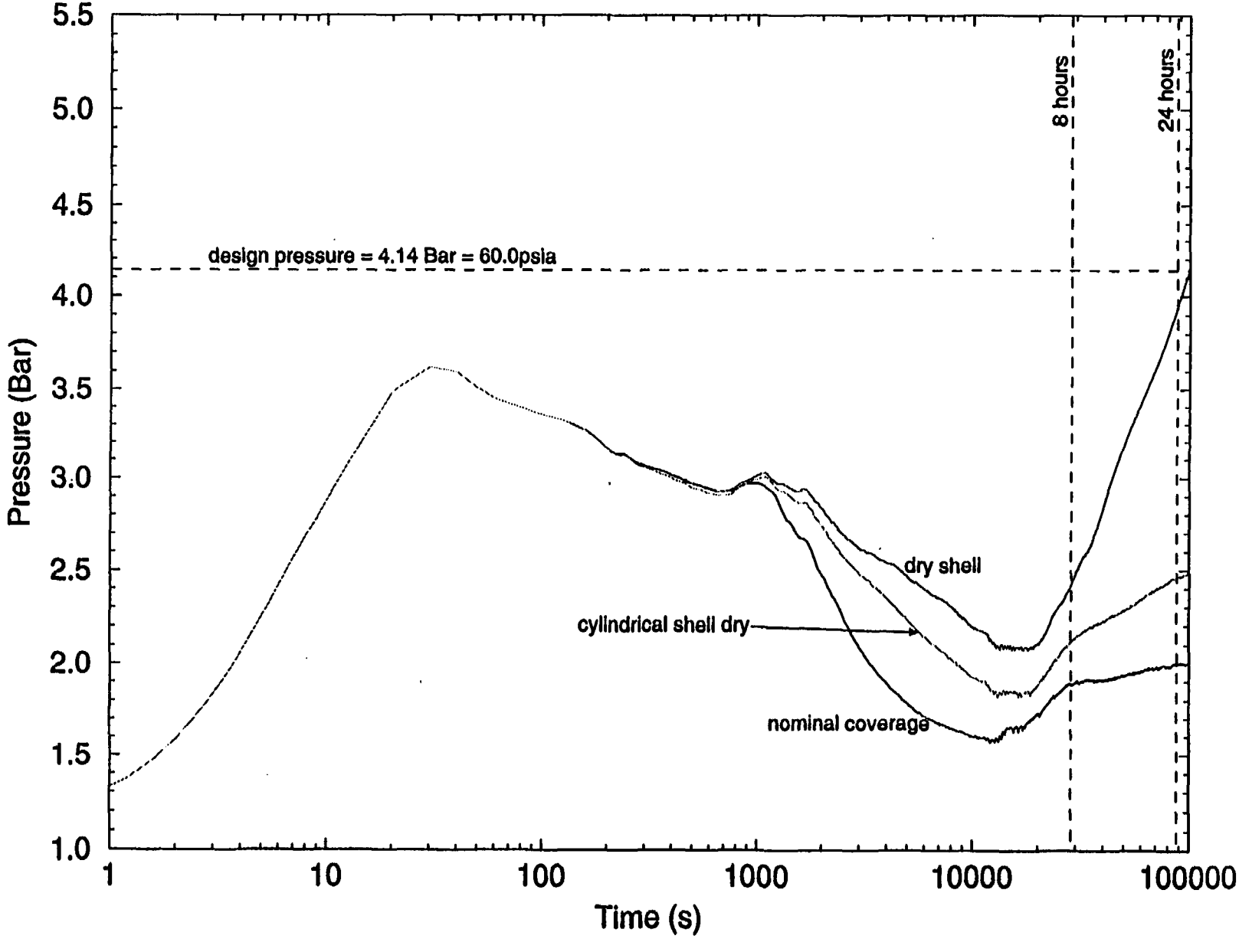

4. CONCLUSIONS

Even though RELAP5 containment models are not well assessed, the code has been benchmarked against a limited set of analyses using well known containment codes. In those cases, the RELAP5 calculated containment pressure is comparable to CONTAIN and WGOTHIC results, when the same FSAR mass and energy release is used, and when CONTAIN outer shell heat transfer coefficients are used.

By using the integrated RELAP5 RCS/containment model, which calculates "best-estimate" RELAP5 mass and energy release to the containment, the second and highest containment pressure peak disappears. This is because: (1) the FSAR energy release in the evaluation models is significantly higher than the "best-estimate" release calculated by RELAP5, and (2) the excess energy in the FSAR release goes upward as steam to the upper containment. This is because Westinghouse assumes a conservative energy partition between water and steam coming from the break, based on an accepted and approved methodology for licensing analysis.

A factor of three reduction in the inside shell heat transfer coefficient still does not result in a high second containment pressure peak for the integrated model with "best-estimate" energy release.

Calculations using a "best estimate" energy release from an integrated RCS/containment model show significant margin for the time required to cool the containment shell , even for severely degraded PCCS cooling.

5. REFERENCES

1. G. N. Lauben, Containment/RCS Modeling of a One-Inch Small Break Loss-of-Coolant Accident in the AP600 Using RELAP5 and CONTAIN, RPSB-98-01, April 1998.

2. J. Woodcock, et. al., WGOTHIC Application to AP600, WCAP-14407 (Revision 1), July 1997.

3. K. Campe & J. Kudrick, Evaluation of AP600 Containment Thermal Hydraulic Performance, NUREG-1632, June 1998.

4. C. B. Davis, et. al., Evaluation and Assessment of RELAP5/MOD3 Version 3.2.1.2 for Simulating the Long-Term Phase of Small Break Loss-of-Coolant Accidents in AP600, INEL-96/0395, October 1996.

5. Westinghouse Electric Corporation, AP600 Standard Safety Analysis Report, DE-AC03-90SF18495, Revision 22, April 6, 1998.

6. W. L. Jensen, Design Basis Containment Pressure Analysis for AP600 Using the CONTEMPT Code, transmitted via memo from R. Caruso to R. Barrett, August 3, 1993.

7. J. Tills, Letter to R. Griffith - Revised CONTAIN Calculations of an AP600 SBLOCA, June 20, 1996.

8. RELAP5/MOD3 Version 3.3 Code Manual - Volume IV: Models and Correlations, to be published.

9. D. Bessette, et. al., Phenomenology Observed in the AP600 Integral Systems Test Programs Conducted in the ROSA-AP600, APEX, and SPES-2 Facilities, RPSB-98-04, April 1998.

BGE Life Cycle Management Project

Calvert Cliffs Plant Aging Management Activities and Lessons Learned

Water Reactors Safety Information Meeting
October 28, 1998

Barth Doroshuk
Marvin Bowman
Life Cycle Management Project

Slide 1

LCM 98-061

BGE Life Cycle Management Project

Presentation Objectives

- Provide overview of aging effects findings for Calvert Cliffs
- Discuss new inspection activities to support long term operation
- Discuss timing of implementing activities at Calvert Cliffs

Slide 2

LCM 98-061

BGE Life Cycle Management Project

Calvert Cliffs Aging Management Activities for License Renewal

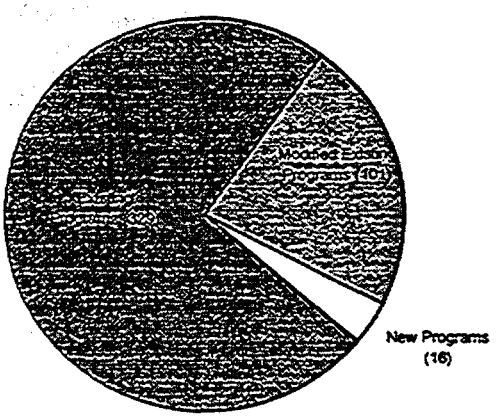

Slide 3

LCM 98-061

BGE Life Cycle Management Project

Existing Calvert Cliffs Aging Management Programs & Procedures Relied on for License Renewal

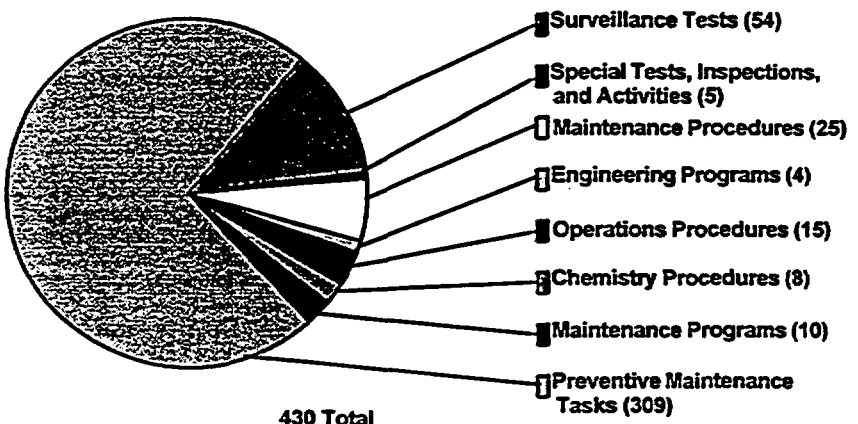

Slide 4

LCM 98-061

BGE

Life Cycle Management Project

New and Modified Aging Management Programs and Analyses for Calvert Cliffs

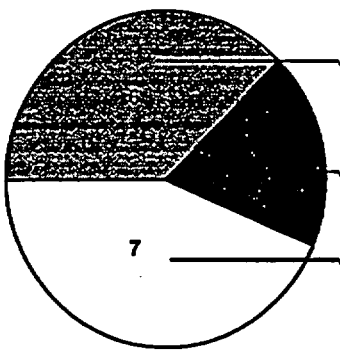

Category	Program	LRA Sections
Extend Existing Engineering Analyses	RCS non-Pressure Boundary Alloy 600 components	1
	Spent Fuel Rack Neutron Absorber	1
	Fatigue Evaluations	7
	LTOP & PT Curves	1
	Containment Tendon Prestress Loss	1
	SCC of CEA Shroud Bolts	1
New Engineering Analyses	Leak-Before Break for RWST Penetrations	1
	Stress Relaxation of CEA Shroud Bolts and Core Shroud Tie Rods	1
	Thermal Aging of Cast Austenitic Stainless Steel	2
New Inspection Programs	ARDI - Mechanical & Piping	21
	ARDI - Electrical & Cables	2
	ARDI - Civil & Component Supports	1
	Buried Pipe	2
	Caulking & Sealants	1
	DFO Tank Internals	1
	Supports Baseline Walkdowns	1

Slide 5

LCM 96-061

BGE

Life Cycle Management Project

Extend Alloy 600 Program beyond Pressure Boundary Components

- **Aging Statement**
  - Alloy 600 components develop stress corrosion cracks in primary coolant environment
- **Inspection Activity**
  - Evaluate susceptibility to cracking of non-pressure boundary Alloy 600 components
- **Schedule -**
  - Add non-pressure-boundary components to existing program - spring 1999
  - Perform susceptibility analysis and initiate plan for inspection or replacement if necessary - spring 1999

Slide 6

LCM 96-061

BGE Life Cycle Management Project

Evaluate Refueling Water Tank Penetrations

- **Aging Statement**
  - Penetrations with stiffener plates may establish environments conducive to stress corrosion cracking
- **Inspection Activity**
  - Determine if refined inspections are advisable
- **Schedule**
  - Perform engineering evaluation to confirm adequate structural integrity remains upon detection of leakage caused by stress corrosion cracking - summer 2001
  - alternatively, include penetrations in Age Related Degradation Inspection program

Slide 7

LCM 98-061

BGE Life Cycle Management Project

Age Related Degradation Inspection of Piping

- **Aging Statement**
  - Stagnant portions of systems may degrade differently than portions exposed to the normal flow stream
- **Inspection Activity**
  - Confirm effectiveness of chemistry controls
  - Establish applicability of existing inspection results
  - Focus inspections to obtain the best value
- **Schedule**
  - Develop methodology - complete
  - Prepare administrative procedure and technical requirements document - winter 1998
  - Prepare inspection plan - spring 1999

Slide 8

LCM 98-061

Age Related Degradation Inspection of Electrical Cables

- Aging Statement
  - Cable insulation degrades with extended exposure to elevated temperatures
- Inspection Activity
  - Establish the population of cables that will exceed service limits
- Schedule
  - Perform thermal survey to define bounding locations - complete
  - Install temperature probes and collect data - complete
  - Compare peak cable service temperatures to 60-year service limiting temperatures - complete
  - Establish corrective actions where limits will be exceeded - 2010

Age Related Degradation Inspection of Electrical Panels

- Aging Statement
  - Panels and enclosed terminal blocks may degrade with time
- Inspection Activity
  - Incorporate all panels into program of periodic inspections
- Schedule
  - Establish the population of panels not presently subject to periodic inspections - complete
  - Establish inspection requirements and implement inspections - first quarter 2001

Age Related Degradation Inspection of Component Supports

- **Aging Statement**
  - Certain component supports may not be accessible but have degradation bounded by accessible supports
- **Inspection Activity**
  - Determine if augmented inspections are advisable
- **Schedule**
  - Establish action items to develop and implement inspection program for inaccessible supports - spring 1999

Buried Pipe Inspection

- **Aging Statement**
  - Degradation rates of buried piping can vary significantly as a result of design, installation, and operation factors
- **Inspection Activity**
  - Confirm effectiveness of design features (installation practices, coatings and cathodic protection)
- **Schedule**
  - Establish action item milestones for program development & implementation - complete
  - Complete assessment to provide basis for scope - fall 1998
  - Develop, review, and approve program - spring 1999
  - Implement program - fall 1999

BGE Life Cycle Management Project

Caulking and Sealants Inspections

- **Aging Statement**
  - Elastomeric sealants degrade with time
- **Inspection Activity**
  - Determine if existing inspection practices (e.g. plant walkdowns, fire barrier inspections) need augmentation for barrier seals with other functions (e.g. internal flooding)
- **Schedule**
  - Establish and implement action plan - spring 1999

Slide 13

LCM 98-061

BGE Life Cycle Management Project

Fuel Oil Storage Tank Internals Inspections

- **Aging Statement**
  - Degraded internal coatings of carbon steel storage tanks can lead to corrosion
- **Inspection Activity**
  - Confirm effectiveness of coatings and cathodic protection
  - Confirm effectiveness of operating practices
- **Schedule**
  - Establish milestones for program development & implementation - complete
  - Establish PM tasks to schedule and perform the inspections - winter 1999

Slide 14

LCM 98-061

Extend Component Supports Baseline Walkdowns

- Aging Statement
  - Environmental conditions may degrade component supports
- Inspection Activity
  - Conduct sampling inspection of in-scope supports that were not subject to Seismic Verification Project or ISI
- Schedule
  - By winter 1998 develop action plan to
    - » Establish inspection criteria and sample size
    - » Perform walkdowns & document results

Summary Observations

- Aging Effects
  - no aging unique to license renewal has been discovered
- Inspection Activity
  - Current Inspection activity on site plus some additional will more than reasonably assure aging is managed regardless of "age"
- Benefits of Early Efforts
  - By applying engineering resources with a "long term" perspective, BGE has been able to plan for the long term safety and reliability of Calvert Cliffs

Technical Challenges for Life Cycle Management — Oconee Nuclear Station

Rounette K. Nader, Debra V. Ramsey, Michael G. Semmler, R. Paul Colaianni, Gregory D. Robison

Duke Energy Co.

Abstract

Life Cycle Management (LCM) is one of the keys to the future operation of Oconee Nuclear Station, since thinking, planning, and acting within a structured business-minded process is required now more than ever. Plant staff and management must recognize the need for integrated, holistic processes that identify and address the life limiting issues that are facing Oconee.

The potentially life limiting issues for nuclear power plants (NPPs) come from a variety of sources but can be grouped into five categories of concern: Technical, Regulatory, Environmental, Political, and Economic. With focus on these five categories, engineers are able to view issues based on the source of the concern and to measure their impacts on their nuclear business. Many common LCM concerns exist, but the importance of each will vary from NPP to NPP depending upon relative significance of the source to that particular NPP. This paper stresses the following technical challenges faced by Oconee Nuclear Station:

- Obsolescence of component technology
- Lack of spare parts
- Material aging

The Business of Nuclear

Each NPP in operation today was conceived as a way to provide needed power generation with a corresponding value returned to the plant's owners and investors. This statement defines the business of nuclear power just as it describes businesses in many other sectors of society. The business of nuclear power has never been simple, but the struggles required to deal with the complexities have been more than offset by the value added by the operation of these plants. Oconee Nuclear Station is a three-unit site licensed in 1973 and 1974 with a combined generating capacity of 2538 megawatts. The station continues to be a valuable generating asset for Duke Power, and through a systematic process of thinking, planning, and action, future plant operations can continue to provide needed generation while corresponding value is returned to Duke Energy and its investors. For Oconee, this process is called Life Cycle Management.

Importance of Life Cycle Management

The driving force behind LCM at Oconee is the desire to predict and address the challenges that the plant will face in the future. Many of these challenges, if not appropriately addressed, can significantly limit or even end the life of the station. Each year, an increasing amount of nuclear generating capacity is lost due to extended outages and shutdowns associated with LCM issues. Implications of this lost generation range from decreased revenues for the utilities to the possibility of power outages in the regions with a limited surplus of electricity. In the long run, the future operation of today's NPPs depends largely on how well the staff and management of operating facilities are able to master the challenges of LCM.

Challenges for Life Cycle Management

The potentially life limiting issues for NPPs come from a variety of sources but can be grouped into five categories of concern: Technical, Regulatory, Environmental, Political, and Economic. While the topic of this paper focuses on the technical challenges, key aspects of each group of challenges are noted here:

Technical

- Obsolescence of component technology
- Lack of spare parts
- Material aging

Regulatory

- More stringent regulations that, in turn, could direct physical plant changes and have an economic impact
- Industry operating issues that again, in turn, could direct plant changes and have an economic impact

Environmental

- Impact of increased amount of spent fuel
- Disposal sites for low level radioactive waste

Political

- Strategic objective of the utility, region and country
- Concerns of surrounding residents and neighboring area

Economic

- Deregulation
- Privatization or change of ownership
- Return on investment and meeting financial targets
- Cost of production

For Oconee Nuclear Station, each of these areas has been and continues to be analyzed in order to understand how our future business may be affected by these concerns and risks. Several iterations of these reviews were performed with increasing levels of detail. Our initial reviews in the early 1990s concentrated on the economic viability of continued operation, while our more recent analyses have focused on plant level details in preparation for plant license renewal.

Technical Challenges: A Systematic Approach

In an effort to effectively think, plan, and act on specific technical LCM concerns, a systematic approach was adopted at Oconee Nuclear Station. Engineering assessments investigated applicable aging and regulatory issues to determine the future plant equipment replacements and improvements needed for optimum operation within the regulatory environment. A long-range plan was instituted to capture all of the issues and provide a means for collectively reviewing the issues. The need for a solution to a particular problem related to obsolescence or aging can be prioritized relative to all other issues. Some examples of these particular issues at Oconee Nuclear Station are presented herein.

Obsolescence of Component Technology

Obsolete component technology can cripple the operation of a NPP. Oconee Nuclear Station is dedicated to upgrading components to avoid the crippling effect of obsolescence. Many large components have been replaced recently, particularly computer-related components. As obsolescence becomes an issue for a particular component or component type, engineering studies are performed to determine feasible replacement options. Management has taken an active role in authorizing and allocating money for replacement of these components.

Oconee Nuclear Station recently completed a replacement of obsolete computer technology on each unit. The Operator Aid Computer (OAC) performs plant calculations, event alarming, and extensive equipment condition monitoring for the operator. The operation of the OAC is not required by regulation but is a vital part of the operator's collective unit control and monitoring system. Loss of the OAC function increases operator work for Technical Specification surveillance and may result in reduced unit capacity or even loss of the ability to run the unit. The OAC was procured in the late 1960s and was connected in tandem with computers that were added in the 1980s. Spare parts for the computer had become unavailable or obsolete, and custom manufactured parts had become cost prohibitive. Hardware maintenance and software programming expertise had become unavailable within Duke Power and in the rest of the industry. Finding someone with maintenance or programming support experience for these computers had become increasingly difficult. Additionally, the computers were not Year 2000 compliant. The computers have now been replaced on all three Oconee units at a cost of $27 million. The expected life of the replacement OAC systems is ten years due to the advancing technology and expertise required to maintain them. The replacement systems have been specified so that individual components of the systems can be replaced as older technology becomes obsolete, without requiring replacement of the entire OAC system. This example demonstrates that the issue associated with obsolescence of component technology will continue to challenge Oconee Nuclear Station.

Lack of Spare Parts

Duke Power's Commercial Grade Program is dedicated to managing the spare parts challenge at its NPPs. Procurement Engineering personnel are responsible for the program implementation as well as for performing the analysis required to dedicate commercial components for nuclear applications that require quality assurance (QA).

Due to the age of Oconee, many of the original equipment suppliers, particularly those of electronic equipment, are no longer in business or simply no longer support their previous product lines. Often, a procurement engineer does not learn that the product is unavailable until he reorders a part. Lack of spare parts is a growing problem that is difficult to assess for the future because it occurs with greater frequency as time passes.

When the ability to obtain spare parts for a given component is discovered, interim solutions vary. In some cases, Duke has purchased all the items in the manufacturer's stock. In other cases, we have worked with the Oconee NSSS vendor group, Babcock & Wilcox Owners' Group (BWOG), to procure parts from other plants. These "fixes" only resolve the spare parts issue momentarily; eventually, these components will have to be replaced.

Unique equipment challenges exist for Oconee because of the separate hydro-electric facility (as opposed to diesel generators) which provides emergency power to the nuclear station. Many parts for the hydro station components are not available under a vendor's QA program. For example, none of the replacement parts for the Westinghouse voltage regulator are available under the Westinghouse QA program and in many cases are no longer manufactured by Westinghouse. There are a few critical spare parts in inventory, but the time quickly approaches when the decision on an alternative must be made before the issue impacts the operation of the nuclear station. Duke will probably be forced to replace the regulator in the next few years.

Lack of spare parts requires a dedication from the site in the form of an allocation of Engineering resources and a budget for replacement modifications. Based on the experiences at Oconee Nuclear Station, lack of spare parts will become more of a reality, especially if the operating license is extended for an additional twenty years. Lack of spare parts is an issue that must be considered when analyzing and planning for future operation.

Material Aging

It was recognized early in the Oconee License Renewal process that planning for License Renewal would not only position the facility for extended operations, but would also be beneficial in optimizing operations for the remainder of the facility's currently licensed plant life. Further, conducting the systematic technical analysis required for license renewal would provide important technical information in a more sophisticated and well-documented manner that would prove valuable in managing the life of plant hardware as related to material aging.

The development and processing of the Oconee License Renewal application is one endpoint of the more detailed approach to Oconee LCM. The main purpose of the License Renewal Application is to demonstrate to the United States Nuclear Regulatory Commission (USNRC) that Oconee can be operated in a safe manner for twenty years beyond the existing forty year licensed life. Embodied within license

renewal is the principle that the current regulatory process is adequate to ensure that the licensing basis of all currently operating plants provides and maintains an acceptable level of safety, with the possible exception of the detrimental effects of aging on the functionality of certain plant systems, structures, and components (SCCs) in the period of extended operation.

To prepare the License Renewal Application for Oconee Nuclear Station, the License Renewal Project Team followed a systematic process to assess material aging in the plant. Age-related degradation of active components are fairly easily detected; normal pump operation or performance testing will indicate a declining performance trend, or motor-operated valve stroke time testing will indicate declining motor performance. The License Renewal approach was designed to focus on the passive components in the plant, i.e., components without moving parts whose gradual degradation will not be monitored through normal operation or performance testing. By following the approach laid out by the License Renewal Rule, the Oconee License Renewal Project Team mechanistically determined the aging effects that could cause loss of function of these passive components and the programs and activities needed to manage material aging. For the purposes of operating Oconee Nuclear Station to the end of its current license term, the license renewal results have provided needed insight into aging issues and the kinds of activities required to manage the material aging challenge.

The following sections provide some examples of technical issues that were addressed during the license renewal evaluation for Oconee.

Structures

One of the structural issues associated with the extended period of operation was loss of prestress over time in the Containment post-tensioning system. Loss of prestress is due to material strain occurring under constant stress. Loss of prestress over time was accounted for in the design of the post-tensioning system. By assuming an appropriate initial tensile loading stress and using appropriate prestress loss parameters, the magnitude of the design losses and the final effective prestress at the end of 40 years were calculated at the time of initial licensing. Extending the analysis to 60 years was crucial in determining whether the post-tensioning system would remain capable of performing its intended functions as installed for an additional 20 years, need to be re-tensioned, or need to be replaced.

The analysis (as described in Oconee Selected Licensee Commitment and developed using the guidance of Regulatory Guide 1.35) determined that the final effective prestress after 60 years of operation would reasonably ensure the ability of the post-tensioning system to perform its intended functions for the extended period of operation.

Mechanical System Components

One mechanical issue that was identified while analyzing thermal fatigue effects of piping designed to USAS B31.1 was excessive thermal cycling of one section of piping. Piping designed to this Code is allowed 7000 thermal cycles over its lifetime, unless a stress range reduction factor is applied to the analysis. Extrapolating from past performance, it was determined that the pressurizer sample line would exceed this number of cycles during the current license period. When the analysis was performed with the stress range reduction factor applied, modifications were required to bring the piping into Code compliance. These modifications have been completed on all three Oconee units.

Another issue in the mechanical area for the period of extended operation is aging of the external surfaces of buried mechanical components. Depending on the material of construction, buried mechanical components are susceptible to loss of material due corrosion and selective leaching, and cracking due to stress corrosion cracking. The aging of these buried components occurs when the protective coating degrades to the point where soil and ground water contact the material surface.

During plant construction, buried mechanical components were externally coated. Twenty-five years of operating experience has identified only two local failures, neither of which impacted system function. This good operating experience indicated that the coating has continued to provide protection for the buried components. However, no direct evidence exists that verifies the actual condition of the coating. Directly determining the condition of the external coating would require excavation, which is costly and increases the likelihood of damage to the coating that accelerates its degradation and the onset of material aging. However, the condition of the external coating can be determined indirectly by inspecting a portion of the interior surfaces of these buried components.

Every five years, the interior surfaces of a large portion of the buried mechanical components are inspected. Approximately 460,000 square-feet of interior surface are directly inspected for signs of degradation from either the interior or exterior environment. The two local failures that have occurred were from the external environment with one being identified by the internal inspection. Through periodic inspection of the interior surfaces, an increase in the number of local failures from the external environment would be an indication of general degradation of the coating. This periodic inspection will ensure that the system will be capable of performing its intended function for the period of extended operation.

The Reactor Coolant System (RCS) received special focus during the license renewal review because of its importance in the radioactive release line-of-defense. Aging management of the RCS components was addressed for Oconee primarily through the BWOG. The results of the BWOG efforts were integrated into the Oconee license renewal application. Aging issues that were addressed ranged from those that are well understood to emerging issues that are under research. Management of these aging issues ranged from analytical solutions to plant maintenance programs. Issues such as reactor vessel embrittlement and the potential cracking of reactor vessel Alloy 600 parts were addressed. Emerging issues on the reactor internals bolting were investigated and a new baseline program was introduced to begin further characterization of aging of these internals parts. Also, steam generator aging management issues were reviewed and emphasis has been placed on the steam generator tubing inspection program that has been implemented at Oconee over a number of years. These issues demonstrate the broad range of aging management issues covered in this important mechanical system.

Electrical Components

In recent years, electrical cables in nuclear power plants have been seen as one of the greatest challenges for operating a plant beyond the originally licensed 40 years. Management at some plants have even expressed the idea that a decision on applying for an extended operating license would depend on the outcome of a plant cable evaluation. At the same time, no complete plant evaluation of electrical cables had been performed at a nuclear plant. This was the setting when planning began for the electrical cables evaluation for license renewal at Oconee Nuclear Station.

The technical challenge of the evaluation was determining which cables were within the scope of the NRC's license renewal rule (10 CFR §54.4) and how to adequately evaluate aging of these cables for the twenty-year extended period of operation. At the time, no clear path to a resolution of these challenges was evident.

At first glance, the most straight-forward process to identify the electrical cables was believed to begin with the plant mechanical systems. The first step of the process would be to identify mechanical systems that are within the scope of the license renewal rule. Following this, the electrical equipment that supports the mechanical system intended functions and the cables that connect the electrical equipment would be identified.

As a demonstration of this process, a single component, known to be within license renewal scope, was chosen — the motor-driven emergency feedwater pump. A review of the electrical connection diagrams for power and control of the pump identified more than twenty separate electrical cables. The specific license renewal intended functions of the pump were identified as were the electrical equipment and cable intended functions. Research was performed to determine the construction and primary insulating material for the cables. The route of each cable was mapped between each piece of electrical equipment involved, and the plant areas through which the cables traveled were identified. The service environment in each of these areas was determined as was the applicable self-heating temperature rise. Once the service conditions of each cable and its primary insulating material were identified, the cable's expected life could be determined.

This demonstration revealed that the electrical cables in the demonstration were routed in the same areas as many other cables that are probably within license renewal scope. For these other in-scope cables, the same process would need to be followed. If bounding values for cable materials, service environments, and self-heating temperature rise could be determined, individual parameters for each cable would not need to be identified. In addition, by using a bounding approach, it may not be necessary to specifically identify all the cables that are within license renewal scope and may only be necessary to ensure that the bounding values include the characteristics of all in-scope cables. Identifying specific and individual functions for in-scope cables was also a major task. Therefore, coupled with the bounding cable review was the idea that reasonable assurance must be provided that all cable functions need to be maintained which in essence is a bounding set of functions that includes all license renewal intended functions.

The use of this bounding approach rather than a specific component identification approach led to numerous economies during the review process. These economies in process made it possible to overcome the technical challenges and complete the evaluation of electrical cables for the Oconee Nuclear Station license renewal application. This bounding approach for evaluating cable aging represents enormous success not only for Oconee Nuclear Station, but for the industry as a whole.

Summary

The challenges that face aging NPPs are expansive in nature and require systematic solutions. License renewal planning for Oconee has been a strong motivator in establishing a larger LCM perspective that aids in providing a structured and systematic method to approach these technical challenges. The Oconee License Renewal Project Team continues to work closely with other industry groups to develop technical processes and common solutions to aging management issues associated with license renewal. These groups included the B&W Owner's Group (BWOG), the Westinghouse Owner's Group (WOG),

Electric Power Research Institute (EPRI), the Nuclear Energy Institute (NEI), and the Institute of Electrical and Electronics Engineers (IEEE). The technical issue examples demonstrate that solutions to the technical challenges that face Oconee Nuclear Station can be engineered such that the issues are managed. As long as the financial analyses determine that resolution and management of these issues does not impact the economic viability of Oconee, these issues will not limit the life of the station. We can reap the benefits of future operation only if we are committed to investing in LCM today.

PLANT LIFE MANAGEMENT : AN INTEGRAL PART OF OPERATION AND MAINTENANCE POLICY AND STRATEGIES

Jean - Pierre HUTIN
Director for Technical Support
Electricité De France, Nuclear Generation Division

Abstract :

Electricité de France is now operating 58 PWR nuclear power plants which produce 75 % of electicity in France. Besides maintaining safety and availability on a routine basis, it is outmost important to protect the investment. That is the reason why EDF is devoting important ressources to implement aging management concern as an integral part of operation and maintenance programs (for example through appropriate data collection, specific repair and replacement projects and important anticipation efforts, taking in account the high level of standardization of the units).

A particular organisation has been set up to continuously observe and analyze all activities so as to make sure that aging concern is correctly taken in account in strategies and that no decisions are susceptible to impair plant lifetime. This "lifetime program" is paying attention to technical issues associated with main components but is also dealing with issues related to economics and industry situation.

1 - INTRODUCTION

Managing ageing and remaining lifetime of an industrial facility is a concern which must be taken in account as soon as possible in daily activities. With that respect, comparison with the human body and health is totally appropriate : ageing is beginning very early, bad practices may be detrimental in the short as well as the long term and the asset is of a considerable value !

EDF recognized very early the importance of that need for its nuclear facilities : 58 PWR units built on 20 sites are producing 75 % of electricity used in France ; between 10 and 20 % of the generated electricity is exported in other european countries, so contributing for a large part to the french commercial balance ; and 50 % of the investment is now amortized. Moreover, building new plants will certainly present much more difficulties than in the past. So that keeping these facilities in good operating conditions as long as possible is absolutely vital for the company which is going to face the reorganisation and deregulation of the european electricity system.

And for nuclear power plants, "good operating conditions" undoubtedly means safety and cost-effectiveness.

2 - LIFETIME MANAGEMENT POLICY

For some components, lifetime is given by the manufacturer as a guaranteed value. But in most cases, manufacturers give only some indications about what they consider as an "average technical lifetime", without any contractual commitment.

The pressure boundaries of the nuclear steam supply system represent a special case. Numbers of expected operating transients are input in the fatigue analysis required by pressurized component regulation. So that the time to undergo these transients may be considered as a "regulatory lifetime" of the NSSS.

An other lifetime value is the one postulated to calculate amortization of the investment. And of course, in many countries, licencing period may be considered as a kind of "lifetime" although it is generally not related to any technical limitations. In France, such a limited licencing period does not exist. The idea is that safety is pemanently under scrutiny with a complete review and reassessment every ten years but without formal authorization process. However, experience shows that this ten-year safety review which is put under control of safety authorities may represent a "re-investment" as big as a formal licence renewal process.

In EDF, the lifetime management policy of the nuclear power plants is based on three principles :

- looking for excellence in daily operation and maintenance activities, with an effective experience feedback organisation taking advantage of the high level of standardization of the units,

- every ten years, a complete review of each facility and an upgrading of its safety level through appropriate modifications while maintaining unit standardization in all the fleet,

- a Life Management Program, at corporate level, which permanently scrutinizes operation and maintenance activities to identify decisions which could impair plant lifetime and which surveys research and development programs related to ageing phenomenon understanding.

3 - INTEGRATION OF LIFETIME CONCERN IN O&M ACTIVITIES

As it has been said, it is outmost important to take in account the lifetime concern in daily operation and maintenance activities. And this must be done as early as possible in plant life. It requires some engineering analysis because this was generally not correctly done in original operation and maintenance procedures.

For example, significant investigations were necessary to realize that pressurizer and steam generator operation practices were imposing significant fatigue loading on some nozzles and branch lines and that it was possible to reduce the fatigue cumulative damage by optimizing procedures. In the same way, optimization of fuel assembly management allows to reduce irradiation embrittlement of the core vessel. Of course, these

optimizations have a cost which must be balanced with the lifetime benefits through appropriate analysis.

Eventhough analysis works generally require engineering capacity, many good ideas may arise from plant staff. And if procedures are "optimized", people will apply them more certainly if they understand the intent. So that increasing lifetime awareness of plant people is also an important feature of EDF strategy.

In many cases, operating experience gives evidences of phenomenons which may impact component lifetime. So it is very important to have an efficient experience feedback organisation. In EDF, events and/or informations are first analyzed by site engineers. Then, the most important informations are provided to the corporate level where specialized departments perform a "second level" analysis, particularly to detect any generic aspect. As a consequence, they may propose relevant measures to be taken on other units and/or initiate appropriate updating of operating and maintenance procedures.

In the following paragraphs, some keypoints of the lifetime concern integration in plant operation and maintenance are described : long term repair/replacement strategies ; collecting relevant data ; surveying industrial capacities.

4 - REPAIR / REPLACEMENT STRATEGIES

Because all the units are quite identical, large ressources may be devoted to problem solving so that a solution found for one unit may be implemented on all the other units. But this high level of standardization could become a weak point if problems are not sufficiently anticipated. It is absolutely necessary to eliminate the risk of a generic problem which would affect all units at once and oblige to shut them down at the same time. For that, EDF must have a very prospective view of all major degradations which could impair component reliability or integrity with appropriate repair/replacement strategies. These strategies must cover periods of time consistent with the capacity of nuclear industry to develop methods and build components (between five and fifteen years).

The "Exceptionnal Maintenance Program" is dedicated to periodic review of design, fabrication and experience feedback of the 30 or 40 most sensitive components in order to identify possible future problems, to estimate potential consequences and to propose appropriate measures to be taken : simple surveillance, development of repair methods, early procurement of spare parts and, possibly, replacement in anticipation if the risk of having all the plants affected at the same time appears too high.

Decisions are made after performing a cost / benefit analysis of various strategies. Probabilistic approaches are often used. But it must be recognized that indirect consequences of some catastrophic scenarios are sometimes difficult to assess.

Of course, consequences of the "anticipation / no anticipation" choice must be integrated on the whole plant lifetime.

Finally, the Exceptionnal Maintenance Program allows to identify large maintenance works which will "probably" have to be performed and to take measures such that, at the proper time, impact on EDF fleet performances is minimized.

Consequences of a prediction error are minimized by a complementary "inductive" analysis : very low probability events are considered and countermeasures may be taken so that if these unlikely events occur, the consequences will be costly but not catastrophic for France electricity production.

5 - COLLECTING RELEVANT DATA

When assessing plant lifetime expectancy, past data about operation and maintenance are needed.

The most common example is the fatigue assessment of the NSSS : to be able to make a prediction about the remaining fatigue resistance of a given component, informations about past fatigue cycles are needed. These fatigue cycles are mainly pressure and temperature transients. Of course, if these informations have not been recorded at the proper time, it is very difficult to find them ten or twenty years later !

The minimum requirement would be to bookkeep the type of each transient occuring on the plant : heat-up and cool-down, load variations, RHRS connection and disconnection and other transients which appear in the design analysis. But, when performing a fatigue assessment twenty years later, it will be necessary to take, for each transient, temperature and pressure variations as they were expected in original design analysis and this is likely to be overly conservative. That is why, for the primary circuit of EDF NPP's, original design transient list has been adapted to obtain a more "operational" reference list so that it fits closely to the actual transients (of course, it required to update design analysis !). And when a pressure and/or temperature transient is detected (with very low threshold), systematic comparison is made with the reference transients to make sure that the actual fatigue loading is not more severe than expected but also, is not too conservative either.

Moreover, it has been recognized that, at some specific locations, global temperature and pressure variations doest not give an exact view of the fatigue loading due to local thermohydraulic phenomenons like stratification. Extensive studies were performed on that subject (mock-up testing, numerical analysis, on-site instrumentation) in order to develop "fatiguemeters" which continuously monitor local fatigue loading and permanently estimate usage factors.

EDF was spontaneously motivated to do all that because it is explicitely required by French Nuclear Pressure Component Regulation.

For other plant components and other types of damage, monitoring programs (beyond regular inservice inspection) depend on the ageing probability and consequences. For exemple, a very sophisticated and extensive approach has been undertaken for cast austeno-ferritic steel elbows.

The operating experience feedback organisation which asks for plant staff to report all significant events to the corporate level, is used as an history recording system (computerized information system used for experience feedback is connected to an historical data bank). These historical data are mainly kept in three formats :

- event description and its causes and potential consequences as they are identified by plant engineering staff, are kept on file. For most interesting events (selected by a specific multidisciplinary committee), the file is completed by corporate analysis conclusions.

- yearly synthesis are made by corporate departments on selected subjects.

- system and component reliability data are separately recorded in order to be easily used as input data in probabilistic type of analysis like Safety Probabilistic Assessment or Reliability Centered Maintenance Approach.

It must be emphasized that the process of collecting appropriate data always begins with plant personnel and that, in order to correctly perform the job, they need to understand the purpose of it and the importance of doing it well. This means a "plant life management awareness" which has to be permanently maintained.

When saying that collecting data must be done as early as possible, it can be added that "early" is never "early enough" . Indeed, it was often experienced that problems arising during plant operating life were related to events which had occured during pre-operationnal tests and for which most of the informations were lost.

6 - SURVEYING INDUSTRIAL CAPACITIES

To build 58 units in twenty years, France had to create specific industrial capacities and to adapt existing facilities. At the same time, many countries were doing the same. Now, the future of NPP construction is not very clear. Even in France, there is no real need for new plants before 2010 or 2015 : this is clearly a drawback of the good life management of existing plants !

Some design and construction companies were able to turn to maintenance activities. But even maintaining the equipment they built does not give as much work as construction. And there is a strong competition with companies the core business of which has always been maintenance. And last but not the least, there is companies which designed and built so reliable components that there is almost no maintenance to perform !

For all these reasons, there is a high risk for some of these "nuclear" companies to go out of business. And the question is : if some components need large repair, revamping or replacement, will the utility find appropriate industrial capacities to do the job and provide the spare parts.

To cope with this issue, EDF set up a "world industrial capacity observatory" which permanently surveys international situation and try to identify "product / company" pairs which are "critical" and "sensitive" :

- "critical" because the company has no sufficient activity perspective so that it is likely to disappear and because the market is so slim that industry has no incentive to keep the capacity to provide the required product or service (this is particularly true with companies which have been totally dedicated to specific nuclear component design and manufacturing)

- "sensitive" because their disappearance would put EDF in a difficult situation

When a "critical and sensitive" case is identified, EDF brings the matter up for discussion with the concerned companies in order to look for possible solutions.

7 - PLANT LIFE MANAGEMENT PROGRAM

As it has been explained, the best way to correctly manage plant life time is, first, to seek quality in everyday operation and maintenance. However, because of the importance of the issue, EDF decided to give itself complementary guarantees : the Ten-Year Reviews and the Plant Life Management Program.

Before the first ten-year outage of a series, a new set of safety references is defined and discussed with Safety Authorities. All component/system/structure situations and operating conditions are reviewed, taking in account experience feedback. The results of these reviews are compared with references and a modification and upgrading program is defined.

During the ten-year outage of each plant of the series, these modifications are implemented. Extensive inspections, verifications and large maintenance works are performed, including an important set of anticipation measures. A complementary investigation program is also implemented, specifically to look for unexpected ageing phenomenons.

Beyond that, a particular organisation has been set up at corporate level to continuously observe and analyze all activities so as to make sure that ageing concern is correctly taken in account in strategies, that everything is done to reach expected lifetime goals and that nothing is done which could impair plant lifetime. This Plant Life Management Program is paying attention to technical issues associated with main components but is also dealing with issues related to economics and industry situation.

The Plant Life Management Program also supports research and development works related to plant life and ageing concern (for exemple, development of methods and tools to correlate operation conditions and lifetime expectancy or research on degradation mechanisms and kinetics). It has close relationships with other companies and international organisations sharing the same concern.

The Plant Life Management Program periodically reviews EDF and world situation and reports its conclusions to EDF General Manager, then to Safety Authorities.

8 - AGEING SITUATION OF EDF NPP COMPONENTS

Component ageing is certainly not the only factor impacting plant lifetime... but it is however an important one ! With that respect, EDF has a rather satisfactory situation, partly due to an early awareness.

Core vessel embrittlement is not really an issue : due to low level of residual elements, the end-of-life Rtndt should not exceed 100 ° C. Moreover, optimized fuel arrangements are

now implemented to reduce even further the level of vessel irradiation. And the original embrittlement monitoring program is to be extended by putting new specimens in place when old ones are removed for testing.

As far as fatigue of reactor coolant system is concerned, actual usage factors are less than expected in most locations and this can be demonstrated with the results of the transient monitoring and bookkeeping program. However, it must be recognized that some locations require specific attention due to unexpected thermohydraulic phenomenons. Fatiguemeters are now under development to address this issue and, in any case, repair is possible.

The 900 MW plant containment buildings are not a concern. But 1300 MW plant ones will certainly require some repair because of unsufficient tightness of their inner wall.

Cables do not rise severe questions but need some monitoring.

The instrumentation and control life expectancy has been very carefully analyzed through a specific project, looking both at technical and industrial aspects. For 900 MW plants, almost nothing is to be done before the third ten-year outages, except for some revamping of a few systems and for in-advance spare parts procurement (we are just entering the second ten-year outages on oldest plants). For 1300 MW plants, the same assessment is under progress.

Pressurizer is not an issue but replacement feasability has to be studied.

So that, if other than technical aspects are correctly handled and if current operation remains safe and cost-effective, EDF nuclear power plants should easily last at least fourty years.

9 - CONCLUSIONS

As it has been shown, plant life management is a very important issue for any utility, and particularly for EDF. And to correctly handle this issue, appropriate measures have to be taken immediately, without waiting for the last years. Many of these measures are of technical and/or industrial nature but the importance of personnel and manager awareness should not be neglected.

Ultimately, it must be recognized that many industrial facilities are obliged to shut down for reasons which are not directly related to equipment situation or utility activity but which are the consequences of external changes : country energy policy, regulation evolution, public acceptance, etc.

Of course, utility must keep a constant watch over these external changes which may impact its survival, with enough anticipation. But the fact that, in such evolving context, a utility defends its own interest will be well accepted only if it has a high level of credibility. And this credibility may only arise from excellence in daily safe and cost-effective operation : in any way, such excellence is the best guarantee for long, long, very long nuclear power plant life !

PLANT LIFE MANAGEMENT ACTIVITIES OF LWR PLANTS IN JAPAN

Akiyoshi Minematsu, Hiroshi Noda, Yuji Takahashi, Kanji Kinoshita
Tokyo Electric Power Company

ABSTRACT

Plant life management activities of LWR Plants has started substantially since 1994 in Japan and it's been conducted by the utilities and MITI co-operatively.

In Japan , it's not same as US ,there are no limitations for an operation period or plant life because we have no laws or rules which prescribe a licensed operation period for nuclear power plants. If an annual inspection checked by the regulatory authority ,MITI, is completed without any problems , one year operation renewal is permitted. This cycle can be repeated without limit.

However , we consider it very important to evaluate the long-term integrity of major systems,structures and components of an aged nuclear plant and to ensure the safe ,steady and highly reliable long-term continued operation. So,we've come to recognize the importance of the Plant Life Management Activities.

Japanese Plant Life Management study consists of two phases. Part 1 study started in 1994 and was already conducted and made public in 1996. Part 2 study is now on-going and be scheduled to be completed in near future.

1. PLANT LIFE MANAGEMENT ACTIVITIES

1.1 Introduction

Already more than twenty-five years have passed since the first nuclear power plant went into operation in Japan. Nuclear power plants, both new and old have been operated, maintained and managed using methods that are very similar and not differential to plant age.

In the 1990's, as Europe and the United States began their technical study of long term operation of nuclear power plants, Japan also recognized the necessity to study measures against the aging factor in the degradation of power plants in Japan. Therefore, a program was established for plant life management in nuclear power plants. The study is currently on-going according to the management program which was established.

This paper briefly introduces the current status of the on-going activities of plant life management of LWR plants in Japan and outlines the future plans.

1.2 BASIC CONCEPT

Part1 study was carried out as a feasibility study to obtain the outlook for nuclear plant soundness over the representative components assuming 60 years operation. To confirm the soundness of plant life time , three candidate power plants that had been in service for many years were selected ,those were Fukushima Dai-ichi Nuclear Power Station Unit 1 (BWR), Tsuruga Power Station Unit 1 (BWR), and Mihama Power Station Unit 1 (PWR).

For the technical assessment , seven or nine typical components were chosen for evaluation such as the reactor pressure vessel , the reactor internals, the primary containment vessel and so on. These components were chosen because of their importance in the safe operation and in the event of any degradation of these components during operation, repair or replacement cannot be performed easily.

The purpose of Part 2 study is to improve plant reliability and thus we should review components not only a safety point of view , but from the perspective of avoiding a forced shutdown, considering a wider range of components (consisting of thousands of items) of the three candidate power plants. It's intended to develop measures against aging degradation and

establish the methods and period of inspections from this assessment for future implementation.

1.3 THE RESULTS OF PART 1 EVALUATION

Through the technical assessment, it was discovered that some of the components should be provided with adequate measures in operation and inspections to insure proper operation for a 60 year period. For example, in the case of BWR plants, it was discovered that planned measurement against thinning of carbon steel pipe wall thicknesses was necessary. Furthermore , in the case of Reactor Internals , it is necessary to have scheduled inspections to avoid the damage due to IGSCC at which non-low carbon stainless steel is applied as basic material. In the case of PWR plants, it was discovered to be necessary that measures be taken against stress corrosion cracking of parts made of Inconel 600 alloys.

In both BWR and PWR plants, it was also discovered that certain aging degradation phenomena had to be monitored by periodical inspection on the components that were susceptible.

It was confirmed, however, that plant integrity can be preserved basically by the continuity of present maintenance methods.

2. PART 2 EVALUATION METHOD

2.1 THE PROCEDURE OF PART 2 EVALUATION

The evaluation methods of Part 2 study is as follows.

An outline of Part 2 of the study is summarized. (See Fig-1)

2.1.1 Selection of Components for Assessment

Aiming to further improve the reliability of nuclear power plants, the components to be assessed are classified into three categories as follows:

a.Important Components for Safe Operation
b.Important Components for the Avoidance of a Forced Shutdown
c.Other Important Components

a. "Important Components for Safe Operation" include components falling under the PS-1, PS-2, MS-1 and MS-2 categories in the publication "The Guidelines for Classification of Important Components":

In the case of a BWR, the components include:
The reactor pressure vessel, the high pressure core injection system pump, the main steam isolation valve, the feedwater piping, the emergency diesel generator, the central control room air conditioning system, etc.

In the case of a PWR, the components include:
The reactor pressure vessel, the heat removal pump, the pressure removal valve of pressurizer, the auxiliary feedwater piping, the emergency diesel generator, the sea-water pump, etc.

b."Important Components for the Avoidance of a Forced Shutdown" include components that are required for continuous power generation, which fall under the PS-3 category in the publication "The Guidelines for Classification of Important Components"

In the case of a BWR, the components include:
The turbine, generator, generator excitation system, condensate system (including main condenser), feedwater system, circulating water system, switchgear, main transformer, switching station, etc.

In the case of a PWR, the components include:
The turbine, generator, generator excitation system, condensate system, extracting

system piping, switchgear, main transformer, switching station, etc.

c."Other Important Components" means all components which belong to "The Guidelines for Classification of Important Components" except "Important Components for Safe Operation" and "Important Components for the Avoidance of a Forced Shutdown"

In the case of "Other Important Components",there isn't so many differences between BWR and PWR. Other Important Components include:
Fire protection system, Radwaste disposal system, House boiler, Sea water intake system, etc.

Note: The publication "The Guidelines for Classification of Important Components for Light Water Reactor Facilities", which is published by the Nuclear Safety Commission (NSC), provides the following definitions:

PS - Abnormality Prevention System: Loss of function may subject the reactor facilities into an abnormal condition and thereby cause excessive radiation exposure to the general public or personnel.

MS - Abnormality Mitigation (or Suppression) System: The spread of abnormality in reactor facilities will be prevented or put under control promptly, thereby preventing or suppressing excessive radiation exposure to the general public or personnel.

2.1.2 Classification and Selection of Typical Components

The components chosen for assessment as noted previously were divided into groups of similar items, such as, type, construction, operating circumstances (which include operating location, fluid properties, etc.) and materials. Typical components were then selected from among these groups based on importance, operating conditions (pressure, temperature) and other critical criteria.

2.1.3 Assessment

The typical components selected under paragraph (b) will be broken down to a part level and technically assessed by considering the phenomena of aging degradation. This technical assessment will verify the preservation of plant integrity and on the appropriateness of current inspection and maintenance programs (additional items may or may not be required), assuming that the plants are to remain in long term service.

The next step will be to apply the results of the assessment of the typical components to other components in each group with consideration to the differences between components.

2.1.4 Formulation of Maintenance Plans Based On Long-Term Operation

Plans will be formulated to adopt for an actual power plant the assessment results which were made considering the aging degradation. Specifically, the maintenance activities and the research and development plans will be developed.

2.1.5 Selection Process of Aging Degradation Phenomena to be Considered in this Assessment

There are many aging degradation phenomena in nuclear power plants. It is impossible to consider every possible phenomenon for each component.

Therefore a selection process was created to select those phenomena of great importance and pertinence.

The aging degradation phenomena that will be considered in this assessment will be selected as follows (See Fig-2):

a.Phenomena with Respect to Industrial Materials and Products
The aging degradation phenomena that may be researched to occur in industrial materials and products (both electrical and mechanical) will be selected. The research will be done through a survey of literature and a study of past abnormalities, including those of other industries and based on the latest technological information.

b.First Phase Screening of Phenomena with Respect to Nuclear Power Plant Environment
The aging degradation phenomena that do not pertain to light water reactors will not be included.
For example, it is not necessary to address halogenated corrosion (necessary in the case of chemical plants) and sigma phase embrittlement (necessary in cases of temperatures between 565 (C) to 930 (C).

c.Second Phase Screening of Phenomena with Respect to Material Environment
The aging degradation phenomena that relate to materials being subjected to abnormal conditions or environments will not be included. For example, carbon steel corrosion does not need be addressed due to the anti-corrosive water quality environment. Also, it will not be necessary to address the thermal aging embrittlement with regard to parts used at low temperatures.

d.Third Phase Screening of Phenomena with Respect to Material Specification Limitations
The aging degradation phenomena that can be identified when material test data, in comparison with operating conditions, can obviously provide technical justification, will not be included. In the screening process, operational records and special factors specific to plants will be taken into account.
For example, it will not be necessary to address inter-granular stress corrosion cracks of austenitic stainless steel (304 stainless steel) in the aqueous environment with a low concentration of dissolved oxygen (below 8 ppm) and at low temperatures (below 100 (C)).

2.2 THE SEISMIC SAFETY EVALUATION CONSIDERING AGING DEGRADATION

2.2.1 The Purpose of Evaluation

It's important to make sure whether the components with aging degradation are remained sound or not under seismic load.

2.2.2 Selection of Components for Evaluation

Components for evaluation are the same as Part2 evaluation, such as "Important Components for Safe Operation","Important Components for the Avoidance of a Forced Shutdown" and "Other Important Components".

2.2.3 Selection Process of Aging Degradation to Evaluate

The aging degradation phenomena that will be considered in this seismic safety evaluation will be selected as follows:

a.The aging degradation which must not have something to do with the seismic related destruction modes, such as Insulation degradation of electric components.

b.The aging degradation which cannot take place as long as the practice of the existing maintenance program will be taken.
For example, the thinning of structure by general corrosion cannot be considered in the condition that the structure is coated with paint and will be repainted appropriately.

c.The aging degradation which cannot affect seismic phenomena judging technically.
For example, the thinning of the internal surface of the valve by general corrosion need

not affect seismic phenomena, because it has thick wall.

2.2.4 The Seismic Safety Evaluation Procedure

The seismic safety evaluation will be carried out according to the following procedure.

a.To select components which should be evaluated corresponding to the aging degradation that will be chosen 2.2.3.

b.To calculate the seismic force in accordance with seismic classification.

c.To combine seismic force with other loads such as inner pressure etc.

d.To conduct seismic response analysis with the load which is calculated above, considering the aging degradation after 60 years operation, such as wall thinning by erosion, irradiation embrittlement, cracking by IGSCC etc.

e.To compare the stress to the allowable stress of the material.

3. THE RESULTS OF PART 2 STUDY

Basically confirming that there is no problem in continuing the practice of the existing maintenance program against aging degradation assuming 60 years operation.

Throughout the Part 2 study, some recommending items are pointed out to improve maintenance methods for long term operation. They should be reflected to the existing maintenance program. For example, in the case of foundation bolts ,it is common to every components, it cannot be inspected as it is burried in concrete. So it is necessary to conduct sampling inspections on proper occasions.

Conservative seismic evaluation against aging components shows there is not any problems for the earthquake resistance. (See Table-1)

4. CONCLUSION

In Japan, appropriate and adequate inspections and maintenance are performed on the LWR nuclear power plants which have been in operation for over twenty-five years. In addition, these plants are provided with adequate preventive measures based on detailed surveys of troubles experienced with plants in foreign countries, and the latest available technical knowledge. Accordingly, there have been no correlations between the plant operating years and the number of abnormalities in Japanese domestic plants.

However , in order to improve plant reliability, it is important to take proper maintenance and management measures against aging degradation on those nuclear power plants that have been in service for a considerable length of time.

Furthermore, through the evaluation of the numerous components in this study, those items that are susceptible to aging degradation can be realized.

And it is important to develop rational inspection and maintenance methods against younger power plants with this study.

Fig-1 PLM EVALUATION PROCEDURE in PART 2

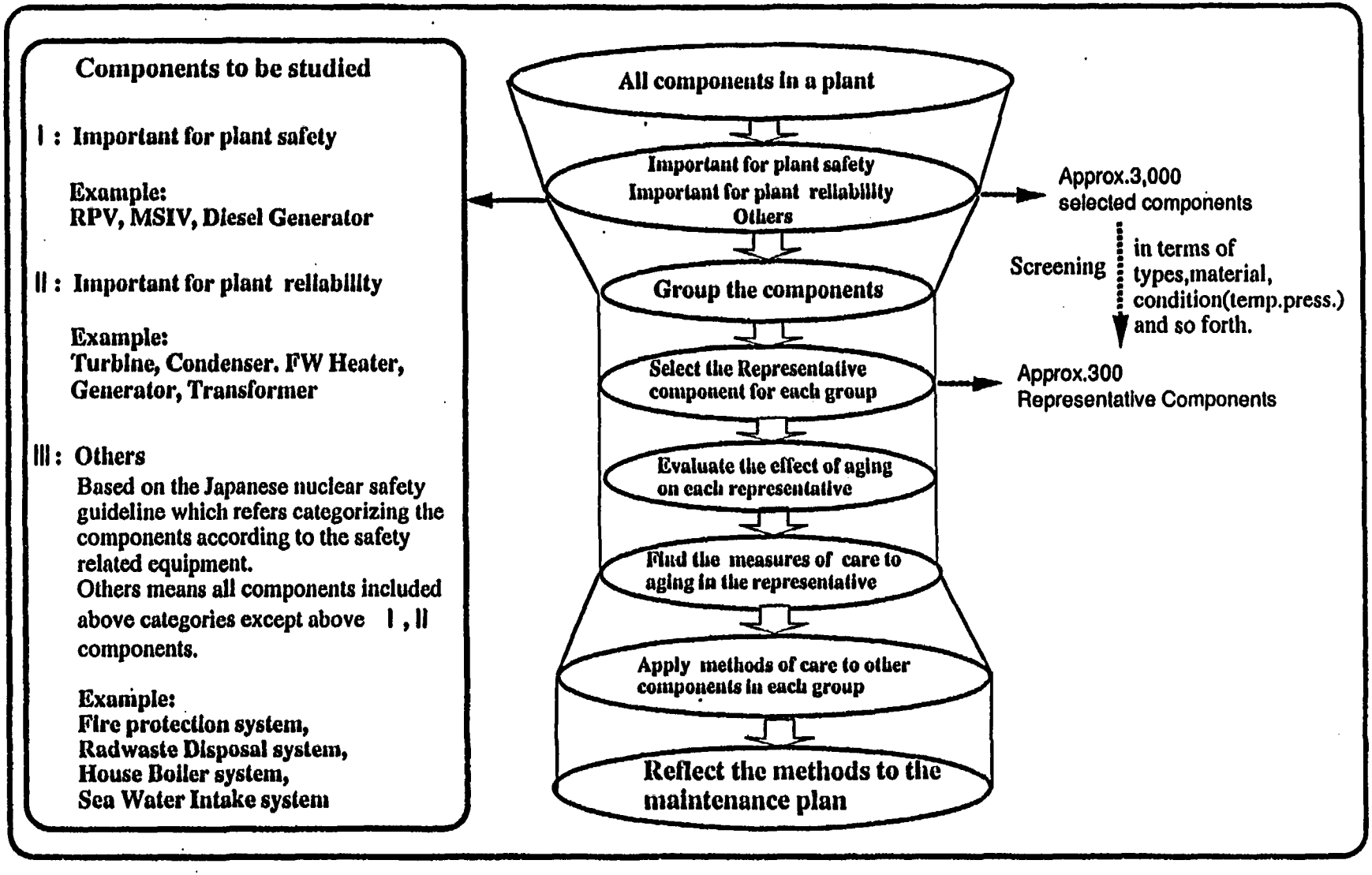

Fig-2 Principles of Identifying Possible Aging Degradation Phenomena

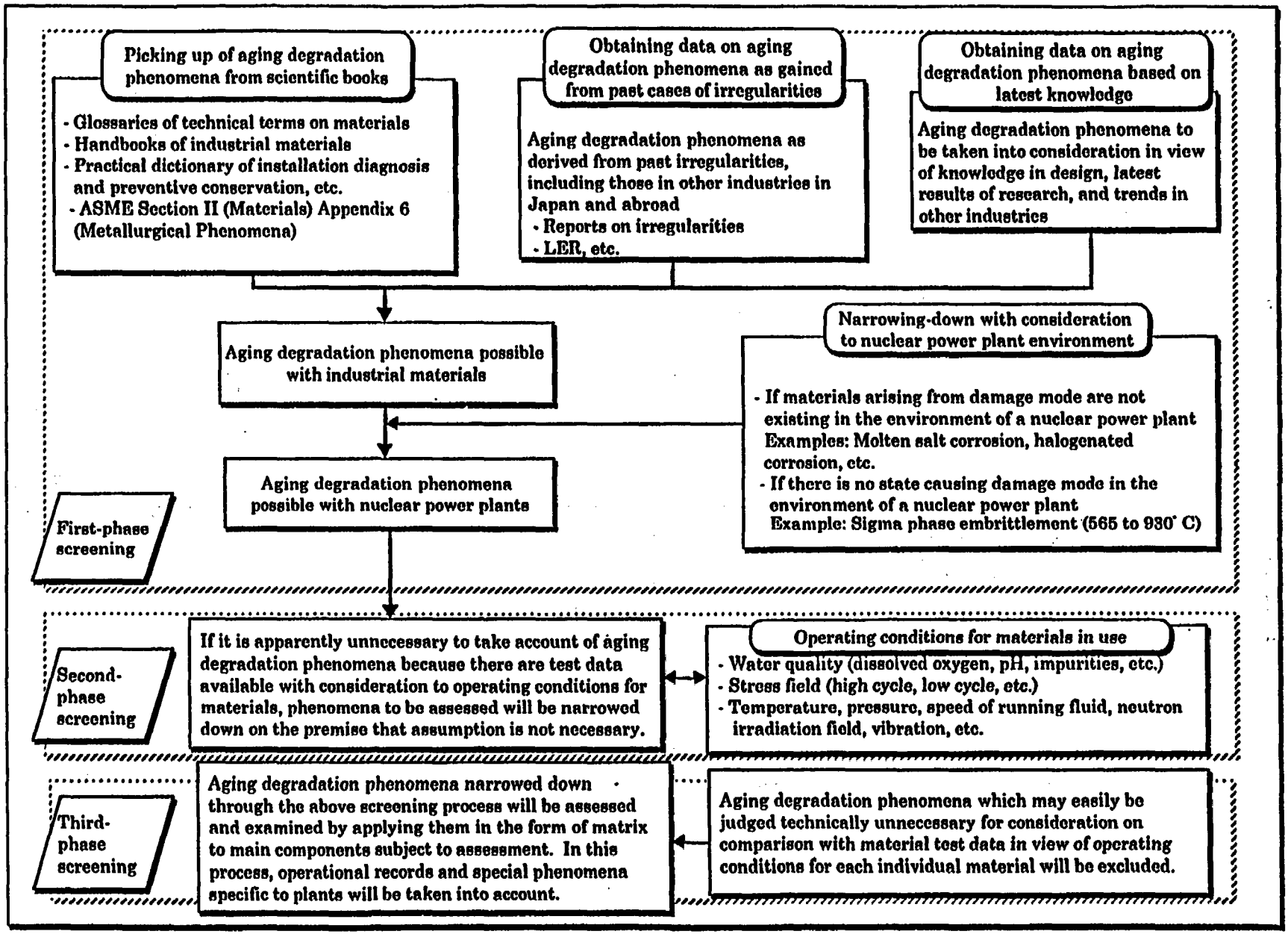

Table-1-1: PART 2 Evaluation results for Fukushima-1 Unit No.1 (Example)

Component		Aging	Long-term integrity evaluation	Existing maintenance service	Measures against aging degradation
RPV Internals	Core Shroud	IGSCC	The present material is susceptible to IGSCC	Visual inspections were conducted by an under water TV camera	Continuing scheduled inspections, and planning to take preventive measures including replacement
	Shroud Support	IGSCC	The material is high-nickel alloy that has lower IGSCC sensitivity than stainless-steel	Visual inspections were conducted by an under water TV camera	Continuing scheduled inspections, and improving the environment by HWC
Primary Containment Vessel	PCV steel plates	Corrosion	PCV was designed with no corrosion margin, so we have to manage the wall thickness	Whole and local leak rate tests and painting film management	Measuring the plate thickness at typical parts of the PCV

Table-1-2: PART 2 Evaluation results for Fukushima-1 Unit No.1 (Example)

Component		Aging	Long-term integrity evaluation	Existing maintenance service	Measures against aging degradation
Heat exchangers (Regenerative H/T in CUW)	the water chamber and shell	Corrosion	The material is carbon steel, which is subject to Corrosion	leak test, but no other inspection has been carried out since replacement	In the future, its integrity will have to be checked
Turbine	inner-casing	erosion	The material is carbon steel, which is subject to Erosion	-Visual inspection -Penetrant inspection (at welding part)	Measuring the plate thickness at typical parts of the Casing
Anchor bolts (common)		Corrosion	No problem with the parts of the bolts burried in concrete	The bolts cannot be inspected	Conducting sampling inspections on proper occasions

EPRI Life Cycle Management Technology Program: Current Activities

John Carey
EPRI

Abstract

Life Cycle Management (LCM) of nuclear power plants can be viewed as the integration of all those various activities which establish the useful operating life of a nuclear power plant. These activities include engineering, operations, maintenance, economic evaluations, environmental assessment, aging management, license renewal and other activities. Since its inception in the mid-1980's, the EPRI LCM program has focused on providing products to assist nuclear utilities in obtaining maximum benefit from their existing nuclear facilities. This paper is intended to provide an overview of several current projects and activities within the EPRI Life Cycle Management Technology Program, in the areas of asset management, aging management, license renewal, and life cycle management implementation. Specific projects reviewed include the EPRI Options Model for Plant Valuation and Management, the Concrete Structures Aging Reference Manual (COSTAR), Generic License Renewal Technical Issues and the issue of fatigue reactor water environmental effects, Calvert Cliffs Life Cycle Management Program, the Life Cycle Management Implementation Guide, and the LCM Implementation Plant Demonstration Project.

Introduction

Life Cycle Management (LCM), as applied to nuclear power plants, is the systematic integration of activities in engineering, operations, maintenance, licensing, environmental and economic planning, and other areas to 1) manage aging and assets, 2) optimize operating life (including the options of early retirement and license renewal), and 3) maximize return on investment while maintaining safety. Since its inception in the mid-1980's, the EPRI LCM Technology Program has focused on providing information and tools to utilities for aging management of important components and structures, asset management, and license renewal of nuclear power plants. This paper is intended to provide an overview of selected, current EPRI LCM projects and activities in the areas of asset management, aging management, license renewal, and life cycle management implementation.

1.0 Asset Management

In general, asset management is a process based on quantitative consideration of uncertainty and risk for making resource conservation and allocation decisions at every level of every business unit of a corporation. These decisions must support corporate objectives and contribute value to all stakeholders.

Nuclear Power Plant Economics and the Options Model

Many of the tasks associated with LCM include input to corporate strategy and interaction with many corporate elements not directly associated with plant operations. These activities include economic evaluations of alternatives for major refurbishment or replacement projects as well as strategic decisions regarding use and disposition of the plant. From the viewpoint of investors and owners, the operating life of a nuclear unit will be determined primarily by its economics relative to other available generation options.

As the marketplace for electricity in the U. S. becomes more competitive and revenues are no longer a result of rate regulation, capital investment is being closely scrutinized. Potential improvements that are not driven by safety or regulatory considerations must meet a more stringent test of value. Developing an operating strategy for a nuclear unit has become increasingly difficult. There is a high degree of uncertainty about key planning factors such as regulatory treatment, the market price of power, capital investments, and decommissioning costs.
Decision analysis and options valuation are being used by U.S. utilities to evaluate the feasibility of license renewal as well as major capital improvements. EPRI has developed a nuclear plant valuation model based on option pricing principles commonly used in the financial community. The model calculates the value of a nuclear plant in a competitive environment and provides guidance for determining optimal management policies in a competitive market.

An option is a contract that permits the holder to buy or sell an asset for a specified price on (or before) a specified future date. In addition to option contracts, option terms are embedded in many corporate securities, such as callable bonds and convertible preferred stock.[1]

[1] Almost all lending agreements, household as well as business, entail an explicit option to prepay and an implicit option to default. Options are pervasive in the financial markets.

The salient feature of an option contract is that it is a right, not an obligation. This means the holder will exercise an option only if it is profitable to do so. In this respect, many characteristics of real assets (i.e., generating units) are analogous to option contracts. Options arise when managers have the flexibility to revise investment and operating plans as new information becomes available. For example:

- A nuclear power plant that can either repair or replace a steam generator has an equipment replacement option, since managers can choose to operate at reduced power to slow the rate of steam generator degradation.

- Up-rating a plant involves an investment timing option, since deferring the investment decision may reduce the odds that the project will turn out to be unprofitable.

- A plant with high operating costs provides a shutdown option, since managers can close the plant in the event operating costs exceed the avoided costs of alternative generation and decommissioning.

There are at least two important embedded options that could confer substantial value on nuclear assets. One, the "early retirement" option, is the ability to retire a unit prior to the expiration of its operating license. This flexibility has value because it may allow plant managers to mitigate losses in the event plant economics are or become very unfavorable (e.g., low power prices or high operating costs). The other embedded option, "life extension", is the ability to apply for license renewal and, if granted, continue to operate the unit after its initial license expires. This flexibility has value because it may allow managers to generate additional earnings in the event that plant economics are very favorable (e.g., high power prices and/or low operating costs).

Options can be important sources of value. Unfortunately, when there is a high degree of uncertainty about important underlying variables, such as electric power prices, asset values can be very difficult to determine. These uncertainties complicate the tasks of forecasting cash flows and selecting risk-adjusted discount rates. Applications of conventional discounted cash flow analysis overlook the possibility that investment and operating policies can be adapted to changing market conditions. Conventional appraisals of nuclear units are prone to neglect the value of embedded options. They assume (implicitly if not explicitly) that nuclear units will operate throughout the license period regardless of plant economics. They therefore neglect the potential savings from early retirement and the potential earnings from life extension. Options always have positive value because they will only be exercised if it is advantageous to do so. Thus by neglecting options, conventional cash flow analysis tends to understate the value of nuclear generating units.

The EPRI Options Model

A large body of theory and methods for pricing options and other derivatives exists in the financial market. EPRI has adapted this theory and methods to develop a model [1] which calculates the market value of a nuclear power station taking into account the early retirement and life extension options. The

model also provides operating guidance as to optimal management policies. Resources are valued at market rather than book value for decision making purposes. A distinction is make between avoidable costs - those which have not yet been incurred - and "sunk" costs. The model can also be used to estimate the value of "regulatory" assets.[2]

The following steps are used to calculate the market value of a nuclear unit and its optimal management policies.

- Identify major events and management decisions that will affect the value of the station over its potential economic life.
- Describe the relationship of station cash flows to important underlying variables and decisions.
- Construct a numerical "grid" that spans the range of possible outcomes for electric power prices over the time horizon of the station.
- Calculate the value of the station recursively, beginning at the terminal date and working backward one period at a time.
- At each possible outcome (i.e., "node" on the numerical grid) compute the value of the station under the alternative courses of action and choose the action for which value is a maximum.

The valuations and optimal policies are derived based on an explicit model of uncertainty about future market prices of electric power. Other underlying variables -- capacity factors, operating costs, capital additions, and decommissioning costs-- are modeled as deterministic variables. However, the model, prepared using Microsoft Excel (version 5.0), allows users to specify a set of scenarios for the non-price variables and thus capture in a heuristic fashion the valuation effects of other uncertainties.

One of the advantages of using valuation procedures of the sort introduced by this model is that managers can determine not only the value of their assets but also the optimal (i.e., value maximizing) management policies. For example, they can find the threshold price of power below which it is optimal to retire a nuclear unit and above which it is optimal to continue operating. This optimal threshold price is substantially less than the threshold price one would arrive at based on conventional analyses. In Figure 1, the "Myopic Early Retirement Policy" is depicted by the dashed line. This line is the "breakeven" point. If the price of power is less than this amount the plant is losing money on an out-of-pocket basis and a traditional cash flow analysis would indicate the need to discontinue operations. However, the Options Model tells us to keep operating unless the price of power falls below the "Optimal Retirement Policy" (solid line) because there is a substantial potential for making money over the longer term.

Figure 1 also provides guidance as to life extension policies. The boxed line indicates the price at which keeping open the option for life extension should be abandoned. The boxed line corresponds to years in which life extension capital investment is required. (These life extension investments are input directly into the spreadsheet by the user.)

---

[2] An example of a "regulatory" asset would be an entitlement to recover stranded investment through (for example) a competitive transition charge.

Figure 1

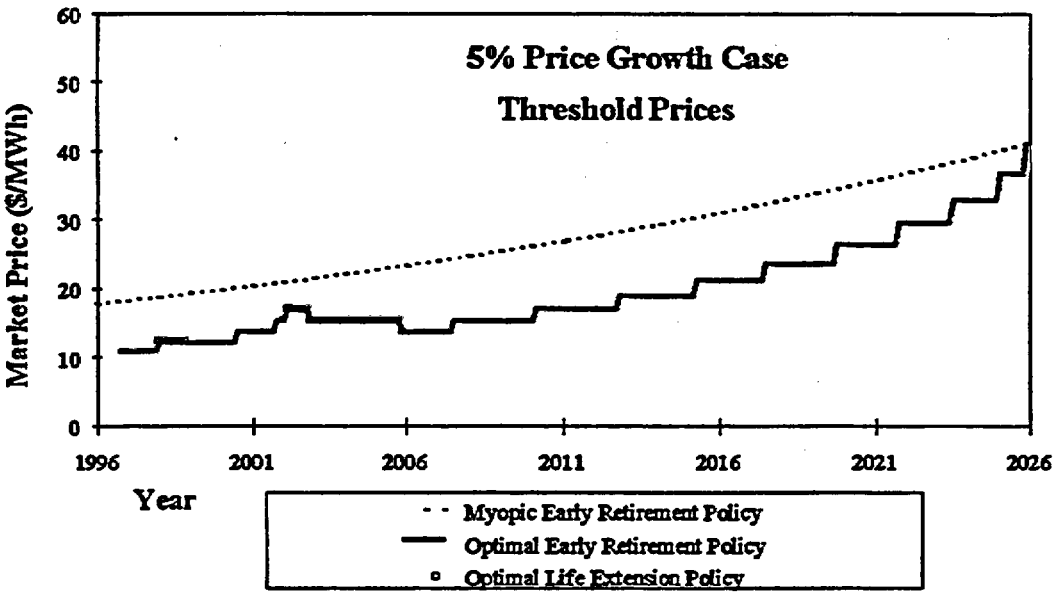

Case Studies - Preliminary Results

Results from site visits to various utilities confirmed initial impressions gained by developing the model. Namely,

- Early retirement and life extension options can be a major source of value, and for some high-cost utilities may be the only source of value. Option values depend in part on the level and trend in power prices. The value of the early retirement option goes up as the market price of electricity falls whereas the value of the life extension option goes up as the price of electricity rises. Option values also depend on the volatility of prices – the dispersion of possible future prices about their expected value. The higher the volatility, the greater the value of both the early retirement and the life extension options. Thus, understanding how to value embedded options is crucial to the management of nuclear assets in a volatile energy market.

- The optimal threshold price for closing a nuclear unit is well below the short-run breakeven price of power.

- The cost of preparing an application for license renewal is so small in relation to the potential payoffs that applying for license renewal seems a foregone conclusion unless the economics of the station are so poor that early retirement is imminent.

- Decommissioning costs, or more precisely, the escalation rates of decommissioning costs, can have a large effect on optimal shutdown decisions. An increase in the escalation rate of decommissioning costs means that the cost of decommissioning the station is higher at each future retirement date, including the planned retirement date. The value of the station without options goes down when the escalation rate of decommissioning costs goes up. An increase in the escalation rate also increases the value of the early retirement option and decreases the value of the life extension option. This is because if decommissioning costs are rising rapidly, they provide an added incentive to retire sooner rather than later.

These applications by utilities and feedback from utility users have also led to improvements in the model. A revised version of the EPRI Options model will be published in early 1999.

Conclusions

This model is useful in that it gives an understanding of what the value of the station would be if the competitive market were fully imposed today. For example, if one combined the station value, the station's remaining unrecovered capital, and the current balance of all decommissioning funds then one would have an indication of the potential stranded (if net liability) or windfall (if net asset) investment associated with the station today. A clear understanding of the market value of the station can be enormously valuable in working out a transition plan with regulators.

The model represents the way operating decisions should be made in a competitive bulk market. It does not rely on regulated rates in its decision making; it selects the course of action that maximizes present value of incremental cash flows.

The results of the model can provide useful information and insight into current decisions and regulatory discussions. It provides nuclear asset managers further insight into how nuclear stations will be valued and managed in the arriving competitive electricity markets.

2.0 Aging Management

Aging management consists of engineering, operations, and maintenance actions to control, within acceptable limits, age-related degradation of systems, structures, and components in a manner that maintains safety while minimizing life cycle cost. Aging management of important nuclear plant systems, structures and components has been and continues to be a significant research activity by NRC, U. S. DOE, EPRI, utility owners groups and various international organizations. One current EPRI LCM research project has focussed on providing utilities with information and methods, in a convenient form, to manage aging effects for concrete structures.

Concrete Structures Aging Reference Manual for Nuclear Power Plants (COSTAR)

Concrete structures have long been thought of as relatively benign structures, capable of functioning well beyond the normal life of the plant. The initial life extension studies carried out under EPRI and DOE

sponsorship, identified a number of concrete structures as "Critical Components," meaning that repair or replacement due to potential degradation would not be feasible, or at least prohibitively expensive, for some of these structures. Effective aging management and early detection of degradation are the principal assurances that the structures will be capable of supporting extended operating lives and that degradation does not advance to a stage which could cause early retirement of the plant. The nuclear utility industry has recognized the importance of concrete structures to safe and long term plant operation. The Nuclear Energy Institute (NEI) has produced a guideline for monitoring the condition of structures [2] and the Westinghouse Owners Group Life Cycle Management Program has produced an aging assessment field guide for structural monitoring, which includes guidance for concrete structures [3]. A significant amount of research has been conducted by NRC and the industry and extensive plant experience has been collected, to where a consensus can be established regarding good practices of aging management and degradation assessment for concrete structures.

EPRI has developed a Concrete Structures Aging Management Reference Manual (COSTAR) [4] to provide a tool for utility engineers to assist in the development or enhancement of aging management programs for nuclear power plant concrete structures. This was accomplished by providing a comprehensive electronic reference manual in the form of a CD-ROM, containing current concrete aging and degradation knowledge and applying this information in a quasi expert format to perform an initial screening and ranking of plant structures with respect to degradation susceptibility and functional importance. The program also contains a condition assessment option to accomplish evaluation of existing or postulated degraded concrete structure conditions and to select supplemental investigation techniques and aging management options.

Available information and experience was screened to extract the most pertinent data and entered into a MS ACCESS data base, modified to suit the specific purpose. From the review of a variety of plant Safety Analysis Reports, Maintenance Rule Structural Monitoring Programs in use at various utilities, and other sources, over 140 plant structures were identified and categorized into 12 concrete structure groups of similar function and exposure. For each structure group, the applicable degradation mechanisms were determined, as well as the associated degradation and mitigation attributes which could accelerate or lessen the degradation. Recognizing that each plant has a unique set of conditions, exposure and service history, the degradation and mitigation attributes can be selected by the user and their relative rank determined based on the known or postulated conditions. In this way, an initial plant inventory of concrete structures and their relative degradation potential can be established, to focus perhaps on those of utmost importance and with the highest degradation potential. The individual steps for the structures screening module are shown in Figure 2.

Similarly, a condition assessment module was developed, utilizing the same data base and principles, but substituting aging effects for aging mechanisms. Aging effects are the conditions observed in the field, such as cracks or leakage, and are evaluated based on specific acceptance criteria for the effects and the known exposure and service conditions. A menu of recommended supplemental investigations and effective aging management options is provided for the user to select for his plant. In addition, the recommended inspection period and the suggested disposition under the Maintenance Rule are provided. The individual steps for the condition assessment module are also shown in Figure 2.

Lastly, the complete electronic copies of 17 key references used to develop the COSTAR Program are provided in the CD-ROM with word search capability, as well as in WORD text form to facilitate cut and paste options. A large number of these references are NRC documents or NRC contractor reports.

Throughout the development phase of the program, a utility review group, consisting of several structural and civil engineers provided oversight and tested developmental versions of the COSTAR program. Two beta versions of the program were submitted to the group members for review, testing and feedback. A third and final beta version was issued, following implementation of enhancements and development of test cases, and is included in the EPRI report. This final version was submitted to an expert panel review committee with the specific assignment to review the technical basis and to establish an expert consensus regarding the data and information provided in the data base. As a principal guideline, the process gave precedence to the data and criteria established in recognized industry standards, familiar to structural engineers. The technical data, descriptions, criteria and methods contained in the data base, are referenced to the original sources and key references where available and appropriate.

FIGURE 2

COSTAR PROGRAM FLOW CHART

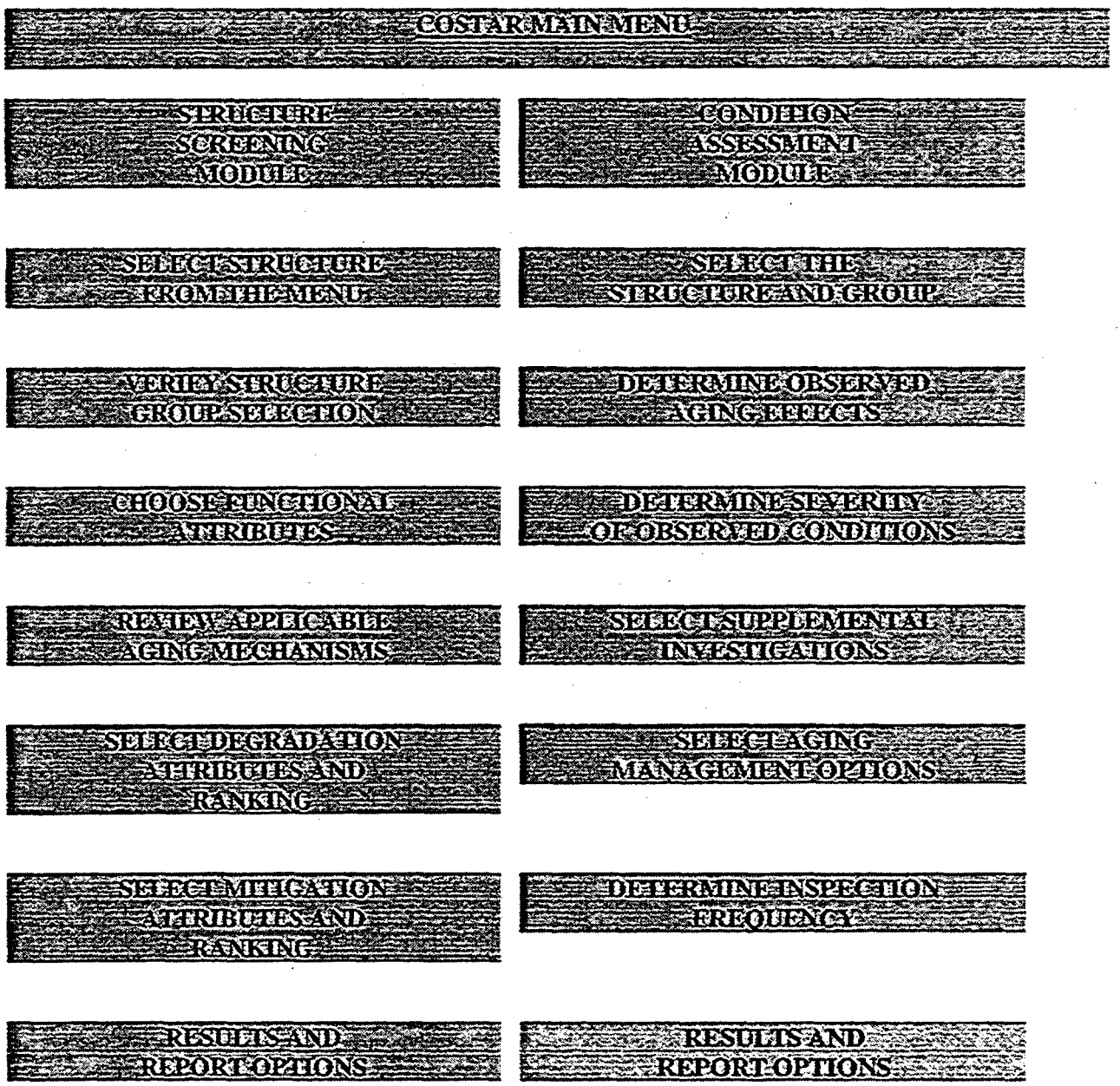

Worked planned for 1999 includes workshops and training to assist utility engineers in using the COSTAR program, additional expert review of data and criteria used in the program, and demonstrations of program implementation at both a PWR and BWR facility. Based on experience gained in implementation of COSTAR and other work to be performed in 1999, a revised version of the COSTAR program is planned to be published in early 2000.

3.0 License Renewal

A major activity of the EPRI LCM Program is to provide technical support for the establishment and demonstration of nuclear power plant license renewal. Efforts by the U. S. nuclear power industry to renew the operating licenses of commercial nuclear power plants has been underway for over ten years, with technical issues related to the cost-effective management of aging effects and regulatory acceptance of the associated aging management programs one area of concern. In order to resolve as many of these technical issues as possible generically, EPRI and the U. S. Department of Energy (DOE) cooperated on the preparation and submittal of ten License Renewal Industry Reports (IRs); see for example [5]. These License Renewal Industry Reports covered major plant systems, components, and structures and were submitted to the U. S. Nuclear Regulatory Commission (NRC) staff for review and comment.

As the result of IR review, many technical issues were resolved. Over 95 % of the technical findings in the IRs were accepted by the NRC and have been incorporated into the License Renewal Standard Review Plan (SRP-LR) Working Draft dated September 1997 [6]. However, some 17 open generic technical issues remain from the IR and other topical report submittals by utility owners groups. Generic license renewal technical issues are, in general, differences of opinion between NRC and Industry on the significance of an aging effect or the adequacy of an aging effects management program affecting many LWR components or structures

The industry has worked through EPRI to develop consensus technical positions on these remaining generic issues, and to assemble existing information and additional data in support of the positions. The 17 generic technical issues are identified below in Table 1.

Table 1

Generic License Renewal Technical Issues

1. Fatigue of Metal Components
2. Environmental Qualification of Electrical Equipment
3. Thermal Aging Embrittlement of Cast Austenitic Stainless Steel Components
4. Irradiation-Assisted Stress Corrosion Cracking of Reactor Internals components
5. Stress Relaxation of PWR Internals Components
6. Primary Water Stress Corrosion Cracking of High-Nickel Alloy Components
7. Stress Corrosion Cracking in PWR Reactor Coolant System Components
8. Degradation of Class 1 Small-Bore Piping
9. Neutron Irradiation Embrittlement of Reactor Pressure Vessel Beltline Materials
10. Ultrasonic Inspection of Pressure Vessels and Components
11. Visual Examination of Components and Containments
12. One-Time Inspections of Concrete and Steel Structures
13. Freeze-Thaw Damage in Concrete Containment Structures
14. Alkali-Aggregate Reactions in Concrete Containment Structures
15. Differential Settlement of PWR Containments and Class I Structures
16. Reinforcement Corrosion in PWR Concrete Containments
17. Void Swelling of Reactor Internals

An EPRI report [7] documenting industry positions on each of these 17 generic technical issues was prepared and submitted to the NRC by NEI in June, 1998. For each generic issue the following information is provided: Description of Issue, Industry Position, Background, Technical Basis for Industry Position, Recommendations for Issue Closure, and References. Early resolution of these generic technical issues will provide greater predictability for the license renewal process and reduce the work by utilities and the NRC in preparing and reviewing license renewal applications.

Fatigue Reactor Water Environmental Effects

One important aspect of the fatigue issue is the influence of reactor water environment on fatigue usage factor and crack initiation. The concerns about the influence of the reactor water environment are based on observations from laboratory testing that indicate a potential lack of conservatism in the fatigue design allowables in the ASME Code Section III. Regulatory interest in these laboratory observations first became evident during the review of and comment on several of the License Renewal Industry Reports in the late 1980s and early 1990s. The principal technical concern is the extension of the fatigue design basis through the license renewal term, considering recent laboratory information on the effect of oxygenated water environments on fatigue crack initiation and growth. As a way of addressing the oxygenated reactor water influence, USNRC contractors prepared a set of modified ASME Code Section III fatigue design curves that were based upon the continuity of the influence over the life of the component. These curves were published in NUREG/CR-5999 [8] and applied to fatigue-sensitive component locations in all light-water-cooled reactor classes in NUREG/CR-6260 [9]. The results in

NUREG/CR-6260 show that there are several component locations in the various NSSS designs for which the CUF is significantly greater than 1.0 at 60 years. The NRC has identified the adequacy of fatigue life of metal components for the license renewal term as Generic Safety Issue (GSI) 190.

EPRI Fatigue Environmental Effects Methodology

EPRI has developed a methodology [10] that accounts for appropriate reactor water environmental effects in fatigue evaluations. This method selectively applies an environmental correction factor to the Code fatigue evaluation procedures. As described in the EPRI methodology, the detrimental effect on fatigue life can be large for the worst combinations of environmental parameters, however, these worst case combinations generally are not typical of LWR operating conditions. The combination of very low strain rates and relatively large strain ranges that could result in large environmental effects do not seem to be typical of events in operating plants. In addition, the high oxygen levels at which much of the environmental data have been obtained are above the levels typical of LWR plants.

An ASME Pressure Vessel Research Committee (PVRC) activity [11], which examined the existing environmental effects database, determined that values of independent parameters listed below should result in only a moderate or acceptable, detrimental effect on the cyclic life of carbon or low-alloy steels.

Parameter	Range
Strain Amplitude	$\leq 0.1\%$
Strain rate	$\geq 0.1\%$/Sec.
Oxygen content	≤ 0.1ppm
Temperature	$\leq 150^0$C
Sulfur content	$< 0.003\%$
Fluid velocity	> 10 ft / sec

Note that independent means that only one criteria needs to be satisfied, regardless of the values of the other parameters, in order that the environmental effects be moderate or acceptable. These environmental effects thresholds or screening criteria are used in the EPRI methodology [10] to selectively correct for reactor water environmental effects only on applicable load state pairs for which environmental effects should be significant.

EPRI Fatigue Environmental Effects Evaluations

In order to determine the significance of fatigue environmental effects and develop information which could be used to help resolve GSI 190, EPRI recently completed several projects to evaluate the effects of reactor water environment on fatigue sensitive locations, using the EPRI/GE fatigue environmental effects methodology, for several NSSS designs. These projects included: (1) a fatigue evaluation of three piping systems at the Calvert Cliffs Nuclear Power Plant (a Combustion Engineering NSSS design) [12];

(2) a fatigue evaluation of several fatigue sensitive component locations in a two-loop Westinghouse plant [13]; (3) a fatigue evaluation of the same component locations examined in NUREG/CR 6260 for a modern BWR, using existing design-basis transient information [14]; and (4) a fatigue evaluation of fatigue-sensitive BWR component locations, using actual operating transient information [15].

The three piping systems at the Calvert Cliffs Nuclear Power Plant that were evaluated are: (1) the feedwater piping system, a Class 2 system with an ANSI B31.1 implicit fatigue design basis; (2) the pressurizer surge line, a Class 1 system with an explicit fatigue design basis (ANSI B31.7, Class 1, essentially equivalent to the ASME Code Section III, Subsection NB-3600); and (3) the chemical volume and control (charging/letdown) system, which is a combination of components with explicit and implicit Class 1 and Class 2 fatigue design bases.

Among the major findings from the Calvert Cliffs fatigue project were:

- The EPRI/GE fatigue environmental effects methodology produced much lower effective environmental fatigue multipliers, F_{en}, than did the application of an environmentally-adjusted design fatigue curve (NUREG/CR-5999) in NUREG/CR-6260. The maximum F_{en} applied to the bounding fatigue-sensitive component locations was found to be in the range of 1.4 to 1.6, well below the fraction of the low-cycle factor of 20 contained in the ASME Code Section III design fatigue curves to account for the conversion of smooth specimen laboratory fatigue data obtained in air to design applications.
- The conservatism implied by the definition of design-basis thermal transients relative to actual thermal transient histories was studied parametrically and was found to have an effect on the calculated fatigue usage equal to or greater than the maximum calculated F_{en}.

The Calvert Cliffs results, as well as the results from the three other fatigue evaluation projects identified above [13, 14, 15] provided evidence that selective application of the effects of reactor water environments, in accordance with the EPRI/GE fatigue environmental effects methodology [10], produces worst-case environmental multipliers that are already compensated for by two existing conservatisms in Class 1 ASME Code fatigue analysis procedures – the low-cycle portion of the design fatigue curve margin factor of 20 that is appropriately ascribed to moderate environmental effects (a factor of from 3 to 4) and the design-basis definitions of thermal transients. The combination of these two existing conservatisms is such that explicit treatment of reactor water environmental effects in fatigue design analysis should not be necessary. The EPRI fatigue evaluation reports have been provided to the NRC for review.

Recent Argonne National Laboratory (ANL) data on austenitic stainless steel fatigue life in both air and reactor water environments [16] is being assessed by EPRI relative to its potential applicability to nuclear power plant component fatigue evaluations, and to the results obtained in the EPRI fatigue environmental effects evaluations described above. Preliminary assessment indicates that the conclusions reached on moderate reactor water environmental effects, using selectively applied environmental shift factors, as described above remain valid.

4.0 Life Cycle Management Implementation

In 1990, EPRI and Baltimore Gas and Electric Co. initiated collaborative studies on Life Cycle Management evaluations for Calvert Cliffs. The results of these studies are documented in over 20 EPRI reports published since the beginning of the program. These studies were undertaken to establish a strategic plan for long term operation of Calvert Cliffs and to reduce current production costs. Life Cycle Management assessments were performed for several systems, structures and components including the Reactor Pressure Vessel [17] Containment Building [18] and Service (Salt) Water System [19]. In addition to technical evaluations of plant equipment, an Asset Management Case Study [20] was performed at Calvert Cliffs to examine the influences on decisions necessary to build a strategy for future operation of the plant. This study documented a strategic decision process for long-term plant operation and demonstrated methods for identifying key uncertainties and evaluating their probable impact, and represents the first documented application of Strategic Asset Management to nuclear power plants. The study identified the long-term market competitiveness of Calvert Cliffs in a deregulated environment, the attractiveness of license renewal, and was a major input to BG&E's decision to apply for license renewal. This study also helped BG&E to focus on several initiatives to enhance the long-term economic viability of Calvert Cliffs, such as developing high level waste disposal contingency plans, and increasing energy production through plant modifications and longer fuel cycles. Current EPRI efforts are to document the lessons learned in the pioneering Calvert Cliffs LCM program for use by other utilities, and to provide technical assistance to BG&E for plant implementation.

Life Cycle Management Implementation Guide

Based on the LCM studies at Calvert Cliffs and other LCM projects conducted by EPRI and other organizations, an LCM Implementation Guide [21] will be published in early 1999. The guide has been prepared to point out the benefits of plant LCM programs and serve as a primer for getting started or improving both the technical and economics aspects of existing plant LCM programs. The guide will:

- Serve as a primer for the technical, economics, and organizational aspects of LCM programs
- Define the elements of a cost-effective plant LCM program (whether or not license renewal is pursued) and how to identify the majority of those elements likely to be already in place at a plant
- Identify potential benefits of LCM programs
- Provide an LCM self-assessment checklist for pinpointing possible gaps in current utility LCM programs, and
- Describe existing EPRI and owners group LCM-related products that can fill current gaps

LCM Implementation Plant Demonstration Project

Recently EPRI initiated a LCM implementation plant demonstration project designed to provide utilities with guidance on how to implement or improve LCM programs at their plants. This project will demonstrate how implementing LCM programs can reduce life cycle costs, manage economic risk, and optimize operating life (including early retirement and license renewal), thereby maximizing the return on investment while maintaining safety.

The first phase of this project will deliver a generic manual and software for preparing plant, system, structure, and component SSC LCM Plans, along with pilot applications to specific systems in participating plants. Two utilities, Duke Energy and Northern States Power are participating in this three-year (1998-2000) project.

The objectives of the LCM Implementation Plant Demonstration Project are to (1) develop a structured approach and provide EPRI members with guidance and tools for improving or establishing cost-effective LCM programs in all nuclear plants and (2) demonstrate the approach with trial implementations of selected elements of LCM programs in participating plants. Project results will demonstrate and, to the extent possible, quantify the benefits of dedicated plant LCM programs. Among the types of expected benefits from implementing LCM are:

- Improved business planning practices and demonstration of management prudence
- Increased long-term profitability with reduced forced outage time and improved capacity factor
- Reduction of financial risk (e.g. reduced refurbishment and replacement costs and forewarning of aging degradation in costly items)
- Insurance against needed capital additions being a surprise so that they wind up being handled in a crisis situation
- Insurance against the early closure experienced recently by several plants
- Deferral of decommissioning and construction of replacement capacity
- Preservation of the option for license renewal

References

1. EPRI TR-106842, "Valuation and Management of Nuclear Assets–Options Model and Case Studies," January, 1997.
2. Nuclear Energy Institute, NEI 96-03, Revision 0, "Guideline for Monitoring the Condition of Structures at Nuclear Power Plants," September, 1997
3. Westinghouse Owners Group LCM Program, "Aging Assessment Field Guide: Structural Monitoring," 1995
4. EPRI TR-110025, "COSTAR (Beta Version 3.0); Concrete Structures Aging Reference Manual for Nuclear Power Plants," June, 1998
5. EPRI TR-103844, "PWR Reactor Coolant System License Renewal Industry Report; Revision 1," July, 1994

6. U.S. NRC Standard Review Plan for the Review of License Renewal Applications for Nuclear Power Plants, Working Draft, September, 1997

7. EPRI TR-107521, "Generic License Renewal Technical Issues Summary," April 1998

8. NUREG/CR-5999, "Interim Fatigue Design Curves for Carbon, Low-Alloy, and Austenitic Stainless Steels in LWR Environments," April 1993

9. NUREG/CR-6260, "Application of NUREG/CR-5999 Interim Fatigue Curves to Selected Nuclear Power Plant Components," March 1995

10. EPRI TR-105759, "An Environmental Factor Approach to Account for Reactor Water Effects in Light Water Reactor Pressure Vessel and Piping Fatigue Evaluations," December, 1995

11. W.A. Van Der Sluys and S. Yukawa, "Status of PVRC Evaluation of LWR Coolant Environmental Effects on the S-N Fatigue Properties of Pressure Boundary Materials," ASME PVP-Volume 306 (1995)

12. EPRI TR-107515, "Evaluation of Thermal Fatigue Effects on Systems Requiring Aging Management Review for License Renewal for the Calvert Cliffs Nuclear Power Plant," December, 1997

13. EPRI TR-110043, "Evaluation of Environmental Fatigue Effects for a Westinghouse Nuclear Power Plant," April, 1998

14. EPRI TR-107943, "Environmental Fatigue Evaluations of Representative BWR Components," June, 1998

15. EPRI TR-110356, "Evaluation of Environmental Fatigue Effects on Selected Components in a BWR Plant," April, 1998

16. Chopra, O. K. and Smith, J. L., "Estimation of Fatigue Strain-Life Curves for Austenitic Stainless Steels in Light Water Reactor Environments," presented at the 1998 ASME/JSME Joint Pressure Vessel and Piping Conference, San Diego, CA, July 26-30, 1998

17. EPRI TR-104509, "Calvert Cliffs Nuclear Power Plant LCM/LR; Reactor Pressure Vessel Evaluation," April, 1995

18. EPRI TR-104777, "Calvert Cliffs Nuclear Power Plant LCM/LR; Containment System Component Evaluation and Program Evaluation," March, 1995

19. EPRI TR-102204, "Service (Salt) Water System Life Cycle Management Evaluation," May, 1993

20. EPRI TR-104615, "Calvert Cliffs Nuclear Power Plant LCM/LR Program; Nuclear Plant Asset Management Case Study," March, 1995

21. EPRI TR-106109, "Nuclear Plant Life Cycle Management Implementation Guide," December, 1998

ESTIMATING THE UNCERTAINTY IN REACTIVITY ACCIDENT NEUTRONIC CALCULATIONS[1]

David J. Diamond, Chae-Yong Yang, Arnold L. Aronson
Brookhaven National Laboratory
Upton, NY 11973-5000

ABSTRACT

A study of the uncertainty in calculations of the rod ejection accident in a pressurized water reactor is being carried out for the U.S. Nuclear Regulatory Commission. This paper is a progress report on that study. Results are presented for the sensitivity of core energy deposition to the key parameters: ejected rod worth, delayed neutron fraction, Doppler reactivity coefficient, and fuel specific heat. These results can be used in the future to estimate the uncertainty in local fuel enthalpy given some assumptions about the uncertainty in the key parameters. This study is also concerned with the effect of the intra-assembly representation in calculations. The issue is the error that might be present if assembly-average power is calculated, and pin peaking factors from a static calculation are then used to determine local fuel enthalpy. This is being studied with the help of a collaborative effort with Russian and French analysts who are using codes with different intra-assembly representations. The U.S. code being used is PARCS which calculates power on an assembly-average basis. The Russian code being used is BARS which calculates power for individual fuel pins using a heterogenous representation based on a Green's Function method.

INTRODUCTION

Background

This study (and others) have been carried out for the U.S. Nuclear Regulatory Commission (NRC) to understand fuel behavior at burnups beyond the current licensing limits. When behavior is sufficiently understood, new acceptance criteria may be proposed for design-basis reactivity initiated accidents (RIAs) in high burnup fuel (and perhaps for fuel at burnups already experienced in operating plants). Acceptance criteria have traditionally been expressed in terms of maximum fuel pellet enthalpy, and hence it is of interest to know what is the fuel

[1]This work was performed under the auspices of the U.S. Nuclear Regulatory Commission.

enthalpy during an RIA. "Best-estimate" methods are available to answer this question, but it is necessary to also understand the uncertainty in the calculated fuel enthalpy.

The above explains the principal motivation for this study which focuses on the design-basis reactivity accident for a pressurized water reactor (PWR). However, it should also be noted that NRC licensees may be moving away from the traditional, conservative methods for calculating fuel enthalpy toward best-estimate methods, and these methods will require an uncertainty analysis. Hence, the study reported upon herein may have a role in regulatory decisions approving new methods for, and the results of, analyzing RIAs.

In a previous study at Brookhaven National Laboratory, the uncertainty in calculating fuel enthalpy for the rod drop accident in a boiling water reactor (BWR) was addressed [1]. That study indicated that the random error in the calculated fuel enthalpy could be approximately $\pm 75\%$ at the 2σ level. It also showed that there could be an additional systematic error of 25% due to the way the intra-assembly power peaking was calculated. This latter error in combination with the random error meant that the calculated fuel enthalpy has to be *increased* by approximately 100% to obtain results at the 95-95 confidence level.

The current study looks at the RIA for a PWR--namely, the rod ejection accident (REA). Because the intra-assembly calculation of power was important for the BWR, it was felt that this should be studied for the PWR and with more rigorous methods than were used for the BWR study. Calculations done as part of a recent Russian study have shown that the peak fuel pin enthalpy during an REA may not be found in the assembly with the peak average fuel enthalpy [2]. In the West, it is typical to use methods that homogenize the assembly and then calculate the assembly response to the REA. The state-of-the-art is changing as flux reconstruction methods are being introduced to improve the intra-assembly representation. Nevertheless, the Russian results are another reason to study the effect of the intra-assembly representation.

Objective

The objective of this study is to improve our understanding of the uncertainty in fuel enthalpy calculated for the REA. The approach is twofold. Sensitivity studies are to be carried out to determine the effect on calculated fuel enthalpy of uncertainties in the important parameters which determine the outcome of the REA. The ultimate objective is to use the sensitivity to estimate the random error in the fuel enthalpy due to random errors in these key parameters.

The second approach in this study is to compare the results for the REA using a code that treats the assembly as an homogenized region and a code that represents each pin in the assembly explicitly. This would give an estimate of the uncertainty in results due to the intra-assembly representation. The PARCS code (Purdue Advanced Reactor Core Simulator) [3], like several other nodal codes in use in the West, treats each assembly as an homogenized region. A newer version of PARCS, with a flux reconstruction method, will soon be available and can be used to obtain additional information about the effect of the intra-assembly representation. The BARS code [2], developed at the Russian Research Centre - Kurchatov Institute (RRC-KI), uses a heterogeneous method wherein each fuel pin is represented explicitly. Hence, it is an

objective of this study to compare results for the REA from PARCS and BARS in order to understand the effect of the intra-assembly representation. It should also be noted that since PARCS is a relatively new addition to the computer tools used by the NRC, the comparison of PARCS and BARS is likely to contribute to the code assessment carried out for PARCS.

Further information on the effect of the intra-assembly representation will come from the same analysis being carried out by the French Institute for Nuclear Safety and Protection (IPSN) and from calculations expected to be carried out using the version of PARCS with the flux reconstruction model.

Scope of this Paper

The results of the sensitivity analysis for the REA are presented in the following section. In the future, these results will be applied to give an estimate of the uncertainty in the calculated fuel enthalpy based on the random errors expected in the key parameters which enter into the calculation. The comparison being carried out between PARCS and BARS is discussed in the next section. This includes some of the limitations of that comparison.

SENSITIVITY STUDIES

Introduction

Although fuel enthalpy is the parameter of interest, the calculations shown in this paper were of the sensitivity of energy deposition. If the event is adiabatic, then energy deposition and fuel enthalpy are essentially identical. The calculations were for total energy deposition rather than for energy deposition at the position of peak power. At a later time, when the edits become available in PARCS, local fuel enthalpy will be considered.

The sensitivity is the relative change in energy deposition (Q) per relative change in key reactor parameter (x). Hence, the sensitivity to x is

$$S_x = \frac{(\delta Q/Q)}{(\delta x/x)}$$

The parameters of interest are well known from previous studies (e.g., [1]) and are related to the reactivity insertion above the prompt critical condition and the negative reactivity feedback from the energy deposition. There are four key parameters which control these phenomena. The first is the reactivity worth of the ejected control rod, ρ_0. This parameter is determined by the core design and by the operating procedures which determine the extent of insertion of the rod and the placement of other control rods at any operating condition. The second parameter is the delayed neutron fraction, β. For a given core design, this parameter changes significantly as the fuel burnup changes. The fuel feedback can be expressed in terms of the fuel temperature (or Doppler) reactivity coefficient, α, and the specific heat, C_p, of the pellet which translates energy into temperature. The Doppler coefficient is determined by core

design and the time during the fuel cycle whereas the specific heat changes relatively little with burnup.

Sensitivity to Key Parameters

The sensitivity to control rod worth is given in Figure 1 where it is plotted versus control rod worth in units of $, i.e., $R = \rho_0/\beta$. The data points on the graph come from PARCS calculations of different reactivity insertion events. Only events with rod worths greater than $1 are of interest. The energy deposition is that deposited during the initial power pulse.

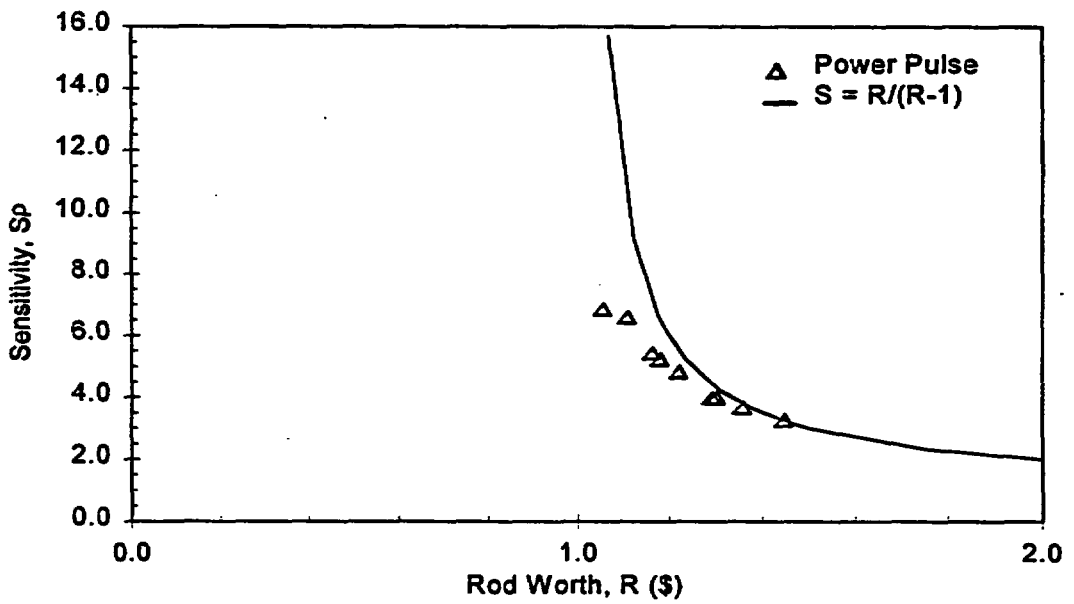

Figure 1 Sensitivity of Energy Deposition to Reactivity Insertion

It is well-known that the power excursion resulting from a reactivity insertion above prompt critical consists of an initial power pulse turned around by feedback followed by a slow decrease in power, due to delayed neutrons, at a level that is still significant as far as energy deposition is concerned. This relatively simple behavior is amenable to simple models.

Using the point kinetics model and the Nordheim-Fuchs approximation an expression for the sensitivity to rod worth can be derived for the time up to the end of the initial power pulse. That expression is $S_\rho = R/(R-1)$ which is plotted on Figure 1. It can be seen that the data points are in good agreement with the theory for the range shown. As the rod worth approaches $1 (from above), corresponding to prompt critical, the simplified expression has

a singularity and is no longer valid. Nevertheless, the sensitivity does increase as rod worth approaches $1. Although this is true, it is also true that the energy deposition becomes smaller and this sensitivity may become less important. The fact that the energy deposition gets smaller has been shown by many analysts. The corresponding result for the energy deposition from the simplified model introduced above also shows this trend:

$$Q = 2(\rho_0-\beta)/(\alpha C_p)$$

The sensitivity of energy deposition to delayed neutron fraction is shown in Figure 2 as a function of reactivity insertion. The data points from PARCS are plotted for both the initial power pulse and by accounting for energy deposition out to three seconds. In addition, the graph shows the curve obtained from the simplified model which predicts a sensitivity of $S_\beta = -1/(R-1)$. Again it is seen that the results for the initial power pulse are in agreement with the theoretical results for the range shown except that as rod worth approaches $1 from above the agreement begins to fail. The sensitivity to 3 s is less than for the initial power pulse as the energy deposited after the initial power pulse is not dependent on rod worth but only on the delayed neutron decay.

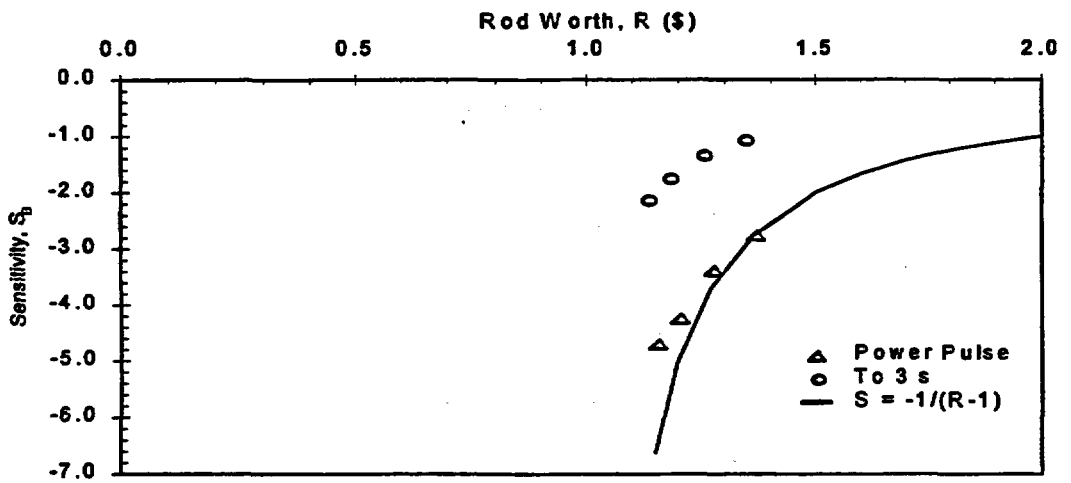

Figure 2 Sensitivity of Energy Deposition to Delayed Neutron Fraction

The sensitivity of energy deposition to fuel heat capacity is shown in Figure 3 as a function of reactivity insertion. Energy deposition is assumed to be to either the end of the initial power pulse or to 3 s to obtain the points plotted on the graph. The corresponding sensitivity from the simplified model is S_c = 1.0 which is also drawn on the graph.

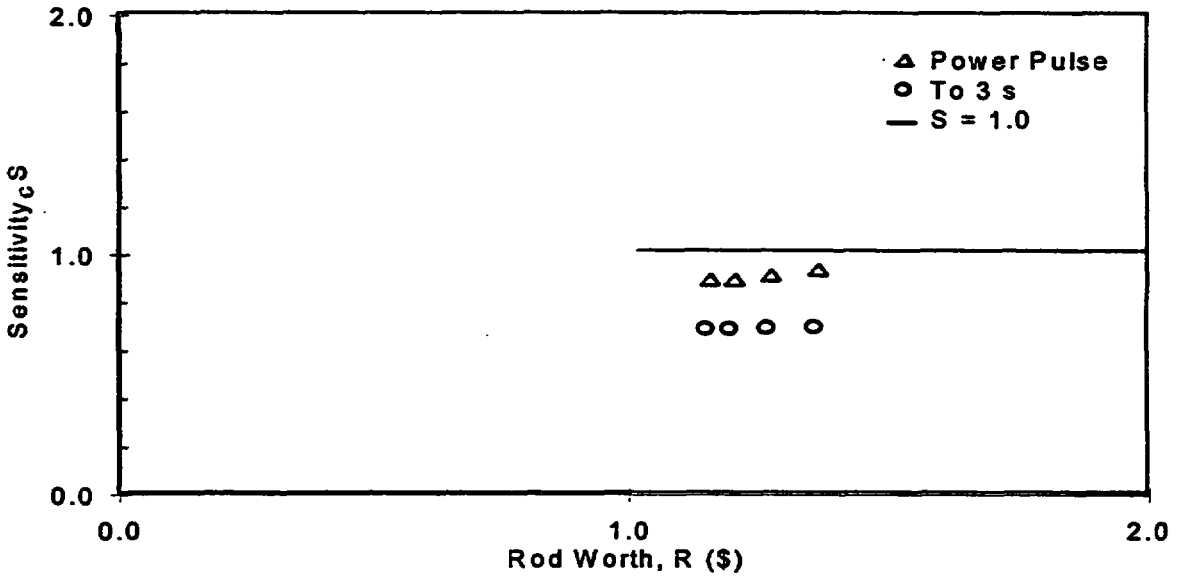

Figure 3 Sensitivity of Energy Deposition to Heat Capacity

It is not possible to plot the sensitivity to the Doppler coefficient as the Doppler coefficient is not a parameter that can easily be extracted from a space-dependent kinetics calculation.

Uncertainty Analysis

The above results are the first step in obtaining an estimate of the local fuel enthalpy during an REA. The sensitivity will be different when it is the local fuel enthalpy rather than the core energy deposition (as above) that is being assessed. This difference will be quantified in the future after the appropriate edits are available in PARCS. An estimate of the uncertainty in fuel enthalpy can be made from the sensitivity if the uncertainty in the fundamental parameters is known. For example, from Figure 2, the sensitivity of energy deposition to delayed neutron fraction is as high as -6 at the end of the initial power pulse and declines to -3 at 3 s. This is the maximum assuming a rod worth just above prompt critical. If we use the -3 value and assume that the uncertainty at the 1σ level for the delayed neutron fraction is approximately 10% then the uncertainty in energy deposition is ±30% due to this key parameter. This type of analysis would have to be done for all parameters in order to complete the analysis.

EFFECT OF DIFFERENT INTRA-ASSEMBLY REPRESENTATIONS

The effect of the intra-assembly representation on the uncertainty in fuel enthalpy is being assessed by comparing codes with different models. The principal codes involved are PARCS the code being used by NRC and BARS, a code developed by the RRC-KI. However, in addition, CRONOS, a code being used by the French Nuclear Protection and Safety Institute (IPSN) and a new version of PARCS with flux reconstruction, will be used to make comparisons.

The PARCS code uses a nodal approximation wherein each assembly is homogenized and the power (flux) is calculated for each axial region in the assembly (or perhaps in a quadrant of the assembly if the mesh is smaller than an assembly). The assembly is homogenized so that neutron cross sections are uniform across the assembly and the thermal-hydraulic parameters are calculated for an average channel representing the assembly. The power in individual fuel rods is obtained by overlaying power peaking factors obtained from an auxiliary calculation. Traditionally, this auxiliary calculation is from a static assembly calculation with reflective boundary conditions, i.e., without consideration of what is happening in adjacent assemblies.

The BARS code uses a Green's Function approach wherein each fuel pin is represented explicitly in the time-dependent calculation. The Green's Functions are based on diffusion theory. Although each pin is represented explicitly in the neutronics calculation, the fuel temperature for each pin is based on an assembly-average calculation. This model will be based on a pin-by-pin calculation in the future.

Although this comparison will provide insight into the effect of the intra-assembly representation, there are other differences between PARCS and BARS which will have a bearing on the calculation of fuel enthalpy. Although the same ENDF/B nuclear data files are used, the data processing codes are different and the nuclear data that enters into PARCS and BARS has a different theoretical basis. For PARCS the CASMO-3 code was used to generate two-group data whereas for BARS, the TRIFON code is used to produce the necessary lambda matrices. The data for BARS is for five energy groups rather than the two that are used in PARCS because the heterogeneous representation puts greater demands on representing changes in spectrum between different regions.

Other differences between the two codes include the axial representation, the time integration method, and the thermal-hydraulics model. Each of these are not expected to have a large effect but the cumulative effect could be significant.

At the time of this paper the specifications of the problem have been completed but no comparisons have yet been done. The specifications refer to the reactor composition and the list of calculations that will be compared. Since the codes do not use the same modeling it is not possible to start from a given cross section data set as has been done in several benchmark exercises in the past. Rather one must specify the composition and geometry of every region within the core: pellet, clad, guide tube, burnable poison rod, control rod, etc. The reactor model is for a core with exposures into the 50 GWd/t range and hence each pellet has a different composition due to burnup.

Prior to comparing results for an REA, results will be compared for steady state calculations of reactivity coefficients, control rod worths, and power distributions. It is only when the differences in results for these parameters are assessed that it makes sense to progress to comparing transient results.

REFERENCES

1. D. Diamond and L. Neymotin, "Sensitivity Studies for the BWR Rod Drop Accident," Letter Report FIN W6382, October 31, 1996.

2. A. Avvakumov and V. Malofeev, "Validation of an Advanced Heterogeneous Model for LWR Detailed Pin-by-Pin Calculations," Proceedings of the International Conference on the Physics of Nuclear Science and Technology, Long Island, NY, October 1998.

3. H. G. Joo, G. Jiang, D.A. Barber, and T.J. Downar, "NRC-PARCS: V1.00, A Multi-Dimensional Two-Group Reactor Kinetics Code Based on the Nonlinear Analytic Nodal Method," PU/NE-98-26, Purdue University, September 1998.

VALIDATION OF A PIN-BY-PIN NEUTRON KINETICS METHOD FOR LWRS

Alexander V. Avvakumov and Valery M. Malofeev

Nuclear Safety Institute of Russian Research Centre "Kurchatov Institute" (NSI RRC KI)
Kurchatov Square, 1, Moscow 123182, Russia
avvakumov@nsi.kiae.ru; malofeev@nsi.kiae.ru

Abstract: This paper describes the pin-by-pin neutron kinetics approach based on an advanced heterogeneous reactor theory to study light water reactor (LWR) transients including reactivity initiated accidents (RIAs). This method has been validated against benchmark numerical and experimental results. Some validation results for reactivity coefficients and a LWR pin-by-pin model are presented. Verification of the transient model was carried out against IGR pulse experiments. To illustrate the capabilities of the pin-by-pin neutron kinetics approach for LWR RIA analysis, an example of control rod ejection accident calculated by the coupled RELAP5 - BARS codes is presented.

I. INTRODUCTION

During some RIAs in LWRs very large deformations in the power distribution over the reactor core can take place. In analysis of these transients it is difficult to evaluate the real uncertainty in calculation of peak fuel enthalpy due to neutronic code because of a lack of adequate experimental data. When large in-assembly power peaking factors occur in LWR, widely used 3 D assembly-by-assembly neutronic codes based on the neutron diffusion theory underestimate to a great extent the peak power in fuel rods and a method for pin-by-pin reconstruction of power distribution requires very complicated procedure of validation for transients. The problem may be solved by comparison of calculational results of assembly-by-assembly diffusion code with ones obtained by qualitatively different, advanced code in the framework of more detailed modeling of the reactor core.

Recently in Russian Research Centre "Kurchatov Institute" an NPP dynamic model for VVER and PWR RIA modeling has been developed. The model is based on coupling of the RELAP5/MOD3.2 thermal hydraulic code [1] with the BARS pin-by-pin neutronic code [2,3].

The model is intended to simulate a wide range of RIAs in LWRs, including unauthorized control rod withdrawal, boron dilution, and steam line break. The thermal hydraulics of the reactor and circulation circuits are simulated by the RELAP5/MOD3.2 code. Thermal hydraulic processes in the reactor core are described by a multi-channel assembly-by-assembly model. An individual thermal hydraulic channel corresponds to each fuel assembly. A number of the hottest fuel rods are also simulated by individual thermal structures.

3 D full-scale neutronic calculation of the reactor is performed by the BARS code using the pin-by-pin model (up to 80,000 calculational cells). This model is based on an advanced method of heterogeneous reactor theory. The heterogeneous reactor method was proposed by A.Galanin and S.Feinberg [4]. For a long time it was being developed and successfully applied in calculations of channel-type heavy water or graphite reactors [2,5-8]. The BARS code has been certified to analyze RBMK reactors by Nuclear Regulatory Body of Russian Federation (GAN).

At present an experience in application of the heterogeneous method in LWR analysis is negligible. So the main aim of this paper is to determine uncertainties in this method for LWR pin-by-pin calculation.

II. FEATURES OF THE HETEROGENEOUS METHOD

The main feature of the heterogeneous method is as follows. Instead of traditional neutron cross sections for cells, heterogeneous equations use matrices of boundary conditions (Λ-matrices). These matrices establish the connection between neutron fluxes and currents at cell boundaries. Traditional neutron cross sections are usually determined on the basis of a single calculation of a cell. Elements of Λ-matrices are determined on the basis of a set of neutron transport calculations with variable neutron currents at cell boundary [9]. Λ-matrices also take into account the effect of the anisotropic diffusion, i.e. the difference in neutron migration lengths in the radial and axial directions. This effect plays an important role in case of a fuel assembly voiding under RIA conditions.

The heterogeneous theory uses analytical representation of the neutron flux distribution in the form of Green's functions superposition. This representation allows to take into account detailed structure of the core including fuel pins, absorber rods, etc. The heterogeneous theory does not require the validity of the diffusion approximation over the reactor. The diffusion equations are used only to determine Green's function shape that weakly influences the reactor calculation accuracy. It is very important for pin-by-pin calculation of LWRs with modern heterogeneous structure of fuel assemblies.

A difference approximation of Green's functions is performed to produce equations to describe relationships only between neighboring cells [7]. Axial dependence of the neutron flux is defined by Fourier series expansion. To describe fast transients, the heterogeneous theory uses "time absorption" matrices [2] instead of the neutron velocities.

The neutron data base of BARS (Λ-matrices) is calculated by the TRIFON code [9]. TRIFON solves the multigroup neutron transport equation in various reactor cells using the collision probability method taking into account detailed structure of resonant cross sections. Strong resonances are taken into account by an additional division of the basic energy mesh within the resonance. Weak resonances are taken into account in the approximation of the effective resonance level [10]. Such resonant treatment was verified by comparison with calculational results obtained by the UNK code [11,12] which uses fine energy structure of resonant cross sections (up to 7,000 energy groups).

Fig.1 shows BWR fuel cell neutron spectrum in energy region of 11 lower resonances of ^{238}U calculated by two codes with ENDF/B-VI library: UNK (3,700 groups in this region) and TRIFON (187 groups; 17 groups per resonance). As shown in Fig.1, the UNK and TRIFON results are very close, although the number of groups in the TRIFON calculation is 20 times lower in comparison with the UNK calculation.

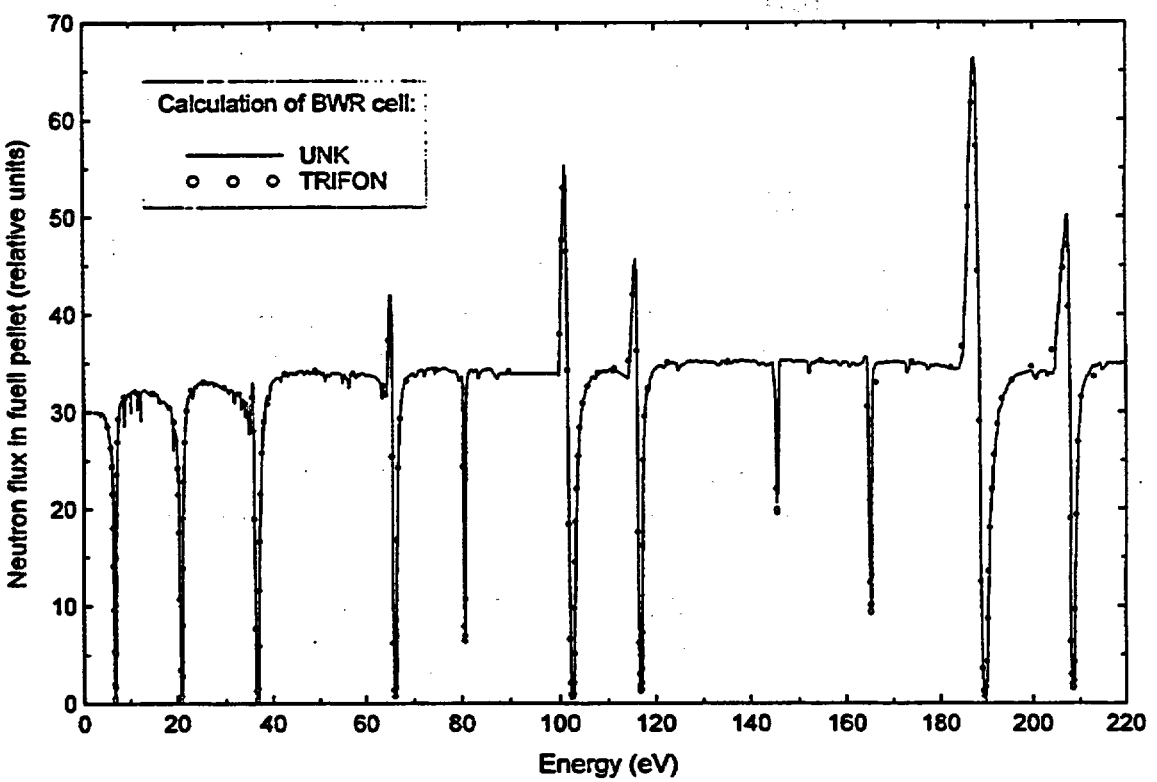

Fig.1. Neutron spectrum in BWR fuel cell averaged over fuel region.

III. CALCULATION OF REACTIVITY COEFFICIENTS

An accuracy in prediction of the reactivity coefficients is a key factor in the analysis of LWR transients, especially for RIA conditions. To analyze uncertainties in prediction of the reactivity coefficients, a number of PWR and BWR benchmark fuel cells [13-15] were calculated by the TRIFON code. All the benchmark calculations were performed using Monte Carlo codes MCNP-3A (with data library based on ENDF/B-V) and MCNP-4A (ENDF/B-VI).

The neutron data base of TRIFON was generated on the basis of ENDF/B-VI. To take into account the resonant structure of cross sections we use information about major resonances of ^{234}U, ^{236}U, ^{240}Pu and ^{242}Pu. As for ^{238}U the data base contains 11 most strong resonances up to 210 eV and 6 effective resonance levels above 210 eV. Practically all of the calculations were performed by using 17 groups per resonance; thus the total number of energy groups was about 350.

Table 1 presents the calculational results for the Doppler coefficient in PWR fresh fuel cells as compared with Monte Carlo benchmark calculations [13,14] for different fuel enrichment (ε_f). Monte Carlo result is given with a single standard deviation (σ) from the mean as an uncertainty; ε is relative deviation in TRIFON result in comparison with MCNP-3A (ε_3) and MCNP-4A (ε_4). Comparison of the presented data shows that almost all the TRIFON results are in excellent agreement with the MCNP calculations.

Table 1. Doppler coefficients α_D (pcm/K) in PWR fuel cells.

ε_f (%)	MCNP-3A $\alpha_D \pm \sigma$	MCNP-4A $\alpha_D \pm \sigma$	TRIFON		
			α_D	ε_3 (%)	ε_4 (%)
0.7	- 5.429 ± 0.760	- 5.468 ± 0.323	- 5.52531	1.77	1.04
1.6	- 3.558 ± 0.310	- 3.388 ± 0.207	- 3.43951	- 3.34	1.51
2.4	- 2.715 ± 0.277	- 2.754 ± 0.157	- 2.82679	4.11	2.64
3.1	- 2.584 ± 0.225	- 2.789 ± 0.137	- 2.51830	- 2.53	- 9.69
3.9	- 2.370 ± 0.187	- 2.534 ± 0.155	- 2.40529	1.49	- 5.08

MCNP-4A (ENDF/B-VI) benchmark calculations for BWR fuel cells [15] were carried out for a wide range of fuel enrichment (ε_f), fuel and moderator temperatures (T_f and T_m), moderator void fraction (v) and the fuel burnup. The total number of calculated fuel cells (except for cells with Gd) is 77.

Tables 2-10 present the TRIFON calculational results for the Doppler coefficient, the void coefficient and moderator temperature coefficient as compared with Monte Carlo calculations depending on fuel burnup. All of the Monte Carlo results are given with three standard deviations (3σ) from the mean as the calculational uncertainty.

Table 2. Doppler coefficients α_D (pcm/K) in BWR cells with fresh fuel.

ε_f (%)	v (%)	$T_{f1} - T_{f2}$ (K)	MCNP-4A $\alpha_D \pm 3\sigma$	TRIFON	
				α_D	ε (%)
0.711	0	300 - 833	- 3.78995 ± 0.30305	- 3.89683	2.82
1.6	0	300 - 833	- 2.86565 ± 0.20779	- 2.95042	2.96
2.8	0	300 - 833	- 2.41922 ± 0.18892	- 2.57283	6.35
3.95	0	300 - 833	- 2.24410 ± 0.17358	- 2.39665	6.80
1.6	0	833 - 1773	- 1.88711 ± 0.12437	- 1.98805	5.35
2.8	0	833 - 1773	- 1.63412 ± 0.11387	- 1.71413	4.90
3.95	0	833 - 1773	- 1.53920 ± 0.10702	- 1.57277	2.18
1.6	40	833 - 1773	- 2.44665 ± 0.15529	- 2.59146	5.92
2.8	40	833 - 1773	- 2.22956 ± 0.13862	- 2.29731	3.04
3.95	40	833 - 1773	- 2.10831 ± 0.12449	- 2.11477	0.31
1.6	70	833 - 1773	- 3.81984 ± 0.21348	- 3.70808	- 2.93
2.8	70	833 - 1773	- 3.10032 ± 0.18410	- 3.13795	1.21
3.95	70	833 - 1773	- 2.91216 ± 0.16348	- 2.75198	- 5.50

Table 3. Doppler coefficients α_p (pcm/K) in BWR cells with fuel burnup of 10 GWd/ST.

ε_f (%)	v (%)	$T_{f1} - T_{f2}$ (K)	MCNP-4A $\alpha_p \pm 3\sigma$	TRIFON	
				α_p	ε (%)
1.6	0	300 - 833	- 3.71859 ± 0.34223	- 3.67232	- 1.24
1.6	0	833 -1773	- 2.47785 ± 0.20181	- 2.45986	- 0.72
2.8	0	300 - 833	- 3.07190 ± 0.27939	- 3.24181	5.53
2.8	0	833 -1773	- 2.22569 ± 0.16147	- 2.20138	- 1.09
3.95	0	300 - 833	- 2.90585 ± 0.25085	- 2.96225	1.94
3.95	0	833 -1773	- 1.88406 ± 0.14804	- 1.90775	1.25
1.6	40	833 -1773	- 3.38408 ± 0.24047	- 3.27364	- 3.26
2.8	40	833 -1773	- 2.88312 ± 0.20159	- 2.83624	- 1.62
3.95	40	833 -1773	- 2.63723 ± 0.17342	- 2.57158	- 2.48
1.6	70	833 -1773	- 5.36560 ± 0.31695	- 4.98304	- 7.13
2.8	70	833 -1773	- 4.36234 ± 0.24622	- 4.26896	- 2.14
3.95	70	833 -1773	- 3.79971 ± 0.21954	- 3.65030	- 3.93

Table 4. Doppler coefficients α_p (pcm/K) in BWR cells with fuel burnup of 35 GWd/ST.

ε_f (%)	v (%)	$T_{f1} - T_{f2}$ (K)	MCNP-4A $\alpha_p \pm 3\sigma$	TRIFON	
				α_p	ε (%)
1.6	0	300 - 833	- 4.39344 ± 0.50901	- 4.32071	- 1.65
1.6	0	833 -1773	- 3.01407 ± 0.30028	- 2.67376	- 11.3
2.8	0	300 - 833	- 4.32288 ± 0.42061	- 4.20512	- 2.72
2.8	0	833 -1773	- 2.77002 ± 0.24888	- 2.74065	- 1.06
3.95	0	300 - 833	- 4.06753 ± 0.39406	- 4.10112	0.82
3.95	0	833 -1773	- 2.92959 ± 0.22850	- 2.57446	- 12.1
1.6	40	833 -1773	- 4.35547 ± 0.36339	- 3.84946	- 11.6
2.8	40	833 -1773	- 4.10445 ± 0.30695	- 3.77828	- 7.94
3.95	40	833 -1773	- 3.96731 ± 0.28726	- 3.72921	- 6.00
1.6	70	833 -1773	- 6.24924 ± 0.46280	- 5.79104	- 7.33
2.8	70	833 -1773	- 5.78185 ± 0.37625	- 5.35503	- 7.38
3.95	70	833 -1773	- 5.55094 ± 0.35852	- 5.30566	- 4.41

Table 5. Void coefficients α_v (pcm/%) in BWR cells with fresh fuel (T_f= 833 K).

ε_f (%)	$v_1 - v_2$ (%)	MCNP-4A $\alpha_v \pm 3\sigma$	TRIFON	
			α_v	ε (%)
1.6	0 - 40	- 156.950 ± 3.24595	- 156.672	- 0.18
2.8	0 - 40	- 156.902 ± 2.89769	- 156.006	- 0.57
3.95	0 - 40	- 152.295 ± 2.65744	- 151.892	- 0.26
1.6	40 - 70	- 422.110 ± 5.62667	- 414.851	- 1.72
2.8	40 - 70	- 380.009 ± 5.03520	- 372.378	- 2.00
3.95	40 - 70	- 341.521 ± 4.40965	- 339.265	- 0.66

Table 6. Void coefficients α_v (pcm/%) in BWR cells with fuel burnup of 10 GWd/ST (T_f= 833 K).

ε_f (%)	$v_1 - v_2$ (%)	MCNP-4A $\alpha_v \pm 3\sigma$	TRIFON	
			α_v	ε (%)
1.6	0 - 40	- 247.102 ± 5.09933	- 241.671	- 2.20
2.8	0 - 40	- 215.470 ± 4.15114	- 211.623	- 1.79
3.95	0 - 40	- 195.310 ± 3.70455	- 194.016	- 0.66
1.6	40 - 70	- 597.351 ± 8.39500	- 602.510	0.86
2.8	40 - 70	- 478.706 ± 6.68053	- 481.648	0.61
3.95	40 - 70	- 411.975 ± 5.98751	- 412.125	0.04

Table 7. Void coefficients α_v (pcm/%) in BWR cells with fuel burnup of 35 GWd/ST (T_f= 833 K).

ε_f (%)	$v_1 - v_2$ (%)	MCNP-4A $\alpha_v \pm 3\sigma$	TRIFON	
			α_v	ε (%)
1.6	0 - 40	- 337.427 ± 7.56898	- 342.941	1.63
2.8	0 - 40	- 313.997 ± 6.31922	- 317.436	1.09
3.95	0 - 40	- 301.364 ± 6.03973	- 303.163	0.60
1.6	40 - 70	- 836.255 ± 12.6691	- 849.050	1.53
2.8	40 - 70	- 706.754 ± 10.3701	- 729.032	3.15
3.95	40 - 70	- 645.497 ± 9.99811	- 667.856	3.46

Table 8. Moderator temperature coefficients α_m (pcm/K) in BWR cells with fresh fuel (T_f= 300 K; v = 0 %).

ε_f (%)	T_{m1} - T_{m2} (K)	MCNP-4A $\alpha_m \pm 3\sigma$	TRIFON	
			α_m	ε (%)
0.711	300 - 600	- 4.23683 ± 0.48924	- 4.47067	5.52
1.6	300 - 600	- 9.40089 ± 0.34691	- 9.47793	0.82
2.8	300 - 600	- 11.0232 ± 0.30170	- 11.0398	0.15
3.95	300 - 600	- 11.5615 ± 0.27272	- 11.5668	0.05

Table 9. Moderator temperature coefficients α_m (pcm/K) in BWR cells with fuel burnup of 10 GWd/ST (T_f= 300 K; v = 0 %).

ε_f (%)	T_{m1} - T_{m2} (K)	MCNP-4A $\alpha_m \pm 3\sigma$	TRIFON	
			α_m	ε (%)
1.6	300 - 600	- 7.62028 ± 0.55428	- 7.12947	- 6.44
2.8	300 - 600	- 15.0195 ± 0.45163	- 14.4955	- 3.49
3.95	300 - 600	- 15.6116 ± 0.40689	- 15.3598	- 1.61

Table 10. Moderator temperature coefficients α_m (pcm/K) in BWR cells with fuel burnup of 35 GWd/ST (T_f= 300 K; v = 0 %).

ε_f (%)	T_{m1} - T_{m2} (K)	MCNP-4A $\alpha_m \pm 3\sigma$	TRIFON	
			α_m	ε (%)
1.6	300 - 600	7.83994 ± 0.84485	8.87828	13.2
2.8	300 - 600	- 11.3586 ± 0.67058	- 11.1990	- 1.41
3.95	300 - 600	- 16.3475 ± 0.64311	- 16.1549	- 1.18

Analysis of the presented results allows to conclude the following. The TRIFON calculations of the Doppler coefficient give very good results for the fresh and slightly burnt-out fuel: the mean square deviation is 3-4 %; as for cells with fuel burnup of 35 GWd/ST this value is 7 % (this is quite satisfactory result). Calculational accuracy to predict the void effect is very high: the TRIFON and MCNP results are in agreement of no more than 4 %. As for the moderator temperature coefficient, almost all the TRIFON results are within 3σ of the MCNP results.

IV. VALIDATION OF THE PIN-BY-PIN REACTOR MODEL ON BENCHMARK CRITICAL EXPERIMENTS

To validate the LWR pin-by-pin model, experimental results obtained at ZR-6 critical assembly [16] were used. These results include measurements of water critical level and pin-by-pin distribution of fuel activation. ZR-6 assembly consists of shortened VVER fuel rods with fuel enrichment of 1.6, 3.6, 4.4 %, absorber rods of different type and water cells. The moderator temperature was 20, 80 and 130 °C. Boric acid concentration in the moderator was up to 8 g/l. The total number of critical configurations with fuel lattice of 12.7 (lattice of VVER-1000 type) selected for validation of LWR pin-by-pin model is 107.

All assemblies may be divided into the following types according to their configurations:

- uniform configurations (single-zone and double-zone);
- Xn type configurations with absorbers or water holes in each n-th lattice position;
- K91 "fuel assembly" type configurations (19 "fuel assemblies", each having 91 cells);
- K271 "fuel assembly" type configurations (7 "fuel assemblies", each having 271 cells);
- K331 "fuel assembly" type configurations (1 "fuel assembly" with 331 cells).

All of the calculations were performed by using the BARS code with 5-group neutron data bases prepared by the TRIFON code with ENDF/B-VI. Detailed calculational results are described in [11].

In Figs.2-17 core loading patterns and radial distribution of the fuel activation (both calculated and measured) are presented. The calculated data were normalized to the mean value over experimental data. Radial distributions of the fuel activation are given in directions, pointed at the core loading pattern: experimental data - by symbols and calculated ones - by curves.

Table 11 presents the BARS calculational results for the multiplication factor and calculational accuracy (ε - mean square deviation) in prediction of the pin-by-pin fuel activation distribution. All data in Table 11 are averaged on each type of assemblies and for all assemblies. Each K_{eff} value is given together with the corresponding mean square deviation for the assemblies of this type.

Table 11. BARS calculational results for ZR-6 assemblies.

Type of assembly	Total Nos. of assemblies	Mean value of K_{eff} multiplication factor	Nos. of assemblies with measurements	ε (%)
Uniform	33	0.99494 ± 0.00165	18	1.33
Xn	39	0.99706 ± 0.00275	11	1.65
K91	11	0.99731 ± 0.00199	6	1.91
K271	12	0.99487 ± 0.00155	-	-
K331	12	0.99614 ± 0.00166	6	1.29
Total	107	0.99608 ± 0.00207	41	1.49

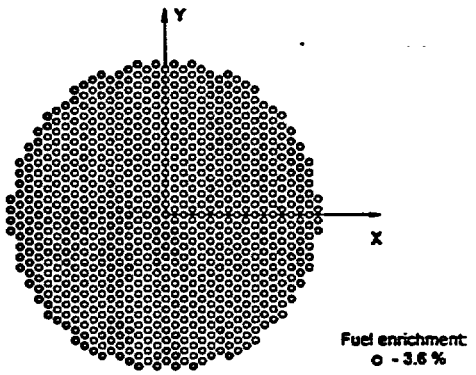

Fig.2. Critical assembly ZR-6. Loading pattern 154/154 (uniform type).

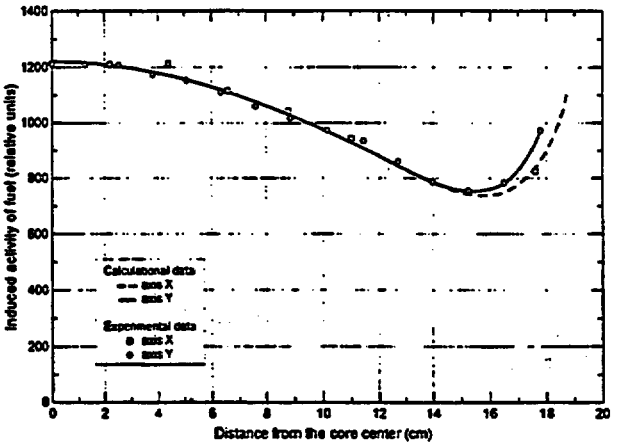

Fig.3. Comparison of calculational and experimental data for assembly 154/154.

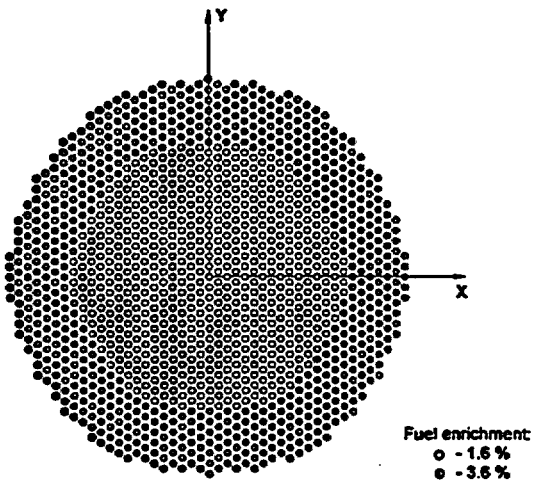

Fig.4. Critical assembly ZR-6. Loading pattern 160/160 (uniform type).

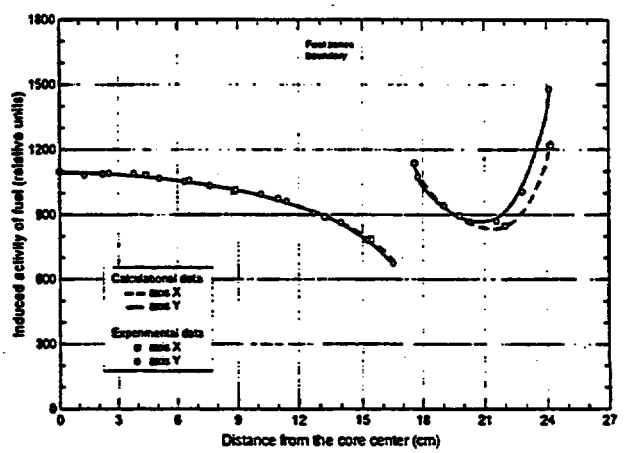

Fig.5. Comparison of calculational and experimental data for assembly 160/160.

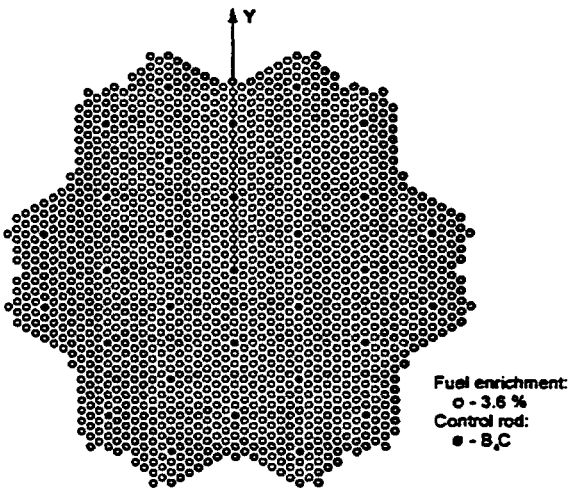

Fig.6. Critical assembly ZR-6. Loading pattern 244/244 (Xn-type).

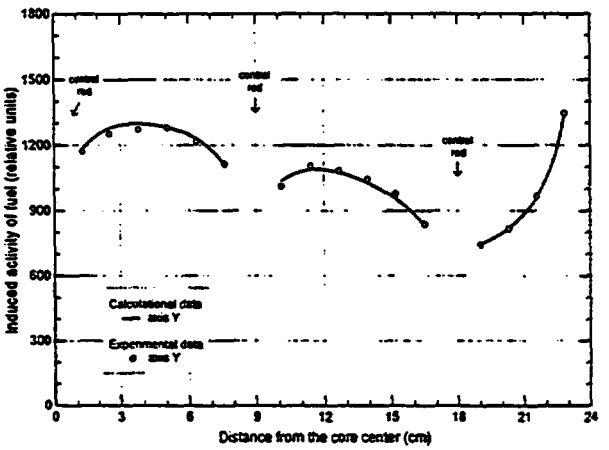

Fig.7. Comparison of calculational and experimental data for assembly 244/244 (moderator temperature is 130 °C).

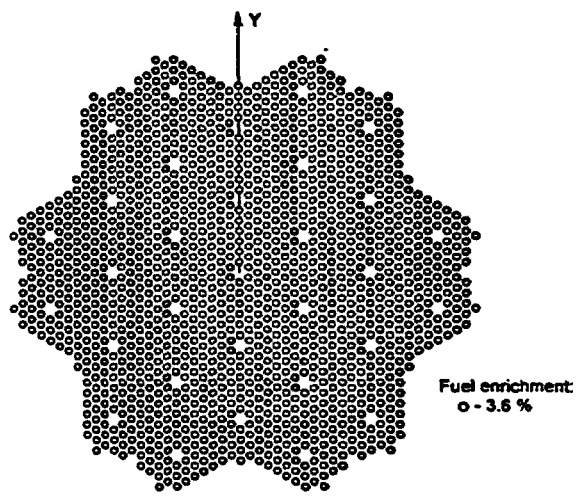

Fig.8. Critical assembly ZR-6. Loading pattern 245/245 (Xn-type).

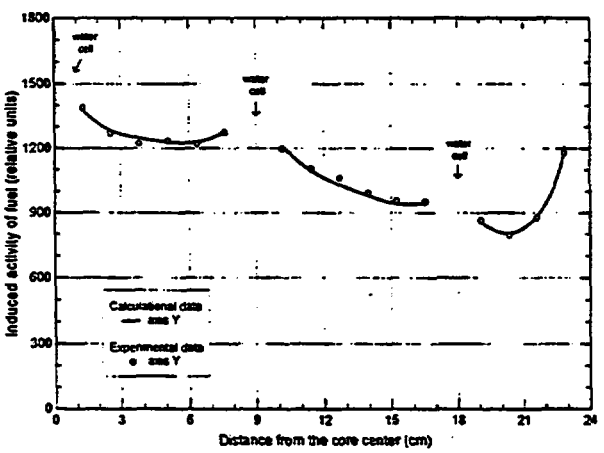

Fig.9. Comparison of calculational and experimental data for assembly 245/245 (moderator temperature is 130 °C).

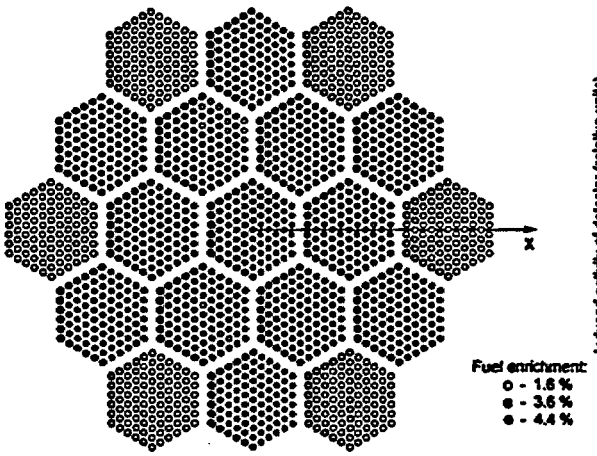

Fig.10. Critical assembly ZR-6. Loading pattern 113/113 ("fuel assembly"-type).

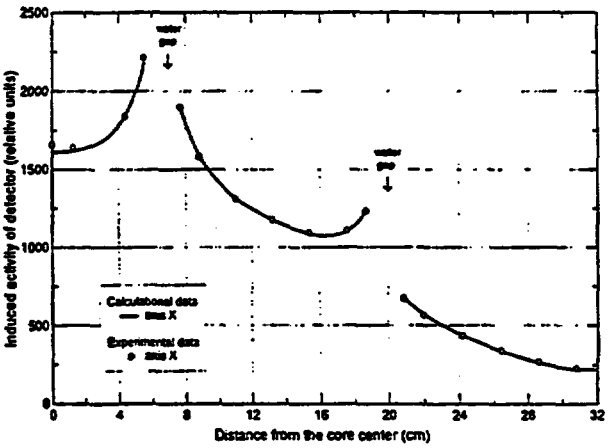

Fig.11. Comparison of calculational and experimental data for assembly 113/113.

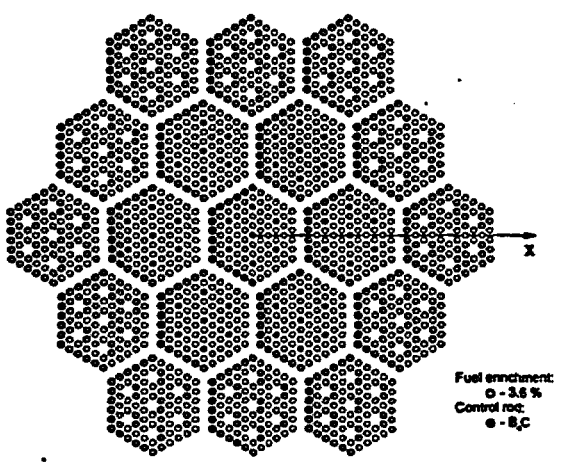

Fig.12. Critical assembly ZR-6. Loading pattern 103/103 ("fuel assembly"-type).

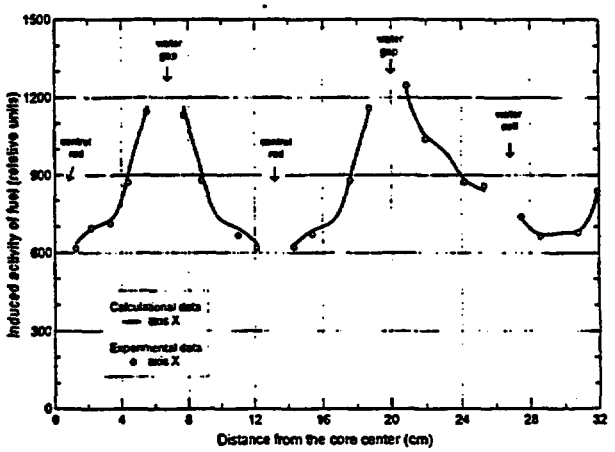

Fig.13. Comparison of calculational and experimental data for assembly 103/103.

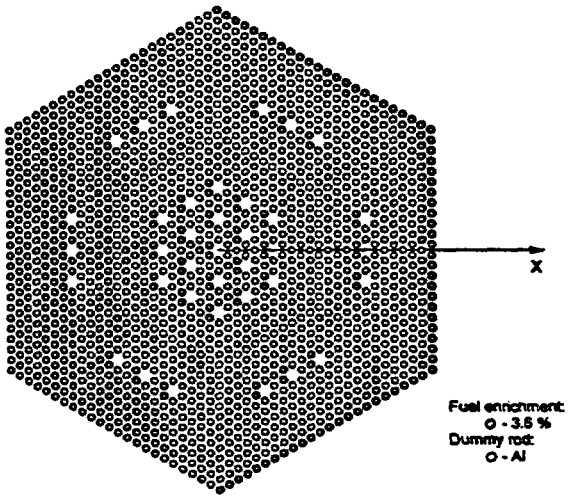

Fig.14. Critical assembly ZR-6. Loading pattern 88/88 ("VVER fuel assembly"-type).

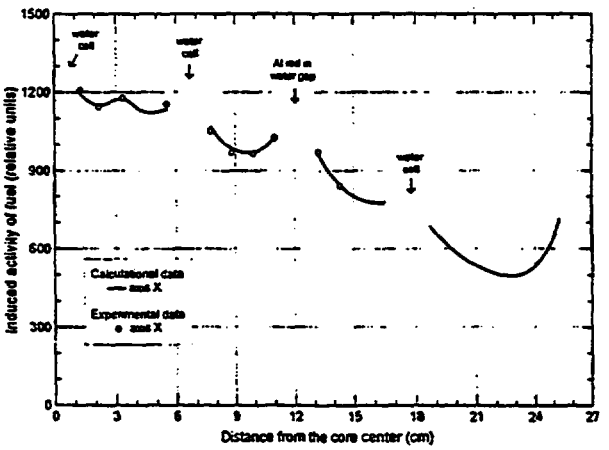

Fig.15. Comparison of calculational and experimental data for assembly 88/88.

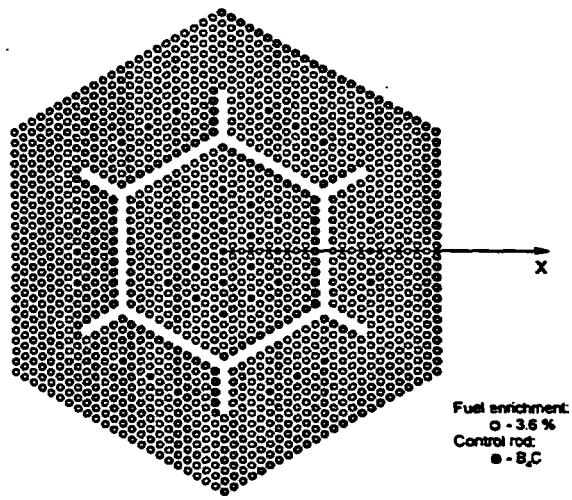

Fig.16. Critical assembly ZR-6. Loading pattern 90/87 ("VVER fuel assembly"-type).

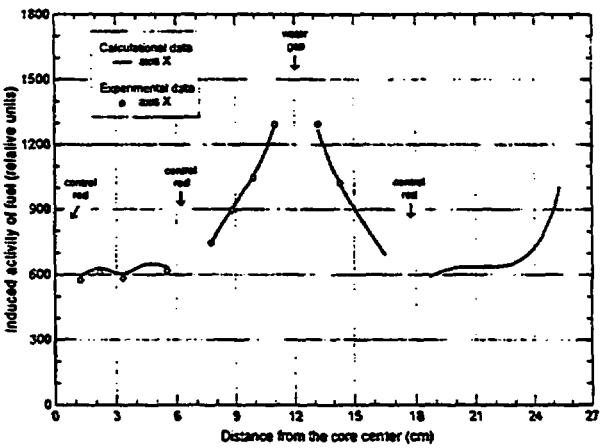

Fig.17. Comparison of calculational and experimental data for assembly 90/87.

Analysis of the calculational results shows that the BARS code with rather high accuracy predicts the multiplication factor and spatial distribution of the fuel activation for the cores of complex geometry with rather strong local deformations in neutron flux due to various types of perturbation (water cells, absorbers, water gap or even trap). It should be mentioned that the BARS calculational accuracy for ZR-6 assemblies is not worse in comparison with the Monte Carlo code KENO-V [17] and the HELIOS code for precise transport calculation of fuel assemblies [18].

V. KINETIC MODELING OF IGR PULSE EXPERIMENTS

To verify the pin-by-pin transient model, experimental results of the power dynamic behavior obtained at the pulsed graphite reactor IGR were used. IGR is intended to test reactor fuel rods under RIA conditions. The basic feature of such transients is the fact that the power surge is initiated by a control rod withdrawal and are suppressed by the negative temperature feedback: the increase in graphite temperature leads to the increase in thermal neutron leakage and, as a result, to large negative reactivity insertion. Such experiments modeling the control rod ejection accident in LWR with temperature feedback are unknown.

The reactor core (see Fig.18) consists of graphite columns impregnated with highly enriched uranium. In the core center there is a central experimental channel where capsule containing test fuel rod samples is to be loaded. The core is surrounded by graphite reflector, thermal shield and water tank. To control reactor operations 16 Gd rods in the core and in the reflector are used. The time dependence of the reactor power was measured by means of a set of out-core ionization chambers in the water tank and in-core detectors located near the experimental capsule.

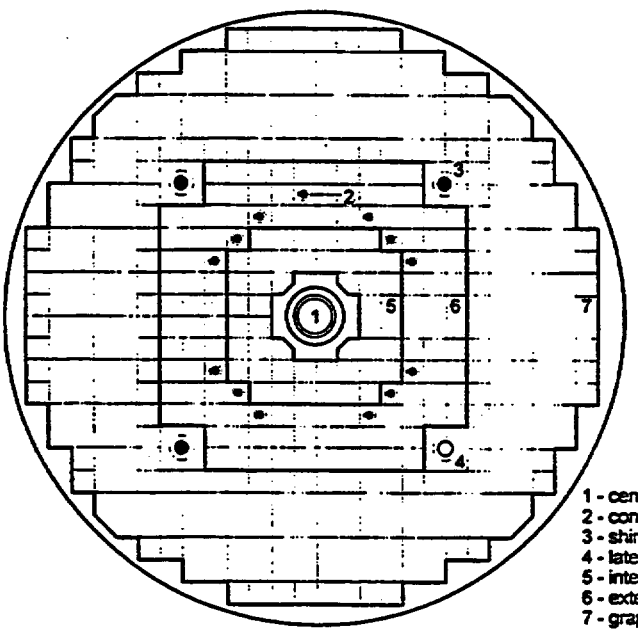

Fig.18. Cross-sectional layout of IGR reactor.

The dynamic behavior of IGR in pulse experiments may be characterized by: sharp changes in the reactor power; significant deformations of the neutron flux; strong heterogeneity in the core graphite temperature distribution; effects of control rod interference and graphite heating up on control rod worth; strong dependence of prompt neutron lifetime and the feedback coefficient on the reactor core temperature.

The verification of the BARS transient module was performed on the basis of experiments carried out at IGR in 1995. The inserted reactivity varied within 0.9 - 1.8 β. The IGR power time profile was recorded by 6 ionization chambers and 3 in-core detectors. Fig.19 shows the comparison of the calculational and experimental results for the test with inserted reactivity of 1.8 β. As shown in Fig.19 calculated and measured power time profiles are in an excellent agreement.

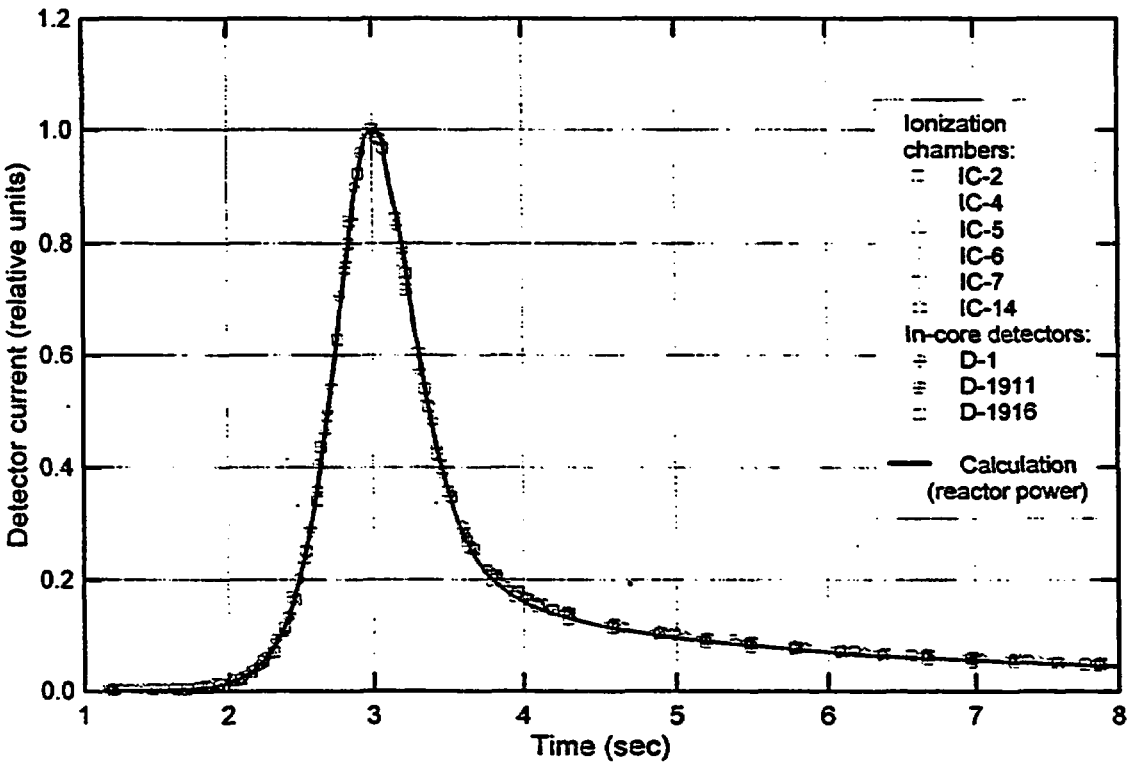

Fig.19. Comparison of calculational and experimental data for the pulse with inserted reactivity of 1.8 β at IGR reactor.

VI. CONTROL ROD EJECTION RIA MODELING

To illustrate the features of LWR dynamics pin-by-pin calculations, some results of control rod ejection RIA modeling at hot zero power conditions for VVER-1000 [19] are presented. The calculations were carried out by the coupled RELAP5 - BARS codes for the initial fuel load of Zaporozskaya NPP Unit 5. Neutronic model consists in 5 energy groups, 6 delayed neutron groups, 5 axial harmonics, and about 75,000 calculational cells including about 51,000 fuel cells.

Fig.20 shows the reactor fuel load and indicates fuel assemblies (1,2) and (2,4) with the maximum fuel rod power after the control rod ejection. Fig.21 illustrates 1/4 part of detailed structure of VVER-1000 load map which takes into account by the BARS pin-by-pin model.

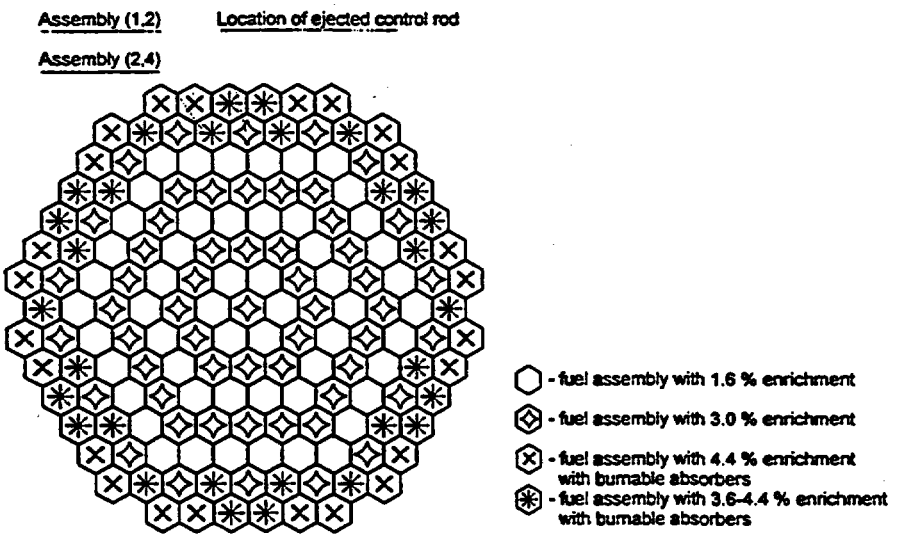

Fig.20. Zaporozskaya NPP Unit 5 initial fuel loading.

The reactor power and reactivity depending on transient time are plotted in Fig.22 (t = 0 corresponds to the beginning of the rod ejection). The reactivity reaches the maximum value of 1.21 β (β = 0.749 %). Pellet averaged fuel enthalpies for the hottest pellet in the reactor core and for the hottest pellet in the average fuel rod of the hottest fuel assembly (FA) are plotted as a function of transient time in Fig.23. The maximum fuel enthalpy is reached in the fuel pellet located in theFAs (1,2) and (2,4) rather than in the hottest FA (2,5) with ejected control rod.

Fig.24 shows detailed pin-by-pin power distribution for the reactor initial steady-state. Pin-by-pin power distribution for time moment when the maximum power is reached is shown in Fig.25. For comparison for the same time moment the assembly-by-assembly averaged power distribution is presented in Fig.26. Near the ejected rod, extremely complicated shape of the pin-by-pin power distribution is observed (see Fig.25). The maximum power is found in accident assembly with ejected control rod whereas in six neighboring assemblies the maximum fuel rod power exceeds the maximum fuel rod power in accident assembly by more then 10 %. Among them, four assemblies located near the reflector have a relatively low power. Obviously, the widely used assembly-by-assembly diffusion model can lead to significant uncertainties in calculations of the peak fuel enthalpy in such assemblies.

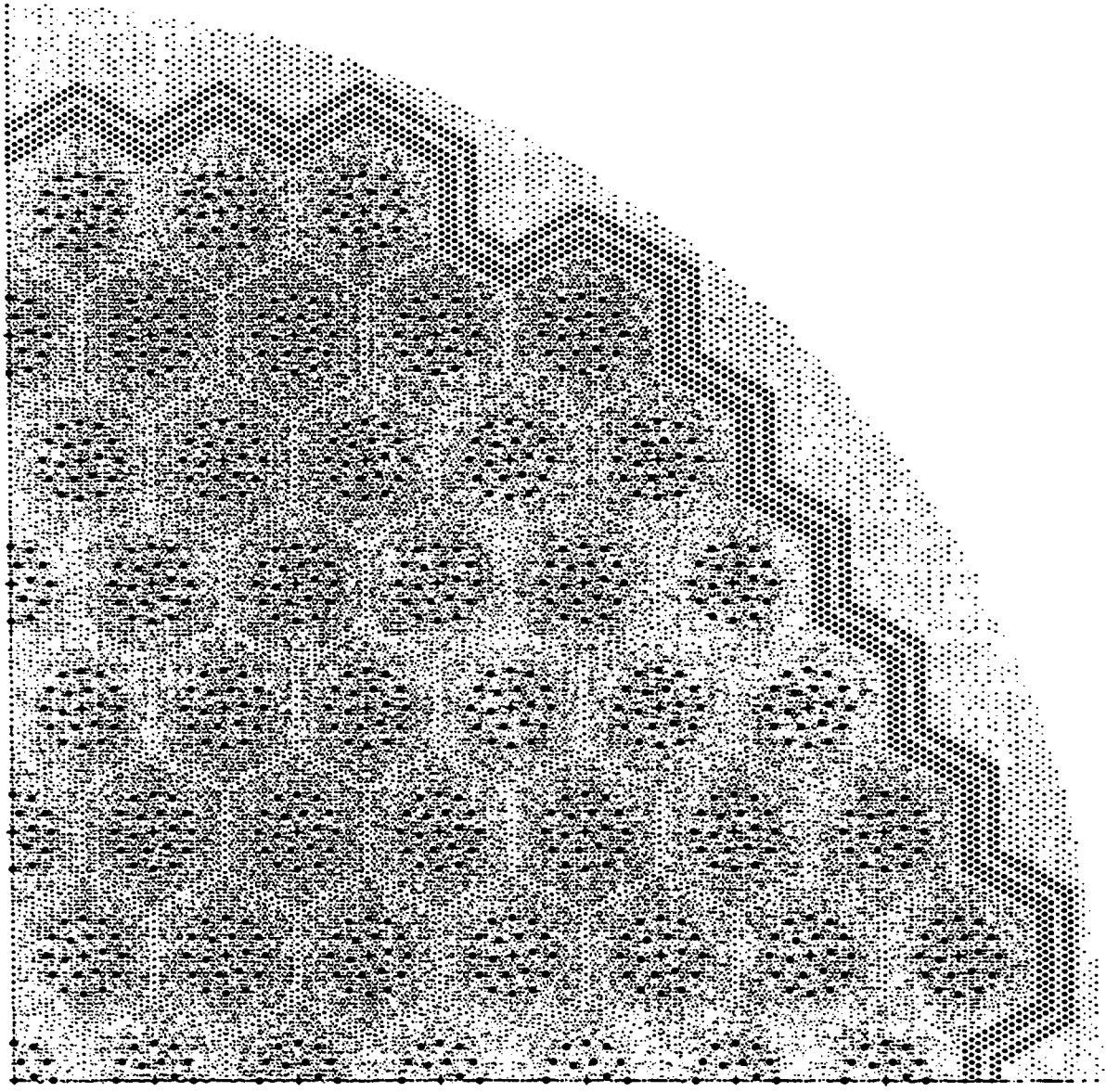

Fig.21. 1/4 part of detailed structure of VVER-1000 load map for the BARS pin-by-pin model input.

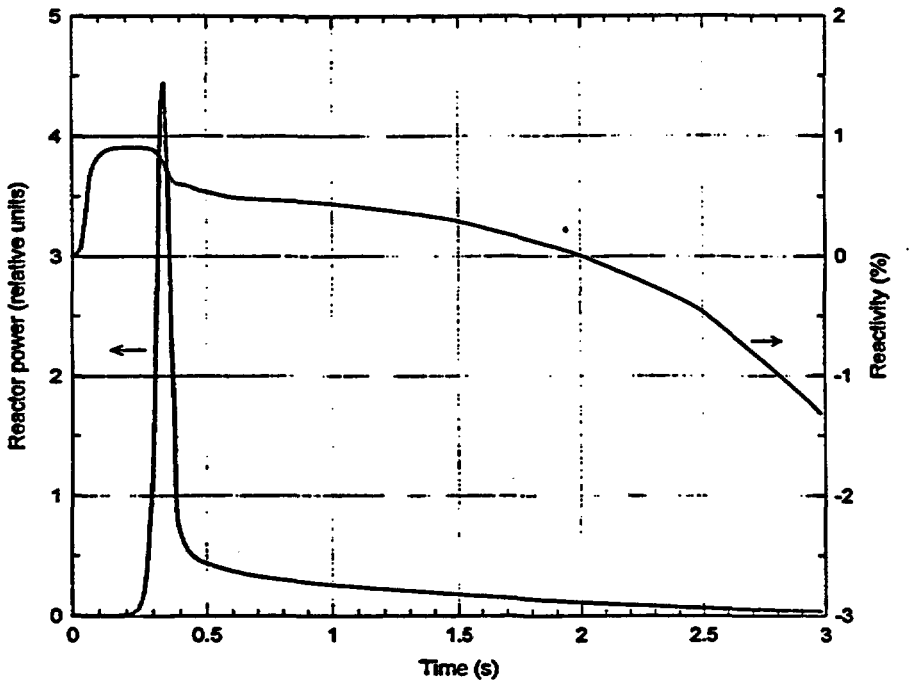

Fig.22. Reactor power and reactivity vs. time.

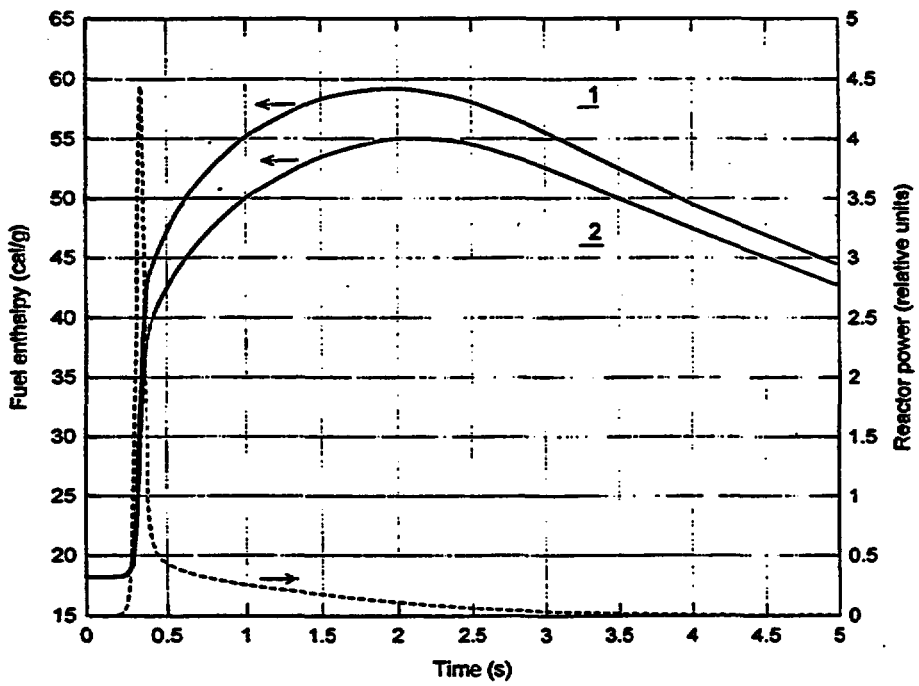

Fig.23. Fuel enthalpy vs. time: 1 - the hottest fuel pellet in the reactor core; 2 - the hottest fuel pellet in the average fuel rod in FA (2,5).

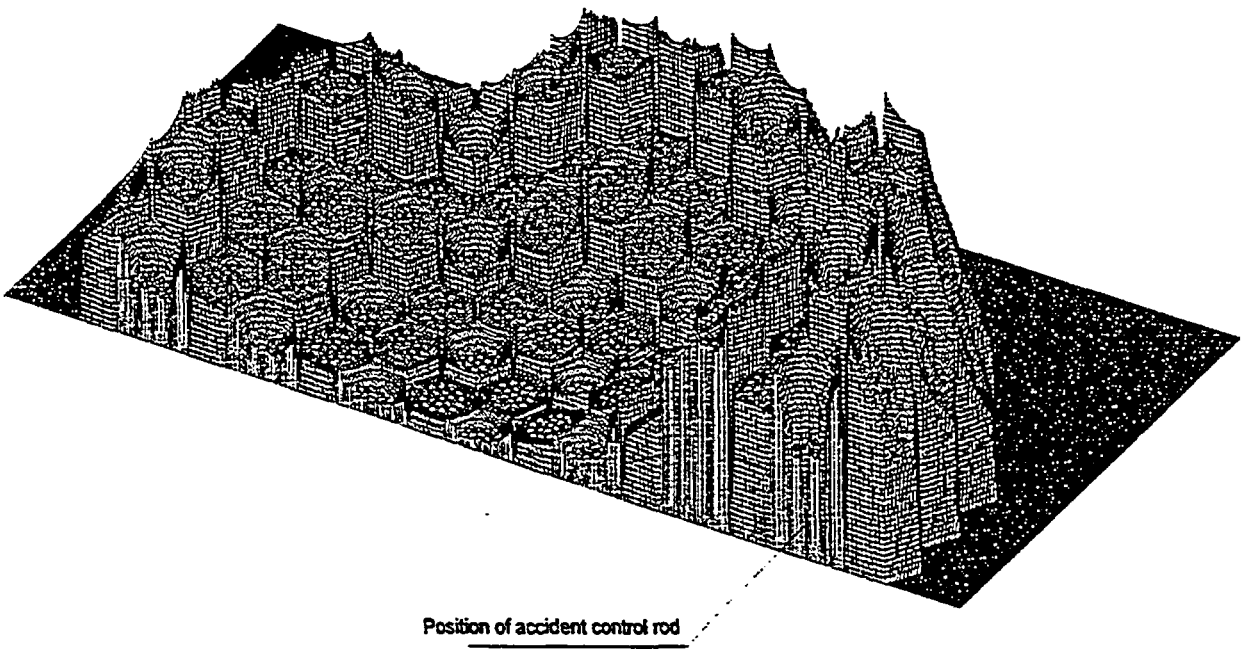

Fig.24. Pin-by-pin power distribution at t = 0 s (steady-state).

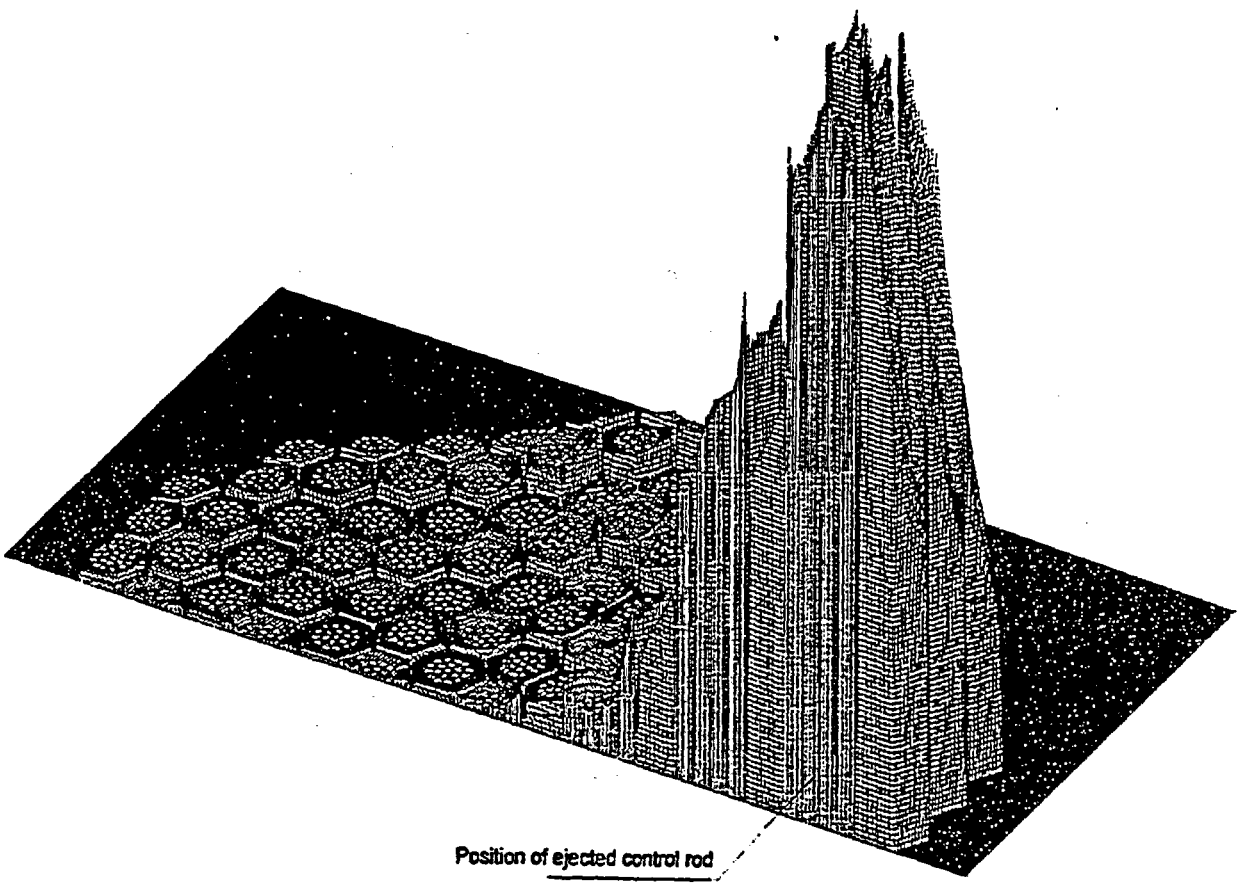

Fig.25. Pin-by-pin power distribution at t = 0.34 s.

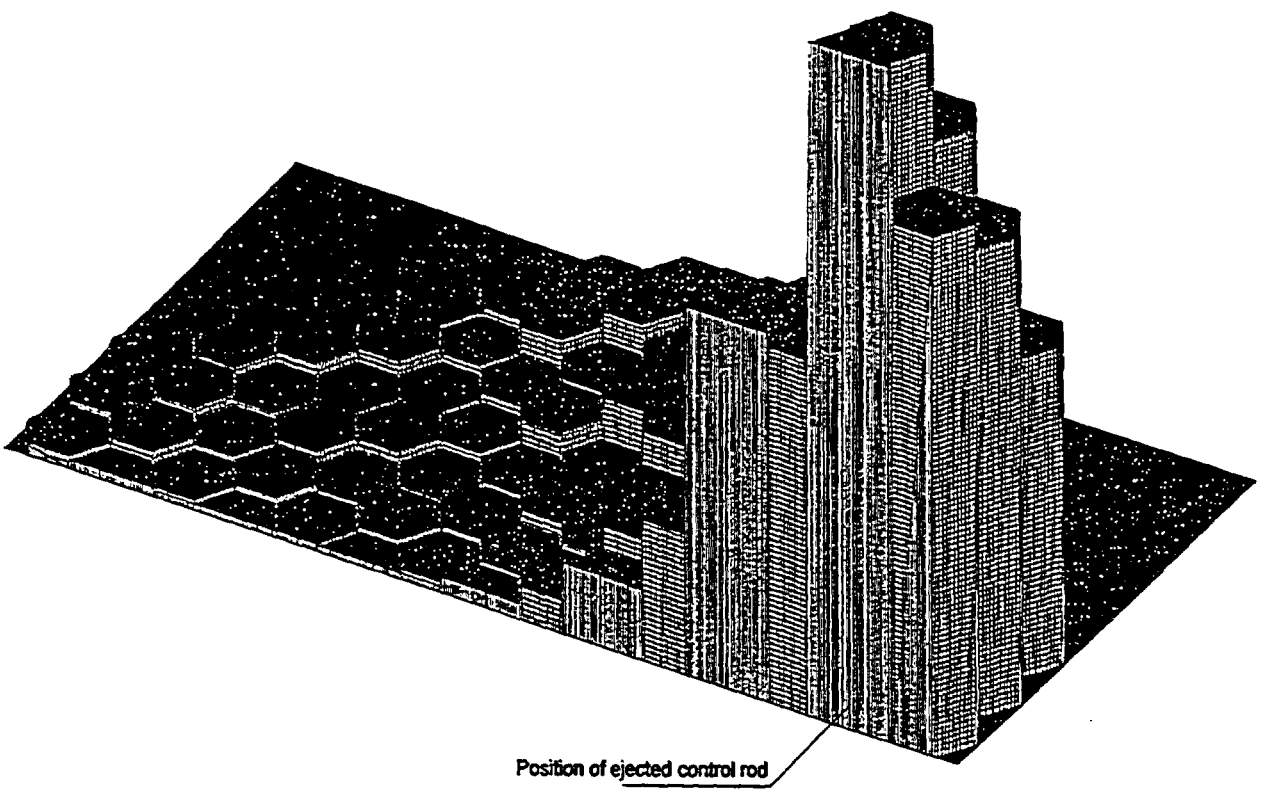

Fig.26. Assembly-by-assembly averaged power distribution at t = 0.34 s.

VII. CONCLUSION

This paper focuses on the problem of validation of the pin-by-pin neutron kinetics method to analyze LWR RIAs with large deformations in the neutron flux over the reactor core. Validation procedure involved the following steps.

The TRIFON code validation was based on comparison with Monte Carlo benchmark calculations of the reactivity coefficients for a large number of PWR and BWR fuel cells. This comparison demonstrates the ability of the TRIFON code to predict the Doppler coefficient as well as the void coefficient and the moderator temperature coefficient with rather high accuracy. It meets accuracy criteria for LWR RIA analysis.

The pin-by-pin reactor model validation was performed using experimental data obtained at ZR-6 critical assembly. Comparison of the calculational and experimental results show that the BARS code predicts correctly spatial distribution of neutron flux in cores with very complex configurations and with various types of perturbations. As the BARS calculations shown, mean square deviations in prediction of the multiplication factor K_{eff} and the spatial distribution of the fuel activation are 0.002 and 1.5 % respectively. These values do not exceed corresponding ones for such codes as KENO-V Monte Carlo code and HELIOS transport code for precise calculation of fuel assemblies.

The BARS neutron kinetics model was verified on experimental results obtained at the IGR reactor. The experiment can be considered as an example of a control rod withdrawal accident with a large negative feedback due to reactor core temperature increase. Comparison of the obtained data shows that calculated and measured power time profiles are in an excellent agreement.

Some features of the pin-by-pin LWR transient model of the BARS code were demonstrated in the control rod ejection RIA modeling at hot zero power conditions in VVER-1000. The calculations were carried out by the coupled RELAP5 - BARS codes. Effects of the local power surge on accident consequences were estimated. It was shown that the detailed pin-by-pin power distribution in the fuel assemblies near the ejected control rod is very complicated. It was found that after the control rod ejection the fuel rods power for a number of fuel assemblies exceeds the maximum fuel rod power in the hottest fuel assembly. Some of these fuel assemblies with rather low power are located near the reflector. The maximum fuel enthalpy was achieved in the fuel rod that is contained not in the fuel assembly with the maximum power, but in one of neighboring fuel assemblies. Therefore, the assembly-by-assembly modeling of such an accident underestimates the maximum fuel enthalpy, and its specification by reconstruction of the detailed power distribution in the hottest fuel assembly may lead to inadequate results.

The results presented in this paper show that the BARS code can be successfully used for LWR RIA modeling and for intercomparison with 3 D diffusion neutronic codes.

REFERENCES

1. "RELAP5/MOD3 Code Manual," NUREG/CR-5535, INEL-95/0174 (1995).

2. A.Avvakumov and V.Malofeev, "Three-Dimensional Simulation of Delayed Neutron Transients in a Heterogeneous Reactor," *At. Energy*, 70 (1) (1991).

3. A.Avvakumov and V.Malofeev, "An Advanced 3 D Pin-by-pin Neutronic Model for the LWR RIA Analysis: Features, Advantages and Validation," Report No.90-12/1-8-97, Nuclear Safety Institute of Russian Research Centre "Kurchatov Institute" (1997).

4. A.Galanin, *Proceedings of the First International Conference on the Peaceful Use of Atomic Energy*, Geneva, 5, 477 (1955). S.Feinberg, Ibid., 484.

5. J.Lugou and C.Magnot, "Three-Dimensional Theory of Heterogeneous Reactors," *Nucl. Sci. Eng.*, 19, 58 (1964).

6. D.Blackburn, "Finite-Difference Formulation of the Multi-Group Source-Sink Equations," *Proceedings of the EAES Symposium on Advances in the Reactor Theory*, Karlsrue (April 1963).

7. B.Kochurov and V.Malofeev, "A Difference Approach to the Solution of Heterogeneous Reactor Equations," *Annals of Nuclear Energy*, 4, 21 (1977).

8. B.Kochurov, "An Advanced Method of Heterogeneous Reactor Theory," *JAERI-Review*, 94-002, JAERI (1994).

9. A.Kvaratshely and B.Kochurov, "A Method for Calculation of Neutronic Parameters in a Heterogeneous Reactor Cell," *At. Energy*, 58 (2) (1985).

10. B.Kochurov, "Effective Resonance Levels", *At. Energy* 60 (3) (1986).

11. A.Avvakumov, V.Malofeev, V.Davidenko and V.Tsybulsky, "Validation of the BARS Code Package with ENDF/B Based Data Library," Report No.90-12/1-4-98, Nuclear Safety Institute of Russian Research Centre "Kurchatov Institute" (1998).

12. V.Davidenko and V.Tsybulsky, "Detailed Calculation of Neutron Spectrum in a Cell of a Nuclear Reactor," *Proceedings of the International Conference on the Physics of Nuclear Science and Technology*, Long Island, New Yourk, USA (October 5-8, 1998).

13. R.D.Mosteller, L.D.Eisenhart, R.C.Little, W.J.Eich and J.Chao, "Benchmark Calculations for the Doppler Coefficient of Reactivity," *Nucl. Sci. Eng.*, 107, 265 (1991).

14. F.Rahnema and H.N.M.Gheorghiu, "ENDF/B-VI Benchmark Calculations for the Doppler Coefficient of Reactivity," *Ann. Nucl. Energy*, 23,12 (1996).

15. F.Rahnema, D.Ilas and S.Sitaraman, "Boiling Water Reactor Benchmark Calculations," *Nucl. Technol.*, 117, 184 (1997).

16. "Experimental Investigations of the Physical Properties of VVER-type Uranium-Water Lattices," Final Report of TIC, Budapest, Akademiai Kiado, 1 (1985), 3 (1991).

17. "The VVER Experiments: Regular and Perturbed Hexagonal Lattices of Low-Enriched UO_2 Fuel Rods in Light Water," Report LEU-COMP-THERM-015, vol.IV, KFKI, Budapest, 1996.

18. S.P.Szabo and R.J.Stammler, "HELIOS: Benchmarking Against Hexagonal TIC Experiments," *Proceedings of the International Conference on the Physics of Nuclear Science and Technology*, Long Island, New Yourk, USA (October 5-8, 1998).

19. A.Avvakumov, V.Malofeev, S.Pylev and V.Sidorov, "3 D Pin-by-pin Modeling of Rod Ejection RIA in VVER-1000," Report No.90-12/1-33-97, Nuclear Safety Institute of Russian Research Centre "Kurchatov Institute" (1997).

Oxidation and Quenching Experiments with High Burnup Cladding under LOCA conditions.

Revision of Previous Data and Main Trends of Recent Tests.

C. GRANDJEAN, IPSN, CEN/Cadarache, France
R. CAUVIN, EDF, Chinon, France
P. JACQUES, EDF, Villeurbanne, France

ABSTRACT

An experimental program has been conducted in France to investigate the oxidation and thermal shock behavior of irradiated cladding under LOCA simulated conditions. Oxidation and quenching experiments were successively performed on as-fabricated, unirradiated but pre-oxidized, irradiated and unirradiated pre-hydrided cladding. The main trends of the tests results on irradiated cladding are summarized. A revision is given of the preliminary analysis of the quenching tests on irradiated cladding. The main trends of the current program tests results relative to oxidation and quench behavior of highly hydrided cladding are discussed.

1. Introduction

Within the framework of burnup extension request, experimental programs have been undertaken in France, jointly by EDF, IPSN, CEA and FRAMATOME, in order to provide the Safety Authority with relevant data concerning the behavior of high burnup fuel under accidental conditions. Relative to Loss-Of-Coolant-Accident, the initial studies were focused on the behavior of cladding alone. As-fabricated cladding as well as cladding bearing a simulated or actual in-reactor corrosion state representative of high burnup reactor operation were studied. With reference to the current LOCA acceptance criteria, the main issues concern the high temperature oxidation kinetics and the resistance to thermal shock upon quench after significant oxidation of the cladding.

2. Background

The TAGCIS test series was first conducted to investigate the thermal shock behavior of unirradiated cladding bearing a pre-corrosion state simulating the end-of-life state of high burnup fuel claddings. Thermal shock experiments (high temperature oxidation terminated by water quench) were performed on different samples : reference bare samples and samples pre-corroded in a pressurized loop. The LOCA transient oxidation configuration was either one-side or two-side, so as to differentiate oxidation development and quench loads for respectively non-ruptured or ruptured rods at ballooning. Nearly 400 tests runs were realized from mid 91 to mid 93 , among which 140 tests results were retained in the data analysis.

The TAGCIR tests series was then performed on actually irradiated cladding samples taken from high burnup rods irradiated over 5 cycles in a commercial EDF PWR and having reached a rod burnup close to 60 GWd/tU. The tests were realized in a hot cell on a test facility very similar to that of the previous

TAGCIS tests ; again the testing configuration was either one-side or two-side oxidation. The test program was completed in 1996 ; 38 tests runs were performed, among which 25 provided usable results.

More details on the experimental features have been presented previously [1]. An overview of these test programs and a preliminary analysis of the results have been presented at the 24th WRSM in October 1996[2].

The main tendencies of the results will be summarized below.

3. Effect of initial oxide grown during in-reactor operation

The initial oxide scale appears non protective relatively to high temperature oxidation and may be considered fully transparent to oxygen diffusion. This is illustrated on figure 1, showing plots of the total thickness of oxide (i.e. initial + transient) measured on external side of irradiated samples after transient testing and compared to predictions with the Cathcart model with and without consideration of the protective effect of the initial layer relatively to transient oxidation. This is coherent with our knowledge of the oxide scale grown during normal operation of the reactor ; this oxide is in fact a porous layer, only the first few microns at the metal-oxide interface being a dense layer.

On the other side, the comparison of the results of the as-fabricated samples and the pre-oxidized ones shows that there is no increase of the thickness of the oxygen rich layers (ZrO_2 and α-Zr(O)) due to the presence of the initial oxide layer.

That's why we can assume that the in reactor corrosion oxide layer may be taken into account simply as for the corresponding reduction in cladding wall thickness.

4. Irradiated cladding behavior

4.1 Qualitative results

Irradiated zircaloy exhibits a slightly enhanced oxidation rate as compared to unirradiated zircaloy, the enhancement effect increasing with temperature. This is shown on figure 2 which plots the measured versus calculated values of the transient oxide thickness for irradiated and unirradiated samples tested in the same facility.

In order to quantify in more detail the oxidation kinetics of irradiated zircaloy a specific test program was undertaken (*CODAZIR program*). The tests consisted in isothermal oxidation runs, without quench, on short cladding rings that were initially stripped of the corrosion oxide by mechanical erosion. The preliminary tests results have shown that the oxidation kinetics of zircaloy is clearly influenced by its hydrogen content ; however, the mechanical erosion for stripping of the oxide layer on irradiated samples had eliminated a more or less wide sublayer of metal with a high concentration of the hydrides accumulated in reactor : the resulting erratic initial conditions thus induced non reproducible effects that led us to interrupt the program.

Tests on irradiated cladding have not indicated any failure below the acceptance limit ECR=17% relative to the transient oxidation alone. Addition of the initial oxidation shifts evidently the observed failure limit towards higher values ; however it raises an important question regarding the physical consistency of adding two oxidation components associated to very different processes and having thus different embrittlement weights ; moreover it makes problem to define the reference initial state (before which oxidation ?) to calculate ECR.

In the preliminary analysis the failure maps indicated a lower brittleness for irradiated cladding than for unirradiated cladding under two-side oxidation ; results for one-side oxidation tests were unclear.

4.2 Quantitative analysis

New tests series was performed on the previous TAGCIR facility with incorporation of significant experimental improvements. Among these was the use of a modified inductive coil, with contiguous turns of square cross section. A detailed analytical investigation of the temperature distribution associated to the successive designs of the inductive coil has indicated that the local increase of the turns spacing near coil midplane, in order to allow the optical pyrometric sighting, induces a local temperature gradient around measurement target ; this should have resulted in small axial and azimutal oxidation differences. Accordingly it was thought that the azimutal variations in oxidation state observed on post-test metallographic examinations, beyond uncertainty on thickness measurements, did reflect the temperature variations. It was therefore considered that the most brittle location and, in case of specimen rupture, the location of rupture inception, should be characterized by the maximum oxidation state (rather than the average) measured on the metallographic cut. These considerations made questionable the results obtained previously from the TAGCIS and TAGCIR tests series, namely the failure limits relative to oxidation amount that were associated to an average state. This finally led us to reconsider the failure limits derived for the two-side oxidation tests series in the TAGCIR experiments. Figure 3 gives a failure map on ECR parameter with, for each test, the ECR interval corresponding to the different measurements performed in the metallographic examination plane : the revised failure limit was drawn as the lowest upper value of ECR interval observed among failed tests : this limit at ECR=28% appears nearly 2% above the limit previously indicated based on average oxidation value, thus indicating a higher margin relatively to the current acceptance limit ECR=17%. This revised limit, compared to recent results of quench tests on as-received cladding, indicates that the quench resistance of irradiated material is very close to , or even slightly higher than, that of unirradiated cladding at same oxidation rate.

Additionally, a further examination of the experimental conditions for the one-side oxidation tests has revealed that the important axial temperature gradient at the bottom of the sample resulting from experimental configuration will have induced locally particular failure conditions, making the measured conditions in central region not representative of actual conditions at the location of failure initiation ; consequently, it was decided to exclude the results of these one-side oxidation tests series from the current data analysis. Very recently, new one-side oxidation tests have been realized with revised experimental conditions avoiding the previous artifact ; the preliminary results of these tests indicate a failure limit close to (but slightly below) that for two-side oxidation, with some evidence of mechanical constraints likely associated to the asymmetric character of oxidation growth and quench loads ; however the acceptance limit remains largely conservative.

5. The current test program

5.1 Objectives and short description of the HYDRAZIR test program

The HYDRAZIR program was undertaken, based on the main TAGCIR outcome that the behavior of irradiated zircaloy under LOCA conditions is essentially borne by the hydrogen charged in the cladding. The objectives of this program are to quantify the influence of hydrogen content on oxidation kinetics and quench resistance. The experimental program consists of different series of oxidation kinetics experiments and oxidation/quenching experiments on unirradiated hydrogen pre-charged zircaloy-4 specimens. The hydrogen content varies from 500 to 5000 ppm weight, thus ranging from the in-reactor corrosion charging (below 1000 ppm) to the transient charging that may occur, after burst, on the inner side of the cladding under steam starved oxidation conditions. LOCA simulation tests on unirradiated rods performed at JAERI[3] have indicated local high contents (>3000 ppm) of hydrogen obtained under

such conditions ; however, similar tests on irradiated cladding are not available to indicate the possibility of such hydriding on irradiated (oxidized on inner side) cladding : transient hydriding on irradiated cladding should therefore be considered potential and need to be confirmed.

The hydrogen pre-charging was realized under gas atmosphere (hydrogen + argon mixture of different compositions) at elevated temperature (around 900°C) allowing charging in the β domain where hydrogen solubility is high.

Two quenching test conditions were applied in quench tests series :

- direct quenching, i.e. immersion of the test sample in the quench tank at the end of isothermal oxidation period ; these conditions are supposed to lead to conservative quench loads ;
- slow cooling (basically -5 K/s) prior quench so as to represent the two-phase cooling of the reflooding ; quenching temperature at 700°C was chosen to allow a large amount of the $\beta \rightarrow \alpha$ phase transformation ; these conditions are supposed to be more realistic than the previous direct quenching conditions.

The program, still under progress for complementary tests series, has provided important results relative to the performance under LOCA conditions of pre-hydrided zircaloy.

5.2 Oxidation kinetics

Results of the oxidation tests experiments indicate an oxidation kinetics enhancement for 500 ppm H content, from 9% at 1050°C to 23% at 1250°C compared to as-received zircaloy kinetics, and increasing with temperature ; this kinetics increase is consistent with the observed kinetics difference between irradiated and unirradiated samples depicted on figure 2. However, the kinetics enhancement vanishes for 1000 ppm and higher H contents, which is consistent with results obtained by Moalem et al [4] who investigated the oxidation rate of H saturated specimens and found a weight-gain rate identical to that of hydrogen free metal. Complementary studies are in progress to refine the enhancement factor and the hydrogen range interval where enhancement occurs.

Figure 4 plots the weight-gain curves derived from isothermal tests on as-received and 500 ppm H charged specimens, illustrating the kinetics increase ; additionally are drawn the weight-gain predictions with the Baker-Just model, clearly evidencing that this model remains fairly conservative for the oxidation kinetics of hydrogen charged specimens, and should therefore keep a similar conservatism for irradiated material.

5.3 Quench behavior

These test series are still in progress and results are preliminary ; therefore, only qualitative results can be indicated here.

5.3.1 Low hydrogen content (in-reactor corrosion)

Results indicate a similar (or possibly slightly better) quench resistance to that of as-received cladding for H content below 1000 ppm, either under direct quenching or under slow cooling prior quench.

5.3.2 High hydrogen content (transient hydriding range)

A first series of oxidation/quenching experiments was conducted with direct quenching at the oxidation temperature., indicating apparently a severely degraded quench resistance at 2000 ppm content and

above. However, it must be pointed out here that the oxidation rate ECR evaluation was derived from the measurements of oxide, α and β layers thickness, assuming oxygen profiles identical to the hydrogen free situation. Metallographic examinations have shown that this assumption is no more valid for high hydrogen content : with increased H content the α layer thickness appears reduced, and since the weight-gain rate remains roughly constant above 1000 ppm H it means that the corresponding oxygen content difference has been absorbed by the β layer. Hydrogen content seems therefore to increase the oxygen solubility in β phase, thus increasing the brittle potential of the material.

A second series of oxidation/quenching experiments was conducted with quenching at 700°C following an intermediate cooling at 5 C/s from oxidation temperature ; preliminary results indicate that the quench resistance is fairly recovered to the level of H free material.

5.3.3 Discussion

Analysis of quenching tests results is still preliminary but metallographic examinations have shown distinct microstructural arrangements within the central metal layer for the two cooling conditions, as illustrated on figure 5 : prevalence of fine martensitic needles for rapid cooling, whereas of α plates and grains for slow cooling. The cooling rate through the $\beta \rightarrow \alpha'$ phase transformation range mainly influences the extent of oxygen redistribution from bulk β to α precipitates, as already evidenced in Chung and Kassner tests[5] ; this effect of cooling appears magnified at high hydrogen content due to the associated increase of oxygen solubility in the β phase. Microanalysis of typical microstructures as those shown on figure 5 have been undertaken ; preliminary results indicate unexpected oxygen contents in α substructures.

A clear understanding of the combined effects of oxygen and hydrogen on the cladding oxidation and quench behavior requires the knowledge of their inter-related distributions in the zircaloy metal phases and evolution during temperature transient ; this requires the acquisition of basic data such as thermodynamic properties with regards to ternary phase diagrams Zr-O-H or preferentially Zy-O-H since, as already observed, the contribution of zircaloy alloying elements to phase changes (and possibly to the mechanical behavior of the cladding), appears not negligible.

It must also be pointed out that hydride precipitation was never observed in optical microscopy, whereas hydride phases (δ and γ) were detected by X-ray diffraction. It is therefore suggested that hydride phase precipitates at cooling as very fine particles, not observable under optical microscopy, and that they consequently may have no direct influence on mechanical resistance upon quench.

Although the high hydrogen content influence is not a burnup extension issue, it points out the need for a proper taking account of hydrogen effects in LOCA transients evaluation. Knowledge gained from experimental testing of irradiated or pre-hydrided cladding under LOCA simulated conditions, as briefly summarized above, indicates that the embrittlement behavior cannot be simply described by oxidation rate which mainly reflects the oxide scale extent ; an alternative parameter would be required to allow the description, on a physical basis, of combined oxygen and hydrogen influences in whole cladding material, including the dependence on cooling rate prior to quench.

6. Conclusions

An experimental program has been conducted to investigate the oxidation and thermal shock behavior of irradiated cladding under LOCA simulated conditions. Oxidation and quenching experiments were successively performed on as-received cladding, unirradiated pre-oxidized cladding, irradiated cladding and unirradiated pre-hydrided cladding.

The preliminary analysis of tests results on irradiated cladding has been updated. Results of the successive tests series indicate that :

1) Initial oxide scale has no impact on high temperature transient oxidation and may be taken into account simply as for the corresponding reduction in cladding wall thickness ;

2) Oxidation kinetics of irradiated zircaloy is slightly higher than that of unirradiated material ; the Baker-Just oxidation model remains largely conservative ;

3) The quenching resistance of irradiated material is similar (and possibly slightly higher) than that of unirradiated material for a same transient oxidation ratio. The failure limit has been revised to ECR=28% with the previous analysis methodology that is supposed to be conservative ;

4) Low hydrogen content (in-reactor corrosion range) may slightly enhance the oxidation kinetics of zircaloy ; however the quench resistance is not affected or possibly improved under slow cooling conditions prior quench.

4) High hydrogen content (potential hydriding under transient) strongly influences the quenching behavior of the cladding, through an increase of oxygen solubility in the β phase, thus increasing the brittle potential of the material. The effect of cooling rate prior quench on oxygen redistribution appears magnified at high hydrogen content : slow cooling prior quench allows a complete recovery of the quench resistance to hydrogen free level.

Understanding of these phenomena should be substantiated by the acquisition of basic thermodynamic data regarding ternary diagrams Zr-O-H or Zy-O-H. A proper description of the combined influences of oxygen and hydrogen requires alternative parameters to the oxidation ratio ECR referred to in the current acceptance criteria.

REFERENCES

1 C. GRANDJEAN, C. LEBUFFE, High Burnup Fuel Cladding Embrittlement under Loss-of-Coolant-Accident Conditions.
ANS International Meeting Safety of Operating Reactors, Seattle, September 17-20, 1995.

2 C. GRANDJEAN, R. CAUVIN, C. LEBUFFE, N. WAECKEL, French Investigations of High Burnup Effect on LOCA Thermomecanical Behavior. Part Two : Oxidation and Quenching Experiments under Simulated LOCA conditions with High Burnup Clad Material.
24th Water Reactor Safety Information Meeting, Bethesda, Md, USA, October 21-23, 1996.

3 H. UETSUKA, T. FURUTA, S. KAWASAKI, Failure-Bearing Capability of Oxidized Zircaloy-4 Cladding under Simulated Loss-of-Coolant Condition.
Journal of Nuclear Science and Technology, 20[11], 941-950, November 1983.

4 M. MOALEL, D.R. OLANDER, Oxidation of Zircaloy by steam.
Journal of Nuclear Materials 182 (1991), 170-194.

5 H.M. CHUNG, T.F. KASSNER, Embrittlement Criteria for Zircaloy Fuel Cladding Applicable to Accident Situations in LWR.
NUREG/CR-1344, ANL-79-48, January 1980.

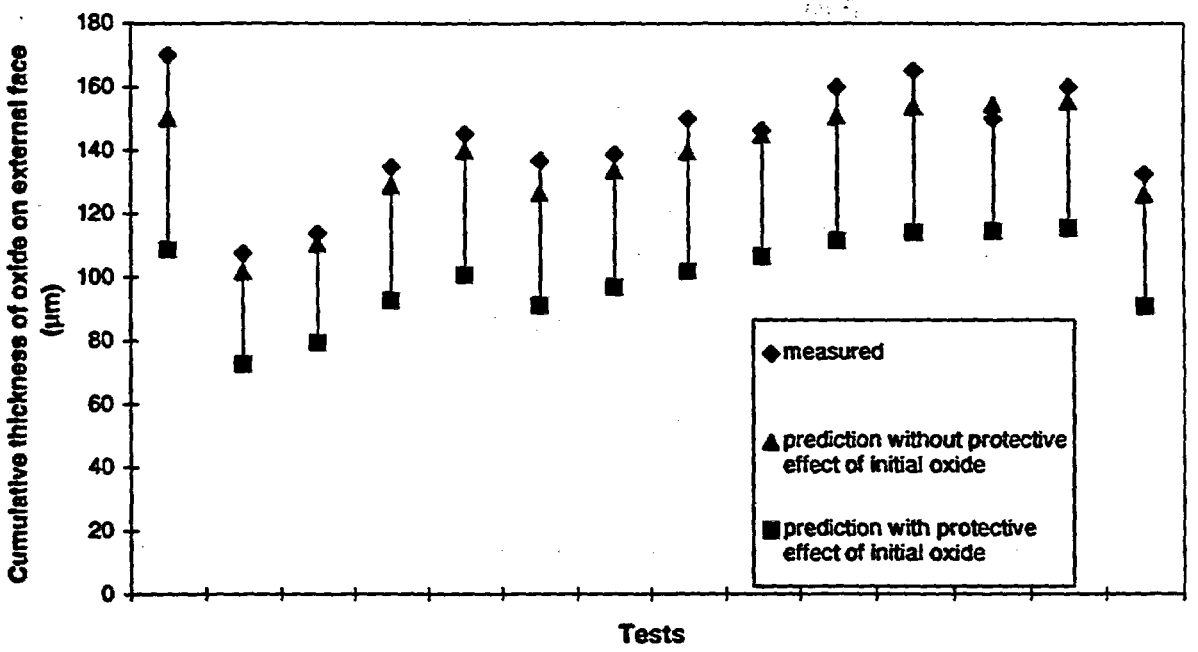

Figure 1. Comparison of measured and calculated oxide thickness with and without protective effect of the initial oxide layer

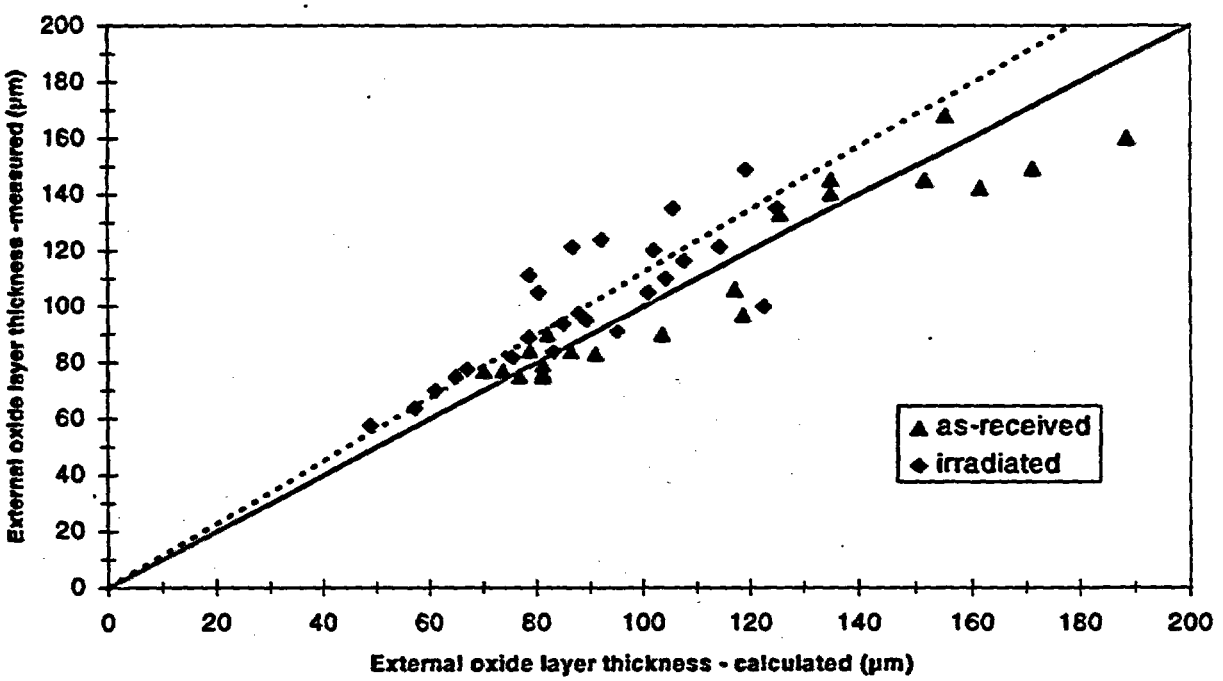

Figure 2. Measured versus calculated transient oxide thickness for as-received and irradiated cladding samples

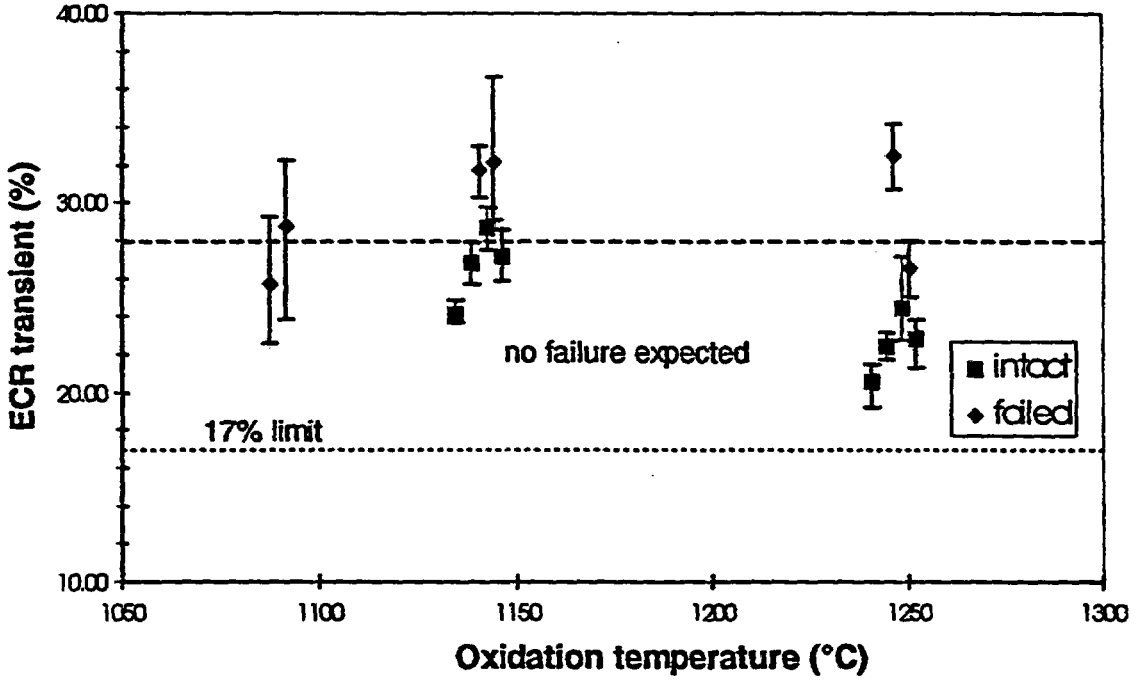

Figure 3. Failure map on ECR parameter for transient oxidation (two-side oxidation tests)

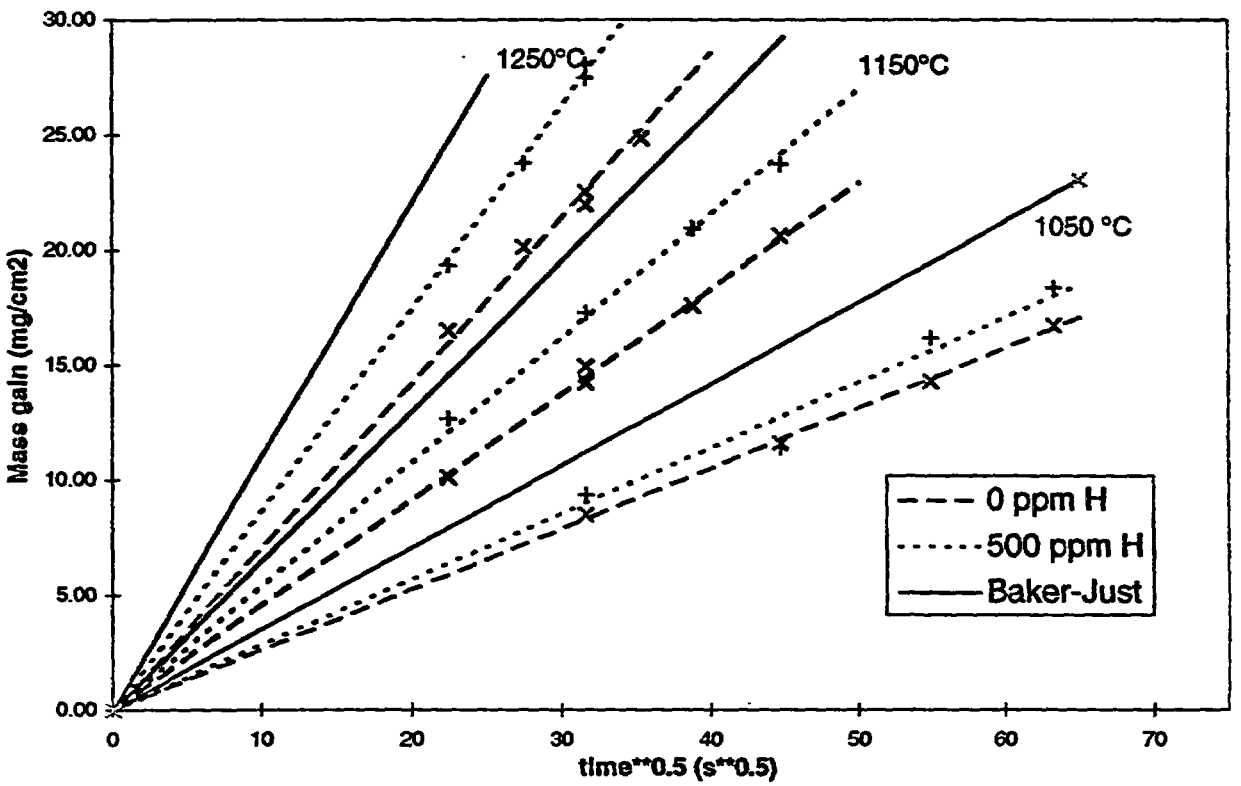

Figure 4. Effect of hydrogen content on oxidation kinetics

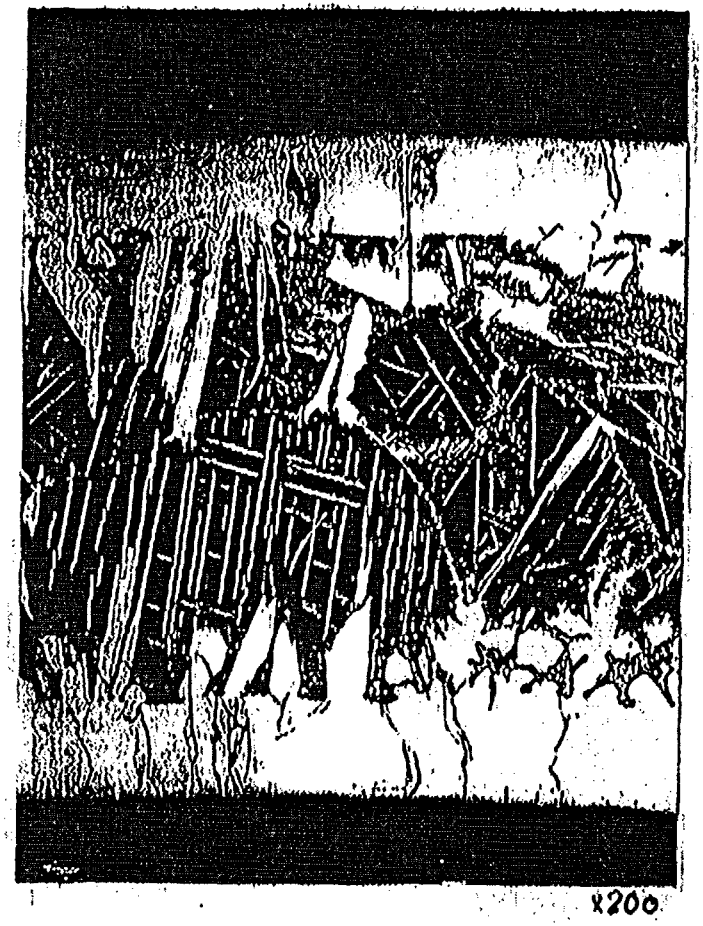

Direct quenching

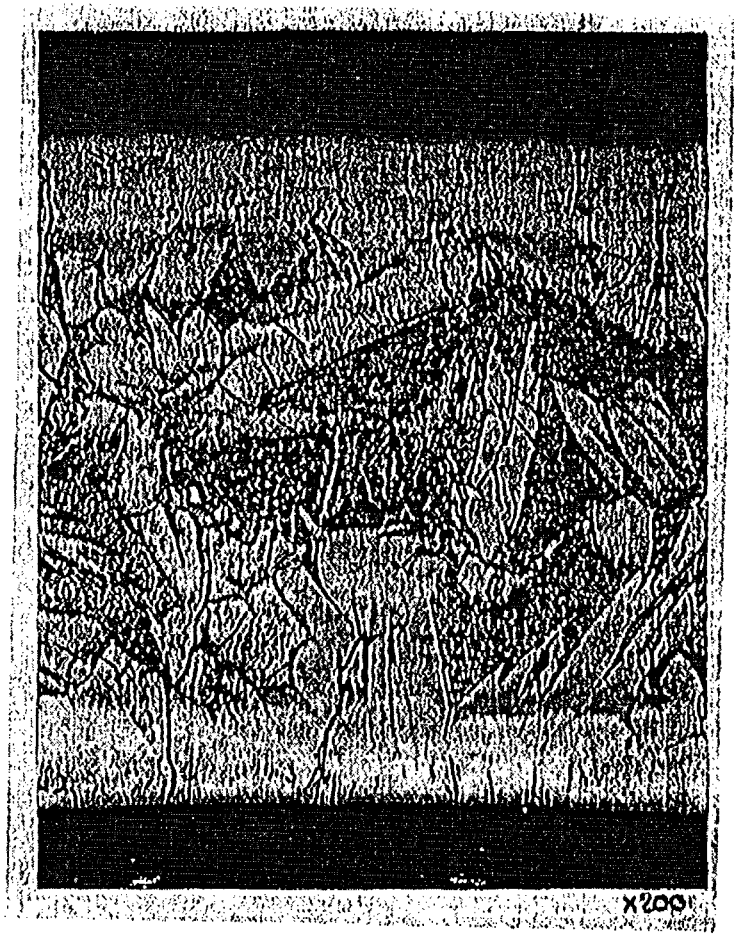

Slow cooling prior quench

Figure 5. Effect of cooling rate prior quench on microstructure.

Zr-1%Nb (VVER) High Burnup Fuel Tests under Transient and Accident Conditions

V. Smirnov, A. Gorjachev, J. Kosvintsev, J. Kungurtsev, V. Mahin,
V. Ovchinnikov, A. Smirnov, V. Tzikanov (SSC RIAR, Russia)

Introduction

The development and licensing of VVER fuel involve the experimental data characterized fuel behavior for all possible burnup ranges including the little-studied burnups of above 45-50 MWd/kgU. At those burnups some negative inner processes are intensified especially under non-steady-state and accident conditions.

The SSC RIAR performs tests on fuel rods under non-steady-state and accident condition in the reactor MIR loops and in the electrically heated apparatus located in the hot cells. Both "fresh" and irradiated fuels, as well as commercial reactor spent fuel, are used in the experiments.

Tests in the reactor MIR are mainly carried out to license and improve the fuel. Some results are also used to improve and verify the codes. The programs of experiments using refabricated and full-scale fuel rods include the following types of the loop tests:

- tests under single power jump (RAMP) and gradual power increase (FGR) at a burnup range of 30-60 MWd/kgU;
- additional irradiation of the refabricated and full-scale fuel rods up to maximal project local burnups and even higher followed by experiment RAMP;
- tests under cycle change in power;
- experiments with VVER fuel assembly segments under conditions of dry out, overheating and quench (LOCA and QUENCH tests);
- tests under reactivity initiated accident conditions (1-5 seconds);
- tests with leaky fuel rods under non-steady-state conditions.

The report considers the principal methodical aspects and some results of the tests of the VVER high burnup fuel with Zr-1%Nb cladding.

1. In-pile fuel rod tests under transient operation conditions

Information on pre-test fuel rod state

The pre-test full-scale and refabricated fuel rod state is examined. The information available allows to select fuel rods, for example, with a particular gap size or fission gas content for the test, as well as to estimate expected fuel rod parameters during the tests taking into account the experience available.

Peculiarities of test methods under power change conditions. Information obtained during experiments.

Taking into account the objective of in-pile experiments both instrumented and non-instrumented fuel rods are used. While using instrumented fuel rods during the tests the fuel temperature, gas pressure in the space volume, change in fuel rod length, change in fuel rod diameter, change in fuel column length, fission gas activity and composition in the coolant are measured.

Some information on experiment RAMP using full-scale and refabricated fuel rods is presented in Table 1. In two experiments of gradual power increase (FGR1, FGR2) the refabricated fuel rods supplied with gas pressure detectors and thermocouples were used. During the experiments the information on gas pressure and temperature change in the centre of fuel pellet while power changing is obtained. The fuel rod time constant was determined.

Table 1

General information on experiments RAMP and FGR using VVER fuel rods in the reactor MIR

Parameter	R1	R2	R3	R4	R5	R6	R7	R8	R9*	RF	FGR1	FGR2
Fuel rod quantity	10	9	10	12	11+6	12	6	6	6	6	6	6
Fuel rod length, mm	265	265	1075	265	265	1075	1075 2500 3840	1075 2500	3840	1075 2500	1075	500 2500
Average burnup, MWd/kgU	8.5-10	8-10.7	47	17	15-30	50	30; 60	50; 60	50	50; 60	50; 60	50; 60
Ramp amplitude rel.units	1.9	2.8	1.9	2.2	2.2	2.2	2.5	2.2	1.5-2	2.2	3.7	3.6
Power increase time, min	8	13	2.5	8	10	113	12	25	30-1800	20	-	-

*Experiment of smooth power increase followed the ramp

Irradiated facility design

Special irradiated facility was developed for tests which allows to test simultaneously both refabricated fuel rods of 1 m long and full-scale ones for VVER-1000 and VVER-440 [1,2,3].

Fig.1 presents the design of the irradiated facility provided possibility to test simultaneously full-scale fuel rods for VVER-440 and VVER-1000 and some refabricated fuel rods (instrumented or non-instrumented) in different composition. The irradiated facility is supplied with the detectors for neutron flux.

Carried out tests and some results

No fuel rod depressurization was noticed in any experiments. The visual inspection and eddy-current defect tests show that there are no test-induced faults on the claddings. The cladding state parameters (oxidation of outer and inner surface, hydrogen absorption and mechanical tensile properties) didn't practically change. The hydrogen content didn't exceed $4.8 \cdot 10^{-3}$% mass.

Fig 2 presents the dynamic change of the linear power (q_l) and gas pressure during gradual power change in one of the FGR experiments.

The tests resulted in the outer cladding diameter increase, especially in the central part of the fuel rods (Fig.3). In the fuel rods with a burnup of about 50 MWd/kgU, the diameter increase was 22-33 μm. In the fuel rods with a burnup of about 60 MWd/kgU, it was 33-54 μm; I.e., in more heated fuel rods the outer cladding diameter changed less than that in less heated ones.

The results of the measurements of the fuel cladding gap in post-test cold state, and their comparison with the pre-test gap testify to the fact that in the fuel rods with a burnup of about 50 MWd/kgU the post-test fuel-cladding gap in the area of maximal power was 40-65 μm and in the fuel rods with a burnup of about 60 MWd/kgU it was 15-33 μm.

The data on change in the post-test outer cladding diameter and fuel-cladding gap were compared and it brought to the conclusion that the fuel column diameter of the heated fuel rods with a burnup of 50 MWd/kgU didn't practically change or even became less. Further fuel column examination supported the conclusion.

Fuel rod test under single ramp and step-by-step power increase brought to some changes in dimensional parameters of the fuel pellets and significant changes in UO_2 structure.

The fuel pellets remained intact along the most part of the fuel rod length and didn't change its configuration. In the area of maximal linear power where it was more than 213 W/cm, the coaxial cracks appeared. The central hole at the linear power of 300-315 W/cm begins reducing and at 343-375 W/cm it is practically absent. In fuel rod 41 (experiment FGR-1) in the area of maximal linear power (about 441 W/cm) a new central cavity of about 0.6 mm was formed (Fig.4).

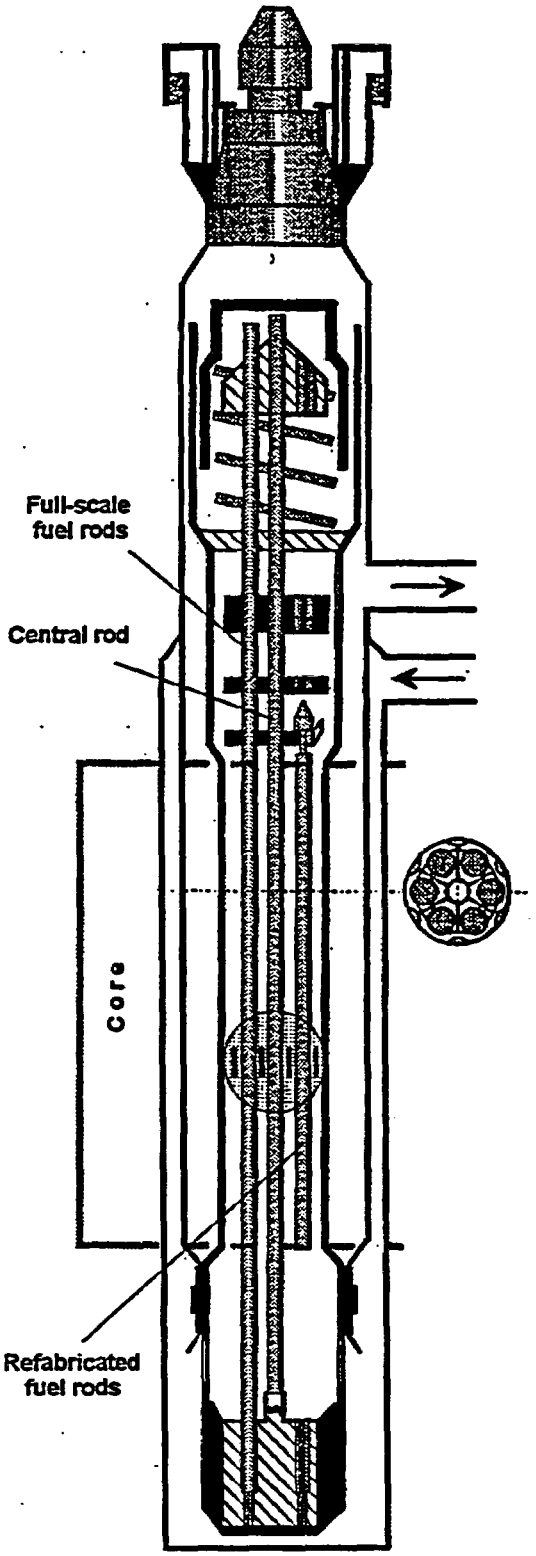

Fig. 1. Irradiated facility to test full-scale and refabricated fuel rods.

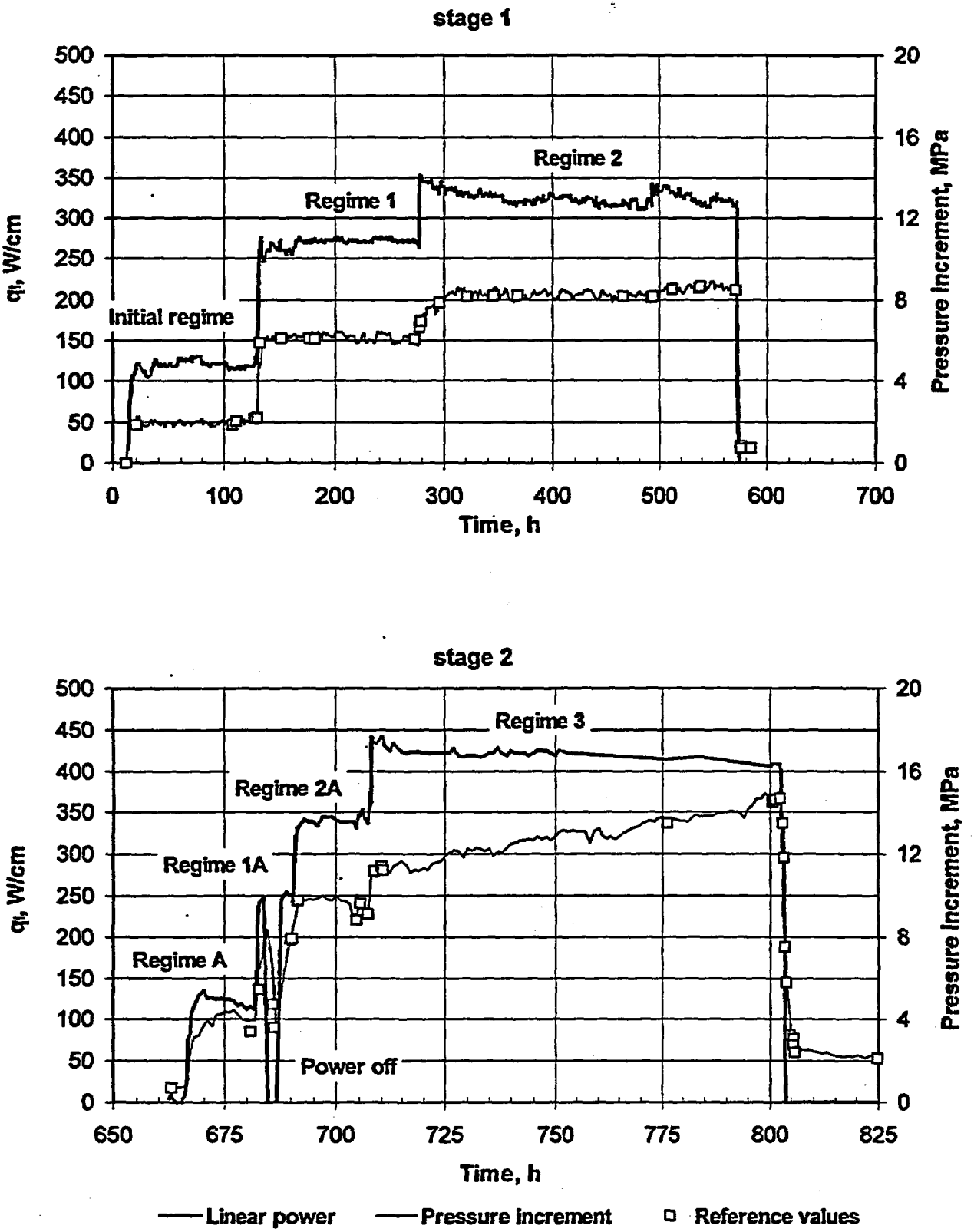

Fig.2. Change in q_l^{max} and gas pressure increment during test FGR1 for fuel rod with a burnup of 50 MWd/kgU

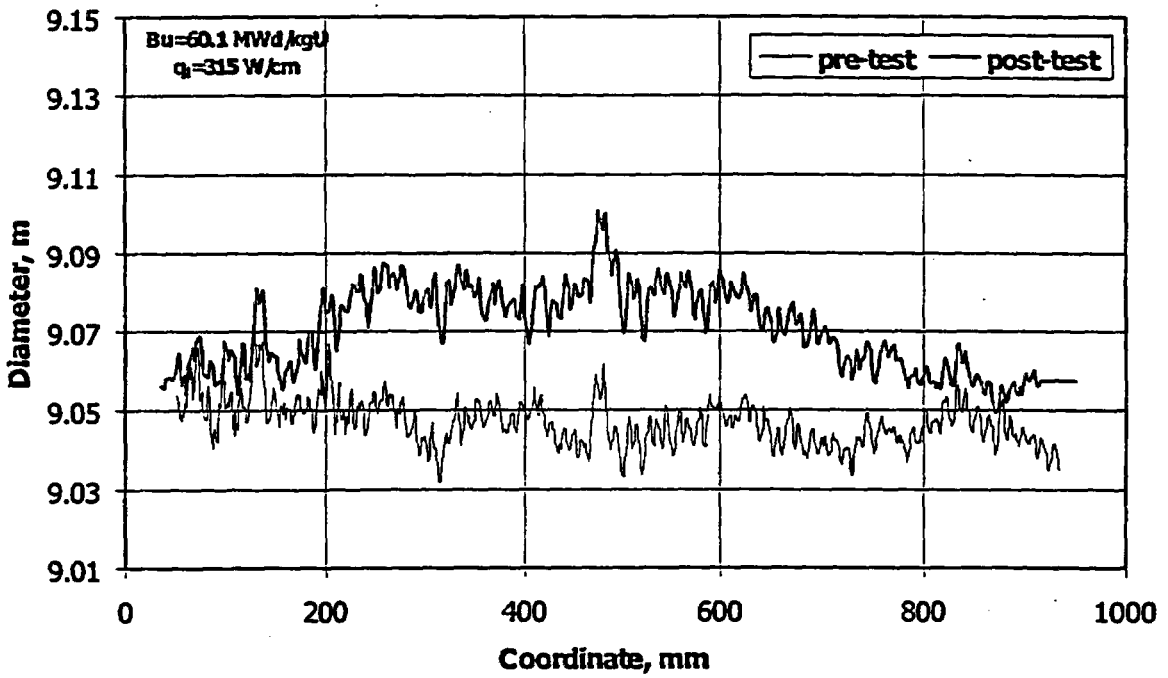

Fig.3. Pre- and post-test fuel rod profile

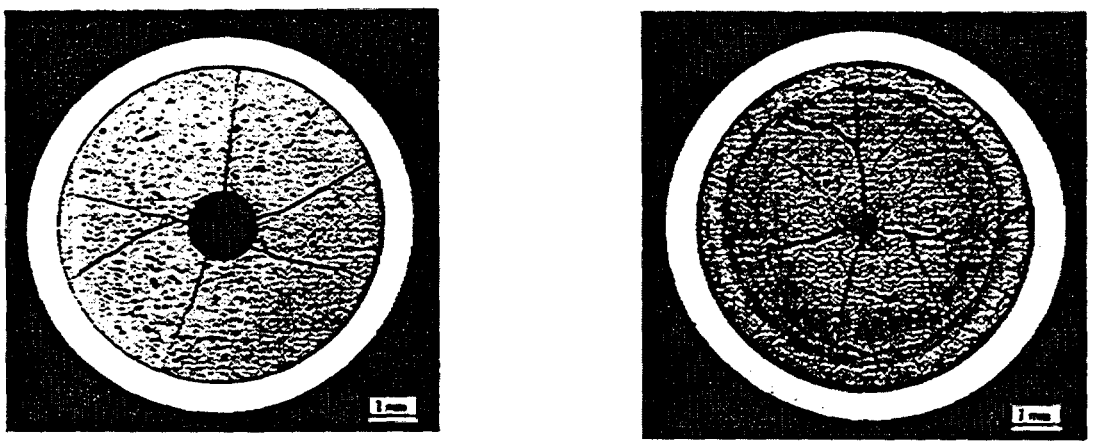

before tests **after test Ql=441 W/cm**
Bu=50 MWd/kgU

Fig.4. Pre- and post-test fuel rod cross-section macrostructure

Change in UO_2 structure was accompanied by increased fission gas release from the fuel under the cladding and Cs nuclide migration in the fuel rod central part in the area of maximal linear power. In the fuel rods with a burnup of about 50 MWd/kgU and with higher linear power, respectively, Cs migration accompanied by Xe and Kr migration occurred more significantly. The results testify to the fact that Cs migration intensification occurs at the linear power more than 285-300 W/cm in the fuel rods with a burnup of 50 MWd/kgU and 220-250 W/cm in the fuel rods with a burnup of 60 MWd/kgU.

Fission gas release upon the whole is proportional to the linear power level and can reach 50% at the linear power of about 440-460 and 330-375 W/cm in the fuel rods with the burnups of 50 and 60 MWd/kgU, respectively. The fuel rod pressure at the operation temperature can rise up to the values equal to the coolant pressure. The fuel with a burnup of 60 MWd/kgU under the same conditions is more subjected to fission gas release as compared with the fuel with a burnup of 50 MWd/kgU.

The program of experiments includes VVER radiation up to higher burnups (75-80 MWd/kgU) followed by RAMP, tests of fuel rods of a burnup of about 50 MWd/kgU under cycle power change regime, tests under non-steady-state conditions of different fuel modifications and further fission gas release examination.

2. Examination of fuel behaviour under accident conditions

Equipment

The fuel assembly construction element and fuel rod properties as well as these elements behaviour under accident conditions of LOCA and RIA type are examined in research reactors and electrically heated apparatus located in the hot cells.

Currently four electrically heated apparatus are used in hot cells designed for:

- examination of radionuclide release from the fuel, study of material structure change under accident conditions as well as cladding and pellet oxidation ;
- examination of cladding and the fuel rod properties by method of inner gas pressurization . For that fuel rod "fresh" and irradiated materials of different degrees of oxidation are used;
- study of behaviour of "fresh" and irradiated rod and guide-channels under thermoshock conditions;
- examination of fuel rod behaviour under conditions simulating different variants of LOCA.

In the research reactors mainly integral experiments are carried out. In particular, in the reactor MIR in the loop PVP-2 the simulated fuel assembly behaviour under LOCA conditions is examined. The fuel assembly includes not only "fresh" fuel rods but also those manufactured of ones operated in commercial reactors. On the fuel rod claddings and along the fuel column center the temperature detectors may be located. Some fuel rods are supplied with gas pressure detectors. At different levels along the fuel assembly height the temperature and coolant vapour content detectors are located.

Apparatus to examine fission gas release, oxidation and irradiated material structure change

The apparatus provides examination in inert, air and vapour gas environment. The apparatus scheme is presented in Fig.5. The principal apparatus element is portable horizontal heating unit provided the required environment and temperature range. The samples in a form of fuel pellet fragments and fuel rod tubes up to 40 mm long are tested on the apparatus to study their oxidation and fission gas release.

Two gamma-spectral channels of Ge(Li)-detectors provide Kr-85 intensity recording during experiments with flowing gas-carrier and change in fission gas intensity in the sample and on the basic filter. Gas mass-spectrometer and gas analyzer measure concentration of not radioactive components of gas flow such as Helium, Hydride, Oxygen .

During annealing the following parameters are recorded:

- temperature;
- gas-carried flow-rate and pressure;
- Kr-85 gamma-activity in gas-carrier;
- fission product gamma-activity on the basic filter or in the sample;
- concentration of gas-flux non-radioactive components releasing from the sample (Helium) or characterizing environment sample interaction (Oxygen, Hydride).

The following post-test sample examination is carried out:

- mass measurement;
- fission product gamma-activity measurement;
- structure examination.

The principal types of the experiments on the apparatus are presented in Table 2.

Table 2
Parameters and results of the test on FGR from the spent VVER fuel on the electrically heated apparatus

Test environment	Temperature range, °C	Burnup, MWd/kgU	Sample appearance
Argon	1000 - 2200	15.8	fuel pellet fragment
Helium	1800 - 2000	45.0	
Argon	800 - 2000	55.2	
	1000 - 2400	59.8	
Argon	1000 - 2100	64.0	fuel rod section
	1250 - 1450	15.8	
air	600 - 1200	36.8 *	fuel pellet fragment
	600 - 2200	0 *	
Argon + vapour	600-1300	55.2	fuel rod section and fuel pellet fragment
		51.7	
		50	

* The sample are additionally irradiated in the reactor MIR to accumulate I-131.

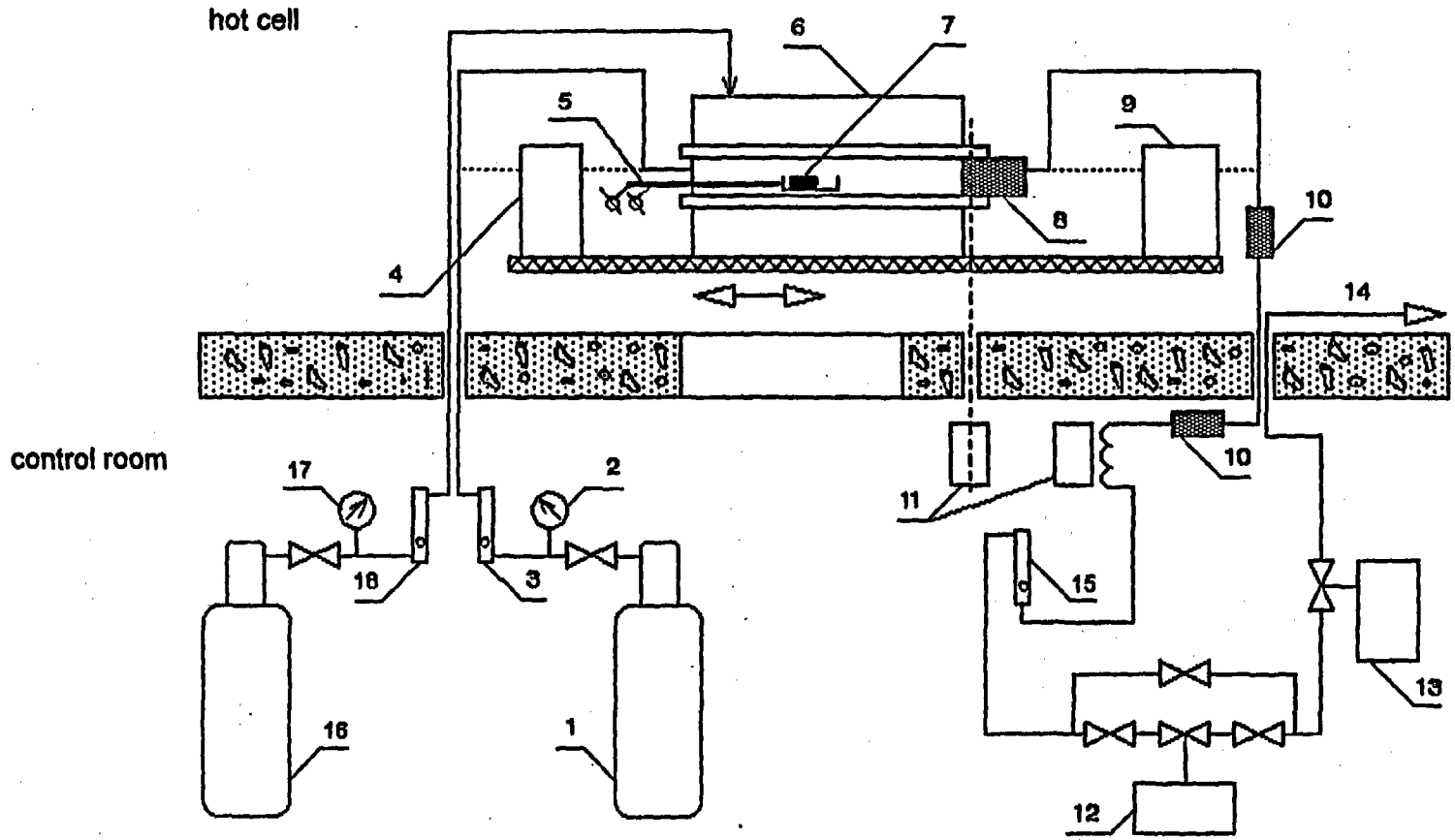

1,16 - argon balloon; 2,17 - manometer; 3,15,18 - rotameter; 4 - steam generator; 5 - thermocouple; 6 - heating unit; 7 - sample; 8 - basic filter; 9 - condensator; 10 - additional filter; 11 - gamma-detector; 12 - mass-spectrometer; 13 - gas-analyzer; 14 - ventilation outlet

Fig.5. Apparatus for examination of fission gas release, oxidation and irradiated material structure change

Typical kinetic dependence of fission gas release from the fuel of high burnup in the inert environment is presented in Fig.6, the temperature dependence for lower and higher burnups is presented in Fig.7.

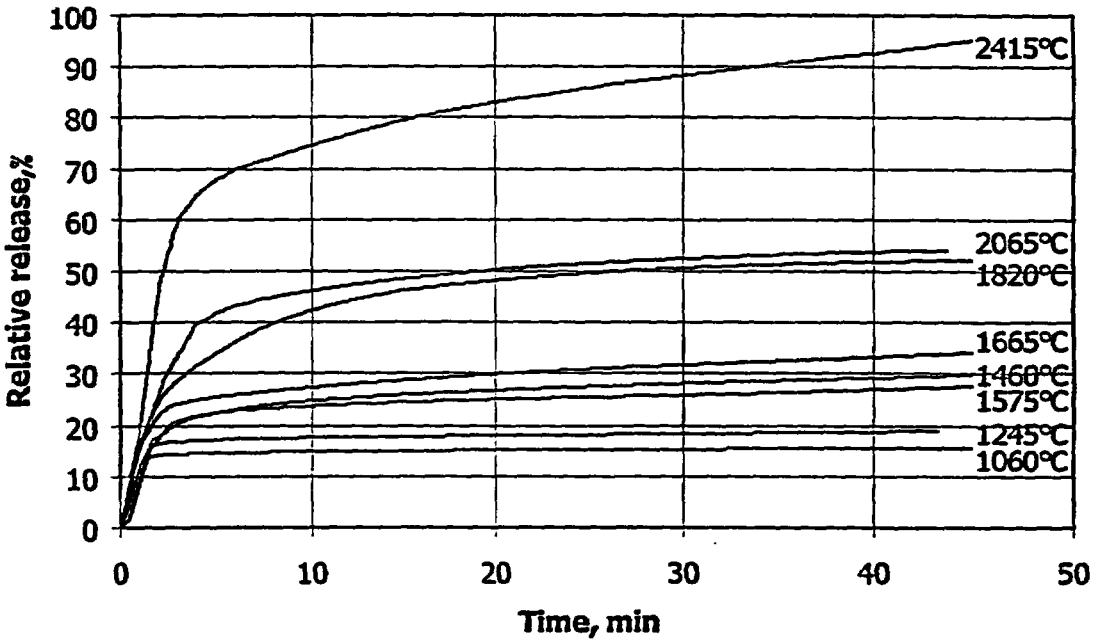

Fig.6. Time dependence of relative Kr-85 release from the fuel pellet fragments of a burnup of 59.8 MWd/kgU in isothermal experiments

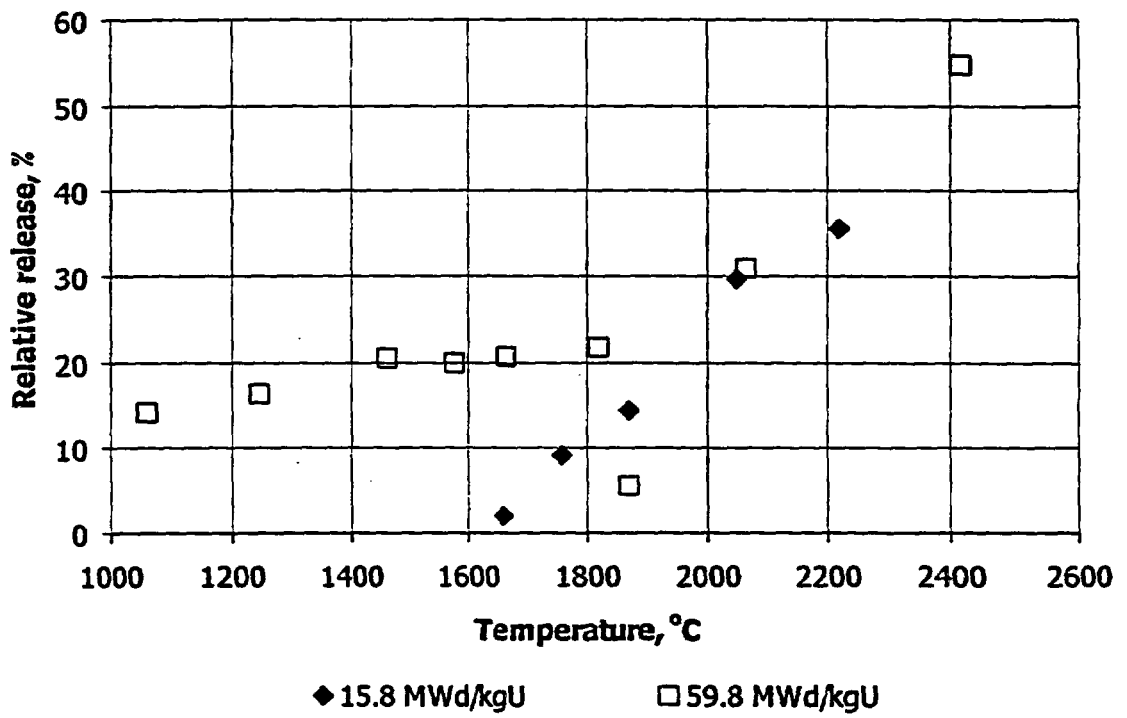

Fig.7. Time dependence of burst Kr-85 release from the fuel pellet fragments

The spent fuel cladding oxidation was examined by method [4] applying in-cell electrically heated apparatus. The samples were manufactured of fuel rods operated in the commercial reactors. The fuel pellets were removed mechanically. After quick temperature rise in the inert environment the vapour-gas mixture was supplied into the unit and the sample underwent holdup for particular time under isothermal conditions.

While examining the oxidation of the spent VVER fuel rod claddings from Zr-1%Nb alloy at the temperatures of 1000 and 1100 it was discovered that at little oxidation time the irradiated cladding weight gain is higher than for not irradiated ones and further the difference disappears. The required time to reveal this effect and its scope decreases after temperature increase. During recording the large irradiated cladding weight gain, the oxide film thickness on its inner surface is larger than that on the outer surface and on the surface of not irradiated samples. The experimental data allow to make a preliminary conclusion that large irradiated cladding weight gains are caused by large oxidation of their inner surface.

Apparatus for gas pressurization of irradiated samples

The behavior of the irradiated samples of Zr-1%Nb alloy at the temperatures and pressures typical for maximal design accident of the VVER reactor is studied on the apparatus to determine the mechanical properties of the fuel claddings.

In one of the experiments the samples consisted of the irradiated VVER fuel rod segments of the burnups of 54.4 and 60.5 MWd/kgU (Fig.8). The sample length is equal to 275 mm, the average outer diameter is 9.08 mm and the cladding thickness is 0.7 mm. The plug and adapter of Zr-1%Nb alloy are welded to the sample ends by argon-arc welding. The guiding tube of 550 mm long is connected to the adapter. It has a shroud of stainless steel. The shroud serves to prevent destroying the adapter at gas pressurization. Inside the tube there is a thermal converter of chromel-alumel type.

The apparatus for gas pressurization (Fig.9) includes the following:

- electrically heated furnace with an ampoule (the furnace working part length is 500 mm, the maximal temperature is 1200 , the sample heating rate is 1 /s);
- steam generator;
- sample pressurization system;
- antiaerosol filters.

Conditions to carry out three experiments:

1. The working samples temperature under isothermal regime was 700, 800 and 1000 .

2. Excess inner pressure in the sample (3.5, 3.75 and 5.44 MPa) simulated pressure drop (fuel rod - circuit).

3. In-ampoule outer pressure was atmospheric.

4. In-sample gas environment was argon.

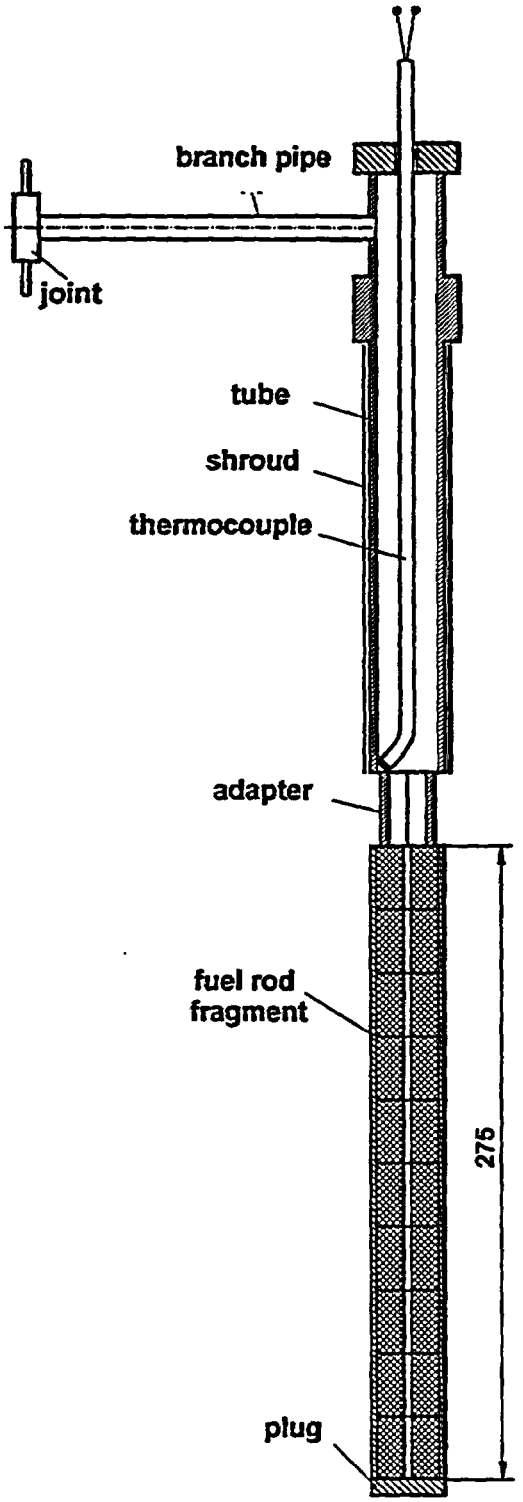

Fig.8. Sample design to test by gas pressurization

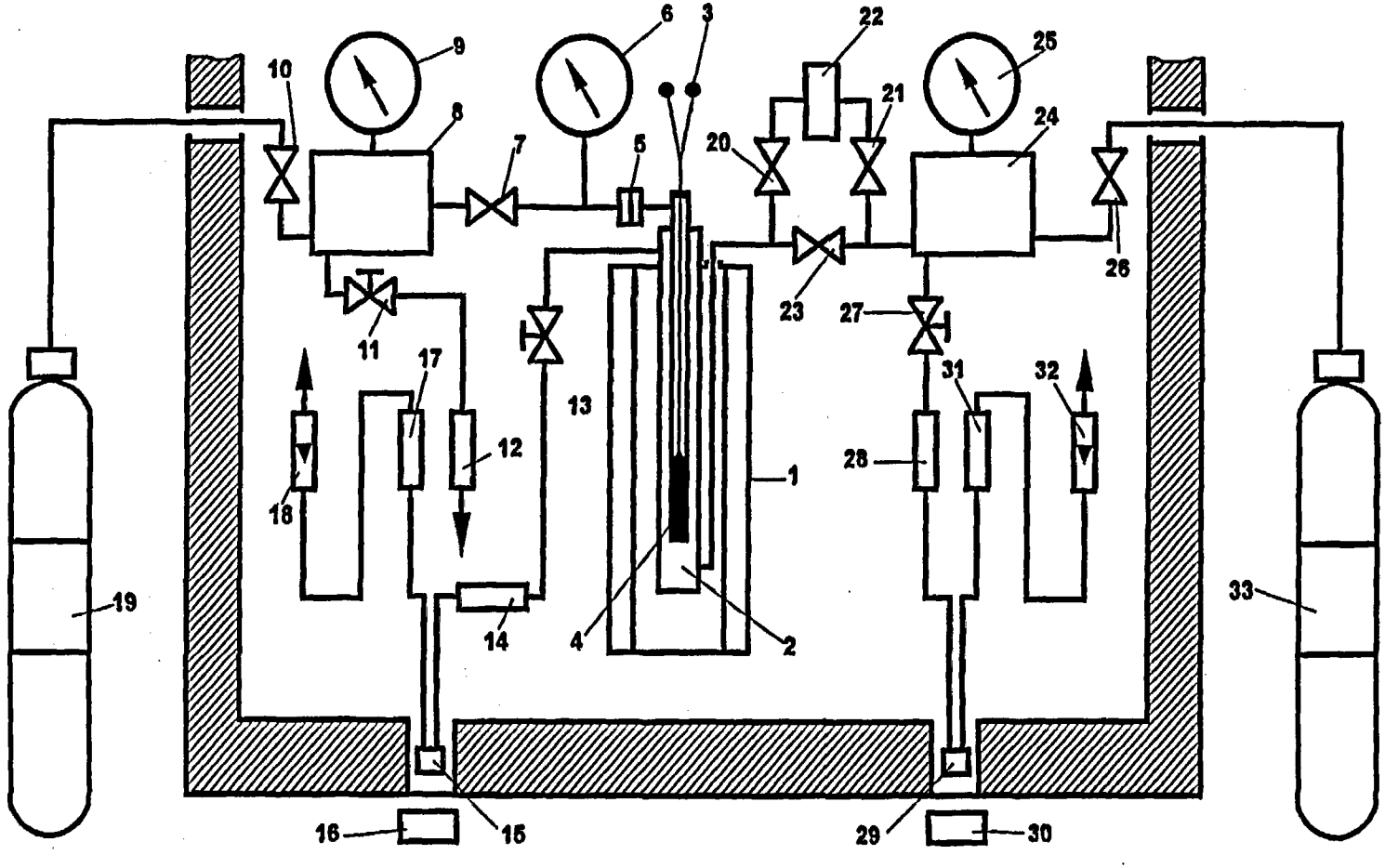

1 - electrical furnace; 2 - ampoule; 3 - thermocouple; 4 - sample; 5 - joint; 6,9,25 - manometer; 7,10,20,21,23,26 - screw; 8,24 - stabilizing balloon; 11,27 - reducing value; 12,17,14,28,31 - filter; 22 - steam generator; 18,32 - rotameter; 15,29 - accumulating chamber; 16,30 - detector; 19,33 - gas balloon

Fig.9. Gas pressurization apparatus

Oxidizing environment at constant velocity vapour argon mixture (flow regime) was reached by means of systems of steam generator of 40 g/hour.

During experiment the time to rupture of the pressurized samples under isothermal conditions at the constant inner pressure was measured. The sample was located into the furnace at the temperature of 25 and was heated up to set temperature at the rate of 0.3-0.5 /s. At that time the in-sample pressure was atmospheric. When the set temperature was reached the excess pressure was supplied with a rate of 10 MPa/s. Since then the time to rupture is observed up. The sample depressurization moment is determined by pressure drop.. After that the heating was stopped and the sample was cooled together with the furnace at the rate of about 1.5 /s.

During the test the following was recorded:

- sample temperature;
- sample heating rate;
- in-sample gas pressure;
- in-ampoule gas pressure;
- sample holdup time under isothermal regime;
- sample cooling rate.

Quantitative analysis of the information obtained during metallography was made using digitizing and image processing system. Table 3 shows principal characteristics of experiment.

Table 3

The results of the experiment on irradiated samples under simulating LOCA conditions

Parameters	Exper.1	Exper.2	Exper.3
Burnup, MWd/kgU	60.5	60.5	54.4
Sample temperature, °C	700	800	1000
Excess pressure, MPa	3.50	3.75	4.52
Time to rupture, s	2085	150	2

Accident condition simulating

We started work to study the behaviour of the separate fuel rods manufactured of those operated in the commercial reactor within standard fuel assemblies. For that purpose an apparatus was developed which is able to create the necessary fuel rod pressure and temperature.

The principal parameters of the fuel rods under examination are presented in Table 4 and the experiment conditions are considered in Table 5. Distribution of the fuel rod temperature and difference in inner and outer environment pressure during experiment are presented in Fig.10.

Table 4
Irradiated sample parameters

Parameter	Sample number					
	1	2	3	4	5	6
Fuel rod number	111	111	123	58	58	57
Fuel assembly number	222	222	222	222	222	198
Cladding lot	1390-4-1/2	1390-4-1/2	795-4-1/2	1390-4-1/2	1390-4-1/2	34-4-1/2
Burnup, MWd/kgU	59.2	59.2	56.5	60.5	60.5	54.4
Sample length, mm	275	275	275	275	275	275

Table 5
Experiment conditions simulating accident regime with separate fuel rods

Experiment No.	Excess internal pressure ΔP, MPa	Sample temperature, °C	In-sample gas pressure, MPa	Fuel burnup, MWd/kgU	Time to rupture, s	FGR, %		
						Kr-85	Cs-134	Cs-137
1	+3.5	800	1.0	59.2	-			
2	-0.15	1100	1.0	59.2	-			
3	-1.4	800... 1200	1.0	56.5	485	1.5	3.2	2.4
4	-3.5	700	1.0	60.5 0	2085 1836	0.6	0.5	1.3
5	-3.8	800	1.0	60.5 0	150 1440	1.3	4.2	2.9
6	-4.5	1000	1.0	54.4 0	2 2	3.9	3.6	2.0

Diameter distributions along the cladding length before and after experiment are shown in Fig.11. The time to rupture and fission gas release are presented in Table 5.

In the experiments when outer gas pressure is more than inner gas pressure and insignificant inner pressure increase the fuel rod depressurization didn't occur. In other experiments the local cladding diameter increase of ballooning type occurs together with the general one, followed by formation of through out cross cracks.

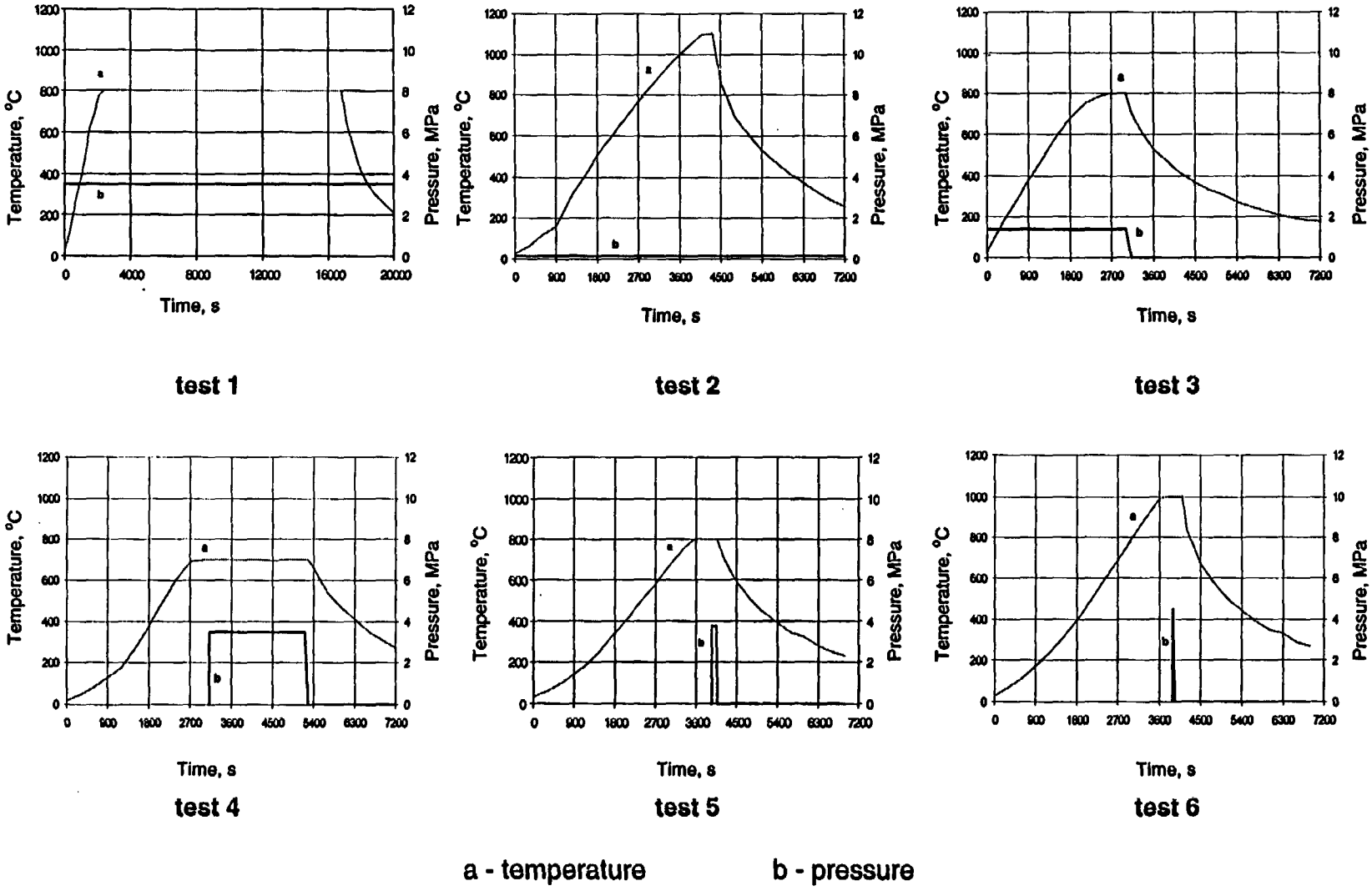

Fig.10. Time profile of temperature and pressure in the samples

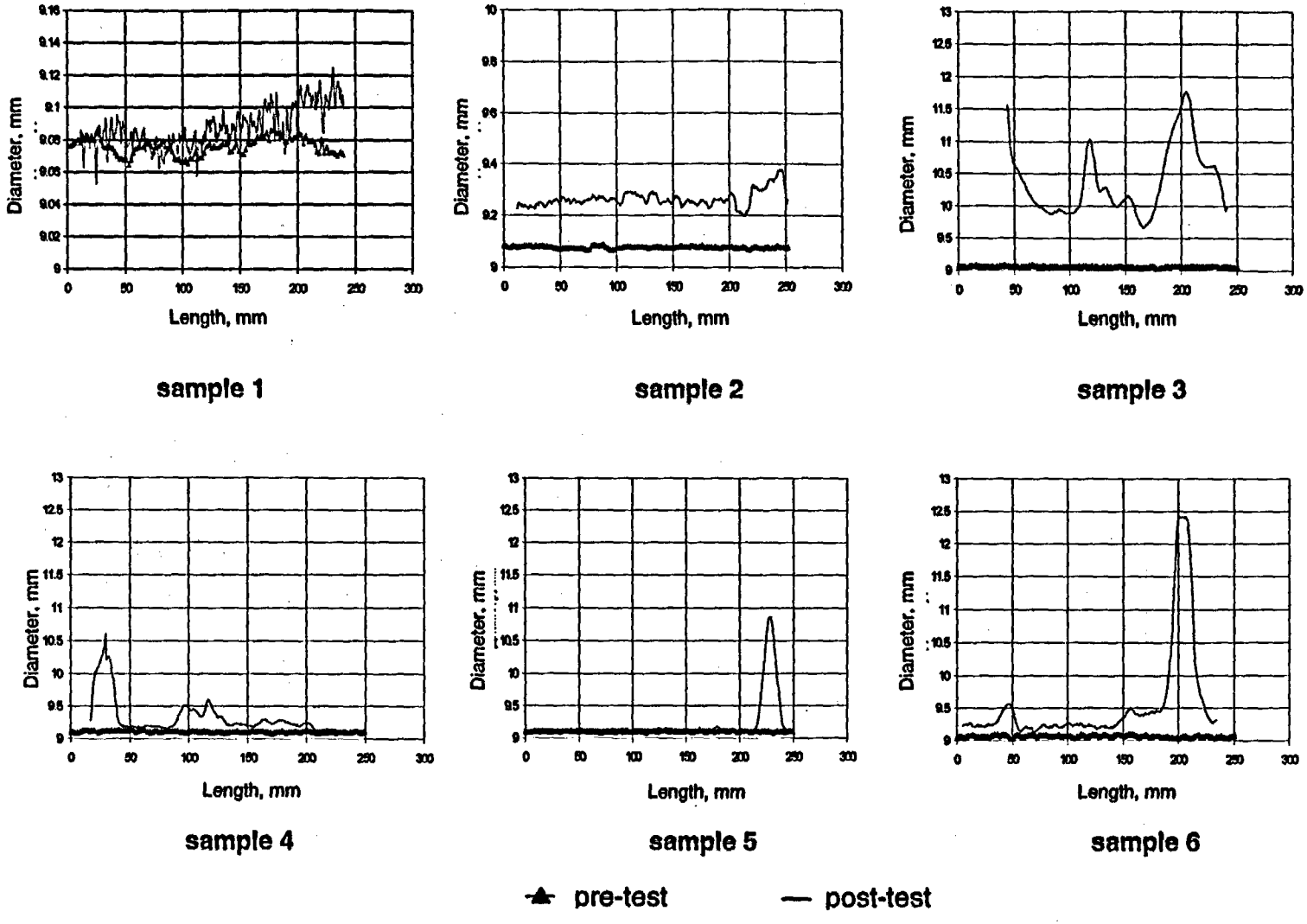

Fig.11. Longitudinal diameter profile in the samples

3. Integral experiments

At the present time, four integral experiments have been carried out using VVER fuel rods under simulating LOCA conditions (Table 6). In the last experiment together with "fresh" fuel rods spent ones were tested. Simulating fuel assembly consists of six fuel rods with "fresh" fuel and central one with spent fuel with a burnup of up to 56.9 MWd/kgU. The test objective is to compare the behaviour of "fresh" and spent fuel.

Table 6
General information on LOCA test

Experiment number	1	2	3	4
"Fresh" fuel rod quantity in fuel assembly	18	19	19	6 and 1 spent
Coolant parameters:				
• pressure, MPa;	12	12	4	6
• temperature at inlet, °C	~320	~320	~80	~270
• flowrate, kg/s	0.04	0.04	0.04	0.008
Fuel assembly power, kW:				
• under steady-state conditions;	500	500	500	100...120
• under LOCA conditions	≤100	≤100	≤70	~35
Maximal fuel rod temperature, °C	550*	1200	720	920
Holdup time at maximal temperature level, min	72	3	25	6
Post-test fuel assembly state	sound.	leaky.	sound.	sound.

* - in one of the fuel rods the temperature was 950°C for a short period of time.

The "fresh" fuel rods are supplied with the temperature detectors in the fuel column and cladding. To smooth out the energy release in "fresh" and spent fuel the "fresh" pellet enrichment was 2% by U-235.

To show the test regime Fig.12 presents the fuel column temperature values for fuel rod 4 and the cladding temperature for fuel rod 2 in experiment No. 4. The coolant pressure during the test was higher than that within the fuel rod. The maximal fuel and cladding temperature was within the range of 900-1000 °. Dry out time was about 30 minutes.

As a result of post-reactor examination the following was determined. The fuel rod bundle is not deformed, the "fresh" fuel rod claddings are under outer pressure in the dry out area, the spent fuel rod cladding is not deformed (Fig.13). All fuel rods remained hermetic. In the fuel assembly dry out area the grain size of both claddings increased. Zirconium dioxide layers on the outer cladding surface in these cross sections have maximal thickness up to 10 μm. On the outer and inner cladding surfaces an alpha-zirconium layer appeared which is stabilized by oxygen. No significant changes in fuel structure before and after experiment are observed. The hydrogen content in "fresh" and spent claddings doesn't differ, hydrogen content increased as compared with the value of $5 \cdot 10^{-3}$ %mass. at the fuel assembly bottom – up to $(1\text{-}2) \cdot 10^{-2}$ % mass. in the dry out area.

Coolant temperature at fuel assembly outlet

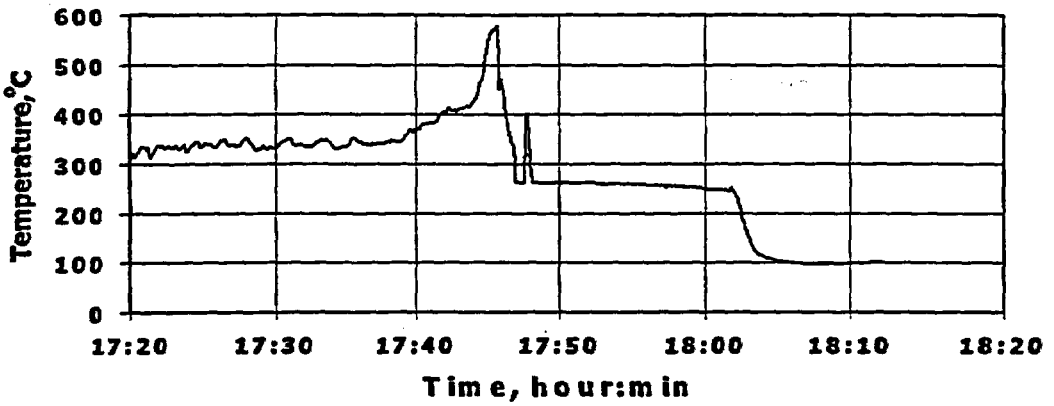

Fuel rod 2 cladding temperature at the elevation of 745 mm

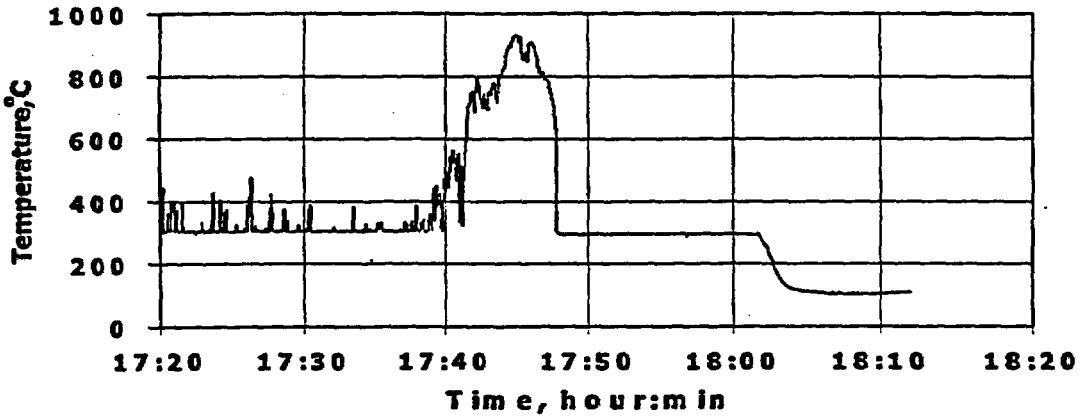

Fuel rod 4 fuel column temperature at the elevation of 895 mm

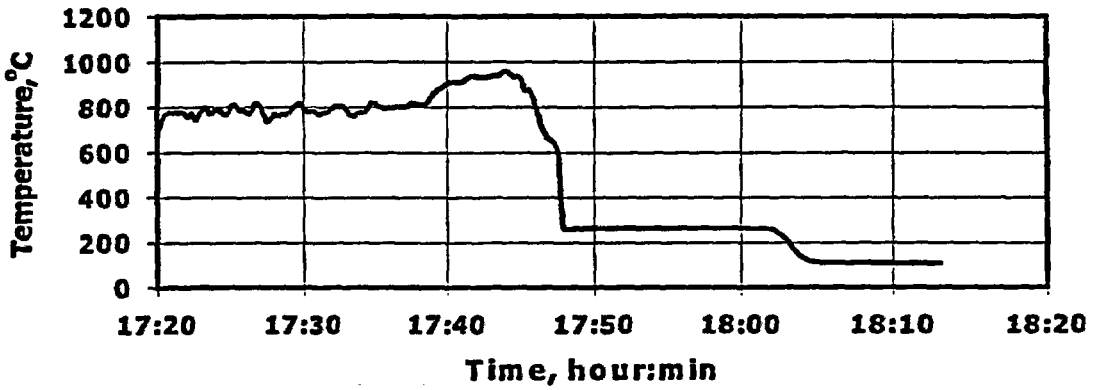

Fig.12. Temperature regime of fuel assembly tests in experiment No. 4 under LOCA conditions

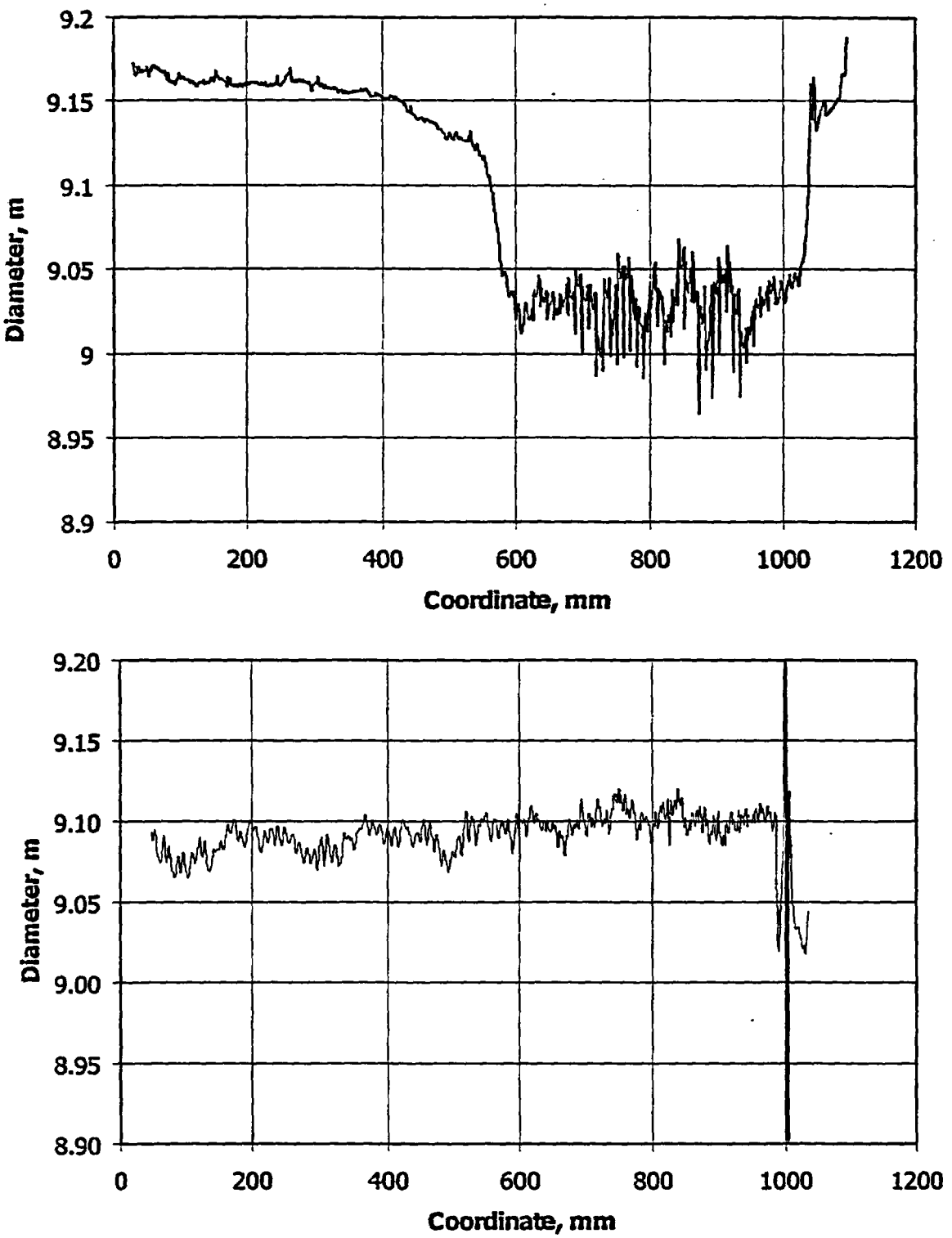

Fig.13. Fuel rod outer cladding diameter after the test of LOCA type a - non-irradiated fuel rod; b - irradiated fuel rod, Bu=56.1 MWd/kgU

The obtained post-test mechanical cladding properties using ring samples are presented in Table 7.

Table 7
Mechanical cladding properties

Fuel rod	Sample coordinate, mm	Test temperature, °C	σ, MPa	$\sigma_{0.2}$, MPa	$\delta_{uniform}$, %	δ_{total}, %
7	315-345	20	472	423	7.2	25.8
		350	272	233	7.6	28.2
	770-800	20	585	504	5.6	6.5
		350	323	279	6.7	17.6
4	320-360	20	380	328	11	31.6
		350	217	187	10.8	33.8
	775-808	20	434	365	7.6	15.1
		350	265	222	8.5	26.0

Based on the results of the tests one may conclude that the behaviour of "fresh" and irradiated cladding materials under accident conditions with temperature up to about 900 ° and excessive outer pressure is identical.

References

1. Цыканов В.А., Грачев А.Ф., Клочков Е.П., Куприенко В.А., Шамардин В.К., Устройства для облучения твэлов в реакторах СМ-2 и МИР при переменных режимах работы. Атомная энергия, т.58, вып.2, 1985 г., с 97-100.

2. Bibilashvili Y.K., Grachov A.F., Kalygin V.V., et.al. I.S.METHODS OF PERFORMING THE POWER RAMPING EXPERIMENTS WITH VVER FUEL RODS AT DIFFERENT BURNUPS. Technical Committee meeting under accident conditions (SSR RIAR, in Dimitrovgrad, Russia. 9-13 October, 1995). IAEATECDOC-921, 1996, p.101-116.

3. Ю.К.Бибилашвили, А.Ф.Грачев, В.А.Куприенко. Экспериментальные исследования влияния скачков мощности на состояние твэлов типа ВВЭР при различных выгораниях. Сборник докладов четвертой межотраслевой конференции по реакторному материаловедению. Том 1. Димитровград, 1996, с.125-140.

4. И.А.Кунгурцев, В.П.Смирнов, В.А.Жителев и др. Исследования кинетики окисления при температуре 1000 °С в пароаргоновой среде образцов оболочки твэла ВВЭР-440, отработавшего до выгорания 42.4 МВт·сут/кгU, в сборнике докладов 5-й межотраслевой конференции, Димитровград, 1997 г.

NSRR PULSE IRRADIATION EXPERIMENTS AND TUBE BURST TESTS

Toyoshi FUKETA, Fumihisa NAGASE, Takehiko NAKAMURA,
Hiroshi UETSUKA and Kiyomi ISHIJIMA
Department of Reactor Safety Research
Japan Atomic Energy Research Institute
Tokai, Ibaraki, 319-1195 JAPAN

To provide a data base for the regulatory guide of light water reactors, behavior of reactor fuels during reactivity-initiated accident (RIA) conditions is being studied in the Nuclear Safety Research Reactor (NSRR) pulse-irradiation experiments and related separate-effect test program of the Japan Atomic Energy Research Institute (JAERI). Recent results obtained from the NSRR experiments with high burnup PWR and BWR fuels are described and discussed in this paper. In addition to the NSRR data, the paper presents results from tube burst test with artificially hydrided cladding samples.

I. INTRODUCTION

To study behavior of light water reactor (LWR) fuels under reactivity-initiated accident (RIA) conditions, twenty-eight pulse-irradiation experiments have been performed with test fuels sampled from irradiated commercial reactor fuels. The tested fuel rods consist of twenty PWR fuels and eight BWR fuels. Fuel failure observed only in the tests series HBO and TK with high burnup PWR fuels. Table 1 lists test conditions and results of the HBO and TK experiments. The results from the HBO-1 through HBO-4[1] and from the HBO-5 through HBO-7[2] were presented in the documents separately. The fuel rods in the HBO series were sampled from a mother rod irradiated in 48 MWd/kgU lead-use program, and these rods had 1.5%Sn Zircaloy-4 cladding. However, fuels with 1.3%Sn (low tin) Zircaloy-4 cladding were adopted for 48 MWd/kgU regular-use in Japanese PWRs. Accordingly, we started new series of experiments with the fuels with the low tin cladding, as TK test series.[3] As for BWR fuels, NSRR data had been limited to five TS experiments with 26 MWd/kgU 7x7 type rods.[4] From 1996, we started FK test series with high burnup 8x8 type rods. This paper describes the most recent results from the TK experiments with high burnup PWR fuels and from first three experiments of the FK test series, and discusses possible sequence of fuel rod behavior during an RIA.

To answer pending questions regarding the fuel rod behavior, various separate-effect, out-of-pile tests have important role in combination with integral, in-pile experiments. The on-going separate-effect tests

include transient tube burst experiment, modified ring tensile test with machined specimen, and fuel pellet annealing test. The paper introduces test conditions and results from the transient tube burst experiment with artificially hydrided cladding.

Table 1 Test conditions of tests HBO and TK (High burnup PWR fuels)

Test ID	Fuel Type	Span	Oxide Layer (μm)	Fuel Burnup (MWd/kgU)	Peak Enthalpy (cal/g)	Result
HBO-1	A	3rd	40 to 48	50.4	73	Failed at 60 cal/g, 100% fuel dispersed
HBO-2	A	4th	30 to 40	50.4	37	No failure, FGR=17.7%
HBO-3	A	5th	20 to 25	50.4	74	No failure, FGR=22.7%
HBO-4	A	6th	15 to 20	50.4	50	No failure, FGR=21.1%
HBO-5	B	2nd	35 to 60	44	80	Failed at 77 cal/g, 5% fuel dispersed
HBO-6	B	4th	20 to 30	49	85	No failure, FGR=10.4%
HBO-7	B	3rd	35 to 45	49	88	No failure, FGR=8.5%
TK-1	A	5th	7	38	126	No failure, FGR=20.0%
TK-2	B	2nd	15 to 35	48	107	Failed at ~60 cal/g 7% fuel dispersed
TK-3	B	4th	4 to 12	50	99	No failure, FGR=10.9%
TK-4	A	3rd	(25)	50	98	No failure, FGR=8.3%
TK-5	A	2nd	(30)	48	101	No failure Tested on October 1, 1998
TK-6	A	3rd	(15)	38	(125)	No failure Tested on October 7, 1998
TK-7	B	3rd	(8)	50	(100)	To be performed on November 20, 1998

Fuel type A and B are manufactured by Mitsubishi Heavy Industries, ltd. and Nuclear Fuel Industries, ltd., respectively.

Span of 1st denotes the highest. FGR is an acronym for fission gas release.

Values in parentheses are from preliminary evaluations.

Fig. 1 Cracking occurred in the TK-2

II. NSRR EXPERIMENTS

The most recent experiment resulting in fuel failure is the TK-2, and the horizontal cross-section of failed cladding shows an appearance similar to those observed in the HBO-1 and HBO-5. An enlarged photograph of the cracking in the TK-2 is shown in Fig. 1. The penetrating crack shows brittle nature in the cladding peripheral region where hydride blisters are precipitated, but shows ductile nature in the inside. During the early stage of the transient, incipient cracking occurs in the outside due to PCMI loading, and the crack propagates to the inside. Figure 2 summarizes the relative elevation of the sampling position of the test rods in the HBO and TK test series. Fuel failure occurred in the HBO-1, HBO-5 and TK-2. It is apparent that the failed rods are sampled from the higher elevation where corrosion and hydrogen absorption of the cladding are more significant. The correlation of the oxide thickness with peak fuel enthalpy is shown in Fig. 3. Since the hydrogen

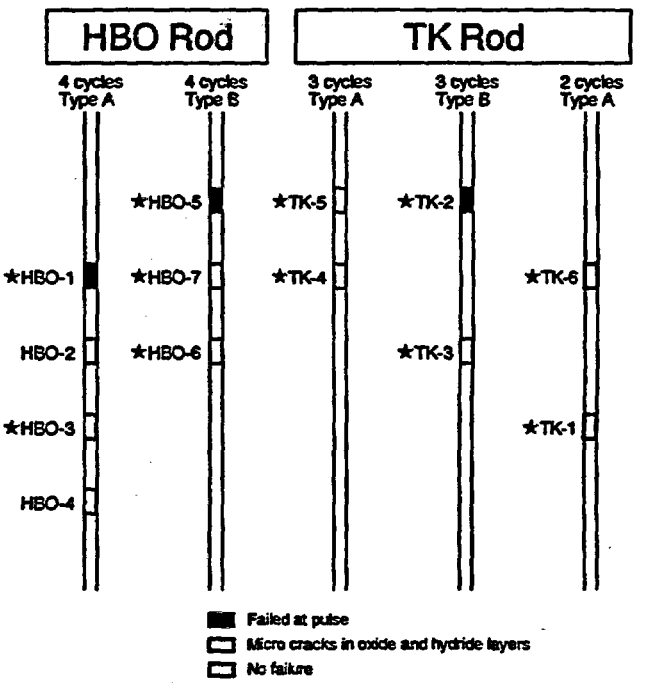

Fig. 2 Relative elevation of test rod sampled

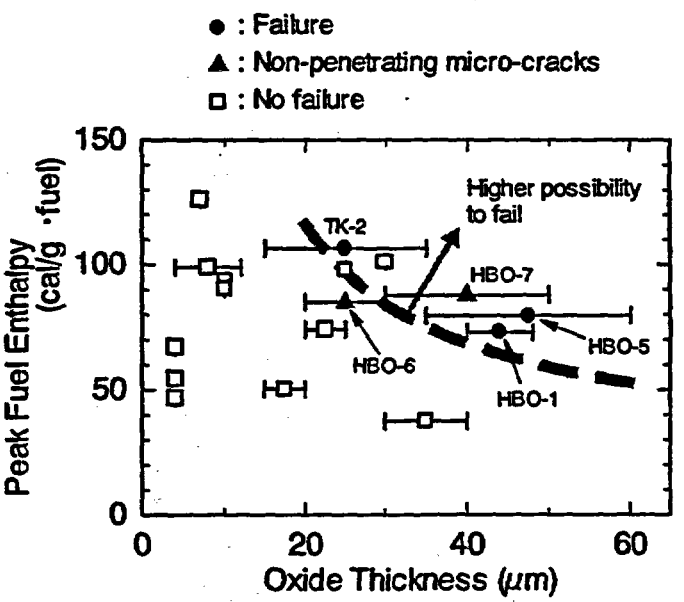

Fig. 3 Correlation of oxide thickness with peak fuel enthalpy

absorption in the cladding is almost proportional to the oxide thickness, the oxide thickness is an indicator including the hydride effect. The peak fuel enthalpy denotes the severity of the transient in the NSRR experiment. As seen in the figure, data points from the HBO-1, HBO-5 and TK-2 resulting in failure are in the region with thicker oxide layer and higher fuel enthalpy. It must be generally accepted that the PCMI failure of the high burnup PWR fuel correlates with corrosion, and with hydrogen absorption and resulting radially-localized hydride layer (hydride rim) which gives decreased cladding ductility.

Figure 4 schematizes anticipated processes of fuel behavior during the transients. Fuel pellet temperature increases promptly at the onset of the event, and fuel pellet expands rapidly due to thermal expansion and most likely due to fission-gas-induced swelling. The fission-gas-induced swelling is caused by thermal expansion of fission gas accumulated in fuel grain boundaries, as shown in Fig. 5. Then, expanded fuel pellets contact with cladding inner surface, and push the surface. When hydride clusters precipitate in cladding periphery, ductility of the cladding is reduced significantly due to the radially-localized hydride layer. Incipient cracking occurs in the cladding periphery, and the crack propagates to the inside. This hydride-assisted PCMI failure occurs in the early stage of the transient when cladding temperature remains low. In the NSRR experiments, the hydride-assisted PCMI failure occurred when cladding surface temperature was 100 deg C or lower. In order to clarify and evaluate the early phase PCMI process, out-of-pile, separate-effect tests are being performed as well as in-pile, integrated experiments. As for mechanical properties of hydrided cladding, material tests, such as machined-ring tensile stretch test and tube burst test, are being conducted in number of organizations. Hence, pending questions in the anticipated PCMI process exist in fuel pellet behavior as well as cladding integrity. A key question of the pellet behavior regards with the fission-gas-induced swelling due to high pressure loading of heated fission gas confined in grain boundary. Expansion of irradiated fuel pellets is much larger than that of un-irradiated fuels in the NSRR experiments. Figure 6 shows residual hoop strain of post-test cladding as a function of peak fuel enthalpy. The higher peak fuel enthalpy resulted in the larger strain, and in the TK-1 the strain reached almost 25%. The fission-gas-induced swelling has a significant role in the large deformation. However, the information regarding pellet expansion and resulting rod deformation is limited to that from the final stage, i.e. post-test, residual cladding deformation, and we do not know how much of expansion occurred in the early stage, the PCMI loading process. In the experiments resulting in the large deformation, 2% strain or higher, cladding surface temperature increased to 300 to 700 deg C at maximum due to an occurrence of DNB. The large deformation occurs during post-DNB phase. It can be expected that the fission-gas-induced swelling in combination with thermal expansion provides a PCMI load to the cladding during the early stage as well as the later post-DNB phase, but it is unknown at present that how early and how fast pressure elevation and reduction occur in fission gas accumulated in grain boundaries. Since the rod deformation during the early stage is critical information to evaluate the PCMI loading, a transient method to measure

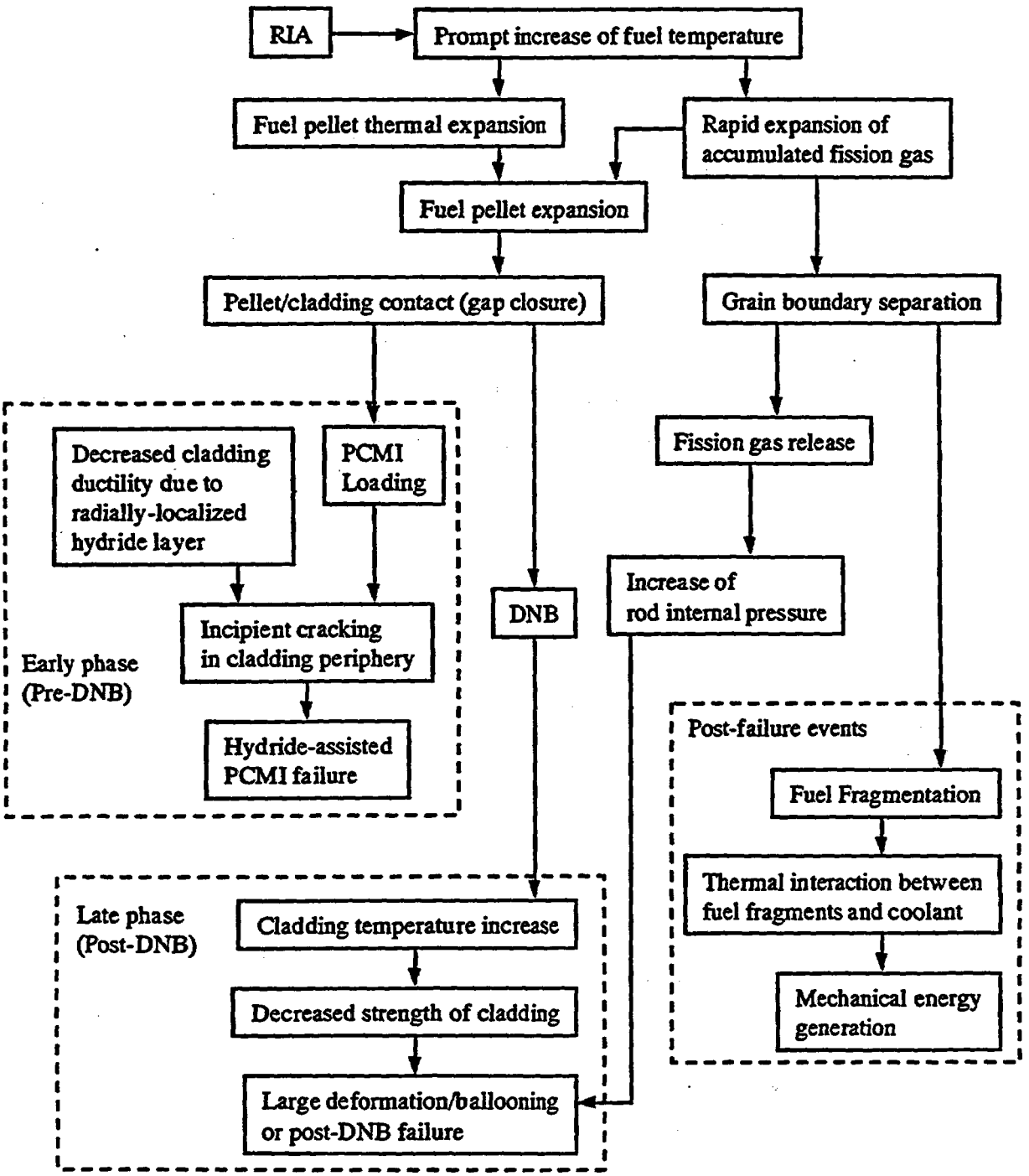

Fig. 4 Anticipated process of fuel behavior during an RIA

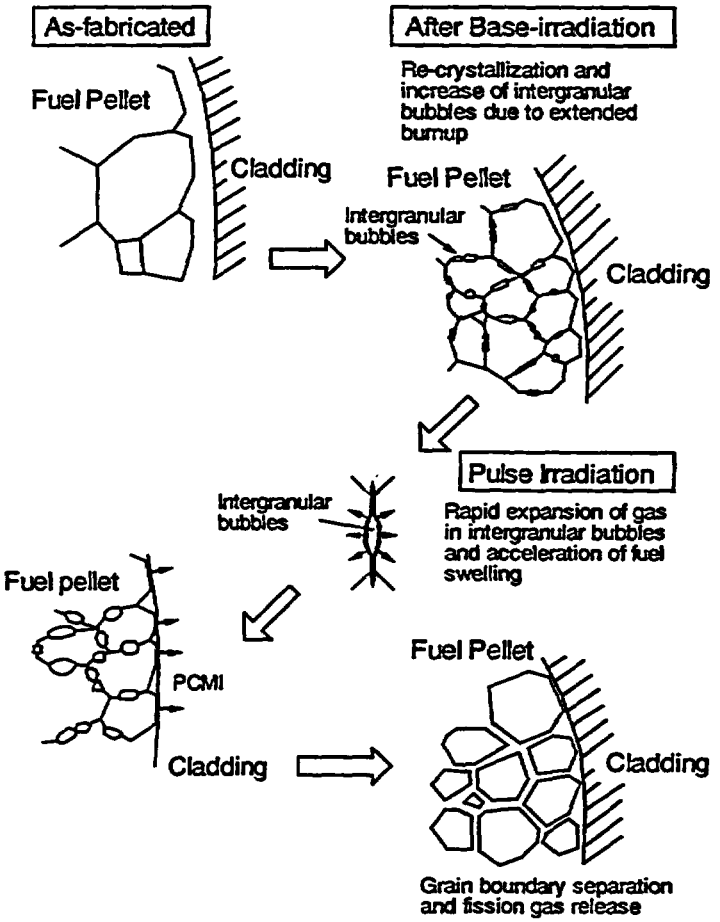

Fig. 5 Fission-gas-induced swelling and grain boundary separation

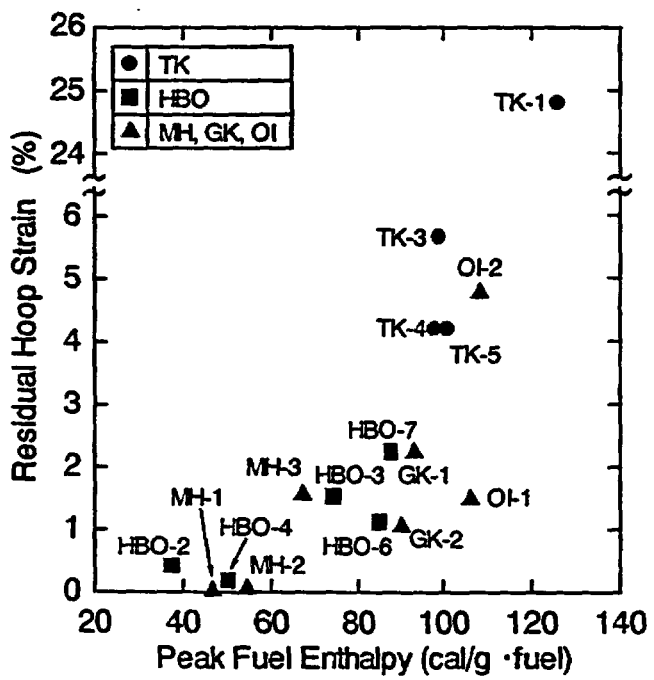

Fig. 6 Residual hoop strain of post-test cladding as a function of peak fuel enthalpy

cladding outer diameter during the pulse-irradiation is being developed with eddy current sensors. The method has been verified in experiments with un-irradiated fuels, and is to be applied to irradiated fuel tests in the NSRR.

Figure 7 shows fission gas release during pulse-irradiation as a function of peak fuel enthalpy. Except HBO-2, -3 and -4, the higher fission gas release correlates with the higher peak fuel enthalpy. In the HBO-2, -3, -4 and TK-1, fission gas release reaches about 20%, and it corresponds that all of fission gas accumulated in grain boundaries is released in these experiments.

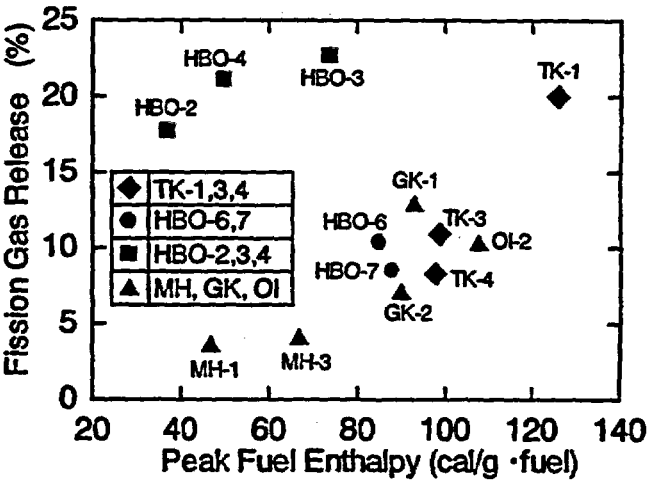

Fig. 7 Fission gas release during pulse-irradiation as a function of peak fuel enthalpy

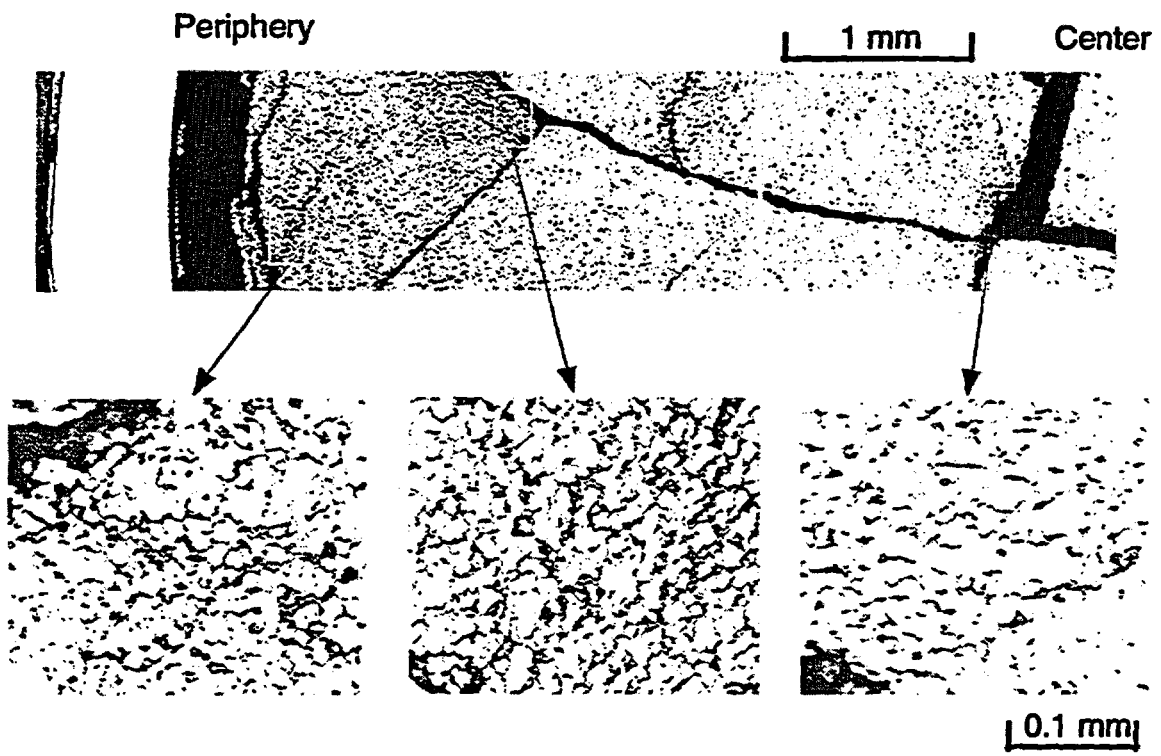

Fig. 8 Fuel pellet micro-structure of post-test TK-2 fuel pellet

As it can be seen in Figs. 6 and 7, the experiments with high fission gas release resulted in the large rod deformation except the HBO-2, -3 and -4. This fact indicates a significant role of fission gas in rod deformation. In the HBO-2, -3 and -4, DNB did not occur and cladding temperature remained in low, so the rod deformation were limited in these experiments. A transient signal from thermocouple in the HBO-3 showed about 400 deg C at maximum, but duration of stable film boiling is very short, and must be limited to local area.

The loading from fission gas expansion appears as grain boundary separation in post-test fuel pellets. Figure 8 shows fuel pellet micro-structure of post-test TK-2 fuel pellet. The pictures show horizontal, as-polished cross-section of the pellet. Significant grain boundary separation can be seen in extensive area of the cross-section. In the TK-2 resulting in fuel failure, about 7% of fuel was recovered as fragmented particles from capsule water after the experiment. Cross-sectional view of the fuel particles is shown in Fig. 9, and SEM images are in Fig. 10. The collected fuel particles are not once-molten, as it can be expected from the maximum fuel temperature (about 2900 K or lower) during the pulse-irradiation. Although the fragmented particles remain in solid, thermal to mechanical energy conversion ratio was about 0.08%. It suggests vigorous thermal interaction between the particles and coolant water.[4]

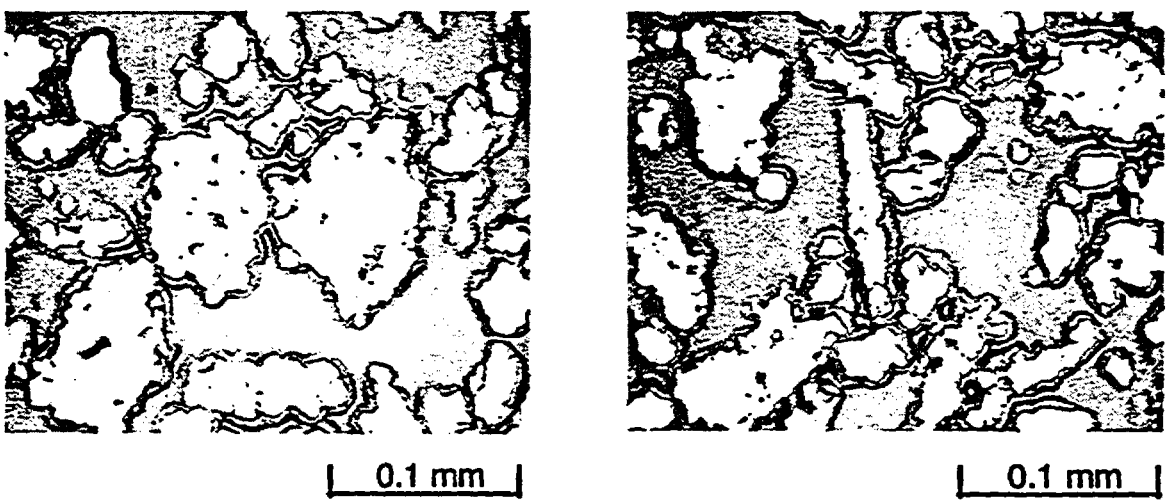

Fig. 9 Cross-sectional view of fragmented fuel particles recovered from coolant water in the TK-2

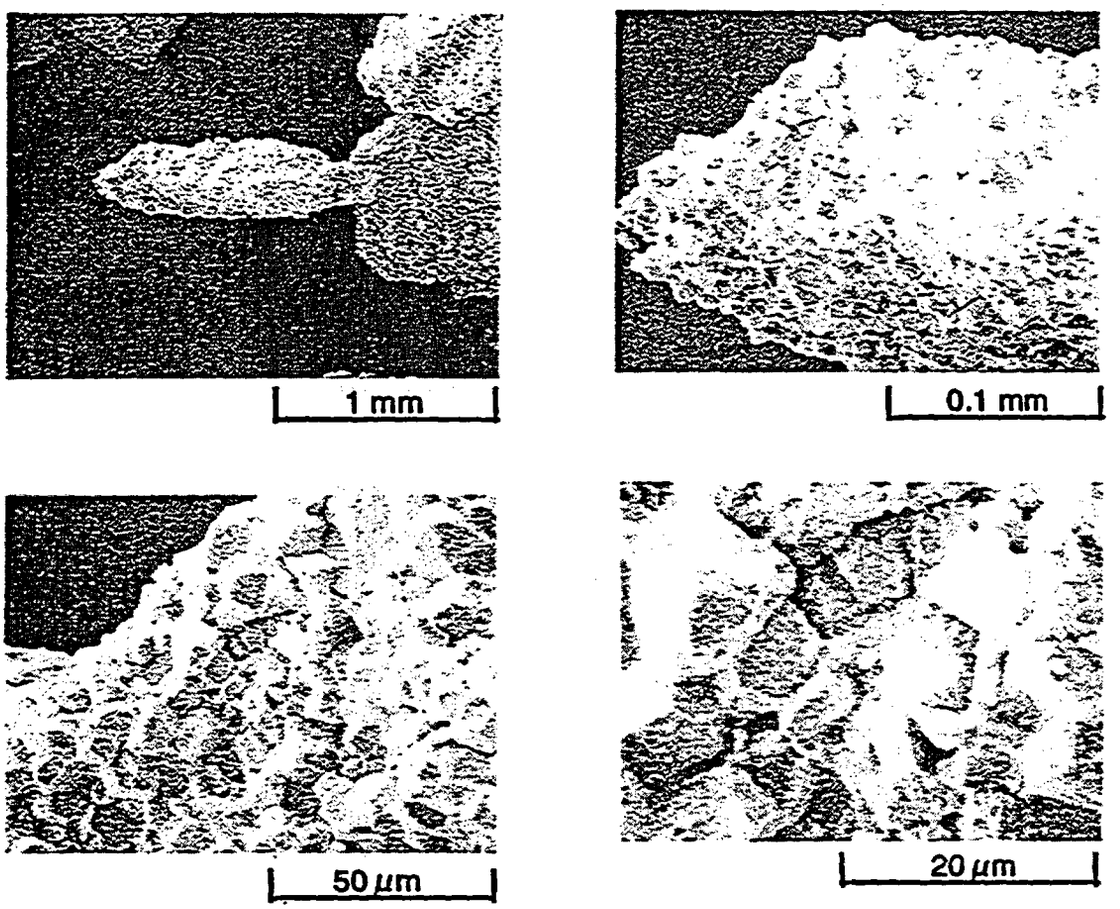

Fig.10 SEM images of fragmented fuel particles recovered from coolant water in the TK-2

As stated previously, BWR data had been limited to five TS experiments with 26 MWd/kgU 7x7 type rods. The test fuel rods in newly initiated FK test series are high burnup 8x8 type rods. The test conditions of the FK test series are listed in Table 2. The test fuels for the FK-1 through FK-3 are Step-I fuels from Fukushima First plant #3 reactor, and the test fuels for the FK-4 through FK-7 are Step-II fuels from Fukushima Second plant #2 reactor. We have performed three experiments so far, and fuel failure has not been observed in these tests. Since creep down of cladding is less significant in BWRs in comparison with that in PWRs, wider gap between fuel pellets and cladding inner surface (P/C gap) exists in BWR fuels before pulse-irradiation in the NSRR. The pre-test wider P/C gap provides BWR fuels with weaker PCMI loading in the early phase, and reflects smaller fuel rod deformation during the transient. Figure 11 shows residual hoop strain of post-test cladding as a function of peak fuel enthalpy, and the figure includes both of BWR and PWR data. The larger strain correlates with the higher peak fuel enthalpy also among BWR data, but the strain data of BWR fuels are much smaller than those of PWR.

Fission gas release in the BWR tests shows in Fig. 12 with those in PWR data as a function of peak fuel enthalpy. The BWR data points in the figure are scattered, and fission gas release in the TS tests with 26 MWd/kgU fuels is higher than that in FK experiments with higher burnup fuels. Fission gas release during base-irradiation in commercial reactor is much higher in TS test fuels, 19.7%, than those of FK test fuels. This fact suggests that release paths generated during base-irradiation contribute to fission gas release during pulse-irradiation.

Table 2 Test conditions of test FK (High burnup BWR fuels)

Test ID	Span	Oxide Layer (μm)	Fuel Burnup (MWd/kgU)	Peak Enthalpy (cal/g)	Result
FK-1	3rd	20	45.4	130	No failure, FGR=8.2%
FK-2	3rd	20	45.4	70	No failure, FGR=3.1%
FK-3	2nd	20	41	(145)	No failure
FK-4	3rd	N/A	56	(140)	To be performed on January 26, 1999
FK-5	3rd	N/A	56	(70)	To be performed on February 19, 1999
FK-6	-	N/A	60	(130)	To be performed for FY1999
FK-7	-	N/A	60	(70)	To be performed for FY1999

Values are from preliminary evaluations.

FY1999 is a Japanese fiscal year from April 1, 1999 to March 31, 2000.

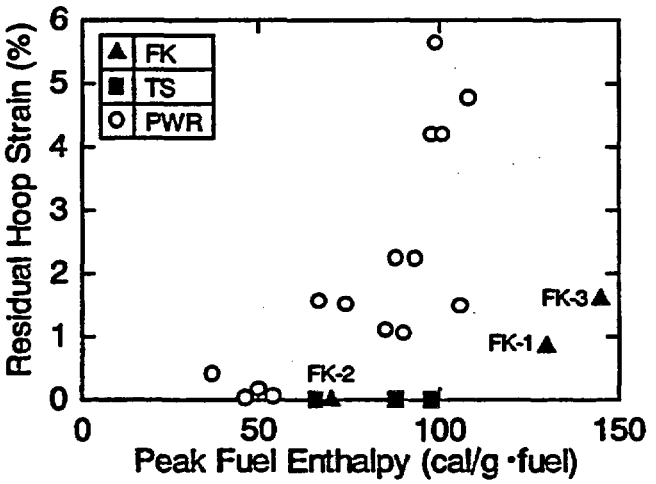

Fig. 11 Residual hoop strain of post-test cladding as a function of peak fuel enthalpy

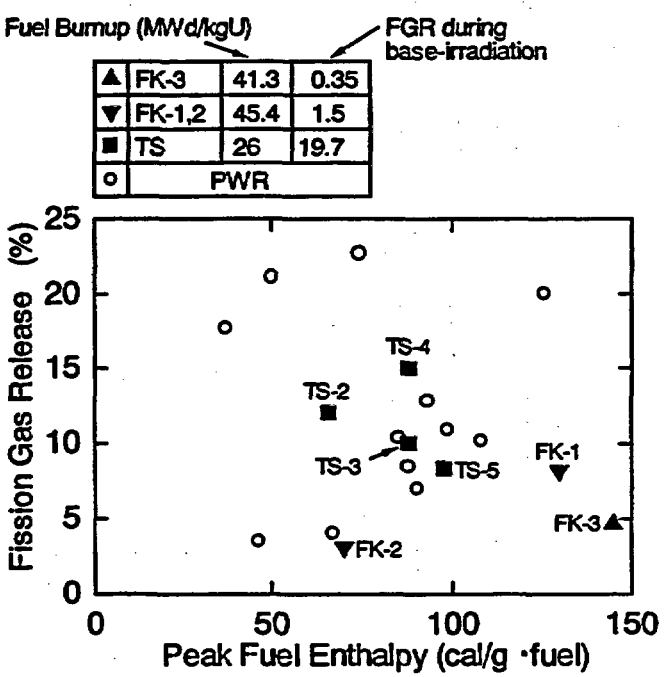

Fig. 12 Fission gas release during pulse-irradiation as a function of peak fuel enthalpy

III. CLADDING TUBE BURST TEST

To understand high burnup fuel behavior during RIA conditions, it is very important to know mechanical properties of cladding materials, in particular, ductility reduction due to radially-localized hydride precipitation. As stated previously, the influence of the hydride deposition has a critical importance in the early phase, PCMI process. The effect of the hydride deposition cannot be described by hydrogen concentration averaged at cross-section, and the effect of radial and circumferential localization of hydride clusters is very important. The influence of hydride precipitation on cladding mechanical properties is being examined in out-of-pile, separate-effect tests at JAERI. The separate-effect tests comprise of highly-transient tube burst experiment and modified ring tensile test on machined specimen. In addition to as-fabricated sample, artificially hydrided cladding has been tested in the burst test and is to be tested in the ring tensile test. This paper describes test method, test conditions and results at room temperature in the tube burst experiment.[5]

Figure 13 shows a schematics of the burst test apparatus. The apparatus consists of a high pressure line (pump, pressure booster and tank), a sample holder, a solenoid valve, and data acquisition system. The pressure medium is diffusion pump oil. Cladding sample is fixed to the sample holder at lower end, while upper end of sample is free for axial movement of sample. Pressure of the tank is elevated to about 150 MPa, and then the solenoid valve is opened. Pressure change in the sample is measured by high capacity transducers with frequency of 250 kHz. Pressure increase rates are 0.002 MPa/ms and 1.9

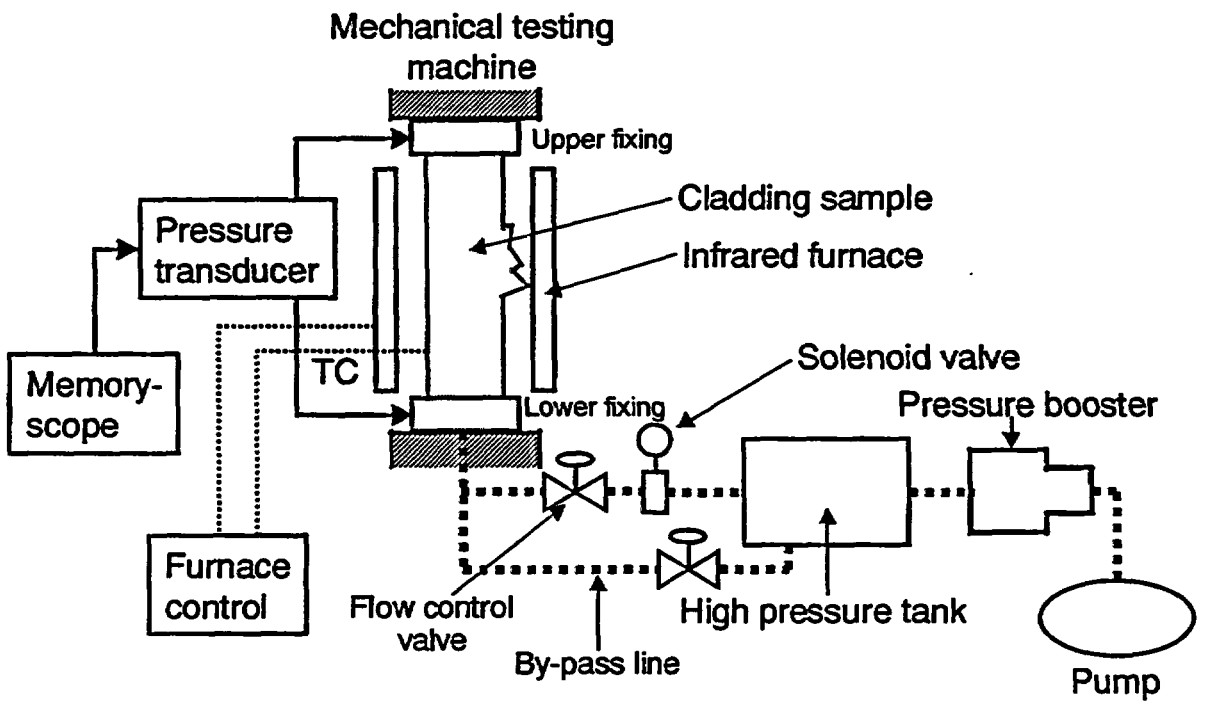

Fig.13 Schematics of the burst test apparatus

MPa/ms, and samples are at room temperature in the current study. Tests will be performed at elevated temperature and the pressure increase rate will be 3.4 MPa/ms for succeeding tests.

Test specimens subjected to the burst test are low-tin (1.3wt%Sn) Zircaloy-4 cladding tubes which are currently used in PWRs in Japan. The inner and outer diameters of the sample are 9.50 mm and 8.36 mm, respectively, and the length is 160 mm. The tests were conducted on three types of specimens consisting as-received sample (non-hydrided); uniformly hydrided sample (without hydride rim); and hydrided sample with radially-localized hydride layer (with hydride rim). Hydrogenation was performed in mixture gas of hydrogen and argon at about 600 K, and samples with hydrogen concentrations of 100 to 600 wtppm were produced. Variation in hydrogen concentration throughout a sample was estimated to be within ±30% from the analysis of reference sample. Hydride clusters are uniformly distributed through the cladding thickness in the sample without hydride rim, while hydride clusters are localized in peripheral region of the sample with hydride rim. The difference of hydride distribution between the two types of samples can be seen in Fig. 14. In the sample with hydride rim (below in Fig. 14), hydrides are localized in 50 to 150 μm of sample periphery. Under assumptions of 400 wtppm for radial-average concentration and 100 wtppm (solid solubility of hydrogen in Zircaloy at 600 K) for concentration in the interior region, hydrogen concentration in the hydride rim is estimated to be 1200 to 3600 wtppm.

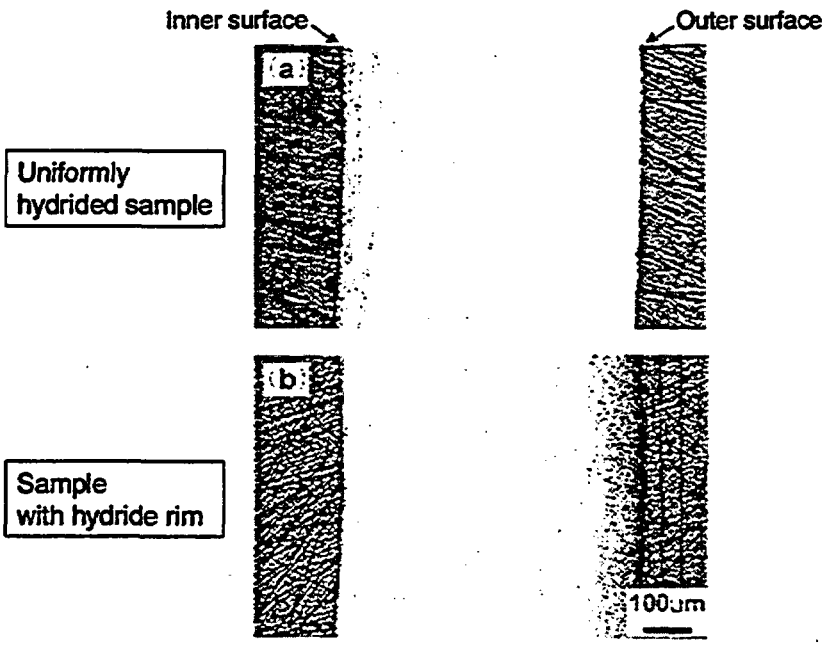

Fig. 14 Hydride morphology in radial cross-section of hydrided samples used in tube burst test; (a) uniformly hydrided sample, and (b) sample with hydride rim

Figure 15 shows post-test appearances of samples in the burst tests. The non-hydrided sample (top in the figure) exhibits a typical burst opening of 30 mm long. On the other hand, axially extended openings are formed in the hydrided samples (middle and bottom in the figure). The average hydrogen concentration of the two hydrided samples are 450 wtppm for that without hydride rim and 360 wtppm for that with hydride rim, respectively. The axial crack in the sample with hydride rim is shorter than

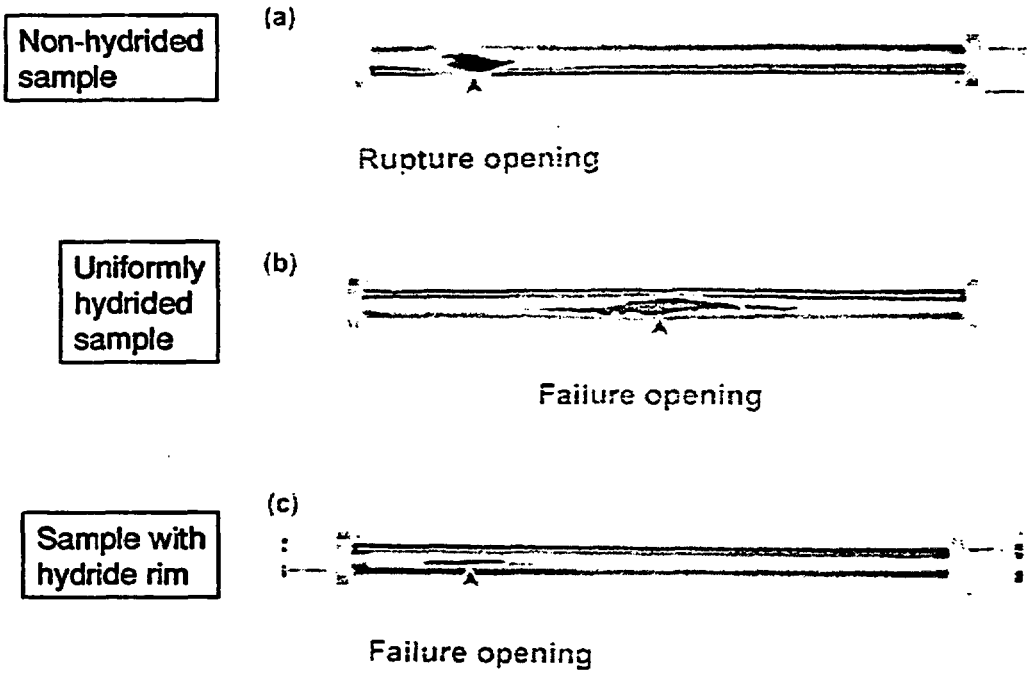

Fig. 15 Appearances of cladding samples after tube burst test; (a) non-hydrided sample, (b) uniformly hydrided sample, and (c) sample with hydride rim..

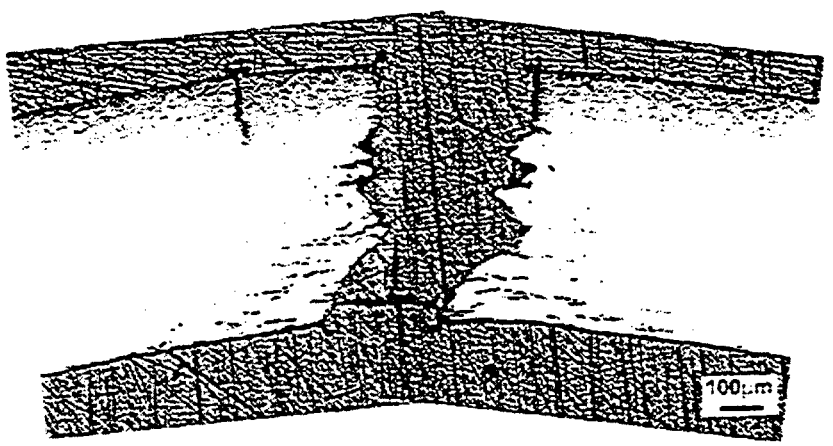

Fig. 16 Cracking observed in sample with hydride rim (tube burst test)

that in the sample without hydride rim. It can be expected that interior region with higher ductility resists to crack propagation in the sample with hydride rim. The axial cracking appeared in the hydrided samples are similar to those observed in the NSRR experiments with high burnup PWR fuels. Horizontal cross-section of tested sample with hydride rim also gives a morphology similar to those in the NSRR experiments, as shown in Fig. 16. Brittle fracture is seen in the hydride rim, while ductile fracture appears in the interior region.

Figure 17 shows transient histories of sample internal pressure in the burst tests with pressurization rate of 1.9 MPa/ms. The upper figure shows the histories for non-hydrided samples and for uniformly hydrided samples (without hydride rim) containing 148 to 461 wtppm of hydrogen. Non-hydrided samples failed at about 150 ms after the pressure increase initiated. The duration from the initiation to sample failure decreases with increased concentration of hydrogen. In terms of burst pressure, however, a difference does not appear between non-hydrided samples and uniformly hydrided samples. The burst pressure of the samples ranges 120 MPa to 126 MPa corresponding to hoop stress at failure of about 900 MPa. The lower of Fig. 17 shows transient records for samples with hydride rim. The samples with hydride rim have 302 and 305 wtppm for radially-averaged concentration of hydrogen. The samples with hydride rim fail at 25 to 30 ms after the pressure increase initiated, and burst pressure is 97 to 104 MPa. The lower burst pressure and the earlier failure suggest reduction of strength and ductility due to the hydride rim. Figure 18 shows influence of hydrogen concentration on burst pressure. Burst pressure is not affected by hydrogen concentration

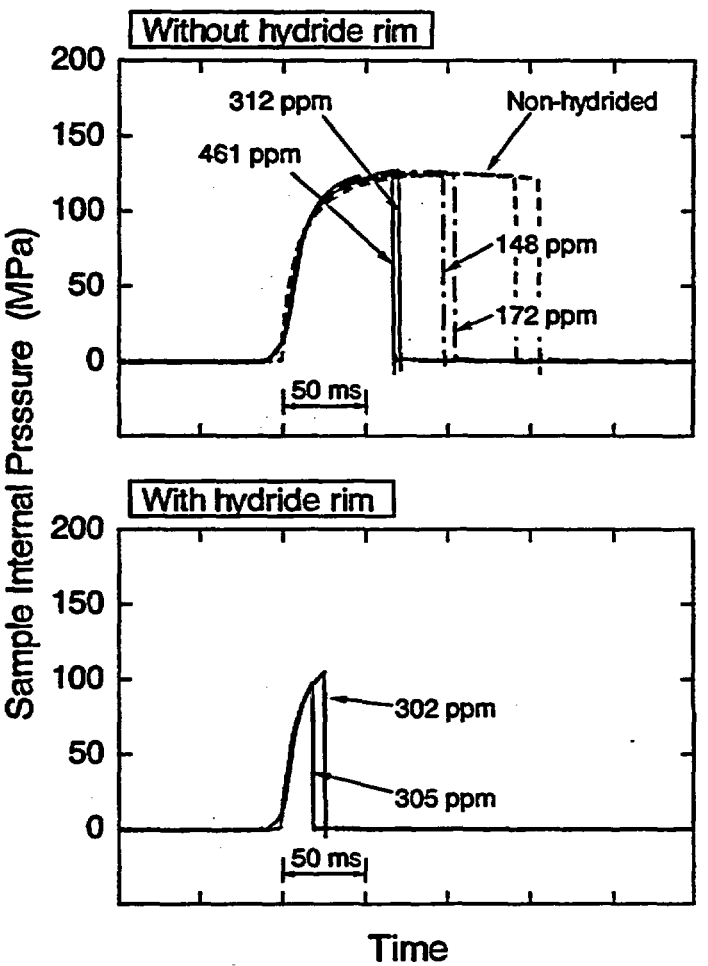

Fig. 17 Transient histories of sample internal pressure in the burst tests with pressurization rate of 1.9 MPa/ms; samples without hydride rim (upper), and samples with hydride rim (lower)

when samples are uniformly hydrided, but decreases in samples with hydride rim. The burst pressure becomes 77 MPa in the test with a sample with hydride rim (520 wtppm of radially-averaged hydrogen) and with pressurization rate of 0.002 MPa/ms.

Through photo-image analysis on radial cross-section at the axial position where the maximum deformation occurred in post-test sample, residual hoop strain was measured at both the inner and the outer surfaces. The residual hoop strain is shown in Fig. 19 as a function of hydrogen concentration. Larger hoop strain was always seen at the inner surface. The maximum and the minimum values of the error bar correspond to hoop strains at the inner and the outer surfaces, respectively. Hydrogen concentration was measured with hot extraction method for the sliced piece sampled from the vicinity of the position where the hoop strain was evaluated. The hoop strain decreases with the increase of hydrogen concentration, and the reduction becomes remarkable in hydrogen concentration of 300 wtppm or higher. The hoop strain data from the high-pressurization-rate (1.9 MPa/ms) tests are lower than those from the low-pressurization-rate (0.002 MPa/ms) tests in the same hydrogen concentration level. It should be noted that the samples with hydride rim failed with significantly low hoop strain, less than 1% in average between the inner and outer surfaces. In particular, the hoop strain in the outer surface is almost undetectable. A crack initiates from the embrittled hydride rim with very low strain,

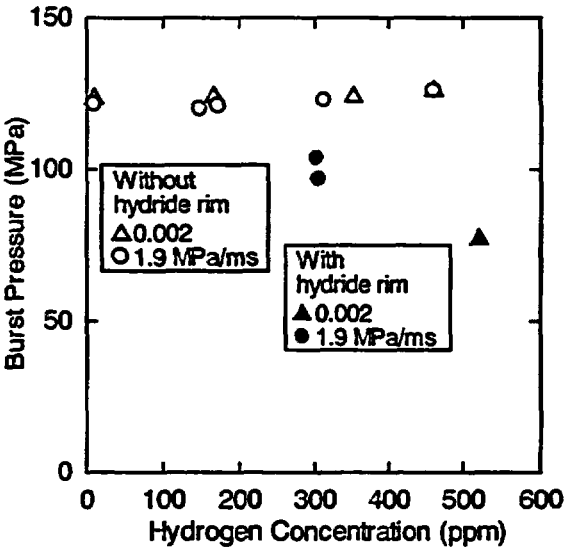

Fig. 18 Burst pressure as a function of hydrogen concentration

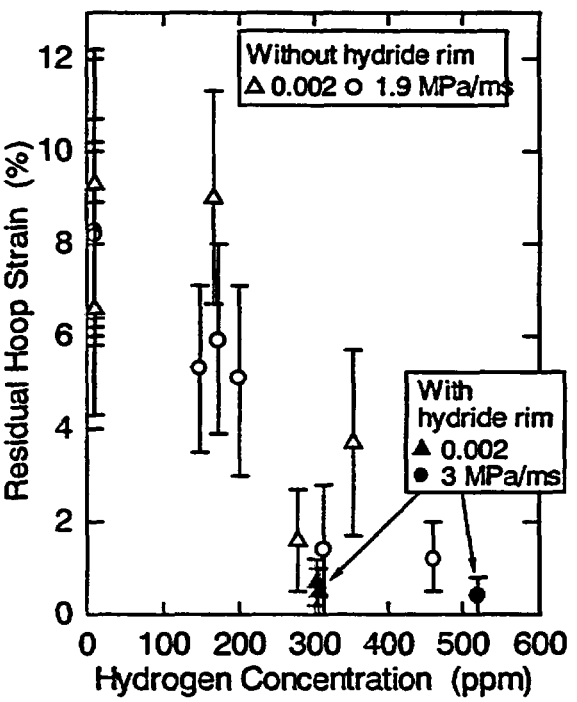

Fig. 19 Residual hoop strain in failed samples as a function of hydrogen concentration

and stress concentration causes crack propagation through the wall. This corresponds to the earlier failure of the sample with the hydride rim at the lower internal pressure. The results from the tube burst test show that cladding with hydride rim fails with the lower internal pressure and with the very small residual hoop strain, and these facts corroborate observation in the NSRR, i.e. hydride-assisted PCMI failure.

IV. SUMMARY

The results from the NSRR experiments with high burnup PWR fuels are summarized as follows.

- High burnup PWR fuels with low tin cladding (1.3%Sn) were subjected to the pulse irradiation, and test fuel rod sampled from the higher elevation, with thicker oxide layer, failed at 60 cal/g.
- Larger fuel deformation occurred at higher fuel enthalpy level, and reached 25% increase of cladding outer diameter at maximum.
- Almost all amount of fission gas accumulated in grain boundaries released in Tests HBO-2, -3, -4 and TK-1.
- Water hammer was detected during TK-2. 7% of fuel dispersed into coolant, and thermal to mechanical energy conversion ratio was 0.08%. Collected fuel particles were not once-molten. The result indicates vigorous thermal interaction between the particles and coolant water.

To understand fuel behavior during the transient, information regarding cladding integrity and loading provided from fuel pellet expansion is inevitable. The existing data suggest a particular importance to study a role of fission gas on the fuel pellet expansion in pre- and post-DNB phase, in particular, in early stage, pre-DNB phase. To evaluate the transient PCMI loading, eddy current sensor for transient measurement of fuel rod deformation is developed, and is to be applied to NSRR experiments with high burnup fuels. Comparison between NSRR experiments with high burnup fuels and with un-irradiated fuels could provide valuable information regarding fission-gas-induced swelling in high burnup fuels.

Experiments with high burnup BWR fuels, i.e. FK test series, initiated in the NSRR, and first three tests FK-1 through FK-3 were successfully performed. 41 to 45.4 MWd/kgU BWR fuels were subjected to the pulse irradiation, and fuel enthalpy reached 145 cal/g at maximum in the FK-3.

- Fuel did not fail in the three experiments. Due to pre-test wider P/C gap, PCMI loading and resulting fuel deformation are less significant in BWR fuels than those in PWR fuels.
- Fission gas release in BWR fuels during pulse-irradiation is strongly influenced by

base-irradiation conditions, such as linear heating rate. Fuel with large fission gas release during base-irradiation gives large fission gas release at pulse.

The tube burst tests were performed with artificially-hydrided Zircaloy-4 cladding samples at room temperature.

- Artificially hydrided sample ruptured with a long axial crack similar to those observed in high burnup PWR fuel rods in NSRR experiments.
- Burst pressure is not influenced by uniformly distributed hydride. However, samples with radially-localized hydride layer (hydride rim) ruptured with the lower burst pressure.
- Residual hoop strain of failed tube decreases at the higher hydrogen concentration, and becomes less than 1% for samples with hydride rim.

The NSRR experiments will continue to perform with LWR fuels including irradiated MOX fuels. Test conditions will be improved by development of test capsule at high temperature and high pressure conditions, in-pile video system for pulse-irradiation experiment, eddy current sensor for transient measurement of fuel rod deformation, etc. In addition to the efforts on in-pile experiments, out-of-pile tests including tube burst test at elevated temperature, modified ring tensile test with machined specimen, fuel pellet annealing test will be conducted.

ACKNOWLEDGMENTS

The authors would like to acknowledge and express their appreciation for the time and effort devoted by numerous engineers and technicians in JAERI, in particular, NSRR Operation Division for performing pulse-irradiation experiments, Department of Hot Laboratories for conducting extensive PIEs, and Process Technology Division in Department of NUCEF Project for inevitable contribution on evaluation of energy deposition. The HBO and TK experiments have been performed as collaboration programs between JAERI, Mitsubishi Heavy Industries, Ltd. and Nuclear Fuel Industries, Ltd. by using fuel rods transferred from Kansai Electric Power Company, Inc. The FK experiments have been conducted with fuel rods from Tokyo Electric Power Company, Inc.

REFERENCES

(1) Fuketa, T., Mori, Y., Sasajima, H., Ishijima, K. and Fujishiro, T., "Behavior of High Burnup PWR Fuel Under a Simulated RIA Conditions in the NSRR", Proc. CSNI Specialist Mtg. on Transient Behavior of High Burnup Fuel, Cadarache, France, September 12-14, 1995, NEA/CSNI/R(95)22, pp.59-85, (1996).

(2) Fuketa, T., Nagase, F., Ishijima, K. and Fujishiro, T., "NSRR/RIA Experiments with High-Burnup PWR Fuels", Nuclear Safety, Vol.37, No.4, pp.328-342, (1996).

(3) Fuketa, T., Nakamura, T. and Ishijima, K., "The Status of the RIA Test Program in the NSRR" , Proc. 25th Water Reactor Safety Information Mtg., Bethesda, Maryland, October 20-22, 1997, NUREG /CP-0162, Vol.2, pp.179-198, (1998).

(4) Papin, J. and Schmitz, F., "The Status of the CABRI-REP-Na Test Programme: Present Understanding and Still Pending Questions", Proc. 25th Water Reactor Safety Information Mtg., Bethesda, Maryland, October 20-22, 1997, NUREG /CP-0162, Vol.2, pp.199-216, (1998).

(5) Schmitz, F. and Papin, J., "REP-Na 10, another RIA Test with a Spalled High Burnup Rod and with a Pulse Width of 30 ms", Proc. 26th Water Reactor Safety Information Mtg., Bethesda, Maryland, October 26-28, 1998, to be issued.

(6) Sugiyama, T., Fuketa, T. and Ishijima, K., "Mechanical Energy Generation During High Burnup Fuel Failure Under Reactivity Initiated Accident Conditions", submitted to 7th Int. Conf. on Nuclear Engineering (ICONE-7) to be held in Tokyo, Japan, April 19-23, 1999.

(7) Nakamura, T., Yoshinaga, Y., Sobajima, M., Ishijima, K. and Fujishiro, T., "Boiling Water Reactor Fuel Behavior at Burnup of 26 GWd/tonne U Under Reactivity-Initiated Accident Conditions", Nuclear Technology, Vol.108, No.1, pp.45-60, (1994).

(8) Nagase, F., Otomo, T. and Uetsuka, H., "High-pressurization-rate Burst Test of Hydrided Zircaloy-4 Fuel Cladding at Room Temperature", JAERI-Research 98-064, (1998) [Text in Japanese].

REP-Na 10, another RIA Test with a Spalled High Burnup Rod and with a Pulse Width of 30 ms.

Franz SCHMITZ and Joelle PAPIN
Institut de Protection et de Sûreté Nucléaire (IPSN)
Département de Recherches en Sécurité
CEA - Cadarache 13108 Saint Paul lez Durance (France)

1. Summary :

The response of a PWR fuel rod to the design basis, reactivity initiated accident (RIA) conditions was originally considered to be dominated by two global parameters : the maximum mean fuel enthalpy and the burnup of the fuel.
The results and analysis of the CABRI REP-Na tests have shown that two additional parameters have a significant influence on the high burnup fuel rod behaviour under the RIA : the level and the structure of clad - corrosion and, last but not least, the fuel - enthalpy increase rate, which is related to the pulse width of the power excursion. This conclusion was based essentially on the 3 experiments REP-Na 1, REP-Na 4 and REP-Na 8 which produced very different results for almost identical energy deposition and fuel burnup conditions.
The demonstration of the favourable influence of a larger power pulse from the test REP-Na 8 by comparison with REP-Na1, with regard to fuel dispersal after failure, needed confirmation. Therefore an additional test was decided in close co-operation between IPSN and NRC with the aim to reach a better phenomenological understanding, both for REP-Na1 (spalling effect) and for REP-Na8 (pulse-width effect). This new test, REP-Na 10, was performed in the CABRI reactor on July, 30 - 1998.
From the results of the latest two experiments, REP-Na8 and especially REP-Na10, a breakthrough could be reached in the understanding of the key phenomena and parameters of the early phase of the reactivity initiated accident. The state of the understanding is presented in this paper.

2. Introduction :

The experiment REP-Na8 was originally designed as the cornerstone of the original series of RIA experiments with UO2 fuel in the sodium loop of the Cabri test reactor. High corrosion with incipient spalling and a reactor representative pulse width were the characteristic parameters for comparison with the earlier tests REP-Na1 and REP-Na4.
A very detailed analysis of the detector signals of the Cabri instrumentation and finally the confirmation by visual inspection and destructive post-test examination were needed to conclude formally that the test rod had ruptured during the REP-Na8 test. No fuel dispersal was observed. The precise value of the enthalpy at failure is still under investigation and the uncertainty for this important value is presently still very high : 42 to 83 cal/g.
Two major questions motivated IPSN and NRC to perform one further experiment, the test REP-Na10 :

- is the beneficial effect of the slow pulse still valid at ~ 30ms ?
- does more severe spalling influence the post failure behaviour under the conditions of a slow power pulse ?

This test has been performed successfully on July,30 - 1998.
The presently available results of this test are presented in this paper together with the test analysis data and the post test examination results of REP-Na8 which were obtained since the last WRSM meeting. In fact, at the time of the last meeting, REP-Na8 was still considered as not having failed.

Table 1 has therefore been corrected and updated and replaces the one of the proceedings of the 1997 WRSM [1].

Table1 : The Cabri REP-Na Tests

Test (date))	*Tested rod*	*Pulse (ms)*	*Energy at pulse end (cal/g)*	*Corrosion (μ)*	*RIM (μ)*	*Results and remarks*
Na-1 (11/93)	EDF Grav5c span 5 4.5 % U5 64 GWd/t	9.5	110 (at 0.4 s) (460 J/g)	80 important initial spalling	200	Brittle failure at H = 30 cal/g Hmax = 115 cal/g; Fuel dispersion: 6 g including particles other than RIM, Sodium pressure peaks.
Na-2 (6-94)	BR3 6.85 % U5 33 GWd/t	9.5	211 (at 0.4 s) (882 J/g)	4		No rupture Hmax = 210 cal/g Δϕ/ϕ (max): 3.5 % average value FGR/5.54 %
Na-3 (10/94)	EDF 4.5 % U5 53 GWd/t	9.5	120 (at 0.4 s) (502 J/g)	40	100	No rupture Hmax = 125 cal/g Δϕ/ϕ (max): 2 % max FGR/13.7 %
Na-4 (7/95)	EDF Grav5c span 5 4.5 % U5 62 GWd/t	80	97 (at 1.2 s) (404 J/g)	80 no initial spalling	200	No rupture Hmax = 99 cal/g Transient spalling Δϕ/ϕ (max): 0.4 % average value FGR/8.3 %
Na-5 (5/95)	EDF Grav5c span 2 4.5 % U5 64 GWd/t	9 .0	105 (at 0.4 s) (439 J/g)	20	200	No rupture Hmax = 115 cal/g Δϕ/ϕ (max): 1 % max FGR/15.1 %
Na-6 (3/96)	EDF MOX, 3c span 5 47 GWd/t	~35	165 (at 1.2 s) (690 J/g)	40	-	No rupture Hmax = 145 cal/g Δϕ/ϕ (max): 3.2 % max FGR/21,6 %
Na-7 (2/97)	EDF MOX, 4c span 5 55 GWd/t	~ 40	175 (at 1.2 s) (732 J/g)	50	-	Rupture at 120 cal/g Hmax = 140 cal/g Pressure peaks Fuel dispersal Examination currently carried out.
Na-9 (4/97)	EDF MOX 2c span 5 28 GWj/t	~ 40	228 (at 1.2 s) (953 J/g)	<20	-	No rupture Hmax = 200 cal/g Examination currently carried out Δϕ/ϕ (max): 6.8 % max
Na-8 (7/97)	EDF Grav 5c span 5 4.5 % U5 60 GWd/t	75	106 (at 1.2 s) (440 J/g)	130 cladding presenting some spalling	200	Rupture at 83 cal/g * Hmax = 109 cal/g gas blow-out, no fuel dispersal Examination currently carried out
Na-10 (7/98)	EDF Grav 5c span 5 4.5 % U5 62 GWd/t	31	107 (at 1.2 s) (450 J/g)	80 important initial spalling	200	Rupture at 79 cal/g * Hmax = 110 cal/g no fuel dispersal Examination to be performed

* Still provisional and subject to modification on basis of results from destructive examination

3. Results :

Cabri test results are obtained from four major sources of diagnostics :

- Cabri driver-core instrumentation
- test section instrumentation
- non-destructive examination at Cabri
- non-destructive and destructive examination at the Hot Cell Laboratory.

Up to the test REP-Na8, these very complete diagnostics allowed in particular to determine unrefutably the failure of the test rod, if occurring, and to establish the time and location of the failure. The relevant detection systems for failure are :

- microphones (failure noise)
- flow-meters (coolant flow disturbances due to gas expulsion or fuel ejection)
- void detectors (passage of large gas bubbles in the coolant channel)
- thermocouples (hot fuel contact)
- DND-delayed neutron detection (leaching of fission products into the coolant)
- hodoscope (at high neutron flux: gross fuel motion, in-pin or external)

Doubtfree and coherent signals had been measured in the failure experiments REP-Na1 and REP-Na7. However only relatively weak signals from a limited number of detectors were measured for the first time in REP-Na8 and furthermore in REP-Na10.
The hot cell observations of the REP-Na8 test rod revealed finally multiple rather narrow, axially extended cracks in the cladding. After this clear evidence only, the Cabri diagnostics could be used for the determination of failure time and location.
In the case of REP-Na10 we are in a similar situation and at the time of writing this paper the hot-cell observations are not yet available (more possibly at the meeting).

3.1 REP-Na8 :

The major test characteristics are given in table 1 for comparison with the other REP-Na tests. The corrosion at the level of span 5 was important, with a mean maximum value of 130 microns ZrO_2 and peaking azimuthally at 145 microns. The incipient spalling was limited azimuthally and axially to 8cm in length and ~30 degrees of circumference. A very detailed test rod characterization program was performed and all the characteristics were well documented and accepted prior to the test.
The detailed test objectives aimed at reaching the mean maximum fuel enthalpy of 105±5 cal/g with a power pulse of 60 ms half-width within the experimental uncertainties.
In Fig.1 are shown the recorded signals from Cabri core neutron flux detectors, test channel flow meters and microphones attached to the test rod.
The origin of noises which are detected coherently on the two microphones is localized , dated in deposited energy and named as events 'A', 'B', 'C', 'D' and 'E'. A significant flow deviation coincides with event 'D'.
Fig.2 summarises the observations from the visual inspection of the test rod after extraction from the test device : two major cracks are identified on both sides of the peak power location, and situated azimuthally outside the zone of initial spalling. The visual inspection was complicated by the important transient spalling so that the existence of further cracks could not formally be excluded.
On basis of Fig.2 the program of destructive examinations has been defined and decided.
Fig.3 and Fig.4 show aspects of the radial cut CR3 located at 315 cm from BFC (bottom of fissile column) corresponding to the microphone event 'B'. This result is of significance as it reveals a penetrating crack and shows a mixed brittle/ductile failure mode. In fact, without the result of the cutting, the weak microphone signal 'B' and the visual rod inspection together with the absence of a flow deviation at the time of signal 'B' could have been understood as the signature of a non-penetrating crack at this level. However the observation is not sufficient to postulate that the open rupture really occurred at the time of the signal i.e. at the level of 42 cal/g. Finally, Fig.4 shows that the failure location on CR3 coincides with a large hydride blister which possibly has initiated the failure at this level. Fig. 5 shows the cut at level 395 BCF together with details of two brittle failures at this level.

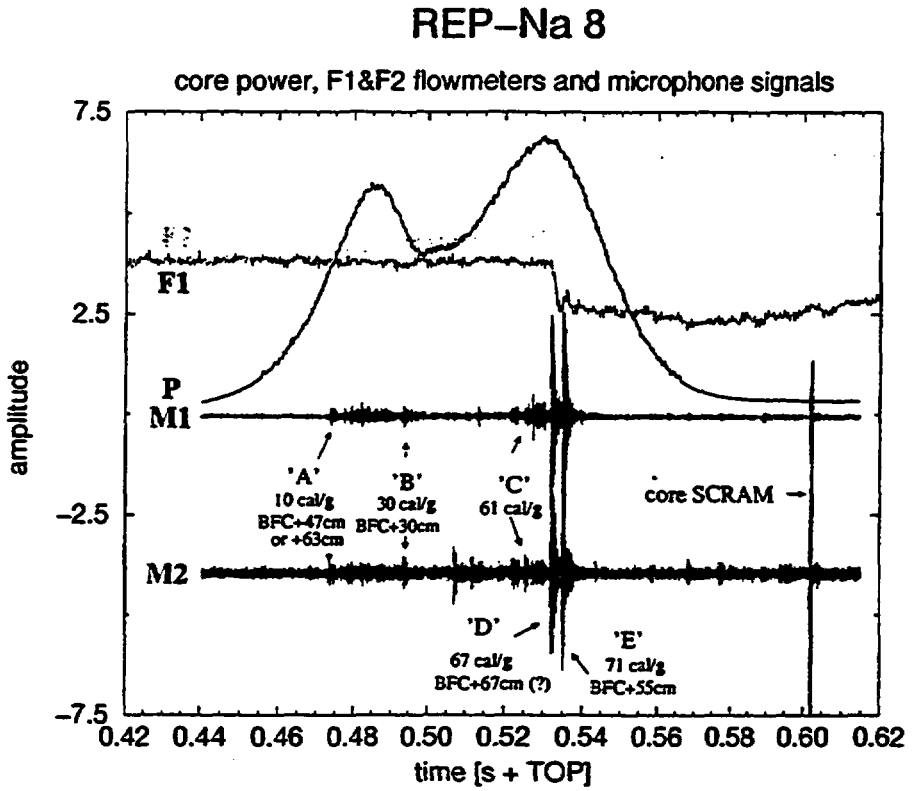

Figure 1: REP-Na8, Cabri on-line recordings showing the the coïncidence of the flow deviation and the microphone event "D" and the timing of the events with regard to the power pulse.

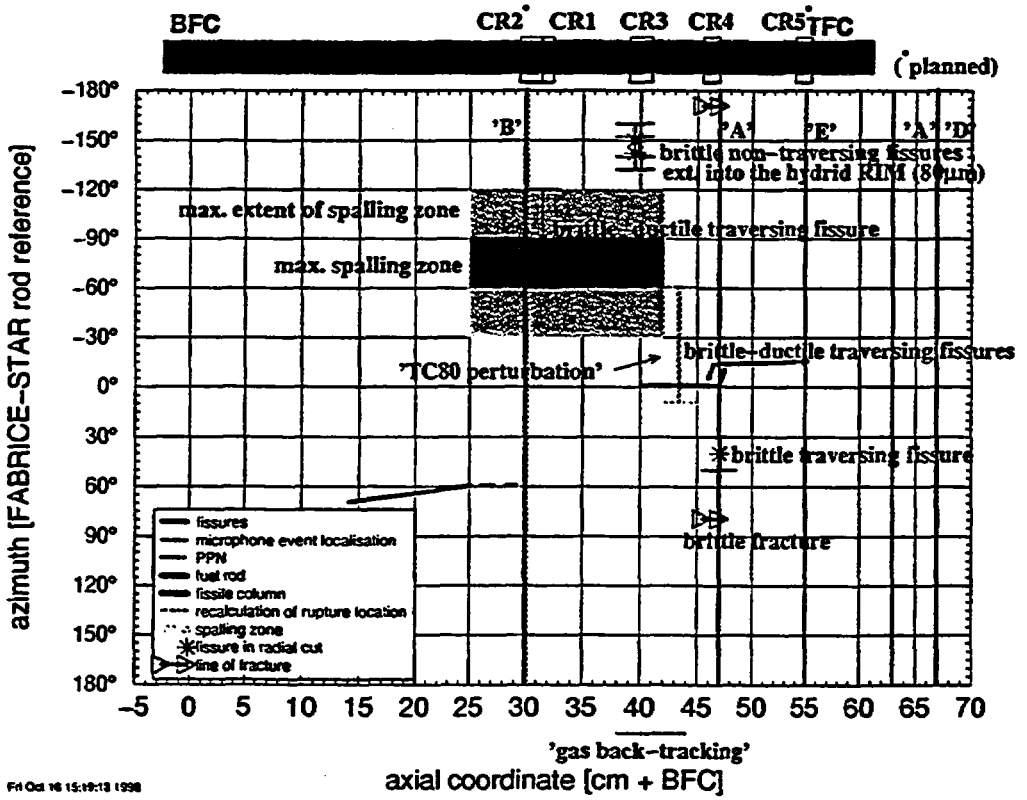

Figure 2: Schematic presentation of the REP-Na8 test rod, including results from the pre-test characteri- sation (spalling), visual inspection after the test (fissures) and metallographic examination (cuts)

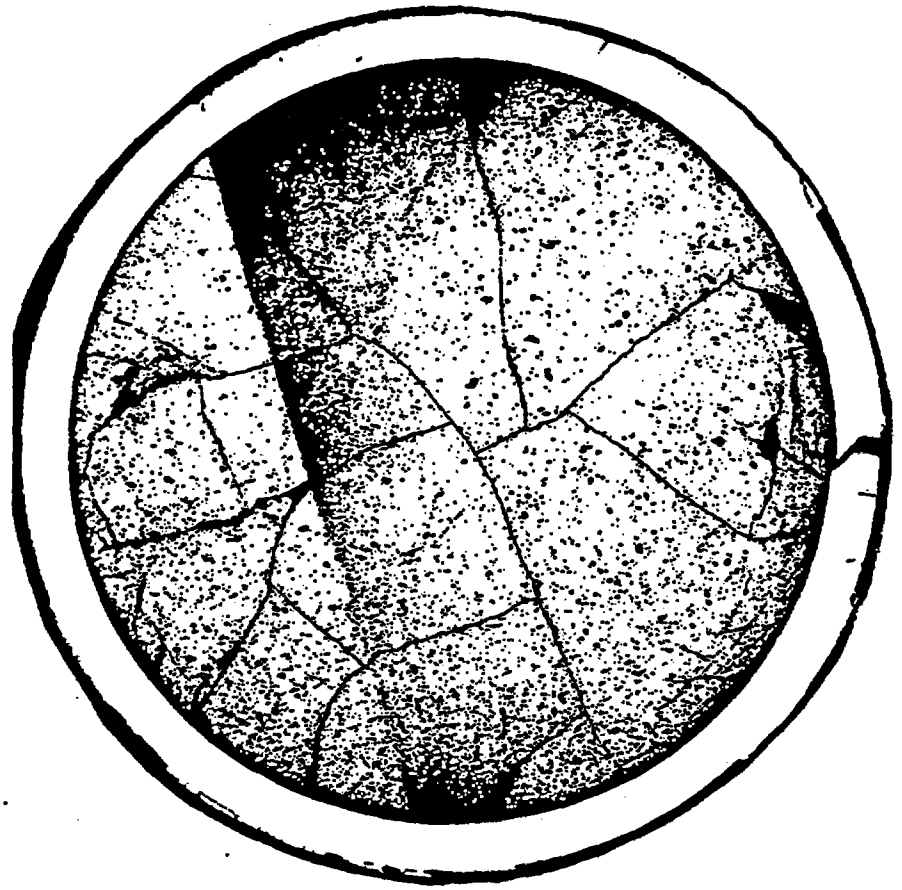

Figure 3: Metallographic cut of REP-Na8 at level 315 bfc (CR1) showing a brittle/ductile failure.

Figure 4: Detail of fig.3, the failure coïncides with a hydride blister which was formed during the reactor irradiation, prior to the Cabri test.

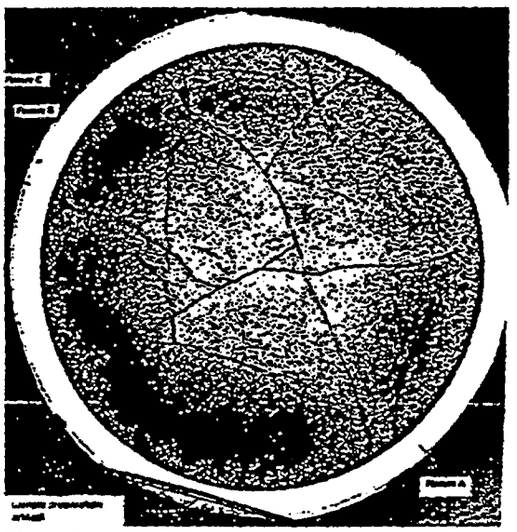

Figure 5a: Macrograph showing a non-penetrating clad fissure and fragmented fuel at level 394 bfc.

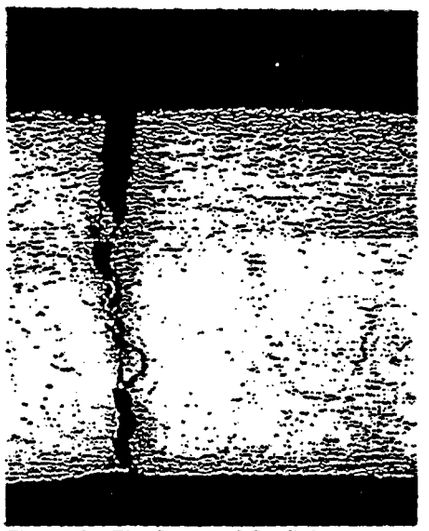

Figure 5c: The fissure of fig.5b becomes a penetrating crack at level 395 bfc.

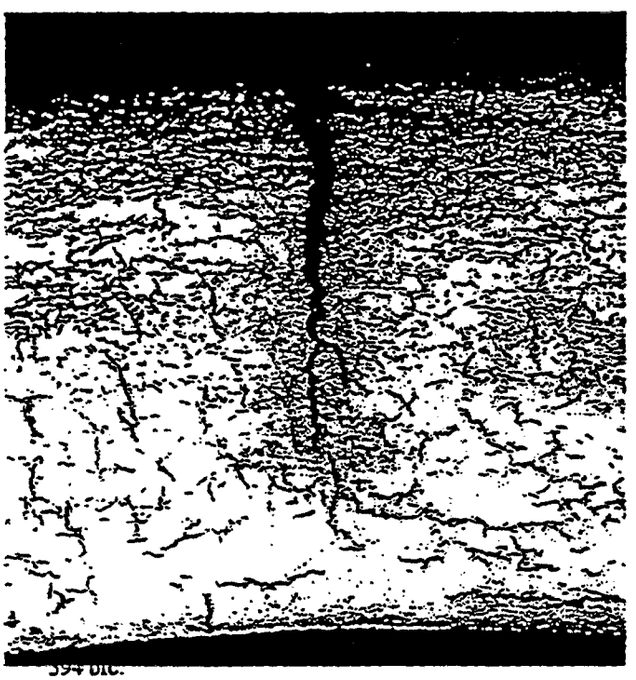

Figure 5b: Detail of the fissure at level 394 bfc.

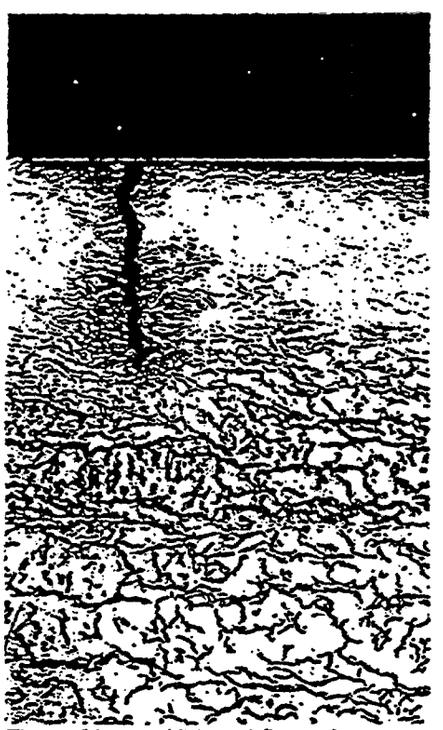

Figure 5d: An additionnal fissure is observed at level 395 bfc., a characteristic heterogenity in the clad material is observed.

Figure 5: Metallographic examination of REP-Na8 at level 394 to 395 bfc.

3.2 REP-Na10 :

The two major objectives which justified the test REP-Na 10 have already been mentioned and the pin characteristics and test conditions are given in table 1.
The absence of fuel dispersal after failure in REP-Na8 represented the principal argument for the attempt to reach a better phenomenological understanding and for performing a new test.. Furthermore, if the slower energy injection rate was the crucial parameter for this behaviour, it was important to perform a test with an intermediate power ramp in between REP-Na1 and REP-Na8, at the lower limit of uncertainty established on basis of the very "in vogue" 3D neutronic calculations.
Finally, the availability of a sibling rod of REP-Na1 allowed to perform a test with only one changing parameter, i.e. the width of the power pulse. In this sense, REP-Na10 represented a REP-Na1 repetition test under more realistic conditions.
As detailed test conditions were defined: 35 ms pulse width and full use of the Cabri core performance capabilities and a resulting maximum mean fuel enthalpy of ~ 110 cal/g.
The experimentally achieved test conditions were very close to the defined values (see table 1).
Fig.6 shows the enregistered significant signals obtained during REP-Na10 : power pulse, flow meter signal and registrations of the test rod microphones. The flow-meters did not show any flow disturbance except the small and well known so-called TOP-effect. No response either from the void detectors, however, from previous Cabri experiments it is known that very small bubbles can escape without being detected.The delayed neutron detection (DND) in the test channel indicates a weak but significant signal, which, together with the acoustic signature and in analogy with REP-Na8, leads to postulate that the pin has failed without any fuel dispersal into the coolant. Fig.7 shows the normalised DND signal amplitude for all Cabri REP-Na tests. The two tests with observed fuel dispersal, REP-Na1 and REP-Na7, give the picture of the originally typical failure detection signal.

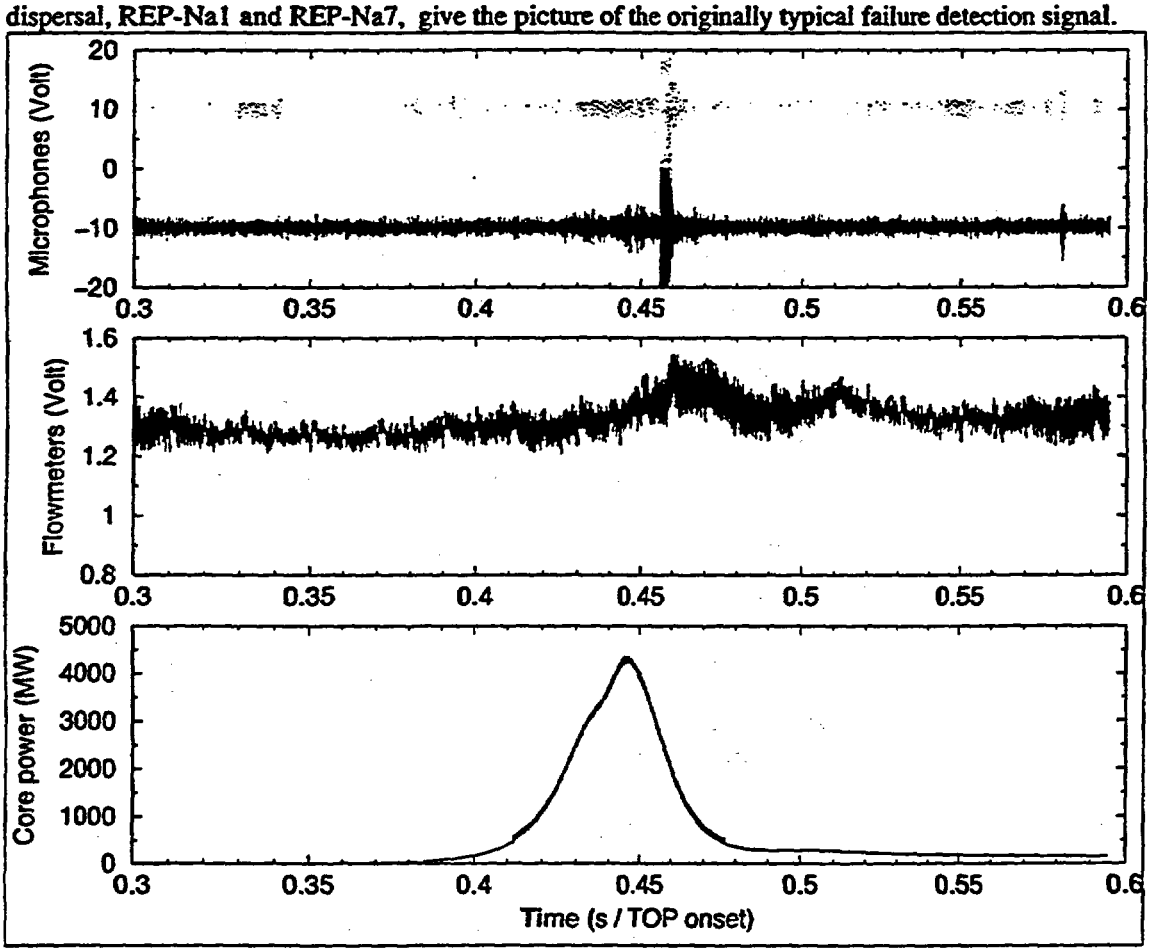

Figure 6: REP-Na10, Cabri on-line diagnostics showing the power-pulse, flow-meter signals and very strong and coherent microphone events (which saturate the scale of the recording system).

In REP-Na8, for the first time, the test rod failure was evidenced and only a weak DND signal was observed. The difference is explained by the different mode of transfer of the delayed neutron emitters to the detectors : fuel debris in the case of strong signals, gases bubbles or even single atoms , emitted into the coolant, in the case of weak signals. The REP-Na 10 signal is weak but still significantly above the noise signal characteristic for unfailed pins.

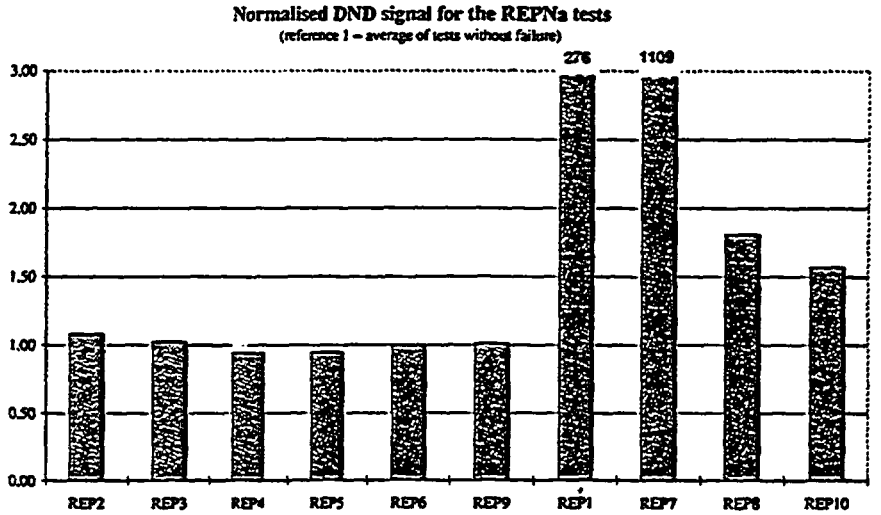

Figure 7: Normalised signals of the delayed neutron detectors which monitor the presence of delayed neutron emitting fission products in the Cabri test channel coolant. These short living fission products are indicators of the loss of the test rod integrity.

4. Discussion :

For the discussion of this paper we will assume that the REP-Na10 test rod has failed during the transient. The correctness of this assumption is highly probable on basis of the microphone signals and by analogy with REP-Na8. As previously, the proof will be given by the results of the visual inspection of the test rod after extraction from the test device in the Hot Cell Laboratory (possibly) and at the latest from the destructive, metallographic examination.
Finally, as will be seen from the following arguments, even if no failure occurred, the valuable contribution from REP-Na10 to our understanding will be unchanged and the conclusions remain valid.
In table 2 are presented the test parameters and the final outcome of the five REP-Na experiments at high burnup. A very clear and complete degree of qualitative understanding is obtained from the analysis of this table.

1. No failure for unspalled cladding up to 80µ corrosion thickness and UO_2 fuel up to 62GWd/t, even under fast power transient conditions - REP-Na4 and REP-Na5.
2. Failure for spalled cladding - REP-Na1, REP-Na8 and REP-Na10.
3. Early failure and fuel dispersal in case of spalled cladding and fast transient conditions - REP-Na1.
4. The high corrosion in REP-Na8 is favorising multiple cracking and crack propagation in the zones rich in hydrides.

A quantitative contribution to the understanding is given by the clad straining and the fission gas release (FGR) in the non-failure experiments REP-Na5 and REP-Na4 as can be seen from table 1 :

- high straining and high FGR under fast pulse conditions - REP-Na5.
- low straining and low fission gas release under slow pulse conditions - REP-Na4.

Evidently, the tight coupling of the thermal, mechanical and FGR phenomena requires a detailed analysis and interpretation. This work is performed presently with the RIA code SCANAIR and with use of the transient mechanical property data from the PROMETRA program.

It can globally be stated that the ongoing analysis confirms and quantifies the above, simplified understanding but its demonstration would go beyond the scope of the present paper.

Table 2: Test parameters and final outcome of the five REP-Na experiments at ~ 60 GWd/t

	REP-Na1	REP-Na 4	REP-Na5	REP-Na 8	REP-Na 10
Cladding	standard ZY4	standard ZY4	standard ZY4	standard ZY4	standard ZY4
Burnup (GWd/t)	64	60	64	60	62
Corrosion (μ ZrO2)	85	80	20	130	85
Spalling	yes	no	no	incipient	yes
Energy Depos. (cal/g)	110	97	105	106	107
Pulse Width (ms)	9.5	80	9.0	75	31
Rupture	YES	NO	NO	YES	YES
Dispersion	YES	-	-	NO	NO

Last but not least, the absence of fuel dispersal under slower pulse conditions is the outstanding contribution of the two latest experiments. Especially REP-Na10 allows the direct comparison with REP-Na1 due to the almost identical, severely spalled yet moderatly corroded state of the test rods which were refabricated from sibling rods, extracted from the same fuel assembly, irradiated in the GRAVELINES power plant of EDF under load follow conditions..

The fundamentally different phenomena observed in these two experiments must be attributed to the variation of the power pulse kinetics and its impact on the thermal-mechanical and fission gas dynamic behaviour.

PROMETRA tensile tests, performed with specimens from this cladding and, later in time, with the ones from the REP-Na8 father rod, have shown a large scattering of the ductile properties. The measured values of uniform elongation are spread over the region from 0 to ~1% as can be seen from Fig 8.

The values of zero ductility are understood as to be attributed to test specimens with hydride blisters within the gauge region.

The totally brittle mechanical behaviour allows to explain the very early failure of REP-Na1.

Furthermore, the rapid power pulse heats up the RIM region of the fuel adiabatically which liberates the fission gas in the RIM and causes the undelayed mixed loading (gas and thermal) of the brittle cladding., leading to failure and dispersal of the pressurised fuel.

This is the scenario observed in REP-Na1.

In REP-Na8 and 10, failures are initiated at the locations of blisters or high hydride concentrations and propagate axially. The smoother power pulse reduces significantly the temperature increase rate in the fuel and shifts the maximum fuel temperature towards the inner part of the fuel pellet. The direct impact on the fission gas action is less well understood and a special analytical program (SILENE) is under preparation in order to fill up this lack.
The present working hypothesis is that, under slower transient conditions, the local peak pressure inside the fuel is significantly lowered. The pressure decrease might be explained by the permeability of the fuel.
In the case of a fast transient, the higher pressure peak and the full availability of all the released gas as additionnal contribution to the pin loading are the driving forces for failure and fuel dispersal.

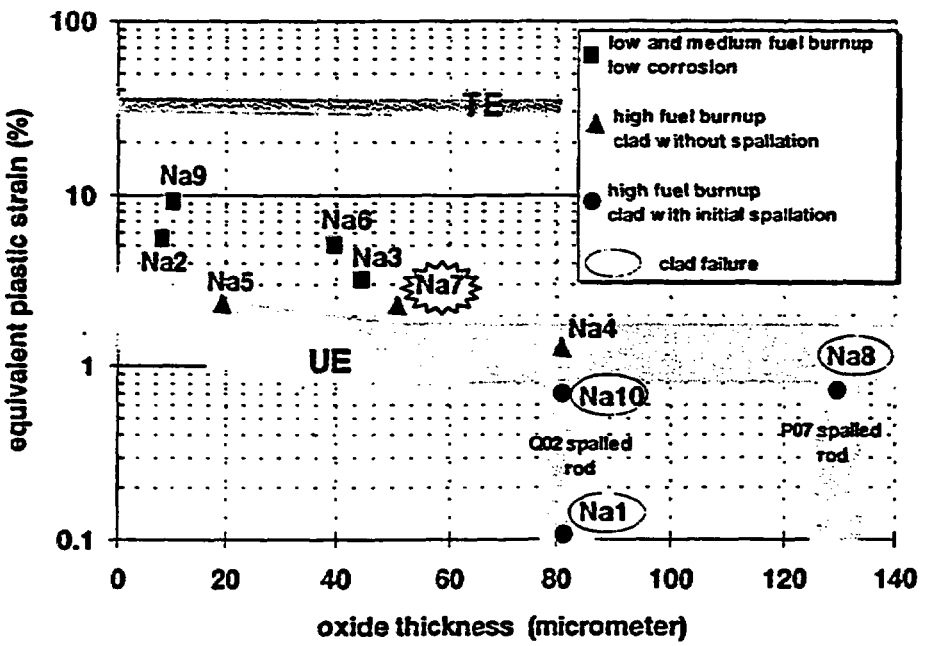

Figure 8: Failure map of the Cabri REP-Na tests. The hydride assisted failure mode is clearly evidenced. The "MOX-effect" failure mode of REP-Na7 may be understood as a precursor of a "RIM-effect" failure mode at very high burn-up (> 65 GWd/t).

5. Conclusion :

From the results of the two latest REP-Na experiments, a breakthrough could be reached in the understanding of the key phenomena and key parameters of the early, thermal/mechanical loading phase of the reactivity initiated accident (RIA) and the risk of pin failure..
The high burnup clad corrosion during reactor operation, especially if it leads to localized spalling of the oxide layer, is the major cause of the test rod failures observed in the REP-Na program.
Cracks are initiated at the location of so-called « blisters » or at spots of high hydrogen concentration and propagate radially and axially under sustained loading.
The "natural" loading by thermal expansion under heating-up of the fuel is assisted by pressure built-up from fission gas release. This contribution is amplified when the reactivity transient is very rapid, because the released gas is still confined in small free volumes at

extremely high pressure. The initial pressure decreases rapidly when the gas flow into open porosities of the fuel becomes effective i.e. under slow power transient conditions.
Fuel rod failure occurs under the mixed loading mode at the level of the uniform elongation for the material which has still some residual ductility, at a level of ~ 120cal/g (PROMETRA). The presence of blisters can be the cause of a totally brittle behaviour and very early failure can occur for a mean fuel enthalpy lower than 50 cal/g as observed in the tests REP-Na1 and possibly in REP-Na8.

6. Acknowledgments :

The theoretical preparation, technical realisation and analysis and finally the post-test examination of the Cabri REP-Na experiments is the work of a large number of scientists, engineers and technicians from IPSN/DRS and from CEA/DRN (especially the LECA Hot Cell Laboratory).
Frequent and fruitful discussions with the partner organisations EDF represented by Nicolas WAECKEL and US-NRC represented by Ralph MEYER have provided highly valuable contributions to the success of the CABRI REP-Na Program.
The authors of the present paper are pleased and honoured to have the opportunity to present these results to the interested public.

7. Références

[1] J.PAPIN, F.SCHMITZ - *The Status of the CABRI - REP-Na Test Programme : Present Understanding and Still Pending Questions.* 25th WRSM - Bethesda (1997) Vol. 2
[2] D.J. DIAMOND and L. NEYMOTIN - *Analyzing the Rod Drop Accident in a BWR with High Burnup Fuel.* Proceedings International Meeting on LWR Fuel Performance, Portland (USA), March 1997

Loads To Be Considered In Qualifying Cables For LOCA

Dipl.-Ing. Wolfgang Michel, Siemens AG, KWU, Germany
Dipl.-Ing. Lueder Warnken, Siemens AG, KWU, Germany

Abstract

The experience gained qualifying electrical and I&C equipment for LOCA and LOCA like conditions will be introduced based on the examples of cable insulation materials used in German NPP's, focusing primarily on our findings and some additional test results supporting our speculations. To facilitate the understanding, the different test steps of qualification, their objectives, and how they go together are addressed at the beginning. Finally some conclusions are drawn and some recommendations on how established procedures could be improved are made.

1 Introduction

The intention of this presentation is to introduce the experience gained qualifying electrical and I&C equipment for LOCA and LOCA like conditions and maintaining it.

This will be done based on the example of cable insulation materials used in German NPP's. To facilitate the understanding, specifically for those who are not familiar with the qualification procedures and the different test steps to be passed, we would like to start with a short introduction addressing the different test steps, their objectives, and how they go together.

After that short introduction we will focus primarily on our findings and some additional test results that support our assumptions regarding partly the correct way some test loads are applied and partly the necessity of test steps that correspond to these objectives.

Finally we will draw some conclusions and make some recommendations on how the established procedures could be improved.

2 Acronyms

EPR	Ethylene Propylene Rubber
EVA	Ethylene Vinyl Acetate
IEC	International Electrical Commission, International Electrotechnical Standards
KTA	Kerntechnischer Ausschuß, Safety Standards for Nuclear Power Plants

LOCA	Loss of Coolant Accident
MSLB	Main Steam Line Break
PVC	Poly Vinyl Chloride
R_{ISO}	Insulation Resistance
SIR	Silicone Rubber
VDE	Verband Deutscher Elektrotechniker, Electrotechnical Standards of the Association of German Electrotechnical Engineers
XLPE	Cross-linked Poly Ethylene

3 Qualification procedure and objectives

3.1 General

The qualification objectives are generally to demonstrate that the equipment to be qualified is able to withstand a LOCA or LOCA like conditions even shortly before the end of it's intended life time. That is, the test specimen has to be put in a condition as if it was 40 to 60 years old, depending on the planned life time of the power plant.

To achieve these conditions it is necessary to apply the loads expected during the operational period at the intended location before the LOCA test is performed. Keeping in mind, that a period of 40 to 60 years has to be emulated (or at least it's consequences) and that the innovation rate of electrical and I&C equipment is in the range of 5 to 10 years, one can imagine that reasonable results can only be achieved if the loads are applied in an accelerated way.

Relevant loads for the normal operation of cables are generally temperature and partly radiation. Those for the so called harsh environment (containment, annulus, main steam valve compartment) are temperature, pressure and the corresponding transients, moisture and partly radiation

Although in reality these loads act simultaneously, in the test practice they are applied mostly sequentially.

Trying to meet the above mentioned objectives, it becomes clear that

- the acceleration values,
- the fact that in most cases the loads are applied sequentially and

- the choice of the order of test steps

can have an influence on the qualification results and consequently that they have to be chosen carefully.

In the following the different test steps as they have been applied for in-containment use in the past and their objectives are described.

3.2 Test steps

3.2.1 Test step I (thermal ageing)

Objective: Application of the operational thermal loads, dominated by the ambient conditions, because safety grade equipment is rarely operated, thus temperature increases caused by self heating of power cables is irrelevant. I&C cables don't suffer self heating at all.

Test values: Stipulated either by Arrhenius' Law or by the n-Degree Rule, aming at the simulation of an operational period of 40 years, limited by the maximum allowable temperature of the relevant material. Table 1 shows some typical examples.

Example	Activation energy	Nominal operational ambient temperature	Aging parameters to simulate 40 years operation		Acceleration values	Parameters to simulate post-accident conditions of 1 year	
			Test temperature	Test duration		Test temperature	Test duration
	[eV]	[°C]	[°C]	[d]		[°C]	[d]
Power cable	1,089 [1]	60	135	14	1042	85	8
Coax cable	1,15 [1]	50	120	10	1460	85	7
Power cable	K = 8 [2]	65	135	26	561	90	12
I&C cable	K = 8 [2]	55	135	11	1327	90	12

Table 1 Typical examples of thermal cable ageing parameters
[1] Arrhenius'-Law
[2] modified Arrhenius'-Law (n-Degree-Rule)

3.2.2 Test step II (radiation part 1)

Objective: Application of the operational radiation loads and the short term (see fig. 1) accidental radiation loads.

Test values: Dose 50 kGy
Dose rate 0,5 kGy/h.

3.2.3 Test step III (LOCA and MSLB)

Objective: Application of the accidental loads temperature, pressure, their transients and moisture short or medium term (see fig. 1).

Test values:	Temperature	160 °C ± 5 K
	Pressure	corresponding to saturated conditions (including the initial content of air of the test vessel)
	Rise time $\leq$	10 s
	Moisture $\geq$	95 %
	Duration	short term 2 h
		medium term 24 h

For further details see fig. 1.

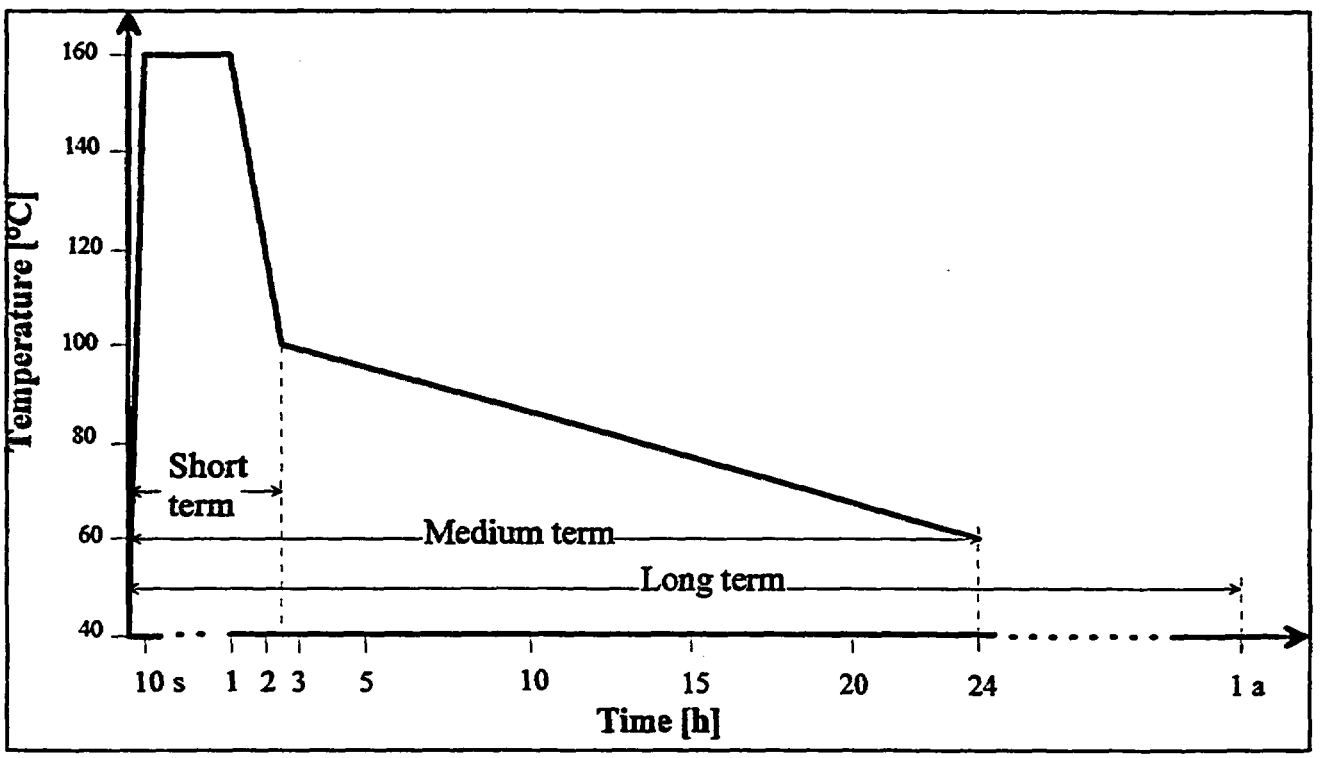

Fig. 1 Standard test curve for PWR 1300 MW containment

3.2.4 Test step IV (radiation part 2)

Objective: Application of the operational radiation loads and the medium and long term (see fig. 1) accidental radiation loads.

Test values:	Dose	200 kGy
	Dose rate	0,5 kGy/h.

3.2.5 Test step V (post-accident (LOCA and MSLB))

Objective: Application of the accidental loads temperature and moisture long term (see fig. 1).

Test values:

Temperature	85 °C
Pressure	atmospheric
Moisture	100 % (the specimen are completely submerged during the test)
Duration	according to Arrhenius' Law or n-Degree-Rule

Some typical examples are shown in table. 1.

3.2.6 Electrical measurements

Objective: To assure the electrical function of the equipment to be supplied during and after LOCA / MSLB.

Test values: See table 2 and 3.

Test step	Test values	Relevant standards
High voltage test prior to test step III	2,500 V AC / 1min	VDE 0472, part 508; VDE 0530, part 1 paragraph 17 table 5
Continuous voltage test During test step III and V	460 V AC ($1{,}2 \times U_N$)	KTA 3403, paragraph 7.2.2.6
Voltage impulse test	1900 V ($3{,}5 \times \sqrt{2} \times U_N$)	VDE 0432, part 2 KTA 3403, paragraph 7.2.2.6
Measuring of the insulation resistance • before, during and after test step III and V • before and after test step II and IV	≥ 200/0.5/200 MΩ related to 20 m cable length, measuring voltage 500 V DC	VDE 0472, part 502
High voltage test after test step III	1500 V AC / 1min	VDE 0472, part 508; VDE 0530, part 1 paragraph 17 table 5

Table 2 Test steps and values for power cables

Test step	Test values	Relevant standards
High voltage test prior to test step III	1500 V AC / 1min	VDE 0472, part 508
Continuous voltage test During test step III and V	60 V AC	KTA 3403, paragraph 7.2.2.6
Voltage impulse test	300 V (5 x U_N)	VDE 0432, part 2 KTA 3403, paragraph 7.2.2.6
Measuring of the insulation resistance • before, during and after test step III and V • before and after test step II and IV	≥ 200/0.5/200 MΩ related to 20 m cable length, measuring voltage 100 V DC	VDE 0472, part 502
High voltage test after test step III	400 V AC / 1min	VDE 0472, part 508

Table 3 Test steps and values for I&C cables

4 Findings

4.1 Designed life time

The uncertainties introduced by the use of

- applying the n-Degree-Rule using assumed K-Factors
- high acceleration values for thermal and radiation ageing (which reduce the damage caused by oxidation (= reduced time for oxygen diffusion)) and
- the necessity to apply the loads sequentially

led already 19 years ago to the conclusion of Siemens to start a long term experimental programs for on-going qualification of cable insulation materials used in German NPP's. This program also includes comparative investigations of cables aged under the natural environment inside containment during normal operation and cables aged under various accelerated conditions in the laboratory. Clear evidence of material and manufacturer dependent dose-rate effects should be made, investigations on the influence of different temperatures at low dose irradiation was and still is also included in the program, permitting an estimation of synergistic effects[1].

[1] Practical experience and intensive studies point to various uncertainties in time-accelerated and sequential simulations of the usually 40-years operating period of the power plant. In general, these uncertainties do not constitute an unacceptable problem for plant operation as long as the power plant has not been in operation for more than 10 to 15 years, since the consequences of these uncertainties increase with time.

What are the most important results up to now?

- Synergism
  From the physical point of few effects of synergism can not be excluded; technically they can be neglected: With very view exceptions, high dose rates (and doses) and high temperatures do not appear in the same places, and additionally, only very few pieces of equipment are mounted in high dose rate areas. Table 4 shows that the relevant long term average temperature is about 33 °C. Fig. 2 shows that roughly 20 out of 170 positions are in areas of higher dose rates (note: dosimeter positions equal equipment positions).

time interval	1 year	
number of measuring points	41	
long term average temperature	33 °C	
individual short term max. temperature	51 °C	(top of steam generator)
next lowest short term temperature	45 °C	(near primary loop line)

Table 4 Typical results from long term and continuous temperature measurement

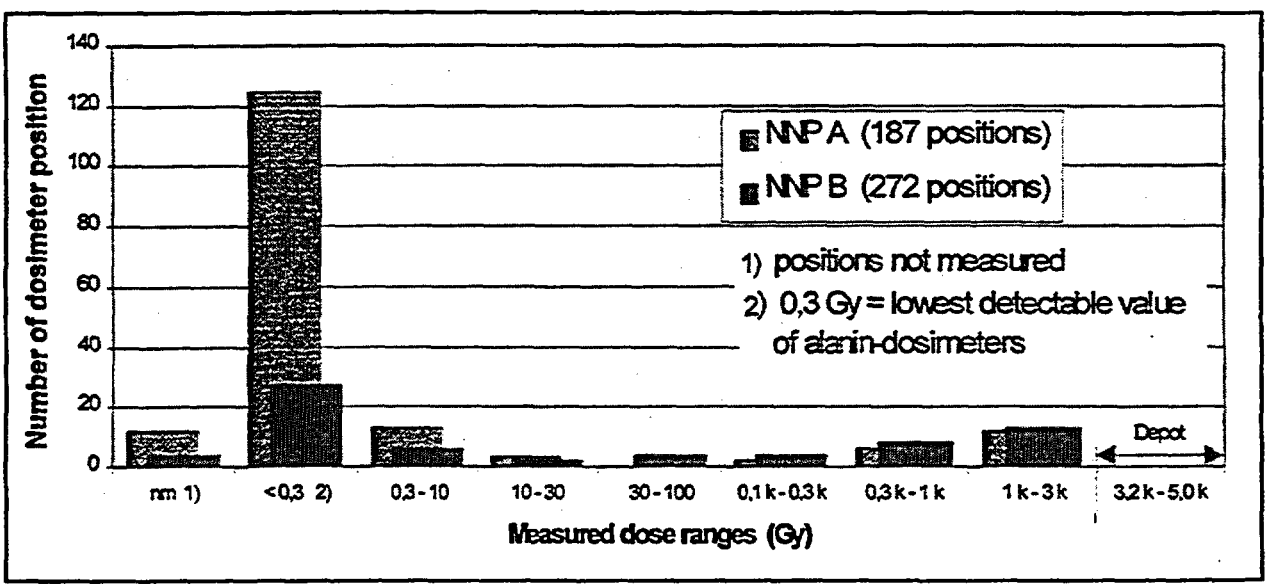

Fig. 2 Long term radiation measurement in PWR 1300 MW containment

- Designed life time
  The designed life time of silicone rubber and ethylene-tetra-fluorethylene can be predicted corresponding to the local dose rate, but the acceptable accumulated doses are less than 250 kGy, the total dose used for qualification ((ETFE = 17 kGy, loss of function, SIR = 60 to 70 kGy, 50 % elongation at break absolute value) ⇒ dose rate effect).

That is, these materials showed strong material degradation after comparatively short periods of time. In some cases replacement strategies had to be developed
The designed life time of cross-linked poly ethylene (XLPE), ethylene vinyl acetate (EVA), ethylene propylene rubber (EPR), and poly vinyl chloride (PVC) allow today a prediction of 25 years of operation. The determination of the total designed life time will be possible when the values, taken in appropriate intervals, show a sufficient degree of degradation, which is not yet the case.

- **Radiological ageing**
  Dose-rate effects are responsible for lower material degradation, when the same dose is applied at an increased dose-rate and vice versa. The presence of oxygen and its specific diffusion rate for a given insulating material (density) are the dominating factors for the dose-rate effect. Oxygen increases material damages caused by radiation.
  That is, the theory, that equal dose leads to equal damage, can not be kept any longer. As already mentioned above, there are materials that show significant dose rate effects. On the other hand, once dose rate effects are determined (which requires some effort), a life time prediction is possible or in other words, regardless of the applied dose for given qualification doses and dose rates, the life time for a given location can be predicted (see fig. 3).

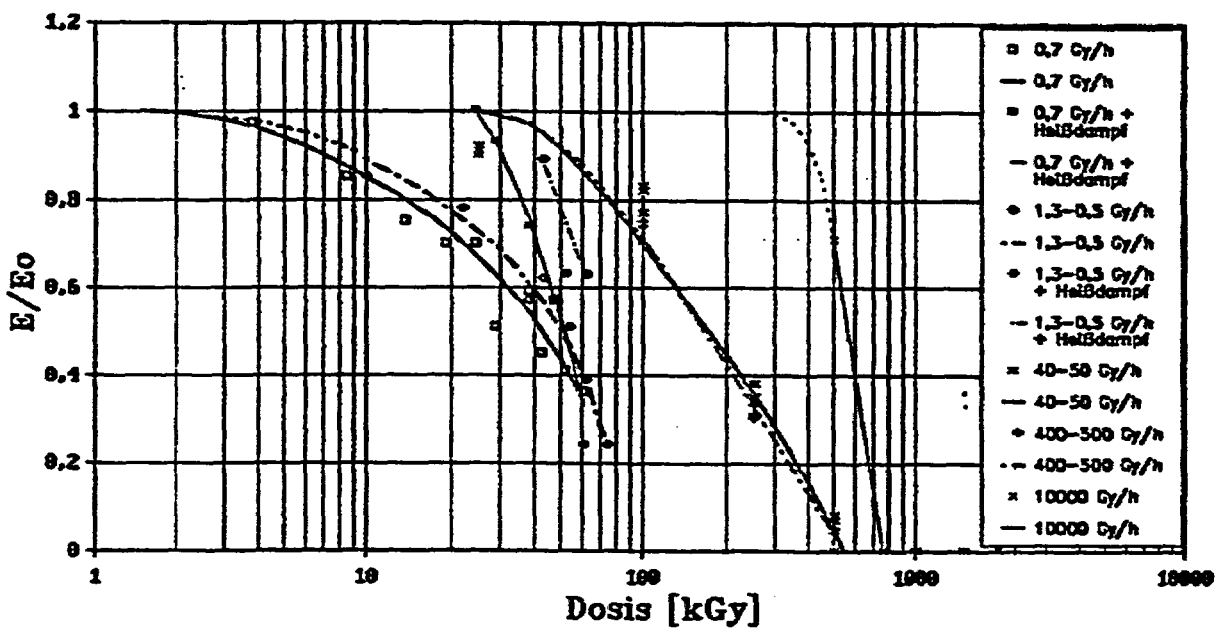

Fig 3 Elongation at Break of SIR as function of dose and dose rate

- **Threshold values**
  Defining threshold values for LOCA and LOCA like tests, one should be aware on the one hand of the fact that the piece of equipment to be qualified is only a part of the function chain effected, and on the other hand that the threshold values should be derived considering primarily the function under accident and post-accident conditions. Insulation resistance values drop already several orders of magnitude caused by the normal operational temperature without any interference of function. That is, provided the

insulation material is able to tolerate the additional increase of the temperature caused by the accident, it is sufficient to assure that there is no danger that

- protective devices like over load protection are initiated or
- the signal to distortion ratio of I&C equipment becomes unacceptable.

Following this, the acceptable threshold values can be significantly reduced compared to the ones to be used qualifying new equipment in normal ambient temperature conditions (see fig. 4).

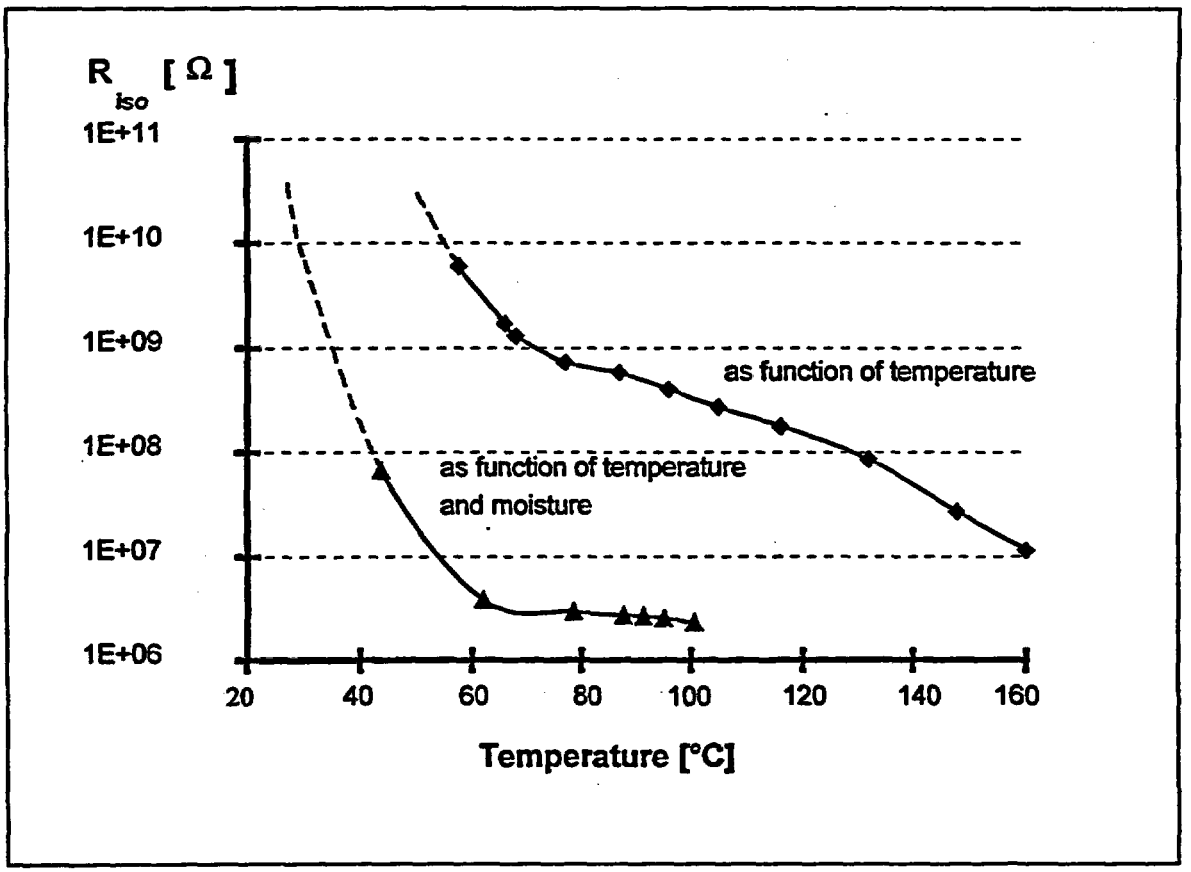

Fig 4 R_{iso} as function of temperature

4.2 Influence of the sequence of test loads applied on the result

During one of the last on-going qualification tests we measured the elongation at break of the insulation material of two cables after every single test step in order to get some insight on the impact of each test step and to verify the chosen order. The results, for SIR shown in fig. 5, are,

- if thermal ageing is performed prior to radiation ageing healing effects caused by temperature can be observed and, even more important,

- that the post-accident test may be redundant.

Alerted by the latter result, additional tests were performed to cover our conclusions.

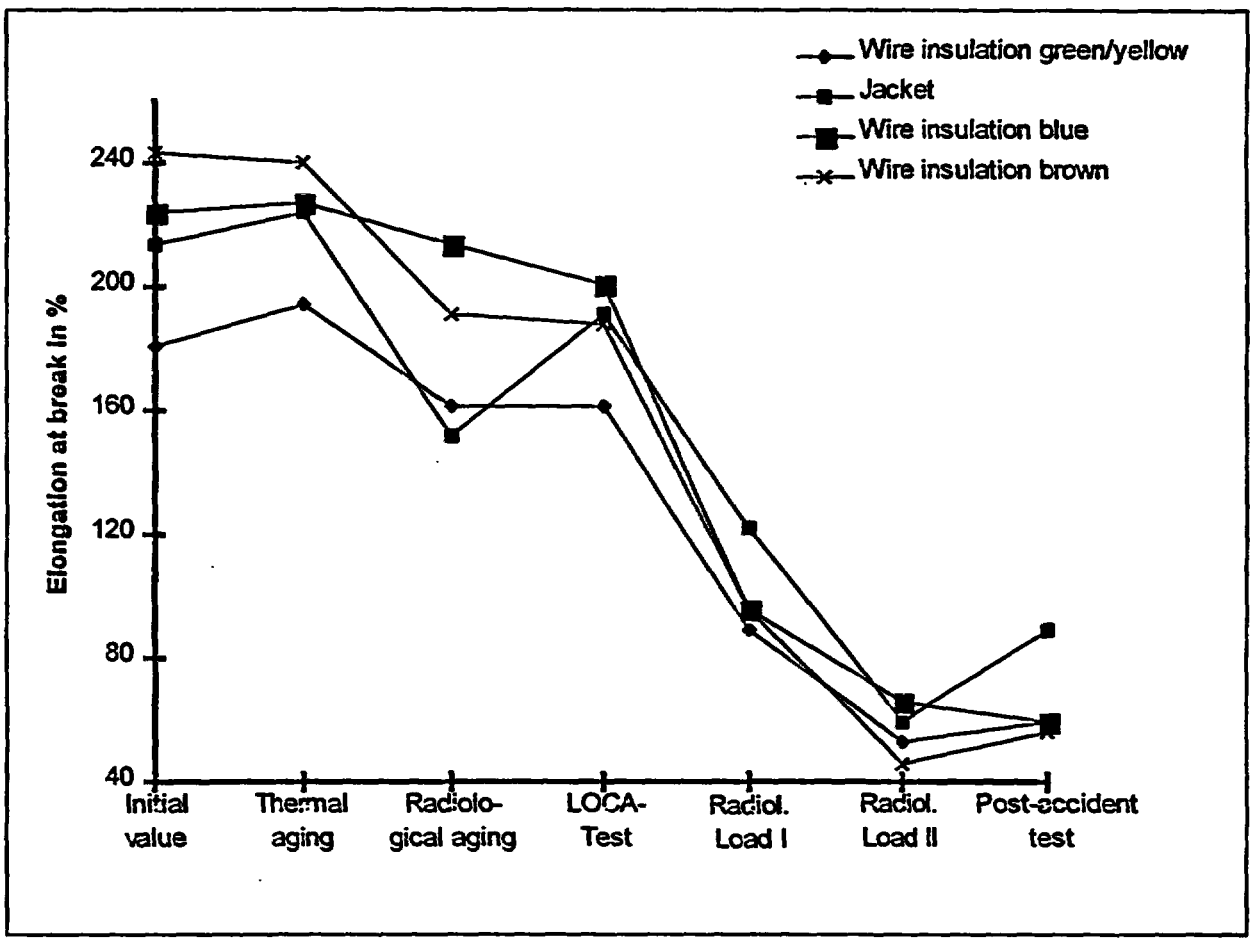

Fig 5 Influence of the sequence of test loads applied on SIR

4.3 Necessity of post accident test steps

4.3.1 General

Regarding to the above mentioned results (see 4.2) we decided to investigate in some more detail the consequences of post accident tests in order to judge whether they are necessary or not.

4.3.2 Supporting additional tests

The materials included are VPE, EPR of two different manufacturers and SIR.

The questions to be answered are at least, what are the decisive parameters for life time prediction, and is it possible to link the parameter elongation at break with the parameter insulation resistance, the decisive parameter for the electrical function during accidents.

As soon as the results are available, published and accepted by the international experts we shall try to introduce necessary improvements into the relevant standards like the German KTA 3706 and the international IEC 780. Besides others, the improvements should address the proper

- consideration of dose rate effects
- stipulation of threshold values
- objectives and necessity of post-accident tests and
- the influence of the cable jacket on the measured values, specifically when used for life time prediction purposes.

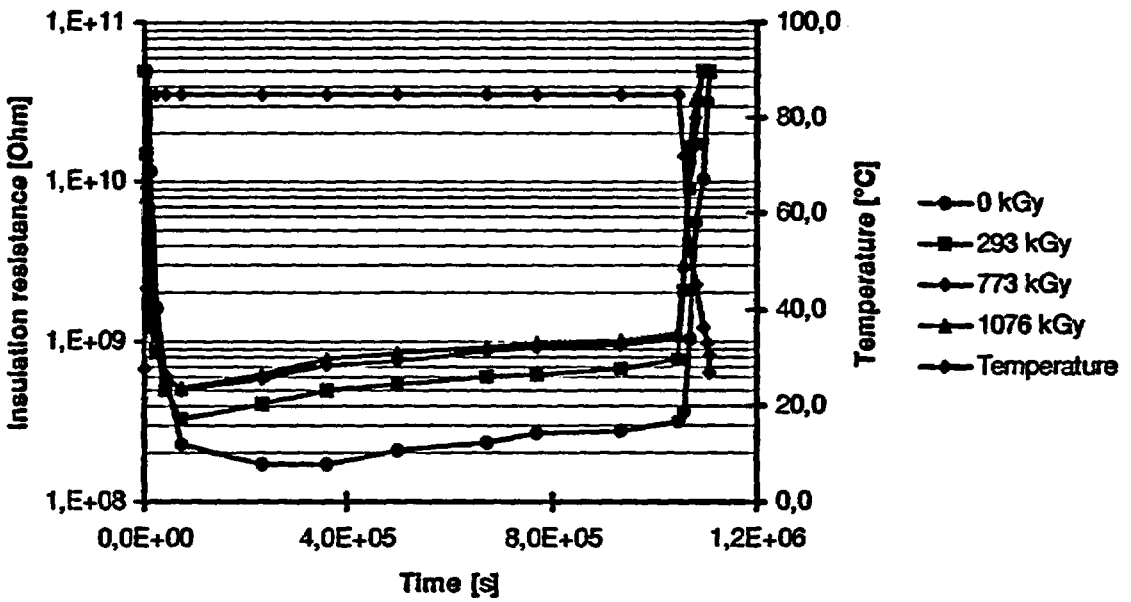

Fig. 6: EPR I, Insulation resistance versus time depending on applied dose

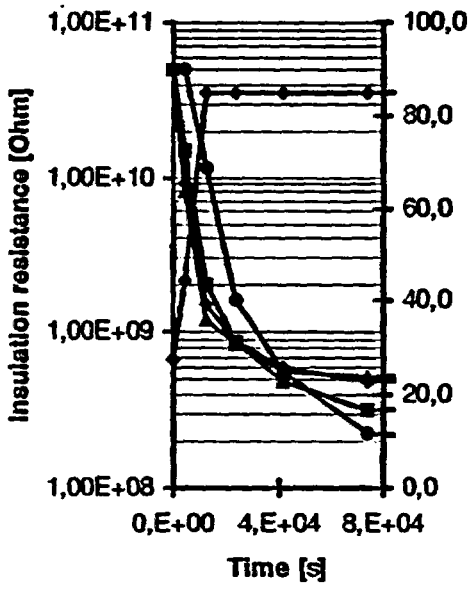

Fig. 7: EPR I, Insulation resistance versus time depending on applied dose
, expanded scale at test start

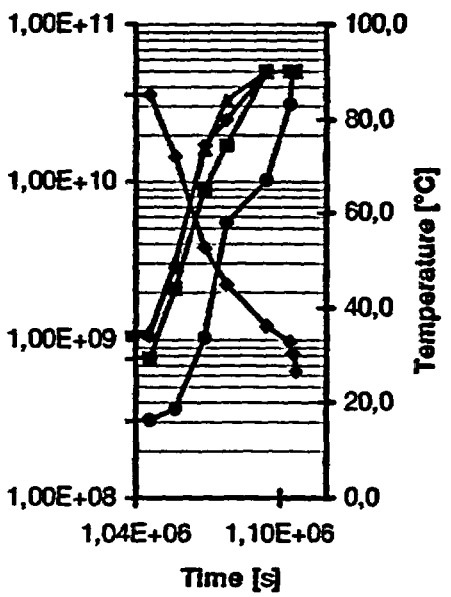

Fig. 8: EPR I, Insulation resistance versus time depending on applied dose, expanded scale at the end of test

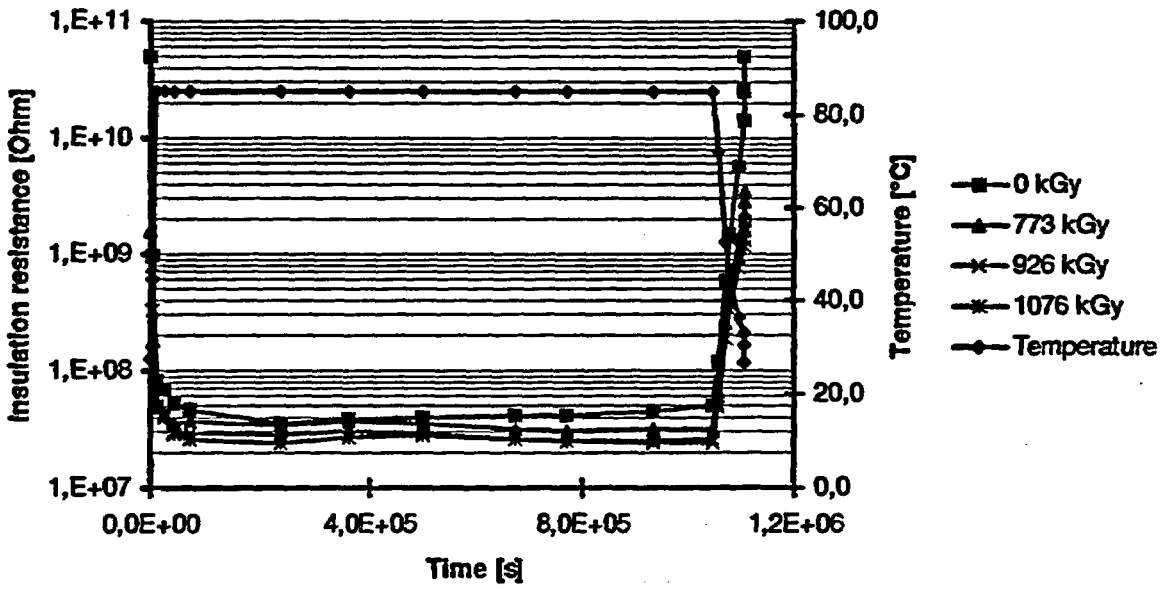

Fig.9: EPR II, Insulation resistance versus time depending on applied dose

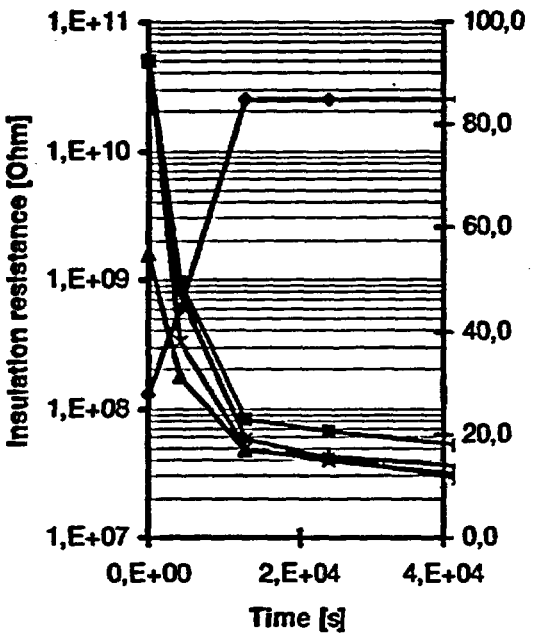

Fig. 10: EPR II, Insulation resistance versus time depending on applied dose, expanded scale at test start

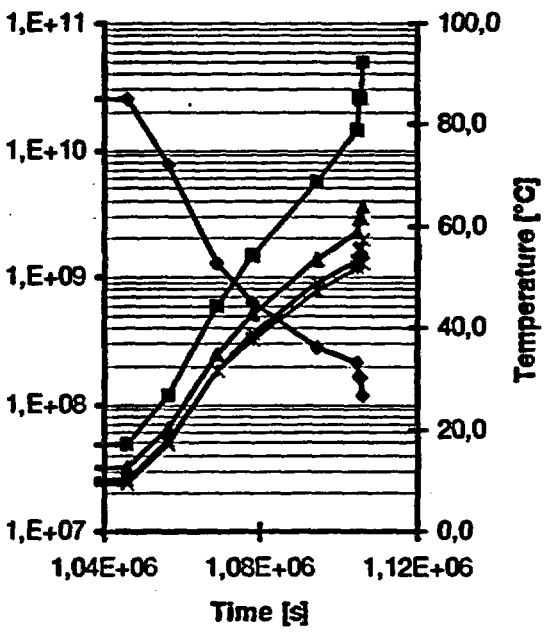

Fig. 11: EPR II, Insulation resi-stance versus time depending on applied dose, expanded scale at the end of test

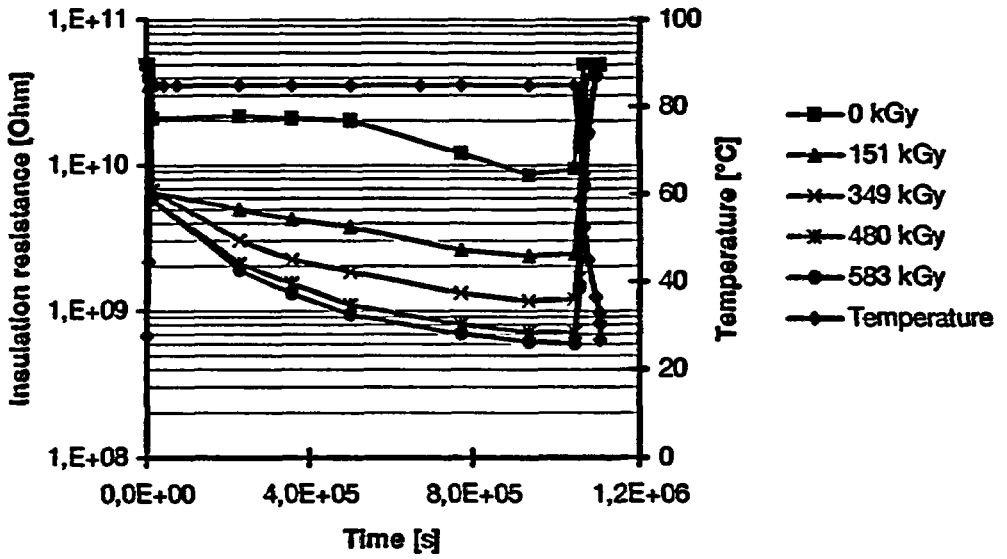

Fig. 12: SIR, Insulation resistance versus time depending on applied dose

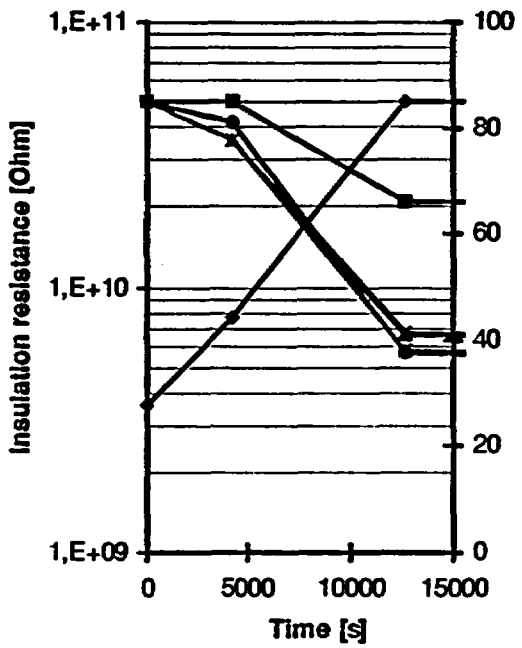

Fig. 13: SIR, Insulation resistance versus time depending on applied dose, expanded scale at test start

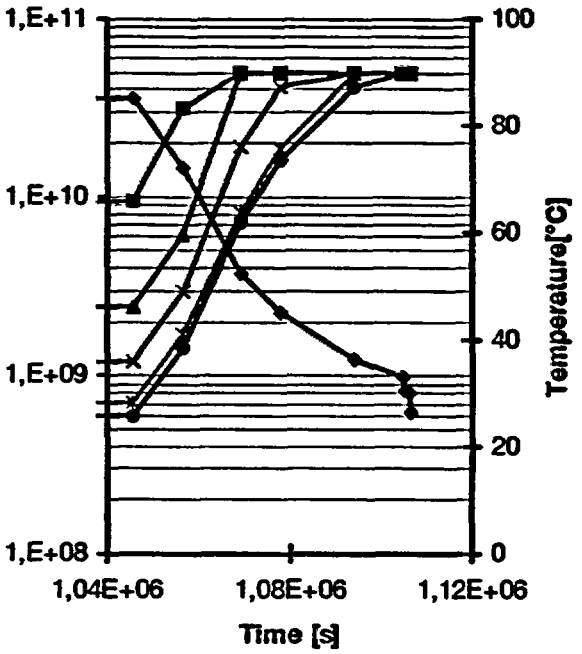

Fig. 14: SIR, Insulation resistance versus time depending on applied dose, expanded scale at the end of test

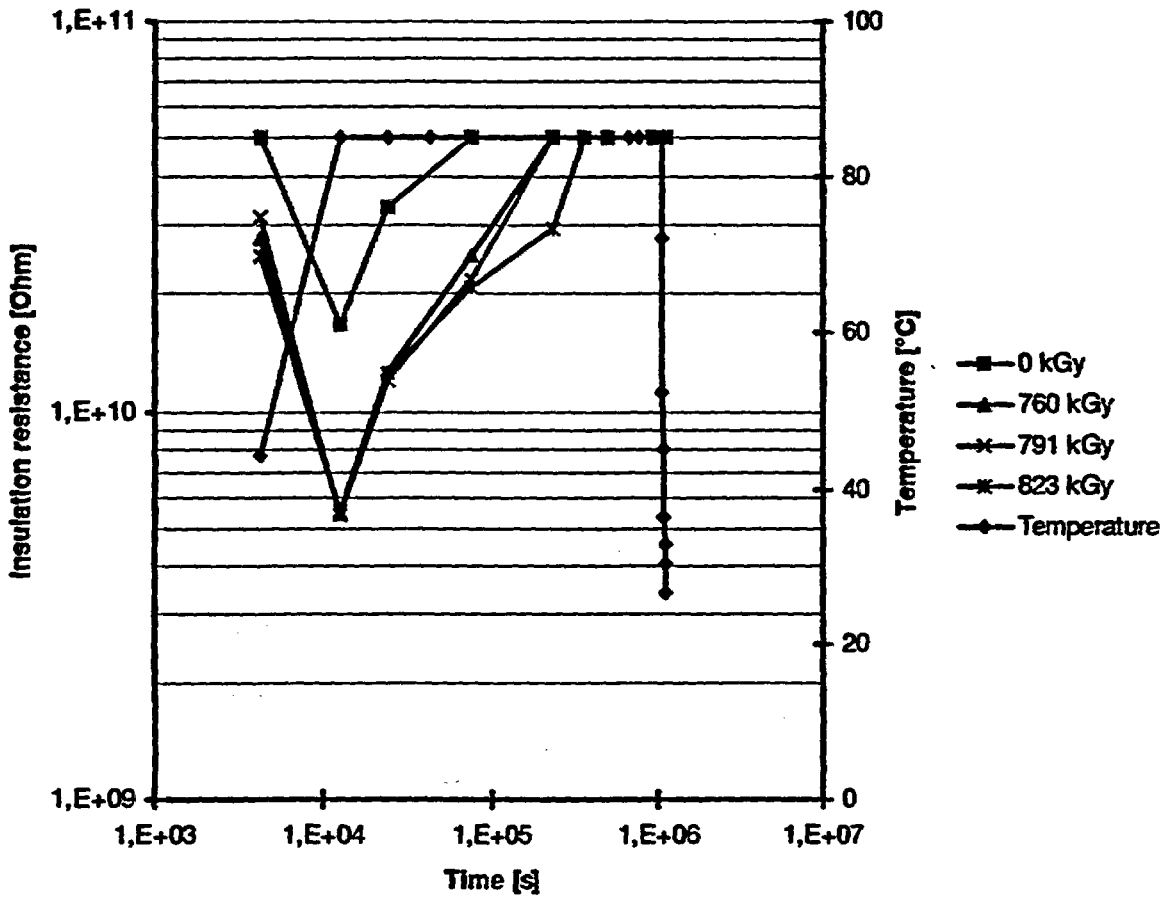

Fig. 15: VPE, Insulation resistance versus time depending on applied dose

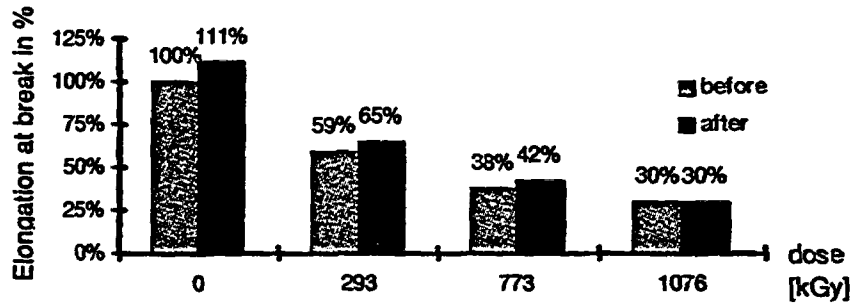

Fig. 16: EPR I, Influence of post-accident test on elongation at break values

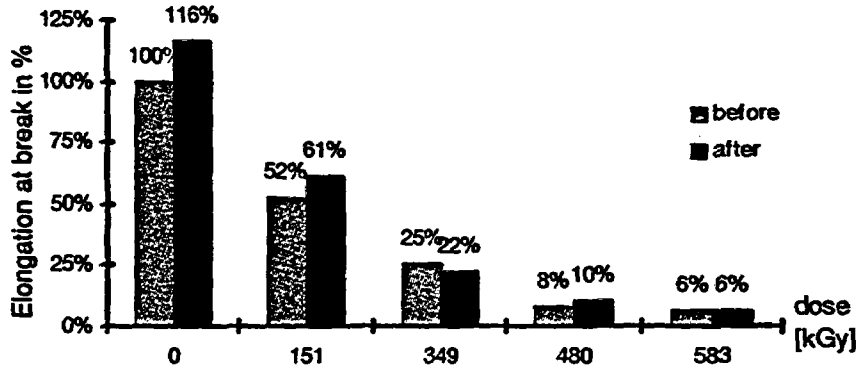

Fig. 17: SIR, Influence of post-accident test on elongation at break values

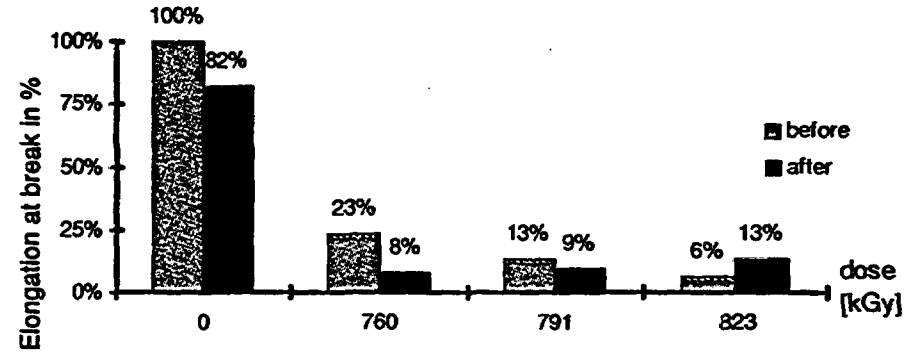

Fig. 18: VPE, Influence of post-accident test on elongation at break values

Correlation between physical degradation of artificially aged cables and their dielectric behavior during LOCA

Kjell Spång, Ingemansson Technology AB, Göteborg, Sweden

Abstract

Consideration of aging in initial qualification of components for nuclear power plants is mostly taken care of by subjecting the components to accelerated aging before they are exposed to the DBE test. Since it is often not possible to determine the acceleration factor with a sufficient degree of confidence, the possibility to supplement the initial testing with a condition monitoring program has been investigated. Indicators are then used to establish the condition of the component after the accelerated aging before the component is subjected to DBE test. It is assumed that the component's qualified life is not consumed as long as the value of the indicator does not exceed the value measured before a successfully passed DBE test.

It is important for a successful condition monitoring program that indicators used for establishment of the condition are correlated to the electrical behavior of the component during DBE. This correlation has been studied for some possible indicators (indenter modulus, dielectric loss factor, OIT) and components (including cables of type Lipalon, Rockbestos and Dätwyler) as part of a research program in Sweden. The program has been supported by the Swedish Nuclear Inspectorate and the Swedish utilities..

For the cables which were degraded to such a degree that they showed significant changes in dielectric behavior during or after LOCA, there was a positive but not very high correlation between the measured degradation after the aging and the values of dielectric loss factors during LOCA.

1 Background

A number of investigations made in Sweden and elsewhere have shown that it is often not possible to reliably predict the life of a cable purely from performance of a drastically accelerated laboratory test. On the other hand, use of moderate acceleration factors and still qualifying for very long life (e.g. 40 years) requires unrealistically long test periods before the cable can be accepted for installation. Various means to overcome the problem have been suggested and to some extent used. Some of the most promising methods involve condition monitoring as a complement to the initial qualification.

A comprehensive experimental study of methodologies for artificial aging of components intended for installation in nuclear power plants has been performed in Sweden. The results are reported in references /1/ and /2/. The study has included investigation of correlation between degradation due to aging, measured by various indicators and dielectric behavior during LOCA testing. This is important for finding suitable indicators, which can be used in a condition monitoring program.

2 Condition monitoring as part of the environmental qualification program

Cables intended for use in safety applications in nuclear power plants are subjected to an initial qualification program, including subjection of cable samples to various environmental stresses, followed by a DBE test. The cables are normally artificially aged before being subjected to LOCA simulation. If condition monitoring shall be used for control of residual life at selected intervals after installation, the

degradation trend of the cable material must be determined as part of the initial testing. A suitable degradation indicator must be chosen for this, which can then be used for the condition monitoring.

There are two basic criteria to be fulfilled for a condition indicator to be useful for the purpose. Firstly, the value of the indicator should vary in a easily measurable and consistent way with the degree of aging of the cable insulation material. Secondly, there should be a reasonable correlation between the dielectric behavior of the cable insulation during LOCA and the value of the indicator before LOCA.

This paper presents the results of the part of the Swedish experimental study which is related to these criteria.

3 Cables and condition indicators included

3.1 Cables

The cables investigated included Lipalon type FSSR7x1, Dätwyler type FEAR-PG 8x(2x1) and Rockbestos Firewall 3, RXSR-G 5x1.

The Lipalon cable has a conductor insulation and jacket of CSPE (chlorosulphonated polyethylene, Hypalon). The Dätwyler cable has a conductor insulation of black EPDM (ethylene-propylene rubber). The jacket material is blue EPDM. The Rockbestos cable has a conductor insulation of XLPE (crosslinked polyethylene) The jacket material is CSPE.

The cables and leads used for LOCA testing had been treated in the ends to avoid humidity intrusion from the ends and the leads were fitted with pins in one end to allow dielectric measurements, see Figure 1 below. The other end was sealed by means of a sealing compound. The cables had a length of 3 m and were wound on bobbins.

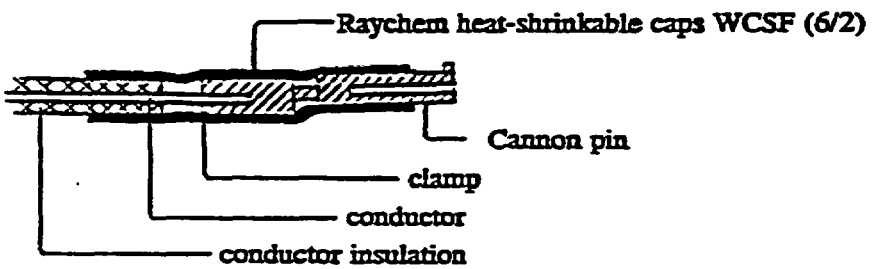

Figure 1 *Treatment of lead ends*

3.2 Condition indicators

The condition indicators used for the study of correlation with dielectric behavior during LOCA included indenter modulus, dielectric loss factors, and oxygen induction time (OIT). The dielectric behavior during LOCA was measured as insulation resistance and dielectric loss factor.

The indenter principle uses a device measuring the force needed for pressing an anvil of a certain shape into the material with constant velocity. The slope of the force versus the intrusion depth is defined as the indenter modulus.

The results of the indenter measurements are presented in terms of indenter ratios, defined as the ratio between the indenter modulus of the aged specimen and the indenter modulus of the unaged specimen.

Table 1 shows the modulus values of the unaged samples. The values are mean values from measurements on a rather large (>10) number of samples. The deviations between values of different unaged samples are very small. The modulus values of the aged samples can be achieved by multiplying the ratios given in this paper by the modulus values given in Table 1.

Table 1 *Indenter modulus of unaged samples*

Component	Indenter modulus before aging, N/mm
Cable Lipalon	3,23
Lead Lipalon	1,04
Cable Dätwyler	3,38
Lead Dätwyler	1,28
Cable Rockbestos	1,50
Lead Rockbestos	19,2

The slope of the force versus intrusion is not always linear. It is then important where on the slope the indenter value is determined. In such cases the determination of the modulus has been based on the first part of the curve, before the slope becomes significantly nonlinear.

Measurements of indenter values on cable jackets were made in three points on the periphery of two different sections of the cable sample. The values presented are the mean of these six values. Measurements of indenter values on leads were made in two points on each lead sample.

Manual measurements of dielectric loss factor and insulation resistance were made before and after the LOCA testing. In order to achieve a more sensitive detection of changes, the test objects were subjected to a humidity conditioning before the dielectric values were measured. The humidity conditioning included 108h at a temperature of 55°C±2°C and a relative humidity of 93%±3%. Continuous registration of dielectric loss factor and insulation resistance was used during the LOCA. In addition, intermittent manual measurement of insulation resistance was made during LOCA.

The loss factor measurements were made at 20Hz, 60Hz, and 1kHz (5V). The measurement of insulation resistance before and after LOCA testing was made with 250V DC (1Mohm serial resistance). The measurement during LOCA was made with 50V, because of the highly degraded test objects.

4 Test conditions

4.1 Thermal aging

The thermal aging was performed in dry heat test chambers, fulfilling the requirements for testing in IEC Publication 68-2-2, test Bb: Dry Heat Testing of Non Heat-Dissipating Specimen. The variation of

temperature in time was kept within ± 0,5°C and the spatial temperature variation was kept within ± 3°C.

4.2 Humidity aging

Some of the test specimens had been humidity aged at the earlier tests, reported in reference /1/. This had been made in conditions according to IEC Publication 68-2-3 Test Ca: Damp Heat, Steady State, with a relative humidity maintained at above 95% in a temperature of 95 ± 2°C for 24 and 48 days.

4.3 Vibration

Some of the test specimens had been subjected to sinusoidal vibrations at the earlier tests, reported in reference /1/. For these specimens, the thermal conditioning had been interrupted once per week by sweep sinusoidal vibration testing between 2 and 200 Hz with a sweep rate of one octave per minute during 30 minutes. Two different severities were used: amplitude 3,5 mm 30 m/s^2 and amplitude 7 mm 60 m/s^2. The cables and leads were mounted in a fixture as illustrated in Figure 2, which was fixed to the table of the electrodynamic vibrator used.

4.4 Ionizing radiation

The irradiation was performed in materials testing reactor R2 at Studsvik. The radiation source was spent reactor fuel elements. Ambient and material temperatures during irradiation were 35°C and 45°C. The dose rate was 10 kGy/h = 1 Mrad/h. The testing continued for 50 h; total dose 500 kGy = 50 Mrad.

The test specimens were encapsulated in plastics and sealed in a container, which was tilted 180° after 25 h. The monitoring method used was Reuter-Stokes Gamma Ionization Chamber RSG - 12A.

The irradiation was intended to simulate the exposure during a LOCA event.

4.5 LOCA simulation

The LOCA simulation was performed in ABB Atom's test loop LOKE. The temperature-pressure conditions are obtained with a system controlling electric heated elements at the pressure vessel, saturated steam generation, overheating of the steam, and outlet flow. The cables were subjected to overheated steam for 3 hours at 181°C and 0.4 MPaG (gage pressure), followed by 160°C and 0.4 MPaG for 3 hours and 120°C at normal laboratory pressure for 44 hours.

5 Study of the relationship between the severity of the aging simulation and the corresponding values of the condition indicators

Samples of the cables were artificially aged at 95°C for 48, 96, 144, 192 and 384 days, at 120°C for 12, 24, 36, 48, 96, 144 and 192 days and at 142°C for 3, 6, 9, 12, 24 and 48 days. Two samples were used for each combination of temperature and duration. In order to achieve significant degradation, the aging included more severe thermal conditions than would normally be used for qualification of the cables for installation in Swedish nuclear power plants.

Figure 2 shows the ratios between the values of the indenter (modulus) determined for the aged cable samples and for the unaged cable samples. The modulus have been determined for the complete cable and mainly reflect the degradation of the jackets.

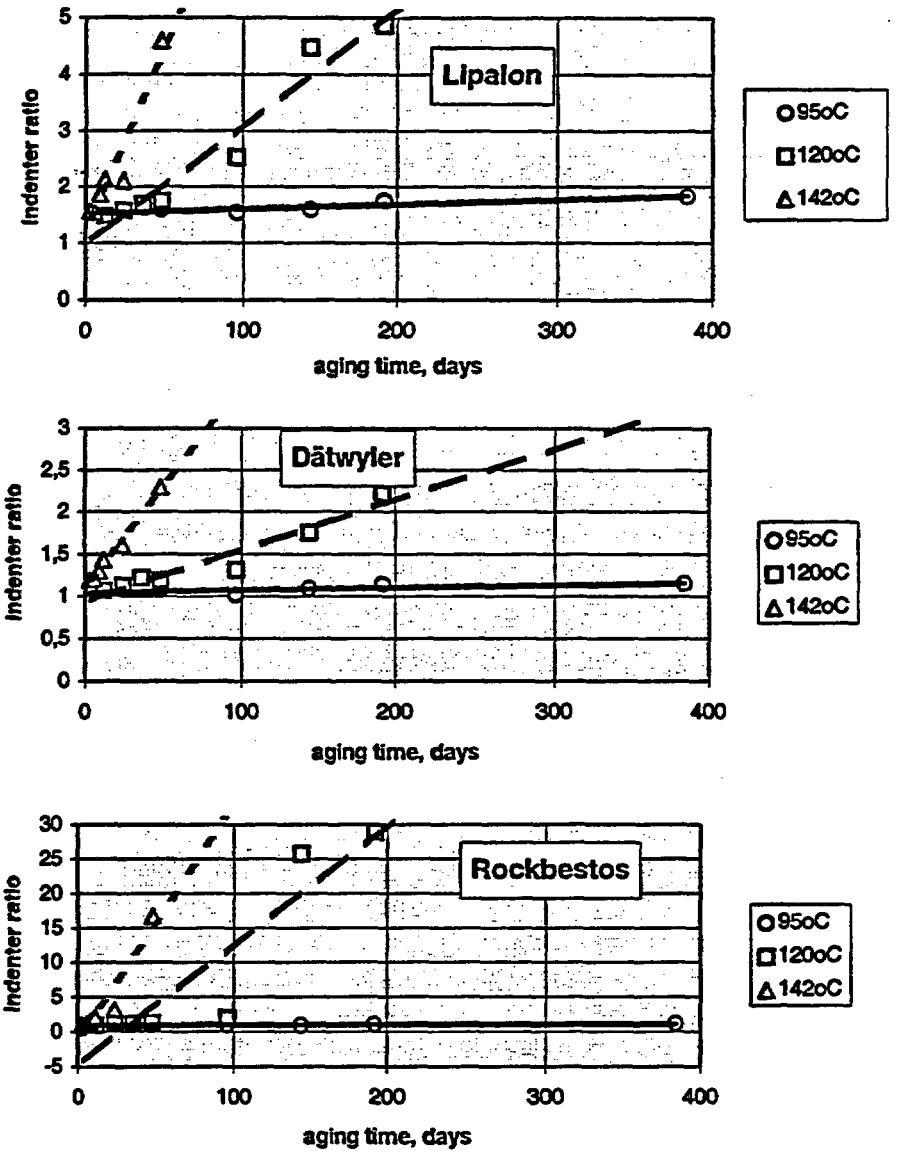

Figure 2. Indenter ratios of thermally aged cables (measured on the jackets)

The coefficients are high (in the order of 0.95 to 0.99) for the linear correlation between duration of aging and indenter ratios for the cables aged at 120°C and at 142°C. The cables aged at 95°C were very little affected by the thermal aging. Measurements of indenter ratios were also made on the conductor insulation material, having been subjected to the same thermal aging. The results showed significant degradation at the severe combinations of temperature and duration for the Lipalon and Dätwyler conductor insulation (CSPE and EPDM), but insignificant degradation of the Rockbestos conductor insulation (XLPE).

Figure 3 shows the dielectric loss factors, measured at 60 Hz. Only aging at severe conditions showed any effect on the dielectric loss factors. The figure only includes results from aging at 120°C for 48,96 and 192 days and at 142°C for 12,24 and 48 days.

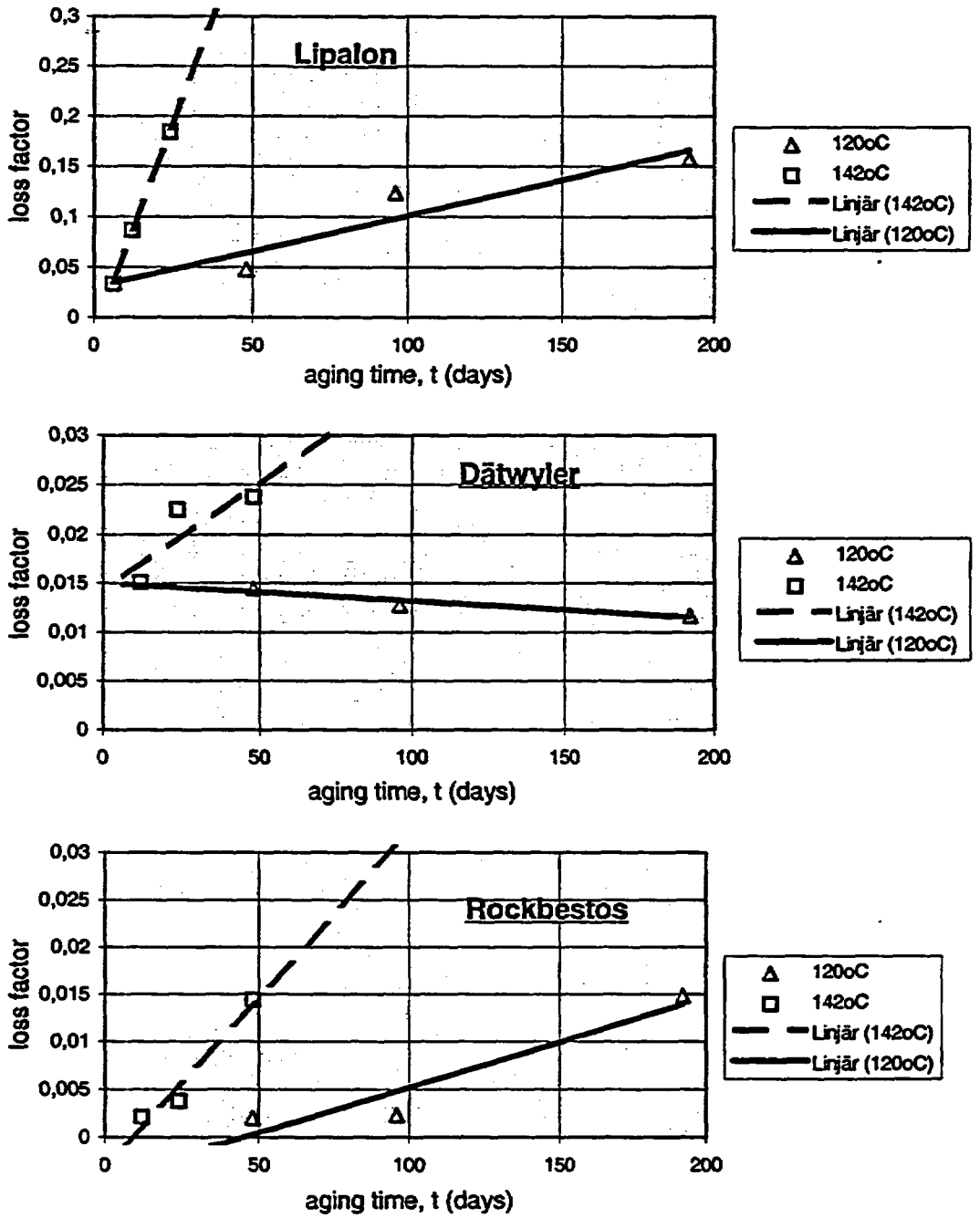

Figure 3. Dielectric loss factors at 60 Hz of thermally aged cables.

The linear correlation coefficients vary from 0.85 to 0.99.

Figure 4 shows the OIT values from measurements on thermally aged conductor insulation. Measurements were made on cable samples artificially aged at 95°C for 96, 192 and 384 days, at 120°C for 48, 96 and 192 days and at 142°C for 12,24 and 48 days. The Dätwyler cable aged at 142°C for 48 days went below measurable values. The conductor insulation of the Rockbestos cable samples exposed to 120°C and 142°C were too severely degraded to give reasonably reliable results.

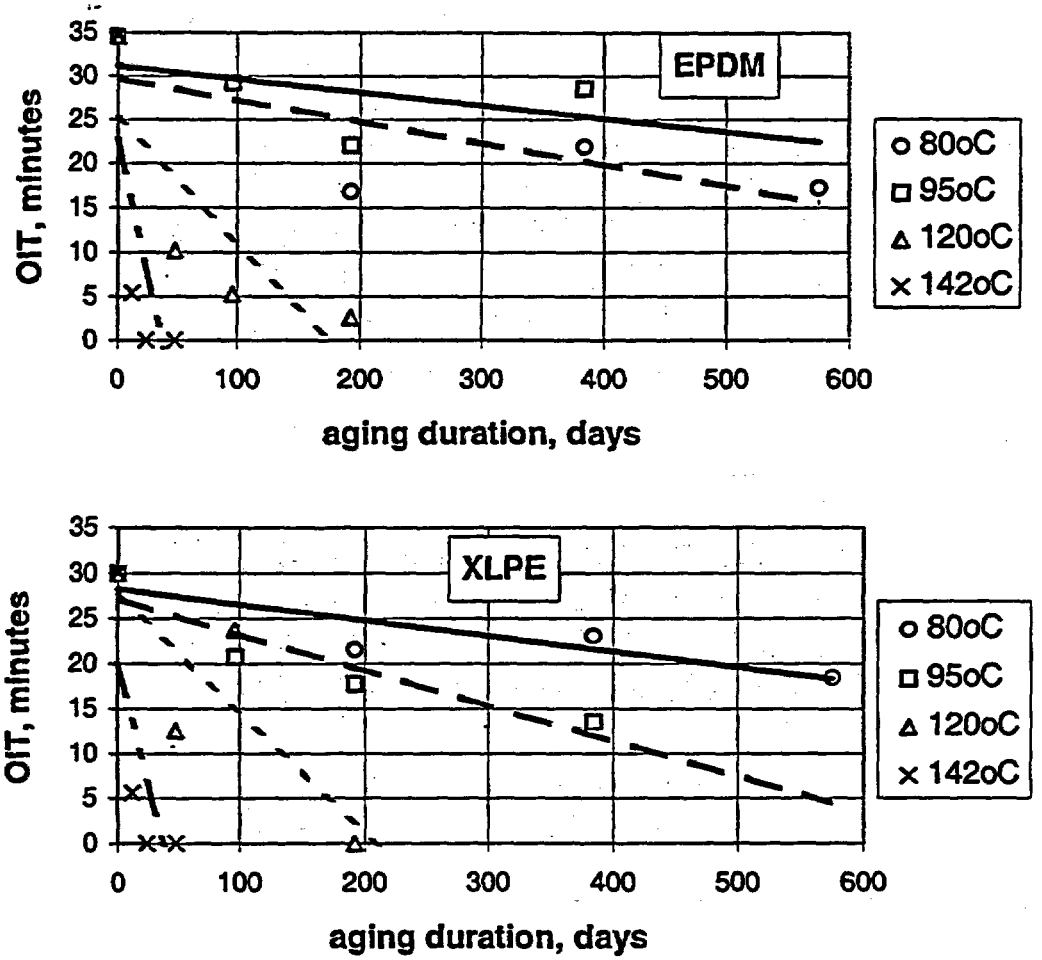

Figure 4. OIT values of thermally aged conductor insulation.

The coefficients of linear correlation are as follows

Dätwyler conductor insulation aged at 95°C: R=0.10
aged at 120°C: R=0.94
aged at 142°C: R=0,80
Rockbestos conductor insulation aged at 95°C: R=0,99

6 Irradiation and LOCA tests, results

6.1 General

The measurements of degradation due to thermal aging in terms of the three indicators studied show a reasonably good correspondence between the severity of the aging conditions and the degradation.

The study of the behavior after irradiation and during LOCA included a selection of samples which had been subjected to aging in the studies presented in reference /1/ and /2/. This included aging for 3-4 different durations at 95°C, 120°C and 142°C, for the Lipalon cable samples also at 80°C.

The dielectric parameter values during LOCA used in the comparison are the extreme values (highest for loss factor, lowest for insulation resistance) achieved during the first 6 hours of LOCA (marked LOCA I in the figures) and the value at the end part of the LOCA (marked LOCA II in the figures).

6.2 Cable Lipalon

In general, the irradiation had a slight degrading effect on the mechanical behavior of the Lipalon jackets in terms of increased indenter modulus. Also the dielectric loss factors increased after irradiation. The results are illustrated in Figure 5 for indenter modulus, in Figure 6 for dielectric loss factor.

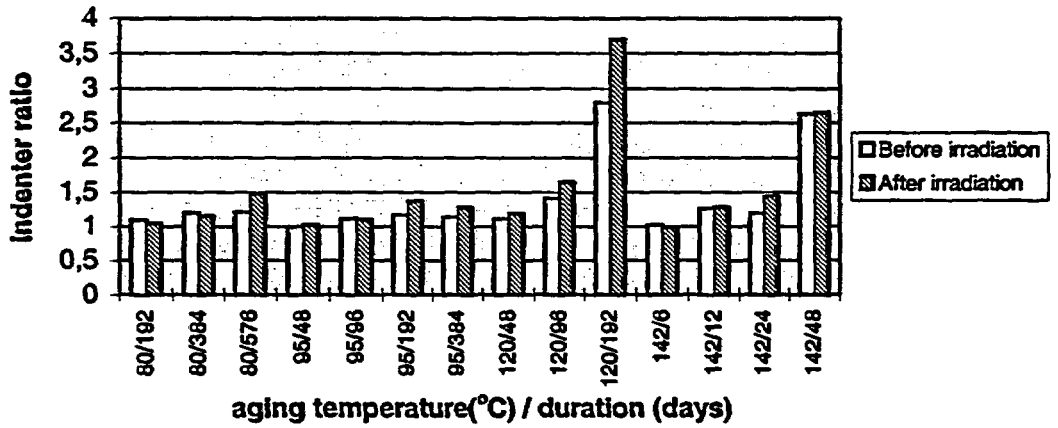

Figure 5. Cable Lipalon. Indenter ratios before and after irradiation

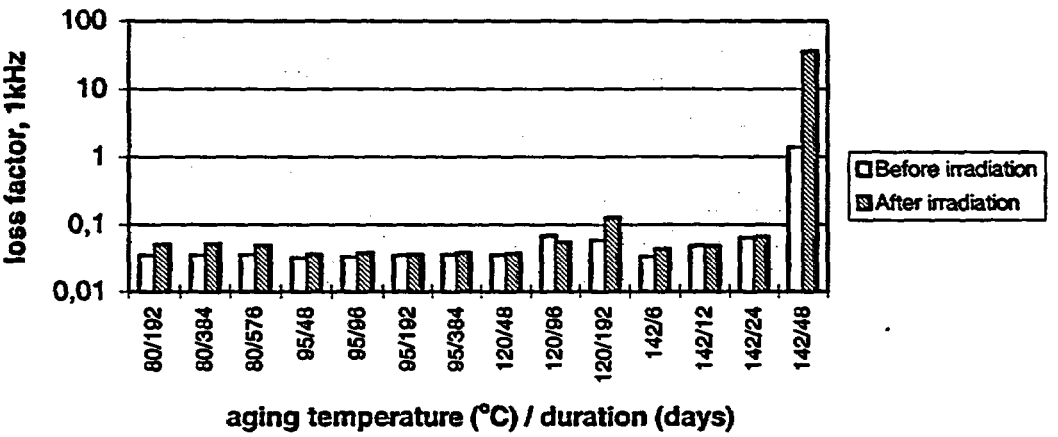

Figure 6. Cable Lipalon. Dielectric loss factor at 1 kHz before and after irradiation

The relationship between indenter ratios measured before LOCA (after thermal aging and irradiation) and the insulation resistance (normalized to 1 meter cable length) during LOCA is shown in Figure 7. There is a significant tendency of lower insulation resistance for cables with higher indenter ratios, even if the correlation is rather low (correlation coefficient approx. 0.4).

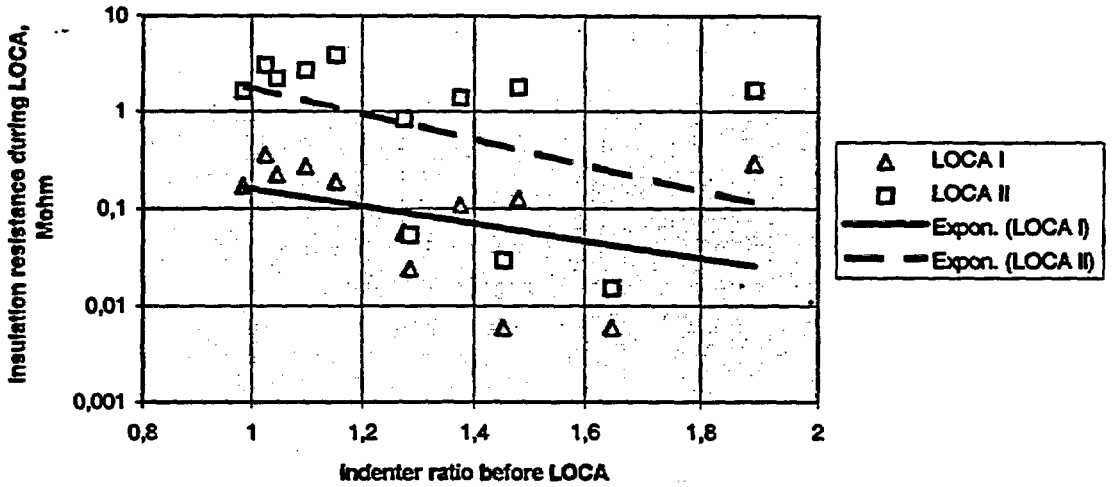

Figure 7. Cable Lipalon. Relationship between indenter ratios before LOCA and insulation resistance during LOCA

The result for comparison of the relationships between indenter ratios before LOCA and loss factors during LOCA is shown in Figure 8. In Figure 8 is also shown the result for comparison of the relationship between loss factor measurements before and during LOCA.

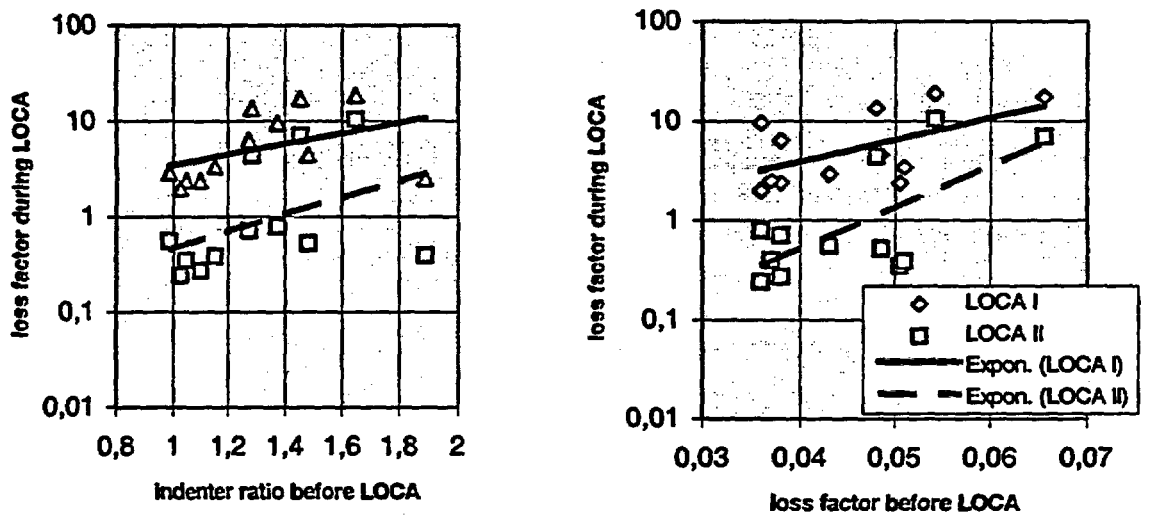

Figure 8. Cable Lipalon. Relationships between dielectric loss factor at 1 kHz during LOCA and indenter ratios before LOCA (left figure) or dielectric loss factor at 1 kHz (right figure) before LOCA

The regression lines for the data show that there is a positive correlation between the condition of the cable sample before LOCA, measured as indenter ratio or dielectric loss factor and dielectric loss factor during LOCA. The correlation is somewhat higher for the use of the loss factor (0.5-0.7) as condition indicator than for the indenter ratio (0.4) as condition indicator.

6.3 Cable Dätwyler

In general, the irradiation had a degrading effect on the mechanical behavior of the Dätwyler jackets in terms of slightly increased indenter modulus. The dielectric loss factors are not sensitive enough to show an increase after irradiation. The results are illustrated in Figure 9 for indenter modulus, in Figure 10 for dielectric loss factor. Figure 9 also includes the effect of the LOCA test on the mechanical condition of the cable. It can be noted that especially the LOCA exposure has had a very strong effect on the most severely aged cable (thermally aged at 142 °C for 48 days).

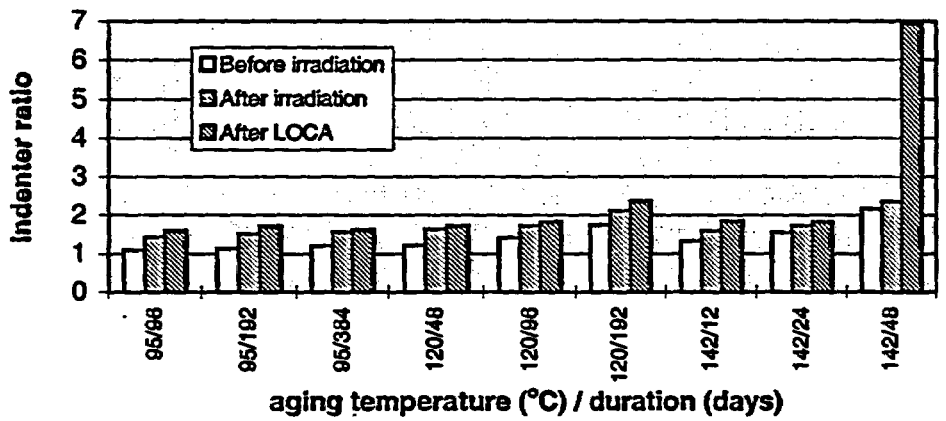

Figure 9. Cable Dätwyler. Indenter ratios before radiation, after irradiation and after LOCA

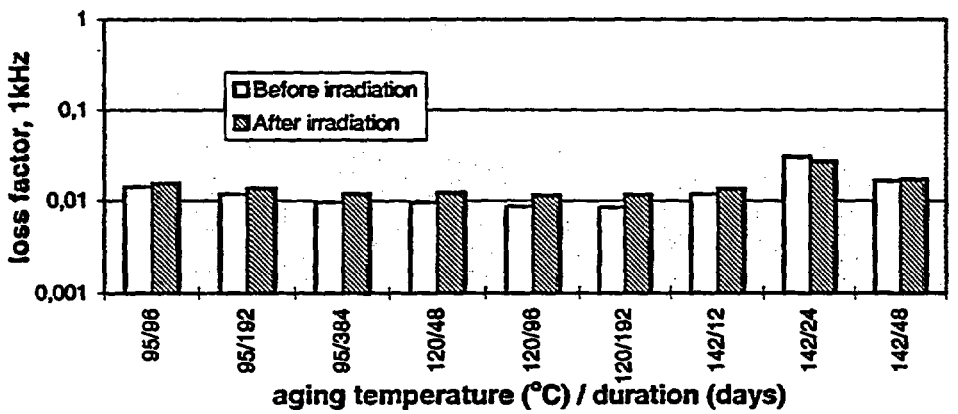

Figure 10. Cable Dätwyler. Dielectric loss factor at 1 kHz before and after irradiation

The insulation resistance and the dielectric loss factor during LOCA didn't show any consistent variation with the duration for which the cable sample had been exposed at a certain aging temperature. A comparison with the mechanical condition before LOCA is therefore not meaningful. The Dätwyler cable was very resistant to thermal aging which hadn't proceeded in our tests to a degree where significant aging related effects were shown in the dielectric behavior during LOCA.

There is, however a reasonable positive correlation between the variation in oxygen induction time (OIT, minutes^{-1}) measured on the cable samples after thermal aging and the variation in loss factor during LOCA, although the variation didn't follow any consistent pattern with the severity of the thermal aging. The relationship is shown for the measurement of loss factor at 1 Hz in Figure 11.

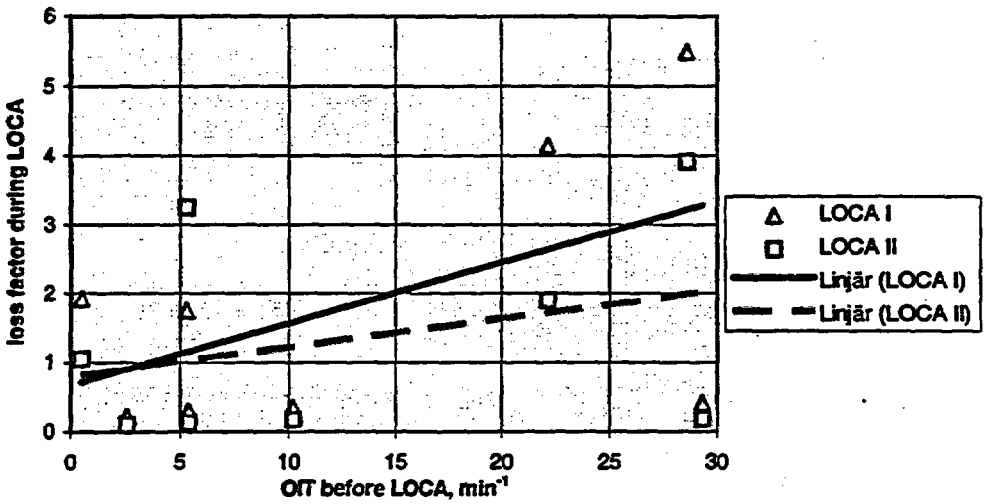

Figure 11. Relationship between OIT before LOCA and dielectric loss factor at 1 kHz during LOCA

The correlation is 0.5 for LOCA I and 0.3 for LOCA II. Similar results were achieved for the loss factors at 20 Hz and at 60 Hz.

6.4 Cable Rockbestos

In general, the irradiation had a rather limited degrading effect on the mechanical and dielectric behavior of the Rockbestos jackets.

The dielectric loss factor couldn't be measured during LOCA for the cables which had been aged at 120°C for 192 days and at 142°C for 48 days - they were in too poor conditions for that. Only the dielectric loss factor at 60 Hz could be measured for the cables which had been aged at 142°C for 24 days. The higher loss factors after LOCA for those cables indicate that the dielectric losses during LOCA was considerably higher than for the cables which had been subjected to less severe aging.

A comparison of the indenter ratios of the cables before LOCA and the dielectric loss factors after LOCA should be reasonably representative for investigating to what extent the behavior during LOCA is related to the mechanical condition before LOCA. The result of such comparison is shown in Figure 12.

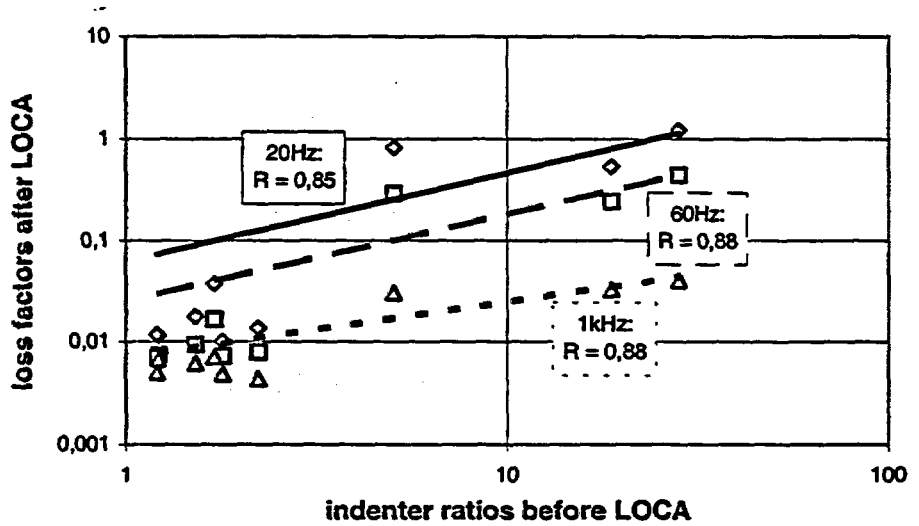

Figure 12 Cable Rockbestos. Relationship between indenter ratios before LOCA and loss factors after LOCA

The (exponential) correlation between indenter ratios before LOCA and dielectric losses after LOCA is rather good, but it should be noted that there are only a few points at the upper side which gives a higher correlation than we would probably find if we had more evenly distributed points.

Figure 13 shows the relationships between loss factors before LOCA and loss factors after LOCA

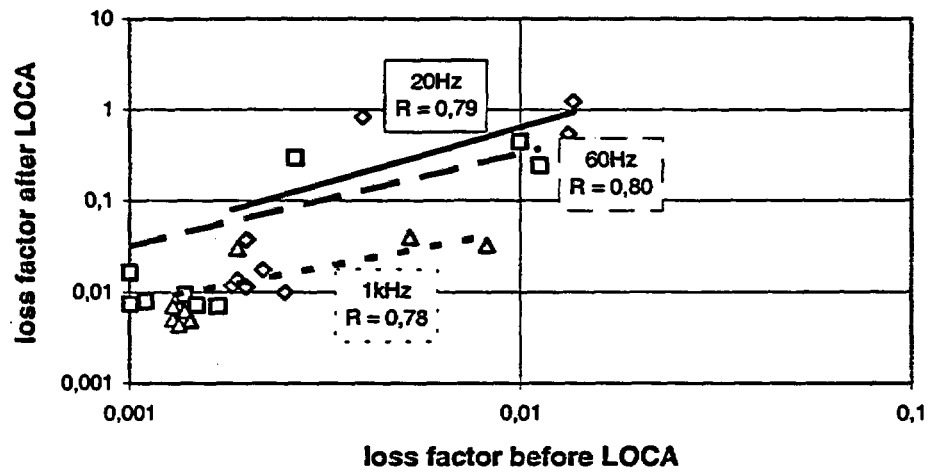

Figure 13 Cable Rockbestos. Relationship between loss factors before and after LOCA

The correlation between the loss factors before and after LOCA is lower than between indenter modulus before LOCA and loss factor after LOCA.

7 Testing for evaluation of the influence of humidity as part of the long-term exposure

7.1 Purpose

The results of earlier tests, presented in ref. /1/, indicated an increase in the degradation due to exposure to high humidity as part of the thermal aging. Samples of Lipalon cables which had been subjected to humidity in the thermal aging were included in the LOCA test presented here, with the purpose of evaluating to what extent the additional degradation because of the humidity factor in the thermal aging program had an influence on the dielectric behavior during LOCA.

7.2 Test results

A comparison of insulation resistance and dielectric loss factors during LOCA was made for cable samples which had been subjected to dry heat in the thermal aging and cable samples which had been subjected to a combination of high humidity and heat in the thermal aging. In all cases the aging temperature used was 95°C. Table 2 shows the results.

Table 2. Results of measurement of dielectric parameters during LOCA for Lipalon cable samples which had been thermally aged in low and high relative humidity.

			Insulation resistance Mohm for one meter		Loss factor at 60 Hz		Loss factor at 1 kHz	
Temp °C	Humidity %	Duration days	Before LOCA	During LOCA	Before LOCA	During LOCA	Before LOCA	During LOCA
95	low	48	99000	0.3564	0.050	15.6	0.036	2.00
95	low	96	119700	0.2700	0.052	17.3	0.038	2.41
95	low	192	103500	0.1107	0.051	33.3	0.036	9.55
95	low	384	105300	0.0558	0.058	27.0	0.038	6.35
95	>95	24	110700	0.0252	0.066	16.29	0.048	2.28
95	>95	48	99000	0.0234	0.077	16.73	0.050	2.35

The insulation resistance is significantly lower during LOCA for the cables which have undergone humidity exposure as part of the thermal aging. The difference is not as pronounced for the dielectric loss factor, but the dielectric loss factor is somewhat higher for the cable pieces which were exposed to humidity during the thermal aging.

8 Testing for evaluation of the influence of vibration as part of the long-term exposure

8.1 Purpose

The results of earlier tests, presented in ref. /1/ indicated no significant increase of the degradation due to exposure to vibration as part of the thermal aging. The components which had been intermittently subjected to vibration during the thermal aging were included in the LOCA test presented here, with the purpose of evaluating to what extent the additional degradation, because of possible cracks due to the vibration in the aging program, had an influence on the dielectric behavior during LOCA.

8.2 Test program

The test program included cable samples of all three types (Lipalon, Dätwyler and Rockbestos). The comparison is made of cable samples which were all aged at 120°C for 48 days. The cable samples which were intermittently exposed to vibration were vibrated at an amplitude of 3.5 mm and 7 mm (see clause 4.3 above); which is high compared to what cables are normally subjected to in their installation.

8.3 Test results

8.3.1 Effects of thermal aging and irradiation on vibrated cables

The tables presented below compare the results of measurement of degradation indicators (indenter modulus ratio, insulation resistance, dielectric loss factors) on cable samples which have been subjected to only thermal aging and cable samples which have been subjected to thermal aging and vibration. Insulation resistance is normalized to 1m, since the cables subjected to vibration had a length of 0,5m, whilst the cables not subjected to vibration had a length of 3m.

Table 3 Cable Lipalon. Results of measurement of degradation parameters, before and after irradiation. All measurements made after aging at 120 °C

Vibration	Duration days	indenter ratio		Insulation resistance Mohm[1)]		loss factor 60 Hz		loss factor 1 kHz	
		before irradiation	after irradiation	before irradiation	after irradiation	before irradiation	after irradiation	before irradiation	after irradiation
-	48	2,0585	2.1479	1197	106200	0,048	0,073	0,035	0,037
3,5	48	2,1831	2.4215	185	20500	0,043	0,078	0,034	0,047
7	48	2,2875	2,5284	183	20000	0,044	0,093	0,037	0,073

1) normalized to 1m cable length

There is a rather significant difference in the influence on the insulation resistance of thermal aging for cables aged with and without vibration. The difference in the influence on dielectric loss factor is not significant. This is also the case for the influence of the irradiation.

Table 4 Cable Dätwyler. Results of measurement of degradation parameters, before and after irradiation. All measurements made after aging at 120 °C

Vibration	Duration days	indenter ratio		Insulation resistance Mohm[1)]		loss factor 60 Hz		loss factor 1 kHz	
		before irradiation	after irradiation	before irradiation	after irradiation	before irradiation	after irradiation	before irradiation	after irradiation
-	48	1,194	1,630	299700	299700	0,0145	0,0175	0,0097	0,0122
3,5	48	1,464	1,948	15500	11250	0,0237	0,0148	0,0126	0,0110
7	48	1,468	1,875	13000	12500	0,0226	0,0146	0,0125	0,0110

1) normalized to 1m cable length

There is a rather significant difference in the influence on the insulation resistance of thermal aging for cables aged with and without vibration. The difference in the influence on dielectric loss factor is not significant. This is also the case for the influence of the irradiation.

Table 5 Cable Rockbestos. Results of measurement of degradation parameters, before and after irradiation. All measurements made after aging at 120 °C

Vibration	Duration days	indenter ratio		Insulation resistance Mohm[1)]		loss factor 60 Hz		loss factor 1 kHz	
		before irradiation	after irradiation	before irradiation	after irradiation	before irradiation	after irradiation	before irradiation	after irradiation
-	48	1,277	1,528	268200	375300	0,0020	0,0010	0,0011	0,0013
3,5	48	1,663	2,340	7675	10000	0,0019	0,0014	0,0029	0,0029
7	48	1,635	2,353	7450	9575	0,0020	0,0010	0,0010	0,0027

1) normalized to 1m cable length

There is a rather significant difference in the influence on the insulation resistance of thermal aging for cables aged with and without vibration. The difference in the influence on dielectric loss factor is not significant. There is also a difference in indenter ratios after irradiation.

6.1.1 Effects of LOCA simulation on vibrated cables

Figure 14-16 show the results of the measurements of insulation resistance (left figure) and dielectric loss factor at 1 kHz (right figure) during and after LOCA and for the cables aged at 120°C for 48 days without vibration and for the cables aged at 120°C for 48 days with vibration. The values during LOCA are the lowest values, normally occurring at the end of the 181°C phase of the LOCA.

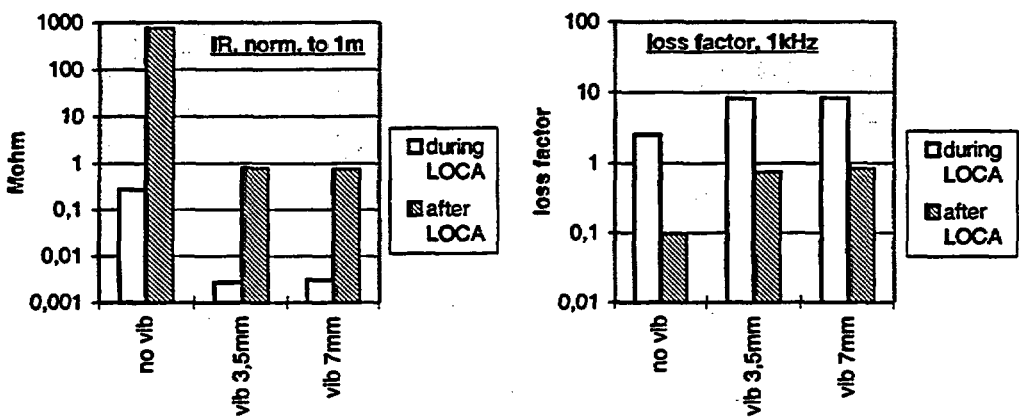

Figure 14 Cable Lipalon. Comparison of LOCA behavior of cables without and with vibration as part of the aging. Insulation resistance, normalized to 1m cable length and dielectric loss factor at 1 kHz.

The insulation resistance is significantly lower during and after LOCA for the cables which have undergone vibration exposure as part of the thermal aging. The inclusion of vibration has also significantly increased the loss factor.

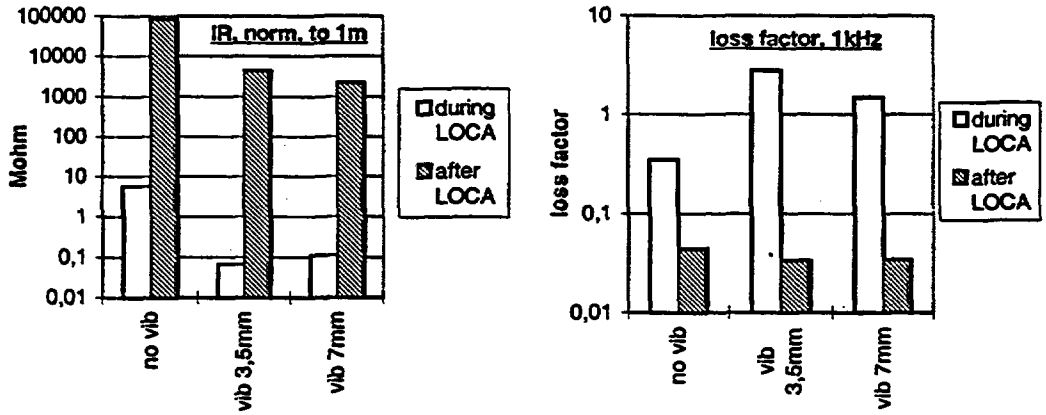

Figure 15 Cable Dätwyler. Comparison of LOCA behavior of cables without and with vibration as part of the aging. Insulation resistance, normalized to 1m cable length and dielectric loss factor at 1 kHz.

The insulation resistance is significantly lower during LOCA for the cables which have undergone vibration exposure as part of the thermal aging. The loss factor during LOCA is 3-5 times higher for the cables which have been subjected to vibration.

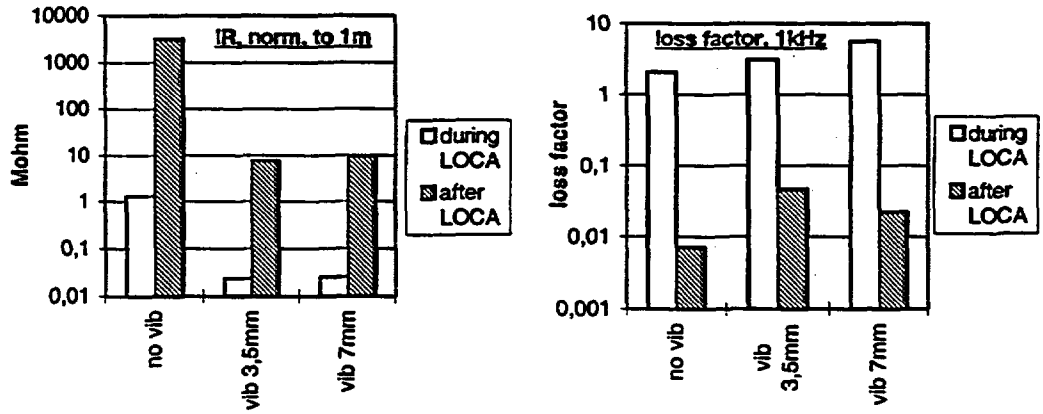

Figure 16 Cable Rockbestos. Comparison of LOCA behavior of cables without and with vibration as part of the aging. Insulation resistance, normalized to 1m cable length and dielectric loss factor at 1 kHz.

The insulation resistance is significantly lower during and after LOCA for the cables which have undergone vibration exposure as part of the thermal aging. The loss factor during LOCA is slightly higher for the cables which have been subjected to vibration.

9 Conclusions

The condition indicators tested (indenter modulus, dielectric loss factors and OIT in most cases show a good relationship between the severity of the thermal aging and the degradation of the cable material indicated. The indenter modulus and OIT are more sensitive than the dielectric loss factors measured (the sensitivity of the latter may be increased by measuring at lower frequencies).

Of primary interest has been to establish the relationships between degradation due to thermal aging and the dielectric behavior during LOCA testing. The results for the Lipalon cable show a significant but not very pronounced linear relationship between indenter values measured before LOCA and the maximum dielectric loss factors at 1 kHz measured during LOCA. There is a slightly higher correlation between the indenter values as a measure of the mechanical condition before LOCA and the dielectric behavior during LOCA.

The results of the study on the Dätwyler cable show is a good correlation between the mechanical degradation measured by the indenter and the aging conditions, but the dielectric parameters measured during LOCA are not well related to the degree of aging. The Dätwyler cable is very resistive to thermal aging which hasn't proceeded in our tests to a degree where very significant aging related effects are shown in the dielectric behavior during LOCA. Also OIT measurements after thermal aging correlate reasonably to the dielectric behavior in LOCA.

The results of the study on the Rockbestos cable show a good correlation between the mechanical degradation measured by the indenter and the aging conditions. A good correlation is shown between the indenter modulus before LOCA and the dielectric parameters after LOCA (correlation about 0,85). The dielectric behavior couldn't be measured during LOCA for the most severely degraded cables, but the result indicates a reasonable relationship between mechanical degradation measured by the indenter and the dielectric conditions during LOCA.

The results of measurements of dielectric parameters during the LOCA tests of cables which had been subjected to high humidity (>95% RH) during the thermal aging show that the insulation resistance during LOCA is considerably lower than for cables which had not been subjected to high humidity during the thermal aging.

The results of measurements of dielectric parameters during the LOCA tests of Lipalon cables which had been subjected to intermittent vibration as part of the thermal aging show that the insulation resistance during LOCA is very much lower than for cables which had not been subjected to vibration during the thermal aging. An effect was also shown on the dielectric loss factors.

For the Dätwyler cables significant effects of the inclusion of vibration in the aging is shown both on dielectric loss factors during LOCA and on the insulation resistance during and after LOCA.

For the Rockbestos cables, a significant effect of inclusion of vibration in the thermal aging is shown on insulation resistance during and after LOCA. A slight effect is also shown on dielectric loss factors during LOCA

It should be noticed that environmental stresses (temperature/time in thermal aging, thermal aging combined with high humidity and vibration levels) in excess of what is expected in cables installed in the containment of nuclear power plants were used in the study.

10 Acknowledgement

The study has been sponsored by Statens Kärnkraftinspektion, Forsmark Kraftgrupp AB, OKG Aktiebolag, Vattenfall AB Ringhals and Barsebäck Kraft AB. It has been governed by a steering committee, including

Tommy Appelqvist, Statens Kärnkraftinspektion
Rainer Cebulla, ABB Atom
Reinhold Delwall, Forsmarks Kraftgrupp AB
Karel Fors, Barsebäck Kraft AB
Einar Ströbäck, Vattenfall AB Ringhals
Lars-Olof Ståhle, OKG AB, Oskarshamnsverken

ABB Atom AB has performed the environmental conditioning including LOCA simulation and the measurement of the dielectric parameters and OIT. Gunnar Ståhl, responsible for the work at ABB Atom, has also been a member of the steering committee.

11 References

/1/ Methodology for artificial aging of electrical components in nuclear power plants. Results of experimental studies. K Spång. SKI Technical Report 93:39, December 1993

/2/ Aging of electrical components in nuclear power plants. Relationships between mechanical and chemical degradation after artificial aging and dielectric behavior during LOCA. K.Spång. SKI Technical Report 97:40, October 1997

Insitu Partial Discharge Detection in Power Plant Cables

Nezar Ahmed and Nagu Srinivas
Detroit Edison
2000 Second Avenue, Detroit, MI 48226

Abstract

Partial discharge (PD) monitoring is perhaps the best predictive tool to check the insulation integrity of cables. It is nondestructive and is a reliable test. It is also provides information about the degree of deterioration and about the location of insulation defects. Remaining cable life estimation can be determined with PD testing. PD monitoring rapidly is gaining popularity in replacing hipot testing in cable. Recent PD monitoring equipment advancements allow real-time resolution recording of PD pulses, both in time and frequency domains. Both on-line and off-line PD measurements can be made on cables. Off-line testing normally is conducted by isolating the cable from the system and applying an external voltage to the cable. Voltages higher than the operating voltage of the cable normally are used. On the other hand, on-line PD monitoring technique normally is based on detecting PD produced by the cable-operating voltages. On-line testing is made while the cable is in operation.

This paper presents on-line PD detection system applicable to power cables used in power plants and production facilities. The system can also utilized to test control and instrumentation cables. However, for control and instrumentation cables, off-line testing normally is used. The technique is applicable to both shielded and unshielded cables.

The PD system presented in this paper measures PD in both the time and frequency domains. The system is capable of detecting PD in a very noisy environment such as in power plants and production facilities. The combination of both domains is used to distinguish between PD generated in the cable under test and outside interference resulting from background RF noise and discharges generated in adjacent equipment. Inductive couplers are used to pick up PD from cable under test. Inductive couplers are devices used to convert the magnetic signals resulting from PD to current pulses. They are designed to filter the 60 Hz signals and coupled to the PD higher frequency signals. In general, they detect PD pulses in the frequency range of 200 kHz to 200 MHz. These couplers consist of either high- frequency current-transformers clamped to the cable or high-frequency coils placed in close proximity to the cables.

Introduction

In general, cables used in power plants can be classified in two groups. One group is the power cables and the second is the control and instrumentation cables. Control and instrumentation cables are rated at 600V, regardless of the voltage used. The selection of these cables is oriented more toward physical rather electrical service requirements. These cables are either two-conductor cables or multcionductor cables. On the other hand, power cables are used to supply power to power plant equipment such as large motors, auxiliary transformers, precipitators and backup diesel generators. These cables are rated from 2001V to 15 kV and are either single conductor or three-conductor cables. Both shielded and unshielded cables are used in power plant.

Most of the power plants cables are extruded-dielectric cables. Extruded cables are insulated with organic materials (polymer). Both thermoplastic and thermosetting materials are used for cable insulation. Thermoplastic polymers soften to essentially a liquid state with increasing temperature, and then return to their solid state unchanged on cooling. On the other hand, thermosetting materials tend to retain their dimensional stability with increasing temperature up to their actual decomposition temperature. Thermoplastic materials include: polyethylene (PE) and polyvinyl chloride (PVC). Examples of thermosetting material used in cable insulation include cross-linked polyethylene (XLPE), butyl rubber, ethylene-propylene copolymer (EPR) and ethylene-propylene-dien terpolymer (EPDM), isobutylene (Butyl), styrene butadiene rubber (SBR). Other types of thermosetting materials mainly used in instrumentation and control cables are methyl chlorosilane (Silicone), tetrafluoroethylene (TFE or Teflon), fluorinated ethylene-propylene copolymer (FEP), ethylene tetrafluoroethylene (ETFE or Tefzel), chlorosulfonated polyethylene (hypalon), chloroprene (Neoprene) and polyvinylidene fluoride (PVDE).

Cable Aging

Extruded cables are insulated with polymer materials. Degradation in polymer occurs either by scission reaction or by crosslink reaction. Scission reaction is the breakup of the long, chain-like molecules while growth reaction occurs when many chains join at many points which results in an extensive, insoluble network, crosslinking. Growth reaction often makes the material brittle and crack. There several fundamental types degradation have been recognized. The most important processes that affect polymer in service are thermal, oxidation and electrical stress degradation.

Thermal degradation in the absence of oxygen usually degrades the polymer to lower molecular weight materials, and occasionally crosslinking also occur [1,2]. The breakup of the polymer chain is caused by two mechanics, random chain scission and chain depolymerization. The initial break in the chain may take place anywhere along the molecule with equal probability, producing two polymer radicals. The location of the next scission event will depend upon which of the two mechanism is operative. When chain scission occurs randomly, the next scission may take place at any link producing products with a mixture of large and small molecules. However, in the chain depolymerization, once initiation has occurred, all chain links no longer have an equal probability of breaking. Rather, scission will always occur at the position of the last link, near free radical resulting in large amounts of monomer.

Oxidative degradation in polymer normally does not occur until a given period of time has elapsed [3,4]. During this time oxygen in absorbed by the polymer, and rate at which this occurs depends upon the temperature, the structure of polymer, the degree of crystallinity, and the extent of crosslinking. In order for the polymer to oxidize, polymer free radicals have to be formed. Radiation, heat, mechanical forces, or very reactive species such as atomic oxygen and ozone, which often may be generated by partial discharges, promotes such reaction. Once the radical has formed, molecular oxygen may then combine with it to form peroxides and hydroperoxides.

Oxidation of long-chain polymer molecules usually occurs with an attack upon a tertiary carbon and abstraction of its H atom [2]. This results in chain scission and it represents the first step in degradation. After the first event, the reaction has many varieties, liberates a range of low molecular weight materials and is autocatalytic so that it accelerates with time. Oxidation in underground cable insulation is not a rapid process because the concentration of oxygen is limited. Moreover, antioxidant agents are added to the cable insulation during the formulation process.

Electrical stresses in polymer cause a phenomenon called treeing [5,6]. Generally, trees are classified in two types. One is called a water tree, the other is an electrical tree. In general, there are two distinct time periods in treeing; the first is an initiation period and the second is a propagation period, during which tree-like figures grow in the insulation. Both electrical and water trees usually initiate at imperfections at the interface or in the bulk of the insulation under the stress of an electrical field. In the case of the water tree, water has to be present too. Imperfections that initiate trees can be summarized as follow [7]:

a) Micro voids inherently induced during the curing of polymer, especially by steam-curing method.
b) Defects in the core screen.
c) Cavities due to shrinkage of gas formation in insulation.
d) Inclusion of foreign particles that separate gases, mainly due to moisture in the particles.
e) Bubbles caused by gas evolution in the conductive screen.
f) Cavities caused by field emission from microscopic protrusions at the semiconducting layers.
g) Small cavities can exist at tips of foreign particles, asperities, or needles, due to differential thermal expansion of the polymer and the metal.
h) Cracks produce by mechanical fatigues. High Maxwell compressive forces in the dielectric, caused by the high electric fields at local excrescencies when ac voltage is applied, produce a mechanical fatigue cracking in the polymer.
i) Cracks and brittleness produce by thermal stresses.
j) Cavities induced by charge injection and extraction.

Electrical trees propagate through the occurrence of partial discharge (PD). PD erodes the inner layers of the cavity that produces the PD [8,9]. The bombardment of the high- and low-energy ions produced by PD damages the polymer insulation as they cause scission reactions. Photo emission, ultraviolet light, from the PD my change the chemical structure of insulation. The other effect of PD is the decomposition of polymer through chemical reaction with activated oxygen, excited oxygen molecule or atoms generated by PD. This reaction occurs at the inner surface material of the cavity, which oxidizes and produces mainly water and carbon dioxide, and in turn eroded.

The shape of electrical tree is determined by the intensity of the field enhancement at the site were it is generated. Higher local field produces bush-type tree while branched tree is caused by lower field. Cable failure occurs when the branches of the tree bridge the length of insulation.

Water trees propagate by non interconnected microvoids partially filled with water. The propagation mechanisms involve electromechanical forces, diffusion of water and chemical action including oxidation [10,11]. Water trees can be either Broccoli- or bow tie- types. Broccoli-type tree grows from the conductor or the shield of the cable while bow tie-type originates in the bulk of the insulation. Water three by itself does not cause breakdown. However, if the tree is partially filled with water, an electrical tree will originate at the tip of the tree and can cause an insulation failure. Water trees are more pronounced in medium-voltage class cables as these cables often lacks water barriers.

Cable Testing

Dc test often is used as a diagnostic test in power plants or production facilities cables due to ease and economy of use. However, the continuity of dc testing recently has been questioned due to limited effectiveness and also due to the destructive nature of test. Alternative test methods such as very low-frequency voltage have been developed. However, this technique does not provide information about the

extent of degradation nor does it identify the location of defects, other than the site where the failure occurs during testing.

Partial discharge (PD) monitoring is perhaps the best predictive tool to check the insulation integrity of cables. It is nondestructive and is a reliable test. It also provides information about the degree of deterioration and about the location of insulation defects. Remaining cable life estimation can be determined with PD testing. PD monitoring rapidly is gaining popularity in replacing hipot testing in cable. Recent PD monitoring equipment advancements allow real-time resolution recording of PD pulses, both in time and frequency domains. Both on-line and off-line PD measurements can be made on cables. Off-line testing normally is conducted by isolating the cable from the system and applying an external voltage to the cable. Voltages higher than the operating voltage of the cable normally are used. On the other hand, on-line PD monitoring technique normally is based on detecting PD produced at the cable-operating voltages. On-line testing is made while the cable is in operation.

The organic insulation can not resist the electron/ion bombardment and related events generally inherent to PD. PD pulses attack the insulation causing failure. Therefore, extruded cable is designed to operate free of any PD. If PD develops, it eventually will lead to a failure. Lead-time depends on the size and type of defect and on the cable type. Smaller defects take several months-to-years to cause a cable failure. However, in larger defects, such lead-time is days and sometime minutes. The majority of large defects are the result of smaller defects enlarged over time by PD. Therefore, the PD technique is more useful if it is capable of detecting PD produced by small defects. These PD are usually within the magnitude of the background noise.

Several off–line PD monitoring methods are commercially available for power cables operating at rated voltages below 40 kV[12,13]. Off-line testing normally is conducted by isolating the cable from the system and applying an external voltage to the cable. Voltages higher than the operating voltage of the cable normally are used. These techniques record PD pulses in the time domains. In general, they record both the actual PD pulse and its reflection from the other end of cable. The time interval between the arrival of the actual pulse and its reflection is used to determine the location of the defect producing that pulse. These techniques are designed to somewhat deal with background noise. However, they only can detect PD pulses with magnitude slightly lower or higher than the background noise. Detecting smaller defects is achieved by energizing the cable with voltages of several orders of the applied voltage. Stressing the cables with higher voltages could lead to a cable failure during testing. The off-line testing only can be applied to cables less than 300 feet and no more than 6,000 feet. Moreover, as cable has to be removed from service during testing, cable preparation is one of the main disadvantages associated with off-line testing. The process is expensive and in many cases can not be achieved easily, especially in production facilities, because backup systems often are not readily available.

On-line PD monitoring technique normally is based on detecting PD produced by the cable-operating voltages. In extruded cables, the magnitude of these PD pulses is below the electrical interference of the system. Therefore, an on-line technique can be useful only if it can distinguish between PD pulses and noise. This paper presents on-line PD detection system applicable to power cables used in power plants and production facilities. The system can also be utilized to test control and instrumentation cables. However, for control and instrumentation cables, off-line testing normally is preferred. The technique is applicable to both shielded and unshielded cables.

Partial Discharge Detection

A: Detection Mechanism

PD in cables often occurs in voids or cavities in the cable insulation or at the shield-semiconducting layers. Such PD activity creates high frequency pulses that travel along side the cable conductor and ground shield. Typically, at the source, these electromagnetic pulses have bandwidths in the 1.5-ns range with rise-times in the nanosecond range. Depending on the type of defects, these pulses can be either a single pulse or a cascade of fast pulses. A coupling device with bandwidth of a few hundreds megahertz and a fast display are necessary to display these extremely fast pulses.

Either an inductive or a capacitive coupler is needed to detect PD pulses. Inductive couplers are high-frequency current-transformers that are placed around the cable. These couplers detect the magnetic field disturbance induced by the PD pulses traveling in the ground loop. Inductive couplers are normally utilized during on-line testing. On the other hand, capacitive coupling is accomplished using high-frequency capacitors connected in parallel with the termination of the cable. These capacitors filter the 60 Hz component from the very-high frequency pulses associated with PD. As these capacitive couplers are connected directly to the high-voltage side of the cable, they must be PD free at the test voltage.

B: PD Monitoring Equipment

The on-line PD system presented in this paper measures PD in both the time and frequency domains [14], see Figure 1. The system is capable of detecting PD in a very noisy environment such as in power plants and production facilities. The combination of both domains is used to distinguish between PD generated in the cable under test and outside interference resulting from background RF noise and discharges generated in adjacent equipment.

The frequency-domain testing is conducted using a spectrum analyzer. The analyzer is capable of conducting measurements in both full and zero-span modes. In the full span mode, the frequency range can be adjusted to examine signals in narrow-frequency bands as well as wide-frequency bands. The zero-span mode is used to examine single-frequency pulses in a time domain. The sweep time of the zero spans is used to find PD pulses occurring at one or more cycles of the operating voltage.

The time domain measurements normally are made using a pulse phase analyzer. The pulse-phase analyzer is capable of recording PD pulses sorted by their phase angle and magnitude.

The location of defects is achieved by comparing the frequencies of the detected PD pulses. This also was used to identify PD produced in the equipment the cable is terminated to. Distinguishing PD from interference is achieved as follows: First, the spectrum analyzer is used to display the detected signals in respect to their frequencies. Each signal then is examined in the zero-span modes. PD signals will occur at the crest of the operating voltages. On the other hand, noise will have no pattern to follow. Once the PD-frequency range is identified, the signal then is displayed in the time domain using the pulse-phase analyzer. A filter system is used to allow the pulse-phase analyzer to record only pulses within the frequency range of the partial discharge. Interference outside this frequency window will be rejected. The pulse-phase analyzer is fed with a reference ac cycle of the operating voltage. The phase-angle

pattern will identify if that PD signal is generated in the equipment under test or in adjacent equipment. The pulse count and magnetite are used to indicate the problem's severity.

A differential noise coupling technique was applied to achieve better noise rejection during field measurements. For this purpose, a pick-up RF antenna is placed near the cable. The signal picked up by the antenna is fed to the inverting input of a differential amplifier while the signal from the PD coupler is connected to non-inverting input. This technique is used to deal with both the aerial and broadcast interference. However, since the gain of the antenna and the PD sensor are not identical, the differential coupling technique can greatly reduced the RF aerial noise without completely eliminating it.

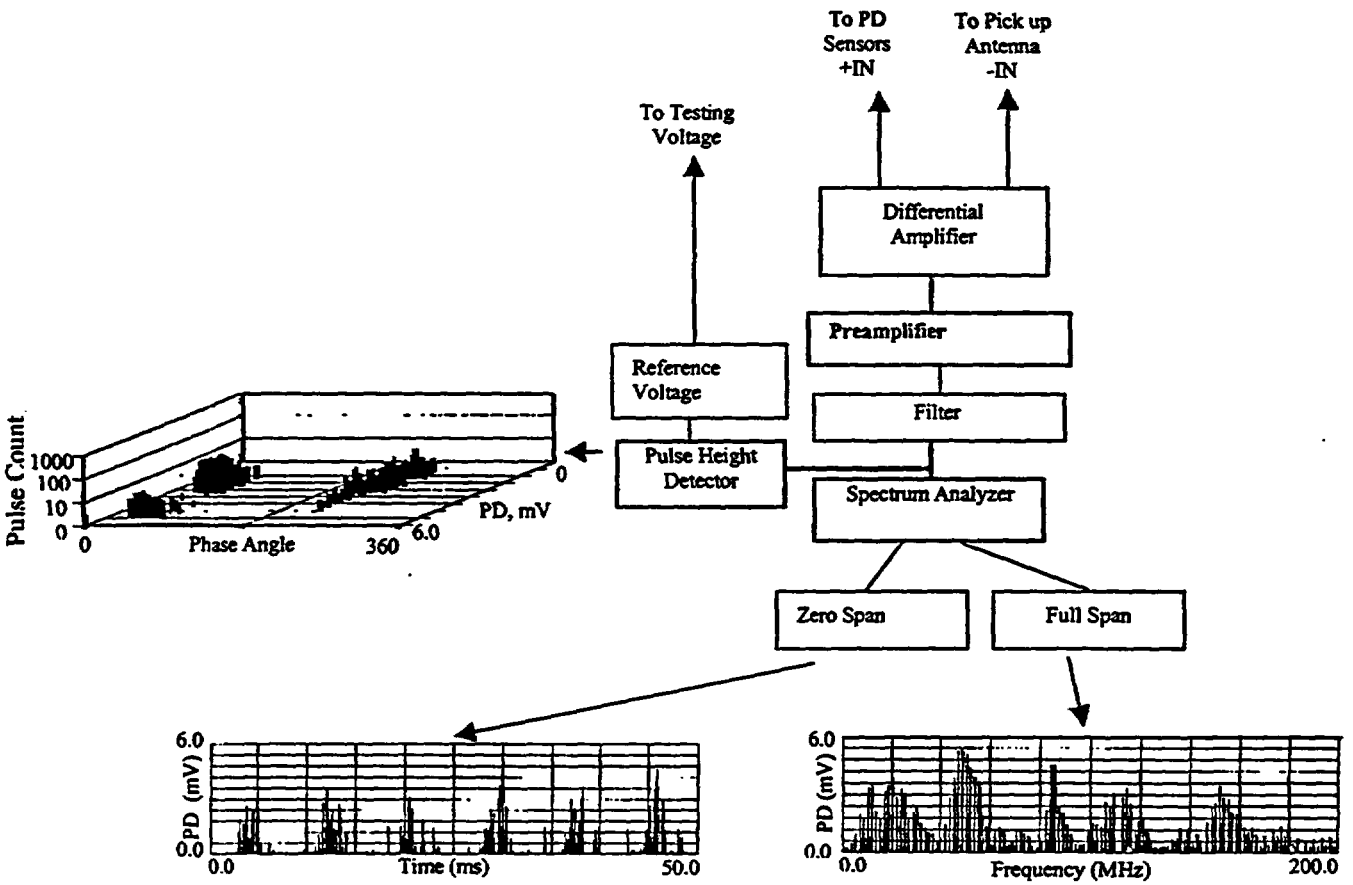

Figure 1 Schematic Diagram of the PD measurement system.

PD Testing in Power Cables

Power cables used in power plant can be tested on-line. This is accomplished by clamping a high-frequency current-transformers around the cables, see Figure 2. For cables shorter than 1000 feet, data is normally collected from both ends of cable, just below the cable termination. For cable longer that 1000 feet, PD measurements are made at both ends of cables as well at every 500 feet.

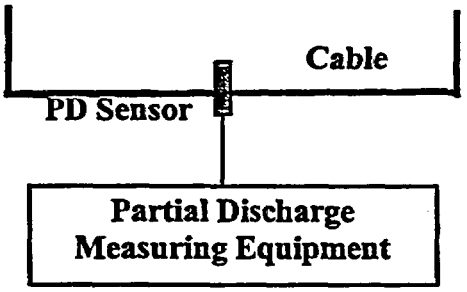

Figure 2 On-line PD testing arrangement.

PD Testing in Control and Instrumentation Cables

The main failure mechanism in control and instrumentation cables is caused by insulation cracks produced by mechanical fatigues and thermal deterioration. These cracks do not cause PD at the cable line voltage. However, higher voltages are needed to introduce PD in these imperfections. Therefore, control and instrumentation cables normally are tested off-line. The cables are removed from service and then energized with 1 to 2 kV from a portable power supply, see Figure 3. PD data collection is made either using a capacitive coupler connected to the cable conductor or through in inductive coupler clamped around the cable.

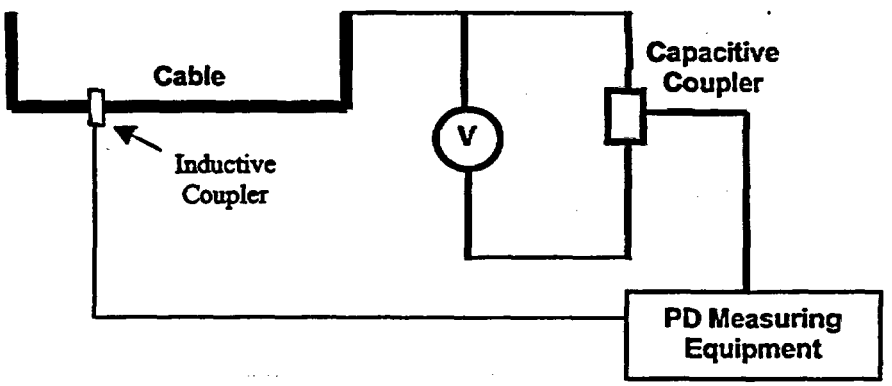

Figure 3 *Off-line PD testing arrangement.*

Noise Treatments

Power cables used in power plants and production facilities often operate at voltages from 2 kV to 15 kV. These cables are laid next to each other in open or closed trays. They are terminated to step-down transformers at one end and often terminated to high- voltage motors at the other end. PD pulses measured from one of these cables also could be the result of PD activities in the adjacent cables, the motors and transformers that these cables are terminated to or could be the results of electromagnetic interference from equipment nearby. This makes conducting on-line PD testing almost impossible. In

such environments, off-line PD testing is also difficult to perform because it requires shutting down almost the entire system to minimize the interference effect.
Generally, the main sources of electrical interference in power plant cable system are:

- Radio and TV station broadcasts and mobile telecommunication
- PD or noise from high-voltage equipment that cables are terminated to, such as transformers and motors
- RF energy (corona) emitted from other high- voltage components such as bushings, busbars and circuit breakers.
- Ground loop
- PD produced in adjacent cables or nearby electrical equipment.

Radio and TV station broadcast noises normally are present in all electrical equipment. However, this type of electrical interference generally is stationary and can be dealt with by a filtering technique. Figure 4 shows the frequency spectrum of some of TV and radio signals picked up from a cable installed in an open tray at the ground level. In general, the magnitude of the broadcast signals depends on the altitude of the cable. The highest noise level usually is encountered in cables installed in overhung trays or on the roof of elevated buildings. At an altitude of 50 feet, the broadcast noise level is about 10 times higher than those measured at the ground level. On the other hand, the noise in underground cables is about five times less than that measured at the ground level.

In the on-line PD measuring technique presented in this paper, the broadcast noise is recognized by its fixed frequency and by its large and smooth bandwidth. Moreover, broadcast noise normally is independent of the measurement sweep-time. It should be mentioned that the zero-span mode also can be used to distinguish broadcast noise from PD. Figure 5 shows the zero span of typical TV, AM and FM stations.

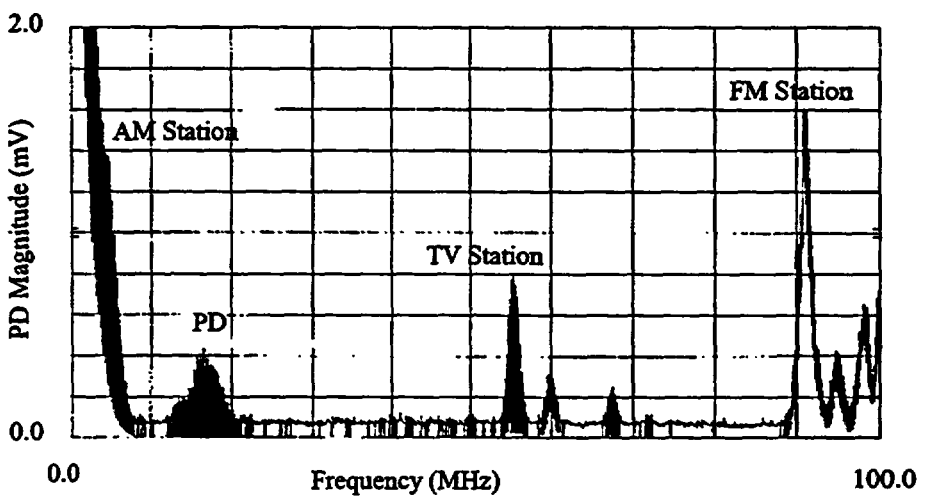

Figure 4 Frequency spectrum picked up from a cable installed in open tray at ground level.

The second type of electrical interference is PD generated in equipment that the cables are terminated to. This type of interference only is encountered in on-line PD testing. Transformers, motors and circuit breakers are the typical equipment that power plant cables are connected to. PD generated in this equipment will be injected in the cable. PD in solid insulation normally produces pulses with frequencies ranging from a few hundred kHz to a few hundred MHz. The attenuation of these pulses is a function of

frequency. The higher frequency components will be attenuated rabidly as they travel alongside the cable. This behavior can be used to distinguish between PD produced in the cable and PD generated in the electrical equipment that the cable is connected to. This behavior also can be utilized to determine the location of the PD site in the cable itself. However, this approach requires multipoint measurements along the length of the cable. In general, for cables less than 1,000-feet, three measurements normally are conducted — two at the cable ends, just below the termination, and one at the middle of the cable. For cables more than 1,000-feet long, measurements are made at both ends of the cable and at every 500 feet. Figures 6a and 6b show PD signals detected from a cable feeding a motor, where PD was observed in both the cable and in the motor. PD measurements were made on the switchgrear end of the cable. Therefore, the low frequency signals were the result of PD occurring in the motor, Figure 6a, while the high-frequency signals were the results of PD occurring in the cable, about a few feet from where measurements were made, Figure 6b.

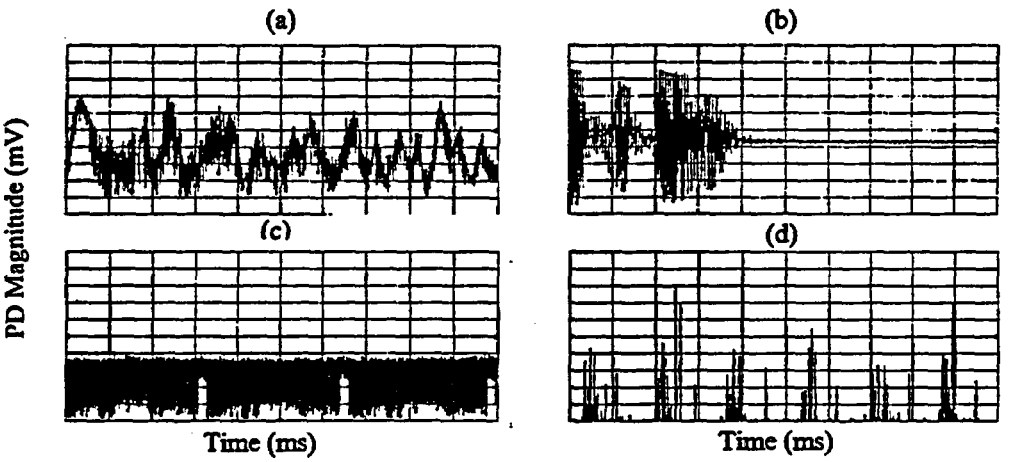

Figure 5 Zero span of some of the signals shown in figure 4. A: AM radio station (760 kHz), B: FM radio station (90.8 MHz), C: TV radio station (channel 4), D: PD signal.

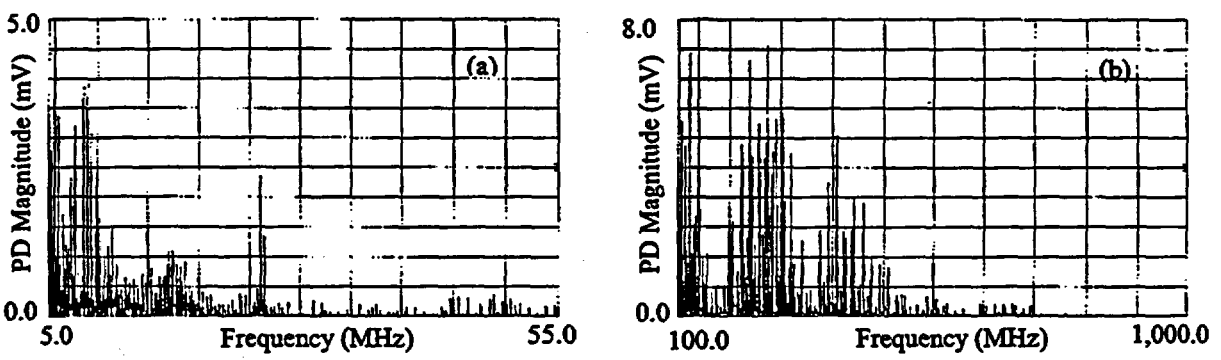

Figure 6 PD signals detected from a cable feeding a motor. A: PD in motor B: PD in cable.

One of the most difficult types of noise to deal with is that resulting from a corona occurring in other high- voltage components such as bushings and busbars. The frequency characteristic of this RF noise is almost identical to that of the PD produced in the cable insulation. In off-line testing, this type of noise

commonly is dealt with using a differential or anticoincidence noise-coupling technique [15]. In on-line testing, noise discrimination is mainly controlled by a skilled operator. Such judgment is based on few phenomena, in which PD produced in air (corona) differs from PD produced in solid insulation. Aerial-corona pulses are introduced into the cable either through direct emission or through the conductors. In either way, the air media controls the pulse attenuation. The RF-signal attenuation rate through air is slower than that through solid insulation. The rise time and duration of corona pulses are smaller than the PD pulses produced in solid insulation. The PD repetition in air normally is higher than that of solid insulation. Magnitudes of the subsequent pulses are almost identical in air. Furthermore, PD in the air is more pronounced during the negative cycle. Figure 7 shows the difference in the zero span between a PD signal generated in the cable and a corona signal induced in the cable from a nearby corona source.

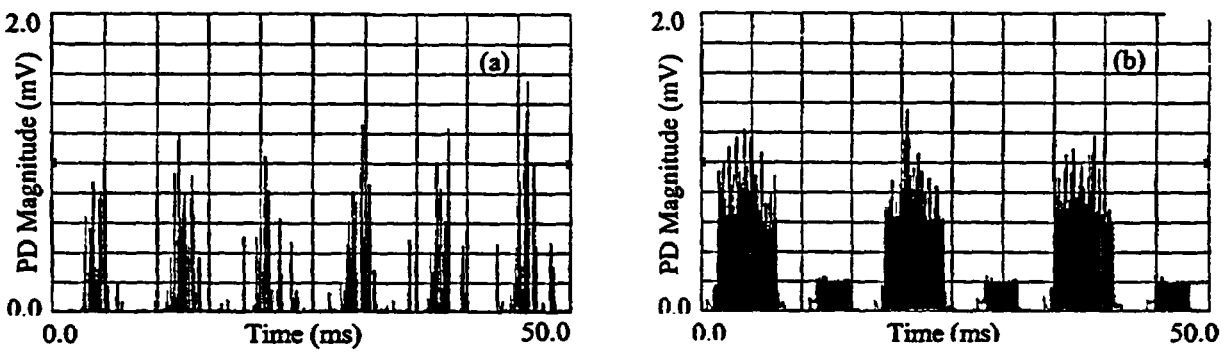

Figure 7 Zero span of A: PD signal. B: corona signaal.

Signals induced in the cable under test because of PD in the adjacent cables, can be recognized from their magnitude and phase angle. This required conducting the PD measurement in the adjacent cables too. Figure 8a show a PD signal detected from a cable without interference from adjacent cables. On the other hand, the source of the PD shown in Figure 8b is likely to be from two adjacent cables with a phase angle of 120 degree between them.

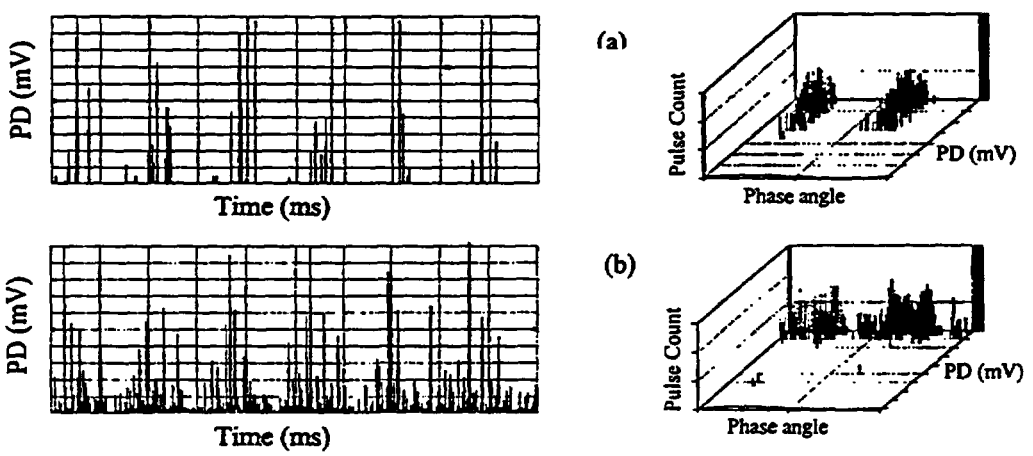

Figure 8 PD signal detected from unshielded cable. (a): without any interference from the adjacent cables.(b): with interference from the adjacent cable.

PD Level (Magnitude)

The magnitude of the detected PD signal normally dermises the severity of the cable degradation. In the traditional off-line PD testing, the magnitude of the PD is normally quantified in picoCoulomb (pC). One pC corresponds to about 10^7 electrons which represents the apparent number of electrons involved in a particular PD event. The attenuation and propagation of the PD pulses depends on the impedance of the cable. Therefore, the tested cable needs to be calibrated in order to quantify the detected PD. In-off line testing, this is made by injecting a known signal in the cable. It should be mentioned here that the traditional off-line testing required direct coupling to the cable conductor both in the calibration and the data collection processes. On the other hand, the PD technique presented in this paper measure the magnetic field outside the cable resulting from the PD pulses. Therefore, the magnitude of the detected signal not only depends on the cable impedance, but also depends on the cable geometry. PD testing also is made on-line making it difficult to calibrate the cable. Correlation between the detected signal and the condition of the cable is made using database information generated through laboratory testing of several types of cables. For example, table 1 shows the PD magnitude detected from several cable types. These data are generated by artificially introducing defects in the cables.

Table 1 PD level detected from several types of cables

Cable type	PD magnitude (mV)
Single conductor, unshielded	10
Single conductor, concentric shield	7
Single conductor, solid shield	4
Shielded three conductor cable	2

Locating the Source of PD

Locating the source of PD is based on the fundamental properties of PD pulses. In solid-insulation defects, PD pulse shapes differ, and several PD pulse with different shapes can be generated simultaneously from the same defect [16]. PD in solid insulation gives rise to electromagnetic pulses having a rise time ranging from few ns to several 10's ns. These pulses become attenuated as they propagate. Strong frequency discrimination occurs as pulses of high frequency are attenuated more intensively than pulses of low frequency [17]. As a result, the rise time of a pulse degrades rapidly after a few feet of propagation, suffering a slower degradation thereafter. For example, the rise time of a 2-ns pulse can increase to 10-ns in the first 300 feet, but only to 30-ns after an additional 1,000 feet of propagation.

PD pulses occurred within less than 30 feet from the point of measurement are expected to maintain their initial shapes due to the short proximity to the source. Therefore, it can be assumed that if the rise time of the detected pulse is less than 10 ns, it is very likely that this pulse has originated near the point of measurement. Likewise, PD pulses originated some distance away from the point of testing will have much wider rise times when measured at the termination end of the cable. In the frequency domain, PD originated near the point of testing will have frequency components as high as 500 MHz. On the other hand, the higher-frequency components of the PD originated away from the point of testing will be

completely attenuated before they reach the testing equipment. Figure 9 shows the PD signal detected at several locations of the cable.

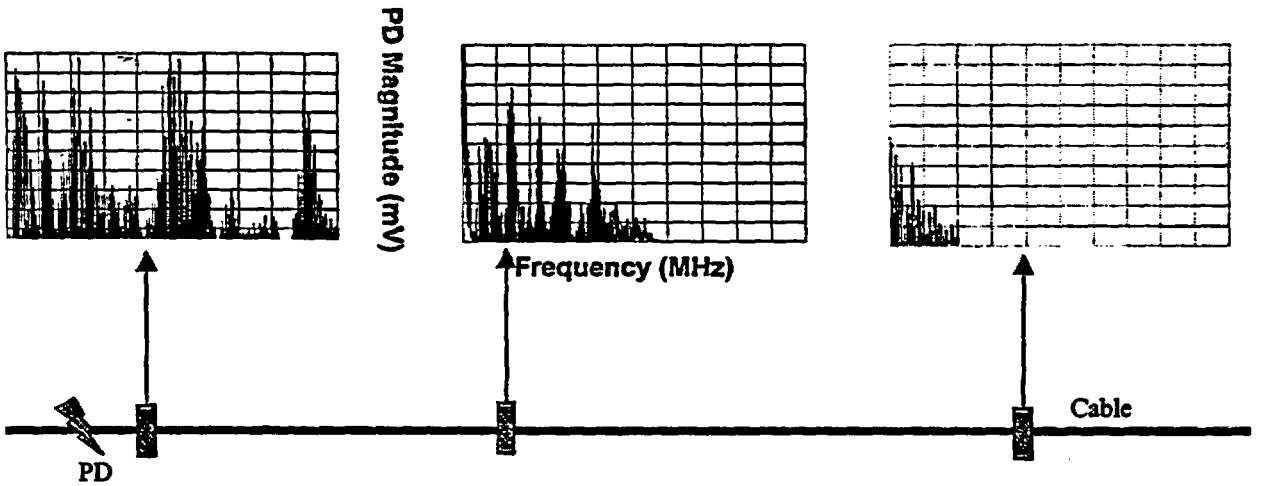

Figure 9 PD detected at several locations of the cable.

Conclusion

This paper describes partial discharge testing technique applicable to power plant cables. For power cables, PD is measured on-line using the line voltage as the excitation voltage of the cable. For control and instrumentation cable, the off-line testing approach is used in which the cable is energized to 1 or 2 kV using a portable power supply.

References

[1] L. Reich and S.S. Stivala, Elements of Polymer Degradation, McGrow-Hill, New York, 1971.

[2] R.T. Conley, Thermal Stability of polymers, Marcel Dekker, New York, 1970.

[3] R. Bartnikas, Engineering Dielectrics, Vol. IIB, ASTM, 1987.

[4] B. Randy, J.F. Rabek, Photodegradation, Photooxidation, and Photostabilization of Polymers, Wiley, London, 1975.

[5] R. Patsch, Breakdown of polymer: tree intiation and growth, CEIDP, Paper No. E6, Washington, 1975.

[6] G. Bahder, T.W. Dakin, and J.H. Lawson, Analysis of treeing type breakdown, CIGRE, paper 15-05, Paris, 1974.

[7] EPRI EL-7090, The aging of extruded dielectric cables, Poceedings: JICABLE/EPRI/CEA Workshop, EPRI, 1990.

[8] Y. Toriyama, H. Okamoto, M. Kanazashi and K. Horii, Degradation of polyethylene by partial discharge, IEEE Transaction on Electrical Insulation, Vol. EI-1, 1967.

[9] IEEJ Committee on Corona Degradation of Insulating Materials, Degradation of insulating materials by corona discharge, IEEJ, Tech. Rep. No. II-43, Tokyo, 1976.

[10] E. Illdstad, Influence of Mechanical stress and frequency on water tree in XLPE cable insulation, IEEE International Symposium, Toronto, 1990.

[11] EPRI EL-7479, Proceeding: water treeing and aging, 1990 EPRI workshop, EPRI, 1991.
[12] M. Mashikian, E. Dorison and N. Qako, "Partial Discharge Location as a Cable Operating Tool", REE, Vol.2, 1997.
[13] E. Pultrum and T. Aabo, "Diagnostic Testing on Cable System", Pennsylvania Electric Association T&D Committee Meeting, 1996.
[14] N. Ahmed and N. Srinivas, "On-line Partial Discharge Detection in Cables", IEEE Trans. On Dielectric and Electr. Insul., Vol. 5, No. 2, 1998.
[15] J.M. Braun, D.J. Horrocks, J.P. Levine and H.G. Sedding, "Development of on-site Partial Discharge Testing for Transmission Class Cable, 1994 T&D Conference, Chicago, 1994.
[16] F.H. Kreuger, "Partial Discharge Part XVIII", IEEE Electr. Insul. Magazine, November, 1993, p.p.14-24.
[17] S. Boggs,"Partial Discharge XXII", IEEE Electr. Insul. Magazine, January ,1996, p.p.9-16.

LIMITATIONS OF THE ARRHENIUS METHODOLOGY

Kenneth T. Gillen, Mat Celina and Roger L. Clough
Sandia National Laboratories, Albuquerque, NM 87185-1407

ABSTRACT

The Arrhenius methodology has been utilized for many years to predict polymer lifetimes in various applications. Unfortunately, there are numerous potential limitations associated with this methodology, many of which can lead to non-Arrhenius behavior. This paper will review several of these limitations, including a brief mention of diffusion-limited oxidation (DLO) effects and a more extensive discussion of the implication of changes in the effective Arrhenius activation energy E_a or in the dominant reactions as the temperature changes. Changes in E_a or in the dominant reactions with temperature can happen for any material, making extrapolations beyond the experimental temperature range problematic. Unfortunately, when mechanistic changes occur, they invariably result in a reduction in effective Arrhenius activation energy, leading to lower than expected material lifetimes. Thus it is critically important to derive methods for testing the Arrhenius extrapolation assumption. One approach that we have developed involves ultrasensitive oxygen consumption measurements. Results from the application of this approach will be reviewed.

INTRODUCTION

The Arrhenius methodology is commonly used to analyze thermal aging data and to extrapolate the data to temperatures outside the range of experimental temperatures. In nuclear power plants, it has been used extensively for polymeric materials and components both as a means of simulating degradation caused by decades of ambient aging and as a method for compressing time scales during LOCA and post-LOCA simulations. In this paper, we describe some of the problems that can result in non-Arrhenius behavior, potentially leading to apparent changes in the Arrhenius activation energy E_a with temperature. Since changes in E_a with temperature can significantly influence predicted lifetimes at temperatures below the lowest experimental conditions used in the Arrhenius analysis, methods are needed for determining whether the E_a changes in the extrapolation region. For polymers that are dominated by oxidation effects, we have introduced the first approach capable of achieving this objective. It is based on the use of ultrasensitive oxygen consumption measurements. For the interested reader, more detailed discussions on the problems associated with the Arrhenius approach and on the use of the ultrasensitive oxygen consumption method to test the Arrhenius extrapolation assumption have been published previously [1-2].

RESULTS AND DISCUSSION

Whenever oxygen is available during the aging of polymeric materials, oxidation chemistry typically dominates the degradation. For the simplest possible example, suppose a polymer *P* chemically reacts directly with oxygen dissolved in the polymer, leading to a degradation product *D*. In chemical kinetic terms, we can write this reaction as

$$P + O_2 \xrightarrow{k} D \tag{1}$$

where classical chemical rate theory gives the rate constant k in terms of E_a, the absolute temperature T and the universal gas constant R as

$$k \propto \exp\left[\frac{-E_a}{RT}\right] \tag{2}$$

Since mechanical properties are typically destroyed after oxidation of 1-2% of the polymer, the concentration of *P* will remain essentially unchanged during the degradation. This leads to the following expression for the rate of oxygen consumption and, equivalently, the rate of growth of the degradation product *D*

$$\frac{dO_2}{dt} = \frac{dD}{dt} = k[O_2][P] = k' = A\exp\left[\frac{-E_a}{RT}\right] \tag{3}$$

Equation (3) implies that the rate of degradation and the rate of oxygen consumption will be given by the same Arrhenius dependence on temperature and that this dependence will not change as the temperature is changed (E_a remains constant). If we therefore measure failure times at various aging temperatures for a property related to the buildup of degradation products and plot the log of the failure time versus inverse absolute temperature, we would expect linear behavior. Figure 1 shows such a plot for an EPDM material. In this plot, the induction (failure) times for several properties are in agreement and consistent with Arrhenius behavior (the E_a of 116 kJ/mol is derived from the slope of the line through the experimental results). From the figure, it is clear that the experimental time required for obtaining data at the lowest temperature probed by conventional measurements (111°C) is approximately 2 years. To make predictions at lower temperatures, it is assumed that the Arrhenius behavior remains constant, so that the linear behavior can be extrapolated (dashed line). This leads to a prediction of a 55,000-year lifetime at 25°C. Although a long lifetime is predicted at room temperature from the extrapolation shown in Fig. 1, it is clear that the distance of extrapolation is very large relative to the data range. This means that a drop in E_a below 110°C could have a profound effect on the extrapolated prediction. Thus, without a method for determining whether E_a remains unchanged, little confidence exists in such extrapolations.

It turns out that there are numerous phenomena that can lead to changes in E_a as the temperature changes [1]. Perhaps the easiest to understand comes from the fact that the oxidation chemistry underlying degradation is seldom as simple as that described by eqs. (1) – (3). In fact, the simplest realistic kinetic scheme for the oxidation of stabilized polymers is given by the following set of chemical reactions [1,3,4]

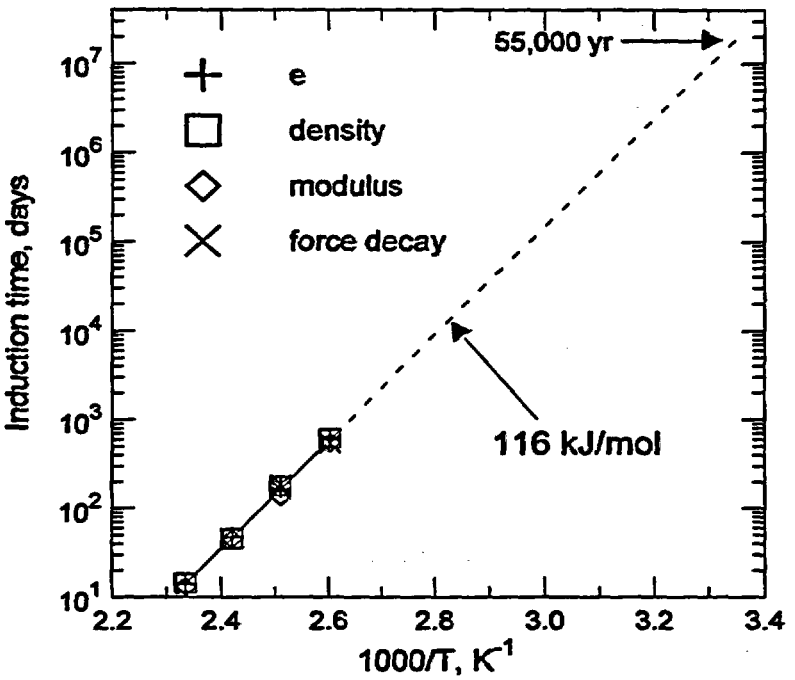

Figure 1. Arrhenius plot of the log of the induction times for the indicated experimental variables versus the inverse absolute aging temperature for an EPDM seal material. The data show Arrhenius behavior with an E_a of 116 kJ/mol. An extrapolation of this behavior (dashed line) to 23°C predicts a room temperature lifetime of 55,000 years.

Scheme 1. Classical oxidation scheme.

Initiation	$\text{Polymer} \xrightarrow{k_1} \text{R}\bullet$
Propagation	$\text{R}\bullet + \text{O}_2 \xrightarrow{k_2} \text{RO}_2\bullet$
Propagation	$\text{RO}_2\bullet \xrightarrow{k_3 = k_3'(\text{RH})} \text{RO}_2\text{H} + \text{R}\bullet$
Termination	$\text{RO}_2\bullet \xrightarrow{k_4 = k_4'(\text{AH})} \text{D}_4\,(\text{Degradation Product})$
Termination	$\text{R}\bullet \xrightarrow{k_5 = k_5'(\text{AH})} \text{D}_5\,(\text{Degradation Product})$
Branching	$\text{RO}_2\text{H} \xrightarrow{k_6} 2\text{R}\bullet + \text{ROH} + \text{HOH}$

Although this scheme has similarities to the earlier scheme (O_2 is used up by the second reaction eventually resulting in the creation of degradation products D_4 and D_5), kinetic analysis leads to very different conclusions concerning the constancy of E_a. By applying steady-state analyses to the free radical species and ROOH, one obtains [1]

$$\phi = \frac{d[O_2]}{dt} = \frac{C_1[O_2]}{1 + C_2[O_2]} \tag{4}$$

where

$$C_1 = \frac{k_1 k_2}{k_5} \tag{5}$$

$$C_2 = \frac{k_2(k_4 - 2k_3)}{k_5(k_3 + k_4)} \tag{6}$$

At low concentrations of O_2

$$\frac{dO_2}{dt} = \frac{k_1 k_2 [O_2]}{k_5} \sim \frac{\exp\left[\frac{-E_1}{RT}\right]\exp\left[\frac{-E_2}{RT}\right]\exp\left[\frac{-\Delta H_s}{RT}\right]}{\exp\left[\frac{-E_5}{RT}\right]} \tag{7}$$

implying that the effective activation energy E_{eff} is given by

$$E_{eff} = E_1 + E_2 + \Delta H_s - E_5 \tag{8}$$

where ΔH_s is the heat of solution for oxygen in the polymer. It is clear from eq. (8) that a constant effective value of E_a is predicted for low oxygen concentrations. On the other hand, at high oxygen concentrations, eqs. (4) – (6) lead to

$$\frac{dO_2}{dt} = \frac{k_1(k_4 + k_3)}{(k_4 - 2k_3)} \tag{9}$$

which, in general, predicts that the effective E_a will change with temperature. In addition, kinetic analysis of the rate of product formation gives for example

$$\frac{dD_4}{dt} = \left[\frac{k_4}{k_4 + k_3}\right]\frac{dO_2}{dt} \tag{10}$$

This result predicts not only non-constant values of E_a for the degradation product D_4 regardless of whether the oxygen concentration is low or high, but also differences in the values of E_a dependent upon which species (O_2 consumption, D_4 production) are being followed.

Although the above discussion indicates that non-Arrhenius behavior and differing values of E_a for different degradation variables might be anticipated from more realistic kinetic schemes, eqs. (9) and (10) show that the changes of the effective E_a with temperature may not be large if E_4 is similar to E_3 and E_1 is considerably larger than either of the other two. This is in fact often the case, implying that the non-Arrhenius character may only show up as a gradual change with temperature. Nonetheless, given the large extrapolations often carried out, even a slowly changing E_a may have profound effects on extrapolated predictions.

Another important mechanism that can lead to non-Arrhenius behavior involves diffusion-limited oxidation (DLO). At the high temperatures typically used for accelerated laboratory experiments, the consumption of dissolved oxygen in the polymer will often occur faster than the oxygen can be resupplied by diffusion from the surrounding air-atmosphere. Although oxidation at the sample surface will be at equilibrium and unaffected by the presence of DLO effects, the amount of oxidation will drop at positions deeper within the sample. Important DLO effects are commonly observed for typical, air-oven aging studies of numerous elastomers, as illustrated by comprehensive studies on SBR [5], nitrile [6], neoprene [5,6], EPDM [7,8] and hypalon [9]. Even though the importance of DLO effects has a complex dependence on time and temperature, these studies show that tensile elongation measurements are typically consistent with Arrhenius behavior. The reason stems from the fact that oxidative degradation of most elastomers leads to hardening of the material. If DLO effects are present, the hardening is greatest at the sample surface. Cracks would be expected to initiate at the hardened surface during tensile testing. Once initiated, if these cracks immediately propagate through the material, the tensile elongation will be determined by the surface degradation, which represents the true equilibrium oxidation rate (uninfluenced by DLO effects). Therefore, quite accidentally, tensile elongation measurements often lead to Arrhenius behavior even in the presence of important DLO effects. If cracks do not immediately propagate through the material, non-Arrhenius behavior can often be observed, as noted for a Kerite hypalon jacket material [9]. Similarly, properties that depend on the entire sample cross-section will not be amenable to Arrhenius analyses when DLO effects are important [2, 9].

Several other mechanisms can lead to important non-Arrhenius behavior. If, for instance, two distinct oxidation pathways underlie the degradation of a material, the mechanism of lower E_a will become dominant when the temperature drops sufficiently. This lower E_a mechanism will not be apparent until the Arrhenius degradation plot begins to curve at lower temperatures, therefore representing an unanticipated surprise if the curvature starts in the extrapolation region. Another problem can occur when the data region or the extrapolation range encompasses a polymer transition region, such as the crystalline melting point region characteristic of many EPDM and crosslinked polyolefin materials [1]. Several non-Arrhenius complications can arise from antioxidant interactions, caused by such things as solubility changes with temperature and various evaporation effects [10,11].

From the above discussion, it is apparent that many possible phenomena can result in non-Arrhenius behavior. It is therefore clear that methods need to be developed to provide more confidence in extrapolated predictions. We will describe one viable method of accomplishing this, involving the use of ultrasensitive oxygen consumption measurements, after we briefly review the concept of time-temperature superposition. The formalism used for time-temperature superposition analysis is needed and is ideally suited for discussing the ultrasensitive oxygen consumption approach.

Earlier in Fig. 1, we used one processed point (the induction time) per temperature to test the Arrhenius equation. This means that most of the data generated versus time at each temperature were eliminated from the analysis. However, if the rate of degradation is constant at each aging temperature, an important consequence is the expectation that the time-dependent degradation curves at any two temperatures will be related by a constant multiplicative factor. This means that the curves at different temperatures should have the same shape when plotted versus the log of the aging time. Normalized elongation results for a nitrile rubber at five different aging temperatures [2] are consistent with this picture, as seen in Fig. 2. Instead of selecting only one point per temperature for the analysis, we apply the principal of time-temperature superposition [1,2,9,12]. We first select the lowest temperature (64.5°C) as the reference temperature. Then for each set of data at a higher temperature T, we multiply the experimental times by a constant shift factor, a_T chosen to give the best overall superposition with the reference temperature data ($a_T = 1$ at the reference temperature). The results of this procedure are shown in Fig. 3, where the time-axis gives the superposed results at the reference temperature. Unlike the analysis given in Fig. 1, this approach utilizes every raw experimental point and yields empirical shift factors that can then be tested by models such as the Arrhenius. If, in fact the empirical shift factors are consistent with the Arrhenius equation, then they would be given by

$$a_T = \exp\left(\frac{1}{T_{ref}} - \frac{1}{T}\right) \tag{11}$$

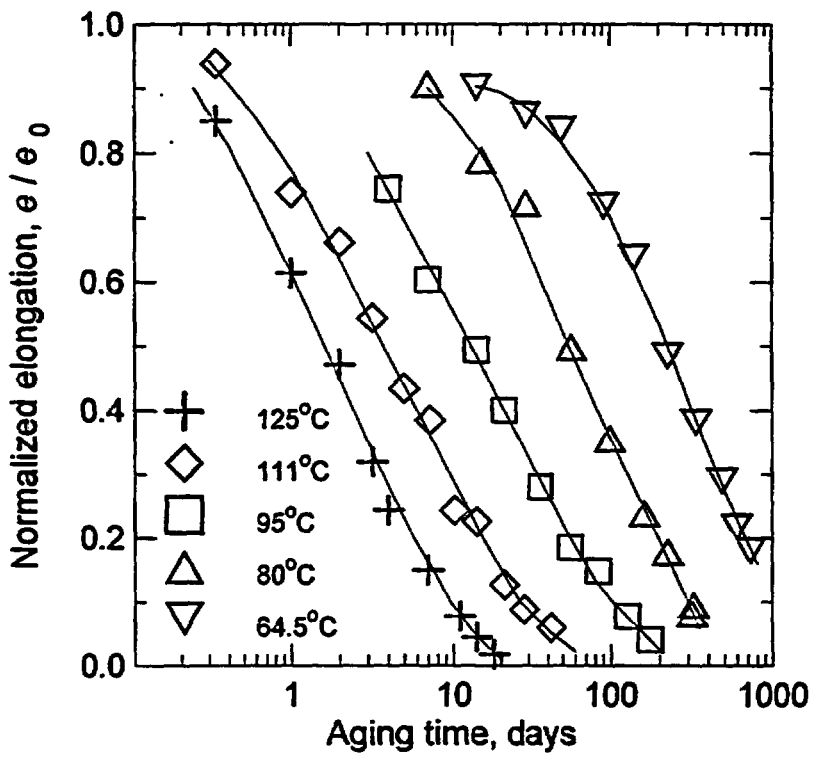

Figure 2. Ultimate tensile elongation (e) of a nitrile rubber normalized to its unaged value (e_0) versus air-oven aging time and temperature.

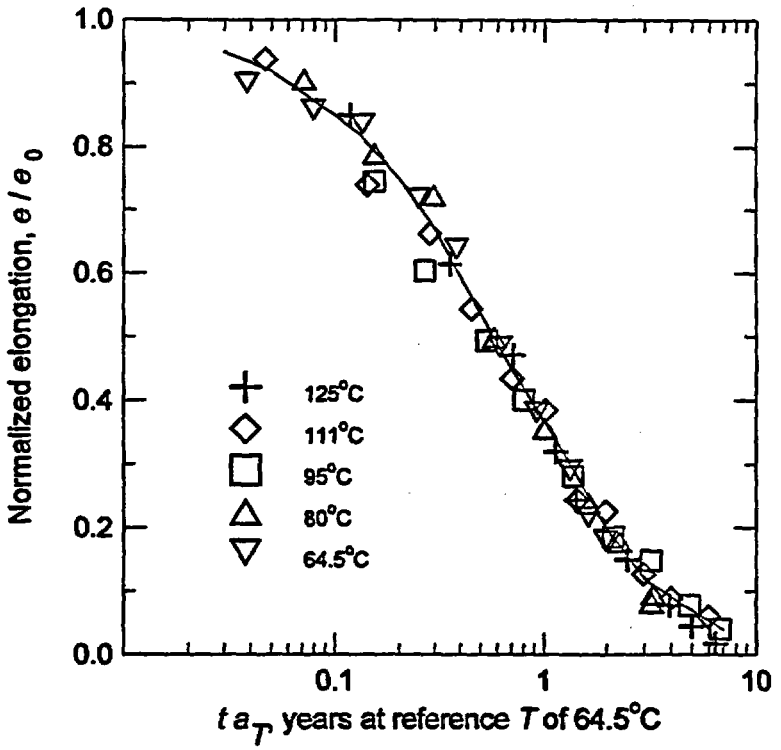

Figure 3. Time-temperature superposition of the data from Fig. 2 using empirically derived shift factors, a_T.

This would predict that a plot of log (a_T) versus inverse temperature would give linear behavior. When the empirical shift factors are plotted in this fashion in Fig. 4, such linear behavior is in fact observed, with a corresponding E_a of approximately 90 kJ/mol determined from the slope. To make predictions at temperatures lower than 64.5°C ($a_T = 1$), the normal procedure would then be to extrapolate (dashed line extension). For instance the extrapolated a_T at 22°C would be ~0.01, implying a lifetime approximately 100 times longer than at 64.5°C.

Given the distinct possibility that non-Arrhenius effects will be important for the extrapolations shown by the dashed lines in Figs. 1 and 4, it would be extremely useful to have methods that give more confidence in any attempted extrapolations. At the lowest temperatures utilized for conventional measurements (111°C for the EPDM material, 64.5°C for the nitrile material), several years of aging were required to see measurable property changes. Thus any technique that accesses lower temperatures must be an ultrasensitive monitor of the degradation. In addition, it needs to measure a property closely correlated to the chemistry dominating the mechanical degradation. One approach that we have developed for thermally oxidized materials involves ultrasensitive oxygen consumption measurements based on gas chromatography techniques [2]. With experimental care, this approach results in sensitivity capabilities of better than 10^{-13} mol/g/s, which typically allows access to temperatures corresponding to expected mechanical property lifetimes of greater than 100 years. One might expect the oxygen consumption rate to be closely related to the tensile elongation since 1) oxidation chemistry is expected to dominate the degradation and 2) surface oxidation leads to the initiation of cracks that quickly propagate and therefore determine the elongation.

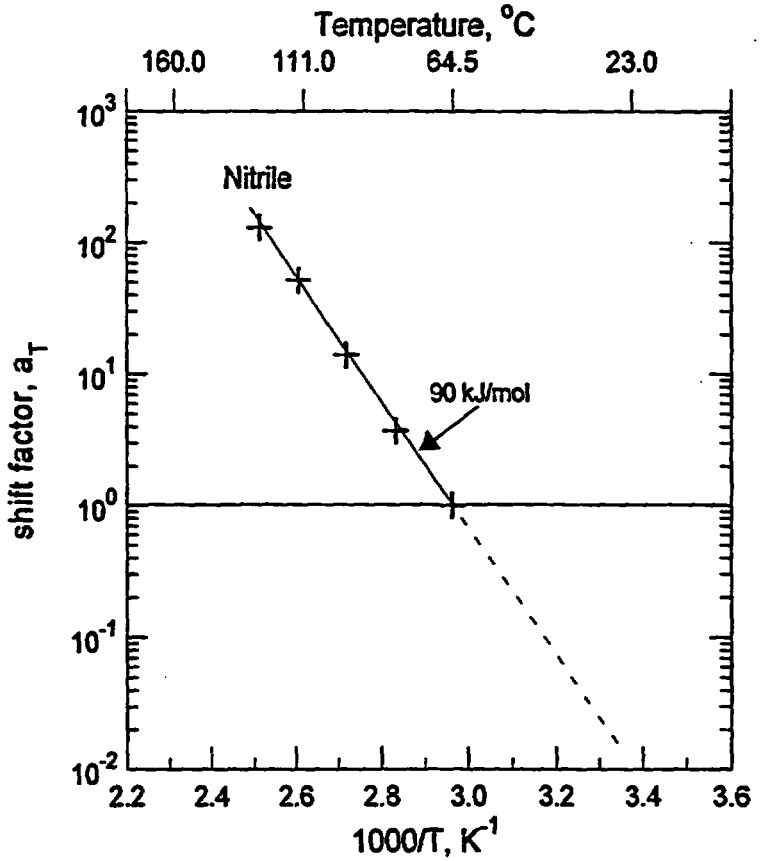

Figure 4. Arrhenius plot of the empirical values of a_T used to achieve the superposition shown in Fig. 3.

To confirm this correlation for the nitrile material, the oxygen consumption rate measurements (Fig. 5) are made at temperatures overlapping the temperatures used for the mechanical property experiments (96°C, 80°C and 72°C) as well as at lower temperatures in the extrapolation region (52°C, 40°C and 23°C). The oxygen consumption results of Fig. 5 were integrated and then time-temperature superposed at 64.5°C so that the shift factors could be directly compared with the mechanical property shift factors given earlier in Fig. 4. The resulting oxygen consumption shift factors are plotted as the triangles shown for the nitrile data on Fig. 6. The results show that the higher temperature oxygen consumption results are consistent with the mechanical property shift values, offering evidence that the two properties are dependent upon the same underlying chemistry. Since the oxygen consumption shift factors at the three lower temperatures are reasonably consistent with an unchanged Arrhenius slope (dashed line) in the extrapolation region, these results offer increased confidence in the validity of the extrapolation.

Similar oxygen consumption measurements spanning the temperature region where conventional measurements were made and continuing into the lower temperature "extrapolation regions" were made for the EPDM material (left set of triangles in Fig. 6) and for a neoprene material (triangles in Fig. 7). For the neoprene material, the results indicate that the Arrhenius behavior determined at high temperatures can be extrapolated with confidence all the way down to room temperature. For the EPDM material, the

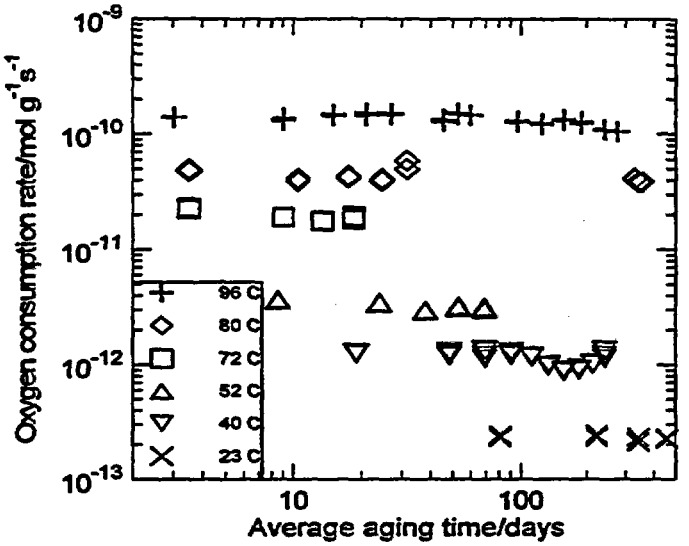

Figure 5. Oxygen consumption rates for the nitrile rubber as a function of time at the indicated temperatures.

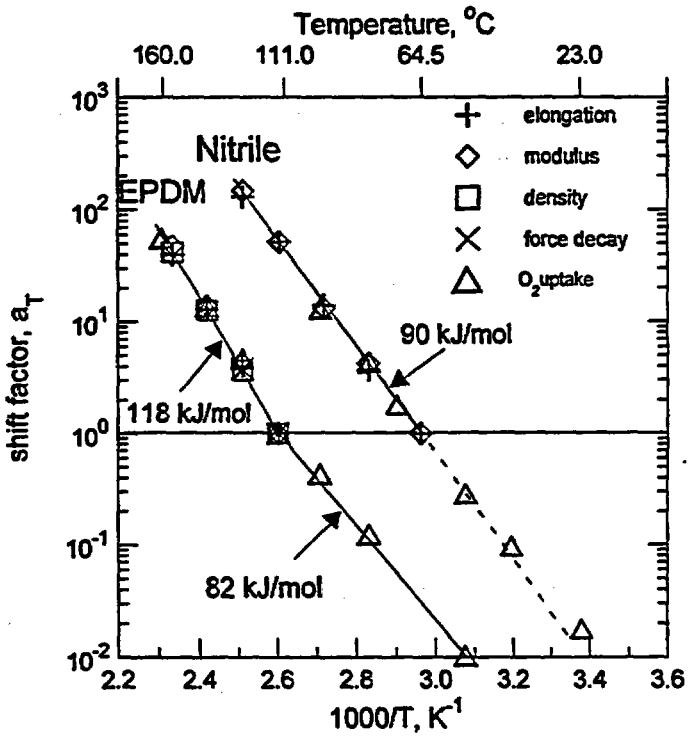

Figure 6. Arrhenius plot of the empirical values of a_T for the indicated conventional parameters and for oxygen consumption measurements (triangles) for the EPDM and the nitrile materials. The results are normalized ($a_T = 1$) to a reference temperature of 64.5°C for nitrile and a reference temperature of 111°C for EPDM.

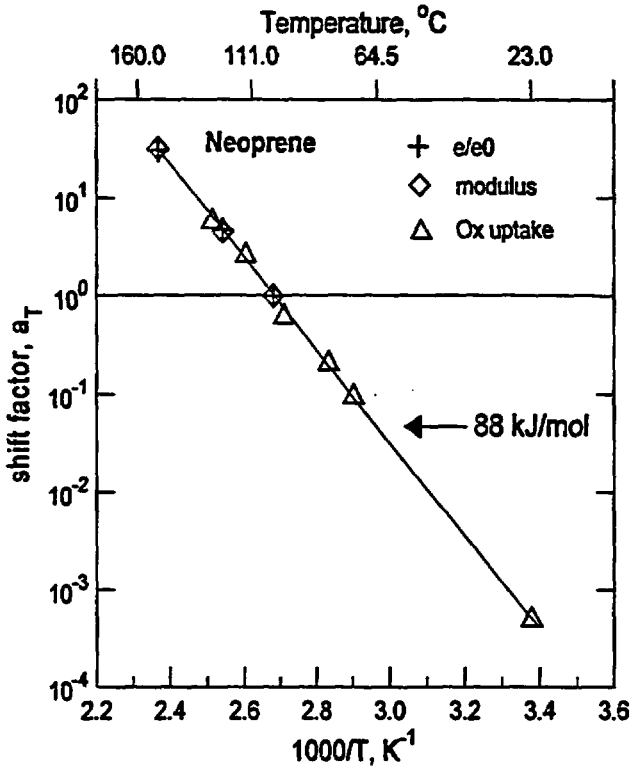

Figure 7. Arrhenius plot of the empirical values of a_T for the indicated conventional parameters and for oxygen consumption measurements (triangles) for a neoprene material.

oxygen consumption measurements at 111°C and above give shift factors consistent with the conventional results ($E_a \sim 118$ kJ/mol), but a change in mechanism leads to an activation energy reduction to ~ 82 kJ/mol below 111°C. Therefore, the straight-line extrapolation used in Fig. 1 is not warranted and the predicted EPDM lifetime is significantly reduced.

ACKNOWLEDGMENT

Sandia is a multiprogram laboratory operated by Sandia Corporation, a Lockheed Martin Company, for the United States Department of Energy under Contract DE-AC04-94AL85000.

REFERENCES

1. K. T. Gillen, M. Celina, R. L. Clough and J. Wise, Trends in Polymer Science, Vol 5, No. 8, 250 (August, 1997).
2. J. Wise, K. T. Gillen and R. L. Clough, Polym. Degrad. & Stabil., 49, 403 (1995).
3. J. L. Bolland, Proc. R. Soc. London, A186, 218 (1946).
4. L. Bateman, Q. Rev. (London), 8, 147 (1954).

5. R. L. Clough and K. T. Gillen, Polym. Degrad. Stabil., 38, 47 (1992).
6. J. Wise, K. T. Gillen and R. L. Clough, Polymer, 38, 1929 (1997).
7. B. Mattson, B. Stenberg, K. T. Gillen, R. L. Clough and E. Ostman, Polym. Degrad. Stabil., 41, 211 (1993).
8. K. T. Gillen, M. Celina, R. L. Clough, G. M. Malone, M. R. Keenan and J. Wise, "New Methods for Predicting Lifetimes in Weapons. Part 1: Ultrasensitive Oxygen Consumption Measurements to Predict the Lifetime of EPDM O-Rings", SAND98-1942 (September, 1998).
9. K. T. Gillen, R. L. Clough, M. Celina, J. Wise and G. M. Malone, Proceedings of the 23rd Water Reactor Safety Information Meeting, NUREG/CP-0149, Vol. 3, p. 133 (1995).
10. N. C. Billingham in Atmospheric Oxidation and Antioxidants, Vol. II, G. Scott, Ed., Elsevier, p. 219 (1993).
11. N. C. Billingham in Oxidation Inhibition in Organic Materials, Vol. II, J. Pospisil and P. P. Klemchuk, Eds., CRC Press, p. 249 (1990).
12. J. D. Ferry, Viscoelastic Properties of Polymers, 2nd Ed., Wiley, New York, 1970.

INSIGHTS AND RESULTS FROM EPRI CABLE AGING RESEARCH PROGRAMS

John Hutchinson, Plant Support Engineering, Electric Power Research Institute
1300 Harris Boulevard, Charlotte, NC 28262

Gary J. Toman, Nutherm International, Inc.
501 South Eleventh Street, Mt. Vernon, IL 62864

Introduction

The Electric Power Research Institute (EPRI) has been developing aging management techniques for environmentally qualified components for the last 14 years. This paper discusses the insights and results from EPRI cable research activities and some of the additional efforts that still remain to allow implementation of condition monitoring for cables. Management of aging of cables may be approached in many ways such as analysis of plant environments, identification and control of hot spots (adverse-localized-equipment environments), and application of condition monitoring ranging from visual/tactile evaluation through sophisticated physical, chemical, or electrical testing. EPRI's more recent activities in these areas are discussed in this overview.

Identification of Adverse-Localized-Equipment Environments

EPRI is developing an Adverse-Localized-Equipment-Environment Guideline for use in identifying environments that can have a significant adverse effect on the aging of components. Adverse-localized equipment-environments are commonly called "hot spots." However, hot spots frequently are thought of as only severe thermal environments, which is too limiting. Localized-adverse radiation, chemical, moisture, and vibration conditions are also of concern. Hence, adverse-localized-equipment environment is used rather than hot spot.

The purposes of the guideline are:

- To establish criteria that define adverse-localized-equipment environments for nuclear plant equipment in general, and specifically for cables and terminations, and
- To develop methods for identifying and documenting adverse-localized-equipment environments to allow appropriate actions to manage the condition to be performed.

An adverse-localized-equipment environment is one that is a significant variation from the specified operating conditions for the equipment. Variations that cause more severe conditions are only of concern. Operating conditions are defined as service conditions, including normal and error-induced conditions, prior to the start of a design basis accident or earthquake.

The guideline first presents a brief background of the historical aspects of the issue. Summaries of related industry and regulatory documents are included. An overview of the sources and causes of adverse-localized-equipment environments are also discussed.

The guideline then presents a systematic approach to managing adverse-localized-equipment environments. The systematic approach emphasizes identifying and refining practices already in place for discovering, correcting, and mitigating adverse-localized environments. Most utilities have already implemented some practices that can help provide reasonable assurance that adverse-localized environments do not pose a significant safety or operational concern.

Once past and on-going efforts to manage adverse-localized-equipment environments are identified and refined, the systematic approach then outlines methods for implementing additional activities for managing these environments. The guideline identifies visual inspections as an effective technique for identifying and managing adverse-localized-equipment environments. The guideline gives two strategies for conducting visual inspections: The *focused approach* and the *general area approach*. In the focused approach, only equipment of a particular type or having specific programmatic requirements (e.g., requiring environmental qualification, or important to safety) is visually inspected based upon analysis that shows that this equipment has higher susceptibility to, or greater consequences of, localized environment induced failure or degradation. In the general area approach, an entire area of the plant is inspected, without prior determination of the importance of the equipment to plant safety or reliability within the area. The guideline also contains an appendix with guidance on how to conduct visual inspections.

Finally, the guideline discusses methods that prevent, correct, and mitigate adverse-localized-equipment environments. Case studies and examples from utilities are also presented.

The report concludes that while many utilities have performed multiple activities to detect, prevent, correct or mitigate adverse-localized-equipment environments, these activities have generally been documented separately and in varying formats. Therefore, the results are often not readily usable when further questions arise. By implementing a systematic approach for documenting adverse-localized environments, utilities can fully benefit from processes they have already implemented and will have a consistent and complete listing of adverse-localized-equipment environments.

Correlation of Natural to Artificial Aging

Thirteen years ago, EPRI embarked on a program in which natural aging would be compared to accelerated aging to validate the Arrhenius thermal-aging model. At the start of the program in 1985, cables and component specimens were placed in 9 plants at 15 locations with environments ranging from 21°C (70°F) to 61°C (142°F). Later, additional cables of the same type as were used in the Sandia qualification research programs for the U.S. NRC were placed at specific sites to allow coordination between the two programs. A last set of cables was placed in a plant location with even higher thermal conditions to provide aging information earlier than the cooler locations would. The cables in the program include Rockbestos with cross-linked polyethylene insulation and neoprene jacket, Okonite with ethylene propylene rubber (EPR) insulation and chlorosulfonated polyethylene (CSPE) jacket, Kerite with EPR insulation and CSPE jacket, and BIW with EPR insulation and CSPE jacket. After 13 years of cable specimen natural exposure in environments up to 61°C, only the neoprene jackets on certain cables are showing signs of limited aging. To date, the results from the natural exposure have been as expected and no surprises have occurred.

In addition to natural aging, accelerated aging has been performed on cable specimens. The naturally aged specimens that have been removed from the plants and the accelerated aged specimens have been subjected to tensile testing and density measurements. As most cable polymers age, oxidative reactions tend to make elongation-at-break decrease and density increase. While the change in elongation-at-break is more dramatic, density can be measured with good precision such that relatively small changes can be used to identify significant differences in aging. Density tests can be performed using a few milligrams of material..

While the goal of the program was to evaluate natural versus artificial aging, the accelerated aging portion of the program has produced correlations of elongation-at break with density, which is of interest from a condition monitoring stand point. Knowing the correlation of density to elongation-at break allows one to determine the expected elongation when only the density is known. Therefore, a small sample subjected to density testing will provide an indication of the remaining elongation, the more common aging evaluation technique. Given that elongation-at-break testing is destructive, removal of a small density specimen that would not destroy the cable represents an essentially non-destructive test.

Figure 1 provides a correlation of the elongation-at break to density for neoprene when aging is performed at 125°C. An orderly curve exists for both elongation-at break and density. A 75 % drop in relative elongation correlates with a 3.5% increase in density. The initial density is 1.6489 g/cm^3 and the final density is 1.7071 g/cm^3. Therefore, if one measured a density of 1.68 g/cm^3, the expected elongation-at-break from Figure 1 would be approximately 200%, which indicates that the neoprene jacket is still very flexible. Given that neoprene is much more sensitive to thermal aging than the underlying cross-linked polyethylene, one could infer that the cross-linked polyethylene insulation has not aged significantly.

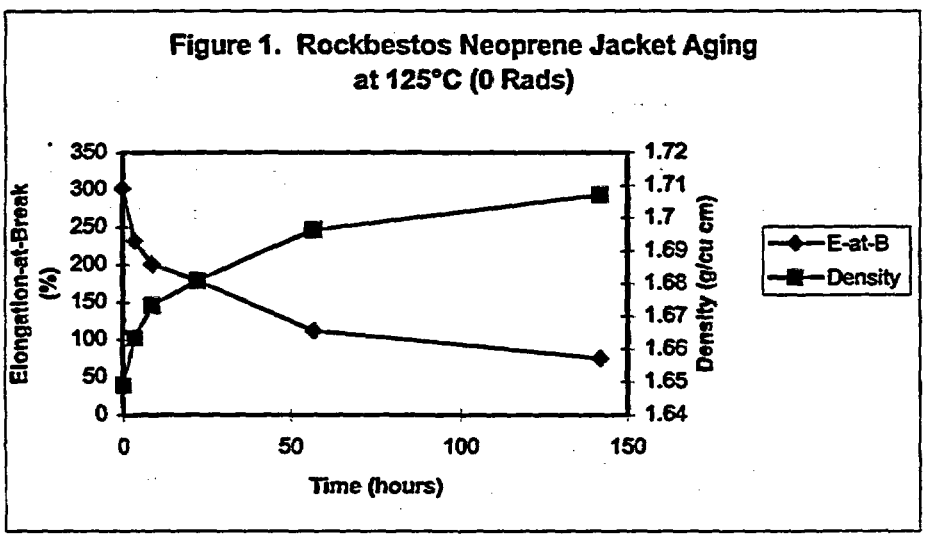

Figure 2 provides the same type of correlation for chlorosulfonated polyethylene (Hypalon) when aging is performed at 125°C. A 50% drop in elongation-at-break correlates with a 3.7 % increase in density.

While the neoprene material had a higher initial elongation-at-break, the Hypalon's elongation-at-break is higher after 140 hours at 125°C than that of neoprene (120% versus 75%). This coincides with the fact that Hypalon ages more slowly than neoprene and can withstand elevated temperatures for longer periods.

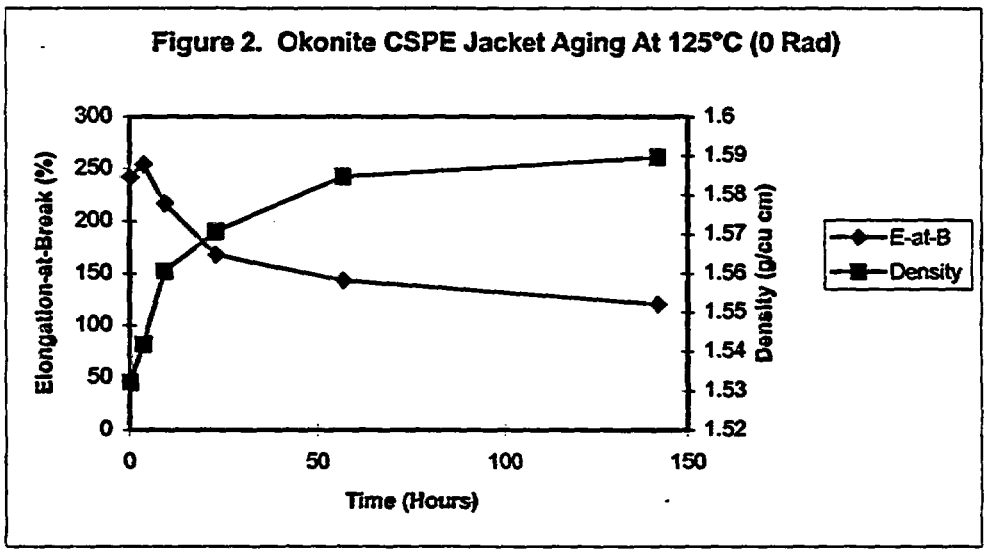

The only material that is showing detectable changes at the plant locations with elevated temperatures is the neoprene jacket material. Figure 3 shows the neoprene data for plant site that has a normal temperature of approximately 131°F. The actual density and the actual elongation-at break are plotted as is the expected elongation-at break taken from Figure 1 based on the density measurements. The expected elongation-at break results are conservative for the samples removed at years 1.3, 2.8 and 3.8. The expected elongation-at break is essentially the same as the actual at year 5.5. These data indicate that the correlation of density to elongation-at break from accelerated aging provides reasonable results for evaluating natural aging. However, persons generating density data from specimens generated by high rate accelerated aging must be careful. The density measurement must be based on material taken from the outer surface of the specimen. Otherwise the resulting density will be based on material that is

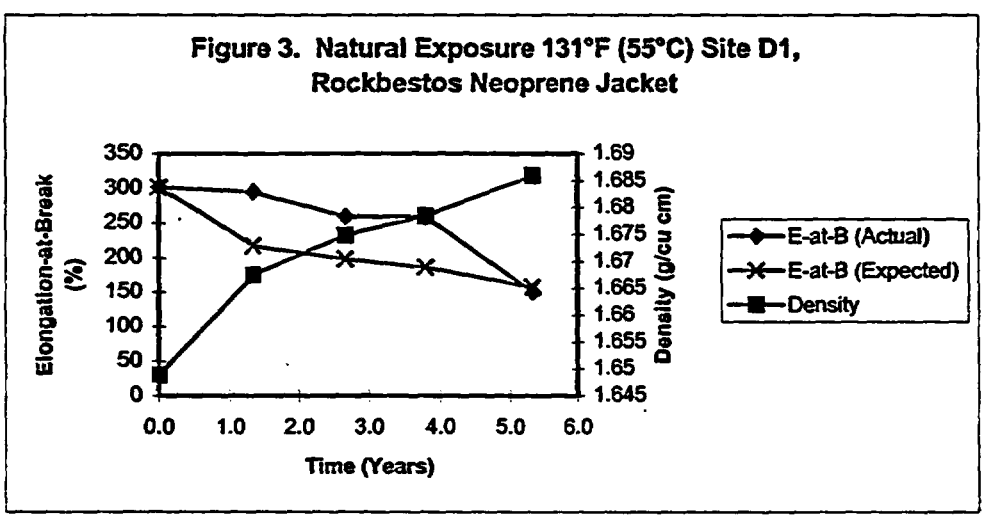

relatively unaged because of oxygen diffusion limited aging of subsurface regions. The resulting density curve will not be representative of the aging occurring at the surface of the material where oxygen diffusion is less restricted. The resulting density curve would be non-conservative.

While the EPRI Natural Versus Artificial Aging Program was intended primarily as a means of verifying the conservative nature of the Arrhenius aging model, large amounts of data have been generated from the natural and accelerated aged specimens. This portion of the discussion has shown one use of the data for evaluating the correlation between elongation-at break and density, and how that correlation may be used to evaluate naturally aged materials.

Condition Monitoring of Cables

IAEA Round Robin Evaluation of Cable Condition Monitoring Techniques

For condition monitoring techniques to be useful, the results should not require all testing to be performed by one laboratory or a specific set of technicians. The results of condition monitoring tests performed by different laboratories and technicians should be comparable. To determine the repeatability of results when tests are performed by different laboratories and to identify where improvements are possible, the International Atomic Energy Agency sponsored round robin testing of unaged and aged cable specimens of cable types used throughout the world. EPRI participated in this project. The monitoring methods that were evaluated included elongation-at break, Indenter modulus, oxidation induction time, oxidation induction temperature, and thermo-gravametric analysis. Twelve international laboratories participated in the effort. Each laboratory performed only those tests within their expertise and equipment capabilities.

There were 15 cable types in the program. Tests were performed on both jackets and insulations. Table 1 lists the jacket and insulation materials included in the program and the thermal aging temperature used in accelerated aging. The period used for accelerated aging was 1008 hours. Only one aging period was performed.

Table 1. Materials and Aging Temperatures

Material Type	Aging Temperature (°C)
Polyvinyl Chloride (PVC)	120
Polyethylene (PE)	100
Cross-linked Polyethylene (XLPE)	110
Ethylene-propylene rubber (EPR)	120
Ethylene-propylene diene rubber (EPDM)	120
Silicone Rubber (SiR)	120
Ethylene Vinyl Acetate (EVA)	120

The goal was not to age any of the materials to the equivalent of a specific condition. Rather, the goal was to have unaged and partially aged cable specimens for each cable type with the entire set of specimens for a cable type being aged to the same condition.

To help assure uniform results, a basic protocol was provided for each of the condition monitoring tests to be performed. The depth of detail given at the start of the test program was thought to be sufficient to provide sufficient direction for the performance of the tests.

Upon gathering the results of the tests, the variations between laboratory results were fairly large for many of the test types. During the week of June 18, 1998, representatives of each of the laboratories met in Bordeaux, France to identify the causes for the differences in results and, where practical, refine the data through further evaluation of the test records.

Elongation-at-Break

Elongation-at-break testing is considered one of the primary means of evaluating the aging of cable polymers. One would expect that protocols for testing cable materials would be well established and variations between laboratories would not be great. In general, a ±10% variation between results of a set of tests would be considered to be good and a ±20% variation in results would not be unusual. Therefore, reasonable reproducibility would have occurred had the variations between laboratories been between ±10 and ±20%. Table 2 summarizes the factors between low and high values for the tests of each specimen type.

Table 2. Evaluation of Elongation-at-Break Results for Unaged Cable Specimens

Factor Between Lowest and Highest Average Result for All Laboratories Reporting Results	Number of Sets of Results in the Range
1.0 to 1.2 (Approximately 0 to ±10 % variation)	1
1.2 to 1.4 (Approximately ±10 to ±20 % variation)	7
1.4 to 1.6 (Approximately ±20 to ±30 % variation)	5
1.6 to 1.8 (Approximately ±30 to ±40 % variation)	2
1.8 to 2.0 (Approximately ±40 to ±50 % variation)	6
2.0 to 2.4 (Approximately ±50 to ±70 % variation)	4
2.4 to 2.8(Approximately ±70 to ±90 % variation)	4

The results for only one set of specimens was in the ±10 % range and the results for another 7 sets of specimens were in the ±10 to ±20 % range. The remaining 21 specimen sets had variations between ±20% to ±90 %.

Discussions among the researchers performing elongation-at-break tests identified a number of issues beyond those stated in the original test protocol that could effect results. The most important of these are:

- How elongation was measured (e.g., between marks on the specimen, between grips, with extensiometers),
- Type of grip used (e.g., mechanical, pneumatic) and the gripping force,
- The point at which the break occurred on each pull. If break occurs in the grip, the value should be excluded from the results,
- The gage length at the start of the pull (section length of zero elongation),

- The ambient temperature and humidity during testing (e.g., One lab was located near the equator and the temperature caused much higher elongation-at-break results. PVC specimens stored in elevated humidity also caused higher elongation results.), and
- Crosshead speed.

Because most of the insulation specimens that are removed from power plant applications will be tube specimens, gripping methods are very important. Because of the nature of elongation-at-break testing, very little change in the outcome of these tests is expected from re-evaluation of the data. Retesting would be required to improve repeatability.

Thermal Evaluation Tests

Oxidation induction time (OIT), oxidation induction temperature (OITemp) and thermo-gravimetric analysis (TGA) tests are all thermally based and most of the factors causing variations in results arise from similar problems. Table 3 presents an evaluation in the variations between lowest and highest measurement for OIT.

Table 3. Evaluation of OIT Results for Unaged Cable Specimens

Factor Between Lowest and Highest Average Result for All Laboratories Reporting Results	Number of Sets of Results in the Range
1.0 to 1.2 (Approximately 0 to ±10 % variation)	5
1.2 to 1.4 (Approximately ±10 to ±20 % variation)	2
1.4 to 1.6 (Approximately ±20 to ±30 % variation)	1
1.6 to 1.8 (Approximately ±30 to ±40 % variation)	0
1.8 to 2.0 (Approximately ±40 to ±50 % variation)	1
2.0 to 2.4 (Approximately ±50 to ±70 % variation)	1
3.3	1
7.8	2
29	1

The variation in results for OIT ranged from minimal to extremely large. The researchers performing the thermal tests identified a number of reasons for the variation in results. A key variation related to whether or not the test pan was covered. Even a cover with holes that would allow oxygen to flow to the specimen caused a significant difference in results from an uncovered pan. The recommended solution was not to use covers. Another source of differences related to interpretation of the OIT plot. Some materials had multiple onsets of exothermal reactions. Some test devices had automatic detection software that would identify the first small change as representing the OIT. Some labs used different criteria for determining which onset was the important one. These problems caused significantly different interpretations of OIT with 7.8 to 29 factors between low and high measurements. Another significant problem with the original protocol for the OIT testing was that the test temperatures were too generic such that some of the unaged tests on EVA and XLPE took 13 hours to perform, which is impractical. An additional item for improving the resolution of the thermogram was to set the start of the OIT test as 3 minutes from the point of starting oxygen flow to the specimen.

Similar problems were identified for OITemp and TGA. In addition, some test machinery from different manufacturers is sufficiently different that results between tests performed on different apparatus cannot agree.

Reanalysis of the thermograms will be performed to improve the round robin results. However, variations from differences in pan covers and basic machinery cannot be resolved for this program.

Indenter Modulus

Table 4 presents an evaluation of Indenter results for unaged cables. While the variations in the initial

Table 4. Evaluation of Indenter Results for Unaged Cable Specimens

Factor Between Lowest and Highest Average Result for All Laboratories Reporting Results	Number of Sets of Results in the Range
1.0 to 1.2 (Approximately 0 to ±10 % variation)	13
1.2 to 1.4 (Approximately ±10 to ±20 % variation)	12
1.4 to 1.6 (Approximately ±20 to ±30 % variation)	3
1.6 to 1.8 (Approximately ±30 to ±40 % variation)	1

results are smaller for the Indenter than for the other test methods, evaluation of the variations by the researchers performing Indenter testing determined that the variations could be significantly reduced by using uniform modulus calculation criteria. The Indenter modulus is the slope of the force versus position curve resulting from pressing an anvil against the side of a cable at a constant velocity. These curves are linear in the portion of the curve where the material properties are in the elastic region. The curves for the Indenter plots were evaluated to identify the intervals where linearity would occur and the best upper and lower force limits for the modulus calculation were identified. The data from the tests will be reevaluated to determine the further improvement in repeatability between laboratories that is possible. Some variations in results related to differences in temperature of the specimen at the time of test were also noted.

Conclusions

The IAEA effort identified a number of significant factors for the test protocols that must be defined to allow results from different laboratories to be comparable. Establishing uniform test protocols for cable condition monitoring tests will be important if one laboratory performs the baseline tests establishing the aging characteristics for a cable type, and another performs tests on the cables from the power plant. Understanding the protocols used in performing condition monitoring baseline testing is critical to using the data properly and performing tests of in-plant cable at a later date.

The IAEA will issue a report of the results in early 2000. The report is being included in an overall report on the development of cable condition monitoring practices.

Practical Condition Monitoring Issues

While the in-plant use of cable condition monitoring (CCM) has been relatively limited to date, the Indenter has been used 10 times in U.S. nuclear plants. These efforts have provided some useful insights related to the practicality of use of CCM and problems that each new method will experience.

Introducing CCM to Plant

Plant operators have faith in cable systems, but are wary of letting CCM practitioners disturb cables or perform CCM tests. Anyone wishing to perform CCM must demonstrate that the activities will not adversely effect the cables. The Indenter is non-destructive and often the point at which the probe had been applied to a cable cannot be detected after a few minutes. Yet, lengthy demonstrations and discussions with plant operators and managers are often necessary before one is allowed to proceed.

Many of the CCM tests under development are based on the concept that very small specimens (10 mg) can be removed from cable jackets and insulations without significantly damaging cables with respect to continued service and accident withstand capabilities. The sample removing technique has not yet been developed or proven. EPRI has just begun this work. It is obvious from the Indenter experience, that plant operators and managers will expect very strong proof that sample removal will not have any significant adverse effect on their cables. We expect that a 10CFR 50.59 safety analysis will be required prior to sample removals on active cables in a plant.

Cable Access

Cable systems were not designed with condition monitoring in mind. Because in-service interactions with cables are generally not required, plant designers often put cables in out of the way places. Therefore, cable trays are located overhead, and junction and pull boxes may be located any place that was convenient during construction. Therefore, finding a particular tray or junction box that contains a specific cable is often time consuming even when the basic location is known and even though the trays and junction boxes have identification numbers. Once found, scaffolds and ladders are often needed to allow CCM to proceed. Many plants now require harnesses to be worn during ladder and scaffold work and also require a period of harness training that adds to preparation time.

In addition to being awkwardly located, vertical spacing between trays is often limited with 12 inches or less not being uncommon. Therefore, CCM equipment must fit between the trays and still allow the technician working space.

Often the physical characteristics of the jacket or insulation of a specific cable circuit are of concern. Most cable circuits are not labeled in field runs. If the circuit is located in an identifiable junction box, one may be able to locate a specific circuit through deduction by evaluating the cable type and the conduits in which it runs to the junction box. In trays, the problem is compounded many times even when the circuits are labeled at wall penetrations. In trays, the cables weave around one another. In addition, cable jackets are generally black or gray, many cables of the same configuration are in the same tray, and light levels are often low where CCM is desirable. Therefore, in less than 1 meter along the run of the tray, one can loose track of the cable one wants to test. Passing a ring of plastic or paper (if one has thought ahead) along the length may help trace the cable, but if the tray is full or the cable dives

deeply into a bundle, this may not work. One could apply a radio tracer signal on the conductor and use a radio receiver to find the correct cable. But if one is trying to evaluate a large number of cables, this is time consuming and impractical.

Often, one cannot find a specific cable in a tray. Then, one must test the condition of all cables having the same physical description (e.g., 5 conductor, 12 AWG, Okonite CSPE/EPR). Testing a larger number of cables takes time but may take significantly less time than tracing one specific circuit. The additional data provides more insight regarding the condition of the population of the cables in the tray. In general, unless one is evaluating the cables in a particular location, finding specific cables to be tested may require more than half of the time required for the condition monitoring effort.

In some cases, a tray may contain one hundred or more cables. Performing condition monitoring tests on every cable in such a tray would be extremely time consuming and expensive. However, in testing specific cables, the tester must manipulate surrounding cables. In doing so, the tester will readily be able to determine if the cable polymers are generally unaged or have experienced significant stress and have hardened. The CCM test documents the condition of a specific cable, but the observations of the tester regarding the condition of the surrounding cables is important also. The observation should be documented as well as the CCM result because of its wider implications.

Most of the CCM tests are being developed with the concept of plant life cycle management and license renewal in mind. However, to date, the uses have often been focused on more immediate problems. The Indenter has now been used to verify that cables are not in the severely aged state that theoretical evaluations have indicated. In two cases, evaluations of the effects of fire wraps and cable ampacities have indicated that cable temperatures were between 110 and 140°C for 10 or more years. Such conditions would lead to severe and readily detectable hardening of the cable insulation and jackets. Yet, Indenter testing determined that the jackets had not hardened indicating that the calculated temperatures for the applications contained inordinately large conservatisms. In another case, the extrapolation of an earlier physical test of a motor lead indicated that end of life would occur at approximately 20 years. Again, Indenter testing determined that the rate of aging was not proceeding at the rate expected from the extrapolation.

Not all of the Indenter tests indicated that cables had not aged. In two cases, the Indenter was used to map the extent of severe hot spot conditions. In one of the cases, the cable was known to have been damaged to the point of needing replacement. The Indenter test was used to identify the boundaries of the hot spot to be able to assess the physical stress imparted to the surrounding structure. Therefore, the cable was being used as an indicator of boundaries of the thermal stress event. The cable's condition provided very precise boundaries for the hot spot in that within 20 cm the cable's hardness changed from an as-new condition to extremely aged and then a few meters further changed back in the same manner. This allowed the plant personnel to more precisely model the extent of the thermal damage on the structure. In another case, the Indenter allowed the region of cable damage to be accurately mapped and helped identify the cause of the most severe damage. The mapping of the results pointed to damaged thermal insulation on a bypass header and helped plant personnel identify areas where additional thermal insulation and cooling air flow were needed to protect cables from additional damage.

Anti-contamination Issues

When working in radiologically controlled areas, test equipment will have to be packaged to prevent contamination. The means of protecting the equipment should be considered prior to entering a plant. If the test equipment must connect to the surface of a cable, cleaning the surface of the cable with dry wipes should be considered to prevent the test equipment from being contaminated. A little care can prevent long delays at control points while the equipment is being decontaminated. In addition, if CCM is to be used in radiological control areas, the technique must be possible with the technician wearing rubber gloves and protective clothing. The anti-contamination clothing greatly reduces dexterity and adds to the technician's discomfort.

If battery powered equipment is being used, consideration should be given to leaving the equipment within the radiological zone and having the charging done during periods when personnel are out of the area. This will reduce the number of times that the equipment must be decontaminated and recovered with protective materials when multiple entries into the radiological control area are required.

Sensory Inspection and Cable Aging Management

While visual and tactile inspection of cable is not a precise means of determining remaining qualified life for cables, they should not be considered useless or unimportant. Cable systems within nuclear plants are huge and CCM testing of large portions of the system is expensive. However, maintenance and operations personnel frequently are able to view or manipulate cables while performing their normal activities. During these activities, unexpected cable polymer deterioration can be identified such that more precise evaluation can be performed and the extent of the problem determined. With relatively little training personnel can be shown how to visually identify cable installation problems and deterioration from adverse stressors. Deterioration is detectable as hardening, discoloration, crazing, spontaneous cracking, and surface bloom of additives. Hardening can be evaluated by light flexure of the cable, especially instrument and control cables. If the evaluator is familiar with the resistance to flexure of a new cable of the same type, hardening is generally easy to distinguish.

As described above, testing of numerous cables within a tray is expensive and time consuming. When CCM testing a limited number of cables, additional information concerning the health of the remaining cables in the tray may be obtained by visual inspection and tactile evaluation. The data gained is important with regard to the overall health of the cable system and should be recorded.

The Westinghouse Owner's Group (WOG) has developed an aging assessment field guide for use in evaluating cable and understanding its problems. The guide provides descriptions of the type of observations that are possible under visual and tactile inspection. EPRI has reviewed the WOG guide and has determined that further development of visual/tactile techniques is not necessary.

Diagnostics Matrix for Selecting Useful Evaluation Techniques

There are numerous types of tests and inspections that may be performed on electrical cables and a number of different reasons for evaluating cable such as pre-service assessment, aging assessment, troubleshooting, and failure evaluation. A particular test may only apply to one assessment type. In

addition, certain tests apply to specific cable configurations and specific cable materials. Selection of an appropriate test method for a particular cable problem may be difficult.

To help plant cable personnel, EPRI has developed a matrix of diagnostic techniques for evaluating low-voltage cable problems. The matrix leads the user from the problem to a set of evaluation techniques that are applicable. The cable component of interest is determined first (e.g., conductors, insulations, shields and drain wires, or jackets). The type of assessment of interest and the concern are determined, and then appropriate tests are listed with reference to the more detailed discussions in the appendices of the document. The applicability of the test to specific materials is provided. Figure 4 is an example of a page from the matrix. This example shows a portion of the matrix related to insulation of multi-conductor cables and portions of the troubleshooting and aging assessment listings. For example, for troubleshooting of low insulation resistance, time-domain reflectometry is a possible test. For aging assessment, there is a list of eight possible tests that have been developed and four more that are either under development or have been partially developed. The test description number refers to the more detailed discussions that describe the test, available acceptance criteria, material applicability, equipment necessary, relative cost and complexity of interpretation of results. References are provided for more detailed descriptions of the test and available data.

The matrix has been issued in a loose-leaf format to allow it to be updated in the future as testing methodology continues to mature. The report is EPRI TR-106108, which was published in November 1997.

Conclusion

The development of useful condition monitoring techniques for cables is progressing. Repeatability of test method results between different laboratories can be improved through formal definition of test protocols and data interpretation methods. EPRI plans to continue to support the development and refinement of cable condition monitoring techniques. A number of techniques are now available when and if nuclear plant personnel need them.

Figure 4. Segment of Low-Voltage Cable Diagnostic Matrix Tracing Insulation Issue through Appropriate Test Technique

Cable Component	Cable Type	Assessment Type	Concern or Problem	Test Name	Test Description No.	Test Nature	Material Applicability*	Comments
Insulation/ Termination Insulation (Cont.)	Non-shielded Multi-conductor (Cont.)	Trouble-shooting	Low Insulation Resistance or Short Circuit	Insulation Resistance/ Polarization Index	E-001/ E-002	Nondestructive	None	Tests between conductor and remaining conductors to ground. Connected equipment should be disconnected from cable to determine component with problem.
				Time Domain Reflectometry	E-005	Nondestructive	None	Might allow determination of location of low resistance without disconnection from equipment.
		Aging Assessment	Embrittlement of Insulation	Hardness	M-001	Nondestructive	Useful for neoprene/EPR and Hypalon®/EPR composites and PVC	
				Indenter Modulus	M-003	Nondestructive	Useful for neoprene/EPR and Hypalon/EPR composites and PVC	
				Density	M-004	Essentially Nondestructive	None	
				Oxidation Induction Time	C-001	Essentially Nondestructive	Useful for EPR and XLPE	
				Oxidation Induction Temperature	C-002	Essentially Nondestructive	Useful for SBR and butyl rubber	
				Plasticizer Content	C-004	Essentially Nondestructive	For PVC only	
				Gel Content/ Swelling Ratio	C-003	Essentially Nondestructive	Useful for PVC and butyl rubber	
				Elongation-at-Break	M-002	Destructive	None	Might be useful if older cable circuit is being removed from service if results will be applicable to other cables.
				Tests in developmental stages for aging assessment	M-005, M-007, E-006, C-005			See individual discussions for state of development and potential uses.

*General applicability is listed. Applicability of a test technique to specific formulations within a generic material category (for example, XLPE) might be more limited.

Temperature and Dose Monitoring of Surroundings, and Accelerated Aging of Electrical Cables in Nuclear Power Plants

Y.Morita, T. Yagi, And T. Seguchi
Takasaki Radiation Chemistry Establishment, Japan Atomic Energy Research Institute
Watanuki-Machi, Takasaki, Gunma, 370-1292, Japan

ABSTRACT

It is essential to estimate precisely degradation of the cables during a use of 40 years that is a legal life time of nuclear reactor. There are two estimation methods of the cable degradation, one is accelerated aging method, and the other diagnostic one. In the accelerated aging, monitoring methods of temperature and average dose rate are developed around the cables in nuclear plants. Alanine-polystyrene dosimeter can be used to measure a dose for a very long term, such as under 40℃ for 200 days. And, a distribution of temperatures along pure silica optical fiber is measured over a length of 1km at accuracy of 1℃ per 1m under low dose rate(about 1Gy/h). In the acceleration of thermal aging, we found that the activation energy of deterioration obtained by tensile rest is 127kJ/mol(30.5 kcal/mol) above 100℃, and 56.5kJ/mol(13.5kcal/mol) below 100℃ for ethylene-propylene rubber(EPR) used as a cable insulation materials. In the simultaneous accelerated aging method, when a life-time of EPR is a time when a elongation at break reaches to 100%, its life-time is estimated 26years by using the degradation condition in which the acceleration factor of a dose rate and a temperature is the same to the standard condition.

The two types of non-destructive diagnostic method are studied on the cable degradation, that is a torque-strain response measurement and a photo-acoustic response measurement.

1. Introduction

Electrical cables for nuclear power plant are essential to safety operation of the plant. It is, therefore, necessary to estimate precisely degradation of the cables during a use of 40 years that is established as a legal life time of the nuclear reactor. The degradation of the cables is dominated by deterioration of the organic insulator and sheath materials which are composed mainly of the polymer materials.

There are two estimation methods of the cable degradation, one is an accelerated aging method, and the other a diagnostic one which is required as non-destructive and more conventional method.

However, in the application of the accelerated aging method containing radiation and thermal to polymer materials, there are three complex problems. At first, radiation degradation of the polymer materials is largely affected by the presence of oxygen, i.e., scission reaction is dominant in the sufficient oxygen atmosphere, such as a surface of polymer sheet at lower dose rate irradiation[1,2], on the other,

cross-linking reaction is dominant in lacking oxygen atmosphere, such as an inner part of polymer sheet at higher dose rate irradiation. In the accelerated aging for simulating a low dose rate irradiation, it is necessary that oxygen diffusion rate into a polymer is superior to radiation reaction rate in a polymer, which is related to dose rate of irradiation. Second, in thermal accelerated aging, apparent activation energy of degradation, obtained by tensile property, is different between higher temperature range and lower temperature range(below 100°C). When we use extrapolation of the activation energy of the higher temperature range, the life-time of polymers is estimated about one order longer than that predicted by the actual activation energy in the lower temperature range[2]. Third, there is a synergistic effect in the radiation-thermal aging. The degradation of polymers is different each other in the combination of dose rates and temperatures, and in simultaneous aging and sequential aging by ordering in radiation-thermal or thermal-radiation.

In a diagnostic method, the monitoring method for high voltage cables has been studied about leakage current of D.C., and comes into practical use. For the most of low voltage cables(below 600V), various detecting methods of non-destructive and more conventional diagnostic ones such as indenter[3], residual voltage method[4], have been investigated, but there is nothing in practical use.

In this paper, we report the progress at JAREI in Japan about monitoring of dose rate and temperature under irradiation for a long term, a simultaneous radiation-thermal accelerated aging test for polymer materials, and a non-destructive diagnostic method of installed cables in the plants.

2. Simultaneous radiation-thermal accelerated aging method of cable

The accelerated aging method is composed of following two stages, first, we monitor temperatures and dose rates, which are main factor of cable degradation, on actual surroundings around the installed cables in the nuclear power plants, and, second, on the basis of these measured condition, various insulator and sheath materials of the cables, such as polyethylene(PE), ethylene-propylene rubber(EPR), polyvinylchloride(PVC) and chlorosulfonated polyethylene(CSM), are tested and evaluated by the simultaneous accelerated aging of radiation and heat to estimate life-time of the cables.

2.1 Monitoring methods of temperature and average dose rate around the cables in nuclear plant

It is difficult to measure dose rates at many points of inside in container vessel by survey meter under operation of the nuclear reactor. Alanine-polystyrene dosimeter(produced by Hitachi cable Co. Ltd.,) which is developed in Japan is useful for these measurement. This dosimeter is a small size(3 mm ϕ ,3cm long), and radicals produced in alanine crystal by radiation are proportional to dose irradiated. The characteristics of the dosimeter is a precise measurement of doses, and of accumulate doses for a very long term, because there is little attenuation of radicals in or after irradiation. Figure 1 shows the change of dose responses of the dosimeter as a function of elapsed time when the dosimeters were stored at various temperatures[5]. There is little attenuation of doses in the alanine-polystyrene dosimeter when it put on the places under 40℃ for 200 days. For example, this dosimeter will be put on places where are to be

measured dose rates around the installed cables during ten months or one year that is an interval of maintenance on the nuclear power plants. If we know the temperatures around dosimeters, and are using these decay data of the dosimeter for a long term, the accumulation doses could be monitored around the installed cables in the nuclear power plants.

About temperatures in nuclear power plant, temperature measurement system using optical fiber as a sensor(produced by Hitachi cable Co. Ltd.,), is developed to apply under irradiation for a long distance. This is based on that the difference of back scattering power of Raman light between Stokes and anti-Stokes light is proportional to temperature of optical fibers, when laser pulse light sends to the fiber placed at various temperature. Figure 2 shows the temperature measurement by optical fibers under irradiation of 2.6×10^{-2}C/kg.h (1×10^{2}R/h)[6] . The Ge doped fiber can not be used to measure temperatures along the fiber because light turns into not to be transmitted through the fiber by color centers produced by

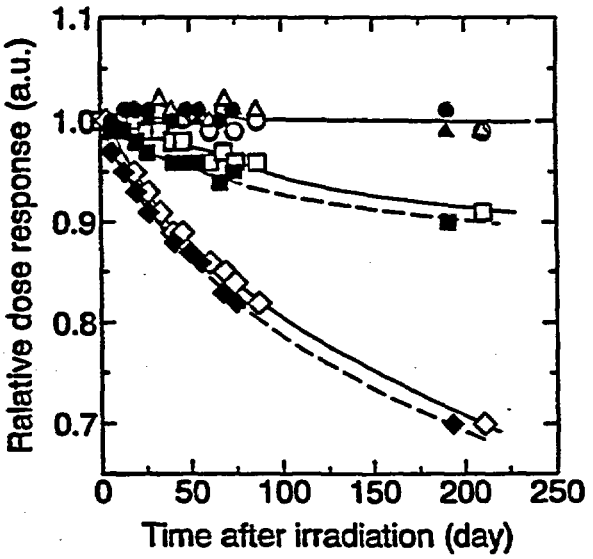

Fig. 1 Change in dose response of alanine dosimeters irradiated 0.1kGy and 1kGy
Dose 0.1kGy stored at ○25℃,△40℃,□60℃,◇80℃
Dose 1kGy stored at ●25℃,▲40℃,■60℃,◆80℃

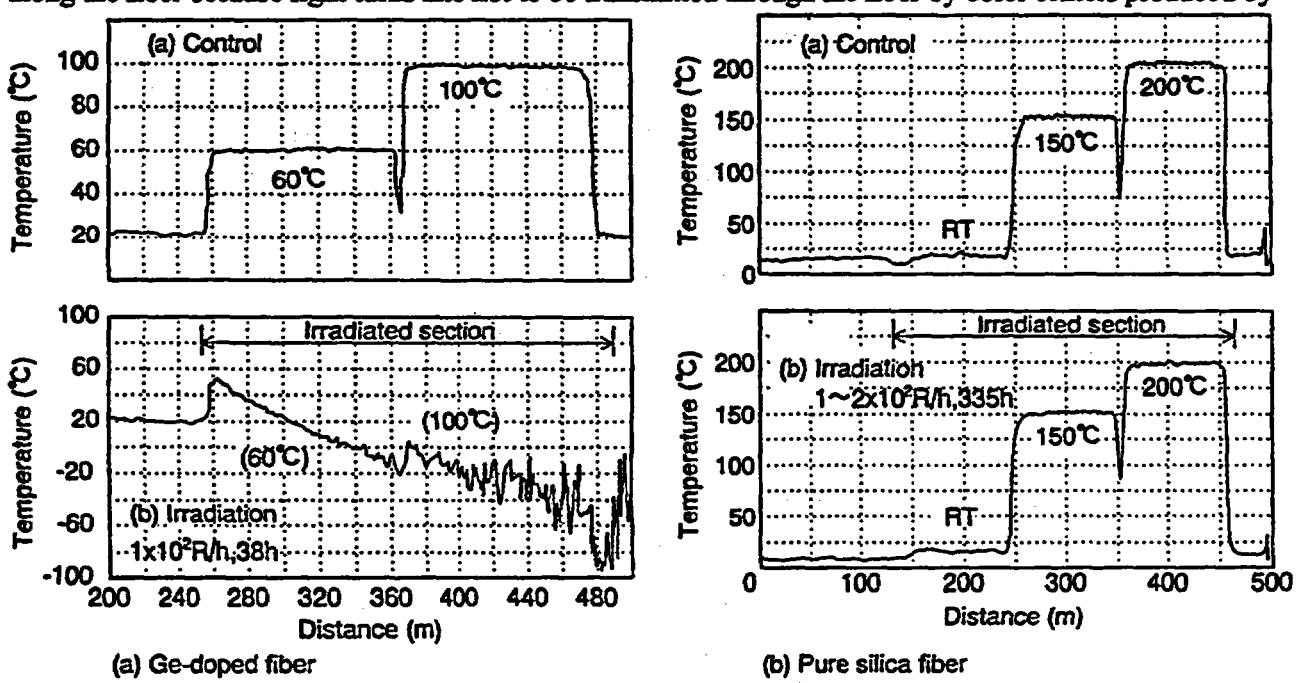

Fig. 2 Temperature measurement of long distance by optical fiber
Wave length of laser light, 854nm; Irradiation, ^{60}Co-γ ray

γ-ray irradiation. On the other hand, the pure silica fiber which has high radiation resistance can be used to measure temperatures along the fiber for a long distance under irradiation environment. Figure 3 shows the comparison with the measured temperatures obtained by optical fiber and by thermocouple under γ-ray irradiation[6]. The differences between these measurements are within ±1°C to the irradiation of 3.1C/kg(1.2x10⁴R). When we use the pure silica fiber as a temperature sensor, a distribution of temperature along the optical fiber is obtained over length of 0.5~1km at an accuracy of ±1 ℃ under the low dose rate of $2.6x10^{-2}$ C/kg.h(about 1Gy/h for organic polymers) for a long time.

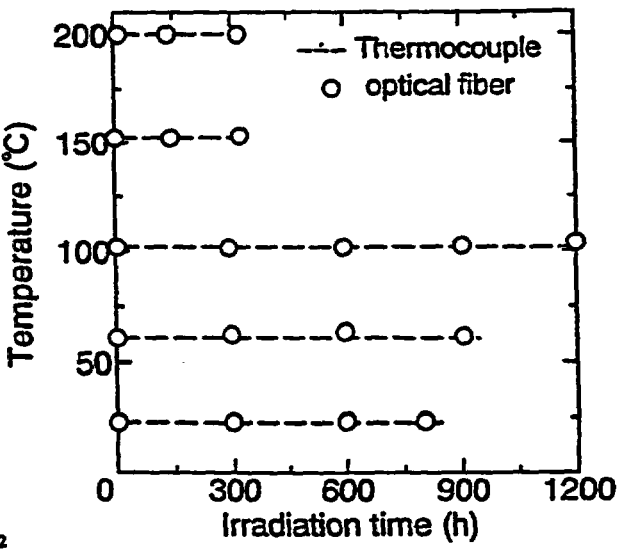

Fig. 3 Comparison with temperatures obtained by optical fiber and by thermocouple
Optical fiber, Pure silica fiber(854nm)
Irradiation, $1x10^2$R/h by ^{60}Co-γ ray

By using these methods mentioned above, we can obtain more accurate surrounding condition about dose rates and temperatures around the installed cables in the nuclear power plants.

2.2 Simultaneous radiation-thermal accelerated aging method for cable

The condition of dose rates and temperatures around the installed cables in a container vessel is said as dose rates less than 1Gy/h and as temperatures of ca.50℃ under normal operation in the nuclear power plants. We must evaluate the simultaneous radiation-thermal deterioration of the cable insulator and sheath materials for 40 years. The degradation of polymer materials in simultaneous radiation-thermal aging is complex, because of the synergistic effects of degradation with radiation and heat. The simultaneous degradation of polymer materials is more severe than those sequential degradation, i.e., degradation by thermal aging followed by irradiation, or irradiation followed by thermal aging. It is because each active region of degradation produced by γ -ray in polymer materials in the simultaneous aging is larger than that in the sequential aging or the only thermal aging.

In the simultaneous accelerated aging for polymer materials, an accelerated aging in dose rate is simply performed by using higher dose rates. For example, when dose rate is 100 times higher than 1Gy/h, we consider that the aging on irradiation is accelerated by 100 times, i.e., the irradiation time of the acceleration test is 100 times shorter than that of 1Gy/h, because in low dose and in low dose rate irradiation, active regions(spur,size2nm) produced by γ -ray in polymer materials do not overlap each other[7]. In acceleration of dose rate, however, it should be noted whether radiation oxidation takes place in an inner part of irradiated polymers. Because oxygen is lacked in an inner part of thick polymer sample by consumption of oxygen in surface region with the higher dose rate over 10^3Gy/h.

In the thermal aging of polymer materials, Arrhenius' equation is used in the acceleration of thermal deterioration, in which we extrapolate higher temperature data to lower temperature ones that are necessary to very long term in actual aging tests. If mechanism in the polymer degradation does not change in wide temperature range, an activation energy of degradation in Arrhenius' equation has a constant value for each polymer.

Figure 4 shows Arrhenius' plot (temperature dependence of degradation rate) of ethylene-propylene rubber(EPR) in thermal and thermal & radiation aging tests[2]. It is found that the apparent activation energy of degradation obtained by tensile test is different between the higher temperature range(above 100 ℃) and the lower temperature range(below 100 ℃). The activation energy(57～69kJ/mol) in the lower temperature range is about the half of that(128kJ/mol) in the higher temperature range. This suggests that, in the degradation of EPR measured by the tensile property, the degradation mechanism is different between the higher temperature range and the lower temperature range. When we use the extrapolation of the activation energy in the higher temperature range, the life time(6.7×10^3h,half of the initial value in the elongation at break) of EPR is estimated about one order longer than that(4×10^2h) predicted by the actual activation energy in the lower temperature range. Figure 5 shows Arrhenius' plots of the reaction rates of EPR under oxidation atmosphere by a chemiluminescence method[8], and a measurement of gas consumption and evolution . The activation energies obtained from both measurements are 58～65kJ/mol in the wide temperature range of 30～140℃ which contained the higher temperature range and the lower temperature range, mentioned above, and are coincided with that obtained from tensile test in the lower temperature range below 100℃. We conclude, therefore, that the activation energy of oxidation reaction on EPR is about 58～65kJ/mol in thermal or thermal & radiation aging tests, and that, in the tensile test, another effect such as micro-cracks on superficial part, or hardening rapidly on superficial part of the polymer, becomes dominant in the degradation of the polymer in the higher temperature range.

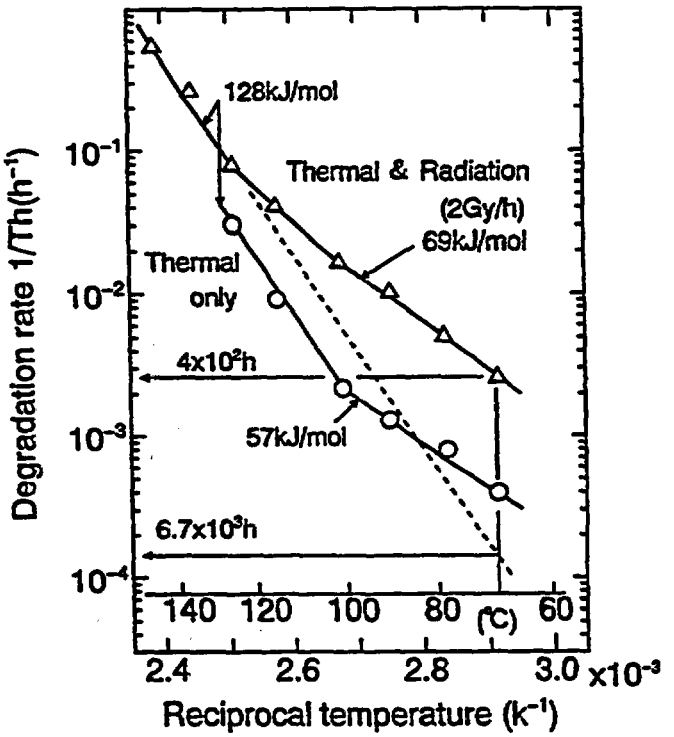

Fig. 4 Temperature dependence of degradation rate of ethylene-propylene rubber(EPR) by thermal & radiation aging in air
Th:Time when elongation is half of the initial value.

By using these different activation energies of the degradation, we get the relationship between

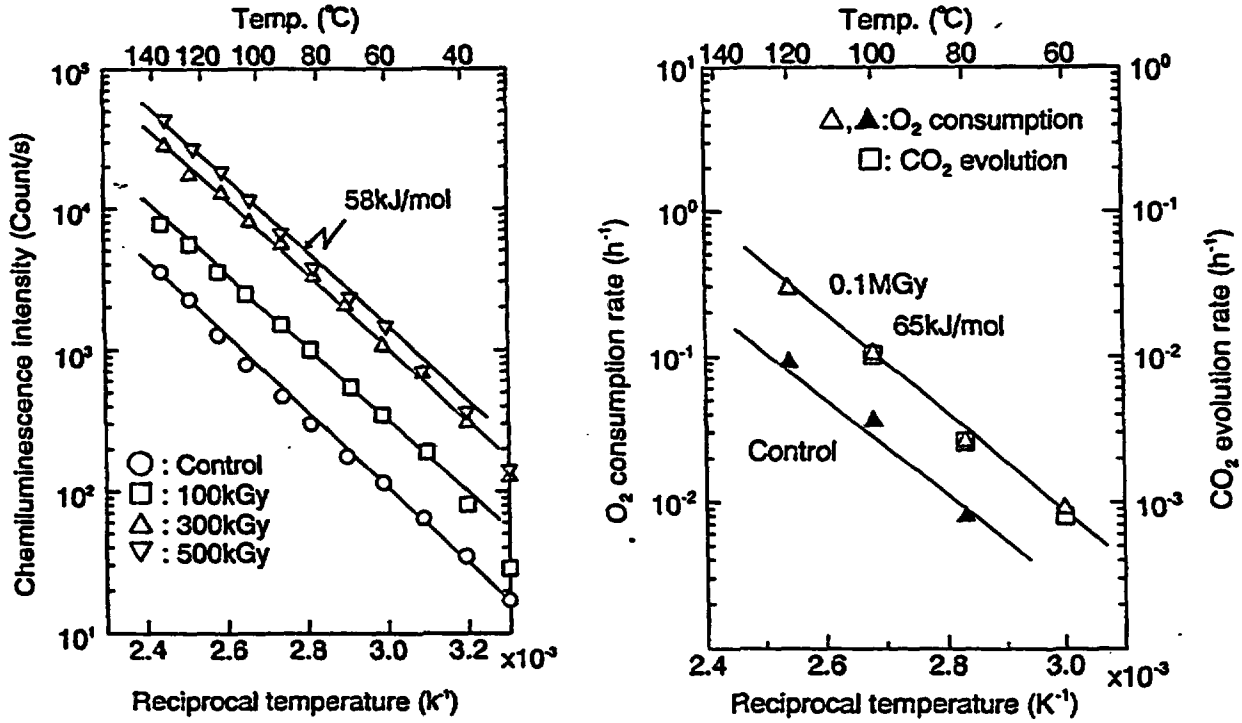

(a) Chemi luminescence intensity
dose rate : 5kGy/h under O_2 flow

(b) Gas consumption rate and evolution rate
dose rate : 5kGy/h under O_2 600torr

Fig.5 Temperature dependence on reaction rate of oxidation of EPR

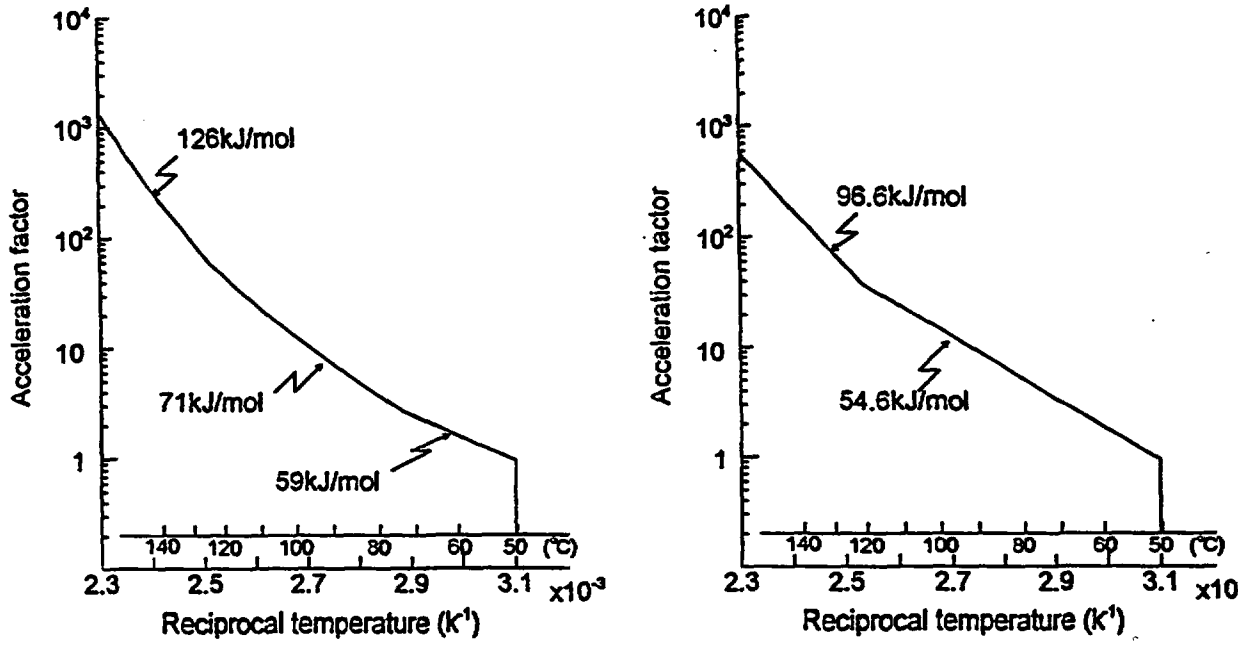

(a) Ethylene-propylene rubber

(b) Chlorosulfonated polyethylene (CSM)

Fig.6 Relationship between acceleration factor (magnification)
and aging temperature for cable materials

acceleration factor and aging temperature for the polymers as cable materials. Figure 6 shows these relationships of EPR and chlorosulfonated polyethylene(CSM) when the standard temperature condition is 50℃. The acceleration factor shows accelerated time in the thermal aging test as the accelerated time is single(one time) for the standard temperature condition. For example, in EPR as the standard temperature condition is 50℃, the aging temperature in 100 times acceleration test is 128℃ from Figure 6. Table 1 shows the conditions in the simultaneous accelerated aging test. To simulate the degradation of the cables in the container vessel for 40 years by our simultaneous accelerated aging method of radiation and heat, we must set up the same acceleration factor in dose rate and temperature for the standard condition which is said as the normal operation condition in the vessel. For EPR as the standard condition is 1Gy/h at 50℃, the dose rate and the aging temperature in 100 times acceleration of the simultaneous aging test are 100Gy/h and 128℃. In this simultaneous aging, synergistic effects of radiation and heat are contained in degradation of the aged polymers.

Figure 7 shows the tensile test result of the simultaneous radiation-thermal accelerated aging of EPR on the condition of 50(50Gy/h at 117℃), 100(100Gy/h at 128℃) times acceleration and so on for the standard condition of 1Gy/h at 50℃. Figure 8 shows the relationship between the life-time of EPR and CMS and the acceleration factor[9] from the simultaneous accelerated aging tests of Figure 7. If we adopt the life-time of EPR as time when a elongation at break reaches to 100%, the life-time of EPR is estimated 30years by extrapolating the line obtained by 50~600 times acceleration test to 1 time of acceleration factor. Using this simultaneous accelerated aging method, we can shorten the deterioration test period from 40 years to several months. By the same procedure, the life-time of CMS is predicted 18 years which is shorter than that of EPR showed more radiation-resistance than the polymers containing chlorine. We also examined the simultaneous accelerated aging test of the cables composed of cross-linked PE and formulated polyvinylchloride(PVC) by using various standard conditions. Table 2 shows the predicted life time of the low voltage cables(600V) having three type of formulated PVC. In these cases, the criterion of the life time is 100% elongation at break in PVC which is sheath material of the cables. The predicted life times of the cables(PVC) scattered from 0.9 year to 81.1 years, depending largely on formulation of PVC, i.e., plasticizer, antirad agent, and so on. It is also pointed out that synergistic effects of radiation and heat are observed above dose rate of 0.5Gy/h on the degradation of PVC.

3. Non-destructive diagnostic method of cable

The two types of non-destructive diagnostic methods are studied on the cable degradation. One is a torque-strain response measurement, and the other photo-acoustic response measurement.

Figure 9 shows a schematic drawing of torque-strain response measurement for the installed cable. There are two chucks apart from 50mm, which grip the cable. The twist chuck moves a small amount of degree(5/360~10/360) with sine wave of low frequency, and the fixed chuck detects torque transmitted through the cable. Figure 10 shows relationship between torque and elongation at break (PVC) of cable

Table1. Condition of simultaneous accelerated aging test

· Standard Aging Condition in Normal Operation(Acceleration Factor =1)

Dose rate : 1Gy/h
Temperature : 50°C

· Simultaneous accelerated aging condition:

Acceleration Factor (Magnification: times)		1	50	100	300	600
Dose rate (Gy/h)		1	50	100	300	600
Temperature (°C)	EPR	50	117	128	143	152
	CSM*	50	124	134	150	161

* CSM : Chlorosulfonated polyethylene

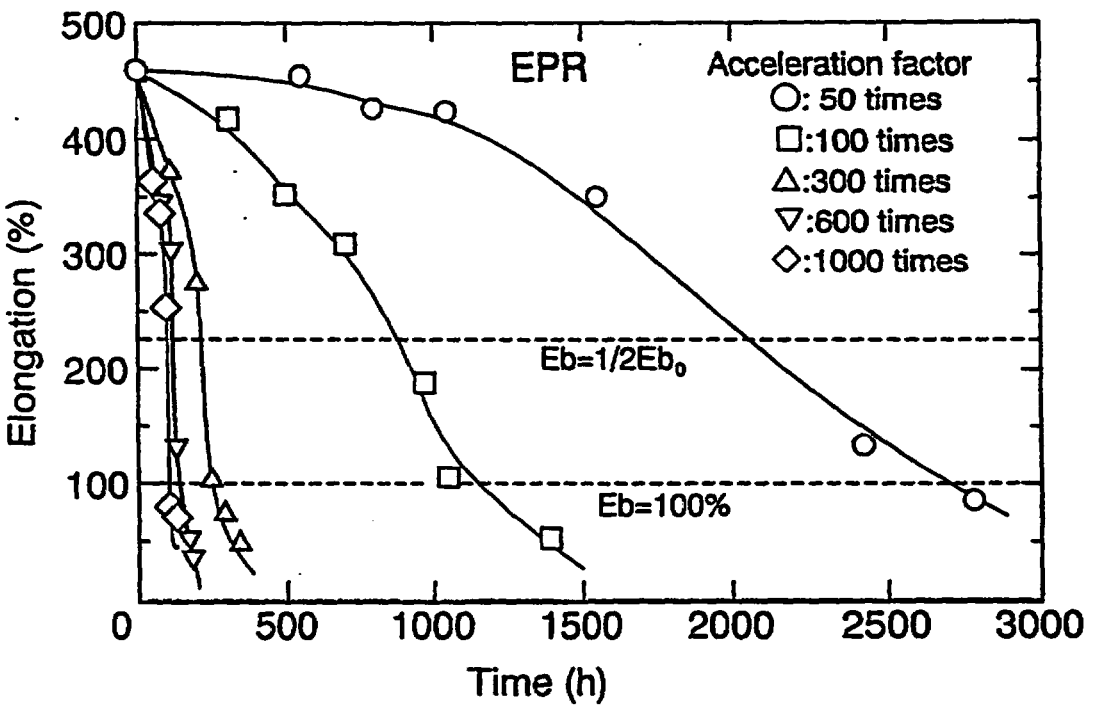

Fig.7 Change in tensile elongation at break of ethylene-propylene rubber (EPR) by a simultaneous acceleratied aging test

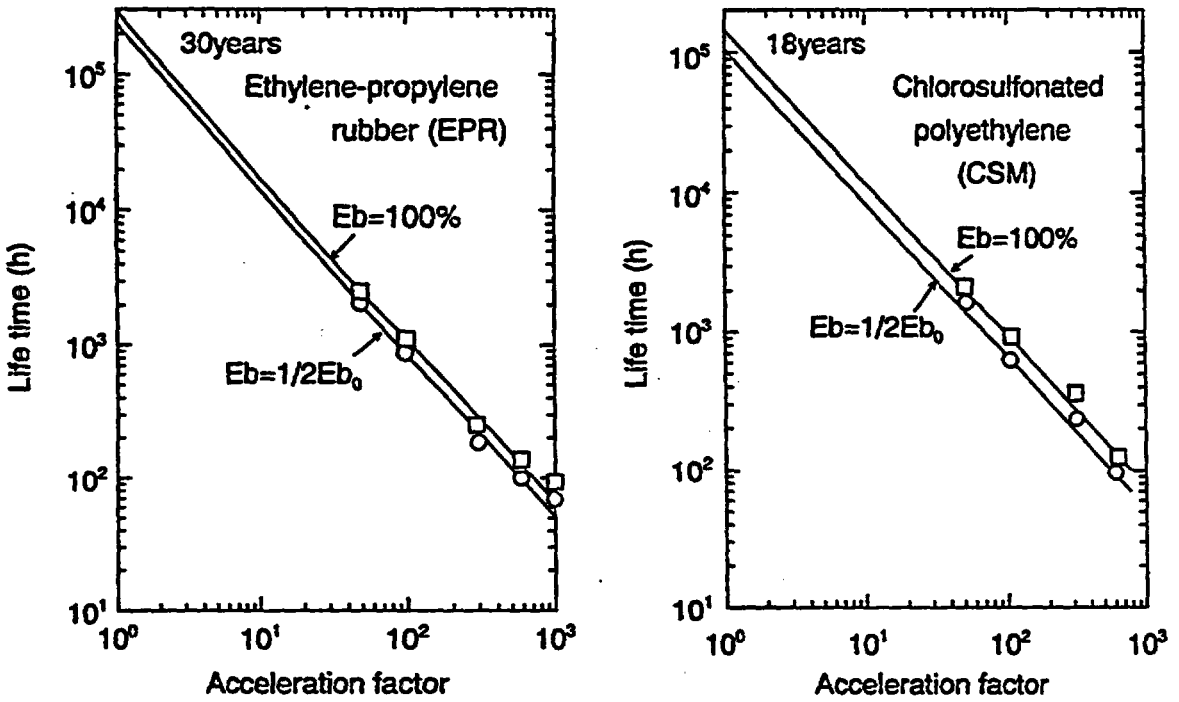

Fig.8 Life time prediction of cable materials by simultaneous accelerated aging test
Eb : Elongation at break of aged sample
Eb_0 : Elongation at break of initial value

Table2. Predicted life time of cable*

Standard aging condition	Predicted life time** of cable (year)		
	cable(No.1)	cable(No.2)	cable(No.3)
heat only, 45°C	2.2	18.3	81.1
0.05 Gy/h, 45°C	2.2	18.3	81.1
0.5 Gy/h, 45°C	2.2	18.3	50.2
5 Gy/h, 45°C	0.9	5.5	11.4

*Cables are composed of cross-linked PE and formulated PVC sheath.

**Criterion : 100% elongation at break .

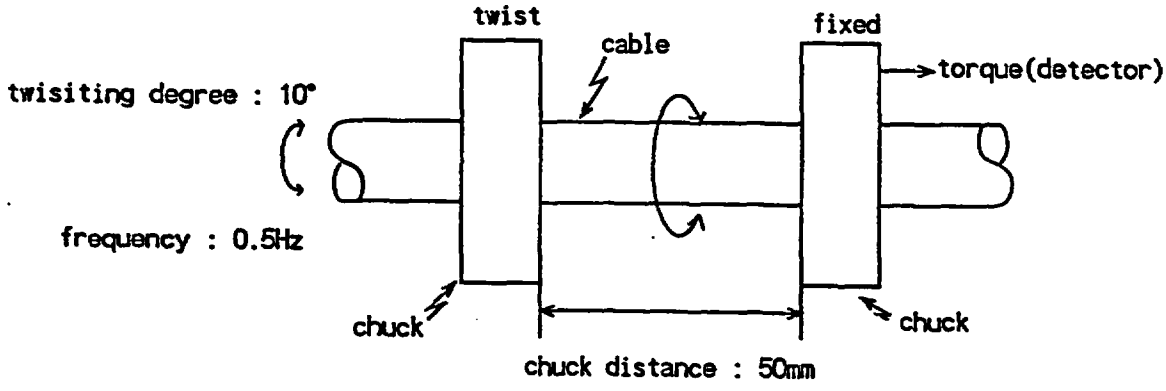

chuck size(cable diameter) : 9.5-16.0mm

Fig.9 Schematic drawing of torque-strain response measurement.

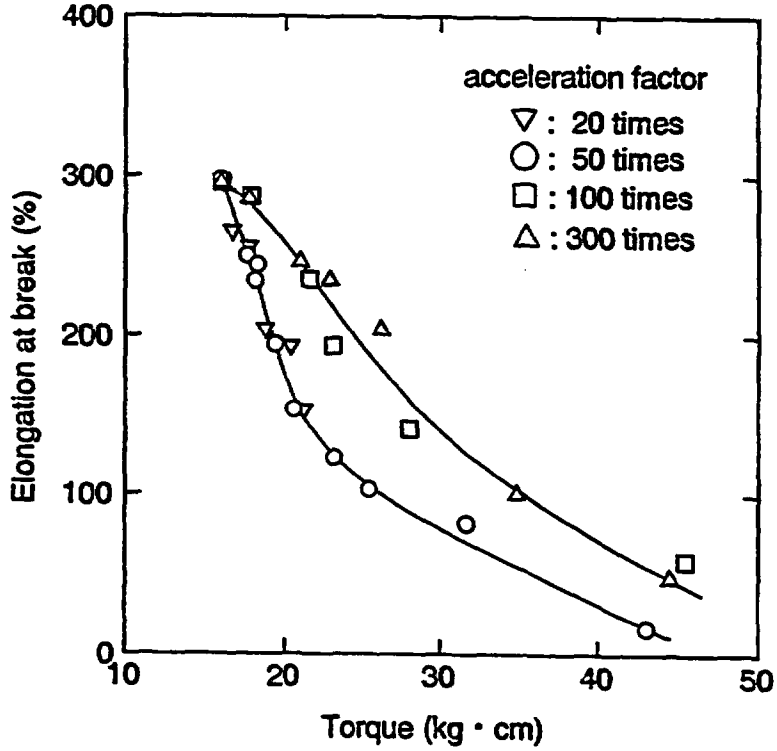

Fig.10 Relationship between torque and elongation at break(PVC) of cable

Cable: Insulator, cross-linked polyethylene

Sheath, polyvinylchloride(PVC)

Standard condition: 1Gy/h at 50°C

performed the simultaneous aging test[10]. We found that the torque response is more sensitive to PVC under ca.150% elongation at break, under which PVC change clearly to brittle, and we want to detect more precisely the degradation of PVC. And, as the torque-strain response is also sensitive to deterioration of surface part on the cable, the severe acceleration condition, such as 300 times acceleration test, bring the larger response for the torque measurement. It is, therefore, better to adopt the torque-elongation curve of the lower acceleration factor(20,50 times acceleration). A instrument of the torque-strain response is so compact that we can carry it to the installed cable in container vessel, and measure deterioration of the cable by it.

Figure 11 shows the schematic drawing of photo-acoustic measurement which is more non-destructive monitoring method of cable deterioration, comparing to the torque-strain method. In this measurement, we detect elastic wave of lateral direction which is very difficult in generating into soft elastic materials such as plastic or rubber by usual ceramic oscillator. Figure 12 shows the photo-acoustic response from PVC sheet. The aged sample which changed to brittle represents clearly higher response, comparing to that of the control sample. In this method, we try to measure a velocity of elastic waves which show more clear difference between an aged sample and a control sample.

4. Estimation and diagnosis of degradation for installed cable

We propose the estimation and diagnosis method of degradation for the installed cables in the container vessel in the nuclear power plants.

1) we measure precisely dose rate and temperature around the installed cables under normal operation, because radiation and heat are main factor for the deterioration of polymer materials which are used as insulator and sheath of the cable.
2) According to the measured condition of dose rate and temperature, we adopt a few standard conditions on normal operation in the plant. For example, a more severe standard condition and a more reduce standard condition.
3) we measure the activation energy of degradation on polymer materials for lower temperature range, especially under 100°C, by measurement of oxygen consumption and gas evolution rates, chemiliminescence, and tensile property.
4) We perform the simultaneous radiation-thermal aging test to the various cable materials under condition of the same acceleration factor of dose rate and temperature. The predicted life times of cable materials are obtained to the various polymers.
5) According to the predicted life time of the cable materials, we measure the deterioration of the installed cable in container vessel by non-destructive diagnostic method
6) Comparing the predicted life time of the cable and degradation obtained by non-destructive diagnostic method, we estimate the degradation of the cable.

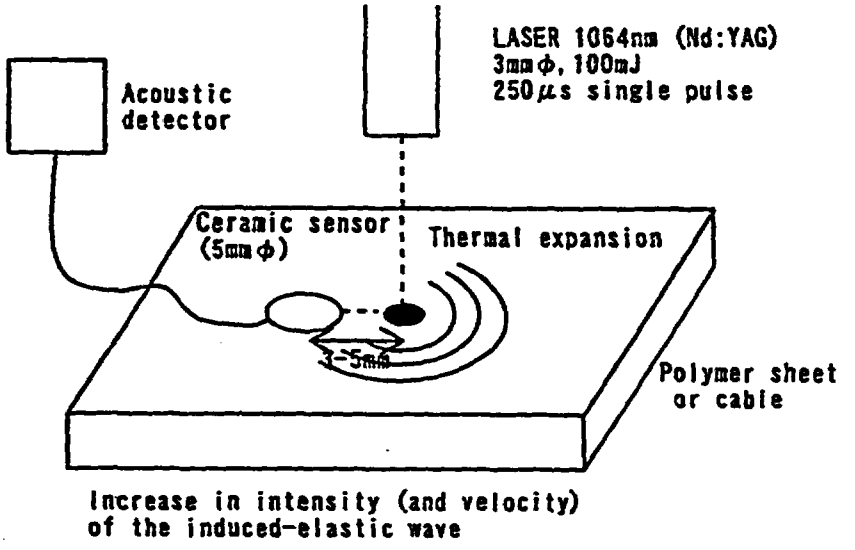

Fig.11 Photo-acoustic measurement for non-destructive monitoring of cable

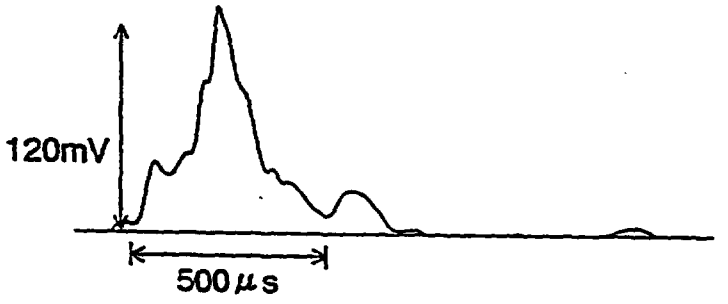

a) Control sample
(Elongation at break : 247%)

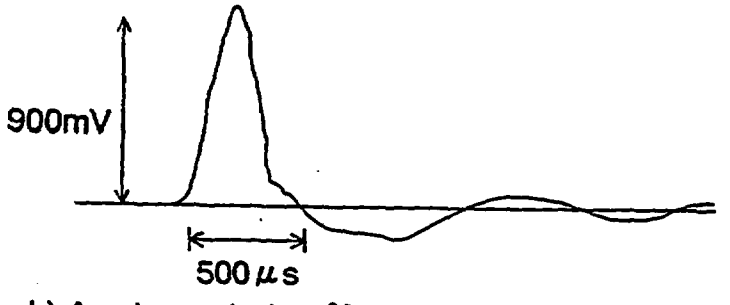

b) Aged sample (132℃,95days)
(Elongation at break : 100%)

Fig.12 Photoacoustic response from PVC sheet

5. Conclusion

The accelerated aging method is composed of following two stages, first, we monitor temperatures and dose rates, which are main factor of cable degradation, on actual surroundings around the installed cables in the nuclear power plants, and, second, on the base of these measured condition, various insulators and sheaths of the cables are tested and evaluated by the accelerated aging of irradiation and heat to estimate the life time of the cables.

Alanine-polystyrene dosimeter and temperature measurement system of optical fiber as a sensor, are developed for a long term under irradiation. In the acceleration of thermal aging, the activation energy of deterioration obtained by tensile rest is 127kJ/mol above 100℃, and 56.5kJ/mol below 100℃ for ethylene-propylene rubber used as a cable insulation materials. In the simultaneous accelerated aging method, its life-time is estimated 30years by using the degradation condition in which the acceleration factor of a dose rate and a temperature is the same to the standard condition.

The two types of non-destructive diagnostic method are studied on the cable degradation, that is a torque-strain response measurement and a photo-acoustic response measurement.

We propose the estimation method of degradation for installed cables in the container vessel in the nuclear power plants. This method is consist of, first, obtaining the predicted life time from the simultaneous accelerated aging test for the cable materials, and, second, measuring the degradation of cable by non-destructive diagnostic method. Combining two methods, we estimate the degradation of the cable in the plants.

Acknowledgement

The authors wish to thank Y.Haruyama(JAERI) for Alanine dosimeter datum, and S.Yamamoto(Hitachi Cable Co. Ltd.,) for data of temperature measurement by optical fibers.

References

1)K.T.Gillen and R.L.Clough;*ACS Symposium Series475, 1990,p457.*
R.L.Clough and K.T.Gillen;*Poly. Deg. and Stability,1992,38,p47*

2)Y.Morita,T.Yagi and W.Kawakami;*ACS Symposium Series475,1990,p485.*

3)S.P.Carfagno et. al.;*International Conference on Operability on Nuclear Systems in Normal and Advanced Environments, 1989,Vol.1,p195.*

4)S.Yamanaka et. al.;*Trans. IEEE of Japan, 1990,Vol.110A(No.3), p181.*

5)Y.Haruyama,H.Tachibana,T.Kojima,J.Okamoto,S.Kashiwazaki,S.Matsuyama,H.Yagyu;*Radioisotopes, 1995,Vol.4(No.8),p507.*

6)Y.Morita,S.Yamamoto,K.Fukuchi,H.Kawakami;*Denkigakkai-Kenkyukaisiryo,1993,DEI-93-166,p21.*

7)J.W.T.Spinks and R.J.Woods;*"An Introduction to Radiation Chemistry",1964,Jhon Wiley & Sons Inc. New York.*

8)T.Yagi,T.Seguchi; *Denkigakkai-Kenkyukaisiryo,1992,DEI-92-114,p63.*

9)T.Yagi,T.Seguchi,T.Okuda,K.Kanamituya,T.Tachibana;*Denkigakkai-Kenkyukaisiryo,1991,DEI-91-126, p45.*

10)T.Yagi,Y.Morita,W.Kawakami,S.Kamimura,H.Yagyu,O.Mochizuki,T.Onishi; *Denkigakkai-Kenkyukai-siryo, 1990,EMI-90-124,p65*

Accident Testing of Artificially Aged and Naturally Aged Electric Cables

R. Lofaro, M. Villaran
Brookhaven National Laboratory
Upton, NY 11973
(516) 344-7191
e-mail: lofaro@bnl.gov

OVERVIEW OF BNL CABLE TESTING PROGRAM

- Addressing 6 Issues related to E.Q.
  - by testing electric cables
- Scope: Low-Voltage I&C Electric Cables

ISSUES ADDRESSED BY TEST SEQUENCES

Issue	Test Sequence Addressing Issue					
	1	2	3	4	5	6
1. Arrhenius Application	✔	✔	✔			✔
2. Activation Energies (a)						
3. Multi-Conductor Cables				✔		
4. Bonded Jacket Cables					✔	
5. Condition Monitoring Effectiveness	✔	✔	✔	✔	✔	✔
6. Condition Monitoring for LOCA Survivability	✔	✔	✔	✔	✔	✔

(a) Activation energy issue to be addressed by separate materials testing at BNL.

OVERVIEW OF TEST SEQUENCES

Test	*Cable Tested*	*Artificial Aging*
LOCA 1	XLPE/Neoprene	20 yrs.
LOCA 2	EPR/Hypalon (unbonded)	20 yrs.
LOCA 3	XLPE/Neoprene	40 yrs.
LOCA 4	EPR/Hypalon (bonded)	20/40 yrs.
LOCA 5	EPR/Hypalon (bonded/unbonded)	20/40 yrs.
LOCA 6	EPR/Hypalon (bonded/unbonded)	60 yrs.
	XLPE/Neoprene	60 yrs.

OVERVIEW OF TESTING

- 6 Test Sequences Planned
  - accelerated aging of new cable
  - naturally aged cable
  - accident (LOCA) testing
  - periodic condition monitoring
- Test Parameters Based on Original Qualification
  - E.Q. report for naturally aged cable used

PREAGING & TEST PARAMETERS FOUR SPECIMEN GROUPS

1. Control specimens ~ no preaging
2. Specimens preaged to match naturally aged cables
3. Naturally aged cables
4. Cables preaged to 20 yrs. per original qualification documentation

ORIGINAL QUALIFICATION FOR ROCKBESTOS FIREWALL III CLASS 1E CABLES

- Parameters from Rockbestos report QR#1806
  - irradiation cross-linked insulation
- Artificial aging to simulate 40 years @ 90°C
  - 1300 hrs @ 150°C
  - 50 Mrad @ 0.51 Mrad/hr
- Accident Exposure
  - 150 Mrad @ 0.51 Mrad/hr
  - steam/chem spray similar to IEEE 323-1974, Appendix A

PLANT SERVICE CONDITIONS FOR LOCA 1 NATURALLY AGED CABLE

- LOCA 1 specimen taken from temperature detector circuit in S/G compartment
- Historical RWP's & HP engineer input used to determine dose rate
- Plant records & operations personnel input used to determine temperature
- Plant purchasing & QA records indicated mfg & installation dates
- Plant operating history records indicated power operation cycle

CABLE SPECIMEN MOUNTING

- Naturally Aged Cable
  - Straight configuration secured in steel Unistrut channel
- Preaged Cables
  - Straight configuration secured in steel Unistrut channel
  - Mounted on mandrel 20 times the diameter of the cable
- Short Specimens for Materials Testing
  - 6 inch pieces of insulation and jacket materials enclosed in stainless steel baskets

TYPICAL STRAIGHT SPECIMENS MOUNTED IN UNISTRUT

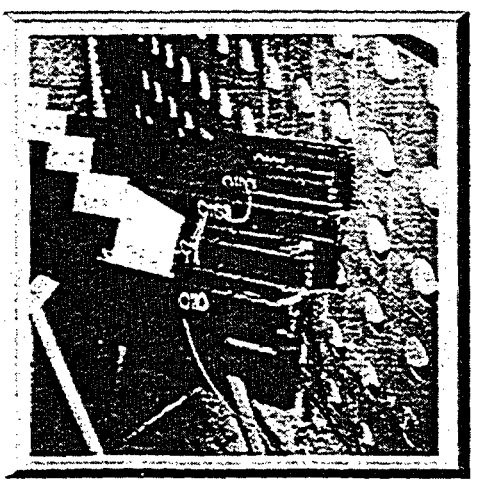

TYPICAL MANDREL MOUNTED SPECIMEN

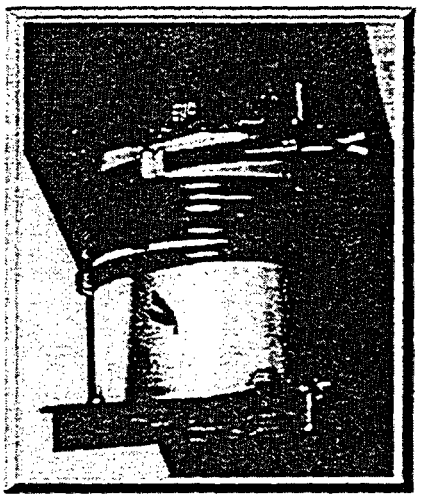

TYPICAL BASKET SPECIMENS

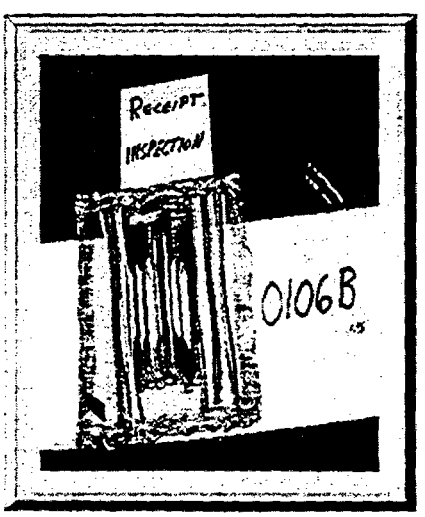

PREAGING PARAMETERS FOR GROUP II SPECIMENS (MATCH NATURALLY AGED CABLES)

- Thermal Aging
  - 2.86 hrs at 120°C using Ea = 1.34eV
- Service Radiation
  - 0.6 Mrad at 0.5 Mrad/hr
- Accident Radiation
  - 150 Mrad at 1.0 Mrad/hr

PREAGING PARAMETERS FOR GROUP IV SPECIMENS (20 YRS EQUIVALENT SERVICE)

- Thermal Aging
  - 650 hrs at 150°C
- Service Radiation
  - 25 Mrad at 0.5 Mrad/hr
- Accident Radiation
  - 150 Mrad at 1.0 Mrad/hr

LOCA 1 TEST PARAMETERS

- Rockbestos QR #1806
  - 346°F/113 psig double peak transient
  - Test duration 7 days
- Chemical Spray
  - 24 hrs starting @ 32 psig test pressure
  - Boric Acid, Sodium Thiosulfate, Sodium Hydroxide

LOCA CHAMBER AT WYLE LABORATORIES

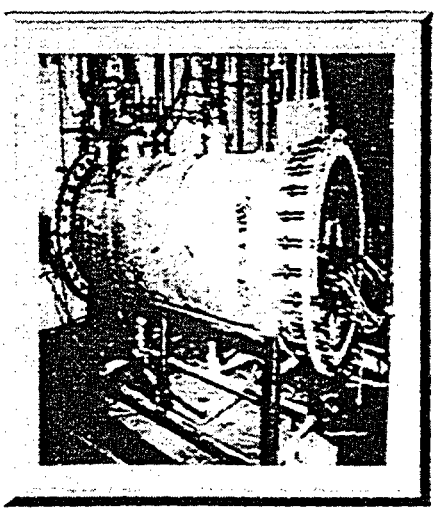

LOCA 1 PROFILE

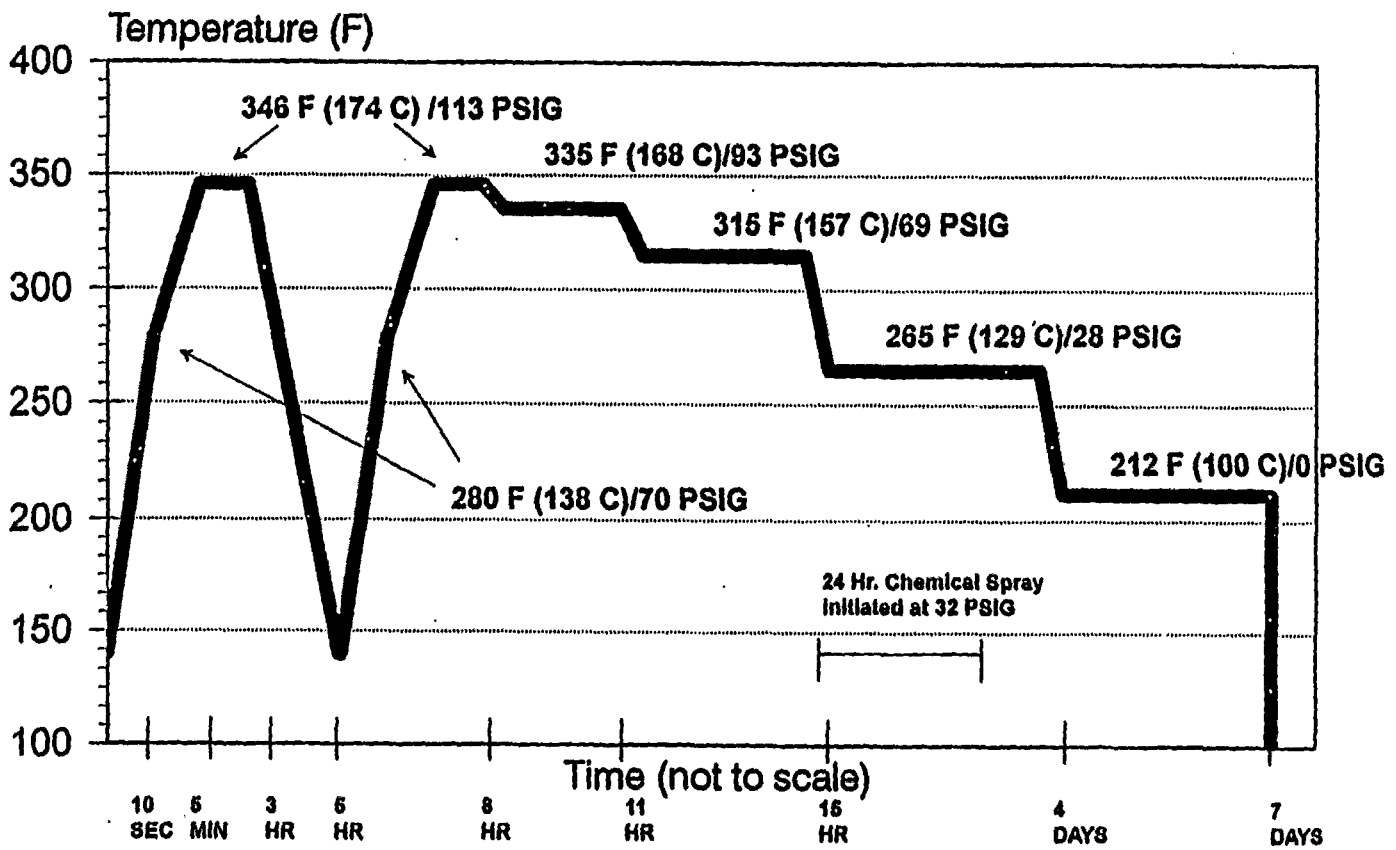

TEST SPECIMENS LOADED INTO LOCA CHAMBER

TYPICAL CONDITION OF MANDREL SPECIMENS AFTER THERMAL AGING TO SIMULATE 20 YEAR AGED CABLE

TYPICAL CONDITION OF MANDREL SPECIMENS AFTER LOCA TESTING

CABLE FUNCTIONAL TEST

- Simulate an actual application for I&C cable
  - Pressure transmitters connected to a manifold
  - 4-20 mA instrument loops
  - 28 Vac power supply protected by a 1/32 Amp fuse
- Monitor circuit parameters & manifold pressure
- Test leads spliced to specimens inside chamber
  - Raychem nuclear grade splices

SUMMARY OF FUNCTIONAL PERFORMANCE ANOMALIES

Group	Maximum Current Deviation (% Full Scale)		Number of Blown Fuses	Maximum Leakage Current (mA)
	Side "A"	Side "B"		
1	4*	4*	0*	0.1
2	4	3	0	0.1
3	2	2	0	0
4	46	3	4	23.7

* Specimen 0105 had a maximum deviation of 96% and blew a fuse; however, this was due to a PT problem.

FUNCTIONAL TEST SUMMARY GROUP 4

Specimen	Max Deviation (% full scale)	Max Leakage (mA)	Ckt Overload Events
0112	2	23.7	1
0113	8	4.3	0
0114	2	0.4	0
0115	4	3.7	0
0116	46	3.7	3

POST-LOCA INSPECTION

- IR test 1 day after LOCA (Specimens wet)
  - Groups 1, 2, 3 acceptable
  - Group 4 all five specimens unacceptable
- IR repeated 2 1/2 weeks later (specimens dried)
  - same results
- Dissection of connections
  - isolated low IR readings inside splices
- All Grp 4 specimens had acceptable IR
  - splices removed

PROBLEMS WITH LOCA 1 SPLICES

- Cracks in specimen jackets provided a moisture pathway into splice
- Inner & outer sleeves too short
- Possible mismatch of shim & test lead diameters
- Ground shield left inside splice uncapped in close proximity to butt splices

MODIFICATIONS FOR FUTURE LOCA TESTS

- Splice kits for test specimens will be specified for this application by Raychem
- Training for Wyle staff on proper splice installation will be provided by Raychem

LOCA 1 FUNCTIONAL TEST CONCLUSIONS

- Performance of test specimens acceptable
- Anomalies attributed to faulty splices & one PT malfunction
- Leakage current alone not a good indicator of instrument ckt. performance

ORIGINAL QUALIFICATION FOR AIW CLASS 1E CABLES

- Parameters from Franklin report #F-C4197-2
  - Ethylene Propylene Rubber
- Artificial aging to simulate 40 years @ 50°C
  - 168 hrs @ 121°C
  - 50 Mrad @ 0.5 Mrad/hr
- Accident Exposure
  - 75 Mrad @ 0.5 Mrad/hr
  - single peak (171°C/60 psig) accident profile

PREAGING PARAMETERS FOR GROUP II SPECIMENS (MATCH NATURALLY AGED CABLES)

- Thermal Aging
  - 30.3 hrs at 121°C using Ea = 1.18eV
- Service Radiation
  - 3.25 Mrad at 0.5 Mrad/hr
- Accident Radiation
  - 75 Mrad at 1.0 Mrad/hr

PREAGING PARAMETERS FOR GROUP IV SPECIMENS (20 YRS EQUIVALENT SERVICE)

- Thermal Aging
  - 84 hrs at 121°C
- Service Radiation
  - 25 Mrad at 0.5 Mrad/hr
- Accident Radiation
  - 75 Mrad at 1.0 Mrad/hr

TYPICAL CONDITION OF MANDREL SPECIMENS AFTER THERMAL AGING TO SIMULATE 20 YEARS OF SERVICE

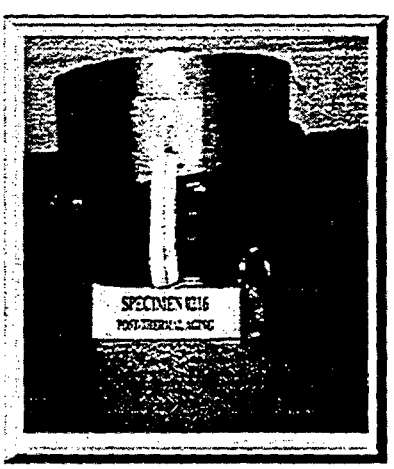

SUMMARY OF FUNCTIONAL PERFORMANCE ANOMALIES

Group	Maximum Current Deviation (% Full Scale)		Number of Blown Fuses	Maximum Leakage Current (mA)
	Side "A"	Side "B"		
1	<2	<2	0	0
2	<2	<2	0	0
3	<2	<2	0	0
4	<2	<2	0	0.1

TYPICAL CONDITION OF SPECIMENS AFTER LOCA TESTING

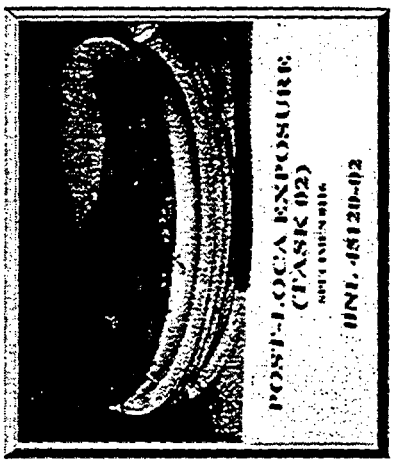

LOCA 2 FUNCTIONAL TEST CONCLUSIONS

- Performance of test specimens acceptable
- No anomalies observed

INSIGHTS FROM LOCA TESTS 1 AND 2

- Arrhenius
  - comparable aging for natural and artificially aged cables (10 yr. And 24 yr. old cable)
  - XLPE/Neoprene and EPR/CSPE cables artificially aged to 20 yrs. indicate conservative aging
- CM effectiveness
  - several CM techniques appear to be effective
  - may need more than 1 CM technique to characterize condition
  - further evaluation needed

NRC FORM 335 (2-89) NRCM 1102, 3201, 3202

U.S. NUCLEAR REGULATORY COMMISSION

BIBLIOGRAPHIC DATA SHEET

(See instructions on the reverse)

1. REPORT NUMBER (Assigned by NRC, Add Vol., Supp., Rev., and Addendum Numbers, if any.)

NUREG/CP-0166
Vol. 3

2. TITLE AND SUBTITLE

Proceedings of the Twenty-Sixth Water Reactor Safety Information Meeting

Thermal Hydraulic Research, Plant Aging I - Plant Life Management, High Burn-up Fuel, Plant Aging II - Cable Aging

3. DATE REPORT PUBLISHED

MONTH	YEAR
June	1999

4. FIN OR GRANT NUMBER

A3988

5. AUTHOR(S)

Compiled by Susan Monteleone, Brookhaven National Laboratory

6. TYPE OF REPORT

Conference Proceedings

7. PERIOD COVERED *(Inclusive Dates)*

October 26-28, 1998

8. PERFORMING ORGANIZATION - NAME AND ADDRESS *(If NRC, provide Division, Office or Region, U.S. Nuclear Regulatory Commission, and mailing address; if contractor, provide name and mailing address.)*

Office of Nuclear Regulatory Research
U.S. Nuclear Regulatory Commission
Washington, DC 20555-0001

9. SPONSORING ORGANIZATION - NAME AND ADDRESS *(If NRC, type "Same as above"; if contractor, provide NRC Division, Office or Region, U.S. Nuclear Regulatory Commission, and mailing address.)*

Same as 8. above.

10. SUPPLEMENTARY NOTES

S. Nesmith, NRC Project Manager Proceedings prepared by Brookhaven National Laboratory

11. ABSTRACT *(200 words or less)*

This three-volume report contains papers presented at the Twenty-Sixth Water Reactor Safety Information Meeting held at the Bethesda Marriott Hotel, Bethesda, Maryland, October 26-28, 1998. The papers are printed in the order of their presentation in each session and describe progress and results of programs in nuclear safety research conducted in this country and abroad. Foreign participation in the meeting included papers presented by researchers from France, Germany, Italy, Japan, Norway, Russia, Sweden and Switzerland. The titles of the papers and the names of the authors have been updated and may differ from those that appeared in the final program of the meeting.

12. KEY WORDS/DESCRIPTORS *(List words or phrases that will assist researchers in locating the report.)*

BWR Type Reactors - Reactor Safety, Nuclear Power Plants - Reactor Safety, PWR Type Reactors - Reactor Safety, Reactor Safety - Meetings

13. AVAILABILITY STATEMENT

unlimited

14. SECURITY CLASSIFICATION

(This Page)
unclassified

(This Report)
unclassified

15. NUMBER OF PAGES

16. PRICE

Federal Recycling Program

UNITED STATES
NUCLEAR REGULATORY COMMISSION
WASHINGTON, DC 20555-0001

OFFICIAL BUSINESS
PENALTY FOR PRIVATE USE, $300

SPECIAL STANDARD MAIL
POSTAGE AND FEES PAID
USNRC
PERMIT NO. G-67